ASTRONOMICAL OBSERVATORY OF ADAM MICKIEWICZ
UNIVERSITY IN POZNAŃ

METEOROIDS 2013

Proceedings of the International Conference held at the Adam Mickiewicz University in Poznań, Poland

August 26-30, 2013

Edited by

Tadeusz J. Jopek
Frans J.M. Rietmeijer
Junichi Watanabe
Iwan P. Williams

WYDAWNICTWO NAUKOWE

POZNAŃ 2014

Editors

Tadeusz J. Jopek
Astronomical Observatory of Adam Mickiewicz University
in Poznań, Poland

Frans J.M. Rietmeijer
University of New Mexico,
Albuquerque, USA

Junichi Watanabe
National Astronomical Observatory of Japan,
Tokyo, Japan

Iwan P. Williams
Queen Mary College,
London, UK

Wydano na podstawie maszynopisu gwarantowanego

Projekt okładki: Helena Oszmiańska-Napierała

Redaktor techniczny: Elżbieta Rygielska

ISBN 978-83-232-2726-7

WYDAWNICTWO NAUKOWE UNIWERSYTETU IM. ADAMA MICKIEWICZA W POZNANIU
61-701 POZNAŃ, UL. A. FREDRY 10
www.press.amu.edu.pl
Sekretariat: tel. 48 61 829 46 46, faks 48 61 829 46 47, e-mail: wydnauk@amu.edu.pl
Dział sprzedaży: tel. 48 61 829 46 40, e-mail: press@amu.edu.pl
Ark. wyd. 32,00. Ark. druk. 24,000
DRUK I OPRAWA: UNI-DRUK, LUBOŃ, UL. PRZEMYSŁOWA 13

Table of contents

Preface

The idea of holding a conference on meteors and interplanetary dust emerged at the commission 22 meetings during the IAU General Assembly in Baltimore and was firmed up at the next meeting in Buenos Aires, where it was decided to hold a conference in Czechoslovakia in 1992. This was 25 years since a meeting "Physics and Dynamics of Meteors" was held at Tatranská Lomnica, Czechoslovakia.

The first Meteoroids Conference was held in Smolenice July 6-10 1992. Interestingly, by the time the proceedings were published (Meteoroids and their Parent Bodies) Czechoslovakia had divided into two independent countries and the book was published by the Slovak Academy of Sciences.

Since that beginning, meetings have been held at roughly three year intervals (Bratislava, Slovakia, 1994; Tatranská Lomica, Slovakia, 1997; Kiruna, Sweden, 2001; London, Canada, 2004; Barcelona, Spain, 2007; Breckenridge, USA, 2010) and this volume publishes papers presented at the eighth meeting held at the Adam Mickiewicz University in Poznań, Poland 26 - 30 August 2013. This meeting, as did the first meeting in Smolenice and some of the others, followed the annual meeting of the International Meteor Organization, thus allowing a continuation of the fruitful collaboration between professional and amateur astronomers that is common in meteor astronomy, by allowing participants to easily attend both meetings. A special session on outreach and relation with amateur meteor astronomers was included in the program.

There were 103 participants from 27 countries at the conference. A significant part of the conference was devoted to the results from the spectacular and large fireball that was observed over Chelyabinsk in Russia on 15th February 2013 and to meteorite falls in general as well as meteoroid interactions with the planetary atmospheres. Other areas of science covered were Observation techniques; Sporadic and shower meteoroids; Physical properties of meteoroids; Meteoroid parent bodies; interplanetary dust and interstellar meteoroids. Some coverage was also given to meteoroid data bases and historical records.

This Volume contains many of the papers that were presented at this meeting. All the papers were refereed and the help of the referees are acknowledged.

Tadeusz J. Jopek,
Iwan P. Williams,
and Junichi Watanabe
co-chairs SOC

Scientific Organizing Committee

Tadeusz J. Jopek (co-chair)	Astron. Observatory of A.M. University, Poland
Iwan P. Williams (co-chair)	Queen Mary College, U.K.
Junichi Watanabe (co-chair)	National Astronomical Observatory of Japan, Japan
Jiří Borovička	Astron. Inst. of the Academy of Sciences, Czech Rep.
Peter Brown	University of Western Ontario, Canada
Guy J. Consolmagno	Vatican Observatory, Vatican
William J. Cooke	NASA Marshall Space Flight Center, Al, USA
Eberhard Grün	Max-Planck-Institut fur Kernphusik, Germany
Robert Hawkes	Mount Allison University, Canada
Diego Janches	GSFC/NASA, Greenbelt, MD, USA
Peter M. Jenniskens	SETI Institute, CA, USA
Detlef Koschny	ESA SRE-SM, The Netherlands
Asta Pellinen-Wannberg	Swedish Institute of Space Physics, Sweden
Olga Popova	Institute for Dynamics of Geospheres, RAS, Russia
Vladimir Porubcan	Astronomical Institute SAV, Slovakia
Frans J.M. Rietmeijer	University of New Mexico, USA
Pavel Spurný	Astron. Inst. of the Academy of Sciences, Czech Rep.
Giovanni B. Valsecchi	IASF, INAF, Roma, Italy

Local Organizing Committee

Tadeusz J. Jopek (chair)
Filip Berski
Małgorzata Bronikowska
Piotr A. Dybczyński
Alicja Gasiorowska
Roman Hirsch
Anna Marciniak
Magda Murawiecka
Dagmara Oszkiewicz
Regina Rudawska

The Local Organizing Committee operated under the auspices of the Astronomical Observatory Institute of the Faculty of Physics of Adam Mickiewicz University in Poznań, Poland.

Acknowledgements

Financial support from the Rector and the Dean of the Faculty of Physics of Adam Mickiewicz University as well as from the Fundacja Uniwersytetu Adama Mickiewicza w Poznaniu are gratefully acknowledged.

List of attendees

1	Shinsuke	Abe	Nihon University, College of Science and Technology	Japan
2	Abedin	Abedin	University of Western Ontario	Canada
3	Željko	Andreic	University of Zagreb	Croatia
4	David	Asher	Armagh Observatory	UK
5	Alexander	Bagrov	Institute of Astronomy, RAS	Russian Fed.
6	Geert	Barentsen	IMO	UK
7	Jiří	Borovička	Astronomical Institute, AS CR	Czech Rep.
8	Małgorzata	Bronikowska	A.M. Univeristy	Poland
9	Peter	Brown	University of Western Ontario	Canada
10	Sebastian	Bruzzone	The Unviersity of Western Ontario	Canada
11	Stijn	Calders	Belgian Institute for Space Aeronomy	Belgium
12	Özcan	Caliskan	Istanbul University	Turkey
13	Margaret	Campbell-Brown	University of Western Ontario	Canada
14	David	Čapek	Astronomical Institute, AS CR	Czech Rep.
15	Juan Diego	Carrillo Sanchez	University of Leeds	UK
16	Apostolos	Christou	Armagh observatory	UK
17	Klim	Churyumov	Kiev Shevchenko National University	Ukraine
18	David	Clark	Western University	Canada
19	Joan	Dergham Sanz	Institute of Space Sciences (CSIC-IEEC)	Spain
20	Alex	Deutsch	University of Munster	Germany
21	Gerhard	Drolshagen	ESA	Netherlands
22	Justyna	Gołebiewska	A.M. University	Poland
23	Mikael	Granvik	University of Helsinki	Finland
24	Piotr	Gronkowski	University of Rzeszow	Poland
25	Ayyub	Guliyev	Shamakhy Astrophysical Observatory	Azerbaijan
26	Peter	Gural	SAIC	USA
27	Maria	Hajduková Jr.	Astronomical Institute of SAS	Slovakia
28	Michael	Hankey	American Meteor Society	USA
29	Robert	Hawkes	Mount Allison University	Canada
30	Peter	Jenniskens	SETI Institute	USA
31	Tadeusz J.	Jopek	A.M. University	Poland
32	Paweł	Kankiewicz	Jan Kochanowski University	Poland
33	Zuzana	Kaňuchová	Astronomical Institute of SAS	Slovakia
34	Anna	Kartashova	Institute of Astronomy, RAS	Russian Fed.
35	Toshihiro	Kasuga	National Astronomical Observatory	Japan
36	Johan	Kero	Swedish Institute of Space Physics (IRF)	Sweden
37	Jean-Baptiste	Kikwya	Vatican Observatory	Vatican
38	Hutch	Kinsman	Pre-Columbian Society at the University of Pennsylvania Museum of Archaeology and Anthropology	USA
39	André	Knöfel	IMO	Germany
40	Tomas	Kohout	University of Helsinki	Finland
41	Gulchekhra	Kokhirova	Institute of Astrophysics, Academy of Sciences of the Republic of Tajikistan	Tajikistan
42	Svitlana	Kolomiyets	Kharkiv National University of Radio Electronics	Ukraine
43	Leonard	Kornoš	Comenius University in Bratislava	Slovakia
44	Detlef	Koschny	ESA	Netherlands
45	Pavel	Koten	Astronomical Institute of ASCR	Czech Rep.
46	Pavlo	Kozak	Kyiv Taras Shevchenko University	Ukraine
47	Tomasz	Kwiatkowski	A.M. University	Poland
48	Herve	Lamy	Belgian Institute for Space Aeronomy	Belgium
49	Grigoris	Maravelias	Hellenic Amateur Astron. Association,	Greece
50	Anna	Marciniak	A.M. University	Poland
51	Anastasios	Margonis	Technical University of Berlin	Germany
52	Sirko	Molau	International Meteor Organization	Germany
53	Netzer	Moriya	siOnet Ltd.	Israel
54	Andrzej	Muszyński	Institute of Geology AMU	Poland
55	Lubos	Neslusan	Astronomical Institute of SAS	Slovakia
56	David	Nesvorný	Southwest Research Institute	USA
57	Nagatoshi	Nogami	Sumitomo Chemical Co., Ltd.	Japan
58	Francisco	Ocaña González	UCM / ISDEFE	Spain
59	Wayne	Oswald	Western University	Canada
60	Sergey	Pavlov	DLR Institute of Planetary Research	Germany
61	Asta	Pellinen-Wannberg	Umea University	Sweden

62	Chris	Peterson	Denver Museum of Nature and Science	USA
63	John	Plane	University of Leeds	UK
64	Petr	Pokorný	Charles University Prague	Czech Rep.
65	Olga	Popova	Inst. for Dynamics of Geosphers, RAS	Russian Fed.
66	Vladimir	Porubčan	Comenius University in Bratislava	Slovakia
67	Sylvain	Ranvier	Belgian Institute for Space Aeronomy	Belgium
68	Jean-Louis	Rault	International Meteor Organization	France
69	Juergen	Rendtel	International Meteor Organization	Germany
70	Hans	Rickman	PAN Centrum Badan Kosmicznych	Poland
71	Frans J.M.	Rietmeijer	The University of New Mexico	USA
72	Elen	Roaldset	University of Oslo	Norway
73	Adriana	Roggemans	International Meteor Organization	Belgium
74	Paul	Roggemans	International Meteor Organization	Belgium
75	Regina	Rudawska	A.M. University	Poland
76	Galina	Ryabova	Tomsk State University	Russian Fed.
77	Mikiya	Sato	Kawasaki Municipal Science Museum	Japan
78	Carsten	Schult	Leibniz Institute of Atmospheric Physics	Germany
79	Aswin	Sekhar	Armagh observatory	UK
80	Lukas	Shrbený	Astronomical Institute AS CR	Czech Rep.
81	Elizabeth	Silber	Western University	Canada
82	Johnny	Skorve	Natural History Museum	Norway
83	Rachel H.	Soja	Universitat Stuttgart	Germany
84	Pavel	Spurný	Astronomical Institute AS CR	Czech Rep.
85	Wojciech T.J.	Stankowski	Adam Mickiewicz University	Poland
86	Gunter	Stober	Inst. for Atmospheric Physics	Germany
87	Edward	Stokan	University of Western Ontario	Canada
88	Dilini	Subasinghe	University of Western Ontario	Canada
89	Jan	Svoreň	Astronomical Institute of SAS	Slovakia
90	Dusan	Tomko	Astronomical Institute of SAS	Slovakia
91	Juraj	Tóth	Comenius University in Bratislava	Slovakia
92	Josep M.	Trigo-Rodriguez	Inst. of Space Sciences (CSIC-IEEC)	Spain
93	Giovanni	Valsecchi	IAPS-INAF	Italy
94	Jeremie	Vaubaillon	IMCCE	France
95	Paweł	Wajer	Space Research Centre	Poland
96	Mark	Walker	Manly Astrophysics	Australia
97	Junichi	Watanabe	National Astron. Obs. Japan	Japan
98	Robert	Weryk	The University of Western Ontario	Canada
99	Iwan P.	Williams	Queen Mary University of London	UK
100	Mariusz	Wiśniewski	Polish Fireball Network	Poland
101	Tomasz	Wiśniowski	Space Research Centre	Poland
102	Ireneusz	Włodarczyk	Polish Astronomical Amateur Society	Poland
103	Bing-Xun	Wu	National Central University, Taiwan	Taiwan

List of invited speakers

1	Jiří	Borovička	Astronomical Institute, AS CR	Czech Rep.
2	Peter	Brown	University of Western Ontario	Canada
3	Margaret	Campbell-Brown	University of Western Ontario	Canada
4	Peter	Jenniskens	SETI Institute	USA
5	Tadeusz J.	Jopek	A.M. University	Poland
6	Jean-Baptiste	Kikwya	Vatican Observatory	Vatican
7	Hutch	Kinsman	Pre-Columbian Soc. Pennsylvania Univer. Museum of Archaeology and Anthropology	USA
8	Detlef	Koschny	ESA	Netherlands
9	Sirko	Molau	International Meteor Organization	Germany
10	David	Nesvorný	Southwest Research Institute	USA
11	John	Plane	University of Leeds	UK
12	Frans J.M.	Rietmeijer	The University of New Mexico	USA
13	Lukas	Shrbený	Astronomical Institute, AS CR	Czech Rep.
14	Rachel H.	Soja	Universitat Stuttgart	Germany
15	Pavel	Spurný	Astronomical Institute, AS CR	Czech Rep.
16	Josep M.	Trigo-Rodriguez	Inst. of Space Sciences (CSIC-IEEC)	Spain
17	Jeremie	Vaubaillon	IMCCE	France
18	Junichi	Watanabe	National Astron. Observ. of Japan	Japan
19	Robert	Weryk	The University of Western Ontario	Canada
20	Iwan P.	Williams	Queen Mary University of London	UK

Participants of the Meteoroids 2013 Conference in front of the Poznań Philharmonic Hall

PART 1

Chelyabinsk superbolide and potentially hazardous objects

Meteoroids 2013, Proceedings of the Astronomical Conference,
held at A.M. University, Poznań, Poland, Aug. 26-30, 2013,
eds Jopek T.J., Rietmeijer F.J.M., Watanabe J., Williams I.P.,
Adam Mickiewicz University Press in Poznań, pp 3–9

Chelyabinsk meteoroid entry and airburst damage

Popova O.[1], Jenniskens P.[2], Shuvalov V.[1], Emel'yanenkoV.[3], Rybnov Y.[1], Kharlamov V.[1], Kartashova A.[3], Biryukov E.[4], Khaibrakhmanov S.[5], Glazachev D.[1], Trubetskaya I.[1]

[1]Institute for Dynamics of Geospheres RAS, Moscow, Russia (olga@idg.chph.ras.ru)
[2]SETI Institute, Mountain View, CA 94043, USA
[3]Institute of Astronomy RAS, Moscow, Russia
[4]South Ural State University, Chelyabinsk, Russia
[5]Chelyabinsk State University, Chelyabinsk,Russia

Abstract. A field study of the Chelyabinsk Airburst was conducted in the weeks following the event on February 15, 2013. To measure the impact energy, the extent of the glass damage was mapped by visiting over 50 villages in the area. To determine how that energy was deposited in the atmosphere, the most suitable dash-cam and video security camera footage was calibrated by taking star background images at the sites where video was taken. Shadow obstacles in videos taken at Chelyabinsk and Chebarkul were calibrated. To measure the nature of the damaging shockwave, arrival times were measured from the footage of 34 traffic cameras, data saved on a single timed server. To measure the impact of the shockwave, some 150 eyewitnesses were interviewed to ask about their personal experiences, smells, sense of heat, sunburn, etc. Meteorite find locations, shape, and size were documented by interviewing the finders and photographing the collections. Some of these meteorites were analyzed in a consortium study to determine what material properties contributed to the manner in which the meteoroid broke in the atmosphere. The results paint the first detailed picture of an asteroid impact airburst over a populated area. This information may help better prepare for future impact hazard mitigation scenarios.

Keywords: Chelyabinsk meteorite fall, airburst, asteroid impact

1. Introduction

The Chelyabinsk airburst of 15 February 2013, was exceptional because of the large kinetic energy of the impacting body and the airburst that was generated, creating significant damage and injuries in a populated area. The meteor and the effects of the airburst were extraordinarily well documented. Previous events with comparable or larger energy include the 1963 August 3 bolide, for which only an infrasound signal was recorded (Silber et al. 2009), and the famous Tunguska impact in 1908. Estimates of the kinetic energy of the Tunguska impact range from 3 to 50 Mt, due to lack of good observations at the time. The Chelyabinsk event is much better documented than both, and provides a unique opportunity to calibrate the different approaches used to model meteoroid entry and calculate the damaging effects of a shock wave from a large meteoroid entry. A better understanding of what happened might help future impact hazard mitigation efforts.

Mass media provided much information about the Chelyabinsk event immediately after the impact. It was immediately clear to us that much of that information

needed to be validated and calibrated, and much work was required to understand the impact and its effects from physical models of meteor entry and airburst propagation.

A fact-finding mission was organized by Institute for Dynamics of Geospheres and Institute of Astronomy (both of the Russian Academy of Sciences). The mission was supported by Peter Jenniskens (SETI institute, USA) and researchers from the Chelyabinsk State University, the South Ural State University in Chelyabinsk, and the Ural Federal University in Yekaterinburg. This collaborative effort aimed to secure as much information as possible to help determine the initial kinetic energy of the impact, the manner in which this energy was deposited in the atmosphere, the nature and properties of the shockwave, and the extent of the damage and injuries it caused on the ground. A better understanding of what happened might help future impact hazard mitigation efforts.

Following the field study on March 9-25, 2013, an international consortium of scientists was formed, the Chelyabinsk Airburst Consortium, to investigate the circumstances of the impact and the properties of the recovered meteorites. Results of the study were published in Science, first online on Nov. 6, 2013 (Popova et al. 2013).

2. Initial kinetic energy

Infrasonic waves are an important source of information about the fireball's initial kinetic energy. Brown et al. (2013) has reported on the infrasound waves detected all around the globe by over 20 stations of the Comprehensive Nuclear-Test-Ban Treaty Organization stations (CTBTO). In our study, we focused on the stations nearest to the impact site in Russia and Kazakhstan, and included infrasound signals recorded at independent infrasound stations in Russia, at locations as far as 1600 km from the impact location.

Estimating the source energy generally relies on empirical scaling relations, which use either the period at the maximum amplitude of the signal or the peak-to-peak amplitude(Ens et al. 2012; Edwards 2010). The period at maximum amplitude is generally less sensitive to propagation effects than the amplitude of the signal.

We used a relation derived from data by Stevens et al. (2006) to calculate a source energy of 432±60 kt (Popova et al. 2013). More recently, this relationship was re-evaluated to arrive at slightly lower value of 415 ± 97 kt from the extended dataset of Russia-Kazakhstan infrasound signals (Rybnov et al. 2013). Figure 1 shows how individual station periods translate to source energy. There are a number of effects which can influence this value, including the reflective properties of the surface (near surface or free-air conditions), the altitude of the energy deposition (different partitioning of energy going into the blast wave at different altitudes), the lack of calibrations at 20-40 km altitude, and the conversion to a chemical equivalent of explosive power. With these corrections, the most probable kinetic energy of the Chelyabinsk meteoroid impact is 570 ± 150kt TNT (Popova et al. 2013).

Further information about the kinetic energy is derived from the fireball's light curve. Space-borne visible and near-infrared observations recorded a total irra-

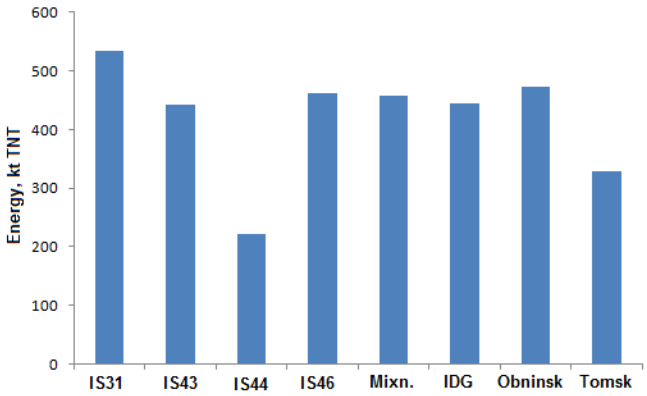

Figure 1. Source energy estimates (without corrections) based on signals from different stations (marked along the OX axes, IS – CTBTO stations, Mixn. – station at IDG Mikhnevo geophysical observatory, IDG – at institute in Moscow, Obninsk – association Typhoon, Tomsk – Tomsk State University).

diated energy of 90 kT (Yeomans and Chodas 2013), corresponding to a kinetic energy of 590 ± 50 kT using the calibration by Nemtchinov et al. (1997). The integral luminous efficiency was determined in the course of hydrodynamical modeling, including radiative transfer modeling, and supplemented by a simplified fragmentation model (Nemtchinov et al. 1997). Results were compared to the light curve derived from video observations, calibrated to the brightness of the Moon in similar dash-cam video cameras. The peak brightness was determined as –27.3 ± 0.5 magnitude, referenced to a range of 100 km. The integrated light curve is consistent with other energy estimates, if the panchromatic luminous efficiency was 7 ± 3%. Theoretical estimates under these conditions range from 5.6 to 13.2% (ReVelle and Ceplecha 2001), in good agreement.

All energy values are uncertain by a factor of two, mainly due to lack of calibration. The conversion of optical energy into kinetic energy is uncertain due to an uncertain luminous efficiency, poor knowledge of real spectral output in different pass bands and a lack of calibration data at those high energies.

3. Energy deposition as a function of altitude

Analysis of video observations of the fireball and it's shadows provided a meteor light curve (Figure 2), deceleration curve and trajectory. The peak brightness occurred at 29.7 km altitude after which a thermal emitting cloud of debris was seen that stopped at 27.0±0.7 km altitude. Modeling of the bolide light curve provides an understanding of how the meteoroid's energy was deposited. For that, we use models previously applied to other ground-based or satellite-based observed bolides (Borovicka et al. 1998; Popova 2011). Attempts to reproduce the observed bolide light curve and deceleration profile (there was almost no deceleration until peak brightness) included ablation and different fragmentation scenarios. Me-

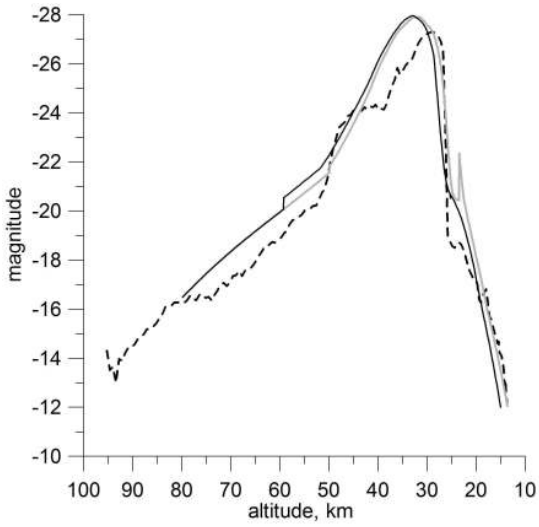

Figure 2. Two model light curves fitted to the data (black and grey; the dashed line is the observed data). These represent two random realizations of fragmentation into three expanding clouds and a number of separated fragments.

teoroid fragmentation occurred in different forms, some part of the initial mass broke in well separated fragments (some of these were later found as meteorites on the ground), while another part formed a cloud of small fragments and vapor united by a common shock wave. The deceleration of this cloud was observed at altitudes of 28-27 km (Popova et al. 2013).

Fragmentation started at altitudes of about 50-60 km, while the meteoroid was catastrophically fragmented at 40-30 km, creating the debris cloud. The conditions in this debris cloud can be derived from the recovered meteorites on the ground. All meteorites recovered just south of the trajectory in a long stretch from Aleksandrovka (0.1g) to Deputatskiy (100g) and Timiryazevsky (3 kg) originated from the rapidly expanding fragmentation around peak brightness. Out of all fragmentation events, only 4,000 to 6,000 kg of meteorites fell on the ground, which is only 0.03-0.05% of the initial mass of the meteoroid. An estimated 76% of the meteoroid evaporated, with most of the remaining mass converted into dust. The reason so little survived is that the radiation was so intense it contributed to evaporating the fragments before they could fall as meteorites out of this cloud.

A few larger fragments survived this fragmentation event and penetrated deeper into the atmosphere. One set of fragments continued to fall apart, further creating dust and debris, while one larger fragment survived in part to the ground and penetrated Lake Chebarkul, leaving a 7-m sized hole in the 70-cm thick ice layer. A large > 570 kg meteorite was later recovered in agreement with model predictions about hundreds kg largest survived fragment (Popova et al. 2013). Borovicka et al. (2013) arrived at a similar answer.

4. Extent of the damage

The extent of the glass damage was mapped by visiting over 50 villages in the area. Interviews were conducted at local grocery markets, and followed up by visits to damaged schools and interviews of eye witnesses encountered on the street. The data gathered in situ from small villages was supplemented by official information from the main damaged areas.

The city of Chelyabinsk, with over a million inhabitants, was right in the path of the shock wave. Locally, the intensity of the shock wave varied considerably as some parts of Chelyabinsk were more severely affected than others. The direction of the damage was not always from the direction of the meteoroid.

There was little structural damage, other than broken windows, window frames and doors. We documented some sites were houses were cracked. One old wall collapsed at a zinc factory in Chelyabinsk. A statue of Pushkin was damaged when it was hit by a window frame blown out by the shockwave.

Injuries seemed to be mostly due to flying glass from windows that were shattered by the shockwave, but we also documented injuries from walking in and handling glass. Some injuries likely occurred from being hit by objects. There were no traffic accidents associated with this event.

For observers near the trajectory, the fireball was brighter than the sun at that time, creating so much ultraviolet emission that some people were sunburned with peeling skin later on. Many reported weak sunburns and sensations of heat. Most eye witnesses avoided lasting eye damage by looking away. No permanent eye damage was reported.

5. Nature of the shockwave

The shape of the damaged area could be explained from the fact that the energy was deposited over a range of altitudes. Figure 3 shows our models of overpressure for different initial source energies and assumptions about the pressure needed to break window glass. It is not known exactly what excess pressure is needed to break window glass. A number of numerical simulations were conducted that attempted a more realistic release of energy along the trajectory and these results were compared with observations of blast wave arrival times and the extent of the glass damage (Figure 3). Reasonable results were obtained for energies of 300-520 kt TNT and over pressures of 500-1000 Pa under assumption that energy release follows the light curve. Such event, with detonations spread over altitudes ranging from 34-27 km and 24-19 km, would cause damage out to a distance of 90-120 km with the observed shape (Figure 3). Only a negligible fraction of the initial kinetic energy was probably deposited below 23 km. This was concluded from the pattern of shockwave arrival times on the ground.

The shockwave continued to travel out to 90-120 km from the meteoroid trajectory, perpendicular to the trajectory, but quickly lost its destructive power in directions along the fireball path. In forward direction, the shockwave was experienced as loud, but not as sharply peaked and no glass damage resulted in Timiryazevsky (Figure 3).

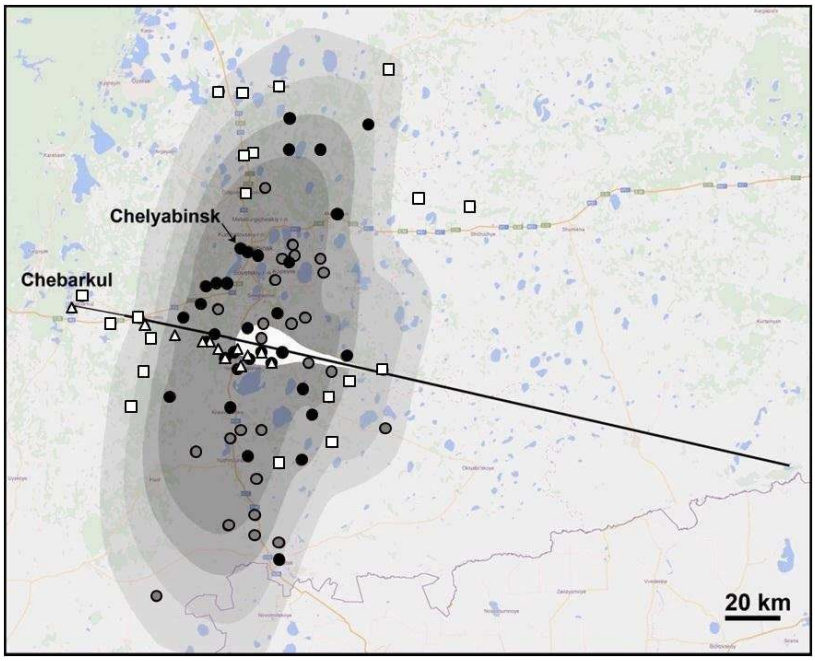

Figure 3. Map of glass damage, with overlay of model calculations. Grey symbols correspond to the official list of most damaged settlements, while black symbols are villages visited that reported damage (white squares: no damage). The black line is the fireball trajectory. The white triangles are locations where meteorites were recovered. From: Popova et al. (2013).

6. Factors that contributed to the damage

Extensive studies of meteorites collected by Chelyabinsk State University researchers shortly after the fall were conducted to investigate its properties in relation to the fragmentation behavior in the atmosphere. We found that the meteorites were riddled with shock veins. Under the electron microscope, some of these veins had deposits of metal grains along the vein boundary, possibly contributing to its weakness.

These shock veins may have been created as long as 4.5 billion years ago, about 100 Ma after the formation of the solar system. At this time, the rock experienced a thermal resetting event in the U-Pb system (Popova et al. 2013).

The orbit of Chelyabinsk was determined and traces LL chondrites with increasing certainty to being ejected from the asteroid belt by the ν_6 resonance, possibly originating in the Flora asteroid family (Popova et al., 2013). Chelyabinsk itself was broken from a larger object only 1.2 Ma ago. This could have been due to a collision in the asteroid belt, or caused by a tidal disruption in a close encounter by Earth. The resulting Chelyabinsk meteoroid itself was probably not a rubble pile based on the measured light curve (Popova et al. 2013).

7. Future work

We still hope to collect more information about the nature of the injuries that were sustained. We are also very interested in the irregular distribution of damaged buildings, reflecting properties of the shockwave at the ground.

Acknowledgements

PJ is supported by the NASA Near Earth Object Observation program.

References

Borovicka J., Popova, O. P., Nemtchinov, I. V., et al., 1998, Astron. Astrophys. 334, 713

Borovicka J., Spurný P, Brown P., et al., 2013, Nature 503, 235

Brown P.G., Assink J.D, Astiz L., et al., 2013, Nature 503, 238

Edwards W.N., 2010, Infrasound Monitoring for Atmospheric Studies. Springer, Dordrecht, Netherlands, 361

Ens T.A., Brown P.G., Edwards W.N., Silber E.A., 2012, J. Atmosph. Solar Terr. Phys. 80, 208

Nemtchinov I.V., Svetsova V.V., Kosareva I.B, et al., 1997, Icarus, 130, 259

Popova O. P., 2011, Proc. Meteoroids Conference (Breckenridge, Colorado, USA, May 24-28, 2010). Edited by W.J. Cooke, D.E. Moser, B.F. Hardin, and D. Janches. NASA/CP-2011-216469., 232

Popova O., Jenniskens P., Emelyanenko V., Kartashova A., et al., 2013, Science, 342, 1069

Revelle D. O., Ceplecha Z., 2001, ESA Special Publ. 495, 507

Rybnov Yu.S. et al., 2013, Dynamic processes in geospheres, Issue 4, GEOS, 21

Silber E.A., ReVelle D.O., Brown P.G., Edwards W.N., 2009, JGR 114, E08006

Stevens J.L. et al., 2006, Defence Threat Reduction Agency, Technical Report ADA446517S

Yeomans D., Chodas P., 2013, NASA NEO Program Office Announcement, March 1, 2013 (NASA, Washington, 2013)

Meteoroids 2013, Proceedings of the Astronomical Conference, held at A.M. University, Poznań, Poland, Aug. 26-30, 2013, eds Jopek T.J., Rietmeijer F.J.M., Watanabe J., Williams I.P., Adam Mickiewicz University Press in Poznań, pp 11–17

A numerical method to investigate the ablation coefficient of the Chelyabinsk superbolide

Dergham J.[1], **Trigo-Rodriguez J.M.**[2]

[1]Institut dEstudis Espacials de Catalunya (IEEC), Edif.Nexus, c/Gran Capit, 2-4, 08034 Barcelona, Spain (joandergham@gmail.com)
[2] Meteorites, Minor Bodies and Planetary Sciences Group, Institute of Space Sciences (CSIC-IEEC), Campus UAB, Fac. Cincies, 08193 Bellaterra, Barcelona, Spain

Abstract. The study of the interaction of large bolides with Earth's atmosphere provides a pleyade of information on relevant physical parameters that allow to predict their behaviour and survival as meteorites. We have developed a computer program based on the drag and mass-loss equations and the Runge-Kutta numerical approximation able to analyze the trajectory of different bolides. This methodology has been applied to dynamic data obtained from three casual video recordings of the Chelyabinsk superbolide.

Keywords: Chelyabinsk superbolide, meteorites, ablation coefficient

1. Introduction

On February 15, at 03.20 UTC, a superbolide overflew Kazakhstan and the southern Ural region in Russia before exploding with a released energy of about 500 kT over the city of Chelyabinsk (Brown et al., 2013). The event was recorded on a large number of videos from multiple locations (Borovička et al., 2013). The progenitor Near Earth Asteroid of about 19 meters in diameter reached the top of the atmosphere with a geocentric velocity slightly over 19 km/s (Borovička et al., 2013). The brightness prior to the explosion was around -17 while during the explosion it reached absolute magnitude -28 (Brown et al., 2013). After recovering different samples, the meteoroid has been analyzed and characterized as a LL5 brecciated chondrite (Kohout et al., 2014; Bischoff et al., 2013). Some information regarding the orbital parameters has been published so far showing the impossibility of being detected using the current NEO surveys (Brown, 2013). In this paper we propose to apply the drag and mass-loss equations (Bronshten, 1983) to understand better the dynamic behaviour of large bolides like e.g. Chelyabinsk during its atmospheric deceleration. We have then applied these equations to get clues on several physical properties.

2. Theoretical modelling of the interaction of meteoroids with the atmosphere

There are two main approaches to study the behaviour of meteors during its atmospheric flight. The single body theory introduced by Bronshten (1983) and the quasi-continuous fragmentation (QCF) introduced by Novikov (1984). Revisions of both disciplines can be found in Ceplecha et al. (1993); Babadzhanov

(1993). The single body theory concepts can be expressed using differential equations based on the laws of motion while the QCF deals with semi empirical formulas. The main disagreement between both disciplines is in the dynamical mass results which do not often agree. One reason of this disagreement is when abrupt fragmentation occurs. For the single body theory we deal with differential equations therefore we need continuity. When a large amount of mass is released in a short time period continuity is not satisfied consequently equations do not describe the movement precisely. Chelyabinsk superbolide presented different explosions over the trajectory, for this paper we study the lower part of the trajectory after the last disruption where continuity is satisfied, as a consequence the main differential equations presented by Bronshten can be used:

$$\frac{dv}{dt} = -K \cdot \rho_{\text{air}} \cdot m^{-\frac{1}{3}} \cdot v^2, \tag{2.1}$$

$$\frac{dm}{dt} = -\sigma \cdot K \cdot \rho_{\text{air}} \cdot m^{\frac{2}{3}} \cdot v^3, \tag{2.2}$$

where, ρ_{air} is the air density, m the mass, v the instantaneous velocity. The factors K and σ are the shape density factor and the ablation coefficient respectively. K can be written as follows:

$$K = \frac{\Gamma \cdot A}{\rho^{2/3}}, \tag{2.3}$$

where ρ is the meteoroid bulk density, Γ the drag coefficient and A depends on the shape of the meteoroid. Some simple shapes and values for the drag coefficient are discussed in Baines et al (1965). Γ and A values used in later studies are reviewed by Gritsevich (2008). The other coefficient, the ablation coefficient (σ) can be expressed as

$$\sigma = \frac{\Lambda}{2 \cdot \Gamma \cdot Q}, \tag{2.4}$$

where Λ is the heat transfer coefficient and Q represent the amount of heat required to ablate a unit mass. This ablation coefficient will determine how easily the mass is released from the meteor as it interacts with the atmosphere. The larger this coefficient is the faster the bolide will ablate and vice versa. Typical values are between 0.01 and 0.3 $s^2 \cdot km^{-2}$ (Ceplecha et al., 1998; Gritsevich 2009).

From video recordings measurements, the velocity evolution of the meteor is normally given in function of the altitude, consequently the main equations are modified using the following relation.

$$\frac{dv}{dt} = -v \cdot cos(z), \tag{2.5}$$

Z is the zenith angle, which is the angle from the zenith to the meteor trail. If the previous relation is used, the main equations (2.1,2.2) become.

$$\frac{dv}{dh} = \frac{-K \cdot \rho_{\text{air}} \cdot m^{-\frac{1}{3}} \cdot v}{cos(z)}, \tag{2.6}$$

$$\frac{dm}{dh} = \frac{-K \cdot \sigma \cdot \rho_{\text{air}} \cdot m^{\frac{2}{3}} \cdot v}{cos(z)}. \tag{2.7}$$

If the two equations are combined the next expression is obtained:

$$\frac{dh}{dt} = -v \cdot cos(z). \tag{2.8}$$

And if we solve the differential equation we obtain:

$$m = m_{\text{o}} \cdot e^{\frac{1}{2}\sigma(-{v_{\text{o}}}^2+v^2)}, \tag{2.9}$$

where v_0 and m_0 are the initial speed and mass of the meteoroid. With m known in terms of the speed, equation (2.5) becomes

$$\frac{dv}{dh} = K \cdot \rho_{\text{air}} (m_{\text{o}} \cdot e^{\frac{1}{2}\sigma(-{v_{\text{o}}}^2+v^2)})^{-1/3} \frac{v}{cos(z)}. \tag{2.10}$$

The instantaneous mass from observations can be obtained if luminosity equation is introduced (explained below). This instantaneous mass is in the initial equations (2.1, 2.2), however this last expression does not depend on the instantaneous mass. Another observation about the last equation is the influence of the zenith angle in the meteor behaviour, the smaller the angle is the more the deceleration is maximized. On the other hand large meteors in grazing angles are able to follow extremely long trajectories or even scape like occurred for the Grand Tetons that for almost 2 minutes overflew different states in the American and Canadian territory (Jacchia, 1974; Ceplecha, 1994).

The last equation describes the velocity evolution for the given values of v_o, m_o, σ, and K. These parameters describing the interaction of the bolide are computed from an accurate study of the bolide dynamics, particularly the velocity evolution over the altitude. Hence some sort of inversion problem must be applied which is described later. From the above mentioned equations, only the values of σ and $m_o^{1/3} \cdot K$ can be obtained. Another equation is needed in to obtain K and m_o separately. This remaining equation is the brightness equation

$$I = \frac{\tau}{2}(-\frac{dm}{dt} \cdot v^2), \tag{2.11}$$

which connects the brightness to the rate of release of kinetic energy. Here τ is the luminosity efficiency, a key but poorly-known factor that inform us about the bolide ability of transforming kinetic energy into light.

Equation (2.10) by defining the product $m_o^{1/3} \cdot K = K'$ becomes:

$$\frac{dv}{dh} = K' \cdot \rho_{\text{air}} (e^{\frac{1}{2}\sigma(-{v_{\text{o}}}^2+v^2)})^{-1/3} \frac{v}{cos(z)}. \tag{2.12}$$

3. Numerical approximation

Equation (2.12) is an ordinary first order differential equation. The most suitable numerical approximation for the problem is the Runge Kutta 4th order method which can be found in any book of numerical analysis. Furthermore the equation

requires the assumption of simplified atmospheric profile to perform the analysis. We adopted a general model widely used in meteor studies: the U.S. standard atmosphere (USSA, 1976). It is a compilation of atmospheric average properties like e.g.: temperature, density, pressure, etc. over a wide range of altitudes.

3.1. Fitting procedure to obtain the ablation coefficient (σ)

The goal is to find the values of K' = $K \cdot m_o^{-1/3}$ and σ that produce the closest curve to the data points. In order to find this curve we introduce the next auto fitting procedure. Firstly a roughly consistent values are chosen for both variables and a single velocity curve is created. The velocities at a determined point are compared by using the next expression

$$\epsilon = (v_{\mathrm{d}} - v_{\mathrm{f}}(K', \sigma))^2, \tag{3.1}$$

where v_d and v_f are the velocity at the height measured from the video recordings and the velocity obtained by our code at the same height respectively. Then ϵ, known as the error factor, is calculated.

Expressions ΔK and $\Delta\sigma$ are defined as small increments in K and σ. Eight more theoretical curves are calculated for the possible combinations of the new variables (K$\pm\Delta$ K; $\sigma\pm\Delta\sigma$) and the error factor is calculated for all of them. The minimum error will show the path to follow in order to obtain the optimal result by incrementing or decrementing ΔK and $\Delta\sigma$. The final result will be achieved when the smallest error factor is obtained from the variable which has no ΔK nor $\Delta\sigma$. These increments can be modified in order to obtain more accurate results.

3.2. Deceleration, relative mass and mass-loss rate

Once the optimal velocity curve is calculated other results can be obtained. For example dv/dh is straightforward and is obtained from

$$\frac{dv}{dh}(h_{2-1}) \approx \frac{\Delta v}{\Delta h} = \frac{v_{\mathrm{h2}} - v_{\mathrm{h1}}}{h_2 - h_1}. \tag{3.2}$$

Equation 2.9 is the relation of mass in function of the velocity. Since σ has been calculated previously, relative mass evolution can be easily obtained. Therefore, the relative mass loss rate evolution can be written as:

$$\frac{d\frac{m}{m_{\mathrm{o}}}}{dh}(h_{2-1}) \approx \frac{\Delta m/m_{\mathrm{o}}}{\Delta h} = \frac{m_{\mathrm{h2}}/m_o - m_{\mathrm{h1}}/m_o}{h_2 - h_1}. \tag{3.3}$$

4. Application to the Chelyabinsk superbolide

The previous equations have been used in order to determine the ablation coefficient of the Chelyabinsk superbolide. Three different videos available in internet have been used to obtain the data of velocity vs. the altitude. The following data was obtained by using fb entry program (Lyytinen and Gritsevich, 2013):

Table 1. Dynamic data of the Chelyabinsk superbolide.

Height (km)	Velocity (km/s)	Height (km)	Velocity (km/s)
18.98	14.04	15.66	9.73
18.78	13.86	15.53	9.46
18.58	13.68	15.39	9.20
18.38	13.49	15.26	8.94
18.18	13.29	15.13	8.68
17.99	13.09	15.01	8.42
17.80	12.88	14.89	8.17
17.62	12.66	14.77	7.92
17.44	12.44	14.66	7.67
17.26	12.22	15.55	7.43
17.08	11.99	14.45	7.19
16.91	11.75	14.34	6.96
16.74	11.51	14.24	6.74
16.58	11.27	14.15	6.52
16.42	11.02	14.06	6.31
16.26	10.76	13.97	6.11
16.10	10.51	13.88	5.92
15.95	10.25	13.80	5.73

Chelyabinsk (1)	61.°29671 E 55.°22055 N	`http://www.huffingtonpost.com/2013/02/`
Magnitogorsk	58.°96572 E 53.°3875 N	`http://www.youtube.com/watch?v=EZlUgCmJE04`
Chelyabinsk (2)	61.°36394 E 61.°36394 N	`http://www.youtube.com/watch?v=gQ6Pa5V_io`

We have used the data present in table 1 as an input for the code. The value of the ablation coefficient obtained by running the program is:

$$\sigma{=}0.035 \pm 0.005 s^2 \cdot km^{-2}$$

Figure 1.a shows the optimal fit for the ablation coefficient obtained, as can be seen the fit is notable. The maximum mass-loss rate value occurs at an altitude of $\approx$ 23.5 km (see arrow in Figure 1d). However even if the value of the ablation coefficient is in the limits, is a bit large if it is compared with other published data, Borovička (2013) obtained a value of 0.01 $s^2 \cdot km^{-2}$ for the same segment. The reason of this difference could be attributed to the fact that different methods are used to obtain the ablation coefficient. For the other study the light curve have been used to obtain the ablation coefficient (QCF), on the other hand we followed the drag and mass-loss equations.

5. Conclusions

We have developed a model able to predict the dynamic behaviour of meteoroids penetrating into the Earth's atmosphere. We applied the model successfully to several meteor events described in scientific literature (Dergham, 2013). Our study of

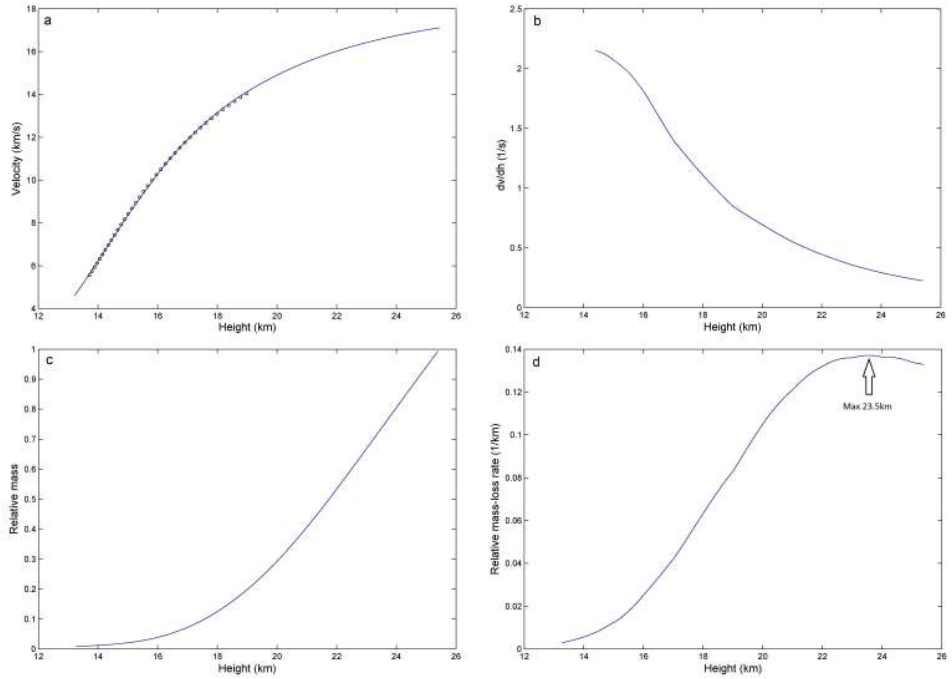

Figure 1. Compilation of results for the Chelyabinsk superbolide, 1a) The velocity as function of height, 1b) The deceleration evolution, 1c) Relative mass evolution, 1d) The relative mass-loss rate evolution.

the deceleration profile of Chelyabinsk superbolide has allowed us to reach the following conclusions:

1) The model when applied to the lower part of the fireball trajectory predicts well the observed deceleration rate of Chelyabinsk in the lower part of its atmospheric path.
2) The best fit to the deceleration pattern measured in the lower atmosphere for Chelyabinsk superbolide provides an averaged ablation coefficient of σ=0.035 $\pm$0.005 $s^2 \cdot km^{-2}$ that is in the range of other derived for chondritic bodies in scientific literature.
3) The ablation coefficient value derived for Chelyabinsk is similar to those obtained for much higher fireballs, even when the atmospheric density is four orders of magnitude higher. Probably the ability of a meteoroid to ablate depends of the mass release and a lower ablation rate can take place independently of atmospheric density.

Acknowledgements

JMT-R thanks the MEC for AYA2011-26522 research grant. JD thanks the fundings received from the Meteorites, Minor Bodies and Planetary Sciences research group crowd-funding provided by IEEC to present this data in the Meteoroids 2013

International Conference. Furthermore JD thanks M. Gritsevich and E. Lyytinen for providing data and guidance for the development of the code.

References

Babadzhanov P.B., 1993, in Meteoroids and their parent bodies, eds Štohl J., Williams I.P., Astron. Inst., Slovak Acad. Sci., Bratislava, p. 295

Baines M.J., Williams I.P., Asebiomo A.S., 1965, MNRAS, 130, 63

Bischoff A., Horstmann M., Vollmer C., Heitmann U., Decker S., 2013, M&PS, 48, 5171

Borovička J., Spurný P., Brown P., Wiegert P., Kalenda P., Clark D., Shrbený L., 2013, Nature, 503, 235

Bronshten V.A., 1983, Physics of meteoric phenomena, Geophysics and astrophysics monographs, D. Reidel Publ., Dordrecht

Brown P.G., 2013, WGN Jour. of the IMO, 41:1, 22

Ceplecha Z., Spurný P., Borovička J., Keclikova J., 1993, A&A, 279, 615

Ceplecha Z., 1994, A&A, 286, 967

Ceplecha Z., Borovička J., Elford W.G. et al., 1998, Space Sci. Rev., 84, 327

Dergham J., 2013, Master Thesis, Univ. Autonoma de Barcelona

Gritsevich M.I., 2008, Solar System Res., 42, 372

Gritsevich M.I., 2009, Advances in Space Res., 44, 323

Jacchia L., 1974, Sky and Telescope, 48, 4

Kohout T., Gritsevich M., Grokhovsky V.I. et al., 2014, Icarus, 228, 78

Lyytinen E., Gritsevich M., 2013, in Proc. Intern. Meteor Conf., La Palma, Canary Islands, Spain, 20-23 September 2012, eds Gyssens M., Roggemans P., p. 155

Novikov C.G., Lebedinets V.N., Blokhin A.V., 1984, Pisma v Astron. Zhurn., 10, 7

USSA, 1976, U.S. Standard Atmosphere, NOAA-S/T 76-1562, Washington D.C., USA, 241

Meteoroids 2013, Proceedings of the Astronomical Conference, held at A.M. University, Poznań, Poland, Aug. 26-30, 2013, eds Jopek T.J., Rietmeijer F.J.M., Watanabe J., Williams I.P., Adam Mickiewicz University Press in Poznań, pp 19–25

Chelyabinsk Superbolide: a detailed analysis of the passage through the atmosphere and orbit determination

Włodarczyk K.[1]**,Włodarczyk I.**[1]

[1]Polish Astronomical Amateur Society, Rozdrazew, Poland
(KW: kwlo@wp.pl, IW: astrobit@ka.onet.pl)

Abstract. A detailed analysis of the passage through the atmosphere of a very bright meteor that exploded in the air near Chelyabinsk, Russia on February 15, 2013 is presented. A number of videos and photographs were examined thoroughly to determine the meteor trajectory beginning from the recorded atmospheric entry height of about 62.5 km until its disappearance at about 9.8 km. The calculated velocity changes as a function time revealed an unusual behavior: during the first 10 seconds the meteor velocity increased from 16.6 km/s up to about 20.6 km/s in the main air burst at the altitude of 26.5 km. Afterwards it decreased rapidly. The light curves derived from videos enabled the total radiant energy and mass loss variations to be calculated. The heliocentric orbit of the meteoroid and possible parent bodies were computed. We proposed an additional 'close approaches' method to the existing method of checking meteoroid/bolide parent bodies based on different D-criteria.

Keywords: bolides, meteor observations, meteoroid orbit, parent body

1. Introduction

On February 15, 2013, shortly after sunrise, local inhabitants in the southern Ural region near Chelyabinsk, Russia, were surprised by a very bright fireball streaking across the sky causing a dazzling airburst followed by a shock wave. This event was witnessed by many people and recorded by dashboard cameras and stationary surveillance systems and observed from an airliner, a meteorological satellite and remote infrasound stations. The next day, dozens of videos were posted on the Internet and became available for analysis. The first preliminary orbital parameters were derived by a group of Colombian astronomers (Zuluaga and Ferrin 2013). Then Borovicka et al. (2013) published their results assuming a linear trajectory of the bolide, while paying attention to several "flares" observed during passage of the meteoroid through the atmosphere. There were also other attempts to determine the orbit. All of them are listed in Wikipedia under 'Chelyabinsk meteor'. The initial results shortly after the event were preliminary based on a few video recordings. Thus we decided to analyze more comprehensive data to describe physical phenomena accompanying the atmospheric flight of the bolide and determine its orbital parameters as well to discuss its origin.

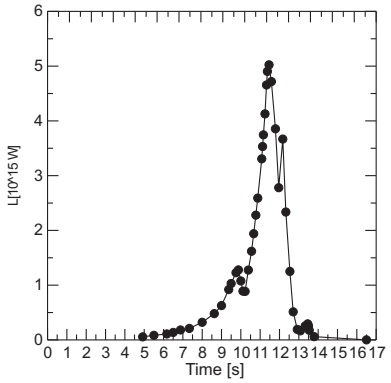

Figure 1. Light curve derived from the video recording taken in Kamensk Uralsky [http://www.youtube.com/watch?v=iCawTYPtehk].

2. Atmospheric passage

The video from Kamensk Uralsky is the most reliable because it has been recorded by a dashboard camera mounted in a car stopped at traffic lights and it covers about a 14.5 second-trajectory from the entry up to the dark flight, i.e. the final phase when the fireball has dimmed and disappears. Another very valuable video recording was also taken in a stationary car located in Korkino, showing the flight of the meteor up to the maximum brightness and the shock wave that arrived 98 seconds later. When analyzing all these videos we first found the trajectory of the meteor. It entered the atmosphere at a velocity of 16.6 km/s at the height of about 62.5 km and vanished after 14.5 seconds at 9.8 km above the ground when its velocity was around 5.5 km/s. The azimuth of trajectory (using Chebarkul Lake, φ=54.951 degrees N, λ=60.313 degrees E) is very well fixed at (280.7±0.15) degs and the entry angle at (12.9±0.3) degs. At its maximum brightness the bolide was at a height of (26.54±0.8) km. This corresponds perfectly with time delays of the acoustic shock wave recorded in Korkino, Chelyabinsk and other sites. Further analysis was focused on the recorded light variations. All recordings posted on the Internet show several maxima of various magnitude, depending on the place of observation. An example of the light curve derived from the video taken in Kamensk Uralsky is presented in Figure 1.

Similar curves were obtained for other sites. All of them indicate a minor flash prior to the maximum burst followed by the two other maxima in the time span of 3.1 seconds. Similar flickering was observed previously in bright fireballs and interpreted as a result of meteoroid rotation and fragmentation, (e.g. Beech and Brown 2000; Beech 2001). In the case of Chelyabinsk an additional feature is the double contrail and clearly twisted final single trace visible shortly after the passage, thus indicating bouncing rather than rotation itself and a dumbbell shape of the impactor. The maximum power emitted as visual light (Figure 1) is 5.33×10^{15}W, while the total radiated energy is 8.12×10^{15} J. The location of crucial points on the superbolide trajectory projection onto the Earth's surface is shown in Figure 2. Initially the temperature rises gradually from about 800 K at entry to 3200 K

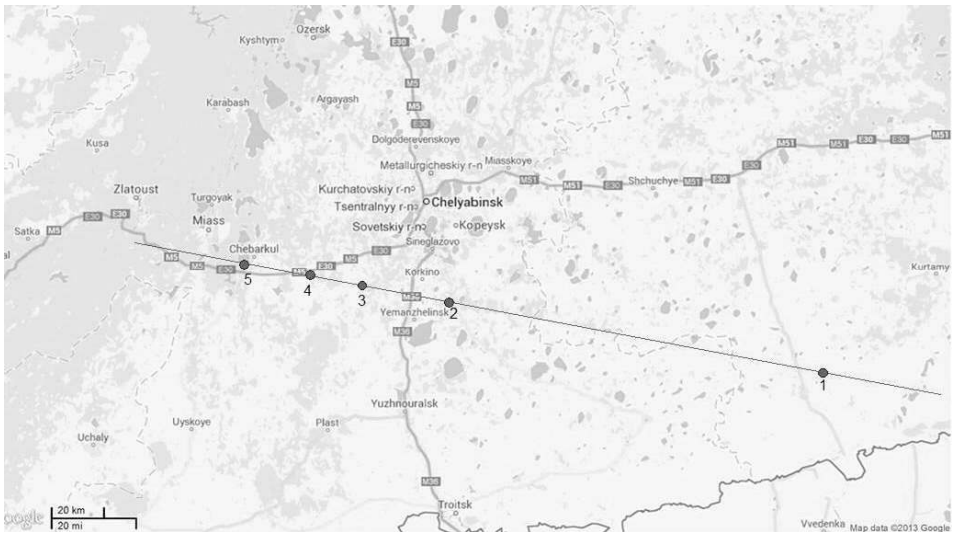

Figure 2. Meteor trajectory projected onto the surface of the Earth. The points numbered from 1 to 5 indicate successively: the entry, maximum burst, last burst, dark flight beginning and impact site.

at maximum brightness and continues to rise up to 3500 K at the final maximum. Afterwards, the temperature falls to 1500 K at the beginning of dark flight. It should be noted that during the last burst the temperature reached the silica stone evaporation point (3500 K) – see Figure 3. This high temperature may explain another unusual phenomenon, namely a dark streak running across the sky and beginning at the spot of last burst, clearly visible from Zlatoust, Satka, Miass and many other places (see an extensive video footage at Chebarkul Meteorite-Google Maps). Such a streak should not be interpreted simply as a kind of smoke cloud shadow. Thus, we may expect not only two large meteorite fragments, viz. one that fell into Chebarkul Lake and the second one somewhere south of it, as suggested by Borovicka et al. (2013), but also the third one somewhere beyond the village of Katka. It is worth to mention that an airplane pilot clearly saw three "burning chunks". When combining the results presented above we can estimate the visual magnitude of the bolide. Assuming the threshold magnitude of -3.7 at sunrise, we find that the superbolide reached its maximum brightness -28.5 magnitude in Korkino and -27.5 in Chelyabinsk, thus was brighter than the rising sun in these locations.

3. Heliocentric Orbit

Knowing the entry time (03:20 UTC, Feb. 15, 2013) as well the entry velocity, azimuth and the inclination angle mentioned above and impact site (Lake Chebarkul, 54.951 N, 60.313 E) we can compute the heliocentric orbit of the superbolide by using the well-known fundamental formulas in celestial mechanics, e.g. Wylie (1939).

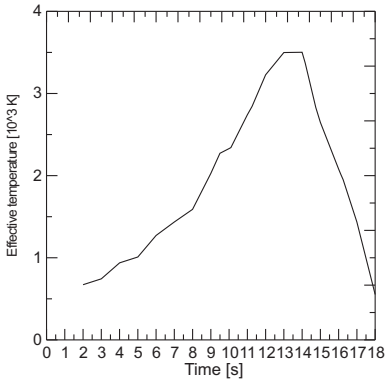

Figure 3. Air temperature in front of the meteoroid. The final part beyond 16.5 seconds is an extrapolation only.

Table 1. The Superbolide Chelyabinsk. Computed orbital parameters

Orbital parameters		1-sigma uncertainty
a (AU)	1.44846	0.0181
i (deg)	2.041	0.931
e	0.46539	0.0051
ω (deg)	108.654	0.774
Ω (deg)	326.424	0.774
Tper., JD0 (days)	2456290.005	0.500
topocentric radiant, right ascension, J2000.0 (deg)	329.39	1.35
topocentric radiant, declination, J2000.0 (deg)	+4.44	1.8
geocentric velocity, vg (km/s)	14.15	1.20
geocentric radiant, right ascension, J2000.0 (deg)	337.04	1.35
geocentric radiant, declination, J2000.0 (deg)	-6.66	1.8

The computed orbital parameters are presented in Table 1. Our results are essentially consistent with those published by Borovicka et al. (2013) and Zuluaga and Ferrin (2013). The differences in semimajor axis and inclination angle originate from different azimuths, zenith distances and assumed apparent velocities. It should be noted that shortly after the Chelyabinsk event there were serious discrepancies reported on the Internet for these principal input parameters. The superbolide trajectory was known more exactly following detailed analysis of numerous video recordings.

Table 1 lists orbital parameters of the Chelyabinsk superbolide with their uncertainties: a – denotes semimajor axis, i – inclination, e – eccentricity, ω – argument of perihelion, Ω – longitude of the ascending node and Tper – moment of the perihelion passage in JD0 (Julian days). Also listed are coordinates of the Chelyabinsk superbolide used in the computations of its orbit. These parameters indicates that before the atmospheric entry the meteoroid was a typical Apollo asteroid.

Table 2. Possible parent bodies for the Chelyabinsk superbolide.

Asteroid	Orbital parameters									
	$D_{(A,B)}$	e	q [AU]	i [deg]	Ω [deg]	ω [deg]	Arc [days]	Δ [AU]	Mag	Diameter [m]
2011 EH	0.027	0.4856	0.7611	2.3499	339.1640	96.6224	2	1.19	28.4	20-50
2013 RN9	0.073	0.468	0.8320	3.5172	324.5682	105.9528	12	2.84	28.8	50-110
2000 SM10	0.084	0.540	0.7647	0.5486	260.6130	176.6892	7	3.04	28.6	50
2013 CV83	0.085	0.453	0.7843	4.5723	339.4706	86.8761	21	0.07	19.2	50-110
2010 SD	0.090	0.406	0.8190	3.5679	336.4478	93.0292	19	2.06	29	30-70
2005 CJ	0.094	0.526	0.8295	1.0837	358.0870	81.6632	2795	3.22	25.7	270-610
2003 BR47	0.096	0.500	0.8136	4.4207	314.5751	112.5060	939	2.28	23.7	150-350

4. Searching for potential parent body

A parent body is the celestial body from which meteorites may originate. Searching for relationships between meteorites, bolides and their parent body like asteroids is an outstanding scientific issue under rapid development (Foschini et al. 2000). Meteorites may be pieces of main-belt asteroids, derived by cratering collisions (Greenberg and Chapman 1983). The efficient delivery of meteorites to the Earth from a wide range of asteroid parent bodies is presented in Vokrouhlicky and Farinella (2000).

We can identify meteor stream and bolides using different D-criteria (Galligan 2001; Jopek et al. 2008). The first D-criterion was introduced by Southworth and Hawkins (1963). We computed their $D_{(A,B)}$ criterion for over 360 000 orbits from the ASTORB.dat catalogue (ASTROB 2013) for the epoch April 07, 2013 updated to April 18, 2013. We selected seven asteroids for which the parameter $D_{(A,B)}$ is smaller than 0.1. Table 2 list possible parent bodies using the $D_{(A,B)}$ criterion, orbital elements, observational arc, distance to the asteroid and its magnitude on February 15th, 2013, and its diameter.

5. New method of checking meteoroid/bolide parent bodies

To study precise orbital computations, f.e. in searching of the possible impacts of dangerous asteroids with the Earth, we compute the list of close approaches of asteroid with the planets. Then we can follow orbital motion of a given asteroid by different authors which used different Solar system models.

Next, we computed 1001 virtual orbits (VO) of our orbit of the superbolide from Table 1 using the multiple method of Milani et al. (2005) for 1-sigma uncertainties and the OrbFit software package, and traced down to 10 000 years ago to find theirs close approaches (CA) to the planets. The results of these computations are presented in Fig.4.

In addition, similar computations were made for several asteroids that might be candidates of being the Chelyabinsk parent body – Fig5. Comparing close approaches with planets of the meteoroid that produced Chelyabinsk Superbolide can be an additional method for selecting its parent body. Analyzing the computed CA of possible parent bodies from Table 2 we rejected all but asteroid 2011 EH. Asteroid 2000 SM10 was rejected because of its CA with Jupiter. Three other asteroids

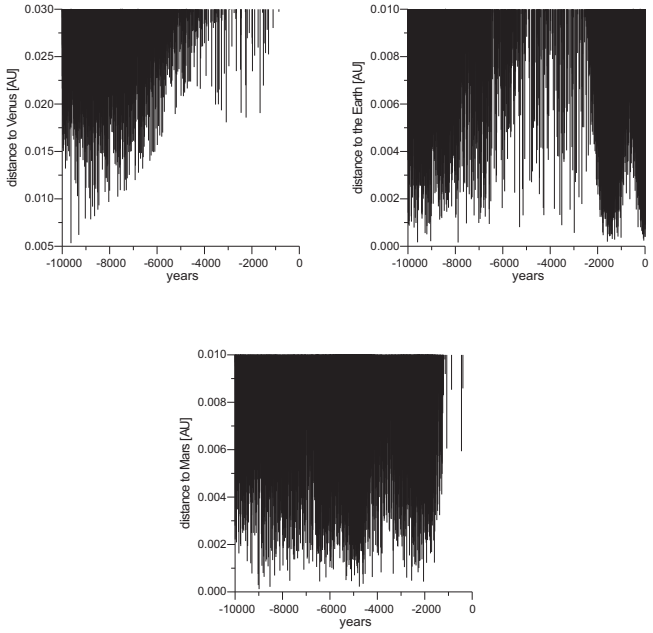

Figure 4. Possible past close approaches of the Chelyabinsk Superbolide to the planets.

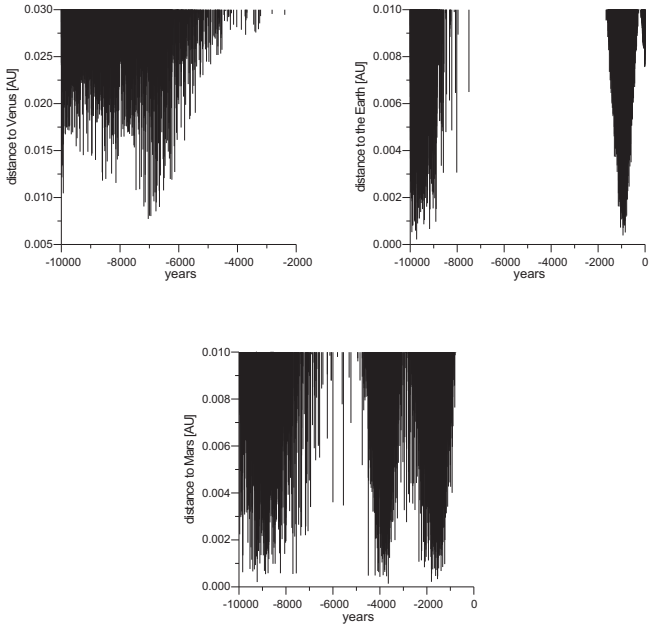

Figure 5. Past close approaches of the 2011 EH.

from the list: 2013 RN9, 2010 SD and 2005 CJ don't have CAs with Venus deeper than 0.1 au. Two asteroids, 2013 CV83 and 2003 BR47 have different CAs with planets than the superbolide meteoroid.

When comparing Fig. 4 and Fig. 5, it seems that only the CA histories of the Chelyabinsk Superbolide and the asteroid 2011 EH are similar, particularly in the case of CAs with Venus and the Earth, and partially with Mars. The computed CAs of all other potential parent bodies from Table 2 are completely different. Thus, amongst the objects listed in Table 2, asteroid 2011 EH is the most probable parent body of the Chelyabinsk Superbolide. Our method of identifying the parent body through CAs analysis can be considered as an auxiliary and qualitative method to the methods based on D-criteria.

6. Conclusions

Our study based on thorough analysis of video recordings and other data allowed the orbital parameters of the Chelyabinsk Superbolide to be determined with high accuracy. The obtained orbit combined with extensive close-approach computations clearly indicates that 2011 EH, a small Apollo Asteroid, is the most probable parent body for the Chelyabinsk Superbolide'. It is interesting that Abe (2013) found the same parent body of the Chelyabinsk superbolide, the asteroid 2011 EH, which is listed in our Table 2.

It should be mentioned that our results predict the final recoverable meteorite mass to be about 1.2 tons. In mid-October 2013 a huge chunk of the meteorite was pulled out of Chebarkul Lake from the depth of 13 m. The stone was quite fragile and broke into three parts during operation. The largest part weighed 570 kg.

References

Abe S., 2013, Meteoroids 2013, in the Conference Program and Abstract, #019, (`http://www.astro.amu.edu.pl/Meteoroids2013/index.php?section=program`)

ASTROB, 2013, `http://www.naic.edu/~nolan/astorb.html`

Beech M., Brown P., 2000, P&SS, 48, 925

Beech M., 2001, MNRAS, 326, 937

Borovicka J., Spurny P., Shrbeny L., 2013, CBAT, Electronic Telegram, 3423

Foschini L., Farinella P., Froeschle Ch., Gonczi R., Jopek T.J., Michel P., 2000, A&A, 353, 797

Galligan D.P., 2001, MNRAS, 327, 623

Greenberg R., Chapman C.R., 1983, Icarus, 55, 455

Jopek T.J., Rudawska R., Bartczak P., 2008, EM&P, 102, 73

Milani A., Chesley S.R., Sansaturio M.E., Tommei G., Valsecchi G.B., 2005, Icarus 173, 362

Southworth R.B., Hawkins G.S., 1963, Smiths. Contrib. to Astroph., 7, 261

Vokrouhlicky D., Farinella P., 2000, Nature, 407, 606

Wylie C., 1939, Popular Astronomy, 47, 297

Zuluaga J. I., Ferrin I., 2013, preprint arXiv:1302.5377

Meteoroids 2013, Proceedings of the Astronomical Conference,
held at A.M. University, Poznań, Poland, Aug. 26-30, 2013,
eds Jopek T.J., Rietmeijer F.J.M., Watanabe J., Williams I.P.,
Adam Mickiewicz University Press in Poznań, pp 27–33

Orbital Evolution and Impact Hazard of Asteroids on Retrograde Orbits

Kankiewicz P.[1], **Włodarczyk I.**[2]

[1]Institute of Physics, Astrophysics Division, Jan Kochanowski University,
Świetokrzyska 15, 25-406 Kielce, Poland, (pawel.kankiewicz@ujk.edu.pl)
[2]Polish Astronomical Amateur Society, Rozdrażew, Poland, (astrobit@ka.onet.pl)

Abstract. We present the past evolutional scenarios of known group of asteroids in retrograde orbits. Applying the latest observational data, we determined their nominal and averaged orbital elements. Next, we studied the behaviour of their orbital motion 1 My in the past (100 My in the future for two NEAs) taking into account the limitations of observational errors. It has been shown that the influence of outer planets perturbations in many cases can import small bodies on high inclination or retrograde orbits into the inner Solar System.

Keywords: main-belt asteroids, near-Earth asteroids, retrograde orbits

1. Introduction

Main aim of our work was the analysis of the orbital evolution of known asteroids in retrograde orbits in the past (1 My) and 100 My in the future for two NEAs. We also took into account the propagation of observational errors. We analyzed the reliability of the initial observational data and the influence of observational data on the limitations of long numerical integration. We show possible scenarios of orbit inversion (if occurred in the past) from prograde to retrograde motion.

2. Observational data and setup

Most of known asteroids in retrograde orbits have long observational arcs and well determined orbital elements. In some cases, observational arcs are relatively short (latest results). Main source of observations was the Minor Planet Center database, known as the ECS (Extended Computer Service). To determine the orbital elements and to generate so-called clones we used OrbFit software developed by Milani (1997). We computed clones of each asteroid with the multiple solution method by Milani et al. (2005) and with the ephemeris JPL DE405/406 (as the source of planetary perturbing forces). Next, the clones were propagated 10^6 years backwards by the numerical integration with the use of the Mercury software (Chambers 1999). During the integration, we averaged orbital elements for all clones of the given asteroid by weighting each element, assuming the Gaussian distribution of observational errors. We also integrated equations of motion of two NEAs (2007 VA85, 2009 HC82) 100 My in the future. In this case we used 900 clones, and took into account more complicated dynamical model with

Table 1. The inclination changes of 18 most known asteroids in retrograde orbits as the result of our first long-term integration of the 'swarms' of clones. Initial nominal i_{n0} and mean inclination (i_{m0}) values correspond to 1 My in the past. Because of a lot 'ejections' of test particles during the integration, we show the probability $P(r < 1000$ AU).

Ast/comet name	i [deg]	i_{m0} [deg]	i_{n0} [deg]	Prob. P	Secular resonances
20461 Dioretsa	160.4	136.3	154.9	0.687	nod./aps. Neptune
65407 2002 RP120	119.1	122.5	110.7	0.606	nod./aps. Neptune, nod. Uranus
1999 LE31	151.9	137.8	178.8	0.801	nod./aps. Neptune
2000 DG8	129.3	125.8	160.2	0.782	nod./aps. Neptune
2000 HE46	158.5	137.0	130.5	0.562	nod./aps. Neptune
2002 CE10	145.5	130.2	73.7	0.759	aps. Neptune, nod. Uranus
2004 NN8	165.5	144.9	166.7	0.192	nod. Uranus/nod. Neptune
2005 SB223	91.4	96.2	91.5	0.515	nod. Uranus/nod. Neptune
2005 TJ50	110.3	106.8	103.4	0.637	nod. Uranus/nod. Neptune
2005 VD	172.8	139.1	132.2	0.696	aps. Neptune
2006 BZ8	165.3	134.1	152.6	0.710	aps. Neptune, aps. Uranus
2006 EX52	150.3	147.9	153.9	0.899	nod./aps. Neptune, nod. Uranus
2006 RG1	133.3	141.2	144.0	0.911	aps. Neptune, nod. Uranus
2006 RJ2	164.7	138.4	166.3	0.809	(fast nod/aps. precession)
2007 VA85 (Amor)	131.9	88.7	86.7	0.248	aps. Neptune, nod. Uranus
2007 VW266	108.3	89.6	67.9	0.385	nod. Uranus/nod. Neptune
2008 KV42	103.5	103.1	103.1	0.997	nod./aps. Neptune
C/2006 GZ2	168.6	148.1	143.1	0.657	nod. Neptune

Table 2. Keplerian elements of two NEA (Apollo and Amor type) asteroids in retrograde orbits, determined from the latest observations. Epoch: JD 2456400.5 TDT.

Asteroid name	a [AU]	e	i_{2000} [deg]	Ω_{2000} [deg]	ω_{2000} [deg]	M [deg]	No. of obs. used	Rms [arc sec]
2007 VA85	4.228	0.7357	131.9	115.6	26.088	237.1	82	0.6413
1-σ rms	7.29E-04	3.89E-05	4.31E-04	7.03E-04	3.18E-03	6.14E-02		
2009 HC82	2.528	0.8075	154.5	294.9	298.5	38.93	104	0.5542
1-σ rms	3.25E-07	1.63E-07	1.99E-05	7.69E-05	7.02E-05	5.11E-05		

the Yarkovsky/YORP effects. We used the modified *swift_rmvsy* software (Broz 2006). Because some needed physical data are not determined yet, we used random or approximate spin and rotation parameters (like spin axes, radius, density, thermal properties, rotation period etc.). These results are shown in Fig. 4, 6 and can be compared with 3, 5 (w/o the Yarkovsky and YORP effect).

3. Results

Probably, part of known asteroids in retrograde orbits have similar dynamical past. They are from different taxonomic groups (Plutinos, Halley-like, SDO, Damocloids, Mars-Crossers, other inner and outer planet crossers). Only two numbered asteroids exist in this group, and the most known is (20461) Dioretsa. Interesting example is the Amor-type asteroid 2007 VA85. In the past, the eccentricity and semimajor axis of its orbit were greater. It is possible that 2007 VA85 changed the inclination significantly (from prograde with high inclination to retrograde motion).

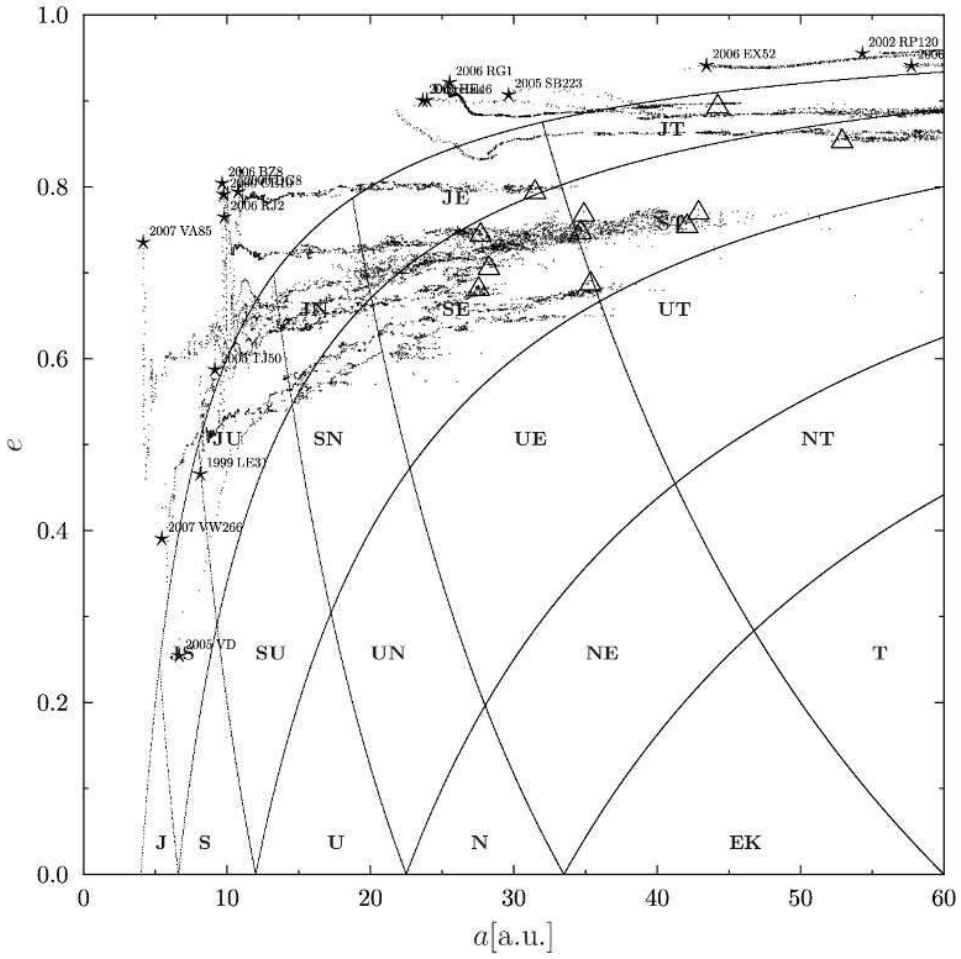

Figure 1. Evolutional paths of most known retrograde asteroids (1 My backward integration, past–marked by triangles, current values marked by stars). The zones of influence of planets are also shown, according to the idea of Horner et al. (2003), where: J-Jupiter, S-Saturn, U-Uranus N-Neptune, EK-Edgeworth-Kuiper Belt, T-Transneptunian.

This scenario is confirmed by the evolution of nominal and averaged orbital elements obtained by Kankiewicz and Włodarczyk (2010b). It is also important to mention that impact predictions based on the first 55 optical observations of 2007 VA85 estimated the probabilities of collision with the Earth from $2.7 \cdot 10^{-10}$ to $6.4 \cdot 10^{-10}$ in 2082, 2083 and 2089 (Kankiewicz and Włodarczyk 2010b). These results were excluded after the update of observational data. The second known example of retrograde NEA is Apollo-type object, 2009 HC82. Among 900 test particles (clones of the nominal orbit) we found one Mars-coorbital solution (after 30 My in the future), with relatively low probability $1.469 \cdot 10^{-4}$.

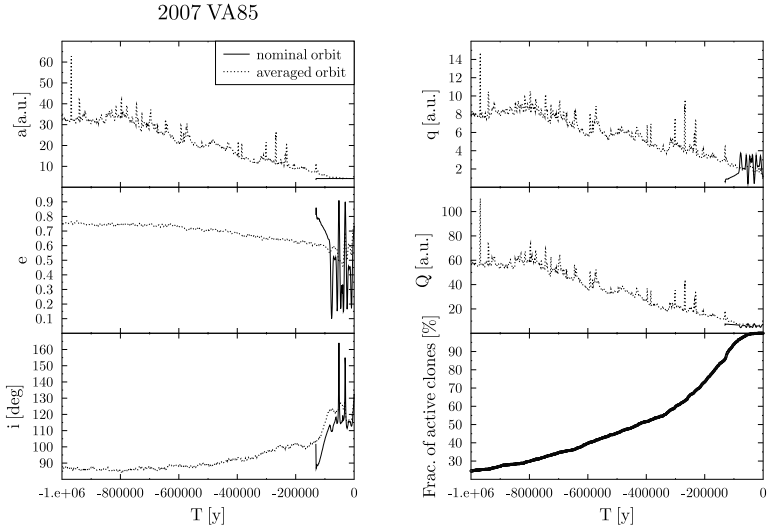

Figure 2. Nominal and averaged orbital elements of the Amor-type asteroid 2007 VA85 as the result of the numerical integration of 1000 test particles ('clones') distributed near the nominal orbit (1 My, past). The fraction of active (no 'ejected' during the integration) clones is also shown (Kankiewicz and Włodarczyk 2010b).

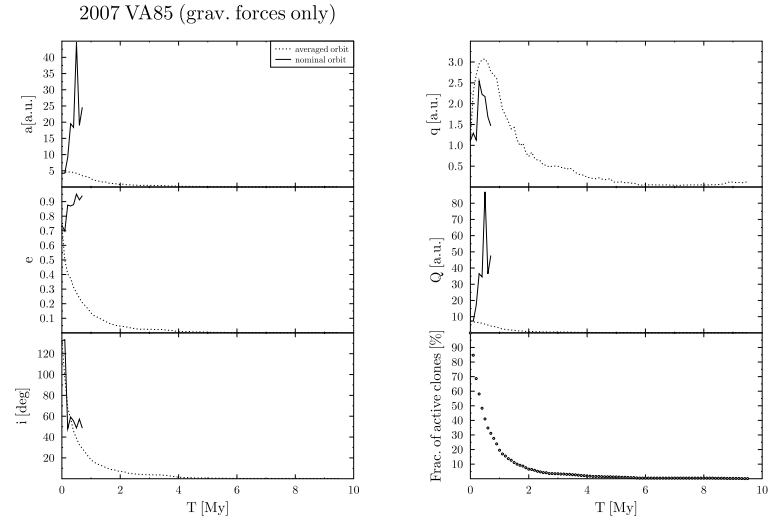

Figure 3. The possible future (10 My) of nominal and averaged orbital elements of the Amor-type asteroid 2007 VA85.

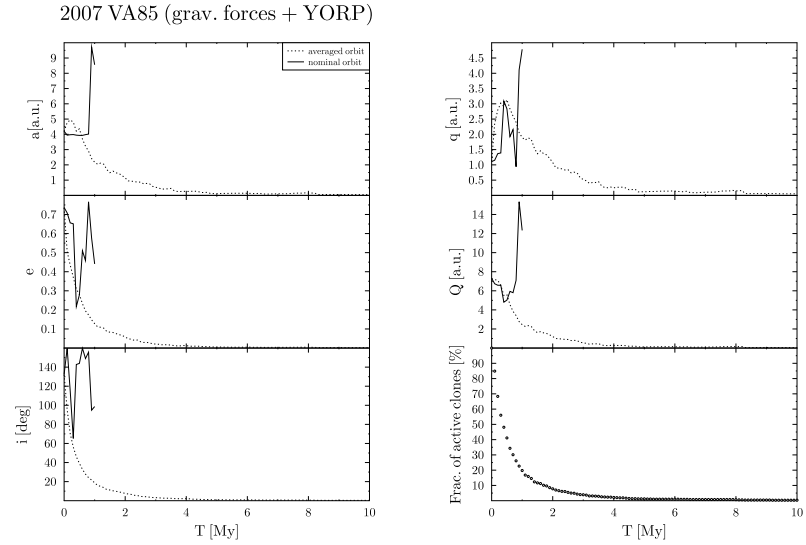

Figure 4. The possible future (10 My) of the Amor-type asteroid 2007 VA85. The Yarkovsky and YORP effects were additionally taken into account.

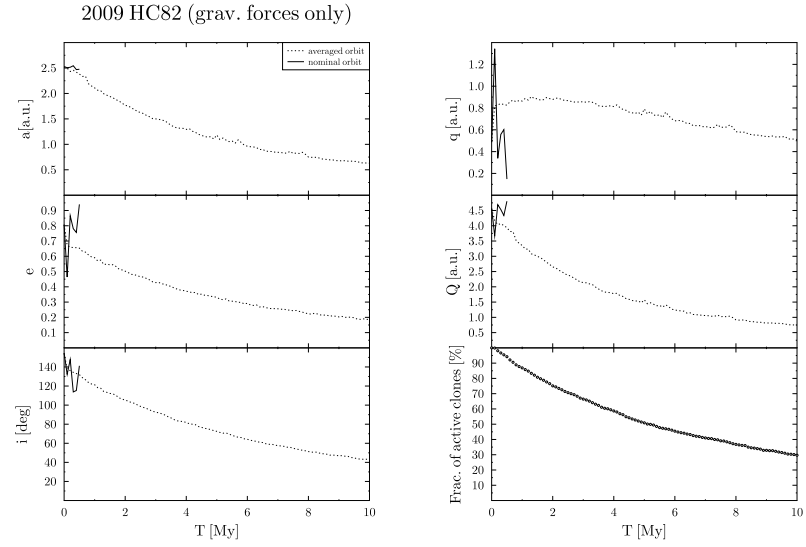

Figure 5. The possible future (10 My) of the Apollo-type asteroid 2009 HC82.

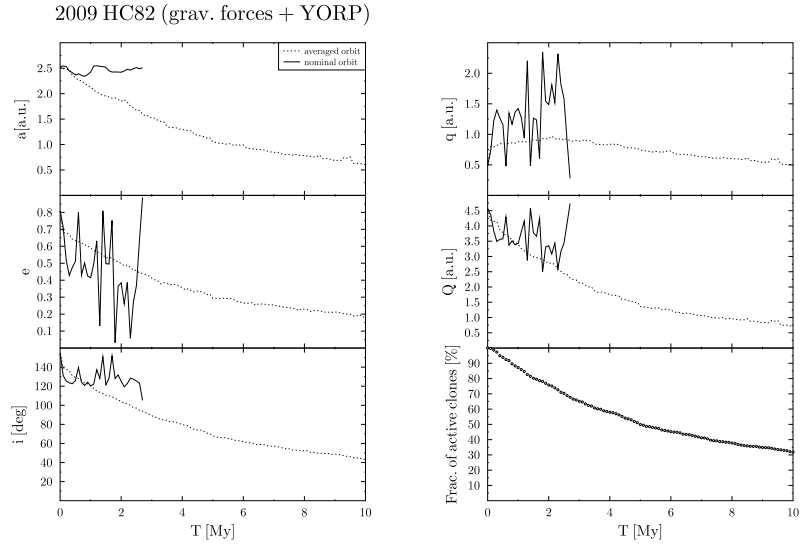

Figure 6. The possible future (10 My) of asteroid 2009 HC82. The Yarkovsky and YORP effects were additionally taken into account.

For most retrograde objects, semimajor axis had greater values in the past and eccentricities were smaller. In some cases orbits changed directions from $i \sim 90^\circ$ during last 1 My. In other cases it happened in the last 100–200 Ky due to planetary perturbations. The role of secular, nodal and apsidal resonances with Neptune is probably the most significant and can be possible cause of inclination changes (Kankiewicz and Włodarczyk 2010a).

4. Conclusions

As a result of this study a few conslusions can be drawn.

1) For the most retrograde objects, inclinations of orbits in the past were smaller.
2) There are two examples of retrograde hazardous objects, Apollo and Amor-type (2007 VA85, 2009 HC82). For now, the application of latest observational results excluded any significant risk of impact.
3) Most of obtained solutions are very sensitive on initial conditions (chaotic and unstable orbits). The long-term predictions have significant limitations.
4) Some results concerning the application of Yarkovsky/YORP effects indicate, that they can play important role. However, this conclusion should be confirmed by more (non-random) physical properties, derived from potential new observations in the future.

References

Broz M., 2006, Yarkovsky effect and the dynamics of the Solar System, PhD Thesis, Charles University, Prague. pp. 184

Chambers J.E., 1999, MNRAS, 304, 793

Horner J., Evans N.W., Bailey M.E., Asher D.J., 2003, MNRAS, 343, 1057

Kankiewicz P., Włodarczyk I., 2010, in Proc. of the Intern. Conf. 'Protecting the Earth against Collisions with Asteroids and Comet Nuclei', eds Finkelstein A.M., Huebner W.F., Shor V.A., (St. Petersburg, Nauka), 52

Kankiewicz P., Włodarczyk I., 2010, in Proc. of the Intern. Conf. 'Protecting the Earth against Collisions with Asteroids and Comet Nuclei', eds Finkelstein A.M., Huebner W.F., Shor V.A., (St. Petersburg, Nauka), 268

Milani A. et al., OrbFit Software 1997-2012, `http://adams.dm.unipi.it/~orbmaint/orbfit/`

Milani A., Chesley S.R., Sansaturio M.E., Tommei G., Valsecchi G.B., 2005, Icarus 173, 362

Meteoroids 2013, Proceedings of the Astronomical Conference,
held at A.M. University, Poznań, Poland, Aug. 26-30, 2013,
eds Jopek T.J., Rietmeijer F.J.M., Watanabe J., Williams I.P.,
Adam Mickiewicz University Press in Poznań, pp 35–39

The potentially dangerous asteroid (99942) Apophis

Włodarczyk I.

Polish Astronomical Amateur Society, Rozdrazew, Poland (astrobit@ka.onet.pl)

Abstract. We computed impact solutions of the potentially dangerous asteroid (99942) Apophis based on 4121 optical observations (of which 34 are rejected as outliers) from 2004 March 15.10789 to 2013 May 27.260672 UTC, and also on 20 radar points from 2005 January 27 to 2013 March 15. Using the freely available OrbFit software package, we can follow its orbit forward in the future searching for close approaches with the Earth, which can lead to possible impacts up to 2110. The possible impact path of risk for 2064 is presented. Also the method of computing path of risk for asteroids is described. It can be useful for computing the path of risk, a locus of possible positions for an impact event on the Earth's surface connected with the parent body of meteorite.

Keywords: Apophis, minor planets, hazardous orbits

1. Introduction

The dangerous asteroid (99942) Apophis was discovered on June 19, 2004 at the Kitt Peak Observatory by F. Bernardi, D. J. Tholen, and R. A. Tucker. Asteroid (99942) Apophis belongs to the Aten group, containing 810 members as of November 11, 2013 and is one of 10 333 known Near-Earth Asteroids at this time (MPC 2013a). Apophis belongs to one of 1433 Potentially Hazardous Asteroid (PHA) (MPC 2013b). PHA are so called the minor planets with the greatest potential for close approaches (CA) to arth. PHA are objects with the absolute magnitude H, brighter than or equal to V=22.0 and Minimum Orbit Intersection Distance from Earth orbit, MOID less than 0.05 AU.

The JPL NASA Sentry Risk Table (JPL NASA 2013) lists, as of November 11, 2013, 451 Near Earth Asteroids which have potential future Earth impact events. Apophis has 10 years observational arc and is still in this Table from 2004 year. Since 2004 many papers have been published with possible impacts computed by different methods: Farnocchia et al. (2013), Królikowska et al. (2009), Wlodarczyk (2008), Wlodarczyk (2013) and many others.

2. Method and Results

The possible impact solutions for asteroids are usually presented in a form such as that used by the NASA's Impact Risk Page (JPL NASA 2013) or by the NEODyS (NEODyS 2013a). They list the name of each dangerous asteroid, the dates of its potential impacts in the next 100 years, the probability of possible impact at each date and the impact energy.

Our computations were made using the free OrbFit Software Package v.4.2 (NEODyS 2013b). Generally, the OrbFit software searches for possible impacts

and give these *standard* solutions. Table 1 lists these parameters for the asteroid (99942) Apophis.

In our calculations we have included the JPL DE405, the perturbations from 25 massive asteroids as was described in Farnocchia et al. (2013), different weighting methods and selection of observations, error model based on Chesley et al. (2010) and the Yarkovsky effects. Observations of Apophis are so precise then the use of these additional small effects was necessary.

Asteroid (99942) Apophis has a 10 years observational arc so it is possible to compute da/dt with the method given by Milani et al. (2009) for asteroid (101955) 1999 RQ36. The value of da/dt computed by us is equal to -11.0×10^{-4} AU/Myr. Moreover, in Farnocchia et al. (2013) the range of possible parameter da/dt is given. Their distribution of da/dt obtained from the assumed physical modeling of Apophis show two maxima: around $da/dt = -10 \times 10^{-4}$ AU/Myr and da/dt=$+10 \times 10^{-4}$ AU/Myr. The probability of the first value is over two times greater. Hence our computed value of da/dt is consistent with the theoretical model of Farnocchia et al. (2013) and we adopted $da/dt = -11 \times 10^{-4}$ AU/Myr in our orbital computations.

Table 1. (99942) Apophis. Possible impact solutions computed with da/dt=–11.0×10^{-4}AU/Myr.

Parameter	Years		
	2064	2073	2075
Impact probability	1.54×10^{-06}	1.41×10^{-07}	3.85×10^{-06}
Date of impact (UTC)	2064 April 13.021	2073 April 13.112	2075 April 13.216
σ_LOV	0.8414	0.6991	0.6126
Mass of Apophis	2×10^{10} kg		
Impact velocity	12.62 km/s		
Energy	3.98×10^{2} MT		

In Table 1 the mass of Apophis is estimated assuming a uniform spherical body with the computed diameter and a mass density of 2600 kg/m^3, Impact velocity is a velocity at atmospheric entry, Energy – kinetic energy at impact, i.e. $\frac{1}{2} \times$Mass$\times$(Impact velocity)^2 measured in Megatons of TNT. The 'ton of TNT' is a unit of energy equal to 4.184×10^9 J, which is approximately the amount of energy released in the detonation of one metric ton of TNT. σ_LOV is the coordinate along the Line of Variations (LOV). This value is a measure how far from the nominal orbit impact occurs. The further away it is from zero, i.e. from the nominal orbit, the less likely is the possibility of impact. About 99% of all the uncertainty region where can be asteroid lies in the range of σ (-3, +3). The JPL NASA explores possible impact out to $\sigma = \pm 5$.

The asteroid (99942) Apophis will be observable for many years so new optical and radar observations can refine the orbit of the asteroid and probably give more precise possible impacts solutions.

3. Impact orbits

Impact orbits, according to Sitarski (1999), are orbits with the orbital elements of the dangerous object at the present date (initial orbital elements) and 7 days before an impact (close orbital elements). As this orbit intersects the Earth, having the precise orbital elements allows us to easily compute the region of impact.

Our method of computing possible impact orbits (Wlodarczyk 2007, 2008, 2012) is based on the method of Milani included in the OrbFit software where the *cloning* is based on the line of variations (LOV) with the largest eigenvalue, where σ_LOV denotes the position of an asteroid on the orbit along the line of variations (LOV) in σ space (Milani et al. 2005a,b).

Using the OrbFit software to integrate alternate (virtual) orbits (VO) ('clones') along the LOV (Milani et al. 2002, 2005a,b) we identify impact orbits and can plot paths of risk for the Earth or any other body in the solar system. For possible impact of the asteroid (99942) Apophis in 2064 the method is as follows. First, we take σ_LOV equal to 0.8414 from Table 1 and compute 5 VOs, i.e. two on each side of the LOV using the multiple method implemented in the OrbFit software. Next, we propagate these VOs 20 days beyond the impact day i.e. to MJD75043 (MJD=JD-2400000.5) equal to 2064-May-03 and search for the close approaches to the Earth in 2064. VO #5 has CA of about 0.0033 AU. We take this orbit and using the multiple method we compute 50 VOs around this orbit with the small value of σ_LOV. It was appeared that with σ_LOV equal to 0.015 we have some VOs which hit the Earth. These VOs are called impact orbits. Table 2 lists initial/close orbital parameters of the impact orbit of the asteroid (99942) Apophis for 2064. Next, we can compute paths of risk for these impact orbits. Using this method we can compute paths of risk for other objects, for example for the parent body of the meteor showers.

Table 2. (99942) Apophis. Initial/close orbital parameters of the impact orbit for 2064. The angles ω, Ω, and i refer to Equinox J2000.0. Epochs: 2013-April-18=JD2456400.5 (MJD56400) for initial orbit and 2064-April-06=JD2475016.5 (MJD75016) for the close orbit.

M = 235°.468506±4E-6	a = 0.9220865017±1E-10 [AU]	e = 0.191164733±5E-9
308°.072372	1.1293765951	0.197565497
ω = 126°.45716±2E-5	Ω = 204°.22381±2E-5	i = 3°.3305675±3E-7
65°.56577	202°.87403	2°.1708679

Fig.1 shows path of risk of the asteroid (99942) Apophis in 2064. Note that path of risk is computed for 3-σ uncertainty. Both ends of the path of risk have lower impact probability than the central places. Hence the probability of hitting Norway by Apophis is very low, about 1.54×10^{-6} as is presented in Table 1.

4. Results and discussion

Because of the different observations used, different method of orbit computations, i.e. selection and weighing of observations, different values of the different nongrav-

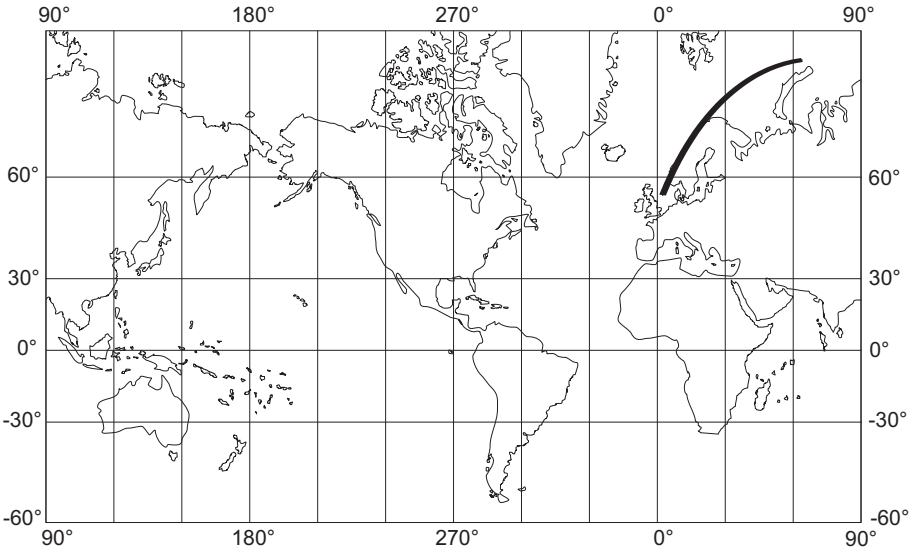

Figure 1. (99942) Apophis. Path of risk of the deepest impact from virtual asteroid in 2064 year.

itational parameters, catalogue biased errors and the different Solar system models used, there are different up to date (2013-Nov-21) impact solutions of Apophis published by different authors such as the JPL NASA, the NEODyS, the Solar Research Center of the PAS and so on.

Table 3. (99942) Apophis. Close approaches with planets of impact orbit for 2064.

Planet	Time, UTC	Distance, AU
Venus	2016/04/24.11796	0.07824181
Earth	2029/04/13.90709	0.00025446
Earth	2044/08/09.82349	0.09939968
Earth	2051/04/15.46873	0.01180630
Earth	2058/04/14.17469	0.00340129

The JPL NASA Sentry Risk Table (see JPL NASA 2013) gives impact solutions of Apophis based on 13 radar delay, 7 Doppler, and 3987 optical observations spanning 3318.0 days (2004-Mar-15.126289 to 2013-Apr-15.15729). They list 12 dates of possible impacts in the range 2060-2105. They computes orbit of Apophis using the Solar system model SB431-BIG16, i.e. the DE431 and 16 massive perturbing asteroids together with nongravitational parameter A2=–2.03E-16 AU/day^2.

The NEODyS Risk Page (NEODyS 2013c) presents 10 dates of possible impacts in the years 2068-2116 using 4105 optical observations (of which 87 are rejected as outliers) from 2004-03-15.109 to 2013-05-07.150.

In July 2013, the Space Research Center of the Polish Academy of Science in their

Main page of Potentially Hazardous Asteroids (see PHA 2013) lists the probabilities of impacts in 2036 and 2037 as nil. They also give old impact results.

Table 3 shows close approaches (CAs) of impact orbit of Apophis for 2064 year with planets. There are many deep CAs which make difficult in prediction of orbital motion of the asteroid. Mainly so called 'keyholes' in 2029 and 2058 can significantly change the possible impact date.

It is possible that asteroid (99942) Apophis can be a parent body of the new possible meteoroid stream visible around 2029.

References

Chesley S.R., Baer J., Monet D.G., 2010, Icarus, 210, 158

Farnocchia D., Chesley S.R., Chodas P.W., Micheli M., Tholen D.J., Milani A., Elliott G.T., Bernardi F., 2013, Icarus, 224, 192

JPL NASA, 2013, August, http://neo.jpl.nasa.gov/risk/

Królikowska M., Sitarski G., Sołtan A. M., 2009, MNRAS, 399, 1964

Milani A., Chesley S.R., Chodas P.W., Valsecchi G.B.,2002, in Asteroids III, eds Bottke W.F.Jr., Cellino A., Paolicchi P., Binzel R.P., Univ. of Arizona Press, Tucson, p. 55

Milani A., Chesley S.R., Sansaturio M.E., Tommei G., Valsecchi G.B., 2005, Icarus, 173, 362

Milani A., Sansaturio M.E., Tommei G., Arratia O., Chesley S.R., 2005, A&A, 431, 729

Milani A., Chesley S., Sansaturio M.E., Bernardi F., Valsecchi G.B., Arratia O., 2009, Icarus, 203, 460

MPC, 2013a, August, `http://www.minorplanetcenter.net/iau/lists/Unusual.html`

MPC, 2013b, August, `http://www.minorplanetcenter.net/iau/lists/Dangerous.html`

NEODyS, 2013a, August, `http://newton.dm.unipi.it/neodys/index.php?pc=4.1`

NEODyS, 2013b, August, `http://adams.dm.unipi.it/$\sim$orbmaint/orbfit/`

NEODyS, 2013c, August, `http://newton.dm.unipi.it/neodys/index.php?pc=1.1.2&n=99942`

PHA, 2013, `http://phas.cbk.waw.pl/Neo/2004MN4.HTM`

Sitarski G., 1999, Acta Astronomica, 49, 421

Wlodarczyk I., 2007, Contrib. Astron. Obs. Skalnate Pleso, 37, 69

Wlodarczyk I., 2008, Contrib. Astron. Obs. Skalnate Pleso, 38, 21

Wlodarczyk I., 2012, Solar System Research, 46, 301

Wlodarczyk I., 2013, MNRAS, 434, 3055

Meteoroids 2013, Proceedings of the Astronomical Conference,
held at A.M. University, Poznań, Poland, Aug. 26-30, 2013,
eds Jopek T.J., Rietmeijer F.J.M., Watanabe J., Williams I.P.,
Adam Mickiewicz University Press in Poznań, pp 41–47

Jovian impact flashes and their implication to meteoroids in outer region of Solar System

Watanabe J.

National Astronomical Observatory of Japan (jun.watanabe@nao.ac.jp)

Abstract. Optical flashes on the surface of Jupiter have been observed by amateur astronomers during 2010. These phenomena were thought to be impact flashes caused by the collision of small bodies of which size is a few to 10 m. They are bright fireballs happened in the Jovian atmosphere. If the frequency and the scale of these phenomena are systematically investigated, the size distribution of meteoroids can be derived down to meteoroids a few meters in size in the giant planet region because the brightness of such flashes depends only on their sizes in the case of Jupiter. We are trying to detect Jovian impact flashes by professional and amateur network over Japan, and to detect much fainter flashes by using larger telescopes. It is a unique method to utilize Jovian planets as natural impact detectors for the small bodies.

Keywords: small bodies, meteoroids, fireballs, impact flashes, meteoroids size distribution, Jupiter

1. Introduction

All the planets have been impacted by small solar system bodies. Most of them happened in the other planets cannot be observed mainly due to their faintness from the Earth together with their low frequency of bright fireball-class. The exception was the bright fireball observed by the spacecraft Voyager 1 in March 1979 at the close approach to the Jupiter (Cook and Duxbury 1979). The reduced absolute magnitude was –12.5, which is similar to the fireballs often observed on Earth. The impactor was thought to be about 11 kg with assuming the density of 2 gcm^{-3}, it was about 0.4 meters in diameter (Cook and Duxbury 1981). Actually Jupiter has so strong gravity that all the objects will have high velocity at the impact compared with the low revolution velocity. The next observed impacts were huge-scale fragments of comet Shoemaker-Levy 9 happened in 1994 on Jupiter. World-wide coordinated observations were carried out including Hubble Space Telescope and Galileo spacecraft on the way to the Jupiter. While the size of fragments of the comet nucleus were thought to be larger than 1 km diameter from optical observations (Watanabe et al., 1994), they were estimated to be less than 1 km from tidal disruption model (Scotti & Melosh, 1993). The latter may have been supported by estimates from various analysis of the impact phenomena (e.g. Knacke, & A'Hearn, 1994). The impact flashes of these fragments could not be directly detected because the impact points were just behind the rim of Jupiter viewed from the Earth. The only direct observations were done by the Galileo spacecraft (Hord et al, 1995). Both the complicated and bright infrared lightcurves after the impacts due to the hot plume (Watanabe et al. 1995) and impact traces

of huge size which were made by the debris fall-back of the debris from the plume (Fitzsimmons et al. 1996) indicated that the scale of these impacts had never been observed in other planets including the Earth in human history. Since 1994 event at Jupiter it is thought that large impacts in Jupiter should leave dark spots or traces at the top of the atmosphere. Tabe et al. (1997) discovered a similar dark spot detected by Cassini from his drawings reserved in the library of Paris Observatory. While this discovery suggested that such impacts seemed to be not rare, it was not proved until 2009 when another single dark spot was discovered (de Pater et al. 2010, Hammel et al. 2010). The impacted body was estimated to be or less than 500 m diameter, which is comparable to the size of smaller fragments of comet Shoemaker-Levy 9.

The direct observation of another impact was serendipitously detected by two amateur astronomers in June 2010. The estimated absolute magnitude was –25.2 and the size of this impactor was 5.5 ± 2.5 m in diameter which is definitely smaller than the 2009 case and resulted in leaving no trace on the surface even when viewed using large telescopes (Hueso et al. 2010). These subsequent events made both amateur and professional astronomers notice the potential for detecting impact flashes or traces in Jupiter even using small telescopes, which led the first detection in Japan two month later.

In this review, we introduce the importance of such impact flashes which can be used to estimate size distribution of small bodies of meteoroid size at the outer planet region, and we present situation of observations together with the first detection by Japanese amateur astronomers in August 2010.

2. First Detection of Optical Flash in Japan

The year of 2010 was a special because two independent impact flashes occurred on Jupiter and detected in June and August. In the former case, the bright flash was simultaneously and independently detected by two amateur astronomers: A. Wesley (Murrumbateman, Australia) and C. Go (Cebu, Philippines) at 20:31:20 UT on 2010 June 3. They used telescopes of 37 cm (A.W.) and 28 cm (C.G.) in diameter together with video recording system using a monochrome Flea3 camera equipped with an ICX618ALA chip. This event is the first case of the Earth-based detection of the superbolide on Jupiter, and detailed analysis was carried out by Hueso et al. (2010). Although the news of this event became popular among the amateur astronomers in Japan, it was unfortunate that no independent observation had been reported from Japan mainly due to the bad weather because of the rainy season.

It was just two month later that another optical flash occurred in August 2010 which was first noticed by M. Tachikawa, who is amateur astronomer in Kumamoto prefecture, Kyushu Island in Japan. He was taking video image of Jupiter for making high-quality images by composing excellent snapshots out of video frames. Usually the atmospheric seeing is not good in Japan, many amateur astronomers are doing so that they obtain high-quality images of the planets, especially Jupiter by utilizing a software such as Registax. Reviewing his video movies on the PC, he

noticed the faint optical flash occurred in the disk of the Jupiter. He contacted to his friend, R. Yamada who is also an amateur astronomer in the same area in Japan. It was also fortunate that he was the acquaintance of the author (J. Watanabe). He immediately did a phone call for reporting this phenomenon. The author recognized the importance of the report, which reminded the author the previous event, and asked him to send the movie file via internet. The movie file sent to the author showed definitely an optical flash. The author tried to analyze the position of the flash, and sent a preliminary report to the Bureau of the IAU Astronomical Telegram.

Figure 1 shows the image of the optical flash taken by M. Tachikawa at 18:21:56 UT on August 20, 2010. The flash location was roughly at planetographic latitude 21.5° north and 337° longitude (system III) in Jupiter's north equatorial belt. The duration of the flash was about 1.5 seconds, and the brightness was 6.2 magnitudes (Watanabe et al. 2012). This is considered to be an equivalent or slightly smaller scale than that in June (Watanabe et al. 2010). the event was later reanalyzed by Hueso et al. (2013) together with other samples detected after this event. We did not ask any follow-up observations by using larger telescope for searching the spot or trace of the impact debris on the Jupiter, because our preliminary analysis showed the scale of this August event is definitely smaller than the previous June event, which showed no trace (Hueso et al. 2010).

I realized that the movie of this flash was valuable to be covered in the press, and tried to contact to several TV press people as a division chief of the Public Relations Center of the National Astronomical Observatory of Japan. As a result, this detection was covered as a news on several Japanese TV channels along with the original movie of M. Takchikawa. the purpose of this publicity was to collect similar data, if any, as soon as possible because many amateur astronomers would erase their data for saving hard-disk capacity after they made an excellent still image by composite frames extracted from the movie they took.

Surprisingly, other detections of the same flash were reported to the observatory immediately after the news released. One was K. Aoki in Tokyo and other was M. Ichimaru in Toyama. They also obtained recordings of the event from locations separated about 800 km from Kumamoto, confirming the Jovian origin for the flash (Watanabe et al. 2010, 2012). A fourth observer, T. Wakamatsu of Arita City, found the impact in his data a few months later but with a lower signal-to-noise ratio. Anyway it is surprising that four amateur astronomers did take data on this precious event. Please note that the time of this event happened at 18:21:56 UT, which was 03:21:56 in Japanese Standard Time. Even if it is considered that it was a Saturday morning, it is proof that many amateur astronomers were taking video of the Jupiter. Moreover, they are not using large telescopes. The telescopes used were refractors with apertures from 12.5cm through 23.5cm, and the camera was Philips ToUcam Pro II attached to the telescopes providing RGB images of the Jupiter operated at 30 or 15 fps. These observation instruments are commonly used by amateur astronomers in Japan, which indicates the potential of such amateur astronomers contributing to the detection of such optical flashes by using small

Figure 1. Example of the optical flash recorded on August 21 by Mr. M. Tachikawa. One frame number corresponds to 1/30 sec. the absolute magnitude is derived as –22.4, and the estimated mass and size are 76 ton and 4.2 m diameter, respectively, with assuming the density is 2 gcm^{-3} (Watanabe et al. 2012).

telescopes. These situation led the author to consider monitoring observations as described later in this review.

It is worthy to note that the reason of the optical flashes were not noticed until 2010. One reason is that we do never think that it is possible to detect impact flashes with such frequency. Many people should be watching Jupiter for bolide impacts but they were overlooked mainly due to their short duration and faintness. Another reason is that amateur astronomers only recently tend to use high-sensitivity detectors, which make them possible to detect the flashes even with using small telescopes.

3. Implication to the Meteoroids in Outer Region

The impact flashes detected so far resemble meteor phenomena in the Earth's atmosphere. Detecting impact flashes on Jupiter is important not only for meteor astronomy as a new field, but also for researches of small solar system bodies in the outer planet region, because the population of the small bodies in the outer planet region is not yet studied in the size range less than 1 km diameter. Actually the re is large uncertainty in the estimate of the size distribution of small bodies in the giant planet region estimated from the crater counting on the solid surface of satellites of Jovian planets (Zahnle et al., 2003). Hence, the impact flashes should be an excellent tool for deriving population down to a few meters in size.

Moreover, there is one big merit to utilize impact flash for studying the size distribution of small bodies. The impact velocity for impactors to the Jupiter should be almost constant at $60 - 64$ km s^{-1} which is almost independent on the impacting direction due to the strong gravity of Jupiter together with the smaller orbital velocity of 13 km s^{-1}. In the Earth's case, the geocentric entry velocity varies from 11 km s^{-1} through 72 km s^{-1}. These value depends on the geometri-

cal situation of meteoroids entering to the Earth. Because gravity of the Earth is not so strong that the meteoroids have wide range value of entry velocity due to the compound of the orbital velocities of meteoroids and the Earth. On the other hand, the meteoroids entering to Jupiter's upper atmosphere should be attracted by its strong gravity, and tend to have similar entry velocities at the final phase of the impact to the Jovian atmosphere. This situation made it possible to know the size of the impactors from the brightness of the impact flashes. In case of Earth, the brightness of meteors depends not only on sizes but also on the entry velocity. On the other hand in the case of Jupiter, the entry velocity becomes almost similar value so that we do not have very small uncertainty for estimating size of impacting bodies just from the brightness of the flashes. Therefore, if the frequency and the scale of these optical flashes are investigated, the size distribution down to size of a few meters can be estimated at around the giant planet region. Of course, actual estimates of each bolide should be performed by constructing appropriate model including Jovian atmospheric properties, which has been well done by Hueso et al. (2013). While it will not be necessary to introduce the details in this review, this is a unique way to explore the population of small bodies by utilizing Jupiter as a natural impact detector.

Actually after 2010, one optical flash was visually detected by D. Petersen in Racine, Wisconsin, USA as a bright two-second flare at 11:35:30 UT on September 10 2012 along Jupiter's eastern limb. Estimated visual magnitude of the flash was to be 6.0. His report was distributed by the Association of Lunar and Planetary Observers, and resulted in appearance of the video record taken by G. Hall in Dallas, Texas, USA, by the 30.5 cm aperture refractor using a Point Grey Flea 3 CCD video camera. This event was also analyzed in detail by Hueso et al. (2013), and it was located at 0.7° planetographic latitude and 265° longitude (system III). The diameter of this bolide was estimated to be $7.8 - 9.7$ m with assuming the density of 2.0 g cm^{-3}. This is the larger than those of previous two cases (Hueso et al. 2013). However all three flashes were the result of serendipitous detections, and number of detections is still small for deriving populations of small bodies even if Hueso et al (2013) tried to make constraint to the size distribution in their latest research. Hueso et al. (2013) shows that the present impact rate estimated from three samples is 14–45 events per year, which is consistent with that predicted by a dynamical model of comets and asteroids (Levison et al. 2000), while it is by one order higher than those estimated from the cratering record in Galilean satellites (Schenk et al. 2004, Zahnle et al. 2003). Anyway, it is too early to conclude on the size distribution of small bodies at this region due to the lack of samples.

4. Monitoring Campaign

In order to derive the population of small bodies more strictly, we have to accumulate the samples. One way for it is to look for optical flashes undetected among the accumulated data until now. Hueso et al.(2013) tried to handle with the data of Planetary Virtual Observatory and Laboratory which is the database of images of the International outer Planets Watch, and those of Association of Lunar

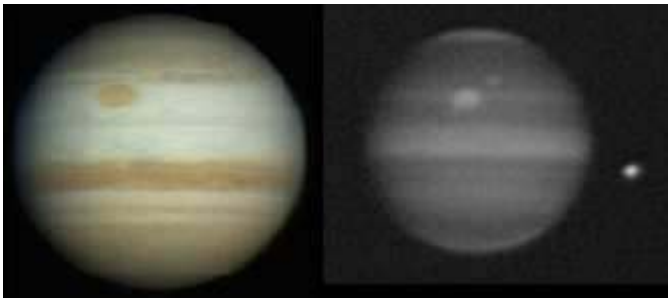

Figure 2. Example of Full color image (left) and methane band image (right) taken by 25 cm telescope of amateur astronomers. This comparison image was supplied by ALPOJ. Methane-band filters should make higher contrast of the impact flashes on the dimmed surface brightness of the Jovin disk.

and Planetary Observers in Japan. However, most of the data taken until now are mainly still images, which are not appropriate for short-time duration events such as optical flashes.

Another way is to perform systematic observations which aim to monitor continuously and widely by involving amateur and professional astronomers. As previously described, the impact flashes having similar brightness to three samples detected so far can be observable for small telescopes along with appropriate detectors connected to the PC or digital movie instruments. the situation is suitable especially for Japanese amateur astronomers, who have the appropriate instruments along with a high level of observational skills. If the size distribution of the small bodies in Jovian region is similar to that of meteoroids near Earth, then fainter impact flashes caused by smaller meteoroids should be more numerous than bright flashes. Using large telescopes of 1 m aperture class, we may be able to catch fainter flashes caused by much smaller bolides which may occur more frequently. In this purpose, we planned to use methane-band filters to reduce the background brightness of Jovian disk. We may be able to pick up fainter impact flashes on the darkened surface of the disk in the methane band as shown in Figure 2.

For this purpose, the author and his colleague coordinated both professional and amateur astronomers in Japan and China, and performed two monitoring campaigns in September and November 2012. the first one was set from August 31 through September 9, 2012. Five telescopes participated including two 1-m class telescopes at Weihai Observatory of Shandong University, China, and Kita-Subaru telescope at Nayoro station of Hokkaido University. It is the irony which the new impact flash happened and detected on September 10 as described in the previous section immediately after the end of this first campaign. The second campaign was set from November 3 through November 10, 2012. Four telescopes participated including 50-cm and 40-cm telescopes. Although total monitoring time was 86 hours, there was no positive detection by using eye inspection and automated detection software developed in our group. In 2013, we performed similar campaign between November 9 and 17. Four telescopes participated including 2-m Nayuta telescope at the Nishi-Harima astronomical Observatory, which belongs to Uni-

versity of Hyogo. The analysis of the data taken in this campaign is ongoing at the present by using our software and automated detection developed by Hueso's group (Grupo de Ciencias Planetarias, UPV-EHU, Spain) which is opened at their web site http://www.pvol.ehu.es/software/.

Considering the astronomical significance of the impact flashes in Jupiter, the author will try to continue such campaign by coordinating amateurs and professionals by involving more amateurs in Asian region, and making an effort for a world-wide campaign.

References

Cook A.F., Duxbury T.C., 1979, Bull. Amer. Astron. Soc., 11, 586
Cook A.F., Duxbury T.C., 1981, JGR, 86, 8815
de Pater I. et al., 2010, Icarus, 210, 722
Fitzsimmons A. et al., 1996, Nature, 379, 801
Hammel H.B. et al., 2010, Astrophys. J. Letters, 715, L150
Hord C.W. et al., 1995, Geophys. Res. Let., 22, 1565
Hueso R. et al., 2010, Astrophys. J., 721, L129
Hueso R. et al., 2013, A&A, 560, A55
Knacke R.F., A'Hearn M.F., 1994, EM&P, 66, 11
Levison H.F. et al., 2000, Icarus, 143, 415
Schenk P.M. et al., 2004, in Jupiter: the planet, satellites and magnetospheres, eds. Bagenal F., Dowling T.E., McKinnon W.B., (Cambridge, UK: CUP), 427
Scotti J.V., Melosh H.J., 1993, Nature, Volume 365, 733
Tabe I. et al., 1997, Pub. Astron. Soc. Japan, 49, L1
Watanabe J. et al., 1994, Pub. Astron. Soc. Japan, 46, L1
Watanabe J. et al., 1995, Pub. Astron. Soc. Japan, 47, L21
Watanabe J. et al., 2010, Abstract in JGU meeting 2011, P-PS22
Watanabe J. et al., 2012, LPI contributions, 1667, 6271
Zahnle K. et al., 2003, Icarus, 163, 263

Meteoroids 2013, Proceedings of the Astronomical Conference,
held at A.M. University, Poznań, Poland, Aug. 26-30, 2013,
eds Jopek T.J., Rietmeijer F.J.M., Watanabe J., Williams I.P.,
Adam Mickiewicz University Press in Poznań, pp 49–53

Impact probability calculations by the Hill sphere method

Wajer P.[1] **Gabryszewski R.**[1]

[1]Space Research Centre of Polish Academy of Science,
Bartycka 18a, 00-716 Warsaw, Poland (wajer@cbk.waw.pl)

Abstract. We present a method of impact probability estimations between a cometary population and terrestrial planets. In this method, the real target, i.e., its collisional sphere, is replaced by a much larger target (the Hill sphere). Knowing the ratio between areas of Hill sphere and collisional surface, the number of objects entering Hill sphere of the planet, the impact probability is estimated. The poster presents the models and results for the two different approaches. The former uses the unperturbed Keplerian orbit of the projectile, while the second uses the elliptic restricted three-body problem (Sun-target-projectile). By comparing the two methods, we have checked if long-time perturbations have any important influence on the results. The method can be applied to the modeling of small bodies dynamics during and after the LHB.

Keywords: impact probability, collisions, Late Heavy Bombardment, Solar System, terrestrial planets, Moon

1. Purpose of the work

We present a method of impact probability estimations between a cometary population and terrestrial planets. Our analysis uses two different approaches: unperturbed Keplerian and elliptic three-body problems. By comparing the two approaches, we have checked if long-time perturbations have any important influence on the results. The method can be applied to the modeling of small bodies dynamics during and after the LHB. It also should allow to conclude on water delivery, climate changes on Mars and effects on other terrestrial planets and Moon. Comparison to the Wetherill analytical method Wetherill (1967) as well as the MOID (minimum orbital intersection distance) method Rickman et al. (2012) were also attached.

2. Hill Sphere Method

Hill sphere method: Collisional sphere of the real target is replaced by much larger i.e. the Hill sphere of the target. If we know the ratio between areas of the target and its Hill sphere, and the number of objects entering the Hill sphere, we can estimate the impact probability:

$$P = \frac{1}{N_{TOT}} \frac{r_t^2}{r_H^2} \sum_{N_H} (1 + \frac{v_e^2}{U^2}) \tag{2.1}$$

where N_{TOT} is the total number of comets on random orbits, N_H – the number of objects entering the Hill sphere of the target, r_t and r_H are the radii of the target and its Hill sphere, respectively, v_e is the the target's surface escape velocity and U is an encounter velocity. The sum is taken over all comets that crossed the Hill sphere.

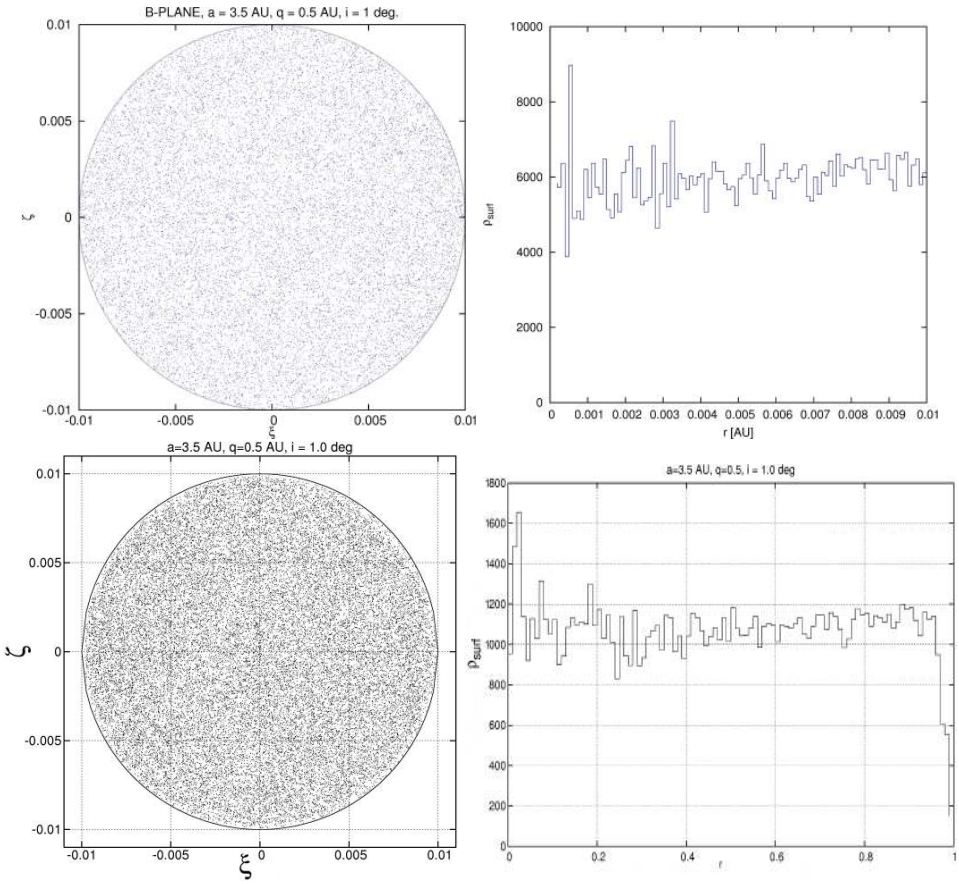

Figure 1. Left: points of intersection projected into b- plane. Right: surface density of these points. Top figures – 2BP approach, bottom figures – ER3BP approach.

3. Numerical models

Simulations were performed in two approaches:

1) two body problem (2BP),
2) the elliptic restricted three-body problem (ER3BP), where the orbit of projectile is perturbed by the target.

We also implemented the Wetherill analytical formula (extension of the Öpik formula to the elliptic case) for comparisons:

$$P_0 = \frac{1}{8\pi^2 \sin i}\left(\frac{R_{coll}}{a_t}\right)^2 \frac{U\rho^{1/2}}{a^{3/2}(1-e_t^2)^{1/2}}\left[2 - \frac{\rho_t}{a} - \frac{a}{\rho_t}(1-e^2)\right]^{-1/2} \tag{3.1}$$

where the subscript 't' concerns the target and e_t is the eccentricity of the target orbit, R_{coll} – the collisional radius of the target, a_t – the semimajor axis of the target, V_t – orbital velocity, ρ_t – the distance of the target from the Sun. The total collision probability is derived from the above formula by averaging over Ω and ω.

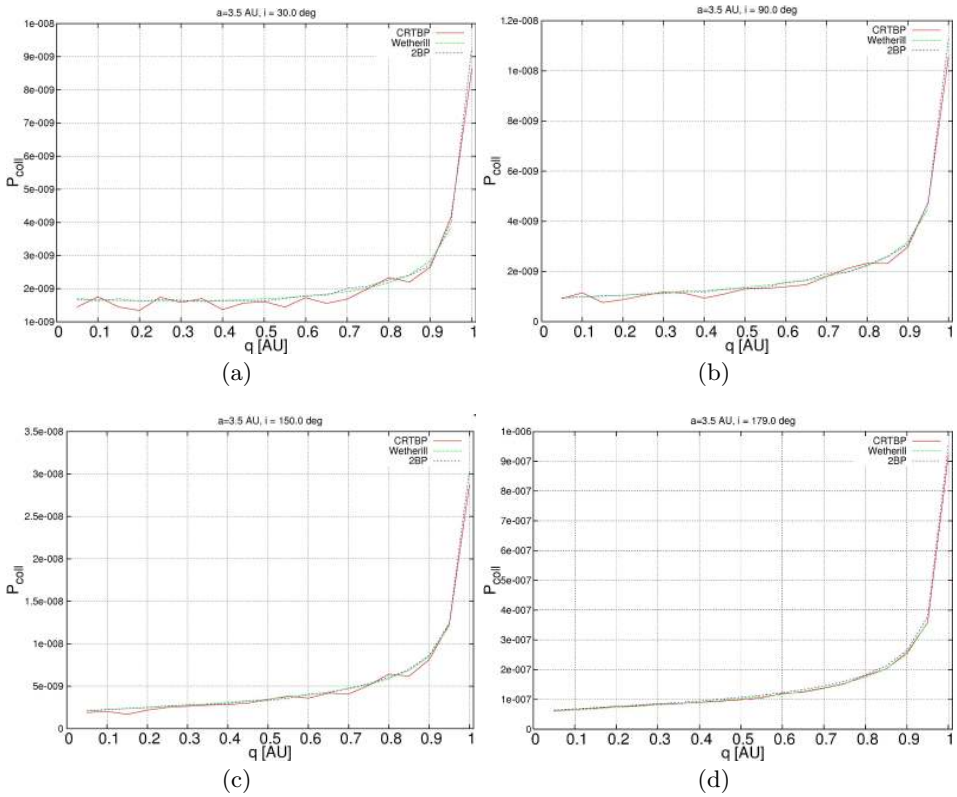

Figure 2. Collisional probability with Earth in a function of perihelion distance of the target, q. In all cases we assumed that the semimajor axes of all impactors are equal 3.5 AU. The eccentricity of Earth's orbit is 0. In figs. a), b) and c), in case of ER3BP approach, we used noticeable smaller value of N_{TOT} (in comparison with 2BP approach), which caused worse agreement between these two methods.

4. Tests

Figure 1 shows points of intersection projected into b - plane, i.e. the plane containing the target and perpendicular to the targetocentric velocity at closest approach

along the unperturbed orbit of the projectile. We should expect semi-uniform distribution because there is no preferred velocity direction.

5. Results

Examples of results: impact probability with Earth, Mars and its behavior near $q_c/q_t = 1$ where q_c is perihelion of the projectile and q_t – perihelion of the planet. We assumed circular orbit of Earth and elliptic orbit of Mars in our calculations.

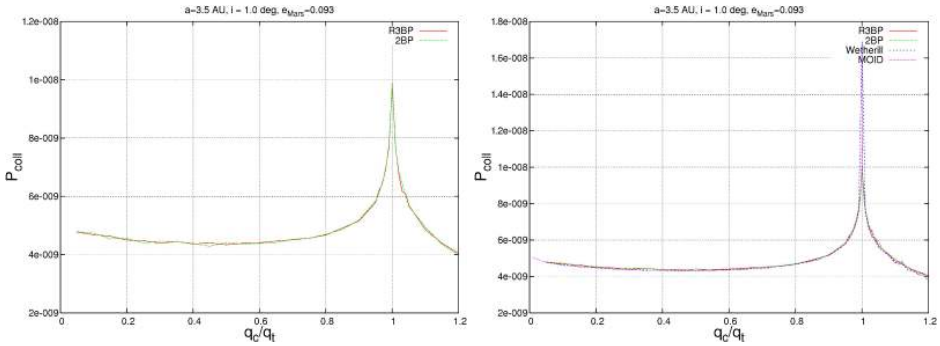

Figure 3. Collisional probability with Mars in a function of perihelion distance normalized by the perihelion distance of Mars. In all cases we assumed that the semimajor axes and inclinations of all impactors are equal 3.5 AU and 1°, respectively.

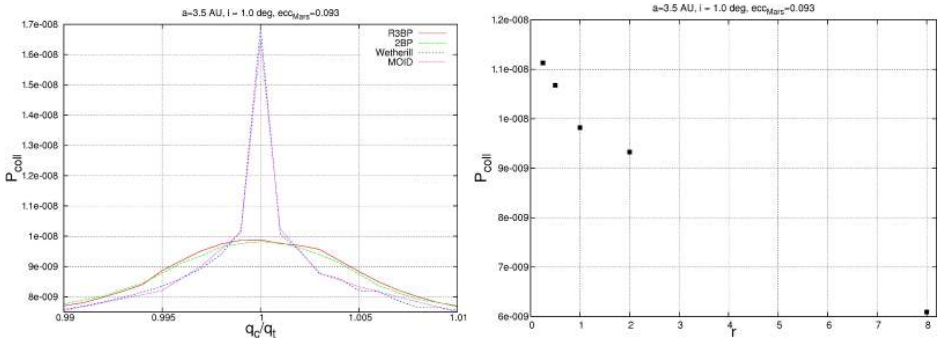

Figure 4. Left: Collisional probability in a function of perihelion distance normalized by the perihelion distance of Mars. In all cases we assumed that the semimajor axes and inclinations of all impactors are equal 3.5 AU and 1°, respectively. Right: Collisional probability calculated for $q_c/q_t = 1$ and different collisional spheres ($r = 1$ means radius of Mars Hill sphere).

6. Summary

The paper shows there is a very good agreement between results obtained numerically within ER3BP and 2BP. Comparing to MOID and Wetherill approaches, Hill sphere method is relatively fast (however slower than MOID and Wetherill methods) and simple to implement. There is also a a very good agreement among impact

probabilities calculated by the Hill sphere method and Wetherill and also MOID methods. The only difference appears for orbits where the perihelion distance of comets is close to the perihelion distance of a planet ($q_c/q_t = 1$). In such a case the Hill sphere method gives us underestimated results comparing to Wetherill and MOID methods.

Acknowledgements

We would like to thank to prof. Hans Rickman and M.Sc. Tomasz Wiśniowski for valuable discussions and helpful suggestions. This work has been supported by research Grant UMO-2011/01/B/ST9/05442 from the Polish National Science Centre.

References

Rickman H., Gabryszewski R., Wajer P., Wiśniowski T., 2012, LPI Contributions, 1667, 6135

Wetherill G.W., 1967, Journal of Geophysical Research, 72, 2429

PART 2

Meteorite falls: recent and historical records

Meteoroids 2013, Proceedings of the Astronomical Conference,
held at A.M. University, Poznań, Poland, Aug. 26-30, 2013,
eds Jopek T.J., Rietmeijer F.J.M., Watanabe J., Williams I.P.,
Adam Mickiewicz University Press in Poznań, pp 57–68

Recent documented meteorite falls, a review of meteorite – asteroid links

Jenniskens P.

SETI Institute, 189 Bernardo Ave, Mountain View, CA 94043, USA
(petrus.m.jenniskens@nasa.gov)

Abstract. Since the previous Meteoroids 2010 meeting, 25 confirmed meteorite falls have been reported, and one additional meteorite was linked tentatively to an observed fireball. All but two of those are classified as ordinary chondrites. Sutter's Mill is a rare carbonaceous chondrite, while Martian meteorite Tissint is a Shergotite. For 18 of these falls the associated fireball was observed, but only four provided a pre-atmospheric orbit derived from video and photographic records. Results were published for Sutter's Mill, Novato, and Chelyabinsk, providing insight into the asteroid belt source regions for CM2, L and LL type chondrites, respectively. Proposed meteorite-asteroid links are discussed.

Keywords: meteorite, meteorite fall, asteroids

1. Introduction

Intense (social) media interest in end-of-the-world predictions for December 21, 2012, coincided with a record number of reported meteorite falls in 2012. Since the last Meteoroids meeting on 24-28 May 2010, 25 confirmed meteorite falls have been reported, as well as one meteorite tentatively associated with an observed fireball (Table 1). The Meteoritical Bulletin (`http://www.lpi.usra.edu/meteor/`) lists details for those meteorite falls that have been reported to the Meteoritical Society and for which the names are approved.

Except for the Martian meteorite Tissint (Aoudjehane et al. 2012), all other meteorites are thought to originate from collisional families in the main asteroid belt. An ongoing scientific endeavor is to identify which asteroid families produce the meteorites we find on Earth. Such links are not easily recognized from asteroid spectroscopic studies alone, because asteroid surfaces redden due to solar wind bombardment, and the larger asteroids are often covered in gravel-sized and sand-sized debris, which changes how they scatter sunlight (Wetherill and Chapman 1988; Cellino et al. 2002; Vernazza et al. 1998).

The dynamical mechanisms involved in bringing the meteoroids from those asteroid families to Earth are well understood (Wetherhill 1985; Bottke et al. 2002; Granvik et al. 2014; Vokrouhlicky et al. 2006, 2014). The evolution has up to three stages. The smallest (m to few tens of m sized) asteroids continue to collide, creating meteoroids that gradually change their semi-major axis due to non-gravitational forces such as the Yarkovsky effect (Stage 1). When their orbital period evolves into a resonance with Jupiter, or when secular orbital evolutions start to resonate with those of the major planets, the meteoroid orbit quickly becomes more eccentric while the semi-major axis stays constant: the aphelion moves out towards

Jupiter's orbit, the perihelion closes in towards the orbit of Earth (Stage 2). Close encounters with the terrestrial planets or with Jupiter can change the semi-major axis to move the orbital period out of resonance. Secular perturbations then will evolve the meteoroid orbit more gradually (Stage 3).

Table 1. List of meteorite falls reported since the Meteoroids 2010 meeting. Names in italic are not yet approved. Bold entries are falls that provided pre-atmospheric orbits. Entries labeled (*) have reports of the fireball, those listed (♯) are finds tentatively associated with observed fireballs. All dates are in local time.

Date	Name (unofficial)	Country	Type	Date	Name (unofficial)	Country	Type
2013.05.09	*Oshika**	Namibia	o.c.?	2012.05.04	Ladkee*	Pakistan	H6
2013.04.23	Braunschweig	Germany	L6	2012.04.22	**Sutter's Mill***	California	**CM**
2013.04.19	Wolcott	Connecticut	o.c.?	2012.03.01	Oslo*	Norway	H5
2013.02.15	**Chelyabinsk***	Russia	LL5	2012.02.11	Xining*	China	L5
2013.01.13	*Planeta Rica*	Columbia	o.c.?	2011.09.14	Boumdeid (2011)*	Mauritania	L6
2012.12.06	Mreïra ♯	Mauritania	L6	2011.07.18	Tissint*	Morocco	**She.**
2012.10.30	*Addison**	Alabama	o.c.?	2011.07.16	Thika*	Kenya	L6
2012.10.17	**Novato***	California	L6	2011.07.13	Draveil	France	H5
2012.10.12	*Beni Yacoub**	Morocco	H5?	2011.06.16	*Wu Jingjie*	China	o.c.
2012.08.22	Battle Mountain*	Nevada	L6	2011.04.30	Soltmany	Poland	L6
2012.07.08	*Jalangi**	India	o.c.?	2011.02.04	***Krizevci****	Croatia	o.c.
2012.06.03	Comayagua	Honduras	o.c.?	2010.07.13	Huaxi	China	H5
2012.05.22	Katol*	India	L6	2010.06.19	Varre.Sai*	Brazil	L5

The collisional lifetime of asteroids (τ, in Ma) is about $\tau = 1.4\sqrt{r}$, with r the radius of the meteoroid in cm (Wetherhill 1985). As a result, the smaller asteroids are most quickly catastrophically destroyed in collisions. Because the yield of fragments is proportional to r^3, most meteoroids impacting the Earth originate from the smallest asteroids that generate enough meteoroids for one to hit Earth before it is destroyed in another collision (or by some other means). Because of this, near-Earth asteroids do not originate in similar proportions from the same source regions as the smaller meteoroids. While the NEO population is dominated by LL-like objects, meteorite falls are dominated by H and L type chondrites (Burbine et al. 2002; Dunn et al. 2013; Thomas et al. 2014).

Because Jupiter scatters the asteroids that approach its orbit, most meteorites arrive at Earth from orbits that stayed inside the orbit of Jupiter. Those evolved predominantly from the inner and central parts of the asteroid belt. The closer the orbit has to evolve to Jupiter's orbit, the less likely the meteoroid will hit Earth before its orbit is drastically changed. Because of that, a relatively large fraction of meteoroids that end up in the $\nu 6$ secular resonance with Saturn (at a $\sim$ 2.0 AU) will hit Earth (Figure 2), while a smaller fraction of those that entered the 3:1 mean motion resonance with Jupiter (a=2.5 AU) will do so, and an even smaller fraction from those that entered the 5:2 resonance (a=2.8 AU). Asteroids in outer belt resonances evolve into orbits intersecting Jupiter's orbit before their perihelion distance moves inside Earth's orbit.

The picture is complicated by the long multi-million year timescale between the collision in the asteroid belt and the impact on Earth. During all stages, collisions with other asteroids continue to happen as long as the meteoroid orbit passes

through the asteroid belt. In Stage 1, meteoroid orbits can jump resonances. In Stage 2, the meteoroid orbit evolution can be quite complicated. To confuse things further, meteorites of one type may well originate from different families. Worse, families can provide more than one meteorite type, as in the case of asteroid 2008 TC3, a ureilite containing also Enstatite and Ordinary Chondrites with some peculiar properties (Jenniskens et al. 2009; Burton et al. 2011). Finally, on a $\sim$ 10 million year timescale other collisions occur in a source region, which can then produce meteorites from a different secondary debris field.

2. Source region insight from recent meteorite falls

That said, some meteoroids hit Earth shortly after entering the source resonance and thus can still point to the asteroid family of its origins. In that case, the time since the last collision, measured by the cosmic ray exposure age (CRE age), and the time since the last Ar-Ar or K-Ar thermal resetting event (presumably the time that the family was formed), can shed further light on which asteroid family is the source region.

There has been an exponential increase in the number of entry trajectory and pre-atmospheric orbits derived from video observations of the fireball since the first such case of Peekskill in 1992 (Brown et al. 1994). At present, 21 orbits have been published: 3 carbonaceous chondrites, 8 H chondrties, 5 L chondrites, 2 LL chondrites, one Ureilite, one Eucrite and one Enstatite Chondrite (Jenniskens et al. 2012).

Eyewitnesses observed the associated fireball from 18 of the 26 recovered meteorites listed in Table 1. So far, orbital elements were published only for the Sutter's Mill, Novato, and Chelyabinsk meteoroids. At the time of writing, analysis of the Krizevci meteorite (a provisional name) is pending, the fall of which was filmed by the Croatian Meteor Network (Segon et al. 2011).

2.1. The April 2012 Sutter's Mill fall and the source of CM2 chondrites

The Sutters Mill fall in California was documented by three digital photographs and two videos. The meteor entered at a record entry speed of 28.6 km/s, the fastest entry so far for which material has been recovered (Jenniskens et al. 2012). Sutter's Mill was the most energetic impact over land (4 kt) since the 1.2 kt impact of asteroid 2008 TC3 in northern Sudan on October 7, 2008 (Jenniskens et al. 2009). A high 48 km altitude disruption created a cloud of meteorites that rained down over the villages of Coloma and Lotus in California, with one of the pieces landing at the Sutter's Mill site, the very location where gold was first discovered resulting in the 1849 California Gold Rush. The falling meteorites were detected by Doppler weather radar, which made rapid recovery possible. Thanks to a large crowd-sourcing effort, in the form of a second Gold Rush, a relatively large number of 77 fragments were recovered (Jenniskens et al. 2012).

The meteorite was a rare mix of CM1-CM2 type materials, stronger than other CM2's because they were slightly heated. This was the first CM2 chondrite to show clear evidence of being brecciated, part of a surface regolith. This fragment

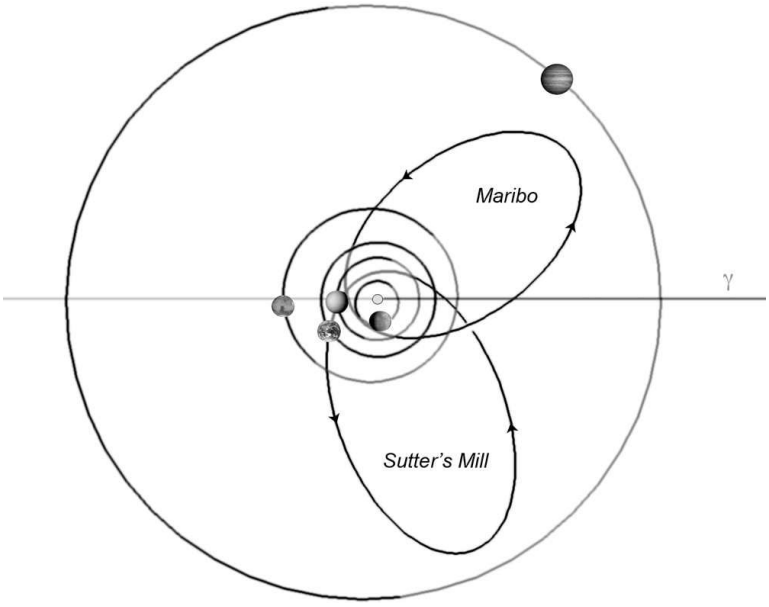

Figure 1. Pre-atmospheric orbits of Maribo and Sutter's Mill (Jenniskens et al. 2012).

originated from near the surface of the CM parent body. The fresh recovery made it possible to recognize some components that are quickly altered by reactions with water (Jenniskens et al. 2012).

CM2 meteorites as a group have a short cosmic ray exposure age ($<$ 2 Ma). Sutter's Mill had one of the shortest on record, only 50,000-90,000 years. This is much less than the collisional lifetime of a 3-m sized asteroid ($\sim$ 24 Ma). The short cosmic-ray exposure age implies that these meteoroid orbits evolved relatively recently from the resonance that delivered them to Earth, and also that they do not survive long (less than 2 Ma) once arriving in the inner solar system, perhaps due to thermal stresses from sides pointed to and away from the Sun.

When the unusual entry conditions of Sutter's Mill became clear, the orbit of the CM2 chondrite Maribo was recalculated, and it was found that this meteorite also arrived at the same entry speed, in a similar low-inclined and low perihelion distance orbit, and also with an orbital period close to that of the 3:1 resonance with Jupiter (Jenniskens et al. 2012). Only the longitude of perihelion was significantly different (Figure 1). CM2 meteorite Murchison, the type specimen of this class, also arrived on a low-inclined orbit. All point to the source region being a C-class asteroid family in a low inclined orbit very close to the 3:1 resonance. This could be the Eulalia family (Table 2, Figure 2), recently identified as a potential source of C-class near Earth asteroids (Walsh et al. 2013).

If meteorites can fall to the ground after entering the atmosphere as fast as 28.6 km/s, then meteorites may one day be found from meteor showers such as the Taurids (Brown et al. 2013) and the Geminids (Madiedo et al. 2013). Geminid

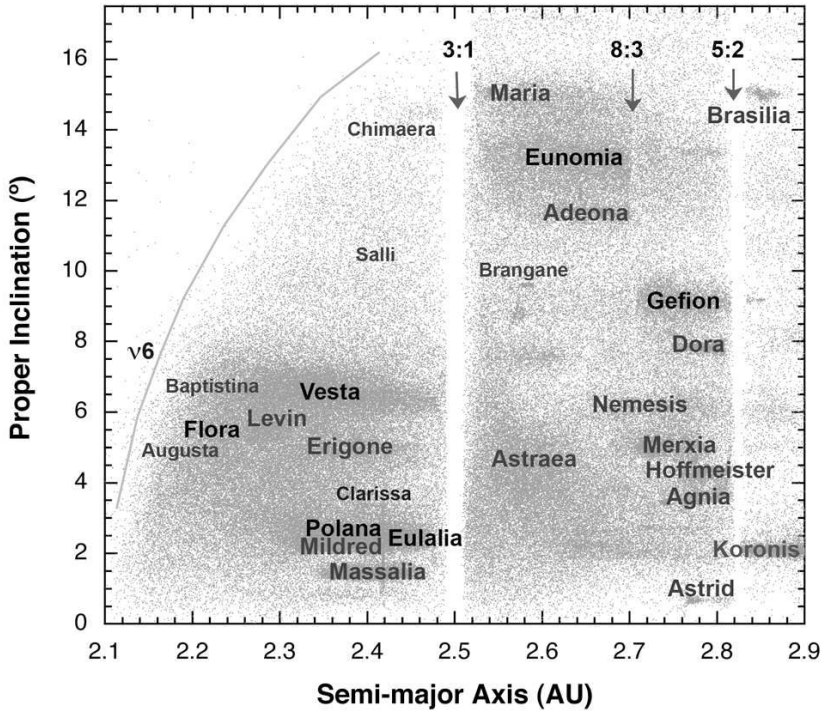

Figure 2. Asteroid families discussed in this paper.

parent body 3200 Phaethon has been linked to the Pallas family, a cratering family from the highly inclined asteroid 2 Pallas (de Leon et al. 2010). In my opinion, this is quite possible, but only if a faster dynamical pathway from asteroid family to the current orbit of 3200 Phaethon is available than proposed by (de Leon et al. 2010). Such pathway may exist via the 5:2 resonance. Until now, no recovered meteorites have been conclusively linked to the Geminid shower (Table 2).

Another CM2 chondrite reported recently is the Paris, a 1.3 kg stone identified in 2001 (bought ca. 1994), which was found in the effects of a former colonial mining engineer, Jean Simon Colonna-Cimera. This meteorite is so fresh that it was likely from a fall. The location of the fall is unknown, presumably a foreign country, perhaps one of the French Colonies. The Paris meteorite is significantly less aqueously altered than other known CM2 chondrites and suffered only low temperature metamorphism (Hewins et al. 2014).

2.2. The Novato fall and the source of L chondrites

California struck gold again with the Novato fall in October of 2012. Novato is a L6 ordinary chondrite fragmental breccia. It was recovered because it crossed the camera fields of the CAMS network in California (Jenniskens et al. 2012). Shocked L6 chondrites have a peak of Ar-Ar ages around 470 Ma, coincident with a time when L type meteorites showered Earth in great abundance. They are thought

to originate from the Gefion asteroid family, which was formed about 470 Ma ago (Nesvorny et al. 2009). The Gefion family (Figure 2) is located close to the 5:2 mean-motion resonance and meteorites can come to us quickly (but not so efficiently) via the 5:2 resonance (as happened 470 Ma ago), or more slowly via the 3:1 mean motion resonance after evolving to shorter semi-major axis (as was suspected to be the case now).

Table 2. Proposed meteorite source regions in the asteroid belt, based in part on meteoroid orbits measured from photographic and video observations of the fireball.

Meteorite Type	Asteroid Family (Class)	Formation Age (Ma)	Resonance	Fall (Asteroid)
Howardites /Eucrites /Diogenites	Vesta (V)	∼1000	ν6	Bunburra Rockhole
L5-6 (shocked)	Gefion (S)	470	5:2 and 3:1	Novato /Jessenice /ParkForrest /Innisfree
LL5	Flora (S)	∼200	ν6, IMC	Chelyabinsk /(Itokawa)
CM1-2	Eulalia (F)	1200±300	3:1	Sutter's Mill /Maribo
Ureilites w. mixed in Enstatite + Ordinary Chondrites	Polana (F)	> 2000	3:1 and ν6	Almahata Sitta (2008 TC3)
H4-5, inclination > 20°	Phocaea (S)	∼2200	ν6	Grimsby /Buzzard Coulee / Morávka
H5-6, inclination < 20°	Maria (S)	∼3000	3:1	Mason Gully /Pribram, Lost City/Peekskill /Košice
Aqueously Altered L6	-.-	-.-	ν6	Villalbeto de la Pena
LL3.5	-.-	-.-	3:1	Benešov
EL6	-.-	-.-	3:1	Neuschwanstein
C2 Ungrouped	-.-	-.-	ν6	Tagish Lake
t.b.d. (Carbonaceous Chondr.)	Pallas (B)	∼500	5:2	Geminid shower

A consortium study showed that Novato has a U, Th-He age of 460 ± 200 Ma, and likely belongs to this group of shocked L6 chondrites (Jenniskens et al. 2014). The cosmic ray exposure age is only about 9 ± 1 Ma, close to the collisional lifetime of this meteorite, which originally had a size of about 45 cm. The measured orbit of Novato, and those of L-chondrites Jessenice (Spurny et al. 2010), Innisfree (Halliday et al. 1981), and Park Forrest (Brown et al. 2004) are consistent with these originating from the 3:1 resonance, but leaves open the possibility that they come to us more quickly from the 5:2 resonance.

The recent observed fall at Varre-Sai (Zucolotto et al. 2012) and Mifflin are of the same meteorite type, possibly Soltmany is as well (Karwowski et al. 2011). Mifflin fell on April 14, 2010, in southwestern Wisconsin, and several videos are available for orbit reconstruction. The meteorite's CRE age is a high 25±3 Ma (Kita et al. 2013).

L chondrite Villalbeta de la Pena (Llorca et al. 2005) does not fit in this scheme, having too high a cosmic ray exposure age (48 Ma). The expected collisional lifetime is only 8.9 Ma, suggesting it spend little time in the main belt recently. With a=2.3±0.2 AU and low inclination, it may have originated from ν6. Interestingly, this meteorite was recently reclassified as having been aqueously altered (Bischoff

et al. 2013), suggesting it may indeed have a different source region than other L chondrites (Jenniskens et al. 2014).

2.3. Chelyabinsk and LL chondrites

Chelyabinsk is the topic of several other papers in this issue. Popova et al. (2013) showed that this LL5 chondrite moves in an orbit, and has a CRE age, consistent with an origin in the $\nu 6$ resonance, possibly deriving from the LL-like Flora family on the inside of the $\nu 6$ resonance (Figure 2). Such association was proposed following the study of asteroid Itokawa, which is of the same spectral type (Michel and Yoshikawa 2006). The 200 Ma age of the Flora family comes from cratering densities on member Gaspra (Vervenka et al. 1994). Chelyabinsk disrupted only 1.2 Ma ago, perhaps from a tidal disruption in a previous encounter with Earth (Popova et al. 2013).

2.4. H chondrite falls

The most recently studied H chondrite fall is that of H5 Kosice (Borovicka et al. 2013). Its semi-major axis has a relatively high value of $a = 2.7 \pm 0.2$ AU, suggesting this meteorite may have originated from the 3:1 mean-motion resonance. Several older falls also have similar high semi-major axis: the H5 Pribram has a=2.40 AU (i=10.5°), while Mason Gully has a=2.47 AU (i=0.8°). Interestingly, almost all H chondrite-like near Earth objects have $a > 1.8$ AU, with orbital elements a, e and i near the 3:1 resonance (Dunn et al. 2013).

A large asteroid, rather than a family, was long proposed as the source of H chondrites. The 185-km large asteroid 6 Hebe (i=14.7°, a=2.246 AU) has an H-chondrite like reflectance spectrum (Gaffey and Gilbert 1998; Akridge 1998). Hebe is near the 3:1 and $\nu 6$ resonances. It does not have an associated asteroid family, however. More recently, Gaffey and Fieber-Beyer (2013) identified two other nearby asteroids as possible fragments from 6 Hebe, with similar H-chondrite like reflection spectra, but it is unclear if smaller debris exists. Bottke et al. (2010) reaffirmed that Hebe could be the source, because it was exposed to the 8.2 Ma Veritas family forming event debris, and therefore could account for the 7-8 Ma CRE age of H chondrites. However, that perhaps more affirms the proposed source of L and LL meteorites, given they were not exposed to collisions. In fact, many S-class asteroid families near the 3:1 region could be the source region for H chondrites (Table 3). One of the largest S-class families close to the resonance is Maria, a more likely source in my opinion (Figure 2). Zappala et al. (1997) pointed out that this family is a likely source of ordinary chondrites.

Not all H chondrites originate from the same source region. The two H4 chondrites with known orbits both impacted Earth from highly inclined orbits ($i > 20°$): H4 Buzzard Coulee, at i=25°, and H4-6 Grimsby at i=28°. H5 chondrite Moravka, too, arrived at a high i=32° inclination. Grimsby has the highest semi-major axis of this set, at a=2.04 AU. Interestingly, there is other evidence that H4 chondrites may have a different parent body than H5-6 chondrites. Fast initial cooling rates of all material suggests fragmentation and re-accretion as an important mechanism in the heating history of these meteorite types (Ganguly et al. 2013). The old

onion model (H4 having been located near the surface, H6 chondrites deep inside the parent body) is not consistent with these meteorite types arriving at Earth on different orbits. The highly inclined S-class Phocaea family (Carruba et al. 2009) is a good candidate for the source region of these meteorites.

2.5. 2008 TC3 and the source of the Ureilites

The orbit of the Almahata Sitta meteorite was precisely measured, because the asteroid 2008 TC3 was observed 20 hours before impact and tracked during its approach to Earth (Jenniskens et al. 2009). 2008 TC3 consisted mostly of ureilites, but contained 20-30 percent enstatite and ordinary chondrites. All Ureilites appear to originate from a single Ureilite Parent Body, suggesting an asteroid family source, Jenniskens et al. (2010) discussed possible source regions, only to resign to the reality that no known spectra of main belt asteroids fit the gray spectrum with weak $0.9\mu m$ pyroxene band of 2008 TC3. Based on the orbit, the most likely source region is in the inner belt. The F-class Polana family was put forth as a possibility, as well as a scattering of unrelated F-class asteroids in the inner belt, but their near-IR spectra do not match 2008 TC3.

Since that time, Meier et al. (2012) have found that the Ureilite parent body did not experience a significant thermal resetting event, enough to affect the Ar-Ar system, since the late heavy bombardment. Hence, the asteroid family responsible is very old. Recently, Walsh et al. (2013) concluded that the Polana family is in fact composed of two unrelated collisional debris fields. One group of asteroids, the Eulalia family, is close to the 3:1 resonance and a good candidate for the source region of the CM2 chondrites (Jenniskens et al. 2012). The other group is more dispersed and much older. In my opinion, this new Polana family may be the source region of the ureilites, based only on its old age.

2.6. Howardites, Eucrites, and Diogenites (HED)

Most basaltic achondrites also appear to originate from one source region. Because there is only one asteroid family with reflectance spectra that show similar deep absorption bands, it is generally believed that the related Howardites, Eucrites and Diogenites originate from the Vesta family. Meteorites come to us from this inner belt family via the $\nu 6$ secular resonance with Saturn, the group of Intermediate Mars Crossers, and the 3:1 mean-motion resonance. The photographed Bunburra Rockhole fall is an anomalous eucrite in some respects (Bland et al. 2009), but the 22 Ma cosmic ray exposure age overlaps with the CRE peak of HED meteorites (Welten et al. 2012). Bunburra Rockhole collided with Earth from an unusual Aten type orbit (a=0.85 AU), whereby virtually the entire orbit was contained within Earth's orbit (Spurny et al. 2012a). In such orbit, the meteoroid would have avoided asteroid collisions, but it broke not much longer ago than other eucrites based on the CRE age. This could point to tidal disruptions from close encounters with Earth, instead.

2.7. Benešov and the LL3.5 chondrites

Benešov is an old fall from May 7, 1991. Only recently were meteorites recovered from this fall and shown to be of LL3.5 type (Spurny et al. 2012b). The 23.7°

inclined orbit and a = 2.43 AU points to a highly inclined S-class asteroid family near the 3:1 mean-motion resonance as the source. Of 96 documented LL falls, 13 are LL3.0-3.9 type chondrites, suggesting a significant source.

Table 3. Possible source regions ($a < 2.9$ AU, close to resonances, inner belt, high inclined, massive, or young) that have not yet been linked to meteorite types (Cellino et al. 2002; Novaković et al. 2011; Madiedo et al. 2013; Milani et al. 2014).

Meteorite Type	Asteroid Family	Class	Type	Formation Age (Ma)	Resonance	a (AU)	i (deg)
(Aubrites)	Hungaria	E	Large	150-200	1:4	1.94	23
(Ord. Chon.)	Augusta	S	Small	-.-	ν6	2.19	5
(Carb. Chon.)	Baptistina	X	Young	80	ν6	2.26	6
(Ord. Chon.)	Levin	S	Large	-.-	ν6, 7:2	2.27	5
(Ord. Chon.)	Hypsipyle	S	Small	-.-	7:2	2.33	25
(CM)	Klio	G	Small	-.-	ν6, IMC	2.36	9
(Ord. Chon.)	Rosseland	S	Small	-.-	ν6, IMC	2.36	8
(Ord. Chon.)	Mildred	S	Large	>1000	IMC, 3:1	2.36	2
(Carb. Chon.)	Erigone	C	Large	280	IMC, 3:1	2.37	5
(Carb. Chon.)	Salli	X	Small	-.-	ν6, IMC	2.40	11
(CM, ureilite)	Clarissa	F	Small	-.-	3:1	2.41	3
(Ord. Chon.)	Massalia	S	Large	150-200	IMC, 3:1	2.42	1
(Ord. Chon.)	13698	S	Small	-.-	3:1	2.45	7
(Carb. Chon.)	Chimaera	C	Small	-.-	3:1	2.46	14
(Carb. Chon.)	Sulamitis	C	Small	-.-	3.1	2.46	6
(Ord. Chon.)	Astraea	S	Large	-.-	3:1	2.57	5
(CO, CV)	Brangane	K	Class	-.-	3:1	2.59	10
(Ord. Chon.)	Gersuind	S	High i	800	3:1	2.59	18
(Ord. Chon.)	Eunomia	S	Large	∼300	3:1, 8:3	2.63	13
(Ord. Chon.)	Hansa	S	High i	1600	3:1	2.64	22
(Ord. Chon.)	Barcelona	S	High i	350	3:1	2.64	33
(Ord. Chon.)	Adeona	S	Large	600	3:1, 8:3	2.67	12
(Ord. Chon.)	Merxia	S	Large	330	8:3	2.74	5
(Carb. Chon.)	Padua	X	Large	-.-	5:2	2.74	6
(Carb. Chon.)	Nemesis	C	Large	-.-	5:2	2.75	6
(Carb. Chon.)	Atalante	C	High i	-.-	5:2	2.75	19
(CO3, CV3)	Watsonia	L	High i	-.-	5:2	2.76	18
(Ord. Chon.)	Gallia	S	High i	450	5:2	2.77	25
(Ord. Chon.)	Agnia	S	Large	1300	5:2	2.78	3
(Carb. Chon.)	Antonia	X	Large	-.-	5:2	2.78	4
(Carb. Chon.)	Zhongolovich	C	Large	-.-	5:2	2.78	8
(CM, ureilite)	Hoffmeister	F	Large	-.-	5:2	2.79	4
(Carb. Chon.)	Tina	X	High i	150	5:2	2.79	21
(Ord. Chon.)	Astrid	S	Young	150	5:2	2.79	1
(Carb. Chon.)	Dora	B	Large	-.-	5:2	2.79	8
(Carb. Chon.)	Brasilia	C	large	-.-	5:2	2.85	15
(Carb. Chon.)	Raybatson	X	Small	-.-	5:2	2.86	16
(Ord. Chon.)	Koronis /Karin cluster	S	Large /Young	1400 5.75±0.05	5:2, 7:3	2.87	2
(CO, CV)	Eos	K	Large	∼1700	9:4	3.03	11
(Carb. Chon.)	Veritas	C	Young	8.3±0.3	2:1	3.17	9

2.8. Neuschwanstein and EL enstatite chondrites

So far, the only enstatite chondrite fall photographed is that of EL6 Neuschwanstein. The orbit was remarkable because it was nearly identical to that of Pribram, an H5 chondrite (Spurny et al. 2003). It is possible that both originated from a rubble pile object that recently fell apart, perhaps in a tidal encounter with Earth.

The enstatite chondrite may have collided with the H5 meteoroid and fragments ended up in the re-accumulated debris. If so, the orbit of Neuschwanstein does not immediately point to the source region of the enstatite chondrites, but the source may be nearby that of H5 chondrite Pribram.

2.9. Tagish Lake and D-class asteroids

The ungrouped carbonaceous chondrite Tagish Lake arrived from a 2.0 AU and low inclination. The spectral reflectance suggested this meteorite may have originated from a D-class asteroid (Hiroi et al. 2001), but those are found mostly in the outer asteroid belt and among Centaurs and Kuiper Belt objects. Instead, the orbit suggests an origin in the inner asteroid belt. The source could have a fairly low yield as no other similar meteorite is known. There are a few candidate C and X class asteroid families (Table 3).

3. Discussion

There are many more potential source regions that have not been linked to a known meteorite type (Table 3, Figure 2). Candidate source regions are large asteroids, rich debris fields, or young debris fields rich in small asteroids. The debris fields, the asteroid families, are named after the largest member in a group, or lowest numbered member, the choice of which is not always clear. As a result, some asteroid families go by different names. Table 3 is a compilation of the most relevant families studied by different authors.

Big asteroids have a large cross section for collisions, and proposed parents include, for example, S-class 6 Hebe (H) (Migliorini et al. 1997a; Akridge 1998), S-class 7 Iris (L/LL) (Migliorini et al. 1997b), G-class 19 Fortuna (CM) (Burbine 1998), E-class 3103 Eger (Aubrites) (Gaffey et al. 1992; Cuk et al. 2012), and K-class 221 Eos (CO) (Bell 1988). However, asteroids 1 Ceres, 19 Fortuna, and 13 Egeria are all large G-class asteroids without known asteroid families and, so far, no associated meteorite type.

The youngest debris fields are the Datura family (age 0.45 ± 0.05 Ma, S-type), the Emilkowalski family (0.22 ± 0.03 Ma, no known type), the 1992 YC2 family (0.15±0.10 Ma, S type), and the Lucascavin family (0.40 ± 0.20 Ma, S type) (Vokrouhlicky et al. 2014). This is younger than the cosmic ray exposure ages of most recovered meteorites. Meteorites from these collisions may not have made it to Earth yet.

Somewhat older, and larger, are the Karin cluster (5.75 ± 0.05 Ma, S class) in the Koronis family, the Veritas cluster (8.3 ± 0.3 Ma, C type), and the Iannini family (< 5 Ma, S class). The signature of these source regions would be a CRE age similar to the breakup age. No spike in CRE ages has been detected so far in corresponding meteorite types.

The large asteroid families (and the background population) have the highest available surface area for collisions. Most likely sources are the large families in the inner and middle belt, and perhaps in the outer belt adjacent to the 5:2 resonance (Table 3). Most easily recognized in fireball orbits are the high inclination

($> 15°$) families, such as those listed by Novaković et al. (2011) and Carruba (2010). Particularly intriguing in Table 3 is the large range of possible source regions for S-class asteroids (presumably resulting in ordinary chondrites). Future meteoroid orbits derived from recovered meteorite falls of ordinary chondrites can perhaps make a distinction between the low and high inclination sources and the inner and middle belt source regions.

Future work will see a number of other meteorite types fall in photographic and video camera covered areas. Meteoroid orbits should be measured for each witnessed meteorite fall. Not just to document the pre-atmospheric orbit of uncommon meteorite types, but also to gather more information about the possible variation in source regions among the ordinary chondrites.

Acknowledgements

This work was supported by the NASA NEO Observation Program.

References

Akridge G., Benoit P. H., Sears D. W. G., 1998, Icarus, 32, 185
Aoudjehane H.C., Avice G., Barrat J.-A., et al., 2012, Science, 338, 785
Bell J.F., 1988, Meteoritics, 23, 256
Bischoff A., Dyl K.A., Horstmann M. et al., 2013, MAPS, 48, 628
Bland P. A., Spurny P., Towner et al., 2009, Science, 325, 1525
Borovicka J., Toth J., Igaz A. et al., 2013, MAPS, 48, 1757
Bottke W.F., Morbidelli A., Jedicke R. et al., 2002, Icarus, 156, 399
Bottke W., Vokrouhlicky D., Nesvorny D., Shrbeny L., 2010, Bulletin of the American Astronomical Society, 42, 1051
Bottke W., Vokrouhlicky D., Nesvorny D., 2007, Nature, 449, 48
Brown P., Ceplecha Z., Hawkes R.L., et al., 1994, Nature, 367, 624
Brown P., Pack D., Edwards W.N., et al., 2004, MAPS, 39, 1781
Brown P., Marchenko V., Moser D. E., et al., 2013, MAPS, 48, 270
Burbine T.H., 1998, MAPS, 33, 253
Burbine T.H., McCoy T.J., Meibom A., et al., 2002, in Asteroids III, eds Bottke W.F. Jr., Cellino A., Paolicchi P., Binzel R.P., University of Arizona Press, Tucson, p. 653
Burton A.S., Glavin D.P., Callahan M.P., et al., 2011, MAPS, 46,1703
Carruba V., 2009, MNRAS, 398, 1512
Carruba V., 2010, MNRAS, 408, 580
Cellino A., Bus S.J., Doressoundiram A., Lazzaro D., 2002, in Asteroids III, eds Bottke W.F. Jr., Cellino A., Paolicchi P., Binzel R.P., University of Arizona Press, Tucson, p. 633
Cuk M., Burns J.A., Gladman B.J., et al., 2012, AAS DPS meeting 44, abstract 105.02
de Leon J., Campins H., Tsiganis K., et al., 2010, A&A, 513, 26
Dunn T. L., Burbine T.H., Bottke W.F., Clark J.P., 2013, Icarus, 222, 273
Ganguly J., Tirone M., Chakraborty S., Domanik K., 2013, Geochim. et Cosmo. Acta, 105, 206
Gaffey M.J., Reed, K.L., Kelley M.S., 1992, Icarus, 100, 95
Gaffey M.J., Gilbert S.L., 1998, MAPS, 33, 1281
Gaffey M.J., Fieber-Beyer, 2013, Proc. Meteoritical Society Meeting, Abstract 5124
Granvik M., Morbidelli A., Jedicke R., et al., 2014, Icarus, (in prep.)

Halliday I., Griffin A.A., Blackwell A.T., 1981, Meteoritics, 16,153
Hewins R.H., Bourot-Denise M., Zanda B., et al., 2014, Geochim. et Cosmo. Acta, 124, 190
Hiroi T., Zolensky M.E., Pieters C.M., 2001, Science, 293, 2234
Jenniskens P., Shaddad M.H., Numan D., et al., 2009, Nature, 458, 485
Jenniskens P., Vaubaillon J., Binzel R.P., et al., 2010, MAPS, 45, 1590
Jenniskens P., Gural P.S., Dynneson L., et al., 2011, Icarus, 216, 40
Jenniskens P., Fries M.D., Yin Q.Z., et al., 2012, Science, 338,1583
Jenniskens P., Rubin A.E., Yin Q.Z., et al., 2014, MAPS, (submitted)
Karwowski L., Pilski A. S., Przylibski T.A., et al., 2011, MAPS Supplement, abstract 5336
Kita N.T., Welten K.C., Valley J.W., et al., 2013, MAPS, 48, 641
Llorca J., Trigo-Rodriguez J.M., Ortiz J.L., et al., 2005, MAPS, 40, 795
Madiedo J.M., Trigo-Rodriguez J.M., Castro-Tirado A.J., et al., 2013, MNRAS, 436, 2818
Masiero J.R., Mainzer A.K., Bauer J.M., Grav T., Nugent C.R., Stevenson R., 2013, ApJ, 770, 7
Meier M.M.M., et al., 2012, MAPS, 47, 1075
Michel P., Yoshikawa M., 2006, AA 449, 817
Migliorini F., Manara A., Cellino A., et al., 1997b, A&A, 321, 652
Migliorini F., Manara A., Scaltriti F., et al., 1997a, Icarus, 128, 104
Milani A., Cellino A., Knezevic Z., Novakovic B., Spoto F., Paolicchi P., 2014, Icarus, (submitted)
Mothé-Diniz T., Nesvorny D., 2008, A&A., 486, L9
Nesvorny D., Vokrouhlicky D., Morbidelli A., Bottke W.F., 2009, Icarus, 200, 698
Novaković B., Cellino A., Knezević Z., 2011, Icarus, 216, 69
Popova O.P., Jenniskens P., Emel'yanenko V., et al., 2013, Science, 342, 1069
Segon D., Korlevic K., Andreic Z., et al., 2011, JIMO, 39, 98
Spurny P., Oberst J., Heinlein D., 2003, Nature, 423, 151
Spurny P., Borovicka J., Kac J., et al., 2010, MAPS, 45, 1392
Spurny P., Bland P. A., Shrbeny L., Borovicka J., et al., 2012a, MAPS, 47, 163
Spurny P., Haloda J., Borovicka J., 2012, Asteroids, Comets, Meteors 2012b, abstract 6143
Thomas C.A., Emery J.P., Trilling D.E., et al., 2014, Icarus, (in press)
Vernazza P., Binzel, R.P., Rossi, A., et al., 2009, Nature, 458, 993
Vervenka J., Thomas P., Simonelli D., et al., 1994, Icarus, 107, 72
Vokrouhlicky D., Broz M., Bottke W.F., et al., 2006, Icarus, 182, 118
Vokrouhlicky D., Broz M., Bottke W.F., et al., 2014, Icarus, (in press)
Walsh K.J., Delbó M., Bottke W.F., et al., 2013, Icarus, 225, 283
Welten K.C., Meier M.M.M., Caffee M.W., et al., 2012, MAPS, 47, 186
Wetherhill G., 1985, Meteoritics, 20,1
Wetherill G.W., Chapman C.R., 1988, in: Meteorites and the Early Solar System, eds J.F. Kerridge and M.S. Matthews, Univ. of Arizona, Tucson, p. 35
Zappalá V., Cellino A., Di Martino M., et al., 1997, Icarus, 129, 1
Zappalá V., Cellino A., Dell'Oro A., Paolicchi P., 2002, in Asteroids III, eds Bottke W.F. Jr., Cellino A., Paolicchi P., Binzel R.P., University of Arizona Press, Tucson, p. 619
Zucolotto M.E., Antonello L.L., Varela M.E., et al., 2012, EM&P, 109, 43

Meteoroids 2013, Proceedings of the Astronomical Conference, held at A.M. University, Poznań, Poland, Aug. 26-30, 2013, eds Jopek T.J., Rietmeijer F.J.M., Watanabe J., Williams I.P., Adam Mickiewicz University Press in Poznań, pp 69–74

The meteorite Moss – a rare carbonaceous chondrite

Bilet M.[1], **Roaldset E.**[2]

[1]Bilet Geoservice, P.O. Box 157, 1430 Ås Norway
[2]Natural History Museum, University of Oslo, Oslo, Norway (elen.roaldset@nhm.uio.no)

Abstract. On July 14, 2006, at about 10:20 a.m. local daylight time (UTC+2), a bright fireball travelling SSE-NNV was witnessed from the Baltic Sea to SE Norway. On the east side of the Oslo fiord, around Moss, an explosion and a rumbling sound was heard, and pieces were observed falling. Rapid recovery of meteorite stones gave an opportunity for detailed petrological and geochemical investigations, including analyses of indigenous organic species, and short lived isotopes. The meteorite is a chondritic stone meteorite, with some carbon (0.21–0.25 wt% C). The cosmic-ray exposure (CRE) age is 14 Ma, i.e. when Moss was ejected from its parent body. Gas retention ages are approximately $3.95 \cdot 10^9$yr (U/Th/He) and $4.43 \cdot 10^9$ yr (K/Ar), respectively. The meteorite has the official name Moss, and is classified as carbonaceous chondrite type CO3.6. It was the first witnessed fall of a CO3 chondrite since Kainsaz in Russia in 1937.

Keywords: meteorite fall, meteorite Moss, carbonaceous chondrite, meteorite composition

1. Fireball, fall, and meteorite pieces

On July 14, 2006, at about 10:20 a.m. local daylight time (UTC+2), a bright fireball travelling SSE-NNV, from the Baltic Sea towards South Norway, was witnessed by many people. A loud explosion and a rumbling sound were heard in the air above Moss, and at least 5 pieces were observed falling (Figure 1). Soon after a small meteorite was heard to land on an aluminium sheet and was recovered by Ragnar Marthinsen. A couple of days later family Johansen coming home from holiday, discovered that a branch of the plum tree was broken, and on the ground laid a meteorite stone. In Moss centre, a piece that had hit a fence was found on July 23, but its total weight has not been shared. On July 30 M. Bilet and M. Farmer drove into an industrial area and discovered a meteorite stone that had hit the concrete basement and been crushed to many pieces. After a heavy rainfall on July 29, 30, and 31, a leakage through the roof of NorgesGruppens building in Moss was discovered. Workmen repairing the roof discovered a meteorite piece that had penetrated the roof and the isolation causing a hole of 10 cm x 10 cm. Searches in the area resulted in the recovery of five stones, with a total weight of 3.76 kg (Table 1, Figure 2).

As rumours about the meteorite fall spread, meteorite hunters from many countries turned up, expecting a viewable terrain with sparse vegetation and not as M. Farmer wrote: *We searched for meteorites day after day, hunting in dense forest in the seaside community. The name Moss is no joke, every inch of ground*

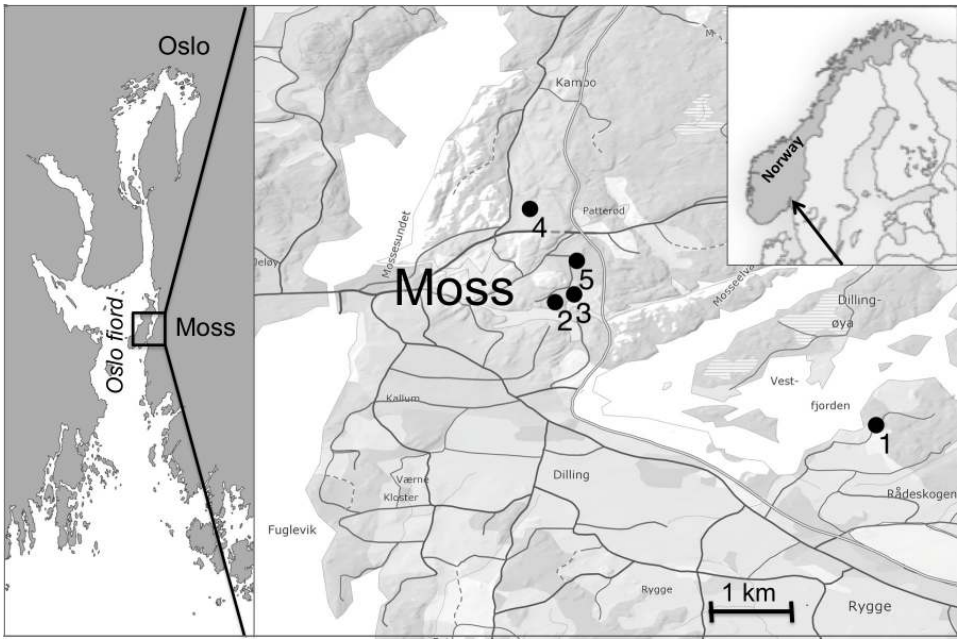

Figure 1. Oslo fiord area, showing Moss and the search area framed, and enlarged with the location of finds.

Table 1. Meteorite stones recovered from the Moss fall (Connollly et al.2007; Meteoritical Bulletin 91). M-S-T: Mass divided between Michael Mazur, Bjørn Sørheim, and Eric Twelker (M-S-T); Natural History Museum (NHM), University of Oslo (UiO).

No	Date 2006	Latitude / Longitude	Mass [g]	Owner	Comments
1	14 July	59° 24.463′ N 10° 45.548′ E	36.7	K.J.R. Ødegaard	Complete stone + some fragments.
2	17 July	59° 25′.908 N 10° 41.778′ E	752	NHM, UiO	Complete stone; hit tree, landed in grass; angular shape.
3	23 July	∼ 59° 26′ N ∼ 10° 42′ E	∼ 1500	M-S-T	Half stone + fragments; hit fence and shattered.
4	30 July	59° 27.005′ N 10° 41.482′ E	∼ 800	M. Farmer, M. Bilet	Many pieces; hit concrete in industrial area.
5	3 Aug.	59° 26.394′ N 10° 42.032′ E	676	NHM, UiO	Complete stone; penetrated roof; angular shape.

was covered with a thick carpet of moss plants, making the search for meteorites very difficult. NorgesGruppen donated stone no. 5 of 676 g to the Natural History Museum, University of Oslo. The museum also acquired stone no. 2 of 752 g from family Johansen. Both stones are of great value and completed the national meteorite collection with the 14th meteorite proven to have fallen in Norway. Rest of this fall is more or less in private collections word wide.

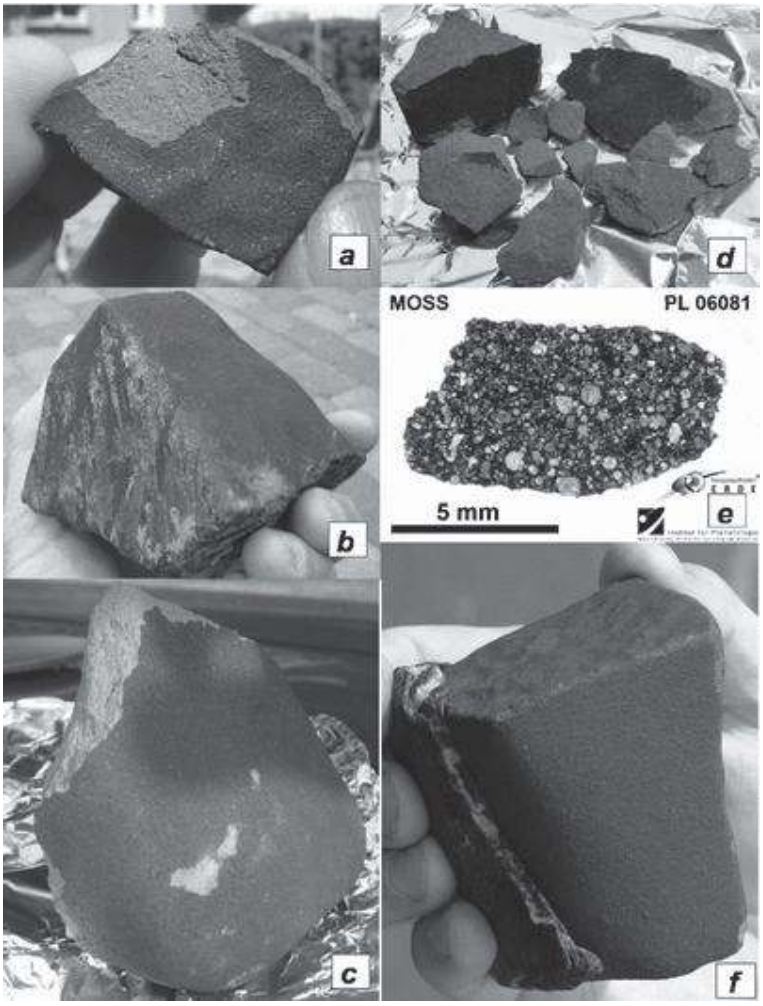

Figure 2. Individual Moss meteorite pieces: a) Stone 1, b) Stone 2, c) Stone 3, d) Stone 4, e) Stone 4. thin section, f) Stone 5. Stones 2 and 5 are kept at Natural History Museum (NHM), University of Oslo (UiO). Photos: M. Bilet, Y. Vogt.

2. Investigations

The observed fall and rapid collection of the Moss meteorite pieces after the fall, gave an unique opportunity for detailed petrological and geochemical investigations, including analyses of indigenous organic species, and short lived isotopes.

2.1. Petrography and mineralogy

The Moss meteorite contains abundant small chondrules (most < 200 μm in diameter), small (< 1 mm) amoeboid olivine aggregates (AOAs) and refractory inclusions, and isolated grains of olivine ($Fa_{0.3-42}$, average $Fa_{19.9}$), troilite (Fe_7S_8-FeS), and kamacite (α-(Fe,Ni)) set in a gray matrix of finegrained olivine and

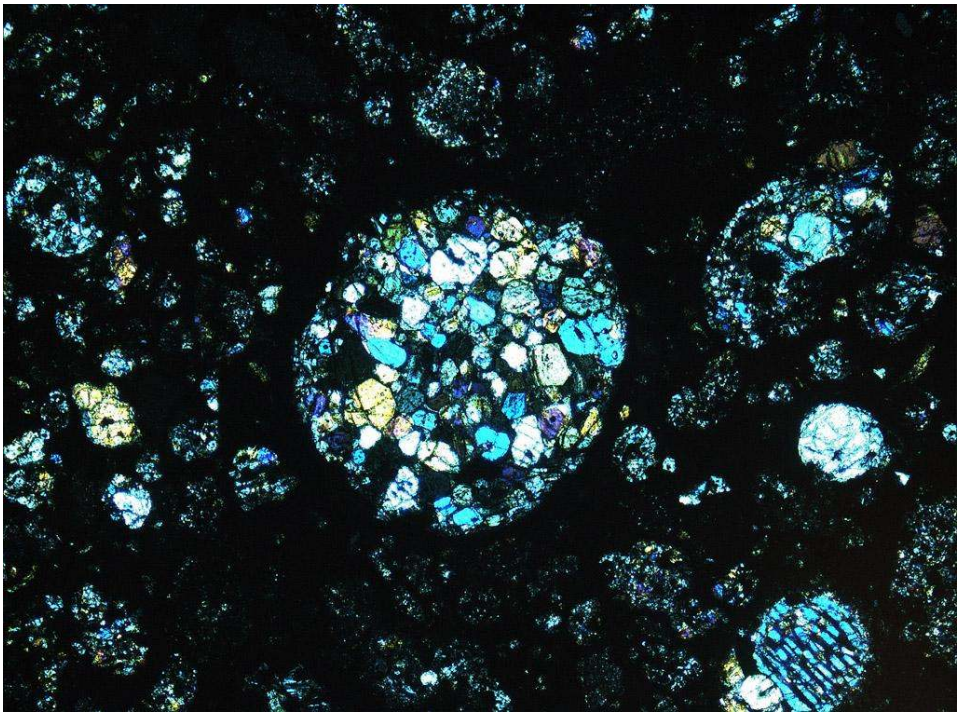

Figure 3. Thin section image in polarized light. The colour of the olivine and pyroxene crystals varies with optical orientation. The height of the picture is 1.7 mm. Photo: R.S.Selbekk.

pyroxene (Figure 3). Diffusional entry of FeO can be observed around edges and along cracks of forsterite grains. Refractory inclusions contain spinel, calcic pyroxene, and abundant nepheline that replace melilite and other primary phases; some perovskite has been transformed to ilmenite. Some amoeboid olivine aggregates contain relict cores of forsterite, but most of the olivine has been converted to more fayalitic compositions. Matrix is mildly recrystallized and sulphur-poor; matrix olivine has similar composition to olivine in fine-grained chondrules and inclusions. Moss contains 0.21-0.25 wt.% C as graphite and organic molecules heterogeneously distributed (Bilet 2007; Greenwood et al. 2007; Pearson et al. 2007, 2008; Bartoschewitz et al. 2010; and Selbekk et al. 2011). Single concentric and Ca, Al-rich inclusions show severe secondary alteration by formation of Fe-rich spinel and by replacement of melilite and perovskite by nepheline and ilmenite (Bischoff and Schmale 2007). The Moss meteorite contains organic molecules of benzene (C_6H_6), toluene (C_7H_8), and up to C_2-alkyl benzenes; besides traces of biphenyl ($(C_6H_5)_2$), benzonitrile (C_6H_5CN) and some aliphatic hydrocarbons. Naphthalene is the highest molecular weight aromatic species evident, but only C_1-alkyl species were identifiable (Pearson et al. 2007, 2008).

Table 2. Gas retention ages of CO chondrite falls (after Bartoschewitz et al. 2010).

Meteorite	Type	K-Ar 10^9 a	U/Th-H 10^9 a	Source
Kainsaz	CO3.1	4.47	4.50	Alaerts et al. (1979a)
		4.02	4.23	Mazor et al. (1970)
Felix	CO3.2	4.19	4.38	Mazor et al. (1970)
Ornans	CO3.3	4.06	4.30	Scherer and Schultz (2000)
		4.56	4.22	Mazor et al. (1970)
Lancé	CO3.4	3.61	3.88	Mazor et al. (1970)
		3.65	2.88	Mainz (Bartoschewitz et al. 2010)
		3.80	2.72	Mainz (Bartoschewitz et al. 2010)
Moss	CO3.5/6	4.51	3.93	Tokyo (Bartoschewitz et al. 2010)
		4.35	3.97	Mainz (Bartoschewitz et al. 2010)
Warrenton	CO3.6	4.64	4.59	Mazor et al. (1970)
		4.34	4.38	Scherer and Schultz (2000)

2.2. Age determinations

Two different samples of Moss meteorite taken 1-2 mm below the fusion crust were analyzed for noble gases at two different laboratories (University of Tokyo and Max-Planck-Institute fr Chemie, Mainz) (Bartochewitz et al. 2010). Calculations based on $^{3}He/^{21}Ne$, $^{22}Ne/^{21}Ne$ and $^{38}Ar/^{36}Ar$ ratios gave cosmic-ray exposure (CRE) ages of about 14 Ma, within witnessed falls the shortest after Lanc. Based on ^{4}He and ^{40}Ar produced by decay of ^{235}U, ^{238}U, ^{232}Th, and ^{40}K, respectively, gas retention ages were calculated (Table 2). The difference in Moss meteorite age between $3.95 \cdot 10^9$ yr and $4.43 \cdot 10^9$ may reflect loss of helium or deviations from the assumed average element composition.

3. Classification and official name

Petrography, mineralogy and oxygen isotope analyses confirm the Moss meteorite to be a carbonaceous chondrite of the Ornans group (CO3). Greenwood et al. (2007) classified it as CO3.4/3.5 according to the classification of Chizmadia et al. (2002) which equates to a CO3.4/5 on the metamorphic scale defined by Scott and Jones (1990), i.e. igneous zoning in chondrule phenocrysts and increasing FeO concentration at the edges and cracks of these phenocrysts. Moss has been classified as CO3.6 shock stage S2 by Connolly et al. (2007, see p. 435) based on mineralogy and petrology of amoeboid olivine inclusions Chizmadia et al. (2002). The meteorites official name MOSS was approved September 25, 2006; final classification January 10, 2007 (Connolly et al. 2007, Meteoritcal Bulletin 91). Moss is by end of 2013 one of 7 approved meteorites classified as CO 3.6, and the first witnessed fall of a CO3 chondrite since Kainsaz in Russia in 1937.

4. Meteorite Moss – Conclusions

1) Petrography, mineralogy and oxygen isotope analysis confirm that the Moss meteorite is a carbonaceous chondrite of the Ornans group (CO3).
2) It is the first CO chondrite fall after a time period of 70yr and the least terrestrially contaminated member of its group.

3) The cosmogenic and trapped noble gas isotopes group Moss as a typical CO-chondrite (Bartochewitz et al. 2010).
4) Gas retention ages are approximately $3.95 \cdot 10^9$ yr (U/Th-He) and approximately $4.43 \cdot 10^9$ yr (K/Ar), respectively (Bartochewitz et al. 2010).
5) Most of the CO chondrite falls were ejected by single events from their parent body between approximately 3.5 (Lancé) and approximately 57 (Felix) Ma ago. Moss shows the second shortest cosmic-ray exposure age and was ejected about 14 Ma ago.

References

Alaerts L., Lewis R.S., Anders E., 1979, Geochimica et Cosmochimica Acta, 43, 1421

Bartoschewitz R., Ott U., Franke L., Herrmann S., Yamamoto Y., Nagao K., Bilet M., Grau T., 2010, M&PS, 45, 1381

Bilet M., 2007, Stein, 34 (2), 3 (In Norwegian)

Bischoff A., Schmale K., 2007, 38th Lunar and Planetary Science Conference, Paper 1561

Chizmadia L. J., Rubin A. E., Wasson J. T., 2002, M&PS, 37, 1781

Connolly, H.C.Jr., Zipfel J., Folco L., Smith C., Jones R. H.. Benedix G., Righter K., Yamaguchi A., ChennaouiAoudjehane H., Grossman J.N., 2007, the Meteoritical Bulletin, No. 91, March., 42, p. 413

Farmer M. 2006, `http://www.meteoriteguy.com/adventures/moss/moss.htm`

Greenwood R.C., Pearson V.K., Verchovsky A.B., Johnson D., Franchi I.A., Roaldset E., Raade G., Bartoschewitz R., 2007, 38th Lunar and Planetary Science Conference, Paper 2267

Mazor E., Heymann D., Anders E., 1970, Geochimica et Cosmochimica Acta, 34, 781

Pearson V.K, Greenwood R.C., Morgan G.H., Turner D., Raade G., Roaldset E., Gilmour I., 2007, 38th Lunar and Planetary Science Conference, Paper 1846

Pearson V.K, Greenwood R.C., Verchovsky A.B., Turner D.C., Gilmour I., 2008, 71st Annual Meteoritical Society Meeting, Paper 5239

Scott E.R.D., Jones R.H., 1990, Geochimica et Cosmochimica Acta, 54, 2485

Scherer P., Schultz L., 2000, M&PS, 35, 145

Selbekk R.S., Roaldset E., Bilet M., 2011, Stein, 38(2), 38 (In Norwegian)

Meteoroids 2013, Proceedings of the Astronomical Conference,
held at A.M. University, Poznań, Poland, Aug. 26-30, 2013,
eds Jopek T.J., Rietmeijer F.J.M., Watanabe J., Williams I.P.,
Adam Mickiewicz University Press in Poznań, pp 75–80

The historical and geological data regarding extraterrestrial matter falls in the Great Poland Lowland

Stankowski W.T.J.

Institute of Geology, Adam Mickiewicz University,
Poznań Poland, Maków Polnych Street 16, 61-606 Poznań, Poland (stawgeo@amu.edu.pl)

Abstract. The multiple falls of meteorites in the Great Poland Lowland provided much historical and environmental data. The most famous site of extraterrestrial matter fall with its morphogenetic effects is at Morasko. Iron meteorites were recognized in Morasko and Oborniki, as well as in Przełazy and Jankowo Dolne. The luminescence and radiocarbon data showed the different time of impacts in Morasko (∼5000 years BP) and Przełazy (∼Late Glacial – Early Holocene). The time of Jankowo Dolne event is not known yet.

Keywords: meteorites, Morasko, Wielkopolska, historical documents, geological data

1. Introduction

The many spectacular falls of meteorites to the Earth's surface as well as the non-spectacular capture of tiny fragments of extraterrestrial material, are natural phenomena. The last well-documented meteorite events in the whole of the Polish territory were in the vicinity of Giżycko in 2011 and the stony meteorites fall at Baszkówka near Piaseczno in 1994. Other cosmic events took place during last one and a half century, the Pułtusk chondrite shower in 1868 and the Łowicz mesosiderite shower in 1935. Further back in time, in the Great Poland Lowland (Wielkopolska) Morasko area near Poznań there occurred the largest iron meteorite shower in Central Europe around 5000 BP (Hurnik 1976; Stankowski 2010; Muszyński et al. 2012), as well as a very probable huge shower on NW Wielkopolska and SW Pomerania at the very beginning of the XIV century (Czajka 2013).

The Great Poland Lowland is a good example of an area where extraterrestrial materials have enriched the environment, as is shown by geological and historical data. The most extensive seems to be the Morasko shower of iron meteorites, as well as the finds near Oborniki and probably at Przełazy (Seeläsgen) and Jankowo Dolne.

2. Historical and press documents

The oldest evidence of falls or flights of meteorites in the Great Poland is the so-called "Great Poland Bolide". Czajka (2013), refers to: reports of probable impact event in Strzelce Krajeńskie at the beginning of the fourteenth century (Brzustowicz 2001; Karwowski and Brzustowicz 2009), fragment of medieval paintings of falling stars in the temple of Paradyż near Gościkowo, the frieze in the northern portal, brick architecture in the fourteenth-century parish church in Rzepin, and finally

the supposition of medieval provenance of star motifs on the heraldic arms of several cities of the Great Poland and Western Pomeranian.

The meteorites falls and bright meteor flights over Wielkopolska and recorded in the press are as follow: in Skalin near Stargard Szczeciński, two stone meteorites, one the size of a human head and the other the size of a goose egg impacted in 1715; at Wilkanowo near Zielona Góra – two small stone pebbles impacted in 1841; in Krobia and Grabianowo near Wschowa and also near Górna świdnica there was an impact in 185 (chunks found in 1957 all metallic matter); observations of bright meteor flights from west to east in 1868, over middle Wielkopolska; impact in 1880 at Ratyń near Konin; impact of stony meteorites 1910 at Grzempy (between Poznań and Piła). Some of the data from meteorites that were found was analytically documented.

3. Morasko and Oborniki iron meteorites

The history of metallic meteorites discovers in this part of Wielkopolska is almost 100 years old. The first chunk with a mass of 77.5 kg was found in 1914. Shortly afterwards, a 4.2 kg chunk and two 3.5 kg chunks were found. The largest chunk was analyzed and exhibited at the Kaiser Friedrich Museum the Spandau Observatory and the Pulsnitz Observatory (Clasen 1978). In the interval 1919–1960, many different size meteorites were collected, the largest having a mass of ∼80 kg. Unfortunately, most of the specimens either fell apart or have since disappeared. This was also the fate of to two medium-size fragments of metallic material, postulated as being meteoritic in origin, found outside the Morasko area, in the "Oborniki forest" about 25 km North of Morasko (Pokrzywnicki 1964; Pilski and Walton 1999). Some of the metallic chunks found near Morasko were used by locals as building material, thus becoming incorporated into walls or floors. An instance is also known were a large meteorite was used for some time as ballast for a treadmill. A small number of the Morasko meteorites are saved in Polish museum collections, including those of the Museum of the National Geological Institute, the Earth Museum in Warsaw, the Polish Academy of Sciences in Poznań (one specimen on loan to the Chorzów Planetarium, another to Wrocław University), in the collections of the Geological Institute of Adam Mickiewicz University in Poznań, and in the Primary School Memorial Hall in Suchy Las near Poznań.

The first Great Poland Lowland meteorite fall (an iron one, with mass of around, 102 kg, though this is not clearly specified) was some time before 1847 (Pokrzywnicki 1964). An attempt to determine the exact place and time of the Przełazy meteorite fall was made by Stankowski and Uścinowicz (2011), checking the iron spherules content in the peat profiles as well as the contents in the superficial deposits in Przełazy surroundings. The most likely place to find the fall could be in today's peat deposit to the SW of the Przełazy area. The time of event seems to be the turn of the Late Glacial and Holocene eras.

In the early years of XXI century small metallic meteorite was found in the Jankowo Dolne (Karwowski 2004). Jankowo Dolne and Przełazy meteorites with almost identical metallic composition are very similar to the Morasko and probably to the Oborniki ones. These four specimens, expressing the sequenced falls line, may

be interpreted as coming from the fall of one original meteoroid. The author does not share this view – according to data obtained, the Przełazy and Morasko falls represent individual events, differing by some thousands of years from each other. The age of Jankowo Dolne meteorite fall is unknown.

The end of the first and beginning of the second decade of XXI century was the especially productive for finding meteorite. In 2006 three chunks with masses of 10–21 kg and one of 164 kg were discovered. In 2011 AD, within the scope of the exploration program *Meteorite Men – episode 302 "Morasko Poland", Science Channel, 2011*, a chunk with a mass of about 34 kg, which is essential to confirm local extent of the extraterrestrial matter fall, was discovered. This is fundamental proof of the impact (contradicting the hypotheses about the Morasko meteorites being brought by an ice sheet/sheets). The chunk was found in the glacitectonically disturb Neogene sediments of the "Poznań series", which is present just beneath the present-day surface. The impact led to penetration of the thin layer of Quaternary sediments (hence fragments of granitic material found in the frontal part of the meteorite – Karwowski et al. 2011). In 2012 the up to now largest Morasko meteorites, with a mass at extraction of 300 kg, and after cleaning of 261 kg, was discovered. At the same time many tiny fragments of extraterrestrial metal matter were found. All specimens were subjected to mineralogical and geochemical research and dosemetric dating. The main aspect of small meteorites research is dating of two specimen surfaces: the melt-weathering and sinter-weathering coating. The obtained data are comparable to the results of previous studies of the Morasko Meteorite matter and Morasko's craters development.

Hot chunks of meteorite falling onto the sedimentary surface penetrated the unconsolidated Quaternary and Neogene sediments. The thermal influence of the chunks on their immediate surroundings has been recorded in the zeroing of luminescence and on the formation of a sinter-like coating. Later weathering resulted in the formation of a compact meteorite coating. All of them include many small fragments of crushed quarts grains, as well as grains which are strongly brecciated, which have a structure that has been altered under the influence of a short-duration high pressure.

The TL dating of the four meteorite coating (chunks differ in mass from ∼10 to ∼160 kg) was carried out at the Institute of Geography of Gdańsk University by St. Fedorowicz. The results are as follow: meteorite of 10.5 kg, 4.7±0.4 ky; meteorite of 11 kg, 5.0±0.7 ky; meteorite 21 kg, 6.1±0.7 ky; and meteorite of 164 kg, 5.2±0.9 ky. There is very little difference between the obtained ages indicating that zeroing of the luminescence occurred in the time interval between 4.5–6.5 thousands years ago.

The earlier luminescence analyses of sinter-weathering crusts of the large Morasko meteorites were compared with new research data regarding the melt-weathering crust of small meteorites (Stankowski et al. 2014). During the passage through the Earth's atmosphere, the exterior part of a meteorite is subjected to distinct heating and simultaneous luminescence resetting. The results of TL dating three small meteorites (done by St. Fedorowicz from Gdańsk University and G. Poręba from Department of Radioisotopes, Institute of Physics, Centre of Science and Edu-

cation, Silesian University of Technology), gave indexes: meteorite 62 g, 4.6±0.8 ky; meteorite 70 g, 4.7±0.7 ky; meteorite 1201 g, 4.9±0.9 ky. It should be add that the mineral material from the immediate surrounding of 70 g meteorite, was also zeroed - sample from above gave data 5.4±0.8 ky, and sample from beneath 5.5±0.8 ky, slightly older than the dates of the melt-weathering crusts (probably not complete resetting of luminescence signal during the impact chunk). The basic dates of both types of material fall within the limits of the measurements errors, so that they should statistically be considered as having taken place simultaneously.

The TL dating of the meteorite coatings was preceded by OSL measurements of the mineral sediments in the beds of the two largest Morasko's depressions/craters. The sample consists of the deformed sediments from the Neogene – few millions years old, and Quaternary ones – not younger than 18–17 ky (Stankowski and Bluszcz 2012). The 101 portions of material were dated. Both the Neogene and Quaternary sediments are often assigned very young luminescence ages. Approximately 47% of all dates show indicators <10 kilo years BP, among which ∼19% are indicators <5 kilo years BP. This indicates a very early time of luminescence resetting. The presence of older age indicators shows that resetting during the impact was characterized by a diverse range of completeness. Luminescence dating provided the verifying data of the origin of the Morasko craters in relations to the previous TL dating of sinter-weathering crusts and melt-weathering crusts, as well as radiocarbon and palynological age estimations of Morasko craters origin.

4. The metallic spherules as an impact indicators

The fine-grained material – micrometeorites, cosmic dust and spherules, rather then meteorites, constitutes the bulk of extraterrestrial sum material reaching the surface of the globe. The amount of this "delivery" varies with time and the concentration is not uniform all over the planet.

In and around the Morasko Meteorite Reserve there exists a distinctly increase in the concentration of tiny metallic fragments. Very often it is observed in the area surrounding the finding meteorites. The metallic dust in which the spherules are observed, come into being as a result of the disintegration of cosmic bodies, both in interplanetary space and in the Earth's atmosphere.

Research into cosmic dust found at Morasko has been curried on since 1976. Initially, indications were found for a variable distribution, sometimes with very high concentrations of such dust, at the northern side of the Morasko Meteorite Reserve (Hurnik 1976). The high concentration was linked to the trajectory of the Morasko meteorites in the atmosphere. These data and the report on the two metallic meteorite chunks found in the "Oborniki forests" in the 1930's led to a search for spherules in the sediment profiles, both mineral Pleistocene and Late Glacial and Holocene organic-mainly peat sections.

In the core of Szlaban site (few kilometers North of Oborniki) and also in some others around, numerous spherules were found. The quantity increases in a peat layer that has been radiocarbon dated as 5070±40 to 4750±40 years BP (respectively no data: Poz-7005 and Poz-7004). This layer formed the surface of the peat bog at the time of Morasko Meteorite shower fall.

Following the results from the researches at Morasko and its surroundings, it was decided to carry out similar investigations around Przełazy. Unfortunately there is insufficient information about the place and time of that meteorite fall. The peat bog nearest to Przełazy (SW of village) was cored. In all of the peat strata the constant supply of magnetic material (single spherules grains) to the gyttia and peat cover the last ten millennia, and over longer. Considerable changes in the concentration of fallen metallic dust took place in the course of this time interval – the distinct increase of spherules in the particular peat layer. If the hypothesis is correct, that a meteorite fall is associated with the increase of spherules content, then the impact at Przełazy can be dated at the end of the Late Glacial or the beginning of the Holocene. The Przełazy impact (with trajectory from NW) seem to be few thousands years older than Morasko one.

5. Conclusion

In the Great Poland Lowland multiple falls of the meteorites were reported - both evidenced by the historical/press documents and geological ones. The most important is the presence of metallic meteorites in Morasko/Oborniki, with the addition of Przełazy and Jankowo Dolne. These sites contain metallic meteorites elaborated in detail by geochemical and morphogenetic methods. The Morasko fall is well-documented in age ∼5000 years BP. The obtained data are consistent with the previous palynological and radiocarbon results. The Morasko area is one of only few places in the Earth, where there exists not only extraterrestrial material, but also impacts effects in the form of craters. The Przełazy meteorite appears to come from another different fall, older by a few thousands of years than Morasko and probably left no effect in the form of craters. The Jankowo Dolne meteorite fall time is not known, but extensive studies are continuing.

References

Brzustowicz G.J., 2001, Nadwarciański Rocznik Historyczno-Archiwalny, 8, 317

Clasen J., 1978, Meteoritics, 13, 245

Czajka W., 2013, Bolid Wielkopolski. Okoliczności spadku meteorytu Morasko, ISBN 978-83-919107-4-0, Biblioteka meteorytyki, Warsaw, Poland (in Polish)

Hurnik H., 1976, Meteorite Morasko and region of its fall, Wyd. Nauk. UAM, Poznań, 64

Karwowski Ł., 2004, in Proceeding of the III Konferencja Meteorytowa, 25-26 Sept. 2004, Poznań, Poland, 24

Karwowski Ł., Pilski A.S., Muszyński A., Arnold S., Notkin G., Gurdziel A., 2011, Meteorites 1, 21

Karwowski Ł., Brzustowicz G.J., 2009, Acta Societatis Metheoriticae Polonorum, 1, 59

Muszyński A., Kryza R., Karwowski Ł., Pilski A.S., Muszyńska J., 2012, Morasko, the largest iron meteorite shower in Central Europe, ISBN 978-83-63400-50-7, Bogucki Wydawnictwo Naukowe 2012, 109

Pilski A., Walton W., 1999, Meteorite 5, 27

Pokrzywnicki J., 1964, Studia Geol. Pol., XV. Wyd. Geol., Warszawa, 176

Stankowski W.T.J., 2010, Morasko Meteorite, a curiosity of the Poznań region (Meteoryt Morasko, osobliwość obszaru Poznania), ISBN 978-83-23221-13-5, Wydawnictwo Naukowe Uniwersytetu im. Adama Mickiewicza, Poznań, 94

Stankowski W.T.J., Uścinowicz G., 2011, Acta Geologica Polonica, 61, 115
Stankowski W,T.J., Bluszcz A., 2012, Radiometric dating, ISBN 978-953-51-0596-1, In-Tech, 115
Stankowski W.T.J., Fedorowicz St., Michalska D., Poręba R., Szyszka M., 2014, Planetary and Space Science, (submitted)

Meteoroids 2013, Proceedings of the Astronomical Conference,
held at A.M. University, Poznań, Poland, Aug. 26-30, 2013,
eds Jopek T.J., Rietmeijer F.J.M., Watanabe J., Williams I.P.,
Adam Mickiewicz University Press in Poznań, pp 81–85

250 Fireballs Observed in Norway 100 Years Ago

Skorve J.

Natural History Museum, University of Oslo
P.O. Box 1172 Blindern NO-0318, Oslo, Norway (skorjoh@yahoo.no)

Abstract. In 1941 the Norwegian Academy of Sciences, presented a study in the Mathematical-Natural Sciences section, by the Norwegian astronomer Sigurd Einbu. In this report, the information of each fireball is presented in a table containing eight parameters, including their radiants. The report also contains several illustrations. For about 60 of the most interesting fireballs, Einbu included additional information, as describing them in more details. Like, those fireballs producing infrasonic sounds, and/or having superbolide brightness. Also, the strong smell of sulfur, have been reported by a number of persons in a meteorite drop zone. Also, a unique incident of four bright fireballs that were observed within a period of 12 hours, all with the same radiant. During this period, we also experienced the brightest fireball that ever has been observed in Norway, the Trysil superbolide, of 1927. This paper discusses Einbu's report. With respect to when it was published, is surprisingly well suited to also to be read and studied by interested researchers.

Keywords: meteoroid, superbolide, fireball, Norway, Einbu

1. Introduction

Between 1903 and 1941, 250 fireballs were observed and categorized in Norway. This was done and published (in German) in 1942 by the Norwegian astronomer Sigurd Einbu. The study was named Observations of 250 fireballs seen in Norway during the 1903-1941 period (Einbu 1942). His report was rediscovered accidentally twenty years ago. It excels in the large amount of fireballs treated and the quality of presentation. The collection includes a number a very bright fireballs and even some superbolides.

Sigurd Einbu (1866–1946) was an astronomer from rural Norway. He collected and coordinated numerous observations of variable stars and fireballs in cooperation with the University of Oslo. In 1912 he discovered a nova (Nova Geminorum II 1912 Enebo) named after him. He received from 1909 a permanent state salary from 1909 which permitted him to work as a full time astronomer. He also established an observatory for magnetic and auroral observations.

His legacy includes 14 scientific publications, popular astronomy books, and variety of astronomical notices to newspapers.

2. Some very bright fireballs and superbolides in Einbus report

Early Christmas Eve 1916, a very bright fireball crossed the border of Swedish Lapland, moving in a SW- direction, in a very shallow trajectory, before reaching the Norwegian coastal area, near the town of Kristiansund. During its more than

400 km long passage through the atmosphere, it had two violent explosions. It must have been a superbolide, according to the description of its impressive appearance. 120 reports were received from people who had seen it. Only 30 minutes later, another very bright fireball was seen moving in the same direction as the first one. However, its trajectory was somewhat further to the south. It split up into two distinctive pieces, and they moved together over a considerable distance. Even more surprising, 24 minutes later, even a third fireball appeared, though it was somewhat smaller that the two others. However, it moved in the same direction as two others, but further to the south. Early next morning, another bright fireball was observed. It had the same radiant as the three others observed the evening before, clearly, a most extraordinary Christmas gift.

Of the 120 reports Einbu received from people who had seen this first and most luminous one, of the bright Christmas 1916 fireballs, only about 20 could be used for locating the fireball path through the atmosphere. The majority of the observers perceived the fireball to be close to them. For some it seemed that it hit the ground in the neighboring area. Some saw it rising from the root of a tree nearby. They immediately went over to the site, but found nothing unusual. Others saw the fireball barely missed, colliding with a tall chimney of a factory. A man walking along a road, told he had to jump into a ditch, to avoid being hit by the fireball! Not many of these observations and descriptions are of direct astronomical value. However, as the geographical location of this superbolide track through the atmosphere, is reasonably well known, it is clear that the majority of these close by observations, actually, were made at distances of more than 100 km. In addition to this superbolides‘ spectacular brightness, it was observed long and widely in its shallow path, over a 400 km long stretch, gradually penetrating the atmosphere.

3. A Presentation of selected fireballs and superbolides from Einbus report

The following image (Figure 1) shows graphically some of the very bright fireballs and superbolides described by Sigurd Einbu. Below each of the selected observations are described in more detail.

No 16.
This has been described above as the first and brightest of the early Christmas Eve 1916, fireballs. During its long passage through the atmosphere, it had two violent explosions.

No 37.
On January 1922, an extremely bright fireball entered the atmosphere, near the border to Sweden. It moved along the southeastern coast of Norway, in a very shallow angle. After a more than 400 km long stretch, it ended in a violent explosion over the North Sea, only about 25 km off the coastal town of Egersund.

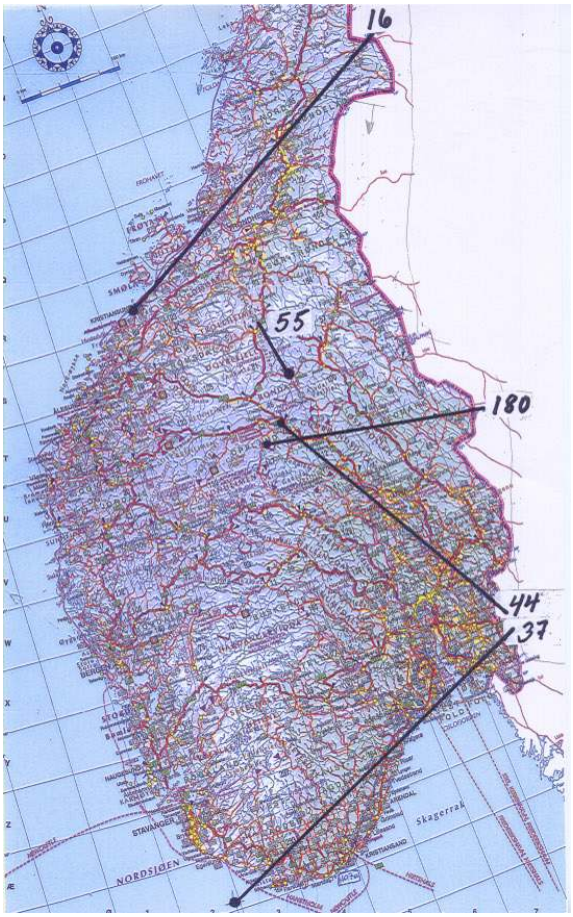

Figure 1. Selected very bright fireballs and superbolides described by Sigurd Einbu.

No 44.
In the evening of February 1923, a very bright fireball came from Sweden into Norway, moving in a NW direction. After it had travelled about 180 km, it had a violent explosion. Below and within a wide area, people felt a strong shock. Some fainted, others sensed a strong smell of sulphur. This same was experienced by some people, in connection with the Tagish Lake superbolide in western Canada in January 2000. After the explosion over SE Norway, three bright objects were seen, continuing moving, in close procession, for about 150 km. Then they disintegrated in the Otta area, where whistling sounds were heard, but no meteorites were found.

No 55.
An impressive fireball moved southward over central, southern Norway, 15 minutes after sunset. Two men saw it approaching from the north, and some minutes later, they saw something hitting the ground close to them. Due to the darkening sky,

they decided to check the area the next morning. Therefore, they did, and they found three holes in the ground, on considerable larger than the two others did. Due to very unfortunately circumstances, these meteorites were never recovered.

No 180.
This extremely bright fireball came across from Sweden, moving in a westerly direction. After having travelled more than 200 km., it exploded violently, at an altitude of about 20 km. From this explosion, strong sounds were heard from widely around, 4–5 minutes later.

4. The Trysil Superbolide

This map (Figure 2) shows the approximate path of this superbolide, that probably was one of the brightest ever observed in Norway. It was first seen from the western coast of Sweden on 21. June 1927, at 6 o'clock in the morning, on this longest day of the year. The Sun had then been up for two hours, and had already reached quit high in eastern sky. Seen from the Swedish west coast, the superbolide moved northward in the western sky. It had probably entered the atmosphere over the central part of Denmark.

Figure 2. The trajectory of the Trysil superbolide.

Some of the observers heard sounds simultaneously when observing the bright fireball. Thus, they thought it was very close to them.

Reaching SE Norway, with decreasing altitude, it became even more overwhelming in brightness, an strong detonations were heard over large areas. In the Oslo area, many people saw the fireball high in the sky, and some surmising it to be passing 300 meters above them. In a nearby area, one person saw it as a flaming lightball moving in a north eastern direction. Felt it being as close as 100 meters, but understood intuitively that it was further away. It was clearly brighter than the Sun.

Moving further north, continuing detonations were heard. Then it changed gradually into an elongated, diffuse object, seemingly containing separated pieces and bright spikes. This indicates that the meteoroid had broken into several fragments. Reaching the Trysil area, it had an extremely violent explosion. The whole area became covered by a black cloud. After some time, this faded gradually away, and finally disappeared.

Within a radius of more than 60 kilometers strong detonations were heard, and the ground was shaking, causing rattling doors and broken windows. This was also the case on the Swedish side of the border. Good measurements from the Swedish side show that the superbolide final explosion, took place 40-20 km above the ground. A few weeks later, a 640 gram meteorite was found. Surprisingly, no search for meteorites was organized by the University of Oslo, which initiated the collection of observations and reports of this superbolide.

5. Some concluding remarks

Interesting in retrospective, is to note that fireballs observations were systematically registered a hundred years ago, but not today until very recently, when the The Norwegian Fireball Network was established in 2013 (NFN 2013).

Einbus report may be used for documentation, comparison and future comparative research. Einbu in a later book reflected on the limitation of visual measurements of fireball sizes. He was convinced that the meteorite bodies had to be much smaller than their appearance.

References

Einbu S., 1942, 250 In Den Jahren 19031941 in Norwegen beobachtete Feuerkugeln-ERRECHNUNG DER RADIANTEN u. a., In Commission by Jacob Dybwad 1942.

NFN, 2013, Norwegian Fireball Network, `http://norskmeteornettverk.no/`

Meteoroids 2013, Proceedings of the Astronomical Conference,
held at A.M. University, Poznań, Poland, Aug. 26-30, 2013,
eds Jopek T.J., Rietmeijer F.J.M., Watanabe J., Williams I.P.,
Adam Mickiewicz University Press in Poznań, pp 87–101

Meteor Showers in the Ancient Maya Hieroglyphic Codices

Kinsman J.H.

Pre-Columbian Society of the University of Pennsylvania Museum of Archaeology and Anthropology
(jhkinsman@gmail.com)

Abstract. Researchers of the ancient Maya culture have long been fascinated with the Maya obsession concerning cyclical calendars and precise visual observations of astronomical bodies and phenomena, in particular the Sun, Moon, visible planets, and solar and lunar eclipses. Although considered possible, heretofore no record of specific sightings of comets or meteor showers in the Maya inscriptions has been firmly established by scholars. Besides difficulties with decipherment of the hieroglyphic script, investigators have had to grapple with an ancient Maya calendar that has not been accurately correlated to the European calendar. Recent examination by this researcher has found that it may be possible to recognize written accounts of meteor showers embedded in the hieroglyphic corpus, especially the codices, the screen-fold books that were the tools of the astronomer-priests of that day. By proposing an alternative decipherment of an astronomical sign and using the accompanying hieroglyphic texts and illustrations with appropriate dates, this researcher believes it is possible to demonstrate that the Maya may have recorded meteor showers occurring in the seventh through the tenth centuries AD.

Keywords: Maya codices, meteor showers, meteor(s), Perseids, Orionids, Dresden codex, Madrid codex

1. Introduction

The Dresden and Madrid codices and some Classic inscriptions† may provide evidence that the Maya observed and tracked certain specific meteor showers including the Perseids, Orionids, Eta Aquariids and a few of the numbered showers (Jenniskens 2006:598-611, Table 1). By comparing dates recorded in the corpus of Maya hieroglyphic inscriptions, including the codices, to known historical dates of observed meteor showers from the same time period, the author could then examine the text and iconography associated with appropriate solar longitudes to decide if a particular inscription applied to a meteor shower outburst.

The word codices is the plural form of the singular "codex" meaning "an ancient manuscript text in book form," (`www.oxforddictionaries.com`). The codex itself

† The Classic period is usually defined from AD 250 to 900, divided into the Early Classic (AD 250-600) and Late Classic (AD 600-900) periods. Classic inscriptions included carvings on stone monuments, panels, doorway lintels and jambs, wooden lintels, paintings on walls, and carvings and paintings on portable objects such as ceramic vessels, seashells, jade objects, turtle shells and the like. The codices were believed to have been painted during the Late Postclassic period (c. AD 1200-1521)(Vail and Hernandez 2013).

Figure 1. Facsimile of the Dresden Codex (Cholsamaj edition, 1998)(Photograph by author).

was a divination tool of the priests, a handbook containing almanacs and tables‡ that pictorially and hieroglyphically displayed astronomical and religious information, including rituals and daily activities (Vail and Hernandez, 2013). Many of the almanacs and tables had been copied from previous codices and thus may contain some historical information. Currently scholars are not clear on which information is historical fact and which is prophecy, however it appears to this author that many of the possible meteor shower events are actual observations.

The Maya codices are accordion style books made with paper from the inner bark of the fig tree. There are four such surviving screen fold books as they are sometimes called; three, the Dresden, the Madrid (also known as Codex Tro-Cortesianus), and the Paris are known by the names of the European cities where they are now housed. Figure 1 shows a facsimile of the Dresden codex, 74 pages long; the Paris Codex is 22 pages long and the Madrid codex is folded into 56 leaves painted on both sides, giving a total of 112 pages.

Given that precise astronomical information recorded in the codices seemed to include all but comets or meteor showers, *was it possible that previously unrecognized astronomical information concerning meteor showers was embedded in the known tables and almanacs?* China, Japan, Korea and Europe also using naked eye astronomy had observed and recorded comets since the 11th century BC (Ho (2) referenced in Yeomans, 1991:362) and meteors since 687 BC (Imoto and Hasegawa, 1958:134). Embodying the physical aspect of visual astronomy, a prominent structure known as the Caracol at the Maya site of Chichen Itza was known to have been used for astronomical purposes (Aveni 2001:92, 272-282).

‡ Almanacs were normally composed of a continuous 260 day cycle while tables were usually anchored in the Maya Long Count, similar to the Julian Day Number system.

2. History

Although the last 20 years have seen great strides in the decipherment of the Mayan hieroglyphics, students of the Maya culture have been hampered by various problems. Following the arrival of the Spanish in 1521, Bishop Diego de Landa burned a great number of hieroglyphic rolls in 1562 (Gates 1937:iii). These destroyed documents themselves may have contained records of astronomical observations.

The exact correlation of the Christian calendar to that of the Maya is still being debated. The problem covers about a 3 day variance. The so-called correlation constants, 584283, 584285, and 584286 refer to the Julian Day Number for the beginning of the current Maya calendar Long Count. Recent literature seems to favor 584286 (Kennet et al. 2013:1-5; Martin and Skidmore 2012:3-16); naturally even a one day difference is critical when talking about a long period meteor shower.

Physical evidence of the knowledge of meteors seems to appear in the Maya area in the AD 300s. It was thought that heavenly gods hurled flaming arrows or darts at each other. A fourth century ball court marker from Tikal depicts a figure holding an atlatl† marked with stars interpreted as a meteor; a stone relief of the founding king of the city of Copan, AD 426, is carved on a structure known as Altar Q, holding a flaming dart, also interpreted as a meteor (Taube 2000:298,274, 295, 296) (figure 2). In Maya mythology, the scarlet macaw is related to meteors by the brilliant red feathers being metaphorically substituted for flaming torches (Christenson, 2007:131). Another metaphor used for meteors was fire-drilling, or the sparks resulting from the friction of the spinning shaft: the fire-drilling scene shown in figure 2 is from the Madrid codex; meteors were also represented by twisted cords, ropes that were used to transfer powerful rotational energy to the spinning shaft (Taube, 2000:294). Caterpillars and worms were also thought to represent meteors because of their drilling capabilities (Taube 2000:290-291; Lenkersdorf 2010:505, 506; Barrera, 1980:188). Meteors and obsidian were both thought of as star excrement; obsidian was thought of as both the meteor and the meteorite (Laughlin 1975:93; Lenkersdorf 2010:333, 571).

Physical seizures and illnesses were thought to result from meteor showers. The term for seizure was "tancas," a contraction of "tamacas" which was also the word for Milky Way [galaxy] (Roys 1965:xviii; Barrera et al. 1980:767, 768). In the Mayan language of Tzotzil, *poslom* means both "sickness in leg" and "falling star seen at dusk," (Laughlin 1975:284). Seizures were treated by shamans, persons who would interact with the spirit world through dance, hallucinogens or incantations. A series of these incantations are translated by Ralph Roys in the volume "Ritual of the Bacabs," (Roys 1965:3-70). The incantations took the form of chants and repeated phrases in an almost hypnotic rendition, sometimes conjuring or invoking deities known as *Bacabs*. The incantation was sometimes directed toward a heavenly realm called the fifth celestial place or *Na Ho' Chan*, "First Five Sky", where fires and some meteors may have originated (Roys 1965:7-9). These meteors that caused the seizures were the offspring of rattlesnake rattles, also known as

† Atlatl, it is a Nahuatl word for a "throwing stick or dart sling" (www.oed.com, Oxford English Dictionary online).

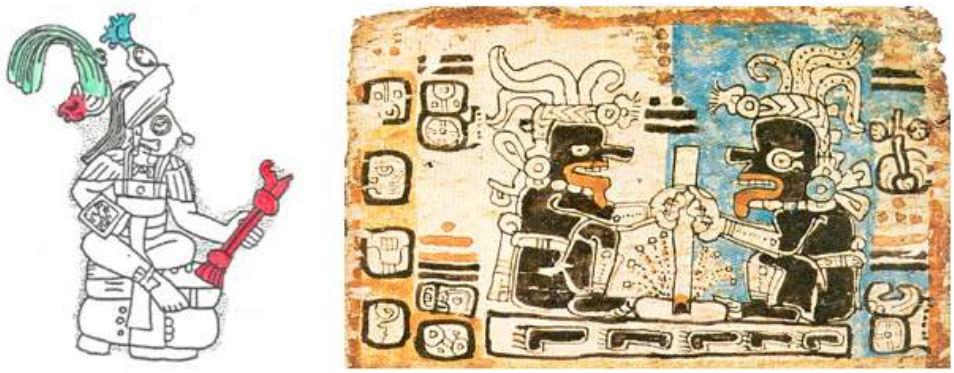

Figure 2. Left: drawing of stone carving of Yax K'uk' Mo', Altar Q, founding king of Copan holding flaming arrow, possibly interpreted as meteor (Taube 2000:274, 295, 296)(Drawing by Linda Schele (shading by author)). Right: two god M figures engage in fire-drilling scene from page 51a, Madrid codex (courtesy Akademische Druck-u. Verlagsanstalt-Graz, electronic document online at famsi.org).

the Pleiades constellation, close to the Perseus constellation and the apparent origination (radiant) of the Perseid meteor shower; the scarlet macaw was responsible for seizures in the incantations (Roys 1965:7-9, xix).

3. Discussion

One important notation used by the Maya was the sky band. The sky band consists of several signs in a horizontal band used in both the Classic inscriptions and the codices to indicate the heavens and celestial activity. Signs such as the sun, moon, a star or Venus, night and the proposed sign for meteor showers make up the sky band (see Figure 3).

This author bases his hypothesis in part on a proposed reading of what is considered a variant of the k'in, "day, sun" sign found in the sky band that is included in many of the pages of the codices. Specifically that sign is a dotted X conflated within the k'in sign, the dotted X containing small circles at the center and at the end of each leg of the X. The conflated k'in sign is known as a k'in variant T544v (Thompson 1962:155-160) or XQ3 (Macri and Looper 2003:197), but neither catalog distinguishes the k'in sign with or without the dotted X contained within the sign itself. The dotted X variant is found occasionally throughout texts in the Classic inscriptions, and whether or not the meteor shower meaning can be attached in those contexts is beyond the scope of this paper. In the codices the dotted X k'in sign seems to be found only in the sky band and not in the glyphic texts themselves. In the sky band of the throne inscription at Uxmal as interpreted by Bricker and Bricker (1996:210), the author interprets the sign shown in figure 3 and a similar sign as the Perseids and Orionids. Meteor shower dates may be associated with and without texts with the k'in variant, therefore the k'in variant may not be an exclusive indicator of showers.

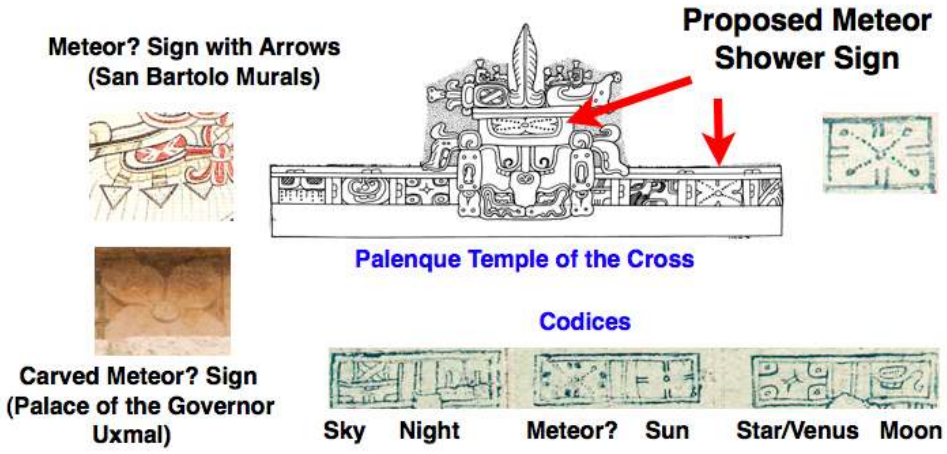

Figure 3. Examples of the k'in sign variant T544v that may signify a meteor shower outburst: Top left: sign with arrows painted on underside of wing of Principal Bird Deity, San Bartolo Murals, circa 100 BC (rendered by Heather Hurst). Bottom left: carving on Uxmal throne inscription, Palace of the Governor, Uxmal, circa AD 900 (photograph by Mauricio Metri Ojeda). Top right: sign carved on Tablet of the Cross, Palenque, on deity G1 forehead and sky band, Classic period (drawing by L. Schele). Bottom right: k'in sign variant contrasted with simple k'in, "sun/day" sign, Dresden codex, late Post-Classic period.

Having a variant of the day or sun sign representing a mostly night-time event may seem contradictory, but there may be a reasonable explanation. First, as noted above, the scarlet macaw was responsible for the meteors from the area of the Pleiades, and the radiants for both the Perseid and Orionids meteor showers are in that vicinity. The macaw, in the form of *Kin-ich-kak-mo* ("sun-eye-fire-macaw"), was also the idol of sun worship at Izamal, where a great number of citizens would bring offerings in times of pestilence (Lizana, Historia de Yucatan. f.4v referenced in Roys 1965:137). The fire of the meteor may have been equated to the fire of the sun, hence the combination.

4. Methodology

The author chose 16 of 34 historically observed showers from China, Korea, Japan and Europe (Jenniskens 2006:598-611, Table 1) for comparison to candidate shower dates in the Maya inscriptions. Since most dates in the Classic Maya inscriptions occur between AD 400 and 900, and many dates recorded in the codices appear to be events that have already occurred from about 700 to 1000, 15 of the 16 historical showers chosen for comparison were observed prior to AD 1000. Shower 15 was an exception as discussed later.

Figure 4 depicts meteor showers that the Maya may have observed arranged according to solar longitudes about a circle. The circular diagram shows the Earth's anti-clockwise direction around the Sun (plan view of the ecliptic plane). Solar lon-

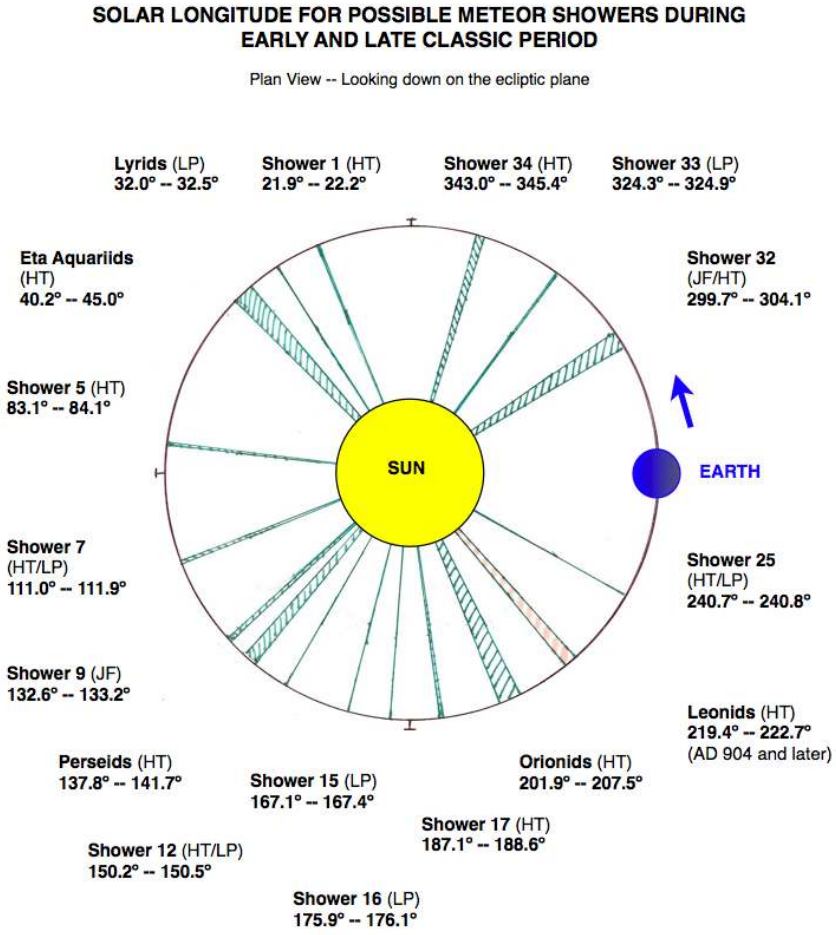

Figure 4. Depiction of solar longitudes of 16 meteor showers that possibly may have been observed by the Maya before AD 1000 (diagram by author)(data from Jenniskens 2006:598-611, Table 1). The Leonids would have only been observed in AD 904 and later (Jenniskens 2006:619, Table 4a).

gitudes measure from the Earth to the Sun using the J2000 reference for the vernal equinox.

Solar longitudes were calculated for known dates in the codices associated with and without the dotted *X* kin sign to see if a correlation could be found to historically observed meteor storms. The number of days that showers or outbursts from 16 individual showers could be observed amounts to about 36 days, or about 10 percent of the days of a year. Candidate showers fell within the solar longitude and chronological limits with an accompanying text descriptive of a possible meteor event (all dates Julian Calendar, UT, unless otherwise noted).

5. Results

Besides the positive results listed in Table One, several groups of data not included in this analysis had little or no correlation. One group concerned the so-called "star wars" glyph, a glyph indicating a war event. Scholars have suggested that it was related to meteor showers because of droplets that appeared to fall from a "star" glyph (Aldana 2005:313, 314). The author however found zero correlation to any of those 27 dates and near zero in reference to a set of 27 dates involving fire rituals (Grube, 2000:103-104). In a third set of 94 dates at Yaxchilan (Tate 1992:271-274), the author found only 4 definite possibilities and 9 dates that had some possibility, i.e. greater than 0.5 degrees and less than 1.0 degree outside of the range of a long-period shower, and greater than 1.0 degree and less than 2.0 degrees outside the range of a Halley-type or Jupiter-family comet.

Table One shows candidate showers considered in this study, both from Classic inscriptions and the codices. All of the codical examples contain text that could be considered descriptive of a meteor storm or its perceived potential for damage. Table One notes are found below.†

6. Analysis: Does the K'in Variant in the Sky Band Indicate a Meteor Shower?

The first set of data is analyzed from Table 2 in terms of the dotted *X* k'in sign found in the sky band, although not all candidates contain a sky band nor the sign itself. In an original sample size of 15 possible candidate showers, 3 samples (nos. 16, 22 and 23) were discarded due to uncertainties in dating and the meteor sign leaving n = 12. First, considering only the sky bands that contained the possible meteor sign, n = 8 (nos. 2, 7, 8, 15, 20, 18, 14 and 21), four (nos. 7, 8, 20 and 18) out of the 8 were acceptable. Two samples were associated with Shower 25, which hasn't yet been determined to be Halley-type or long-period. If Shower 25 is long-period, the solar longitude for each sample is deemed either one degree too high

† a. The date of 736 July 24 (Maya Long Count 9.15.5.0.0) is also recorded on Bench XXI at Palenque; all Ahkal Mo' Nahb III events in Table 1 occur on Temple XIX. b. dates for candidates taken from other than the first row of the table: no. 8, Dresden 45b1, row 6; no. 21, Dresden 39a1, row 20. c. The author translates *y-a-ek'* "of the cosmological throne" as "rain-stars" or "meteors" of the cosmological throne," whereas MacLeod translates the same phrase as "crocodile throne" (personal communication, 2013). d. The author translates *ch'o[j]* as "pierce, perforate, be pierced" from the Mayan language Tzotzil (Laughlin, 1975:137) and Ch'ol, *ch'ojch'on*, "to peck something," (Hopkins and Josserand, 2011:53). e. Both paintings depict what has been suggested as hanging textiles; in the historical record, 19 of the shower descriptions use the term "weaving" and one "fabrics of silk" (Jenniskens, 2006:598-611, Table 1). f. The author discards these two showers due to uncertainty in dating, i.e. almanac 33c-39c has no Maya Long Count anchor (as found in tables in the codices) and the fact that the almanac most likely refers to the 16th century, out of the scope of the author's analysis. g. Two k'in sign variants are located in the sky band on the top of the Sarcophagus lid; dates of deaths (or apotheoses) of several kings are carved on the edges of the lid. h. The k'in sign variant is recorded in the sky band and forehead of GI on the Tablet of the Cross. i. The author considered the possible k'in variant found in the sky band too dissimilar to be included in the data analysis.

Table 1. Meteor shower candidates (correlation constant 584286) found in the codices with and without k'in sign variant, including Classic inscription dates. Shower 1 was not recorded in the historical record after AD 581 and the Shower 25 type is uncertain (long-period or Halley-type). Shower 15 was not noted in the historical record before AD 1037, but its possible occurrence in 731 would be (28)(11.86yr) prior to observed 1063; Jenniskens states that this shower is periodic with the 11.86 year period of Jupiter (Jenniskens 2006:603). Showers marked with "x" may have uncertain dates after AD1500. λ = solar longitude in degrees. Explanations for notes found in footnotes.

No	λ	Date	Meteor Shower	Event	Location	Sign?	Notes
1	22.6	959 Mar 24.3	Shower 1?	"Fire from the sky of Rain god (Chahk). It is chopped."[Chahk with shield and holding torches]	Dresden 36a3	No	
2	43.1	959 Apr 14.3	Eta Aquariids	[Deity (Pawahtun?) with axeand bag standing in rain]	Dresden 37a2	Yes	
3	137.7	156 July 16.3	Perseids	Undeciphered (non-Maya)	La Mojarra St 1	No	
4	141.4	570 July 23.3	Perseids	Apotheosis of Ahkal Mo' Nahb II	Palenque	Yes	g
5	139.7	690 July 22.3	Perseids	Burning of heavenly location?	Palenque	Yes	h
6	141.7	736 July 24.3	Perseids	Ahkal Mo' Nahb III, last event; in the presence of GI Triad Deity	Palenque	No	a
7	139.9	775 July 23.3	Perseids	"(It is) his fire from the sky (of) four macaw place... [macaw holding torches]	Dresden 40b2	Yes	
8	140.5	819 July 24.3	Perseids	"Beast" is chopped. Injury to Lord Fire Macaw-? ?? Death to Maize deity	Dresden 45b1	Yes	b
9	141.3	933 July 25.3	Perseids	[macaw holding torches]	Madrid 12a3	No	
10	167.2	731 Aug 20.3	Shower 15?	Ahkal Mo' Nahb III, event involving G1	Palenque	No	
11	203.3	724 Sep 25.3	Orionids	Ahkal Mo' Nahb III, receives "rain-stars"? of cosmological throne in presence of GI, GII, GIII	Palenque	No	c
12	208.3	775 Oct 1.3	Orionids	Unknown event caused by meteor storm? [Moon goddess hangs by neck under sky band]	Dresden 53b Picture 6	No	
13	204.9	874 Sep 28.3	Orionids	Event: K'awiil combined with GI with Heron headdress	Seibal Stela 3	No	
14	239.3	764 Oct 31.3	Shower 25?	Red/great water/rain over Earth/caves	Dresden 56a Picture 3	Yes	
15	241.9	949 Nov 4.3	Shower 25?	Step/foot? of Rain god Chahk?. Earth/sky is pierced?	Dresden 66a2	Yes	d
16	291.7	949 Dec 23.3	none	Bolon K'uhul Yok Te'..,?	Dresden 68a3	?	i
17	302.4	722 Jan 01.3	Shower 32	Ahkal Mo' Nahb III accession to kingship	Palenque	No	
18	302.3	762 Jan 01.3	Shower 32	Meteor storm? sky, Earth Damage to Man, Earth, caves, sky	Dresden 55a Picture 2	Yes	e
19	324.1	779 Jan 23.3	Shower 33	Damage to sky, earth. Governed by Lady Moon. [Textile? hangs from sky band]	Dresden 54b Picture 7	No	e
20	345.4	950 Feb 14.3	Shower 34	(same event as number 15	Dresden 66a2	Yes	
21	344.8	964 Feb 14.3	Shower 34	(eroded) Rain god (Chahk) fire at? cave place. [Dog/oppossum? holds flaming torches]	Dresden 39a1	Yes	b
22	x	1517?	x	Vulture in text [Rain god Chahk in rain with axe and fish]	Dresden 37c2	Yes	f
23	x	1517?	x	Vulture head in text [Rain god Chahk in rain with axe]	Dresden 39c1	Yes	f

Table 2. Meteor shower candidates from the codices. "Success?" refers to positive candidate.

No	Codex	Sign?	Shower	Valid?	Sky Band?	Comment	Year	Type	Success?
2	Dresden 37a2	Yes	Eta Aq.	?	Yes	storm in 964?	959	HT	
7	Dresden 40b2	Yes	Perseids	Yes	Yes	related to no. 9	775	HT	Yes
8	Dresden 45b1	Yes	Perseids	Yes	Yes	row 6	819	HT	Yes
9	Madrid 12a3	No	Perseids	Yes	No	China 933	933	HT	
15	Dresden 66a2	Yes	25?	?	Yes	2 dates for 66a2	949	HT/LP	
20	Dresden 66a2	Yes	34	Yes	Yes	2 dates for 66a2	950	HT	Yes
18	Dresden 55a	Yes	32	Yes	Yes	Picture 2	762	JF/HT	Yes
14	Dresden 56a	Yes	25?	?	Yes	Picture 3	764	HT/LP	
12	Dresden 53b	No	Orionids	Yes	Yes	Picture 6	775	HT	
19	Dresden 54b	No	33	Yes	Yes	Picture 7	779	LP	
1	Dresden 36a3	No	1?	?	No	not seen after 581	959	HT	
21	Dresden 39a1	Yes	34	No	Yes	row 20	964	HT	
16	Dresden 68a3	?	none	No	Yes	meteor sign??	949		
22	Dresden 37c2	Yes	?	No	Yes	Uncertain	1517?		
23	Dresden 39c1	Yes	?	No	Yes	Uncertain	1517?		

or too low. If Shower 25 is a Halley-type, the two samples are acceptable, yielding 6 out of 8. Sample number 21, Dresden 39a1 is considered unacceptable because a shower does not correlate until the table reaches row 20. Four samples (37a2, 36a3, 39a1 and 68a3) come from the spliced table Dresden 32a-39a, considered somewhat ambiguous since the two spliced sections overlap in dates (Bricker and Bricker, 2011:647). Sample 37a2 correlates to the Eta Aquariids but the translation is unreliable. An additional sample (37a3, not shown nor considered) correlates to the Perseids date but the drawing, sky band, or text seem unrelated to a shower. Sample 8, Dresden 45b1, a Perseid which correlates at row 6 is considered acceptable as explained later. In summary, the success rate is 4 out of 8, or about 50 percent. Therefore, if one finds a dotted *X* k'in variant in a sky band with a descriptive drawing and text possibly relating to a meteor shower or storm, one could expect to have a date that would coincide with a meteor shower about half of the time. If in the future Shower 25 is found to be a Halley-type, the success rate jumps to 6 out of 8, or about 75 percent. Further, if it is determined in the future that Shower 34 is valid for row 20 for page 39a1 of the Dresden table, the number increases to 87 percent.

7. Analysis: Four Candidates in the Pictures of the Dresden Eclipse Table, Pages 51-58

Scholars agree that the table on pages 51 through 58 is an eclipse table, but whether mostly solar (Bricker and Bricker, 2011:249-342) or lunar (Aveni, 2001:173-184) or undecided (Love, 1994:91) is still under debate. Ten "pictures" or drawings are spread throughout the table as an expansion of certain columns, though not part of the counting sequence itself, and seem to record events already completed. The author bases this interpretation in part on the grammatically "perfect" statements *u-kabijiiy/chabijiiy*, "he/she has caused/governed it," (MacLeod, 2004:291-325) that

appear in the text of four of these pictures. Dates associated with four of the pictures, 2, 3 (with a caveat for Shower 25 as discussed above), 6 and 7 coincide with historical meteor shower solar longitudes, well above the one out of ten statistical average. Pictures 2 and 3 have sky bands while pictures 6 and 7 do not, although all four have text and iconography that indicate death, disease and destruction that are consistent with beliefs about meteors mentioned earlier in this paper.

The possibility that the Maya recorded Shower 32 (Picture 2) seems more than coincidental since both Showers 32 (Table 1) fall within the less than 100 year historical record between AD 685 and 764. The showers of January 685, 743, 745 and December 764 combined with the Maya candidates of January 722 and 762 seem to indicate a shower with about a 20 year period. If Kresáková (1987:935-936) is correct that this shower may have been caused by a comet that appeared in December 684/January 685 (observed in Japan and Europe), that might preclude a prediction by the Maya, especially in 722. Picture 3 concerns Shower 25 which is discussed above, although the table seems to allow an adjustment of a day either way. The plausibility that this shower is described as "red or great rain" is credible since one third (118 of 357) of the historical records use the word "rain" in describing falling stars. Picture 6 depicts a deceased female deity hanging from a sky band. The author translates the first line of the text *ch'a?pahal* as "sickness, disease, possibly contagious," (Barrera, 1980:126), possibly caused by meteors as indicated in the last line of text. This shower would have been Orionids, recorded in AD 288, 585, 903 and 930 prior to AD 1000 (Jenniskens, 2006:604). Picture 7, correlating to long-period Shower 33, seems to record damage to the earth and sky although the cause is not clear due to poor understanding of the text. The shower may be indicated by what has been called a textile suspended beneath the sky band. Moonlight would not have been a factor under a new Moon. In summary, the author believes it plausible that Pictures 2, 6, 7 and possibly 3 are records of meteor storms.

8. Analysis: The Perseids, including events at Palenque

The ruler of Palenque Ahkal Mo' Nahb III recorded his last event on the stone platform in Temple XIX on AD July 23, 736 (local), 9.15.5.0.0, 10 Ahau 8 Ch'en, a date that precisely coordinated with the "road-entering" (death or apotheosis) of Ahkal Mo' Nahb II on 9.6.16.10.7, July 22, 570 (local), exactly 166 sidereal Earth years earlier (365.259 days per year, 365.256 actual). The difference between these two dates, 60,633 days, also equals 14 sidereal cycles of Jupiter (4330.929 days, 4332.589 actual) and 152 synodic cycles of Jupiter (398.901 days, 398.88 actual). These two dates in 570 and 736 also correlate to Perseid solar longitudes of 141.4 and 141.7 degrees respectively when Jupiter was positioned in the constellation Virgo. Grofe (2011:85) demonstrates that the Maya knew the length of the sidereal Earth year and may have tried to keep track of it by adding 23 whole days to 90 Haabs of 365 days to reach 90 sidereal years: (90 x 365) + 23 = (90 x 365.2555556). Similarly, in the case of 166 years between 570 and 736, the sidereal year can also

be calculated by adding 43 days to 166 Haab's (one Haab' = 365 days):

60,633 days = (166 Haab's)(365 days/Haab') + 43 days = (2)(83)(365) + 43 = 60,590 days + 43 days = 8.8.5.10 + 2.3 = 8.8.7.13 = (166 sidereal years)(365.259)

The equation is interesting for a couple of reasons. The event immediately prior to 9.15.5.0.0 occurred 43 days earlier inscribed as 6 Kaban 5 Yaxk'in (9.15.4.15.17), a "fire-entering" event. Remarkably, then, counting forward from 9.6.16.10.7, the "road-entering" of Ahkal Mo' Nahb' II in 570, exactly 166 Haab's, or 60,590 days = 8.8.5.10, one arrives at 9.15.4.15.17, the exact date of the "fire-entering" event. Adding another 43 days leads to 9.15.5.0.0, just as in the above formula. The translation of this fire-entering passage is problematic, although Stuart suggests (2005:104-106) it may involve the *o'* bird mentioned in the Ritual of the Bacabs. The *o'* bird is noted in traveler-seizure as being the offspring of the Pleiades (Roys, 1965:9), perhaps a direct reference to the Perseids. First recorded by China in AD 36, the Maya undoubtedly observed the strong annual Perseids regularly (Jenniskens, personal communication 2013). At a normal Zenith Hourly Rate of about 100 meteors and twice that during an outburst (Jenniskens, 2006:649, Table 5c), the Maya would have been interested in predicting future outbursts. In their discussion of the heliocentric sidereal period of Mars and the Upper Water Table of the Dresden codex, the authors state that they know of no reason why the Maya would be interested in such a period [sidereal] (Aveni, et al, 2003:158), yet in the above scenario, the Maya may have been demonstrating the relationship between the sidereal cycle of Jupiter and the Perseid storms and thought that the position of Jupiter was connected to outbursts of the Perseids. Jupiter, in fact, does steer the dust trails [Perseids] of the parent comet 109P/Swift-Tuttle [Jenniskens, 2005:272]).

Continuing with half of the above values, one arrives at a formula using 83 Haab's + 21.5 days that tracks 83 sidereal Earth years and 7 sidereal and 76 synodic cycles of Jupiter:

(83 Haab's)(365 days per Haab') + 21.5 = (83)(365.259) = (7)(4,330.929) = (76)(398.901) = 30295 + 21.5 = 4.4.2.15 + 1.1 (and a half) = 30316.5

Aveni actually derives nearly the same number, 30,316 in a hypothetical exercise deriving the sidereal cycle of Jupiter (2001:87-89). Projecting forward from AD 736, the Maya may have been able to forecast another outburst of the Perseids:

(83 Haab's)(365 days per Haab') = 30,295 days = 4.4.2.15 days;
Long Count 9.15.5.0.0 + 4.4.2.15 days = Long Count 9.19.9.2.15

Interestingly, the date 9.19.9.2.16 is found in column one, row six of the "Mars" table, Dresden pages 44b and 45b. A 19 day interval follows in column two, leaving only 1.5 days short that the Maya would have needed to arrive at 7 sidereal Jupiter cycles and 83 sidereal Earth years. That date in column 2 corresponds

to 9.19.9.3.15, July 23, 819 (local), another possible Perseid storm date at a solar longitude of 140.5 degrees. Although the question of whether the Maya Long Count changed at sunset or sunrise is beyond the scope of this paper, they may have changed over 9.19.9.2.15 to 9.19.9.2.16 at sunset because the event occurred at night and accepted that the Long Count was about a day short in the following column. Only two dates out of 40 total in the Mars table coincide with solar longitudes of actual historical showers, and the text reads in part, "it is destruction to Fire Macaw and death of the Maize deity." The 83 year pattern in the Perseids is also evidenced by China observations in AD 841 and 924 and Japan in 1007 (Jenniskens, 2006:601).

There is another interesting relationship between two Perseid candidates in cognate eclipse almanacs, Dresden 38b-41b and Madrid M10a-13a. In his discussion of these two instruments, Tony Aveni raises the questions of why the intervallic sequences might be different between the two and "can astronomical knowledge incorporated in one almanac be used to date its cognate?" (2004:152). In fact, the adjusted intervallic count in each almanac produces the Perseids date in frame 8 (H) in each almanac, July 23, 775 in the Dresden and July 25, 933 in the Madrid. In the historical tables China recorded the Perseids only hours later on July 25, 933. Drawings in both almanacs depict an anthropomorphic macaw holding a torch in each hand and the text states "it is fire from the sky of four macaw place" (figure 5).

Another Perseid event may have been recorded at Palenque on Maya date "2 Kib 14 Mol," July 22, 690. Highly important but problematic (but see Stuart, 2006:96-98), this "burning" event of possibly a heavenly location involved the Triad Deities GI, GII and GIII followed by "three-times conjuring" the next day. GI or all the Triad Deities are connected to all four major events of Ahkal Mo' Nahb' III's reign with possible connections to meteor showers. Given the "road-entering" of Ahkal Mo' Nahb' II on a Perseid date in 570, it seems the Maya would have been well aware of the Perseids in 690 and "burning and conjuring" are terms associated with meteors in the incantations.

Ahkal Mo' Nahb' III acceded into kingship over 30 years later on a date corresponding with Shower 32. In fact, four of the major events during his reign occurred on dates of possible meteor showers: Shower 32, the Orionids, Shower 15 and the Perseids, statistically a very unusual occurrence. One wonders whether his name itself wasn't related to meteor showers, as the Orionids radiant is near Orion the turtle *Ahkal* and the Perseid radiant is near the Pleiades connected to *Mo'*, "macaw" as discussed earlier. Indeed "Nahb'" may be a homophonic reading for *naab'*, "rain" in a few of the Mayan languages (Kaufman with Justeson, 2003:482).

9. Conclusions

The author believes the Maya recorded at least three Perseid meteor showers: Dresden 40b2 (AD 775), Madrid 12a3 (AD 933, quite possibly the same event recorded by the Chinese only hours later), and the "2 Kib 14 Mol" event in AD 690

Figure 5. Frames 8 (H) from each of cognate almanacs Dresden 38b-41b and Madrid 10a-13a displaying anthropomorphic macaws holding torches on possible Perseid meteor shower dates.

recorded at the Classic site of Palenque. A strong probability exists that the AD 819 date recorded in the Dresden Mars table in row 6, page 45b1 is a prognostication for a Perseid storm derived from a formula for the sidereal Earth year and sidereal cycle of Jupiter from possible Perseid outbursts in AD 570 and AD 736 recorded at Palenque. In the codices there is about a 50 percent (4 out of 8 candidates) chance of a meteor storm indicated by the k'in variant in the sky band, somewhat low due to Shower 25 type uncertainty. There is some likelihood of 3 or 4 occurrences of meteor storms recorded in the group of 10 pictures in the Dresden eclipse table (D.51-D.58), although better translations are needed in the accompanying texts; the verification of a strong Orionids meteoroid stream in AD 775 (Picture 6) might increase this likelihood. The possibility of meteor storms being recorded during Ahkal Mo' Nahb' III's reign remains high, though increased understanding of the associated texts and again a verification of a stronger Orionids meteoroid stream in AD 724 would raise this probability. The resultant solar longitudes for the Perseids (see Table 1) very close to the peak solar longitude of 140.19 degrees may serve to verify the correlation constant of 584286, though this may not discount 584285 due to the meteor showers being a night event; however the use of a 584283 constant may be sufficiently low to render the results of this study questionable.

Acknowledgements

I would like to thank Dr. Tony Aveni and Dr. Harvey M. Bricker for reviewing an earlier draft of the paper, Dr. Barbara MacLeod, Dr. Carl Callaway, Dr. Michael Grofe and Dr. Peter Jenniskens for valuable comments and acknowledge the kind invitation extended by Dr. Jenniskens and Dr. Tadeusz Jopek to present at the 2013 Meteoroids Conference.

References

Aldana G., 2005, Agency and the "Star War" Glyph: A Historical Reassessment of Classic Maya Astrology and Warfare, Ancient Mesoamerica, 16 (2005), 305, Cambridge U. Press

Aveni A. F., 2001, Skywatchers: A Revised and Updated Version of Skywatchers of Ancient Mexico, University of Texas Press, Austin

Aveni A.F., 2004, Intervallic Structure and Cognate Almanacs in the Madrid and Dresden Codices, in *The Madrid Codex: New Approaches to Understanding an Ancient Maya Manuscript*, Eds. Vail, G. and Aveni, A., University Press of Colorado, 2009

Aveni A.F., Bricker H.M., Bricker V.R., 2003, Seeking the Sidereal: Observable Planetary Stations and the Ancient Maya Record. *Journal for the History of Astronomy* 34:145-161.

Barrera Vásquez A., Vermont S.R., Dzul G.D., Dzul P.D., 1980, Diccionario Maya Cordemex, Merida, Yucatán

Bricker H.M. and Bricker V.R., 1996, Astronomical References in the Throne Inscription of the Palace of the Governor at Uxmal, Cambridge Archaeological Journal, 6, pp 191-229 doi:10.1017/S0959774300001712

Bricker H.M. and Bricker V.R., 2011, Astronomy in the Maya Codices, Amer. Phil. Society

Christenson A. J., 2007, *Popol Vuh: Literal Translation.* Electronic version of original 2004 publication. Mesoweb: `www.mesoweb.com/publications/Christenson/PV-Literal.pdf`

Gates W., 1937, Yucatan Before and After the Conquest by Friar Diego de Landa (1566), with other related documents, maps and illustrations, translated with notes by William Gates, Dover Publications (1978)

Grofe M. J., 2011, The Sidereal Year and the Celestial Caiman: Measuring Deep Time in Maya Inscriptions, Archaeoastronomy, Vol XXIV

Grube N., 2000, Fire Rituals in the Context of Classic Maya Initial Series, in *The Sacred and the Profane: Architecture and Identity in the Maya Lowlands*, eds Colas P.R., Delvendahl K., Kuhnert M., and Schubart A., Acta Mesamericana, Vol. 10, pp. 93-110, Berlin.

Hopkins N.A. and Josserand K.J., 2011, A Historical Dictionary of Chol (Mayan), Electronic document at `www.famsi.org/mayawriting/dictionary.htm`

Imoto S. and Hasegawa I., 1958, Historical Records of Meteor Showers in China, Korea and Japan, *Smiths. Contra. Astrophys.*, 2, 131 (updated in 1993)

Jenniskens P., 2006, Meteor Showers and their Parent Comets, Cambridge University Press

Kaufman T. with Justeson, J., 2003, A Preliminary Mayan Etymological Dictionary, Electronic document at `www.famsi.org/mayawriting/dictionary.htm`

Kennett D.J., Hajdas I., Culleton B. J., Belmecheri S. et al., 2013, Correlating the Ancient Maya and Modern European Calendars with High-Precision AMS 14C Dating, Scientific Reports, 3:1597, DOI:101038/srep01597

Kresáková M., 1987, Associations between Ancient Comets and Meteor Showers, A&A, 187

Laughlin R. M., 1975, The Great Tzotzil Dictionary of San Lorenzo Zinacantan, Smithsonian Institution Press

Lenkersdorf C., 2010, Diccionario tojolabal-español 1: idioma mayense de Chiapas, Electronic document, www.webislam.com/media/2011/10/45269

Love B., 1994, The Paris Codex: Handbook for a Maya Priest, University of Texas Press, Austin

MacLeod B., 2004, A World in a Grain of Sand: Transitive Perfect Verbs in the Classic Maya Script, in *Linguistics of Maya Writing*, Ed. Wichmann S., University of Utah Press, Salt Lake City

Macri M. J. and Looper M. G., 2003, The New Catalog of Maya Hieroglyphs, Volume One: The Classic Period Inscriptions, University of Oklahoma Press, Norman

Martin S. and Skidmore J., 2012, Exploring the 584286 Correlation between the Maya and European Calendars, The PARI Journal 13(2), 2012, p. 3

Roys R. L., 1965, Ritual of the Bacabs: A Book of Maya Incantations, (translator and editor), University of Oklahoma Press, Norman

Stuart, D., 2005, The Inscriptions from Temple XIX at Palenque: a Commentary, The Pre-Columbian Art Research Institute

Stuart D., 2006, Sourcebook for the 30th Maya Meetings, UT Austin

Tate C., 1992, Yaxchilan: The Design of a Maya Ceremonial City, University of Texas Press, Austin

Taube, K., 2000, The Turquoise Hearth: Fire, Self-Sacrifice, and the Central Mexican Cult of War, in *Mesoamerica's Classic Heritage: from Teotihuacan to the Aztecs*, Eds. Carrasco, D., Jones, L., and Sessions, S., University of Press Colorado 2002

Thompson J. E. S., 1962, A Catalog of Maya Hieroglyphs, University of Oklahoma Press, 1991

Vail G. and Hernandez, C., 2013, *The Maya Codices Database, Version 4.1.* A website and database available at http://www.mayacodices.org/

Yeomans D. K., 1991, Comets: A Chronological History of Observation, Science, Myth, and Folklore, John Wiley and Sons, Inc., New York

PART 3

Physical and chemical properties of meteoroids, micrometeoroids and dust

Meteoroids 2013, Proceedings of the Astronomical Conference,
held at A.M. University, Poznań, Poland, Aug. 26-30, 2013,
eds Jopek T.J., Rietmeijer F.J.M., Watanabe J., Williams I.P.,
Adam Mickiewicz University Press in Poznań, pp 105–116

Meteor emission spectroscopy: clues on the delivery of primitive materials from cometary meteoroids

Trigo-Rodríguez J.M.

Meteorites, Minor Bodies and Planetary Sciences group, Institute of Space Sciences (CSIC-IEEC), Campus UAB, Torre C5 parells, 2ond. floor, 08193 Bellaterra, Barcelona (trigo@ice.csic.es)

Abstract. Meteor emission spectroscopy is an useful technique to infer bulk chemistry properties of meteoroids. Even for a spectrum calibrated on a relative scale, valuable chemical information about the meteoroid can be inferred. Obviously, the determination of the chemical abundances requires having into account the right physical parameters. A model assuming thermal equilibrium in the meteor head, and computing the radiating volume as a prism is created using four free parameters: temperature, column atom density, surface area, and damping constant. By directly comparing the intensity of Fe lines in the recorded spectrum with a synthetic one, the density of Fe atoms in the meteor column will be determined. Once the fit is established for Fe lines, the abundances of the other elements are changed until reaching a general match between both spectra: the recorded and the synthetic one. That procedure developed by J. Borovička allows to get reliable chemical abundances from meteoroids ablating in the Earth's atmosphere. Currently, several programs around the world study the chemical properties of meteoroids ablating in Earths atmosphere. By using diffraction gratings in front of the optics of video cameras is then possible to infer chemical abundances for the main rock-forming elements. Current state-of-the-art meteor recording instruments can obtain meteor spectra with the needed spatial resolution to gain insight into the chemistry and physical processes at work in meteor columns. Then, a general review of current meteor spectroscopy achievements and future challenges is presented.

Keywords: meteoroids, meteors, fireballs, emission spectrum, emission lines, multiplets, chemical abundances, IDPs, chondrites

1. Introduction

The space between the planets is populated by billions of particles from very diverse sources following heliocentric orbits. This system is in constant replenishment because mm-sized meteoroids tend to fall into the Sun in timescales of tens of millions of years (Ma) as consequence of the loss of kinetic energy caused by non-gravitational effects (Nesvorny et al. 2002). Obviously, the interplanetary space needs to be continuously replenished by small fragments that we call meteoroids. A meteoroid was defined by the International Astronomical Union (IAU) as a particle larger than a micron and smaller than ten meters in diameter following a heliocentric orbit in our Solar System. Most meteoroids are originated from the natural evolution of minor bodies: asteroids and comets.

They are mostly released from asteroids by impacts, while outgassing is the force driving cometary meteoroids to heliocentric orbits. Other dynamic mechanisms to drive meteoroids into heliocentric orbit are at work in the near-Earth region (Trigo-Rodríguez et al. 2007; Jopek & Williams 2013).

It is not surprising the importance of comets because they are fragile undifferentiated objects formed in the outer solar system and composed by a mixture of ices, organic materials and mineral grains (Brownlee et al. 2006). These volatile-rich objects suffer significant ice sublimation when approaching to the Sun. Then, volatile-rich regions produce jets of gas that drive out tons of meteoroids with diameters from dm- to tens of microns. These meteoroids are forming meteoroid streams that can be studied for centuries in order to gain insight into the physico-chemical properties of their parent bodies.

These particles are subjected to interplanetary collisions that disrupt them into their constitutive mineral grains with typical diameters of few microns that are considered dust. Then, the interplanetary space is populated by meteoroids originated by collisions between small bodies or planets, cometary outgassing, catastrophic disruption of rubble-piles, and from rocks escaped from planetary bodies like e.g. the Moon or Mars as a consequence of a grazing impact. Consequently, interplanetary meteoroids have very diverse origins, as meteor studies reveal. Then, by obtaining their heliocentric orbits from multiple-station meteor monitoring plus meteor spectra chemical information of their rock-forming elements is possible to better understand the delivery mechanisms and nature of exogenous material to Earth. Meteor spectroscopy is by itself a valuable remote-sensing technique as only a small mass fraction (about a 8%) of meteoroids in the 10 to 50 micron range survive their entry and arrive unaltered to Earth's surface as micrometeorites (Anders 1989).

This paper will summarize the role of emission spectroscopy of meteors and fireballs to gain insight into the bulk elemental chemistry of meteoroids. I will also review the most significant progress made during the last decades. Meteor spectroscopy is certainly an added-value technique for meteor studies.

2. Modern meteor spectroscopy: looking for new clues on meteoroid chemistry

Meteoroids are moving around the Sun at typical velocities of few tens of km/s. Then, they produce a luminous phenomenon called meteor when they encounter a planetary atmosphere. For Earth the relative geocentric velocity range in which meteoroids reach the top of the atmosphere (before suffering significant deceleration) is $11<Vg<72$ km/s (Ceplecha et al. 1998). When penetrating in the atmosphere at these supersonic velocities the meteoroids suffer increasing collisions with atmospheric components (atoms or molecules) and their surfaces are quickly heated by direct collisions. As a consequence, a physical process called ablation produces the vaporization, fragmentation and sputtering of the meteoroid components. From the ground we observe a meteor phenomenon that basically consists of three differentiated parts: the head or region around the meteoroid in which

the interaction is taking place, the wake left just behind and the train or meteor column. The meteor head is the part that mostly contributes to produce light as is the part where the more energetic collisions take place. Then, the head is the main source of emission lines that are produced by ionization of the meteoroid and atmospheric components (Borovička 1993, 1994; Trigo-Rodríguez et al. 2003). The meteoroid-forming minerals are progressively vaporized and the elements are released suffering excitation or/and ionization as consequence of the exposure of the released particles to the collisions produces a cloud of ions, and free electrons forming a significant part of the ablated material. The electrons are transmitting energy, and the ions emit light through well-defined emission lines, while that surviving dust contributes to a continuum emission. In general, emission lines can be reproduced assuming chemical equilibrium, while the emission lines coming from the meteor train are out of equilibrium. This will be explained in further detail in the discussion.

From the very beginning of this field early in the 20th century, several authors used emission spectra to identify distinctive emission lines from rock-forming elements. The light emitted must be decomposed by a prism or diffraction grating set up in front of imaging systems. The emission lines of main rock-forming elements were identified by pioneers (Halliday 1961), but they were not obtaining a clear modelling of the light generation process (see e.g. Harvey (1971); Millman (1980)). First temptative modelling was made by Ceplecha (1964) who developed a complex cylindrical model for the radiating column assuming local thermal equilibrium. In that approach, the theoretical curve of growth was built up, also describing the self-absorption of the lines and obtaining some physical parameters. Unfortunately, the resulting computed number of Fe atoms in the radiating volume and the involved mass determined from the meteor luminous efficiency were not always accurate. On the basis of previous attempts by Z. Ceplecha, a more simple model was created by Borovička (1993) and tested on the excellent Cechtice fireball photographic spectrum. With such extraordinary emission spectrum, also obtained during routine sky monitoring from the Ondrejov Observatory, Borovička (1993) obtained for the first time a computed meteor synthetic spectrum. It adjusted exceptionally well to the observed spectrum although the physical approach was very simple: thermal equilibrium and constant temperature and density in the whole volume. Meteor spectra consists of two different components: the main spectrum characterised by a temperature of about 4,500 K and one second spectra that reaches usually 10,000 K (Borovička 1994; Borovička & Betlem 1997; Trigo-Rodríguez 2002; Trigo-Rodríguez et al. 2003). The second component is originated in the front wave where high-energy collisions can produce the excitation of atoms increasing the ionisation of the meteoroid components (Borovička 1994).

Many other photographic spectra were available in Ondrejov Observatory at the end of the 20th century, and most of them remained not studied. Trigo-Rodríguez (2002) Ph.D. thesis compiled selected ones, and provided an innovative idea to infer the average elementary abundances and temperature of the incoming particles from the sequential study of the meteor spectrum. On Figure 1 appears

an Andromedid fireball produced by a meteoroid associated with disrupted comet 3D/Biela.

The basic idea is simple, most relative abundances of the elements present in the meteor column are many orders of magnitude over the expected in the atmosphere at the meteor ablation height (see e.g. Trigo-Rodrguez et al., 2003, 2004). Previously cited studies show that it is possible to estimate the chemical abundances relative to one reference element (as e.g. Fe that has many omnipresent emission lines) at different heights as (Trigo-Rodríguez 2002; Trigo-Rodríguez et al. 2003). The results were consistent with the abundances of Interplanetary Dust Particles (IDPs), and CI chondrites (CIs) (see figure 3) Then, it is statistically possible to deduce an averaged composition for the meteoroids as is also suggested by an independent test of the inferred Trigo-Rodríguez (2002) chemical abundances as a function of height that were consistent with the ablation of distinctive minerals (Rietmeijer 2004).

The intensity values of each emission lines recorded on Ondrejov's photographic plates was accurately measured by using a microdensitometer (for full details see: Trigo-Rodríguez (2002)). Then, Trigo-Rodríguez et al. (2003) computed for each fireball a synthetic spectrum and compared it directly with the observed one until finding the best match. A model assuming thermal equilibrium in the meteor head, and computing the radiating volume as a prism was built by using four free parameters: temperature (T), column atom density (N), surface area (S), and damping constant (Γ). First, these parameters are changed until finding a good solution for the Fe lines that are almost present all over the visible spectrum. Once the fit is set, the Fe lines are well adjusted in the synthetic model. Then, we should be able to modify the relative abundance of the different elements, one by one, until having the best match (see Figure 4).

Once the model fits the observed spectrum, the physical parameters and the chemical abundances can be determined. What was really new is that Trigo-Rodrguez (2002) derived relative chemical abundances of incoming meteoroids from the sequential spectroscopy of the luminous trajectories of photographic fireballs during their entry into the terrestrial atmosphere. In that work, the averaged chemical abundances for the main rock-forming elements of meteoroids were obtained, and later were discussed in (Trigo-Rodríguez et al. 2003, 2004; Trigo-Rodríguez & Llorca 2007). I discuss in next section the main implications of these works, and compare with recent work by other authors.

Meteor spectroscopy is then a way to deep into the elusive physical processes occurred during ablation of the meteoroid in the atmosphere. It is not only a way to infer bulk elemental chemistry, but also a pathway to know more about the delivery of exogenous materials to Earth. This is because, emission spectroscopy models can provide also evidence on the survival of pristine materials released during ablation. There are some physical processes capable to drive enough energy to the particles to allow them to escape from the heat associated with the shock wave and the wake. Trigo-Rodríguez & Blum (2009) noted that some meteoroids suffer disruptions in the atmosphere, probably direct consequence of the fragile nature of these bodies that are weakly-bonded aggregates formed by fine micron-sized dust, organics and

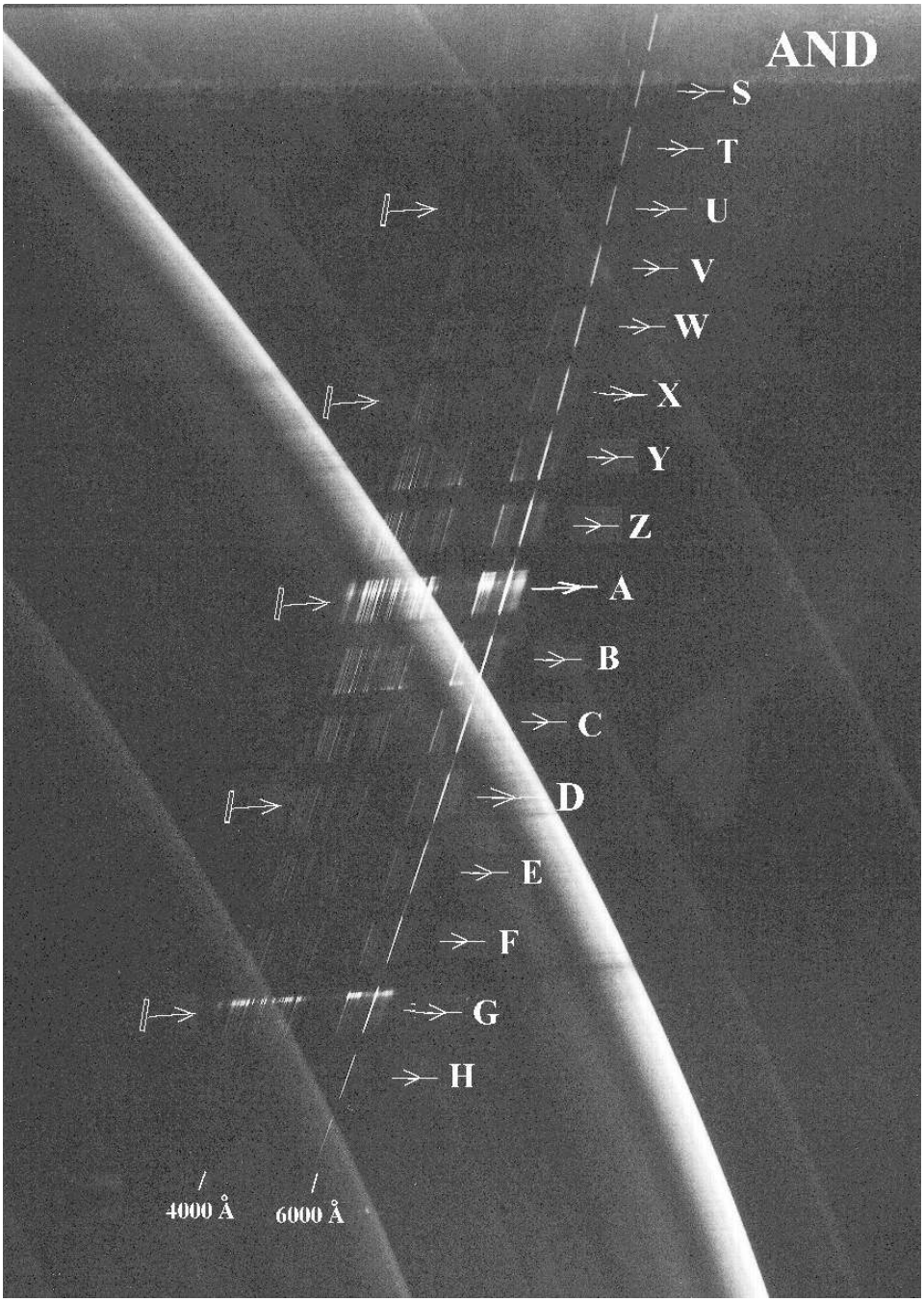

Figure 1. The photographic spectrum of an Andromedid bolide studied by Trigo-Rodríguez (2002). The direction of the different scanning slots made with the microdensitometer are indicated.

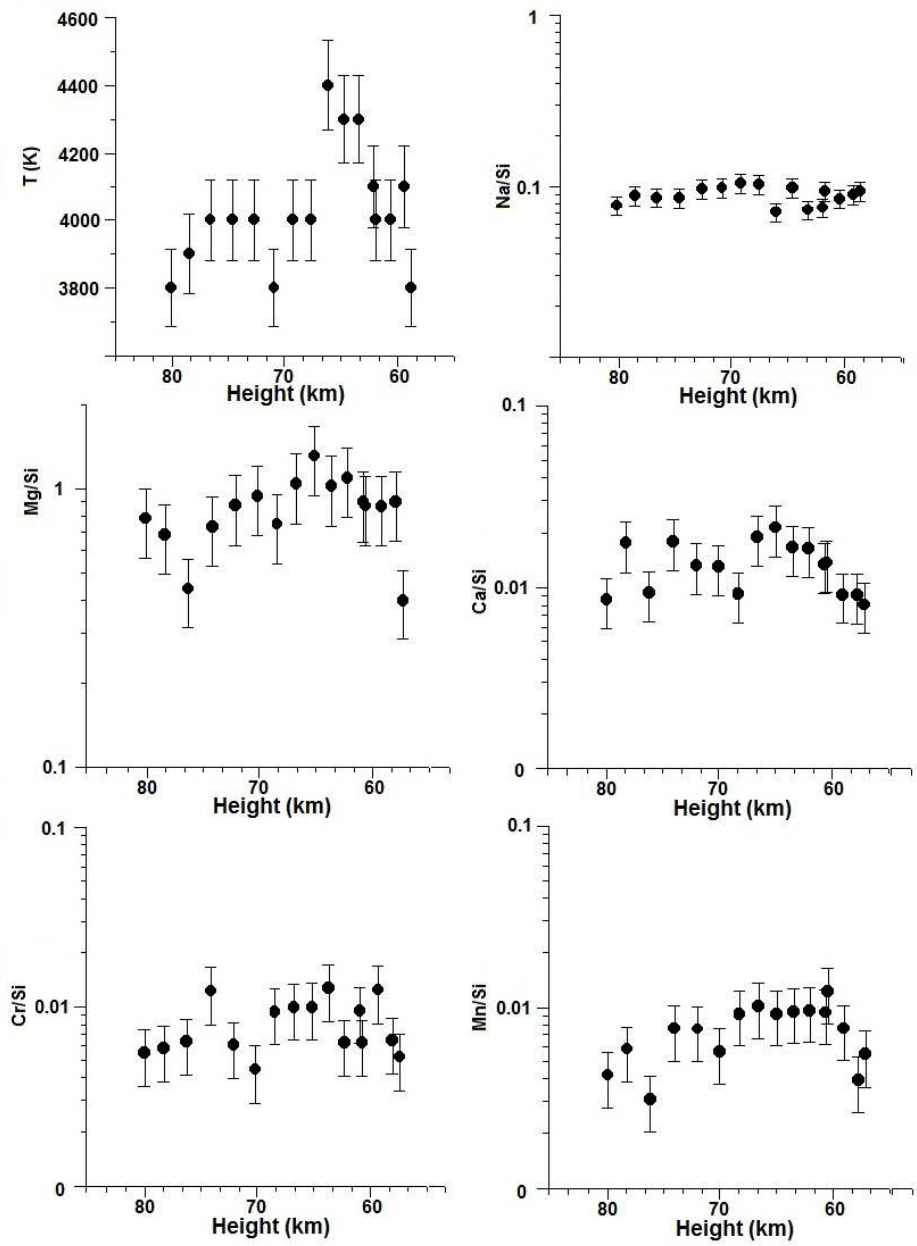

Figure 2. Temperature and relative abundances of main rock-forming elements for an Andromedid bolide studied by Trigo-Rodríguez (2002).

volatiles. Once the tensile strength of the particle is overloaded the particle breaks apart. I think that the study of such disruptive events can be source of scientific

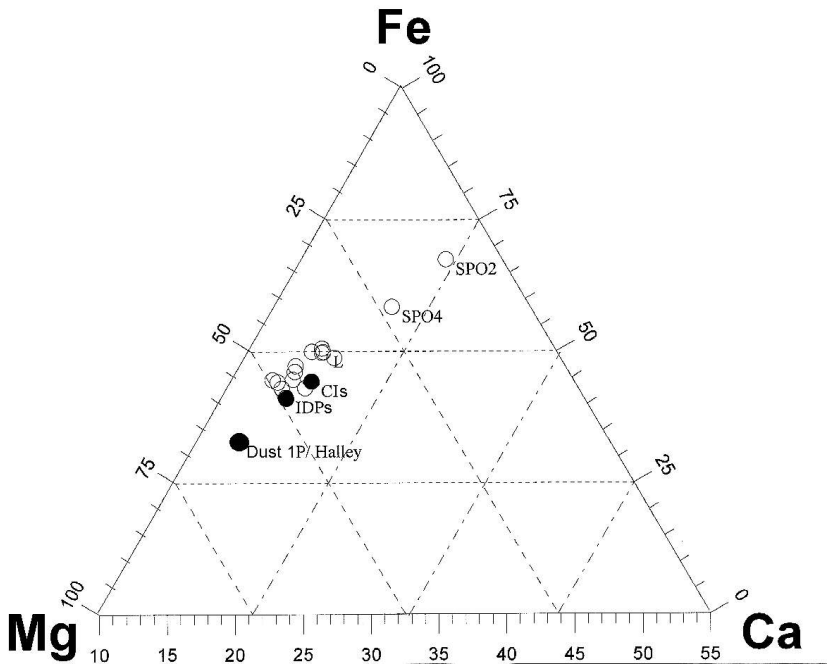

Figure 3. Ternary diagram to show the affinity between the averaged chemical compositions of 13 meteoroids studied from their fireball spectra (open dots), and that corresponding with IDPs and CI chondrites (CIs) as black filled dots. The composition of SPO2 and SPO4, clearly separated in the diagram from the rest of spectra, was probably non-chondritic as inferred from their anomalous Mg content. For more details and implications see: Trigo-Rodríguez (2002); Trigo-Rodríguez et al. (2003).

opportunity because could show the presence of elusive phases associated with volatile compounds.

3. Discussion: survival of meteoroids and future meteor spectroscopy research

Photographic systems were during the 20th century the only way to obtain reliable information, but new CCD and video imaging techniques are providing additional clues on the meteor phenomenon. These systems are far more sensitive than photographic plates and cover a wider wavelengths' window. High-sensitivity video cameras also provide a sequential (frame to frame) evolution of the meteor head, and allows to study the evolution of the ablation. Video can also better separate the wake contribution than photography, and allows to gain insight on the origin of persistent trains (Madiedo & Trigo-Rodríguez 2014). Our continuous monitoring work in the framework on the Spanish Meteor Network (SPMN) is providing medium resolution video spectra of sporadic and stream fireballs from which meteoroid chemical abundances are inferred (see e.g.: Madiedo et al. (2013,b)).

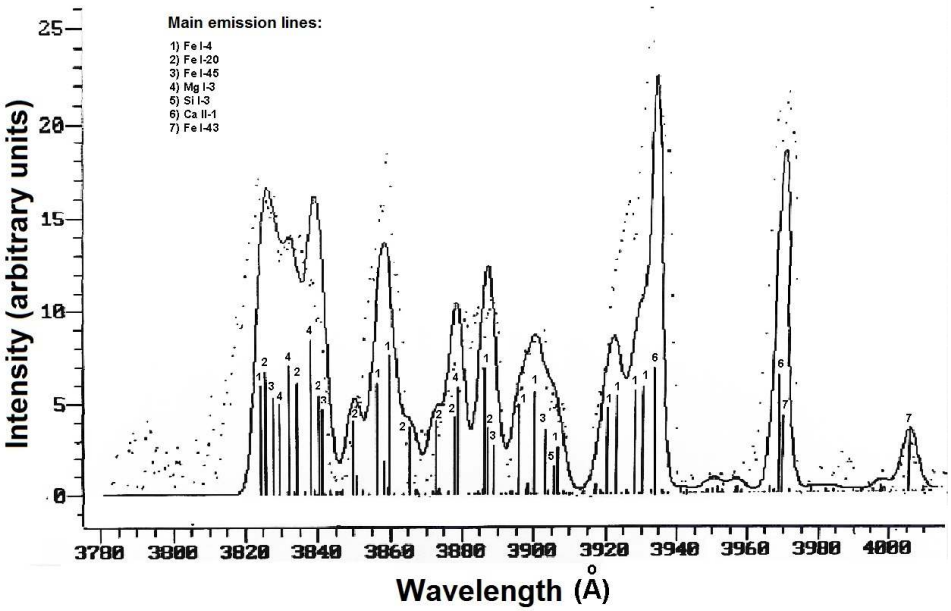

Figure 4. The photographic spectrum (seen here as a discontinuous line) is directly compared in screen with the synthetic one (continuous). At first the intensity of all Fe lines is fitted modifying the free parameters, and after that the relative abundances of the other elements with lines observed. This figure is the final match for the spectrum of a sporadic fireball studied by Trigo-Rodríguez (2002).

Current state-of-the-art instruments can be used to identify elusive bands or radicals in high-resolution meteor spectra, associated with e.g. water and organics. A significant progress and new instrumentation was developed for the Leonid campaigns. The possible decay of organics in meteor columns was e.g. studied by Jenniskens et al. (2004); Jenniskens & Stenbaek-Nielsen (2004). They used high-rate video images that allowed to estimate accurately the cooling rate in the meteor columns. They concluded that insufficient collisions were produced to break apart large organic compounds before most reactive radicals and electrons were lost from the air plasma. It is plausible after all that meteoroid fragments survive if they are in the wake of the meteoroid or its vapor cloud, or if they are decelerated quickly enough by induced backward motion during fragmentation. In reference with water, other studies did not detect the OH Meinel band in meteor spectra produced by 51P/Tempel-Tuttle particles (Jenniskens et al. 2004c). However, that work suggested that a search for water in meteor spectra might also implies looking carefully by the onset of hydrogen atom emission (Jenniskens & Mandell 2004). Such appearance of hydrogen could be evident during fragmentation events in which important amounts of organics could be potentially delivered to the meteor column (Trigo-Rodríguez & Blum 2009; Trigo-Rodríguez & Llorca 2007).

Bright bolides are important sources of radiation and their brightness makes possible the identification of elusive emission lines. Future spectral studies of bolides in the terrestrial atmosphere should focus in detection of key radicals like e.g. the OH Meinel band, or the presence of CN band (Jenniskens et al. 2004c; Abe et al. 2005, 2007). The Leonid campaigns provided significant clues on these radicals and more accurate estimations of the upper detection limit of the CN molecule in the Leonid meteor plasma. It was estimated to be less or equal to one CN molecule per 30 Fe atoms (Jenniskens et al. 2004). Accurate CCD spectra can be also useful to detect and account for the appearance of O lines during meteoroid fragmentation as reported previously (Trigo-Rodríguez et al. 2005).

In the last decade significant papers on meteor spectroscopy have been also published. Some researchers have attempted to get clues on the depletion of moderately volatile elements like e.g. Na. In that sense clear evidence on the onset of thermal desorption for meteoroids exhibiting short perihelion distances was found (Borovička 2005; Kasuga et al. 2006). On the other hand, preferential ablation of moderately volatile elements has been demonstrated to be an evidence of differential ablation in the atmosphere as Na and K are able to evaporate at the beginning of the meteor head at the beginning of ablation (Kokhirova & Borovička 2011).

From our understanding of parent bodies aqueous alteration suffered by chondritic meteorites, Na, K, S or P are also easily mobilized by water from the mafic silicates forming chondrules towards the meteoroid matrix (Trigo-Rodríguez et al. 2006). Consequently, it is possible that the meteoroids exhibit different degrees of Na depletion and several ablation behaviours depending of having Na in the fine-grained matrix that compact the materials or in the chondrules and other inclusions (Trigo-Rodríguez & Llorca 2007). Na-enhancements in cometary-origin meteoroids have been also reported indicating the chemical diversity behind cometary materials reaching the Earth (Trigo-Rodríguez et al. 2004; Borovička et al. 2008).

The study of artificial bolides like e.g. the Hayabusa capsule re-entry (Abe et al. 2011) is also relevant for meteor studies. Such re-entry events are very important to gain insight into light production during the fireball phase due to the well-constrained mineralogical nature and velocity of the projectile colliding with the atmosphere.

The previous results are evidencing that not all meteoroid streams should produce chondritic-like meteoroids. It is true that small meteoroids are randomly formed by few mineral grains that have distinctive bulk chemistry depending of the mostly mafic or refractory nature of the dominant constituents (Rietmeijer 2004). Overabundance of Mg in these particles can be indicative of pristinity as magnesian (mafic) silicates are usually associated with more pristine mineral phases that have been not processed in the protoplanetary disk or the parent body. On the opposite side, by studying resolved fireball spectra is also possible to distinguish the achondritic nature of differentiated meteoroids that can be useful to indicate parent asteroids with such composition (Madiedo et al. 2013d).

SPMN video spectroscopy using widely-distributed Watec cameras has been able to reach the IR until about 800 nm, being able to detect N I and N2 contributions (Madiedo et al. 2013c). Column abundances measured with sequential systems can

provide new clues on the delivery of organics to Earth. Simple molecules or radicals are potentially detectable, depending obviously on their relative abundances in the meteor column. It is particularly detecting the signal of fireball afterglows in order to study the exponential decrease in brightness and the main lines involved (Madiedo & Trigo-Rodríguez 2014). We have particularly found in that work several lines that could be associated with the vaporization of silicates (Mg, Na, Fe) and refractory phases (Ca) so it suggests that the study of fireball afterglows provides direct clues on the survival of meteoroid fragments in the meteor column. The study of a Leonid fireball (Borovička & Jenniskens 1998) revealed that thermal equilibrium is not satisfied for all populated levels, so probably to gain insight into the extent of ablation of meteoroid fragments in meteor columns, the first step should be developing new theoretical studies on non-equilibrium chemistry. In that sense, high-resolution emission spectra fortunately taken with large telescopes offered very valuable information on the distinctive components of meteor spectra (Kasuga et al. 2007; Borovička & Zamorano 1995).

Future outreach campaigns can be useful to inform astronomers about the relevance of obtaining such casual spectra. To study additional cases of emission spectra at very high resolution deserves such effort, and can be focused when the Earth's encounters with cometary dust trails are forecasted. Meteor outbursts or storms provide a higher rate of chance of catching such wonderful records of meteoroids interacting with Earth's atmosphere: an ongoing celestial phenomenon passed down through the eons of time.

4. Conclusions

This review paper provides a general overview of the relevance of promoting emission spectroscopy for meteor science. Some of the main conclusions are:

1) Modern meteor spectroscopy is not only allowing to identify the main rock-forming elements contributing to produce meteor light. Emission spectroscopy can be identified as an unique, remote-sensing technique, that can provide a lot of essential information on the meteor ablation and the physical processes governing the delivery of extraterrestrial materials to Earth.
2) The spectra are mostly dominated by emission lines of rock-forming chemical elements, but high-resolution spectra can provide additional clues on the delivery of volatile compounds to Earth because could separate weak contributions of organic and volatile species. Video spectra have also the potential to allow sequential study of meteor ablation, depending of height and changing temperature.
3) Recent studies by fitting synthetic spectra of optically thin radiation (i.e., considering no self-absorption) to the metal atom ablation lines demonstrate that meteor spectra can be reproduced successfully. The intensity values of each emission lines can be reproduced for each fireball using a synthetic spectrum. It uses a simple model that assumes thermal equilibrium in the meteor head, and computes the radiating volume as a prism. Four free parameters are needed: temperature, column density of atoms, damping constant and effective surface

area. First, these parameters are changed until finding a good solution for the Fe lines that are almost present all over the visible spectrum. Afterwards, when the intensity of the Fe lines is well fitted with the synthetic model, we can modify the abundance of the different elements, one by one, until having the best match among the observed and synthetic spectra.

4) Video spectra allow to separate the radiation emitted from the meteor, and from the persistent train or afterglow of bright bolides. It seems that thermal equilibrium is not satisfied for all populated levels in such conditions, so to gain insight into the survival of meteoroid fragments in meteor columns, new non-equilibrium chemistry theoretical studies are required.
5) The study of the temporal evolution of the intensity of emission lines allows to quantify the relevance of this continuous delivery by meteoroids and obtaining new clues on relevant chemical processes probably associated with the organic enrichment of primeval Earth (Jenniskens et al. 2004).

Then, to conclude, meteor spectroscopy is an added-value technique for meteor studies and should be promoted among meteor scientists and amateurs. Diffraction gratings can be easily attached in front of the optics of high-sensitivity video and CCD cameras to get significant meteor spectra. Due to the intrinsic heterogeneity of the meteoroid aggregates producing fireballs, we could say that each spectrum is different from each other, and as many more spectra will be obtained probably our understanding of the meteor phenomenon will increase.

Acknowledgements

The author acknowledges financial support from the Spanish Ministry (project AYA2011-26522) and the Institut d'Estudis Espacials de Catalunya (IEEC).

References

Abe S., Ebizuka N., Yano H., Watanabe J., Borovička J., 2005, Astrophys. J., 618, L141
Abe S., Ebizuka N., Yano H., Watanabe J., Borovička J., 2007, Adv. Space Res., 39, 538
Abe S., Fujita K.., Kakinami Y., Iiyama O., Kurosaki H., Shoemaker M.A., Shiba Y., Ueda M., Suzuki M., 2011, Pub. Astron. Soc. Japan, 63, 1011
Anders E., 1989, Nature, 342, 255
Borovička J., 1993, A&A, 279, 627
Borovička J., 1994, Planet. & Space Sci., 42, 145
Borovička J., 1994b, A&A Suppl. Ser., 103, 83
Borovička J., Koten P., Spurny P., Bocek J., Stork R., 2005, Icarus, 174, 15
Borovička J., Betlem H., 1997, Planet. & Space Sci., 45, 563
Borovička J., Jenniskens P., 1998, EM&P, 82/83, 399
Borovička J., Zamorano J., 1995, EM&P, 68, 217
Borovička J., Koten P., Spurny P., Stork R., 2008, EM&P, 102, 485
Brownlee D., et al., 2006, Science, 314, 1711
Ceplecha Z., 1961, Bull. Astr. Inst. Czech., 12, 246
Ceplecha Z., 1964, Bull. Astr. Inst. Czech., 15, 102
Ceplecha Z. et al., 1998, Space Sci. Rev., 84, 327
Fomenkova M.N., Kerridge J.F., Marti K., McFadden L.A., 1992, Science, 258, 266
Halliday J., 1961, Publ. Dominion Observatory Otawa, 25, 3

Harvey G.A., 1971, Astrophys. J. 165, 669
Jenniskens P., Mandell A.M., 2004, Astrobiology, 4, 123
Jenniskens P., Stenbaek-Nielsen H., 2004, Astrobiology, 4, 95
Jenniskens P., Schaller E.L., Laux C.O., Wilson M.A., Schmidt G., Rairdn R.L., 2004, Astrobiology, 4, 67
Jenniskens P., Laux C.O., Wilson M.A., Schaller E.L., 2004b, Astrobiology, 4, 81
Jenniskens P., Laux C.O., Schaller E.L., 2004c, Astrobiology 4, 109
Jopek T.J., Williams I.P., 2013, MNRAS, 4, 81
Kasuga T., Yamamoto T., Kimura H., Watanabe J., 2006, A&A, 453, L17
Kasuga T., Iijima T. and Watanabe J., 2007, A&A, 474, 639
Kokhirova G.I., Borovička J., 2011, A&A, 533, A115, 6 pp.
Madiedo J.M., Trigo-Rodríguez J.M., 2014, in Proc. Meteoroids 2013 Conf., held in Poznań, Poland, Aug. 26-30, 2013, eds Jopek T.J., Rietmeijer F.J.M., Watanabe J., Williams I.P, AM University Press, Poznań, p. 133
Madiedo J.M., Trigo-Rodríguez J.M., Konovalova N.; Williams, I.P., Castro-Tirado A.J., Ortiz J.L., Cabrera-Cao J., 2013, MNRAS, 433, 571
Madiedo J.M., Trigo-Rodríguez J.M., Konovalova N.; Ortiz J.L., Castro-Tirado A.J., Alonso-Azcrate J., Lacruz J., Cabrera-Cao J., 2013b, A&A, 555A, 149M
Madiedo J.M., Trigo-Rodríguez J.M., Williams, I.P., Ortiz J.L., Cabrera-Cao J., 2013c, MNRAS, 431, 2464
Madiedo J.M., Trigo-Rodríguez J.M., Williams, I.P., Konovalova N., Ortiz J.L., Castro-Tirado A.J., Pastor S., de los Reyes J.A., Cabrera-Cao J., 2013d, MNRAS, Advance Access, DOI: 10.1093/mnras/stu222
Millman P.M., 1980, in Solid Particles in the Solar System, Halliday I., McIntosh B.A. (eds), IAU Symp. 90, Reidel, Dordrecht, p. 121
Nesvorny D., Ferraz-Mello S., Holman M., Morbidelli A., 2002, in ASTEROIDS III, W.F. Bottke et al. (eds), Univ. Arizona Press, Tucson, p. 379
Rietmeijer F.J.M., 2004, EM&P, 95, 321
Trigo-Rodríguez J.M., 2002, Ph.D. thesis, University of Valencia, downloadable at: `http://www.tdx.cat/handle/10803/9481`
Trigo-Rodríguez J.M., Blum J., 2009, Planet. & Space Sci., 57, 243
Trigo-Rodríguez J.M., and Llorca J., 2007, Adv. Space Res., 39, 517
Trigo-Rodríguez J.M., Llorca J., Borovička J., Fabregat J., 2003, MAPS, 38, 1283
Trigo-Rodríguez J.M., Llorca J., Fabregat J., 2004, MNRAS, 348, 802
Trigo-Rodríguez J.M., Castro-Tirado A.J., Llorca J., 2005, 36th Lunar Planetary Science Conference, League City (TX), abstract #1485
Trigo-Rodríguez J.M., Rubin A.E., Wasson J.T. 2006, Geoch. Cosmochim. Acta 70, 1271
Trigo-Rodríguez J.M., Lyytinen E., Jones D.C., Madiedo J.M., Castro-Tirado A.J., Williams I., Llorca J., Vitek S., Jelinek M. Troughton B., Galvez F., 2007, MNRAS, 382, 1933

Meteoroids 2013, Proceedings of the Astronomical Conference,
held at A.M. University, Poznań, Poland, Aug. 26-30, 2013,
eds Jopek T.J., Rietmeijer F.J.M., Watanabe J., Williams I.P.,
Adam Mickiewicz University Press in Poznań, pp 117–124

CAMSS: A spectroscopic survey of meteoroid elemental abundances

Jenniskens P.[1], Gural P.[2], and Berdeu A.[3]

[1]SETI Institute, 189 Bernardo Ave, Mountain View, CA 94043, USA (petrus.m.jenniskens@nasa.gov)
[2]Leidos, 14668 Lee Road, Chantily, VA 20151, USA
[3]NASA Ames Exploration Academy, Ames Research Center, Moffett Field, CA 94035, USA
[4]SAE Supaéro, 10 Avenue Édouard Belin, 31400 Toulouse, France

Abstract. The main element abundances (Mg, Fe, Na, ...) of some Near Earth Objects can be measured by meteor spectroscopy. The Cameras for All-sky Meteor Surveillance (CAMS) Spectrograph project aims to scale up meteor spectroscopy in the same way as CAMS scaled up the measurement of precise meteoroid trajectories from multi-station video observations. Spectra are recorded with sixteen low-light video cameras, each equipped with a high 1379 lines/mm objective transmission grating. The cameras are operated in survey mode and have recorded spectra in the San Francisco Bay Area every clear night since March 12, 2013. An interactive software tool is being developed to calibrate the wavelength alignments projected on the focal plane and extract the meteor spectra. Because the meteoroid trajectory and pre-atmospheric orbit are also independently measured, the absolute abundances of elements in the meteoroid plasma can be calculated as a function of altitude, while the orbital information can tie the meteoroid back to its parent object.

Keywords: meteoroids, video spectroscopy of meteors

1. Introduction

Atmospheric ablation induced breakdown spectroscopy of meteors is the only way of measuring the main element composition of meteor shower parent bodies, short of visiting the responsible Near Earth Objects (NEO). Meteoroid orbits identify the source, adding to abundance measurements from collected meteoroids (Rietmeijer 2007). Meteor spectroscopy is a widely applied technique, but its application has been limited by the labor-intensive effort of extracting and reducing the spectra (Borovicka 1993, 1994; Jenniskens 2007; Abe et al. 2007; Trigo-Rodriguez and Llorca 2007; Kasuga et al. 2007; Berezhnoy and Borovicka 2012; Gomez et al. 2013).

The low yield during mostly sporadic nights adds additional challenges to data collection. The only year-around survey of meteor spectra, with simultaneous triangulation of meteoroid trajectories to determine their pre-atmospheric orbit, was that of Borovicka et al. (2005). They reported on 94 meteor spectra and confirmed that there are sodium-poor meteoroids in long-period comet orbits (Jenniskens et al. 1997), hinting at the existence of compositional diversity among Oort cloud comets. They also discovered short-period meteoroids that consist almost entirely of iron (lacking magnesium and sodium), possibly arising from an asteroidal source.

In prior work, we developed the Cameras for Allsky Meteor Surveillance (CAMS), a night-time meteor video surveillance system that deployed 60 low-light video

cameras at three stations in the San Francisco Bay Area (Jenniskens et al. 2011; Gural 2012). CAMS measures the meteoroid trajectory, light curve and deceleration in the Earth atmosphere, as well as the meteoroid pre-atmospheric orbit in space for meteors brighter than about m_v=+4 visual magnitude (typically +3 to −1). As of August 11, 2013, about 130,000 meteoroid orbits have been measured with a precision better than ±2° in radiant direction and ±1 km/s in speed.

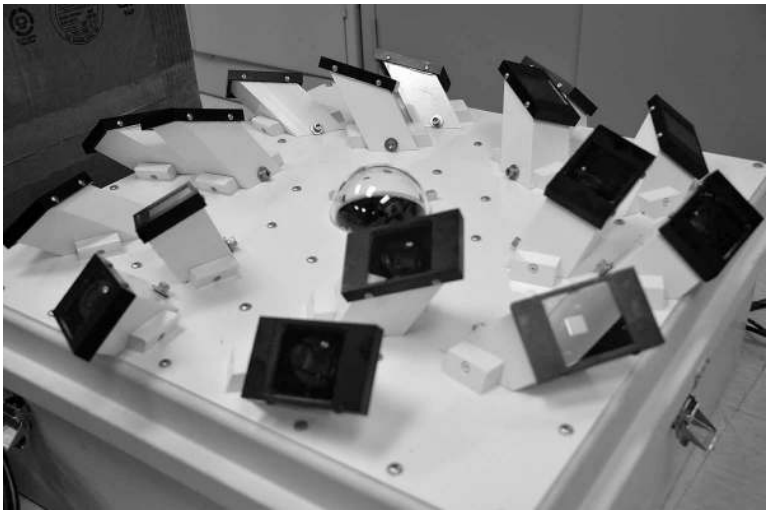

Figure 1. The CAMS Spectrograph consists of 16 spectrographic cameras.

2. Methods

The new CAMS Spectrograph (CAMSS) aims to measure the main element abundances (Mg, Fe, Na,...) of the brightest meteors detected by CAMS (about m_v=+1 and brighter). Coupling the spectral measurements of emission line strengths to a trajectory and orbit estimation capability, provides the unique opportunity to identify the source, mass, density, fragmentation, and chemical abundance properties of each collected meteor record.

CAMSS is based on the same camera as used in CAMS, the Watec WAT-902 H2 Ultimate 1/2" format video camera equipped with the Pentax 12.0 mm f/1.2 lenses (22 x 30 deg. field of view). These are 29.97 frames per second NTSC-type low-light level CCD cameras with 640 x 480 pixel video output dimensions. This choice was based on the cost and limited long endurance of intensified cameras required to facilitate a multi-year spectroscopic survey. Alternatively, using larger format cooled CCD or CMOS cameras would have needed a complete revision of the meteor capture and detect software. Due to the transient nature of the signal, long integrations on the sky background are not advised.

The choices of lens, grating substrate and window materials were determined by what wavelength range is of most use in measuring meteoroid abundances. The most important emission lines are listed in Table 1. Of key interest, are the sodium lines

at 589 nm, the magnesium lines at 518 nm, and the multitude of iron lines. Iron emission lines are found throughout the optical and near-UV spectral range, but the 527-546 nm and 393-386 nm wavelength ranges are most suited for excitation temperature measurements in meteors. Of interest, too, is the 422 nm line of Calcium. In the near-UV below 380 nm, telluric extinction is strong and variable. For those reasons, we adopted the 380–880 nm wavelength range. The standard Pentax 12mm f/1.2 lens adopted for this system is a good achromatic lens over the range 410–880 nm, and transparent from 380 nm upwards. No affordable low-f number achromatic lenses are available that also cover the 350–400 nm range.

For the dispersing element, we chose the 1379 line/mm Ibsen Photonics FSTG-VIS1379-911 fused silica grating, a holographic grating with 200 micron groove depth, etched in fused silica. These small 1 x 1 cm gratings are just big enough to cover the Pentax lens' clear aperture. Absence of the resins used in replica style gratings, guarantees that these Ibsen gratings will survive the periodic heating and cooling from continuous day and night cycles.

The dispersion of the CAMS Spectrograph (1.1 nm/pixel) is sufficient to resolve the Fe lines needed to measure excitation temperatures. Based on the typical +5.4 star limiting magnitude of the video cameras in single frame detection, we estimated that meteors of about +1.3 magnitude and brighter should provide a suitable signal-to-noise signal to measure the Na/Mg ratio. Brighter meteors would allow the measurement of more elements from the extracted spectra.

Table 1. Spectral lines most suited for measuring elemental compositions.

Element	Vacuum wavelength (nm)
Li	670.9601-670.9927 (19 lines)
Na	**588.9507/589.1583**
Mg	**516.8760/517.4125/518.5048**; 383.3386/383.3391/383.9381/383.9384
Al	394.5122/396.2641
Si	390.6629
K	766.7021/770.1093
Ca	**422.7918**
Sc	402.1528/402.4814; 391.2923/390.5895
Ti	517.5183; 398.2887/396.3972/394.9789; 363.6499
V	485.2837; 457.8457; 385.6455; 381.9326
Cr	429.0923/427.5999/425.5530; 360.6349/359.4506/357.9706
Mn	403.1892/403.4202/403.5623
Fe	**527.1-545.7; 393.14-385.7466**; 386.1005; 328.5529; 372.0993; 368.0961
High excitation temperature component:	
H	656.2822/656.4610; 486.2681; 434.1682
Ca+	393.4777/396.9592
Si+	634.8864/637.3132; 386.3690/385.7111/385.4758
Mg+	448.2383/448.2407/448.2582

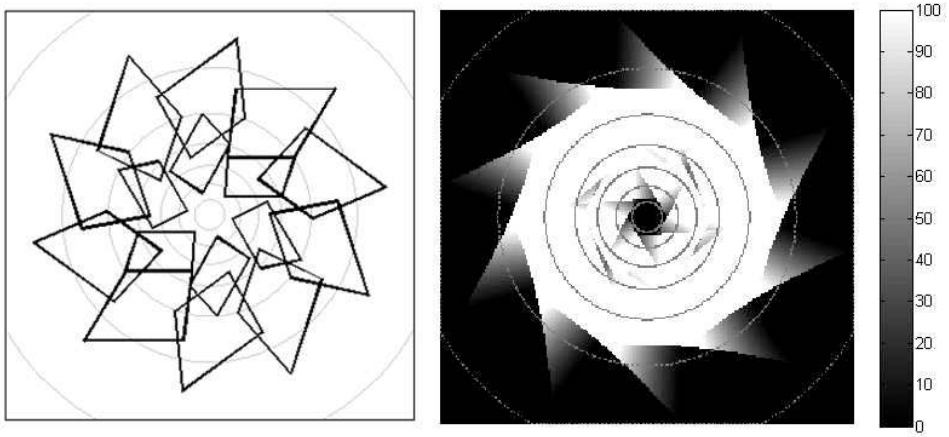

Figure 2. Final result of optimization study: Field of view of each camera in zeroth order shown in gnomonic projection with circles at 10° elevation intervals (left), and the percentage of wavelength range (380-600 nm) covered by the spectrograph in first order (right).

The number of cameras was dictated by the availability of a 16-camera digitizer device (Sensoray 817 capture board mounted internally to a PCI x1 bus), which made it possible to digitize the video and process the meteor detection in real time across all sixteen video channels on a single PC computer with i7 quad-core processor. A pointing optimization study was made to see what camera layout would result in a reasonable zero-order coverage above 30° elevation (Fig. 2, left panel) as well as provide maximum first order (380–600 nm) spectral coverage (Fig. 2, right panel), while also trying to maintain overlapped spatial coverage between zero and first orders. From that, a solution was chosen with 6 cameras pointing at a high 67.5° elevation, rotated with yaw of 25°, and 10 cameras at a low 45° elevation, also with yaw of 25°. This design leaves an uncovered area near the zenith, which can be filled with a planned 17th camera mounted in the central dome of the setup shown in Fig. 1. The central dome was originally intended to facilitate an all-sky spotting camera for triggering the dump of the 16 camera imagery buffers upon bright meteor detection. This turned out to be unnecessary, since the real-time detection performance was adequate on each individual camera on the single PC employed.

The transmission grating on each camera is mounted at an angle of 25° from the camera boresight optical axis, to optimize the responsivity of the first order spectrum. A special grating holder was build that grabs onto the fused silica waver and holds it at the proper angle in front of the lens. The grating holder can be rotated around the camera/lens central axis to align the dispersion direction (perpendicular to the grooved lines) with the horizontal rows of the camera focal plane. This simplifies the spectral line extraction and integration when using interleaved video cameras which flip-flop odd and even row collection at the interleaved frame rate (60 Hz for NTSC). The grating holder provides a clear field of view for

light falling onto the grating for entry angles of up to 65° in the chosen first order dispersion direction.

The grating is isolated from environmental contaminants by placing the camera/lens/grating inside a sealed unit (Fig. 1). This keeps out insects, weather, dust, and pollen, but requires a cover window depicted by the black rectangular box mounted to the front of the white square tube enclosure for each camera. To minimize reflections, the window is mounted at an angle of 45° relative to the boresight of the camera, because the first order spectrum light typically falls onto the camera at a high 45° angle (Fig. 1). The window is a BK7 optical window from Edmund Scientific, with a simple MgF2 anti-reflection coating. This coating is not as efficient in preventing reflections than other coatings, but has a simpler wavelength dependency and good transmission performance over the full wavelength range.

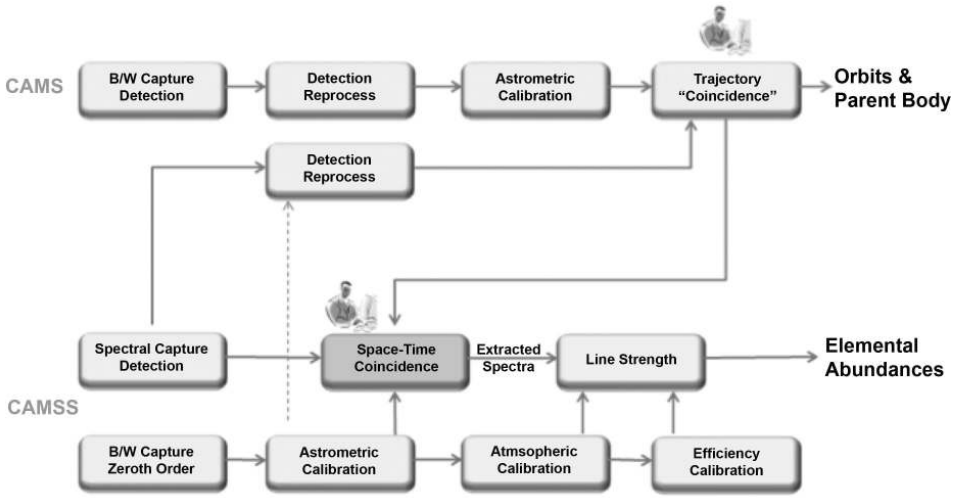

Figure 3. The current suite of CAMSS software as visualized in a work flow diagram showing the inter-connection of CAMS and CAMSS processing.

The standard CAMS system uses a real-time compression technique to retain all the captured video of a given night for post-collection detection processing (Gural 2010; Jenniskens et al. 2011). However, this compression method could lose faint emission lines close to the noise floor of the sensor. Instead, a real-time detection algorithm was developed that was tuned towards spectral line detection. After detection, the algorithm saves the raw video sequence of the spectrum thus avoiding any compression artifacts or losses. This includes a few frames prior to detection and a user specified number of frames after detection, typically one second's worth, to account for a fireball's duration within the CAMSS single camera field of view. The current sixteen channel CAMSS does the real-time video capture and spectrum detection processing using an i7 quad-core processor on a single PC platform. This generates about 500 GB of data every 2 months of operation. Many of the detected spectra are from passing aircraft.

Figure 3. shows the CAMSS off-line processing work flow and associated software components. In off-line data processing at the SETI Institute, first the CAMS-derived meteor trajectories are calculated by pooling meteor detection measurements from multiple video collection sites as well as the zeroth order measurements from the CAMSS system. For each sufficiently bright meteor trajectory determined, the software works through the geometry of grating dispersion and identifies the CAMSS cameras/files that may contain the spectrum. This avoids a pre-sorting and full review effort on all the spectral collection imagery. Only meteors with trajectories are post-processed for spectral estimation. The geometric alignment must be determined for either the first or second order wavelengths given the pointing direction of the grating camera and the position of the meteor on the sky from the perspective of the grating camera. The clock synchronization error between the cameras also needs to be taken into account.

Each CAMS and CAMSS (zeroth order image) video are astrometrically calibrated for pointing boresight, field of view rotational orientation, image scale, and third order warp coefficients. In addition, the grating's pitch, roll and yaw with respect to the camera axis and focal plane are calibrated. The spectral response of the camera (efficiency) as a function of wavelength is obtained by calibrating against opportunistic bright star spectra that appear in the video frames captured periodically through the night. An atmospheric extinction correction needs to be applied as well. The calibration (emission line wavelength alignment) is verified by a user interactive validation process, similar to the Coincidence software in CAMS (Jenniskens et al. 2011). The result is a line strength estimate for identified spectral emission lines yielding elemental abundances.

3. Results

The real-time detection algorithm was first tested in a prototype Matlab application against video data obtained during the 2012 Geminids, resulting in 4 out of 5 spectra being detected, the missing case being too faint to provide useful data. The high efficiency C code for the detection processing was then implemented based on the Matlab code and confirmed to work properly. The optimized settings for the detection algorithm were determined on actual measurement recordings and then put in operation.

The spectrograph saw first light at the Sunnyvale CAMS station on March 12, 2013. In the next two nights, 3 spectra were recorded in each night, meeting expectations. The detection algorithm was further improved in the next months. Figure 4 shows example spectra measured during routine observations at the Sunnyvale CAMS station on the Lyrid shower night of April 21, 2013. These are composites of multi-frame video with spectral emission lines identified. The spectral curvature is due to the three-dimensional grating dispersion that introduces warping for off-normal incidence to the grating surface (both along groove versus cross-groove incidence angles). Note the existence of the Magnesium line in all the spectra, which is useful as an abundance ratio reference.

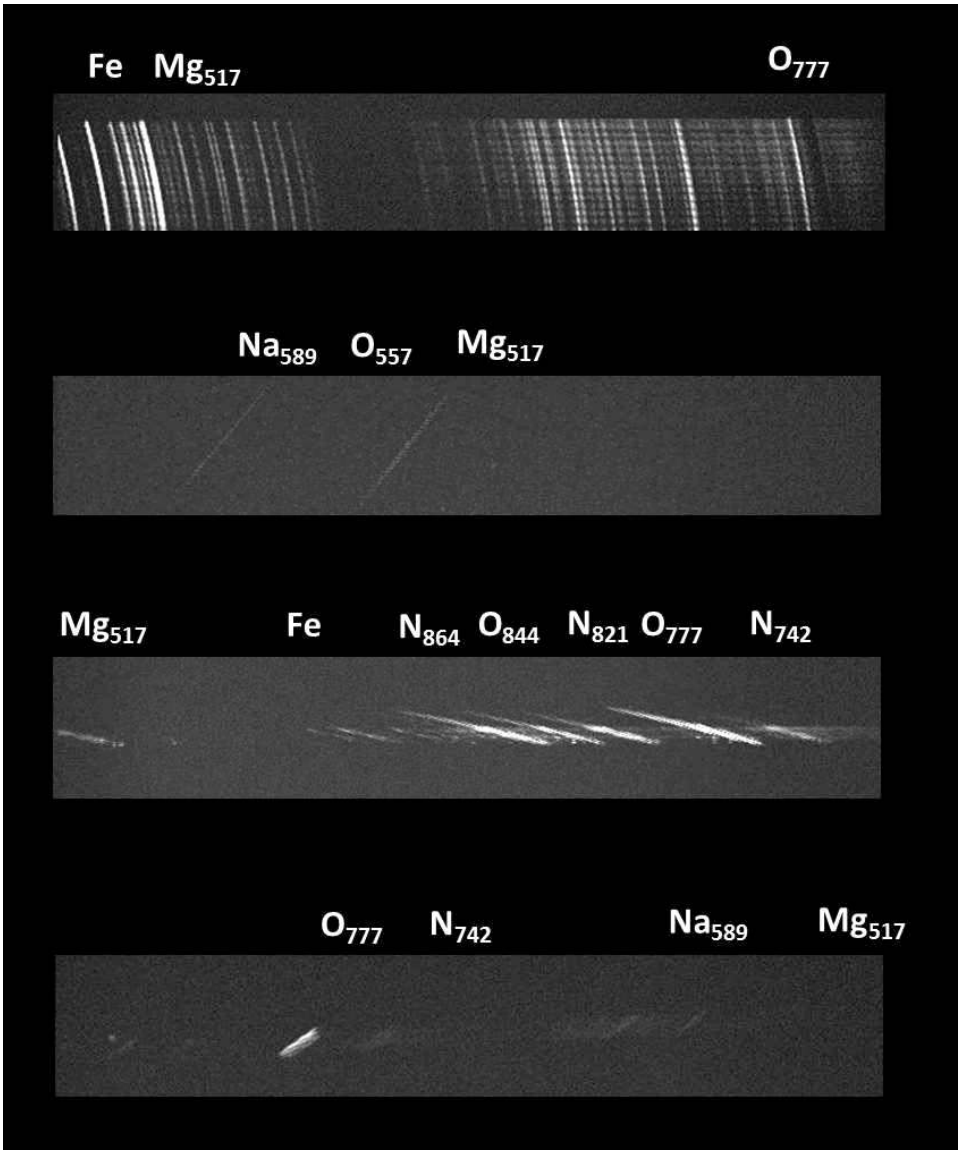

Figure 4. Example spectra. Multi-frame composites of meteor spectra from the night of April 21, 2013, collected at 5:32:10 (SPO), 8:52:53 (LYR), 9:12:22 (SPO), and 11:14:16 (SPO) UTC.

4. Future Work

Parts of the off-line data reduction pipeline are still to be completed. So far, we built and tested the end-to-end prototype Matlab code to calibrate the cameras for grating orientation, spectral response efficiency, atmospheric correction, and for verifying the formulae governing the relationship between a meteor's three-

dimensional propagation track and its focal plane position permitting the extraction of the spectral line signatures.

The product of this work will be a database of elemental compositions for meteoroids on known orbits. This data can then be used to study the diversity of comets in the Oort cloud and in the Jupiter-family (Kuiper belt) population as represented in the population of near Earth objects. This data will be used to address such hypotheses as that the Oort cloud comets may have originated predominantly around other stars in the birth cluster of the Sun (Morbidelli and Levison 2004), and that Jupiter family comets and outer belt C-type asteroids may sample the same original population of outer disc solar system objects (Walsh and Morbidelli 2011).

Acknowledgements

We thank Jim Albers (Sunnyvale), Rick Morales (Fremont Peak Observatory), Bryant Grigsby (Lick Observatory), and Dave Samuels (Single CAMS stations) for support of the CAMS station operations. This work was financially supported by the NASA NEO Observation Program.

References

Abe S., Ebizuka, N., Yano H., Watanabe J.-I., Borovicka J., 2007, Adv. Space Res., 39, 538

Berezhnoy A.A., Borovicka J., 2012, ACM 2012, Abstract 6142

Borovicka J., 1993, A&A, 279, 627

Borovicka J., 1994, A&A Supl. Ser., 103, 83

Borovicka J., Koten P., Spurny P., Bocek J., Stork R., 2005, Icarus, 174, 15

Gural P.S., 2010, in Proc. of the Inter. Meteor Conf., Armagh, Northern Ireland, 16-19 Sept., 2010, eds Asher D.J., Christou A.A., Atreya P. and Barentsen G., International Meteor Organization, p. 28

Gural P.S., 2012, MAPS, 47, 1405

Jenniskens P., Betlem H., de Lignie M., Langbroek M., 1997, ApJ, 479, 441

Jenniskens P., 2007, Adv. Space Res., 39, 491

Jenniskens P., Gural P. S., Dynneson L., et al., 2011, Icarus, 216, 40

Gomez N., Madiedo J.M., Trigo-Rodriguez J.M., 2013, 44th LPSC, Abstract 1239

Kasuga T., Watanabe J.-I., Kawakita H., Yamamoto T., 2007, Adv. Space Res., 39, 513

Morbidelli A., Levison H.F., 2004, AJ, 128, 2564

Rietmeijer F.J.M., 2007, Adv. in Space Res., 39, 583

Trigo-Rodriguez J.M., Llorca J., 2007, Adv. in Space Res., 39, 517

Walsh K.J., Morbidelli A., 2011, A&A, 526, 126

Meteoroids 2013, Proceedings of the Astronomical Conference,
held at A.M. University, Poznań, Poland, Aug. 26-30, 2013,
eds Jopek T.J., Rietmeijer F.J.M., Watanabe J., Williams I.P.,
Adam Mickiewicz University Press in Poznań, pp 125–131

Chemistry of the Benešov meteoroid

Berezhnoy A.A.[1], **and Borovička J.**[2]

[1]Sternberg Astronomical Institute, Moscow State University,
Universitetskij pr. 13, Moscow, 119991 Russia
[2]Astronomical Institute, Czech Academy of Sciences, Fričova 298, CZ-25165 Ondřejov, Czech Republic

Abstract. Based on the quenching theory approach, formation of NO and metal oxides during penetration of Benešov meteoroid into the Earth's atmosphere is considered. Identification of FeO, CaO, AlO, and MgO bands is confirmed in Benešov spectra while Al hydroxides, NiO, and TiO are tentatively detected in meteor spectra for the first time. For large meteoroids NO enrichment and O_3 depletion in the impact-produced cloud is predicted.

Keywords: meteoroids, meteors, spectra, impact chemistry, diatomic molecules, band identification, quenching theory

1. Introduction

The Benešov meteoroid penetrated into the Earth's atmosphere on May 7, 1991. Its initial mass was about 4000 kg (Borovička et al. 1998). The analysis of atmospheric fragmentation and spectra of the bolide was interpreted as an evidence of stony nature of the meteoroid. Bands of diatomic molecules such as CaO, FeO, AlO, and MgO were detected in the spectrum of cooling radiating cloud at 24 km altitude while features of molecular bands were not so intensive in the spectra of fireball at 20–24 km altitude and, except FeO, were absent at higher altitudes (Borovička and Spurný 1996). In spring 2011 several pieces of Benešov meteorite belonging to different classes (H5, LL3.5, and achondrite) with a total mass of 11.3 g were found (Spurný et al. 2012). Benešov meteorite became only second meteorite with detected heterogeneity in its composition, after Almahata Sitta (Bischoff et al. 2010).

2. Equilibrium composition of the impact-produced cloud

Maximal temperature and pressure in the impact-produced cloud formed during entrance of big meteoroids into the Earth's atmosphere are high enough for reaching of the equilibrium chemical composition (Berezhnoy and Borovička 2010). The quenching theory was already applied to study chemistry of the impact-produced cloud formed by Benešov meteoroid (Berezhnoy and Borovička 2010). However, in this paper it was assumed that the Benešov bolide had the elemental composition similar to that of CI chondrite.

We performed new calculations of the chemical composition of the impact-produced cloud for the case of impactor with much lower content of volatile elements (H and C) typical for LL chondrite (Lodders and Fegley 1998), the largest Benešov

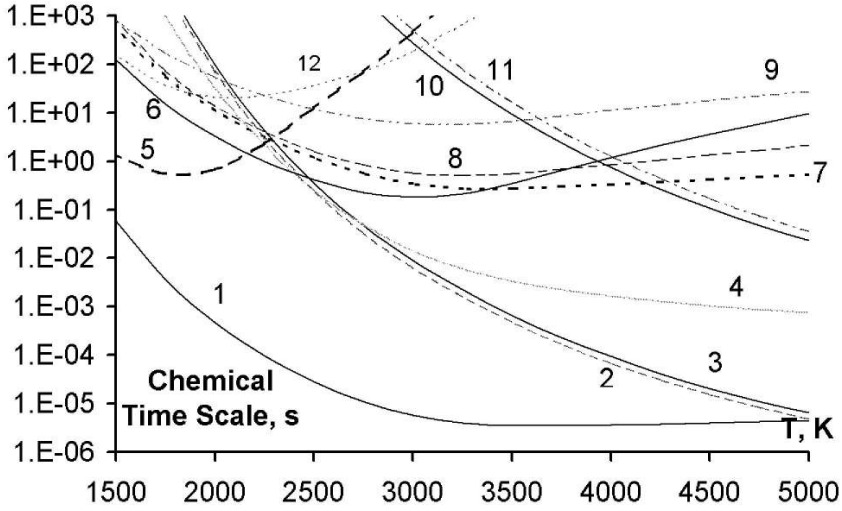

Figure 1. Chemical time scales of most important reactions of NO formation and destruction as function of temperature at 20 km height for the case of the equilibrium chemical composition of the impact-produced cloud. Air-to-meteoroid mass ratio in the impact-produced cloud is 30. Quenching occurs when the chemical time scale is longer than 1 s. Curves 1–12 represent reactions NO + O = NO_2 (1), N_2 + 3 O = 2 NO + O (2), NO + N = N_2 + O (3), O_2 + N = NO + O (4), OH + OH = H_2O + O (5), NO_2 + O = NO + O_2 (6), NO_2 + M = NO + O + M (7), NO + O + M = NO_2 + M (8), O_2 + M = O + O + M (9), N + O = NO (10), NO + M = N + O + M (11), O_2 + 2 OH = H_2O + 3 O (12), respectively.

meteorite (Spurný et al. 2012). The air-to-meteoroid vapor mass ratio was assumed to be 30 according to the results of the analysis of the Čechtice fireball (Borovička 1993). The pressure of the impact-produced cloud is assumed to be the same as the pressure of ambient atmosphere at the corresponding altitude (Berezhnoy and Borovička 2010). Chemical time scales of main reactions with the participation of refractory elements were estimated based on the NIST data base (NIST 2013a). Quenching of chemical reactions occurs at 1500 – 2000 K for the case of pressure equal to 0.05 bar which is corresponding to the altitude of 20 km. Main compounds of refractory elements in the impact-produced fireball are SiO_2, AlO, FeO, and MgO. Difference between the equilibrium chemical composition of the impact- produced fireballs formed after collisions of CI and LL chondrites is negligible because in both cases the content of metal hydroxides is quite low. The same conclusion is obtained for the equilibrium chemical composition of the impact-produced cloud formed by mixtures of air and H5 and achondrite meteorites because the content of volatile elements in H5 and achondrite is also quite low.

NO is among the most interesting impact-produced species of atmospheric origin. NO molecules are produced in meteor tails at 1500 – 4000 K. Based on rate constants of main reactions responsible for NO formation and destruction such as O_2 + N = NO + O and N_2 + 3 O = 2 NO + O (NIST 2013a) formation of NO molecules

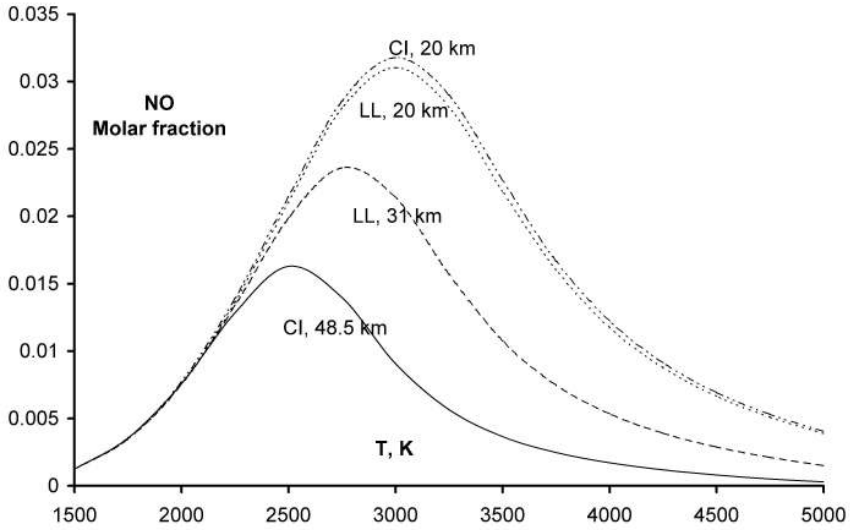

Figure 2. Equilibrium NO mole fraction as function of temperature at different altitudes and chemical compositions of impactors. Air-to-meteoroid mass ratio in the impact-produced cloud is 30.

quenches at about 2000 K at hydrodynamic time scale of about 1 s (see Fig. 1). At this temperature the NO equilibrium mole fraction is almost independent on the meteor altitude and equal to about 1% (see Fig. 2). Assuming the air-to-meteoroid mass ratio in the impact-produced cloud equal to 30 (Borovička 1993; Borovička and Spurný 1996) NO mass can be estimated as about 1 500 kg. Later impact-produced NO molecules react with O_3, it leads to local depletion of O_3 content at the place of the meteoroid impact (Klumov 2001). Thus, we expect O_3 depletion also in the impact-produced cloud formed by Chelyabinsk meteoroid.

3. Identification of molecular bands

Spectra of Benešov bolide were obtained in the wavelength range between 380 and 670 nm with spectral resolution of about 0.1 nm (Borovička and Spurný 1996). The spectrum of a cooling radiating cloud left behind the bolide at altitude 24 km is particularly convenient for molecular studies. The spectrum (Fig. 3) consists of bright continuum, roughly corresponding to a 4000 K Planck function, superimposed with numerous molecular bands. Used spectral resolution is sufficient to study influence of population of rotational levels on the shape of electronic-vibrational bands.

Theoretical spectra of considered diatomic molecules were obtained with usage of PGOPHER program (PGOPHER 2013). Molecular constants of AlO were taken from Saksena et al. (2008), of MgO from Daily et al. (2002), and of TiO, N_2, and CN from NIST (2013b). Molecular constants of other species such as FeO, CaO, NiO, and Al hydroxides are poorly known. For this reason we used laboratory spec-

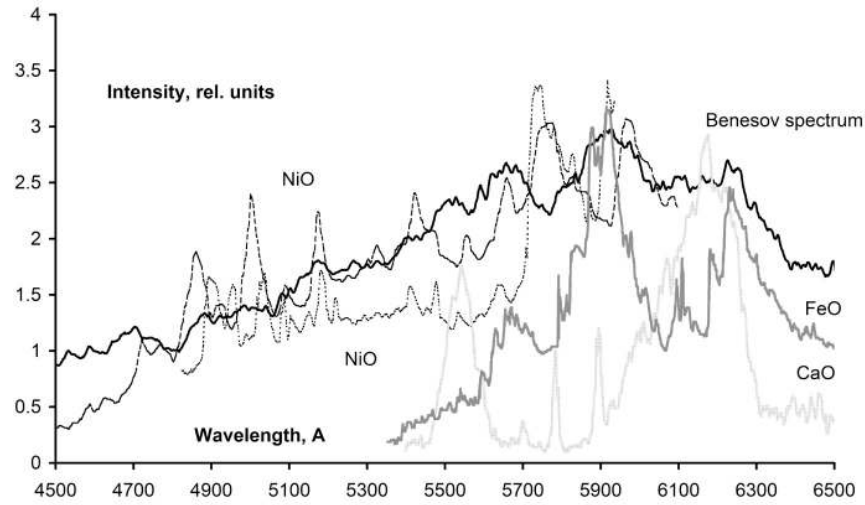

Figure 3. Spectrum of Benešov bolide train at 25 km in comparison with laboratory spectra of FeO, CaO, and NiO. The NiO spectrum at 4800–5900 Å with the higher background at 5200 Å was taken from Srdanov and Harris (1988) while the NiO spectrum at 4500–6100 Å was taken from Burgard et al. (2006).

tra for identification of molecular bands in Benešov spectra. The laboratory spectra of FeO were taken from West et al. (1975), of CaO from Sugita et al. (2003), of NiO from Srdanov and Harris (1988) and Burgard et al. (2006), and of AlO and Al hydroxides from Gole and Kolb (1981). Of course, taking of laboratory spectra for identification of molecular bands in meteor spectra has some disadvantages because laboratory spectra were obtained at quite different conditions (temperature, pressure, chemical composition and so on) in comparison with obtained meteor spectra. For example, CaO emission spectra were obtained after collision of copper projectiles with dolomite target (the impact velocity was 4.85 km/s) and additional Cu, Na, and Ca atomic lines were observed at the wavelength range between 560 and 600 nm (Sugita et al. 2003). The better agreement between FeO laboratory and meteor spectra was achieved for FeO produced during reaction of Fe atoms with O_3 in comparison with that produced during reaction of Fe atoms with N_2O and discharged O_2 (West et al. 1975). NiO molecules were also produced during reaction between Ni atoms and O_3 in laboratory experiments (Srdanov and Harris 1988; Burgard et al. 2006) while reaction Me + O_2 = MeO + O was responsible for formation of metal oxides in the meteoroid impact-produced cloud (Berezhnoy and Borovička 2010).

The most prominent broad bands in the red region (at 560, 565, 590, and 620 nm) are identified as features of FeO orange system; weaker CaO broad bands are identified at 553 and 615 nm (see Fig. 3). Due to significant difference between Benešov spectra and CaO and FeO laboratory spectra (see Fig. 3) additional identification of weaker molecular bands of other species at 550–650 nm range seems to be difficult. Namely, weak features at 559, 617, and 620 nm may be identified with strongest

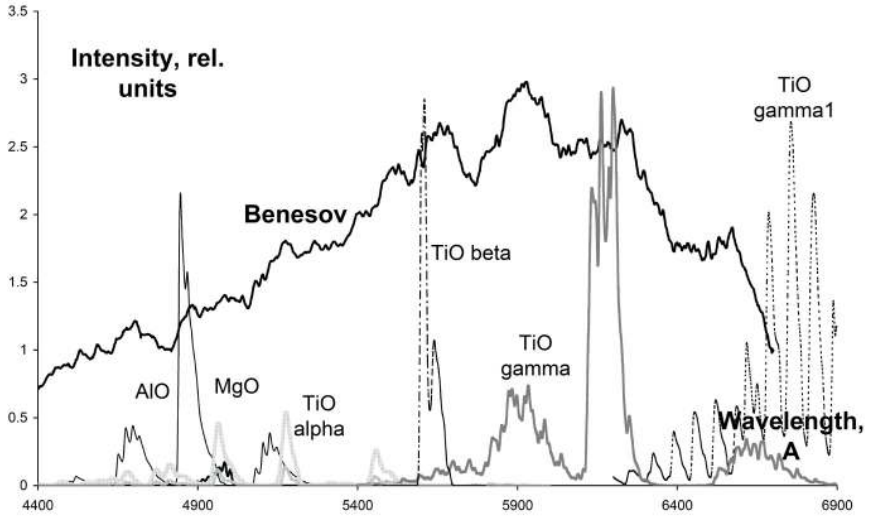

Figure 4. Spectrum of Benešov bolide train at 25 km in comparison with theoretical spectra of AlO, MgO, and TiO.

transitions of TiO beta and gamma systems (see Fig. 4). NiO features are found at 488, 518, and 540 nm (see Fig. 5). However, the absence of the strongest NiO experimental band at 575 nm and the presence of the AlO features at 488 and 540 nm lead us to claim NiO detection as tentative. AlO bands are identified at 454, 468, 488, 513, and 542 nm, the MgO green system is also detected at 496–500 nm while CN bands were not identified (see Fig. 6). Agreement between Benešov spectrum and Al in air spectrum becomes better with adding of the spectrum of Al in water vapor (see Fig. 5). Namely, HAlOH compound may be responsible for existence of 459 and 505 nm bands (Gole and Kolb 1981). The most intensive unidentified band is located at 527 nm; this band may be produced by still unidentified diatomic or triatomic molecule.

Theoretical intensities of AlO and MgO electronic-vibrational-rotational transitions were calculated with usage of the approach of Kovács (1969). The best agreement between theoretical and obtained spectra was achieved for the value of the vibrational temperature of about 4000 K. Electron temperature could not be measured because only MgO and AlO transitions from unique electronic states were detected. Rotational temperature was assumed to be 3000 K. Assuming optically thin emission, the AlO/MgO abundance ratio was estimated to be about 20. This value is higher than that obtained with the usage of quenching theory by a factor of 50. However, emission of molecules in Benešov impact-produced cloud was optically thick and for this reason it is impossible to estimate the bulk chemical composition of the impact vapor and meteoroids from molecular spectra.

Detection of so large amount of molecules in meteor spectra was performed for the first time because Benešov meteoroid is the biggest meteoroid with low altitude of penetration into the Earth's atmosphere among all observed meteors for which

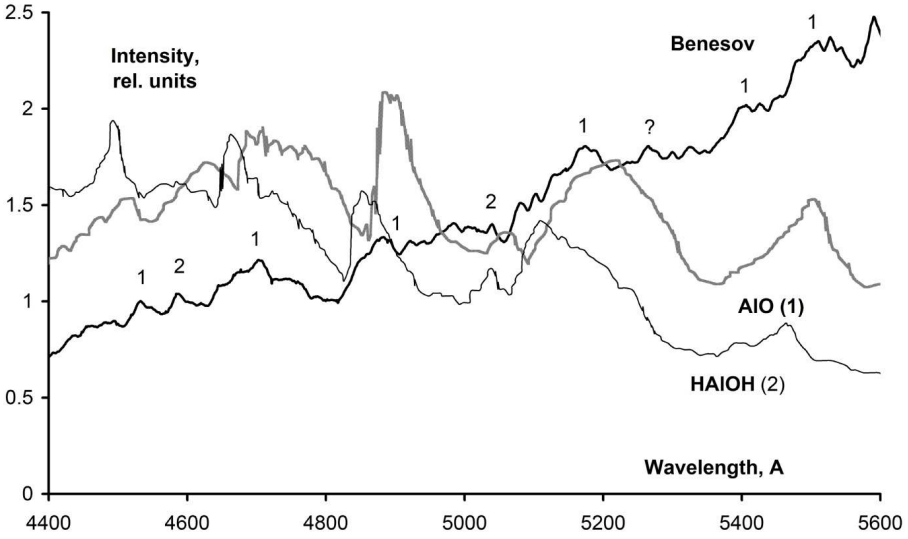

Figure 5. Spectrum of Benešov bolide train at 25 km in comparison with laboratory spectra of AlO and HAlOH. Possible identifications of AlO and HAlOH bands are shown by symbols 1 and 2, respectively.

high-resolution optical spectra are available. Let us note that N_2 and CN optical bands were not detected in Benešov spectra.

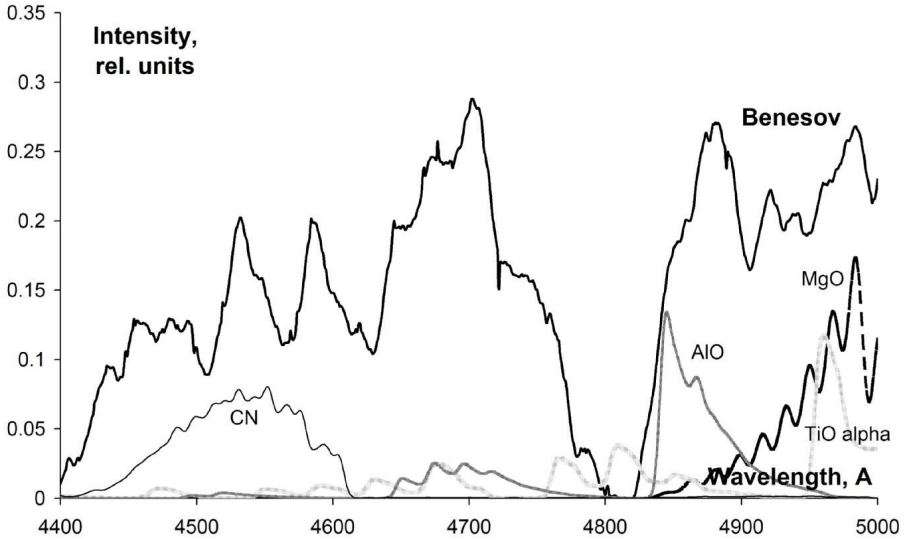

Figure 6. Spectrum of blue part of Benešov bolide train with subtracted continuum in comparison with theoretical spectra of AlO, MgO, TiO, and CN.

4. Conclusions

Based on quenching theory approach, formation of NO and metal oxides during meteor events was considered. Identification of FeO, CaO, AlO, and MgO bands was confirmed in Benešov spectra while Al hydroxides, NiO, and TiO optical features were tentatively detected in meteor spectra for the first time.

Acknowledgements

This research was supported by grant No. P209/11/1382 from the Grant Agency of the Czech Republic. The institutional project was RVO:67985815.

References

Berezhnoy A.A., Borovička J., 2010, Icarus, 210, 150
Bischoff A., Horstmann M., Pack, A., Laubenstein M., Haberer S., 2010, M&PS, 45, 1638
Borovička J., 1993, A&A, 279, 627
Borovička J., Spurný P., 1996, Icarus, 121, 484
Borovička J., Popova O.P., Nemtchinov I.V., Spurný P., Ceplecha Z., 1998, A&A., 334, 713
Burgard D.A., Abraham J., Allen A., Craft J., Foley W., Robinson J., Wells B., Xu C., Stedman D.H., 2006, Appl. Spectrosc., 60, 99
Daily J.W., Dreyer C., Abbud-Madrid A., Branch M.C., 2002, J. Mol. Spectr., 214, 111
Gole J.L., Kolb C.E., 1981, J. Geophys. Res., 86, 9125
Klumov B.A., 2001, JETP Lett., 28, 1159
Kovács I., 1969, Rotational structure in the spectra of diatomic molecules, Akadémiai Kiadó, Budapest, 307 pp.
Lodders K., Fegley B., 1998, The Planetary Scientist Companion. Oxford University Press, 371 pp.
NIST Site, 2013a, November, `http://kinetics.nist.gov/`
NIST Site, 2013b, November, `http://webbook.nist.gov`
PGOPHER Site, 2013, November, `http://pgopher.chm.bris.ac.uk/`
Saksena M.D., Deo M.N., Sunanda K., Behere S.H., Londhe C.T., 2008, J. Mol. Spectr., 247, 47
Spurný P., Haloda J., Borovička J., 2012, in Proc. ACM Conf., No. 1667
Srdanov V.I., Harris D.O., 1988, J. Chem. Phys., 89, 2748
Sugita S., Schultz P.H., Hasegawa S., 2003, J. Geophys. Res., vol. 108, Issue E12, pp. 14-1, CiteID 5140
West J.B., Broida H.P., 1975, J. Chem. Phys., 62, 2566

Meteoroids 2013, Proceedings of the Astronomical Conference,
held at A.M. University, Poznań, Poland, Aug. 26-30, 2013,
eds Jopek T.J., Rietmeijer F.J.M., Watanabe J., Williams I.P.,
Adam Mickiewicz University Press in Poznań, pp 133–139

Emission spectrum of a sporadic fireball afterglow

Madiedo J.M.[1,2] **Trigo-Rodriguez J.M.**[3]

[1]Departamento de Fisica Atomica, Molecular y Nuclear, Facultad de Fisica, Universidad de Sevilla,
41012 Sevilla, Spain (madiedo@cica.es)
[2]Facultad de Ciencias Experimentales, Universidad de Huelva,
Avenida de las Fuerzas Armadas S/N, 21071 Huelva, Spain
[3]Institute of Space Sciences (CSIC-IEEC), Campus UAB, Facultat de Ciencies,
Torre C5-p2. 08193 Bellaterra, Spain

Abstract. We analyze a fireball observed over the south of Spain on April 14, 2013. Its estimated absolute magnitude is -11 ± 1. The event was imaged from two meteor observing stations operating in the framework of the SPanish Meteor Network (SPMN) in Andalusia (south of Spain). On the one hand, the atmospheric trajectory of the bolide and the heliocentric orbit of the parent meteoroid are calculated. The emission spectrum produced during the ablation of this particle was also recorded in the framework of the systematic spectroscopic campaign we are developing since 2006. The relative intensities of emission lines produced by the major meteoroid rock-forming elements (Fe, Mg and Na) clearly indicate a chondritic nature for the progenitor meteoroid. On the other hand, the emission spectrum of the meteoric afterglow was recorded during about 0.12 seconds. The main lines appearing in this signal were identified and their evolution with time is also discussed.

Keywords: meteors, meteoroids, fireballs, meteor spectroscopy

1. Introduction

On April 14th 2013 a fireball with an estimated absolute magnitude of -11 ± 1 was observed over the south of Spain (Figure 1). This sporadic event was simultaneously recorded at $22^h35^m49.8^s \pm 0.1^s$ UTC from two meteor observing stations in Andalusia: Sevilla (latitude: $37^o20'46''$ N, longitude: $05^o58'50''$ W) and El Arenosillo (latitude: $37^o06'16''$ N, longitude: $06^o43'58''$ W). These meteor stations employ an array of low-lux monochrome CCD video devices to monitor meteor and fireball activity, as described below. The bolide was included in the SPMN fireball database with the code 140413, which was assigned after the observing date.

In order to obtain an insight into the chemical properties of meteoroids ablating in the atmosphere, both meteor stations develop a systematic fireball spectroscopy campaign by means of video and slow-scan CCD video spectrographs. These spectrographs have been configured as autonomous devices by means of software developed by the first author. In this way, the emission spectrum produced during the ablation of the parent meteoroid was obtained. Besides, the fireball exhibited a very bright flare by the end of its luminous path, and the afterglow spectrum could also be imaged after this fulguration took place. Here we present a preliminary analysis of the SPMN140413 bolide. Its atmospheric trajectory is obtained and the orbital elements of the parent meteoroid are calculated. In addition, we

Figure 1. Composite image of the SPMN140413 fireball as imaged from Sevilla.

infer information about the bulk chemistry of this particle from the analysis of the fireball emission spectrum. The afterglow spectrum is also discussed.

2. Instrumentation and methods

An array of low-lux monochrome CCD video devices (models 902H2 and 902H Ultimate, manufactured by Watec Co., Japan) operating from the meteor observing stations at Sevilla (lat.: $37^o20'46''$ N, lon.: $5^o58'50''$ W) and El Arenosillo (lat.: $37^o06'16''$ N, lon.: $6^o43'58''$ W) was employed to record the SPMN140413 fireball (Figure 1). The operation of these systems, which work in a fully autonomous way by means of software developed for this purpose by the first author, is explained in detail in (Madiedo and Trigo-Rodriguez 2008; Madiedo et al. 2010). Besides, some of these devices are configured as video spectrographs by attaching holographic diffraction gratings (1000 grooves/mm) to the objective lens (Trigo-Rodriguez et al. 2009). To calculate the atmospheric trajectory and radiant we have employed the AMALTHEA software (Madiedo et al. 2011), which follows the planes intersection method (Ceplecha 1987). Once these data were obtained, the orbit of the meteoroid was calculated with the same software by following the procedure described in Ceplecha (1987). On the other hand, the spectrum was analyzed with the CHIMET application, also developed by the first author (Madiedo et al. 2013).

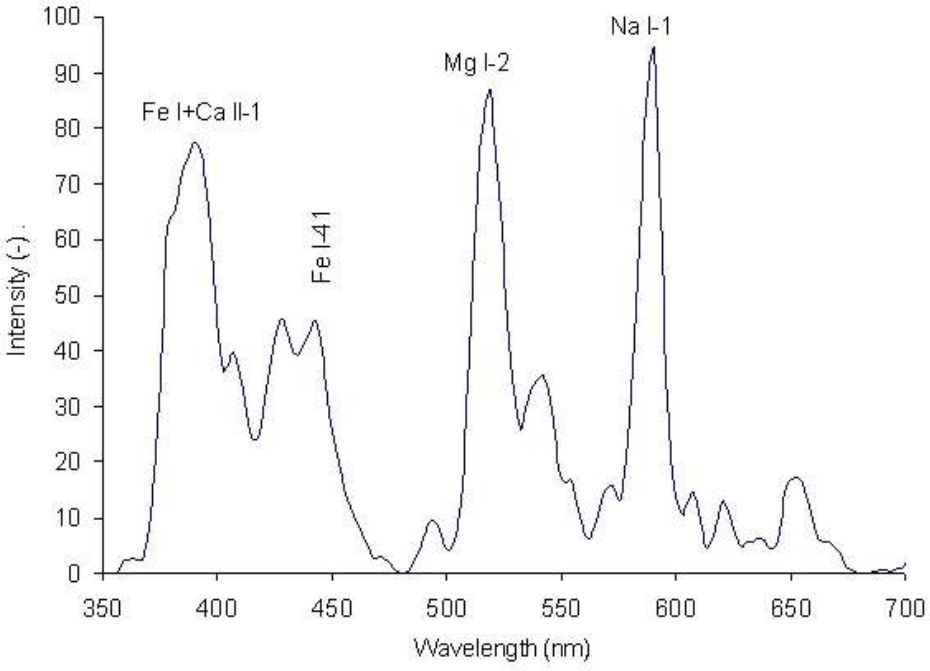

Figure 2. Calibrated emission spectrum of the SPMN140413 fireball. Intensity is expressed in arbitrary units.

Table 1. Trajectory and radiant data (J2000) for the bolide analyzed here. H_b and H_e are the beginning and ending heights of the luminous trajectory, α_g and δ_g the right ascension and declination of the geocentric radiant. V_∞, V_g and V_h indicate the preatmospheric, geocentric and heliocentric velocity, respectively.

H_b [km]	H_e [km]	α_g [deg]	δ_g [deg]	V_∞ [km s^{-1}]	V_g [km s^{-1}]	V_h [km s^{-1}]
104.4±0.5	80.7±0.5	186.30±0.03	-41.6±0.1	28.9±0.3	26.6±0.3	39.7±0.3

3. Results and discussion

According to our analysis, the parent meteoroid impacted the atmosphere with an initial velocity V_∞=28.9±0.3 km s^{-1} and the inclination of the trajectory was of about 74 degrees with respect to the local vertical. The fireball began at a height of 104.4±0.5 km above the ground level and ended its luminous phase at 80.7±0.5 km, with the main flare taking place at 83±0.5 km under an aerodynamic pressure, calculated in the usual way, of (7.4±0.6)·10^5 dyn cm^{-2} (Bronshten 1981; Trigo-Rodriguez and Llorca 2006, 2007). The radiant and orbital parameters (J2000) are shown in Table 2. These data confirm that the bolide was produced by a meteoroid from the sporadic complex. The orbital parameters also show that the meteoroid was following a Jupiter family comet (JFC) orbit before impacting our planet. The fireball emission spectrum, once calibrated in wavelengths and corrected for the instrumental efficiency, is shown in Figure 2, where the most significant lines

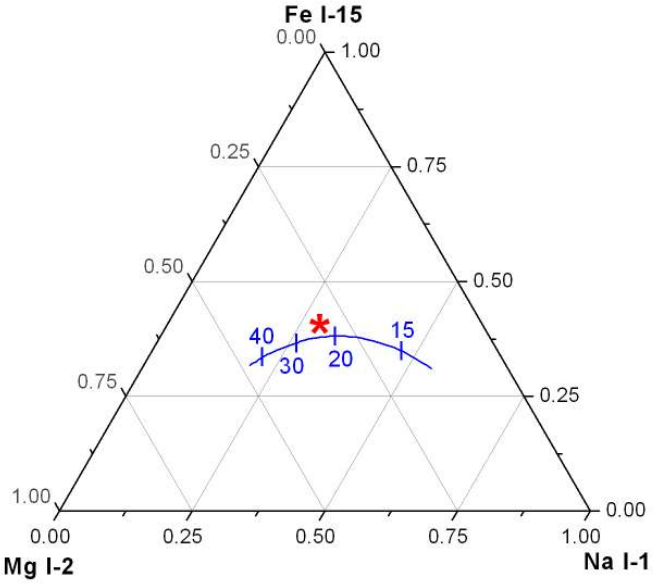

Figure 3. Expected relative intensity (solid line), as a function of meteor velocity (in km s^{-1}), of the Na I-1, Mg I-2 and Fe I-15 multiplets for chondritic meteoroids (Borovicka et al. 2005). The asterisk shows the experimental value obtained for the SPMN140413 fireball.

Table 2. Orbital elements (J2000) for the bolide discussed in this work.

a [AU]	q [AU]	e	i [deg]	ω [deg]	Ω [deg]
4.6±0.4	0.690±0.01	0.85±0.01	27.2±0.2	71.1±0.1	204.9556 ± 10^{-4}

have been highlighted and multiplet numbers are given according to Moore (1945). As can be noticed, the most important contributions correspond to the Na I-1 (588.9 nm) and Mg I-2 (517.2 nm) multiplets. In the ultraviolet, the contribution from the H and K lines of Ca was also identified. However, as usual in meteor spectra, most lines correspond to Fe I. The intensities for the Na I-1, Mg I-2 and Fe I-15 multiplets have provided the intensity ratios Na/Mg=1.08 and Fe/Mg=0.80. These intensities have been plotted on the ternary diagram shown in Figure 3, where the solid curve corresponds to the expected relative intensity, as a function of meteor velocity, for chondritic meteoroids (Borovicka et al. 2005). Thus, the position of the point describing the SPMN140413 fireball spectrum fits well the expected relative intensity for a meteor velocity of about 29 km s^{-1}, which is consistent with a chondritic nature for the meteoroid.

During the first 0.12 seconds after the main flare exhibited by this bolide took place, the afterglow was bright enough to produce an emission spectrum that could

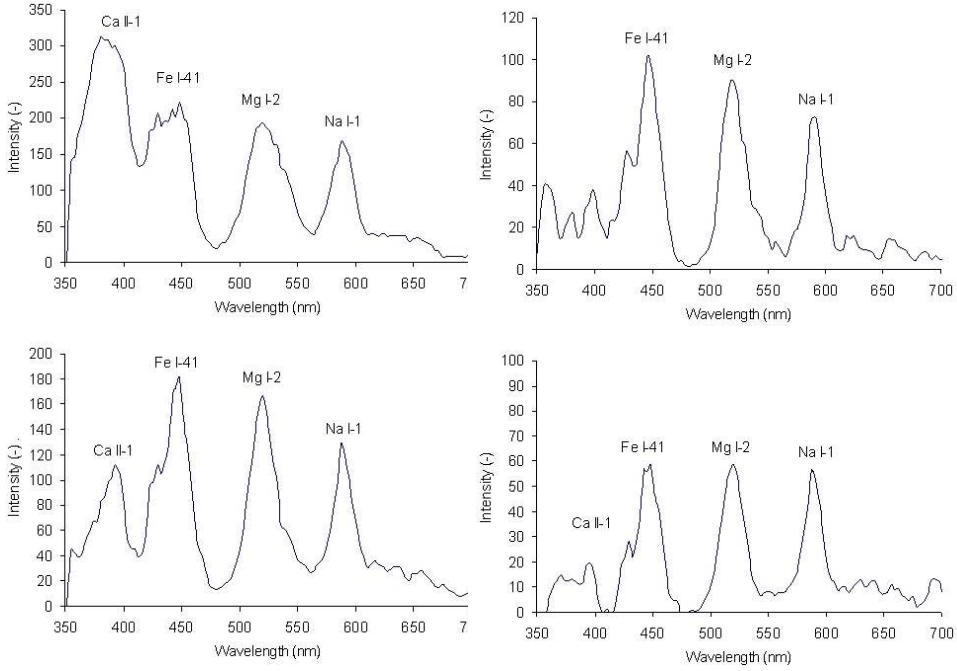

Figure 4. Calibrated emission spectrum of the fireball afterglow at different times. Top panel from left to right, and bottom panel from left to right – these plots correspond to 0.02, 0.04, 0.06 and 0.08 seconds after the main flare took place, respectively. Intensity is expressed in arbitrary units.

be recorded by two CCD video spectrographs. Wake spectra can provide useful information about physical processes taking place in persistent meteor trains. However, such spectra are not abundant in the literature Borovicka and Jenniskens (2000); Abe et al. (2005). These video spectrographs generate interlaced imagery at a rate of 25 frames per second (fps) but once these images were de-interlaced we obtained the evolution of this spectrum with a temporal resolution of 0.02 seconds. In this way, we could analyze the evolution with time of the intensity of the emission lines identified in this signal. The spectrum was also calibrated in wavelengths and corrected according to the efficiency of the spectrograph. Figure 4 shows the calibrated afterglow spectrum at different times after the main flare exhibited by the fireball took place. The contributions from Mg I, Na I, Ca I, Fe I, Ca II and O I were identified in the signal (the latter is not shown in Figure 4), with the Na I-1 and Mg I-2 lines being the most important ones. The brightness of these lines was found to decrease exponentially with time. This behaviour was also found for the lines in the afterglow spectrum of Leonid fireballs (Borovicka and Jenniskens 2000). This is exemplified in Figure 5, where the evolution of the intensity of the Na I-1 line is shown. Additional analysis will be performed in order to establish the mechanism that drives this evolution of brightness with time.

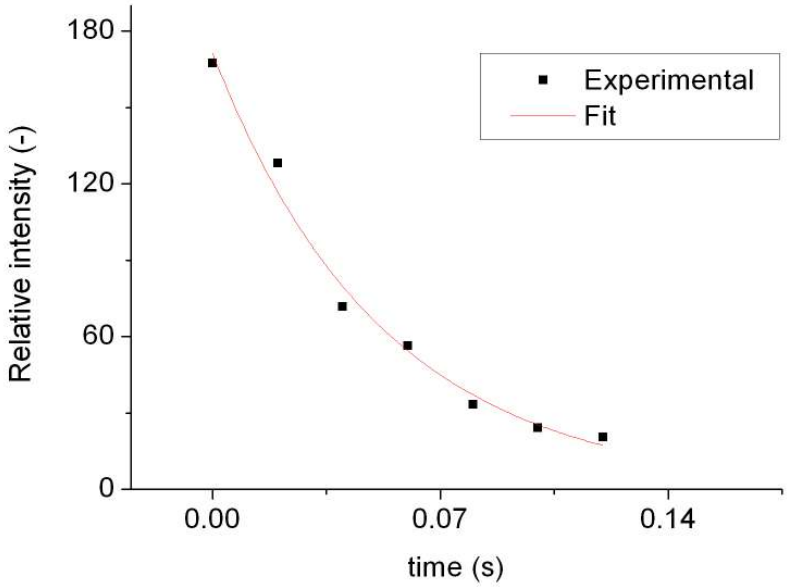

Figure 5. Variation with time of the intensity of the Na I-1 line in the afterglow spectrum.

4. Conclusions

We have studied a mag. −11 fireball observed over the south of Spain on April 14, 2013. From the preliminary analysis of this event we have extracted the following conclusions:

1) The parent meteoroid impacted the atmosphere with a velocity of ∼28.9 km s^{-1}. The fireball began at 104.4 km above the ground level and ended at a height of around 80.7 km. The maximum luminosity of the bolide took place during the flare occurring by the end of its atmospheric path.
2) The calculated orbit, atmospheric penetration and tensile strength of the meteoroid are consistent with a cometary origin for this particle. In particular, the orbital elements show that the meteoroid had a sporadic origin and was following a JFC orbit before impacting the Earth.
3) The analysis of the emission spectrum of this fireball, particularly the emission lines coming directly from the ablation of the main meteoroid rock-forming elements (Fe, Mg and Na), points towards a chondritic nature for the meteoroid.
4) The contributions from Mg I, Na I, Ca I, Fe I, Ca II and O I were identified in the afterglow spectrum, with the Na I-1 (588.9 nm) and Mg I-2 (517.2 nm) lines being the most important ones. The brightness of these lines decreased exponentially with time. Additional analysis will reveal the mechanism that drives the evolution of this brightness.

Acknowledgements

We are very grateful to INTA-CEDEA for its support with the automated meteor observing station at ESAt (Huelva, Spain). We also acknowledge support from the Spanish Ministry of Science and Innovation (projects AYA2009-13227 and AYA2011-26522) and Junta de Andaluca (project P09-FQM-4555).

References

Abe S., Ebizuka N., Murayama H., Ohtsuka K., Sugimoto S. et al., 2005, EM&P, 95, 265
Borovicka J., Jenniskens P., 2000, EM&P, 8283, 399
Borovicka J., Koten P., Spurny P., Boek J., Stork R., 2005, Icarus, 174, 15
Bronshten V.A., 1981, Geophysics and Astrophysics Monographs. Reidel, Dordrecht.
Ceplecha Z., 1987, Bull. Astron. Inst. Cz. 38, 222
Madiedo J.M., Trigo-Rodriguez J.M., 1991, EM&P, 102, 133
Madiedo J.M., Trigo-Rodriguez J.M., Ortiz J.L., Morales N., 2010, Advances in Astronomy, 2010, 1
Madiedo J.M., Trigo-Rodrguez J.M., Lyytinen E., 2011, NASA/CP-2011-216469, 330
Madiedo J.M., Trigo-Rodrguez J.M., Konovalova N., Williams I.P., Castro-Tirado A.J., Ortiz J.L., Cabrera-Cao J., 2013, MNRAS, 433, 571
Moore C.E., 1945, In: A Multiplet Table of Astrophysical Interest. Princeton University Observatory, Princeton, NJ. Contribution, No. 20
Trigo-Rodrguez J.M., Llorca J., 2006, MNRAS, 372, 655
Trigo-Rodrguez J.M., Llorca J., 2007, MNRAS, 375, 415
Trigo-Rodriguez J.M., Madiedo J.M., Williams I.P. et al., 2009, MNRAS, 392, 367

Meteoroids 2013, Proceedings of the Astronomical Conference,
held at A.M. University, Poznań, Poland, Aug. 26-30, 2013,
eds Jopek T.J., Rietmeijer F.J.M., Watanabe J., Williams I.P.,
Adam Mickiewicz University Press in Poznań, pp 141–146

Micro-Raman spectroscopy of meteorite Košice

Kaňuchová Z.[1] **and Baratta G.A.**[2]

[1]Astronomical Institute of Slovak Academy of Sciences, SK-05960 T. Lomnica, Slovakia
(zkanuch@ta3.sk)
[2]INAF-Osservatorio Astrofisico di Catania, Via S. Sofia 78, IT-95123 Catania, Italy

Abstract. The Raman microscope technique was used to characterize 3-5 μm structures in the matrix of the Košice meteorite, an H5 ordinary chondrite. Its fall is associated with a bright fireball that appeared over central-eastern Slovakia on February 28, 2010. Several micro-Raman spectra of the interior part of meteorite Košice sample were collected. On the basis of characteristic frequencies of Raman modes the main types of minerals (olivines, pyroxenes) as well as carbon material were identified. The Raman signature of the carbon material is consistent with the second stage of the amorphization trajectory between amorphous carbon and nanocrystalline graphite.

Keywords: Košice meteorite, Raman micro-spectroscpy

1. Introduction

The Raman microscope technique is a non-destructive spectroscopic technique based on inelastic scattering of monochromatic light (Raman Effect), usually from a laser source. Inelastic scattering means that the frequency of photons in monochromatic light changes upon interaction with a sample. Photons of the laser light are scattered at a different energy by the sample molecules.

The frequency of the scattered photons is shifted up or down in comparison with original monochromatic frequency, which is called the Raman Effect. This shift provides information about vibrational, rotational and other low frequency transitions in molecules. Raman spectroscopy can be used to study solid, liquid and gaseous samples. By applying Raman spectroscopy to meteoritic material it is possible to observe the presence and characterize many minerals and variety of carbon structures (e.g. Baratta et al. 2008; Wang et al. 2004; Larsen and Nielsen 2006).

It is also a sensitive tool for the study of structural properties of carbonaceous materials. In particular, it provides an indicator of the degree of crystallinity of sp^2 graphitic clusters, which is correlated with the metamorphic grade of meteorites (Buseck and Bo-Jun 1985; Pasteris and Wopenka 1991; Busemann et al. 2007; Starkey et al. 2013).

In this contribution we present a Micro-Raman spectroscopy study of the interior part of the piece of the meteorite Košice, carried out at the Experimental Astrophysics Laboratory at the Catania Astrophysical Observatory, Italy.

2. Laboratory equipment and procedure

Micro-Raman spectra were collected using a triplemate SPEX Raman spectrometer equipped with a 1200 groves/mm holographic grating. The spectrometer is coupled to a confocal DILOR xy illuminator equipped with an Olympus BX40 microscope with 10×, 50× and 100× magnification objectives. The Raman spectrometer is equipped with a continuous Ar ion laser beam (514.5 nm) as exciting radiation and a CCD detector in the 0.4–1.0 μm spectral range. Details of the in situ Raman technique can be found in Brunetto et al. (2004). Using the microscope objectives (50×, 100×) to focalize the exciting laser beam we get the spot size of about 4 and 2 microns respectively. An example of the microscopic view of a studied sample area is shown in Fig. 1. The laser power (Ar^+, 514.5 nm) on the sample was kept below 0.3 mW to avoid overheating the sample. The spatial resolution, set by a confocal pinhole, was 4 μm for the 100× objective; and the instrument spectral resolution was 8 cm^{-1} with a peak position accuracy of 1-2 cm^{-1}. The spectrum acquisition time was 60 s and the signal to noise ratio was improved by multiple acquisitions (ten per spot). In addition, in the case of spectra acquired in the 200-1200 cm^{-1} Raman shift region the final Raman spectra were smoothed using 5 points in Svitzky-Golay procedure.

3. Results and discussion

Raman spectra of several different regions of the meteorite interior were taken. On the basis of characteristic frequencies of Raman modes, the main types of minerals were identified. The common minerals found in our sample of the Košice meteorite are silicates. Raman double-band (in a range 800–900 cm^{-1}) indicates olivine (spectra no. 8, 9, 10 in Fig. 2) (e.g. Wang et al. 2004). A Raman "fingerprint" of pyroxene is identified in spectrum no. 7.

The major Raman peaks in the spectra of olivine and pyroxenes result from the coupling of fundamental symmetric and asymmetric stretching vibrational modes of SiO_4 tetrahedra and (Si_2O_6)n chains. The different cations (Mg, Fe, Ca, etc.) that occupy the octahedral sites formed by the silicates affect the peak positions of these fundamental vibrations, with respect to the masses of the cations. The peak-position shift towards higher wavenumbers with increasing Fo content is linked to the decrease of atomic mass and polyhedral volume in octahedral sites, and to the degree of coupling of the symmetric and asymmetric stretching vibrational modes of SiO_4 groups (Kuebler et al. 2006).

As a consequence, molar ratios of the major cations in pyroxene and olivine can be determined from their Raman peak positions (Wang et al. 2004; Baratta et al. 2008; Kuebler et al. 2006). Following the work of Wang et al. (2004), we estimated the Mg/(Mg+Fe) ratio of observed olivine crystals to be 0.7-0.9; and Mg/(Mg+Fe+Ca) ratio of pyroxene around 0.75.

The presence of organic material is evident, when their specific bands, viz. D ($\sim$1360 cm^{-1}) and G ($\sim$ 1582 cm^{-1}), are observed in Raman spectrum. The presence and width of D and G bands in the spectra depends on the degree of order of graphitic material. Both bands are due to sp^2 hybridized carbon sites. The G band

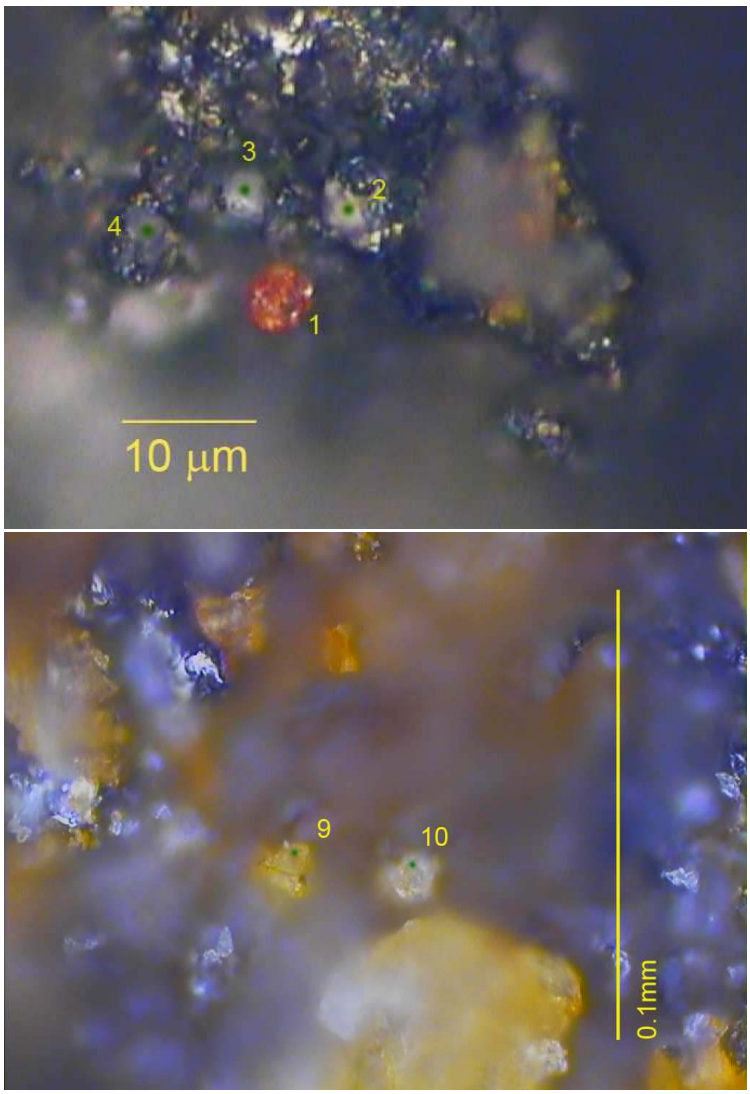

Figure 1. The microscopic views of the analyzed sample of meteorite Košice. Positions of laser spots are indicated and numbered for identification of each spectrum.

is a bond stretching vibration of a pair of sp^2 sites, it occurs wherever the sp^2 sites are arranged as olefinic chains or aromatic rings (Ferrari and Robertson 2000). In the Raman spectra of highly ordered pyrolitic graphite or natural graphite with large ($\gg 1\,\mu$m) microcrystals only one, the G band is observed. Spectra of microcrystalline and disordered carbon show an additional D band (Tuinstra and Koenig 1970). The D band is a breathing vibration of aromatic rings which is activated by disorder, it only occurs when sp^2 sites are in aromatic rings (Ferrari and Robertson 2000).

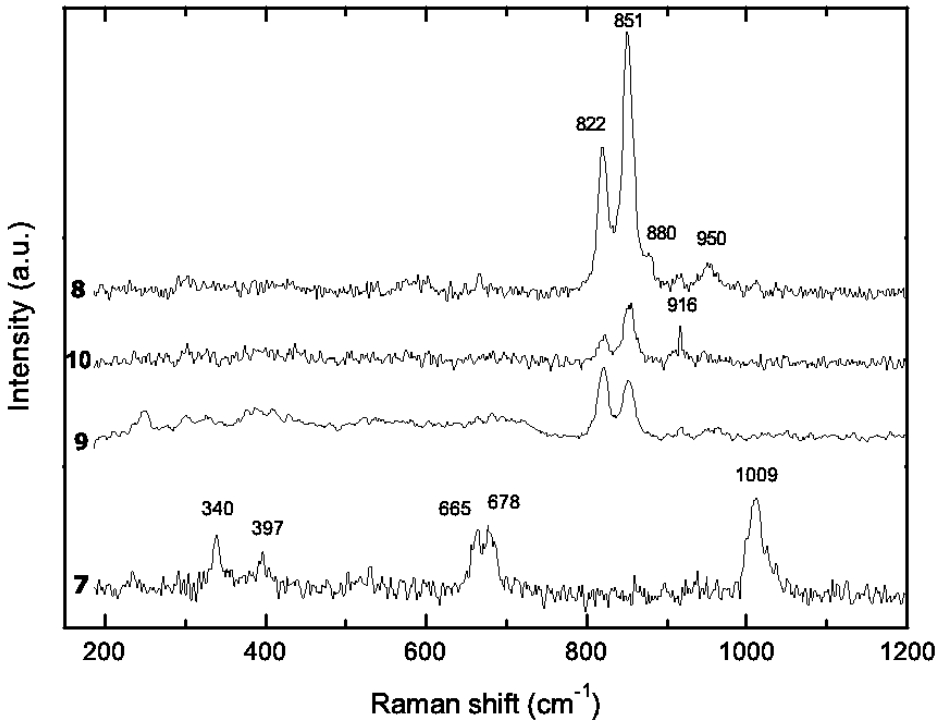

Figure 2. Micro-Raman spectra of silicates in meteorite Košice. Numbers on the left indicate positions of laser spots at the sample (see Fig. 1).

As well known, graphite is composed of planar hexagonal rings of carbon atoms. The parameters characterizing the dimensions of graphite layers are L_a – the average size of graphite layer and L_c – which divided by the interlayer spacing gives the number of layers (Tuinstra and Koenig 1970). Well-crystallized graphite can have L_a values up to several hundreds nanometers, whereas microcrystalline graphite (also referred as amorphous graphite), can have L_a values as low as 20-30 Å (Larsen and Nielsen 2006).

The intensity ratio I_D/I_G is a spectral parameter related with the degree of structural order of carbonaceous material (Ferrari and Robertson 2000). However, the relation is unambiguous, as is described further. The Tuinstra-Keonig relation between the graphite domains L_a and the D – and G – lines intensities (Tuinstra and Koenig 1970):

$$L_a = C_L(\lambda) \times \frac{I_G}{I_D} \tag{3.1}$$

where C_L (λ) is a laser wavelength (λ) dependent factor (C_L(514 nm)=44 Å), is valid for values of the graphitic domain size $L_a > 20$ Å. For the range $L_a < 20$ Å,

Ferrari and Robertson (2000) proposed a new and an opposite relation:

$$L_a^2 = C_L'^{-1}(\lambda) \times \frac{I_D}{I_G} \tag{3.2}$$

where $C'_L(514\,\mathrm{nm})=0.0055\,\mathrm{Å}^2$.

An indication of the degree of order can be provided also by the G and D band widths - the broader the bands, the more disordered is the graphitic material. Broadening of the bands indicates an increase in the bond angle disorder (i.e. bond angle distortions of the three-fold coordinated C atoms from the ideal 120°) and a decrease in the mean size and/or number of crystallites (Baratta et al. 2008). Below a certain size of the basic structural unit of the carbonaceous material, the bands become so wide that they can no longer be recognized as individual peaks (Wopenka 1988). In the studied sample of meteorite Košice, both D and

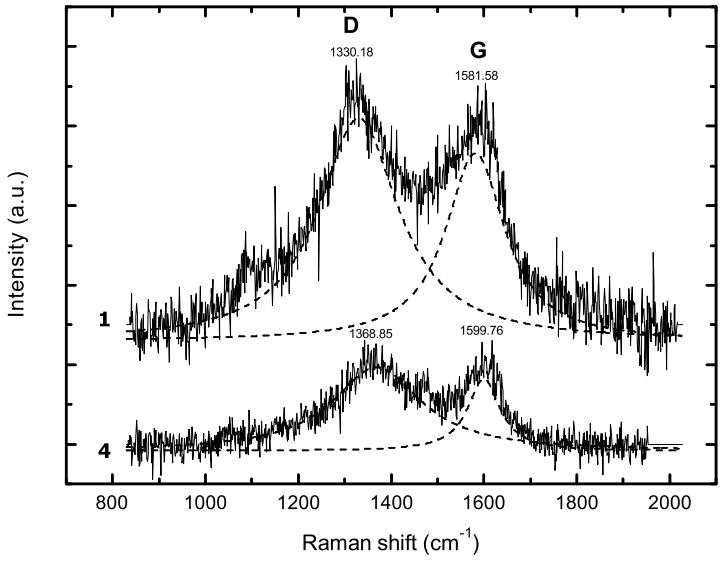

Figure 3. Micro-Raman spectra of carbonaceous matter in meteorite Košice. The spectra were fitted after a linear baseline correction by using a two-Lorentzian band model. The two first order Raman bands D and G are characteristic for disordered carbon. Numbers on the left indicate the positions of laser spots at the sample.

G Raman bands were observed in the 800–2100 cm^{-1} Raman shift region (Fig. 3). After a baseline correction, the Raman spectra were fitted by a two-Lorenzian band model (Ferrari and Robertson 2000; Larsen and Nielsen 2006) and the individual band parameters (center, intensity and FWHM of bands) were extracted.

Raman spectra of thermally metamorphosed meteorites have D and G peaks that are quite narrow and well separated, primitive carbonaceous materials have broad

and blended D and G bands (Busemann et al. 2007). According to work of Busemann et al. (2007) (see Fig.6 in referred paper), increasing metamorphism from CI, CM, CR through types 3.05-3.2 to 3.2-3.7 and the EH chondrites leads to smaller values of D band width, simultaneously, the intensity ratio ID/IG increases up to ∼1.5, following by the steep decrease of intensity ratio with decreasing band width. These trends resemble those described for the transitions from disordered amorphous C through "nanocrystalline graphite" to graphite in terrestrial carbonaceous samples (Ferrari and Robertson 2000; Busemann et al. 2007).

Assuming that carbon material in the Košice meteorite sample is in the stage 2 of the insoluble organic matter (IOM) amorphization trajectory between nanocrystalline graphite and amorphous carbon defined by Ferrari and Robertson (2000), we can use the Eq. 3.2 for the estimation of the graphitic domain size of carbonaceous material L_a. It was estimated to be around 14.6 Å.

The width of the D line found in Košice is similar to that found in the IOM of many ordinary chondrites (e.g. H/L3.6 Tieschitz, H3.7 Brownfield, see Busemann et al. (2007)).

Acknowledgements

This research has been supported by VEGA - The Slovak Agency for Science, Grant No. 2/0022/10.

References

Baratta G.A., Brunetto R., Leto G., Palumbo M.E., Spinella F., Strazzulla G., 2008, J. Raman Spectroscopy 39, 211

Brunetto R., Baratta G.A., Strazzulla G., 2004, J. Appl. Phys. 96, 380

Buseck P.R., Bo-Jun H., 1985, Geochim. Cosmochim. Acta 49, 2003

Busemann H., O'D Alexander C.M., Nittler L.R., 2007, M&PS, 42, 1387

De Angelis S., Della Corte V., Baratta G.A., Rietmeijer F.J.M., Brunetto R., Palumbo P., Ciucci, A., Rotundi A., 2011, Spectroscopy Letters 44, 549

Dresselhaus M.S., Pimenta M.A., Eklund P.C., Dresselhaus G., 2000, In Raman Scattering in Materials Science, Springer Series in Materials Science, vol 42, Weber W.H., Merlin R. (eds), Springer-Verlag: Berlin, 2000, 314

Ferrari A., Robertson J., 2000, Phys. Rev. B 61, No. 20, 14095

Kuebler K.E., Jolliff B.L., Wang A., Haskin L.A., 2006, Geochim. Cosmochim. Acta 70, 620

Larsen K.L, Nielsen O.F., 2006, J. Raman Spectroscopy 37, 217

Pasteris J.D., Wopenka B., 1991, Can. Mineralogist 29, 1

Rull Perez F., Martinez-Frias J., 2003, J. Raman Spectroscopy 34, 367

Starkey N.A., Franchi I.A., O'D. Alexander C.M., 2013, Met. Planet. Sci. 48, 1800

Tuinstra F., Koenig J.L., 1970, J. Compos. Matter. 4, 492

Wang A., Kuebler K., Jolliff B., Haskin L.A., 2004, J. Raman Spectroscopy 35, 504

Wopenka B., 1988, Earth Planet. Sci. Lett. 88, 221

Meteoroids 2013, Proceedings of the Astronomical Conference,
held at A.M. University, Poznań, Poland, Aug. 26-30, 2013,
eds Jopek T.J., Rietmeijer F.J.M., Watanabe J., Williams I.P.,
Adam Mickiewicz University Press in Poznań, pp 147–153

Sampling the constant drizzle of meteoric dust in the upper stratosphere

Rietmeijer F.J.M.[1], Della Corte V.[2], Rotundi A.[3] Ferrari M.[3]

[1]Dept. of Earth and Planetary Science, MSC 03 2040, 1-University of New Mexico,
Albuquerque, NM 87131-0001, USA, (fransjmr@unm.edu)
[2]IAPS-INAF, via del Fosso del Cavaliere; 00133 Roma, Italy
[3]Dip. Scienze Applicate, Universitá degli Studi di Napoli Parthenope,
Centro Direzionale I C4; 80143 Napoli, Italy

Abstract. In our effort to sample the constant drizzle of meteoric dust DUSTER (Dust from the Upper Stratosphere Tracking Experiment and Retrieval) collected a surprisingly mineral-rich population of mostly nanometer, and lesser amounts of micrometer, particles. Our analysis shows that bolide disintegration could be a possible source for this dust in the upper stratosphere.

Keywords: meteoric dust, dust collection, upper stratosphere, bolides

1. Introduction

Meteoroid ablation and evaporation release metal species and molecules into the upper atmosphere where they contribute to the mesospheric metal complex between 100 and 80 km altitude. What happens next is a bit uncertain. It was suggested that vapors of small extraterrestrial particles would condense in the mesosphere followed by settling to lower altitudes (Megie and Blamont 1977). In the sulfate aerosol layer of the stratosphere the smallest ($\leqslant$500 nm) and the largest ($\geqslant$10 μm) sulfate particles had presumably nucleated on this condensed meteoritic dust (Hunten et al. 1980). There is no evidence to connect this putative, condensed meteoritic dust from mesospheric to these sulfate particle nucleation centers. Today we know there is a continuous supply of meteoric smoke nanoparticles, 4 to 20 nm in diameter, between ∼85 km to ∼35 km altitudes, incl. fayalite (Fe_2SiO_4) and pyroxene ($Mg_{0.4}Fe_{0.6}SiO_3$ Hervig et al. (2009)) that act as condensation nuclei for Polar Mesospheric Clouds (a.k.a., noctilucent clouds). Other meteoric nanograin compositions are listed as carbon (C), wüstite (FeO), or magnesiowüstite, $Mg_xFe_{1-x}O$; x = 0.1–0.6 (Hervig et al. 2012). These meteoric dust compositions are inferred from remote sensing data that cannot make unique identifications. If we want to know their chemical composition, size, shape, morphology and structural state (crystalline or amorphous) we need to collect these meteoric particles.

2. Particle Collections and Source Connections

The top of the stratospheric aerosol layer at 30 km altitude (Renard et al. 2008) is a natural lower boundary for any searches of interplanetary materials. The upper stratosphere is quite accessible by high altitude balloons that can carry dust

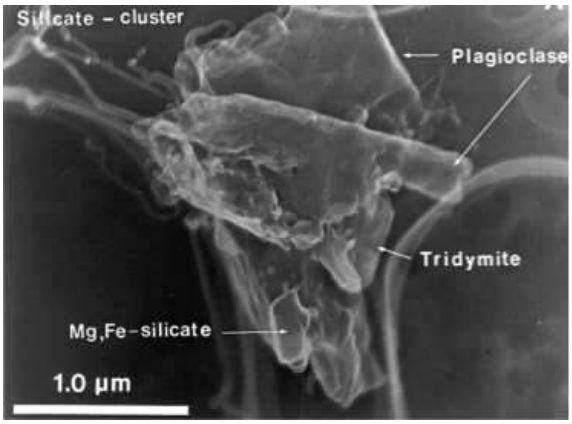

Figure 1. This cluster of Ca,Al- and Mg,Fe-silicate minerals and SiO_2 (tridymite) collected in the stratosphere between 34-36 km during May, 1985 was present in a sample of sub-micron grains that were clearly volcanic ash fines. Occam's razor then dictated that this particle too is volcanic ash. At that time claiming it was extraterrestrial dust from the Zodiacal cloud could not be supported based on the state of knowledge in 1985. Today, the same claim is not preposterous. Reproduced from Rietmeijer (1993); Journal of Volcanology and Geothermal Research.

collectors. Obviously interplanetary dust collections should avoid periods directly following volcanic eruptions of major magnitude, e.g. Mt. Pinatubo, El Chichón and Mt St. Helens, as their fine dust entrained in the rising plume could reach above 30 km (Rietmeijer 1993). The upper part of the stratosphere presents a potentially mixed environment, a crossroads, of terrestrial and extraterrestrial dust. The terrestrial component would be overwhelmingly dominated by the finest volcanic ash particles (Fig. 1). But we learn as we go on. It turns out that 85%–95% of the observed mid-infrared emission of the Zodiacal cloud is produced by particles from Jupiter-Family (J-F) comets and that ∼85% of the total mass influx at Earth is J-F comet dust (Nesvorný et al. 2010). Their atmospheric velocities are typically low; and as low as ∼12 km s^{-1}, which means that many J-F comet particles might survive flash heating. It is then not too farfetched to postulate that this compact aggregate particle of silicate minerals (Fig. 1) could have survived but of course comets do not contain chemically differentiated materials. This notion must be revisited in the light of the mineralogical results from the Stardust mission. The big surprise was that the dust from 81P/comet Wild 2 closely resembled asteroid-like minerals and mineral-grain clusters (Brownlee et al. 2006; Zolensky et al. 2008; Joswiak et al. 2012; Dobrică et al. 2009). Thus, it is not unthinkable that this silicate-cluster has its analogs among the dust in comet Wild 2 that began life as a Kuiper Belt Object that became part of a constant supply of Interplanetary Dust Particles (IDPs) and micrometeorites (MMs) to the lower stratosphere and the Earth surface of J-F comet dust in addition to meteoric dust. Meteoric (smoke) nanoparticles have yet to be collected but for a few possible exceptions. Crystalline metallic noctilucent cloud particles ⩽500 nm in diameter, and clusters

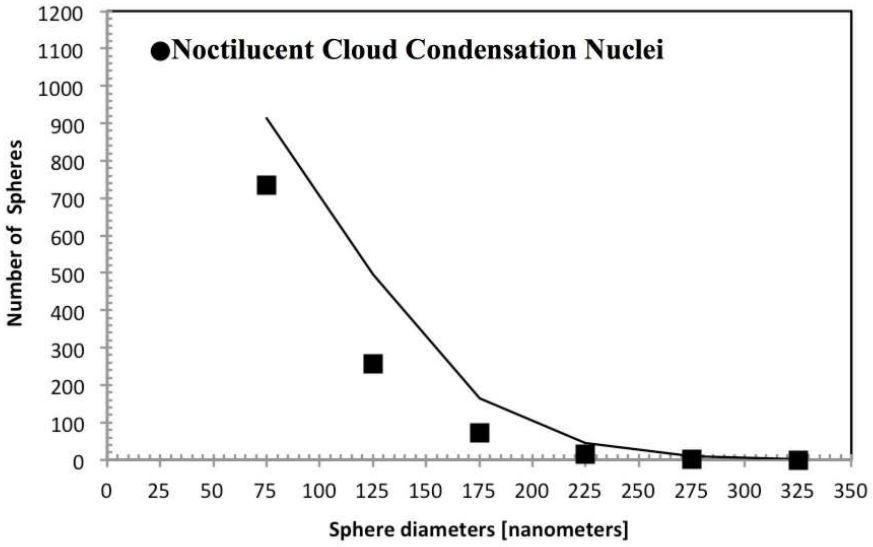

Figure 2. The size distribution of meteoric NiO and taenite smoke nanospheres from 5 to 30 nm in diameter (Hemenway et al. 1961) (solid square) and the smallest meteoric smoke particle, or noctilucent cloud condensation nuclei, size (dot). The solid squares are the midpoints of each of the six size bins listed in Hemenway et al. (1961). The trend shows that these nanospheres could be evolved meteoric smoke particles by a process of grain growth.

thereof ∼500 nm in diameter, had pure iron and FeNi- compositions, while other submicron noctilucent particles had Si and Fe, Si and Ca and pure Si compositions (Witt et al. 1964). The size distribution from 20 to 800 nm supports they could be chemically-evolved meteoric dust (Hemenway et al. 1964). Also, NiO and taenite (high-Ni Fe,Ni-metal) spherical nanometeorites intercepted settling in the lower stratosphere at 20 km altitude in the Arctic November 1960 (Hemenway et al. 1961) could be evolved meteoric smoke (Fig. 2). The NiO and taenite compositions are quite acceptable for extraterrestrial dust but unlikely for natural terrestrial dust in this size range.

Meteoric particles 0.2 to 3 microns in diameter were also collected in the lower stratosphere at ∼20 km altitude. It was concluded that this extraterrestrial component residing in the mesosphere and stratosphere did not have a chondritic composition for Fe, Ni, Mg, Mn, Ca, Na and K (Cziczo et al. 2001). Apparently the tacit assumption was that meteoric dust once it had settled into the lower stratosphere should have the chondritic composition of the annual influx of interplanetary materials to the Earth's atmosphere. The observed Ca abundance was well below its chondritic abundance (Cziczo et al. 2001), while no Al and Ti abundances were reported. It could be an indication that differential ablation (Janches et al. 2009) is on average for all incoming extraterrestrial materials more efficient than anticipated.

3. Do Meteoric Dust Aggregates Exist?

Laboratory simulations of photo-chemical oxidation of mesospheric Mg, Fe and Si metals by O_3 when settling through the upper atmosphere showed potentially diverse meteoric nanoparticle compositions. The ∼10 nm in diameter meteoric dust analogs were open aggregates of SiO_2 (silica), Fe_2O_3 (hematite) and FeOOH (goethite), fayalite, forsterite (Mg_2SiO_4), ferrosilite ($FeSiO_3$), enstatite ($MgSiO_3$), amorphous olivine [$(Mg,Fe)_2SiO_4$] and amorphous pyroxene [$(Mg,Fe)SiO_3$] (Saunders and Plane 2006, 2011). The largest meteoric analog grains in these aggregates were ∼200 nm in diameter showing that initially meteoric nanoparticle sizes could be increased via simple grain growth. The formation of open nanograin aggregates is probably an artifact of high particle densities in the experiments as it is in almost all experiments of this nature (Rietmeijer and Nuth III 2012; Rotundi et al. 1998). It is unlikely that similarly-high particle densities exist in the meso- and stratospheres except perhaps during strong winds. The finding of branched chains of nanograin aggregates with typical lengths of 1–2 microns above 35 km altitude (Bigg 2012) could be interesting evidence that meteoric dust aggregation is possible in the upper atmosphere. Still, lacking compositional data of these branched chains we cannot exclude the possibility that they can be chondritic porous (nano)IDPs. Clusters and short strings of electron-dense spheres (∼10 to ∼100 nm in diameter) collected ⩾35 km altitude were interpreted as melted metallic particles from ablating meteoroids (Bigg 2012) but lacking chemical analyses this interpretation cannot be confirmed albeit also not be denied.

4. DUSTER collecting meteoric dust

DUSTER (Dust from the Upper Stratosphere Tracking Experiment and Retrieval) is an autonomous instrument designed for the non-destructive collection of dust particles, 200 nm to 40 microns in size, between 30 and 40 km altitude (∼12 to 3 mbar) in the upper stratosphere. This balloon-borne instrument has an active sampling system that was specifically developed to minimize and control contamination during instrument assembling and autonomous flight performance (Della Corte et al. 2012, 2013). The instrument contains an active collector operational at altitude and a "blank collector" that functions as a monitor of particulate contamination during all pre- and post-flight operations, and all operations in the laboratory where a class-100 clean room is used. Another unique DUSTER feature is the rigorous protocol to accept an individual particle on the active collector as "collected" during stratospheric sampling. That is, all collection surfaces (standard transmission electron microscope holey-carbon thin films on Cu-mesh grids) are automatically scanned using a Field-Emission Scanning Electron Microscope (FESEM) and any particles present are documented. Upon return after collection these same surfaces are re-scanned and "new" particles are recognized. When the blank's integrity was compromised during the actual period of stratospheric collection, or at any time after closing the actual collector during descent, recovery or transportation to the laboratory in Naples, these added particles (relative to the pre-flight analyses) are proof of contamination. When the blanks integrity was preserved, the difference

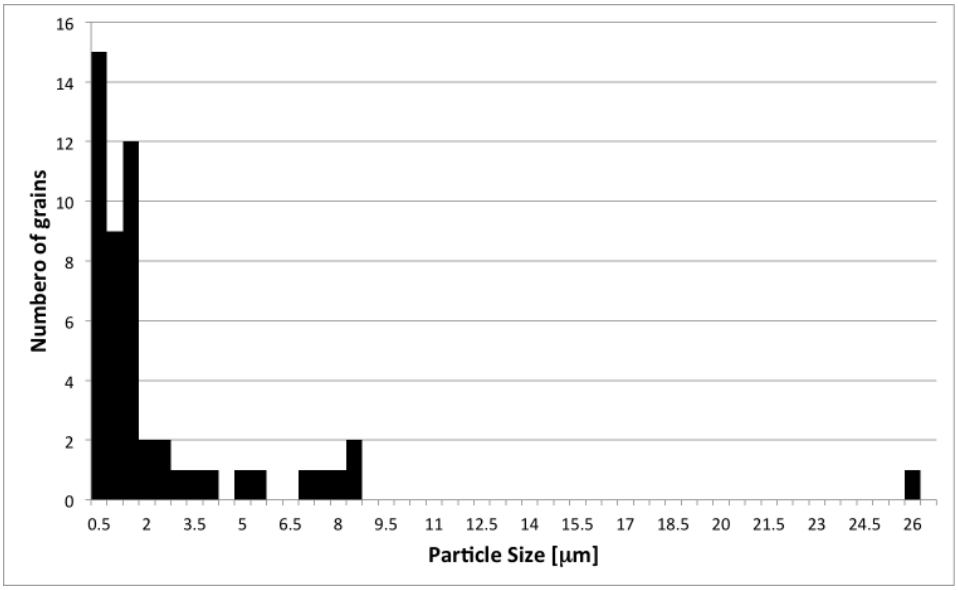

Figure 3. Histogram showing the number of particles collected in the upper stratosphere during 2008 and 2011 as a function of geometric mean particle diameter (microns).

between pre- and post-flight dust loadings on the actual collector are particles that were collected in the upper stratosphere (for more details see: Della Corte et al. (2012) and Della Corte et al. (2013)). It is possible that individual particles can be removed from the collector for further analyses by Fourier Transform Infrared Spectroscopy (FTIR) and micro-Raman spectroscopy (cf. Ciucci 2011). Fifty-one particles 0.2 μm to 26 μm in size were collected at altitudes between 32 and 38.5 km (Fig. 3).

The particles are mostly (1) Ca-bearing calcite and/or aragonite (De Angelis et al. 2011) with evidence of thermal erosion and incipient melting (Fig 4a), (2) irregularly-shaped carbon particles (Fig. 4b), and (3) carbon and low-Si C-O-Si spheres (Fig. 4c). Aluminosilica and aluminum-oxide grains are also present. Rare aggregate particles include (1) massive (Fig. 4d) and smoke-like (Della Corte et al. 2013) carbon aggregates, (2) quenched 'bunch-of-grapes' CaO aggregates (Fig. 4e), and (3) fine-grained CaF_2 aggregates (Fig. 4f).

5. Bolide Disintegration: A possible new source of meteoric dust

Such particles, but more critically, such assemblages of particles were never before identified among dust collected in the upper stratosphere. The grain compositions and morphologies point to an environment wherein each particle experienced flash heating up to ∼4,000K followed by ultra-rapid cooling that caused grain melting and quenching into spheres and formation of liquid spays that quenched into smoke-like aggregates (Figs. 4d, -e, -f). That is, the environment had to provide containment of these grains as a dense cloud. We propose that conditions during

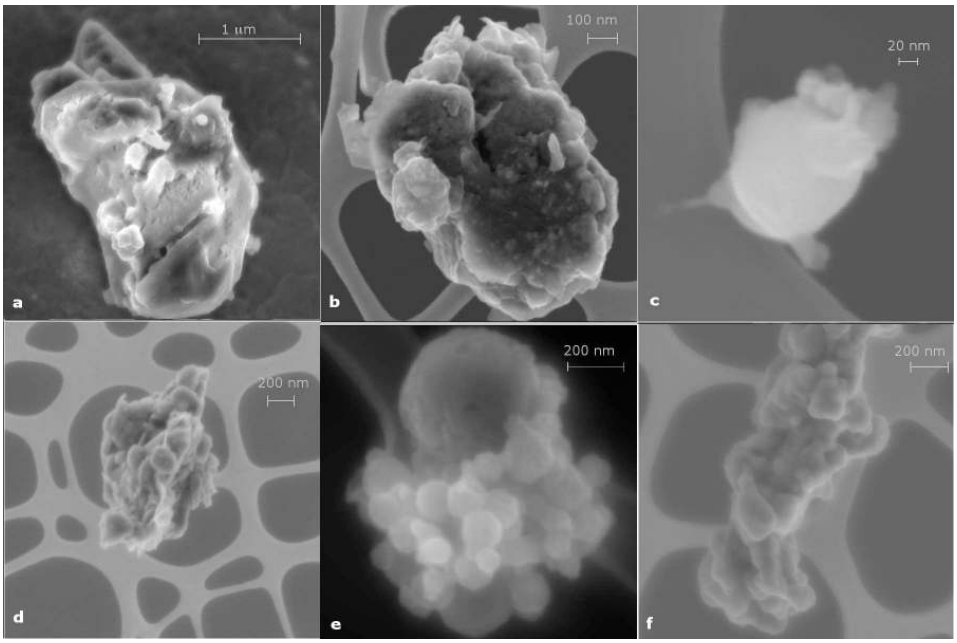

Figure 4. *(a)* thermal erosion of Ca-bearing calcite or aragonite, *(b)* an irregularly-shaped carbon particle, *(c)* a C-O-Si sphere, *(d)* an almond-shaped massive carbon aggregate of (sub)spherical grains (it lacks the typical smoke morphology of soot particles collected in the lower stratosphere, *(e)* an agglomerate of CaO nanospheres ∼10 to 120 nm in diameter attached to a 250 nm CaO sphere (Della Corte et al. 2013), and (f) a compact cluster of fine-grained CaF_2 grains.

disintegration of a low-tensile-strength bolide meet these environmental requirements. We suggest that similar dust particle associations will be found in the dust clouds that are associated with large bolide events, a.o. the Tagish Lake bolide.

6. Conclusions

There is a constant drizzle of nano- to micrometer size dust settling from the mesosphere to the lower stratosphere (and all the way down to the Earth surface) that consists mostly of J-F family debris in the form of most of the collected IDPs and meteoric dust due to meteor ablation in the mesosphere. The collected CaO, spheres were very much part of the dust associations collected by DUSTER but on the basis of size alone they resemble evolved meteoric smoke particles from noctilucent clouds (Hemenway et al. 1961, 1964). They are in fact oxidized mesospheric metal nanograins. Other particles collected by DUSTER are not meteoric smoke particles as they formed during bolide disintegration in the upper stratosphere. They represent a possible new source of meteoric dust that was not previously sampled.

Acknowledgements

FJMR was supported by the National Aeronautics and Space Administration LARS (NNX11AC36G) and Cosmochemistry (NNX10AK28G) grants. DUSTER was developed at the Cosmic Physics Laboratory of the University of Naples Parthenope and Istituto Nazionale di AstroFisica where this project was funded by the Italian Space Agency (ASI), PRIN2008/ MIUR (Ministero dell Istruzione dell Università e della Ricerca), MAE (Ministero degli Affari Esteri), and Regione Campania. The authors also thank E. Zona and S. Inarta at the Laboratorio di Fisica Cosmica for technical assistance. We thank ASI, CNES, ISTAR (International Science Technology And Research) and Università di Roma La Sapienza for supporting flight opportunities and recovery activities.

References

Bigg E.K., 2012, M&PS, 47, 799

Brownlee D. et al., 2006, Science, 314, 1711

Ciucci A., 2011, Stratospheric Dust Collection by DUSTER (Dust in The Upper Stratosphere Tracking Experiment and Retrieval), a balloon-borne instrument and laboratory analyses of collected dust. PhD thesis, 128p, Universita degli Studi di Napoli Federico II, Dept. Aerospace Engineering, Naples (Italy)

Cziczo D.J., Thomson D. S. & Murphy D.M., 2001, Science 291, 1772

De Angelis S. et al., 1993, Spectroscopy Lett. 44, 549

Della Corte V. et al., 2012, Space Sci. Reviews. 169, 159

Della Corte V. et al., 2013, Tellus B 65, 20174; `http://dx.doi.org/10.3402/tellusb.v65i0.20174`

Dobrică E. et al., 2009, M&PS, 44, 1643

Hervig M.E. et al., 2009, Geophys. Res. Lett. 36, L18805, doi:10.1029/2009GL039737

Hervig M.E. et al., 2012, J. Atmos. and Solar-Terrestrial Phys. 84-85, 1

Hemenway C.L., Fullam E.F. & Phillips L., 1961, Nature 190, 897

Hemenway C.L. et al., 1964, Tellus 16, 96

Hunten D.M., Turco R.P. & Toon O.B., 1980, J. Atmos. Sci. 32, 1342

Janches D. et al., 2009, Geophys. Res. Lett. 36, L06101, doi:10.1029/2009GL037389

Joswiak D.J., Brownlee D.E., Matrajt G., Westphal A.J., Snead Ch.J., Gainsforth Z., 2012, M&PS 47, 471

Megie G. and Blamont J.E., 1977, P&SS 25, 1093

Nesvorný D., Jenniskens P., Levison H.F., Bottke W.F., Vokrouhlick D., Gounelle M., 2010, Ap.J. 713, 816

Renard J-B. et al., 2008, J. Geophys. Res. 113, D21303, doi:10.1029/2008JD010150

Rietmeijer F.J.M., 1993, J. Volc. Geothermal Res. 55, 69

Rietmeijer F.J.M. and Nuth III J.A., 2012, In Nature's Nanostructures (eds Barnard A.S and Guo H.), Pan Stanford Publishing Pte Ltd, Singapore, p. 329

Rotundi A. et al., 1998, A&A, 329, 1087

Saunders R.W. & Plane J.M.C., 2006, J. Atmos. Solar-Terrestrial Phys. 68, 2182

Saunders R.W. & Plane J.M.C., 2011, Icarus 212, 373

Witt G. et al., 1964, Tellus 16, 103

Zolensky M., Nakamura-Messenger K., Rietmeijer F., Leroux H., Mikouchi T. et al., 2008, M&PS, 43, 261

Meteoroids 2013, Proceedings of the Astronomical Conference,
held at A.M. University, Poznań, Poland, Aug. 26-30, 2013,
eds Jopek T.J., Rietmeijer F.J.M., Watanabe J., Williams I.P.,
Adam Mickiewicz University Press in Poznań, pp 155–162

Meteoroid structure and ablation implications from multiple maxima meteor light curves

Roberts I.D.[1], Hawkes R.L.[1], Weryk R.J.[2], Campbell-Brown M.D.[2], Brown P.G.[2,3], Stokan E.[2], Subasinghe D.[2]

[1]Department of Physics, Mount Allison University, Sackville, Canada (rhawkes@mta.ca)
[2]Department of Physics and Astronomy, University of Western Ontario, London, Canada
[3]Centre for Planetary Science and Exploration, University of Western Ontario, London, Canada

Abstract. The Canadian Automated Meteor Observatory (CAMO) detects occasional meteors with two maxima in the image intensified CCD based light curves. We report early results from an analysis of 21 of these events. Most of these events show qualitatively similar light curves, with a rounded first luminous peak, followed by an almost linear sharp rise in the second peak, and a relatively rapid curved decay of the second peak. While a number of mechanisms could explain two maxima in the light curves, numerical modelling shows that most of these events can be matched by a simple dustball model in which some grains have been released well before intensive ablation begins, followed by a later release of core grains at a single time. Best fits to observations are obtained with the core grains being larger than the pre-released outer grains, with the core grains typically 10^{-6} kg while the early release grains are of the order of 10^{-9} kg.

Keywords: meteoroid structure, meteor light curve, dustball, intensified CCD, fragmentation

1. Introduction

Light curves provide one of the best indicators of the mode of meteor ablation and fragmentation, and implied meteoroid structure. The intensity of the light produced is indicative of the almost instantaneous mass loss rate. In this paper we consider implications for meteoroid structure and ablation from dual peak meteor light curves, in particular looking at whether these observations support a dustball model.

Jacchia (1955) suggested that photographic observations of shortened trails, flares and meteor wake supported a dustball structure for at least some meteors. However the fragile dustball structure proposed was inconsistent with bright meteors that survived high pressures to low observed heights.

Hawkes and Jones (1975) developed a two component dustball model that would fit both faint and brighter meteor light curves. The key idea of this model was that meteoroids have two components, a grain component with a silicate metallic composition that is responsible for the light production, and a glue component (possibly organic in nature) which has a lower boiling point and does not produce significant luminosity. With this model meteoroids are not necessarily fragile. Under this model some grains will be released early (as the glue reaches its boiling point) while other grains will be separated during intensive light production by

the meteor. Fisher et al. (2000) reviewed the observational evidence in favour of this dual component dustball model (e.g. shorter more symmetric light curves, relative independence of heights of meteors past a certain mass cutoff, good prediction of ablation profiles across a wide mass range).

2. Observations

The Canadian Automated Meteor Observatory (CAMO) described in detail by Weryk et al. (2013) uses image intensified CCD meteor observations at two stations (baseline ≈44.9 km) coupled with automatic detection and analysis software to provide a large sample of faint meteor light curves, atmospheric trajectory and orbital data. At each CAMO station are wide field cameras ($28^\circ \times 21^\circ$) operating at 80 fps. Each station also has a tracking high resolution system at each station with a field of view of $1.5^\circ \times 1.1^\circ$ operating at 110 fps. The tracking system is capable of moving across the sky at 2000 deg/s, and is updated in position at 2000 Hz. Only a subset of the events are well tracked with no transverse smearing or leaving the field of view. The high resolution data will be considered in detail in a subsequent paper. Both wide and narrow field systems use Gen III image intensifiers coupled to CCD cameras with the main spectral response from 500 to 850 nm.

The CAMO system observes some events that have two clearly defined peaks in the meteor light curve. A typical dual peak light curve is shown in Figure 1. We have analyzed 21 double peak events for this paper. Almost all of these events had a qualitatively similar light curve structure such as that shown in Figure 1. The light curves had a rounded first peak, followed by an almost linear (on a plot using the logarithmic astronomical magnitude) increase for the second peak, followed by a rounded but usually short duration end of the second peak.

We studied the atmospheric trajectories and orbital parameters of double peaked meteor light curves, but there were no obvious differences from the general population observed with CAMO. The events studied here ranged in peak brightness between astronomical magnitude -2 and +4, and in beginning heights all but three of the events were in the range from 110 km to 80 km and none were above 120 km (although the triangulation overlap optimization may partly contribute to this). The events were somewhat slow when compared to the general population, with 42% having speeds of 20 km/s or less. We plot in Figure 2 the Tisserand parameter plot for the double peak events which suggests that both cometary and asteroidal origin meteoroids contribute to the double peak events (generally $T_J > 3$ considered asteroidal). Jopek and Williams (2013) discuss alternative methods to classify meteoroid orbits.

While the events studied here were identified from the CAMO records by observers, a subsequent automated search through 198 meteors seeking events with at least a 1 magnitude difference between local minima and local maxima identified 13% of the events as being double peaked.

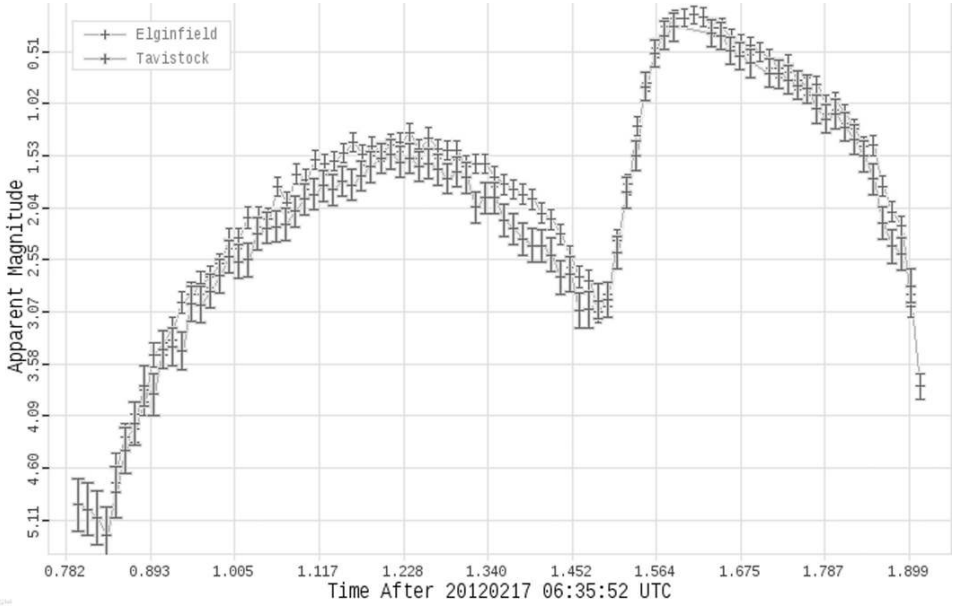

Figure 1. A plot of apparent astronomical magnitude versus time for the light curve for a meteor observed on Feb 17, 2012 at 06:35:52 UT. The dual peaks in the light curve and agreement between the observations at the two stations are clearly evident.

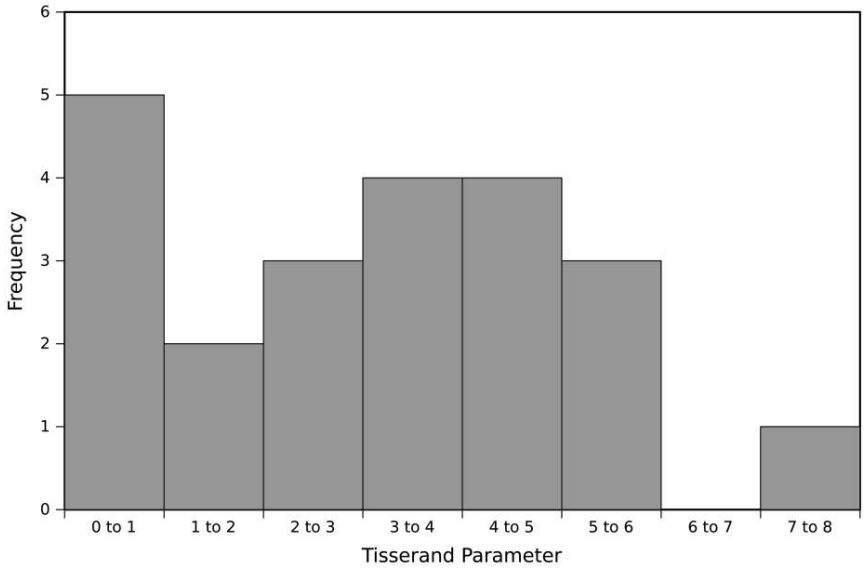

Figure 2. A plot of the distribution of the number of double peak events in this study according to the Tisserand orbital parameter. The double peak events have representation from both cometary ($T_J < 3$) and asteroidal ($T_J > 3$) type orbits.

3. Potential Meteoroid Structures

A number of different mechanisms can produce dual peak meteor light curves. Perhaps the most obvious explanation would be two near simultaneous parallel meteors. If the spatial resolution of the observing system is insufficient to resolve these as parallel light curves, then the result will be a dual peak meteor light curve. At least occasionally such events have been observed with high resolution systems (Kaiser et al. 2004).

A second possibility is that differential chemical ablation occurs, with the peak due to the more volatile chemical species ablating first. While historical theoretical treatments considered meteoroids as chemically homogeneous, clearly actual meteoroids are collections of different chemical constituents with different thermodynamic properties. Vondrak et al. (2008) describe the CAMOD numerical system for predicting meteor ablation when differential ablation is taken into account. Borovička et al. (2007) among others have provided spectral support for the idea of differential ablation.

A third possibility is that there is a single meteoroid, but it has varying chemical or physical structure, with different layers ablating at different rates. This is different from the second model in that different regions of the meteoroid have a different chemical composition (or possibly a different physical parameter such as density). The idea of meteoroids having coatings is broadly consistent with the literature on the structure of much smaller interstellar grains by Greenberg and Li (1999).

A fourth possible mechanism is a conventional meteor ablation profile coupled with enhanced grain release either because of thermal or aerodynamic fragmentation. Simonenko (1968) invoke this mechanism to explain meteor flares in shower meteors.

A final option might be a dustball model with some grains having been released prior to atmospheric luminosity (those producing the first peak) followed by a subsequent major grain release. Hawkes and Jones (1975) saw this as a routine occurrence, although how obvious it would be, and whether it would result in two distinct peaks, will depend on the properties of the luminous grains and the glue. Of course it is quite possible that some combination of these proposed mechanisms is responsible for the light curve.

4. Numerical Simulations

We used a quartic Runge-Kutta approach with fixed step size to numerically model the heating and ablation of dustball grains. The standard equations of meteor ablation were used (Fisher et al. 2000) and the same value for the physical and thermodynamic parameters as in that work. It was assumed that the meteoroids were sufficiently small and high enough in the atmosphere that free molecular flow dominates. The model did not incorporate sputtering as it is of negligible importance in the mass and velocity regimes considered here. The MSISE-90 atmospheric model (Hedin 1991) was used to provide atmospheric density profiles. Results from individual grains are then combined to produce a composite light curve.

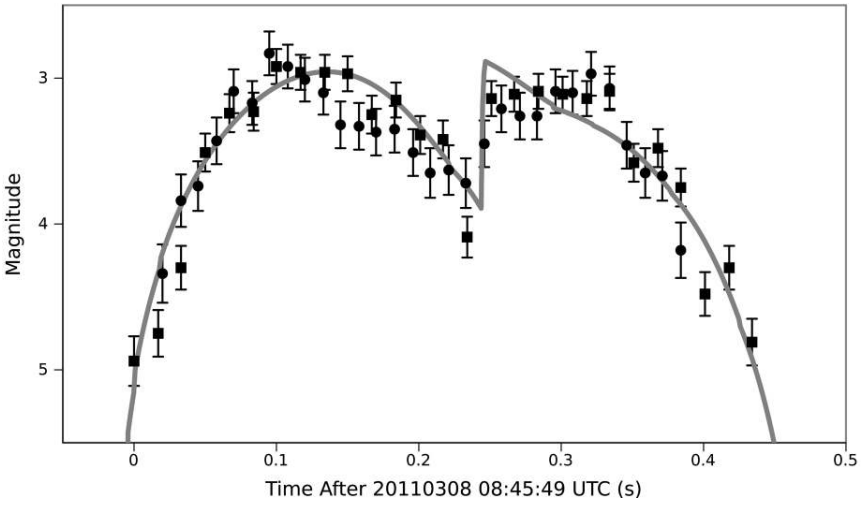

Figure 3. A plot of light curves from both wide field station cameras (square points are from Elginfield and circle from Tavistock station) along with a fit using the grain model. This meteor had a speed of 44 km/s, and the light curve extended from 103 to 86 km. The first peak for this event was modelled with outer grains with the following characteristics: 100 3×10^{-9} kg grains, 500 7×10^{-10} kg grains, 5000 3×10^{-10} kg grains and 50000 2×10^{-11} kg grains. The second peak was modelled with a mix of three grain sizes (all simultaneously released) 100 grains of mass 1×10^{-9} kg, 80 grains of mass 5×10^{-9} and 60 grains of mass 2×10^{-9} kg.

The rapid rise of the second peak in almost all of the dual peak light curves suggested to us a model with sudden release of additional grains part way through the light curve. We assumed that the second release of grains occurs at a single point. We will refer to the grains released high as outer grains, and those released late as core grains. We show in Figure 3 one of the dual peak meteors and the fit to the light curve provided through this model.

Many of the double peak light curves could be adequately matched with this simple model. While the computational model results reported here are preliminary, we have summed over all events that could be successfully modelled to obtain the mass distribution of the core and outer grains. The data for the total mass in each grain mass range is shown in Figure 4. An interesting result is that the core grains are larger in mass than the early release outer grains. The core grains range from 10^{-10} to 10^{-5} kg, with a peak at 10^{-6} kg. The outer (pre-released) grains range from 10^{-12} kg to 10^{-6} kg, with a peak at 10^{-9} kg. It should be noted that we have used the traditional luminous efficiency factor and velocity distribution (that used by Fisher et al. (2000) and many other studies). Weryk and Brown (2013) have recently suggested on the basis of simultaneous radar and electro-optical observations that the video meteor mass scale is an order of magnitude smaller than previously thought. This would not change the result that core grains are larger, but would shift the actual grain sizes to a smaller size.

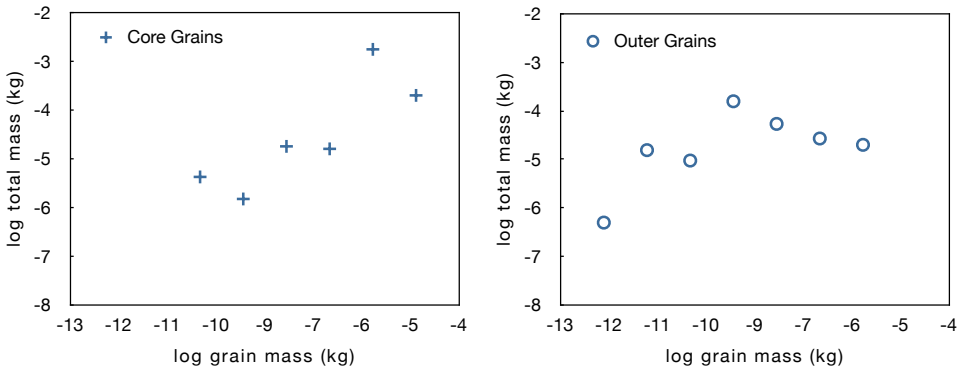

Figure 4. A plot of total mass in different grain mass categories for all events successfully modelled. The core grains released to produce the second light curve peak are shown on the left, and the early release grains on the right. This preliminary finding suggests that the outer grains are smaller in size than the core grains.

5. Conclusions and Discussion

Perhaps the most obvious question is why some meteors, but not all, show a dual peak structure. A related question is why these events have not been more frequently reported in the past. One possibility is that the relatively high response in the near infrared of the CAMO detection systems may play a factor.

One of the most striking aspects of the study was the similarity of different light curves. In almost all cases the first peak is more rounded and symmetric, while the second peak has a sharp almost linear (in a plot using the logarithmic astronomical magnitude as the vertical axis), followed by a fairly sharp rounded decline. This suggests to us that a similar mechanism is producing most of the double light curve events. While other mechanisms can probably also match the results, the simple dustball model used here seems adequate for the events studied. Malhotra and Mathews (2010) have conducted a statistical study of smaller meteoroids observed with large aperture radar, and find that only about one-quarter are consistent with simple single body ablation. They find that 48% seem to show fragmentation, while 20% imply differential ablation is important.

If a more detailed future analysis continues to suggest that the core grains are larger than the early release grains, that is an important and somewhat surprising result. This work suggests that core grains are typically 10^{-6} kg while early release grains are of the order of 10^{-9} kg. A number of previous studies have sought to establish the size of meteor constituent grains. Simonenko (1968) found from an analysis of rapid onset flares on bright meteors a mean grain mass of about 2×10^{-9} kg.

Borovička et al. (2007) have modelled six electro-optical Draconid meteors, using an erosion model in which grains are released over generally the first half of the light curve, although for the brightest meteor a number of grains were resistant

to release and separated later. They generally found agreement using grains from 10^{-11} to 10^{-9} kg. They find a model with total pre-release prior to intensive ablation inconsistent with the meteors in this small sample. Of course it should be kept in mind that these were Draconid meteors, known to have a porous low density structure (Borovička et al. 2007).

Campbell-Brown and Koschny (2004) have modelled Leonid light curves using a thermal erosion two component dustball model. The find that two of the meteors are well matched with Gaussian mass distribution of grains, while the third requires a power law distribution. Grain sizes generally range from 1×10^{-11} to 4×10^{-7} kg, in general agreement with this study. Beech and Murray (2003) used a power-law mass distribution to match Leonid light curves, generally finding the need for grains in the mass range from 10^{-10} to 10^{-7} kg. In an analysis of four Leonid fireball bursts Hawkes et al. (2002) found that relatively large grains 10^{-5} to 10^{-4} kg were needed to match the observations.

It is also interesting to compare the grain size distribution with that obtained by Stardust during encounter with the coma of Comet 81P/Wild 2. Green et al. (2007) show that most grains are smaller than those reported here, although the total range is about 10^{-15} to 2×10^{-5} kg.

It is possible that the outer grains released prior to ablation are produced in a similar manner to the less spatially and temporally constrained clusters of meteoroids occasionally observed (Watanabe et al. 2003; Piers and Hawkes 1993). While Watanabe et al. (2003) discusses possible production mechanisms, there is not yet clarity as to how these clusters occur.

Brosch et al. (2004) point out the many parameters of meteor light curve analysis, and how they can help to constrain meteoroid structure and ablation. Stokan et al. (2013) have studied optical trail widths using the CAMO system and this information will help constrain the possible meteoroid models. We plan to in a later paper incorporate the tracking data for a small number of events in a more in depth investigation of dual light curve events which may help to further constrain possible models.

Acknowledgements

We acknowledge research funding from the Natural Sciences and Engineering Research Council of Canada and the Canada Foundation for Innovation. IDR received research assistantship funding from a MY Bell Research Fellowship at Mount Allison University.

References

Beech M., Murray I.S., 2003, MNRAS, 345, 696
Borovička J., Spurný, P., Koten P., 2007, A&A, 473, 661
Brosch N. et al., 2004, MNRAS, 355, 111
Campbell-Brown M.D., Koschny D., 2004, A&A, 418, 751
Fisher A.A., Hawkes R.L., Murray I.S., Campbell-Brown M.D., LeBlanc A.G., 2000, P&SS, 48, 911

Green S.F., McBride N., Colwell M.T.S.H., McDonnell J.A.M. et al., 2007, ESA SP-643, 35

Greenberg J.M., Li A., 1999, Space Sci. Rev., 90, 149

Hawkes R.L. et al., 2002, in Proc. of the IAU Coll 181 held at the University of Kent, Canterbury, UK, 4-10 April 2000, eds Green S.F., Williams I.P, McDonnell J.A.M., McBride N., Oxford: Pergamon, 2002, 414 p. COSPAR colloquia series, Vol. 15, p. 23

Hawkes R.L., Jones J., 1975, MNRAS, 173, 339

Hedin A.E., 1991, JGR, 96, 1159

Jacchia J., 1955, Astrophys. J., 121, 521

Jopek T.J., Williams I.P., 2013, MNRAS., 430, 2377

Kaiser N.R., Brown P., Hawkes R.L., 2004, EM&P, 95, 579

Malhotra A., Mathews J.D., 2010, JGR, 116, A04316

Piers P., Hawkes R.L., 1993, WGN-JIMO, 21, 168

Simonenko A.N., 1968, in Proc. of the IAU Symposium No. 33 held at Tatranska Lomnica, Czechoslovakia, 4-9 Sept. 1967, eds Kresak L., Millman P.M., Dordrecht, D. Reidel, p. 207

Stokan E., Campbell-Brown M.D., Brown P.G., Hawkes R.L., Doubova M., Weryk R.J., 2013, MNRAS, 433, 962

Vondrak T., Plane J.M.C., Broadley S., Janches D., 2008 Atmos. Chem. Phys, 8, 7015

Watanabe J., Tabe I., Hasegawa H., Hashimoto T., Fuse T., Yoshikawa M., Abe S., Suzuki B., 2003, PASJ, 55, L23

Weryk R.J., Campbell-Brown M.D., Wiegert P.A., Brown P.G., Krzeminski Z., Musci R., 2013, Icarus, 225, 614

Weryk R.J., Brown P.G., 2013, PSS, 815, 32

Meteoroids 2013, Proceedings of the Astronomical Conference, held at A.M. University, Poznań, Poland, Aug. 26-30, 2013, eds Jopek T.J., Rietmeijer F.J.M., Watanabe J., Williams I.P., Adam Mickiewicz University Press in Poznań, pp 163–176

Physical and kinematic characteristics of meteoroids producing bright radio meteors. Meteor showers and associations

Narziev M.

Institute of Astrophysics of Academy of sciences of Tajikistan (mirhusseyn_narzi@mail.ru)

Abstract. This paper contains radiants, velocities, masses and densities of 214 meteor showers and associations identified among more than 6100 radar meteors observed in the Gissar Astronomical Observatory during one year cycle 1968–1969. Part of these streams and associations were observed by the radar technique for a very first time. We have determined the masses and densities of the meteoroids which constitute streams and associations. The mean values of masses fall into interval $7 \cdot 10^{-4} \div 0.3$ g, and densities are in range of $0.3 \div 7$ g/cm^3. For 76% showers and associations, the mean values of the meteoroid densities concentrate between 1 and 4 g/cm^3. For 11% of showers and associations, the particle densities have mean values from 4 up to 7 g/cm^3, and in the case of remaining 13% the mean densities of the particles proved to be smaller than 1 g/cm^3. For the meteoroids, members of showers and associations, our analysis has shown that, with an increase of the average mass of the particle, its average density decrease. Based on the radar observations the density and the porosity of meteoroid streams of common origin (twin meteoroid streams) have been estimated. It was established that the densities and the structure of meteoroid stream particles of common origin are similar.

Keywords: radar meteor, meteoroid, meteor shower, meteoroid association, meteoroid mass, meteoroid density, meteoroid porosity

1. Introduction

Physical characteristics of meteoroids, their masses and densities as well as the radiants and velocities are of great interest not only for meteor astronomy, space science and cosmogony of the Solar System but also for solving important practical and theoretical problems. They provide information about the nature of the meteoroid parent bodies, the nucleus of comets and asteroids.

The radar meteor observations carried out in Harvard, Kharkov, Kazan, Obninsk and Dushanbe resulted in identification of a few dozen to a few hundred of meteor showers and associations†. The catalogues of meteor showers contain radiants, velocities and orbital elements (Korpusov 1970; Kashcheev et al. 1967; Sekanina 1976). However, they don't include information about the masses and densities especially of the minor meteor showers and associations.

† The dividing lines between the terms "shower", "stream" and association" are not ridigly defined. In this paper we use the term "association" for groups of meteors which to our knowledged were discovered in this study.

In 1968-1969 at the Gissar Astronomical Observatory (GisAO) of the Institute of Astrophysics, Academy of Sciences of Tajikistan, we have conducted radar observations of meteors. During this period ∼6100 meteor radiants, velocities and orbits have been obtained. The analysis of these observations, allowed to identify new showers and associations and to determine the masses and densities of meteoroids, members of different showers and associations.

Our results contribute significantly, because:

1) our data correspond to meteors brighter than 5 magnitude, when at the Harvard, Obninsk, Kharkiv and Kazan stations, the radar systems observed fainter meteors (+6.5, +13 magnitude),
2) at the other radar stations, velocity of meteors was determined by the diffraction method only. However, the diffraction patterns are known to form by a part of meteors only, resulting in loss of valuable information. The bearing-time radio method (Chebotaryev 1976) which is applied at the GisAO gives the triple rise in the number of measurements,
3) using the bearing-time radio method the zenith angle of the radiants is determined 25-50 times more accurately than by the diffraction-time method,
4) in this paper, along with the radiants and velocities, we present the physical parameters of the particles, members of meteor showers and associations, such as the mass and density,
5) the geographical location of GisAO contributes to study streams and associations which have more Southern radians, that are not always available some other stations.

2. Apparatus and processing of the observed data

We have observed meteors using the radar complex MIR-2 (Chebotaryev et al. 1970), consisted of a transmitter working at the wavelength $\lambda = 8$ m with the pulse power of 65 kW and four receivers, three of which were located at 3.8 to 4.1 km from the central receiver. For further processing we have used only those meteors, which were recorded by 4 receivers and had at least first maximum in the amplitude-time characteristics (ATX), and which were not substantially distorted by the noise. We have observed: 900 meteors in December, 800 meteors in February, 170 in March, 300 in April, 2000 in May, 200 in June, 700 in July, 260 in August, 350 in September, 430 in October and 52 meteors in November.

The results of the radar observations displayed on the cathode-ray tubes were recorded photographically. For recorded meteors we have found: the date and time of appearance, the distance to the meteor trail from the main central station, the distance to the meteor from each of the four receiving points d_1, d_2, d_3, d_4. For each i-th channel of the amplitude-time characteristics (ATX), the positions of the beginning and of the first four maxima $N_{i1}, N_{i2}, N_{i3}, N_{i4}$ were measured. Using these data, by the method described in Chebotaryev (1970) we have determined the angular coordinates (A – the azimuth and Z – zenith distance) of the mirror point on the meteor trail. Next, using information from all channels the average length of the Fresnel zones in the pulses was calculated, and by the diffraction method

described by Kashcheev et al. (1967) the velocity of the meteor was determined. Independently, the azimuth A_R and zenith angle Z_R of the meteor radiant as well as the velocity V of the meteor were determined by the bearing-time method, using formulae given by Chebotaryev (1976)

$$Z_R = \arctan\left[-\cot Z/\cos\left(A - A_R\right)\right] \tag{2.1}$$

$$A_R = A_1 + \arctan\left[\left(t_2 B_1/t_1 B_2\right)\cdot \csc A_{12} - \cot A_{12}\right] \tag{2.2}$$

$$V = B_i \cos\left(A_R - A_i\right)\sin ZR/t_{im} \tag{2.3}$$

where A_i – the azimuth of the i-th receiving station, $A_{12} = A_2 - A_1$, B_i – the distance between the remote and the central station, t_{im} – the maximum shift of the i-th point relative to the central receiver.

The horizontal coordinates of the radiants A_R and Z_R, were transformed into the equatorial ones, α_R, δ_R. The main sources of measurement uncertainty in the radiant position are discussed in detail in Korpusov (1970); Kashcheev et al. (1967); Chebotaryev (1976). Uncertainties of the meteoroid velocities, determined separately by the first and the second method, amount to 3-4 km. Simultaneous measurements of the velocity by both methods reduced the uncertainty to 2-3 km. For the bearing-time method, the zenith distance of the radiant point is determined with accuracy 0.9°–1.2°; which is better than in the case of the diffraction-time method. In case of the azimuth of the radiant, for both methods the uncertainties are the same.

To identify the meteor showers and associations we have analyzed the radiants coordinates and velocities of the meteors observed within each of the observation period. For each detected group of meteors the mean values of the parameters were calculated. As an example, in case of the Geminids, their radiants occupy an area similar to a circle. More than 70% of the radiants of the members of this shower are concentrated in a circle of a radius of 3 degrees. Our mean coordinates of the radiant and velocities are in good agreement with the mean values obtained for Geminids by the photographic technique. For this shower, the mean square errors of the pre-atmospheric velocity V_∞ (the velocity of meteoroid before it was decelareted by the atmosphere) and radiant α_R, δ_R are equal to:

$$\Delta V_\infty = 2km/s, \quad \Delta\alpha_R = 2.5^\circ, \quad \Delta\delta_R = 2^\circ$$

Finally, by the analysis of radiants and velocities of radar meteors observed during the annual cycle 1968-1969 in GisAO, we have detected 214 meteor showers and associations. Among them, about 30% have negative radiant declinations. In Kashcheev et al. (1967) the radiants with negative declinations constitute about 10% of the observed sample. In Table 1, our results (the shower radiants and velocities) are compared with those obtained at Harvard (Sekanina 1976), Kharkiv (Kashcheev et al. 1967) and Obninsk (Korpusov 1970).

Despite the fact that observations in the GisAO and in the other stations were made in different years, the average values of the coordinates of radiants are in most cases, practically the same. It seems to validate the frequency of the identified meteor streams and the reliability of the results. We have found close similarity among

Table 1. The main radiant coordinates and pre-atmospheric velocities of selected meteor showers obtained by radar observations in Dushanbe in 1969 (this study) and in Kharkiv (Kashcheev et al. 1967), Obninsk (Korpusov 1970), and Harvard (Sekanina 1976).

Source		Dushanbe			Kharkiv			Obninsk			Harvard		
Showers	λ_S	α_R	δ_R	V_∞	α_R	δ_R	V_∞	α_R	δ_R	V_∞	α_R	δ_R	V_∞
Geminids	13 Dec.	111	32.7	37	111	33	36	112	33	36	113	32	36
μ-Geminids	14 Dec.	93	22.1	29	95	24	31	95.3	20	31	94	22	31
Monocerotids	14 Dec.	106	14	40	103	15	39	-	-	-	94	14	42
σ-Hydrids	14 Dec.	133	0.6	55	-	-	-	-	-	-	-	-	-
Dec. Leonids	15 Dec.	144	22	60	-	-	-	141	24	62	150	22	56
Comae-Berenicids	14 Dec.	170	22	65	-	-	-	169	22	67	-	-	-
Ursids	21 Dec.	230	75	36	-	-	-	-	-	-	-	-	-
N. α-Leonids	17 Dec.	159	11	32	-	-	-	155	12	27	-	-	-
S. α-Leonids	17 Dec.	159	0.9	33	-	-	-	-	-	-	-	-	-
N. β-Leonids	17 Dec.	179	8	41	-	-	-	-	-	-	-	-	-
S. β-Leonids	18 Dec.	172	-2	36	-	-	-	-	-	-	-	-	-
N. δ-Virginids	19 Feb.	188	8	40	-	-	-	-	-	-	-	-	-
S. δ-Virginids	17 Feb.	185	-4	39	-	-	-	-	-	-	-	-	-
Virginids	15 Mar.	192	-7	36	193	-9	36	191	-8	31	-	-	-
March Herculids	13 Mar.	261	39.5	37	261	32	34	-	-	-	261	38	34
N. Librids	15 Apr.	225	-10	35	224	-13	28	225	-13	34	224	-13	28
S. Librids	16 Mar.	229	24	37	-	-	-	-	-	-	-	-	-
ζ-Librids	17 Apr.	242	-19	36	237	-19	40	-	-	-	236	-19	36
ν-Herculids	18 Apr.	272	28	37	-	-	-	274	28	38	272	30	34
Cygnids	18 Apr.	305	41	42	-	-	-	-	-	-	303	44	40
γ-Pegasids	10 May	4	18	37	8	21	37	-	-	-	1.6	18	35
ν-Piscids	12 May	13	22	38	17	19	39	-	-	-	12	19	36
ø-Cetids	10 May	22	-3	38	-	-	-	-	-	-	22	-4	38
N. May Arietids	7 May	34	19	29	33	9	31	-	-	-	37	18	27
S. May Arietids	6 May	34	11	30	-	-	-	-	-	-	-	-	-
N. ε-Arietids	10 May	41	22	27	41	23	27	-	-	-	44	21	23
S. ε-Arietids	12 May	46	13	27	-	-	-	-	-	-	-	-	-
ε-Taurids	12 May	55	29	22	-	-	-	-	-	-	59	22	17
μ-Virginids	6 May	227	-4	24	-	-	-	-	-	-	-	-	-
α-Scorpiids	12 May	237	-16	31	-	-	-	-	-	-	-	-	-
Serpentids	7 May	245	11	33	-	-	-	-	-	-	-	-	-
N. May Ophiuchids	10 May	250	-16	33	-	-	-	-	-	-	256	-13	31
S. May Ophiuchids	10 May	248	-29	33	-	-	-	-	-	-	-	-	-
N. θ-Ophiuchids	10 May	262	-17	37	-	-	-	-	-	-	-	-	-
S. θ-Ophiuchids	12 May	263	-28	37	-	-	-	-	-	-	-	-	-
ε-Aquilids	10 May	281	22	35	-	-	-	-	-	-	-	-	-
ξ-Sagittariids	4 Jul.	274	-30	24	-	-	-	-	-	-	290	-26	28
ψ-Cassiopeiids	15 Jul.	27	65	46	-	-	-	-	-	-	-	-	-
S. ι-Aquariids	15 Jul.	319	-17	34	328	-18	33	-	-	-	-	-	-
π-Aquariids	23 Jul.	327	-2.7	36	330	2	36	-	-	-	334	-0.4	37
Perseids	12 Aug.	49	57	58	41	57	60	46	58	60	45	59	58
α-Capricornids	12 Aug.	3	-5	23	-	-	-	319	-8		3	-7	23
N. δ-Aquariids	11 Aug.	345	3	40	337	-5	42	-		-	346	5	39
S. δ-Aquariids	4 Aug.	348	-14	41	341	-16	41	351	-14	40	342	-16	40
γ-Arietids	23 Sep.	31	18	37	-	-	-	-	-8	-	28	18	38
β-Aurigids	22 Sep.	87	43	59	90	41	69	-		-	86	42	59
Oct. Andromedids	4 Oct.	9	22	30	-	-	-	10	25	20	9	27	25
S. Arietids	11 Oct.	32	14	32	40	15	33	-	-	-	32	10	28
N. Taurids	14 Oct.	40	22	36	33	18	30	-	-	-	46	17	27
τ-Taurids	10 Oct.	74	30	57	81	29	58	-	-	-	70	21	57
Oct. Lyncids	14 Oct.	116	57	60	-	-	-	-	-	-	121	55	55

the radiant coordinates determined in this study and those by Sekanina (1976), especially in case of showers γ Pegasids, *o* Cetids, ν Piscids, Arietids observed in May, where the observation periods are virtually identical. Some discrepancies turned out to be due to individual coordinates of the radiants of the particles of

the η-Aquariids shower; we have found that sometimes the radiants were grouped into several active centers. Out of 2000 meteors registered during 6-12 of May, 136 were the η-Aquariids, the members of the most active meteor shower. In this period of time, clearly separable from the background were also the daytime streams o-Cetids (N = 91), ν-Piscids (N = 106). Among the lesser known daytime meteor showers, also clearly distinguishable from the sporadic background, we identified the Northern and Southern May Arietids; the radiants of these streams are concentrated in a circle with a radius of 4 degrees.

A number of showers, such as the Northern and Southern θ-Ophiuchids, δ-Virginids, α-Scorpiids, ν-Hydrids, Southern α-Leonids, Southern Librids as well as many associations have been revealed using the radar data for the first time.

Small differences in the radiants and velocities for some showers may be due to small number of meteors detected for a given group, as well as due to some differences in the period of observations. Despite that our observations were limited to the bright meteors and that the observations covered the period of activity of the Perseids, we have identified only a few members of this stream. Out of 260 meteors observed in August, only 11 belong to the Perseids, what can be explained by the fact that some very bright Perseids gave non-specular echo types. The most numerous shower during this period was the Southern δ-Aquariids (N = 23).

As was mentioned in the introduction, we have made a study of physical characteristics of meteoroids the members of showers and associations. For this purpose, for each individual meteoroid, we have used: the radar echo duration measurements, the height h of the maximum ionization of the meteor trail, the pre-atmospheric velocities V_∞ and the zenith distance Z_R of the radiant point. The analysis of the measurements of the echo duration τ (in seconds), has shown that in the most cases, duration of meteor echoes for small meteor showers and associations does not exceed 4 seconds. For major meteor showers (e.g. the Geminids) duration of echoes reach up to 22 seconds. In case of the high-velocity meteor showers and associations duration of radar echos were less and didn't exceed, as a rule, 1.5 seconds.

For each radar meteor, using the duration of the echo calculated from 4 points, the electron line densities q have been found by

$$q = (\tau e^{-k\tau} + r^2/4D)D/A\lambda^2 \tag{2.4}$$

where r is initial radius of ionozed meteor trail, k is rate of the electof ron attachment to the neutral particles, A is a shape factor (constant), D is an ambipolar diffusion coefficient and λ is a radio wavelength.

For determination D and r we have used the following expressions (Voloshchuk et al. 1989):

$$\lg r = 1.47 \cdot 10^{-10} V^{0.65} \rho^{-1} \tag{2.5}$$

$$\lg D = 0.79h - 6.6 \tag{2.6}$$

$$\rho = 3.3 \cdot 10^{-9} e^{(90-h/H^*)} \tag{2.7}$$

where, ρ – is the density of the atmosphere, h – is the height of homogeneous atmosphere and H^* is the atmospheric scale height.

The mass M (in grams) and the density δ_0 (in g/cm^3) of a meteoroid, accounting for influence of the form of ionization curve were calculated by formulae (Bibarsov et al. 1990)

$$M = (3\mu H^* q_m / 4\beta \cos Z_R (Q - Q_H / Q - (2/3)Q_H)^3 \tag{2.8}$$

$$\delta_0 = \gamma (A\lambda^{'} H^* V^2 \rho_m / 2(Q - 2/3 Q_H) M^{1/3} \cos Z_R)^{3/2} \tag{2.9}$$

where μ is the atomic mass of a meteoroid in grams, β is the ionization coefficient, Q and Q_H are the ablation energy, γ is correction coefficient for fragmentation, $\lambda^{'}$ is the thermal conductivity coefficient, q_m is maximum electron line density, ρ_m is the atmospheric density at the height of maximum ionization.

The values for H and ρ_m were taken from CIRA (CIRA 1972). The values for β, were taken from Table given in Narziev (2003) and k were calculated according to the expressions given in Narziev (2003) and Bibarsov et al. (1990)

$$\lg k = 4.99 - 0.07h \tag{2.10}$$

In our calculations we have adopted: γ=1.31, λ=1, A=1.21, Q=$8 \cdot 10^{10}$ erg/g, Q_H=$2 \cdot 10^{10}$ erg/g and μ=$3.82 \cdot 10^{-23}$ g.

Calculated masses and densities of the meteoroids occupy a wide range of values. For 76% of the identified meteor groups the mean densities of meteoroids for the members of the same group are equal to 1–4 g/cm^3. For 11% of the meteor showers and associations the mean values of densities are equal 4–7 g/cm^3. For remaining 13% of the meteor showers and associations the mean densities were smaller than 1 g/cm^3. In Table 2 for each group, we give the mean values of the radiant coordinates, pre-atmospheric velocity, the meteoroid mass M and density δ_0.

The analysis of the average values of the masses and densities of meteoroids (members of showers and associations) has shown that with an increase of the mass of the particle, the average particle density decreases, see Figure 1. This means that the porosity of the particles increases that would suggest that for the higher mass particles, these particles are becoming more porous aggregates (Rietmeijer 2000). An increasing tendency of the number of particles with decreasing of their masses were found by the other authors. At this point, our analysis confirmed the results obtained during the Vega-1 and Vega-2 missions, as well as the results obtained during the HEOS-2 and HELIOS missions for the interplanetary dust particles (Smirnov et al. 1986).

Decrease of average density with increase of mass of the particle may be due to the internal structure of the particles – they can have a different porosity. The particles which may have the same mass and velocity, can have different cross-sections and therefore they evaporate at different altitudes. Hence, when comparing the average meteoroid densities derived from observations at different sites by different equipment, the differences in the structure of the particles should be noted.

Therefore, it is interesting to compare the mean densities of meteoroids for the same mass. However, the available observational data for meteor showers and associations are not sufficient for such selection. For this reason, we have reduced

Table 2. The radiant coordinates α_R, δ_R and pre-atmospheric velocities V_∞, the masses M and densities δ_0 of meteoroids the members of meteor showers and associations identified in this study. In the last column, for known showers we give the references to the papers where some shower paremeters are given; by an asterisk symbol, we have labeled these meteoroid groups which, to our knowledge, were discovered in this study. In the last column: C– Cook (1973), J– Jopek and Jenniskens (2011), K– Korpusov (1970), Ka– Kashcheev et al. (1967), S– Sekanina (1976), T– Terentjeva (1966).

	Showers and associations (A)	Day of observation	α_R deg	δ_R deg	V_∞ km/s	N	M $\times 10^{-3} g$	δ_0 g/cm^3	Note
				December 1968					
1	Geminids	12-15	110.6	32.7	36.9	220	9.6	2.4	C, J, Ka, S
2	μ-Geminids	12-15	93.9	22.1	29.1	7	18.7	1.2	K, Ka
3	A	12-15	100.7	8.0	39.1	7	3.8	3.8	*
4	Monocertids	12-15	105.9	14.0	42.0	8	8.5	2.1	J, S, T
5	A	12-15	133.1	1.5	60.4	13	1.8	4.8	T
6	A	12-15	111.5	-11	44.9	5	1.8	6.0	K
7	A	12-15	148.8	37.2	53.7	10	1.0	6.9	K
8	A	12-15	143.9	21.8	64.1	10	1.7	5.4	K, S
9	A	12-15	158.1	27.3	67.0	5	1.2	3.3	*
10	A	12-15	160.1	-8.3	62.3	6	3.6	0.5	*
11	A	12-15	165.1	10.6	66.5	8	1.4	4.1	*
12	Comae-Berenicids	12-15	170.3	22.2	64.7	12	1.5	4.7	K, S
13	A	12-15	173.4	31.8	63.8	8	1.4	3.5	*
14	A	12-15	166.1	38.9	63.7	5	3.9	4.7	K
15	A	12-15	183.5	34.6	61.4	5	-	-	K
16	A	12-15	198.1	11.8	59.0	6	-	-	K
17	A	12-15	215.8	58.9	40.7	6	4.2	3.4	K
18	A	12-15	229.7	6.1	42.2	9	2.1	3.7	*
19	A	21-27	112.2	11.7	34.5	9	2.1	2.8	*
20	A	21-27	110.1	-10.7	36.4	6	9.6	1.7	*
21	A	21-27	147.4	7.5	58.7	6	1.4	5.8	*
22	A	21-27	139.3	-7.2	63.8	4	2.5	1.9	*
23	A	21-27	170.4	-8.2	66.0	3	1.1	6.5	*
24	A	21-27	181.4	-12	71.5	5	0.9	2.1	*
25	A	21-27	212.2	-2.9	58.0	6	3.9	2.1	*
26	A	21-27	240.3	-1.4	48.8	7	2.0	2.5	*
27	Ursids	21-27	207.3	76.3	37.1	8	10	0.7	J
28	A	21-27	229.5	75.3	35.6	6	22	0.9	*
				February 1969					
29	A	1-3	163.9	11.8	40.1	7	3.4	5.9	*
30	A	1-3	158.4	-13	44.7	8	-	-	*
31	A	1-3	208.0	-0.5	69.7	7	-	-	*
32	A	1-3	231.9	0.4	66.4	5	1.2	3.1	*
33	N. α-Leonids	1-3	158.7	10.5	31.7	13	12	2.7	K, S, T
34	S. α-Leonids	17-22	159.2	0.9	33.0	9	25	0.4	*
35	N. β-Leonids	17-22	172.2	-2.3	36.3	37	9.1	2.2	*
36	S. β-Leonids	17-22	179.0	8.4	41.1	11	5.2	2.8	K, T
37	S. δ-Virginids	17-22	185.4	- 3.8	39.3	5	-	-	*
38	N. δ-Virginids	17-22	188.4	8.1	40.6	4	2.3	3.5	K
39	A	17-22	196.6	0.6	50.7	6	1.3	1.7	*
40	A	17-22	203.8	-15	58.3	10	11.1	3.6	*
41	A	17-22	211.9	- 0.9	60.7	7	1.7	2.1	*
42	A	17-22	221.4	12.6	65.8	7	-	-	K
43	A	17-22	224.2	7.3	64.8	5	1.4	1.7	*
44	A	17-22	229.0	16.5	67.2	12	0.9	1.4	*
45	A	17-22	232.1	- 1.2	69.7	6	0.6	6.0	K
46	A	17-22	240.1	- 4.5	67.5	8	3.6	0.7	*
47	A	17-22	240.8	17.1	64.3	7	1.2	2.9	*
48	A	17-22	234.5	7.3	61.3	8	2.2	1.9	K
49	A	17-22	242.2	12.2	70.0	4	0.7	3.0	K
50	A	17-22	248.6	6.3	62.3	5	-	-	K
51	A	17-22	249.5	- 5.2	65.0	13	1.7	2.3	*
52	A	17-22	296.6	- 9.1	60.3	9	4.7	2.9	*
53	A	17-22	295.6	- 14.5	36.6	5	8.4	2.6	*

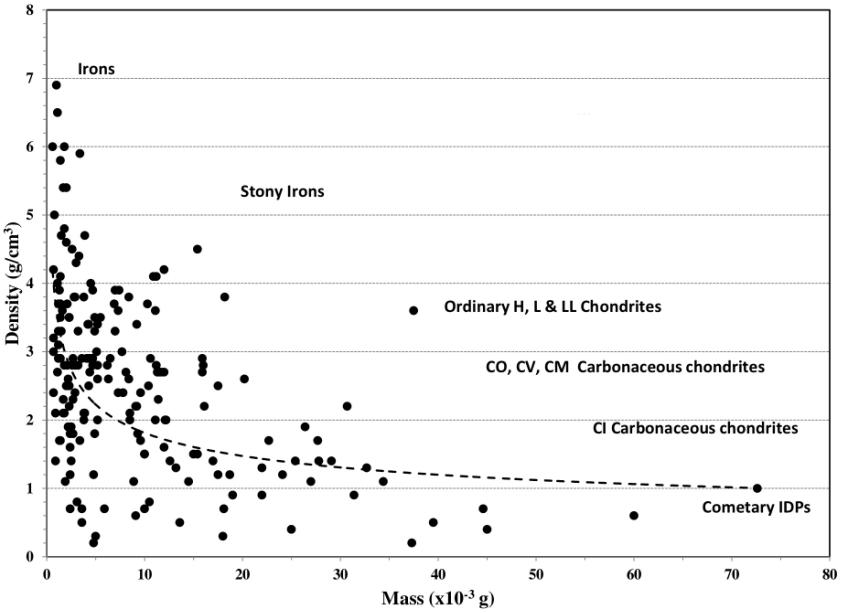

Figure 1. The densities versus masses of the meteoroids listed in Table 2, exclusive of the data points 93 and 143.

the value of the density of meteoroids of masses equal to $M = 10^{-2}g$. As result we have found that the density of meteoroids with equal masses are not the same, and they lie in the interval $0.4 \div 7 g/cm^3$. Such a large spread of the densities of the meteoroids, the members of the showers and associations, is partly due to the lack of statistics, as well as due to differences in the origin, age and evolution of these objects. To verify the last hypothesis, we analyzed the densities of the meteoroids, the members of the same stream twins. The average densities δ_0 for some streams are presented in Table 3. Also, in this table we list the average values of densities δ_{01}, δ_{02} for bright photographic meteors observed in Dushanbe (Babadzhanov 2002; Lebedinets 1987). They correspond to faint photographic meteors and were found taking into account the quasi-continuous fragmentation. Also we list the average mineralogical densities δ_m taken from Benyuh (1974). The average densities δ_{01} and δ_{02} differ slightly, mostly due to low statistics of the data used by Babadzhanov (2002) and Lebedinets (1987).

In Table 3 one can see that in case of the related twin-streams (separated by horizontal lines) the average densities δ of the meteoroids are not significantly different from each other. For unrelated streams, such as the α-Capricornids and the Geminids, the average densities δ differ by a factor two. The particles of the Geminids shower have densities greater than 1 g/cm^3. In case of the α-Capricornids particles, which normally have smaller sizes, the densities are smaller then 1 g/cm^3.

Also, in Table 3 we see that densities obtained by formula (2.9) are systematically smaller than the mineralogical densities δ_m. This can be explained by the fact that formula (2.9) allows to determine only the bulk density. Assuming that the dif-

Table 2. Continuation.

	Showers and associations (A)	Day of observation	α_R deg	δ_R deg	V_∞ km/s	N	M $\times 10^{-3} g$	δ_0 g/cm^3	Note
				March 1969					
54	A	12-16	169.2	-7.0	24.8	4	45	0.4	*
55	Virginids	12-16	192	-7.3	36.4	9	27.8	1.4	K, Ka
56	A	12-16	204.2	-2.2	34.9	5	37.5	3.6	K, Ka
57	A	12-16	235.7	-12	68.0	5	1.6	3.6	K
58	A	12-16	246.7	24.0	46.9	4	0.7	3.2	*
59	A	12-16	262.6	15.2	53.9	4	3.3	4.4	*
60	March Herculids	12-16	261.2	39.5	36.5	4	2.0	5.4	S
61	Herculids-Lyrids	12-16	270.6	37.8	40.4	5	-	-	S
62	A	12-16	269.8	-5.1	61.7	5	2.7	1.8	K
63	A	12-16	284.8	43.2	41.3	5	-	-	*
64	A	12-16	293.2	-20.8	62.2	6	-	-	*
65	A	12-16	318.5	6.1	38.0	8	7.0	3.3	*
				April 1969					
66	A	15-18	217.1	-23.4	30.7	6	15	1.5	*
67	A	15-18	218.7	-6.4	28.2	8	19	0.9	T
68	S. Librids	15-18	225.0	-9.7	35.1	14	27	1.1	K, Ka, S
69	N. Librids	15-18	229.1	-24	36.6	7	16	2.8	T
70	A	15-18	237.3	-4.9	35.1	9	6.3	2.6	*
71	ζ-Librids	15-18	241.7	-18.5	35.7	5	5.2	2.6	S
72	A	15-18	250.7	-1.4	35.0	7	2.9	3.8	*
73	A	15-18	270.7	-11.9	61.7	8	2.6	4.5	*
74	μ-Herculids	15-18	271.8	28.4	37.0	7	5.2	2.0	K, Ka
75	A	15-18	286.0	12.7	59.3	5	12	4.2	*
76	A	15-18	290.4	-1.9	63.5	6	1.4	3.7	K
77	A	15-18	292.4	35.1	35.4	13	10	1.5	*
78	A	15-18	295.9	12.2	70.5	4	2.7	2.3	*
79	A	15-18	297.3	10.0	57.6	7	-	-	*
80	Cygnids	15-18	304.9	40.8	41.6	7	4.9	3.5	Ka, S
				May 1969					
81	γ-Pegasids	5-12	4.0	18.2	37.0	27	7.0	3.9	K, Ka
82	A	5-10	5.1	59.7	34.2	5	17	1.4	*
83	A	5-10	5.6	35.7	39.5	17	7.3	2.4	*
84	ν-Piscids	5-12	13.3	21.7	37.5	106	11.2	2.8	Ka
85	A	5-12	20.3	30.2	34.5	16	4.4	2.7	K, Ka, S
86	o-Cetids	5-12	22.4	-3.0	36.6	91	11.5	2.7	C, J, S
87	A	5-12	23.7	14.6	35.1	31	12.1	2.0	Ka
88	A	5-12	25.1	26.8	33.8	27	8.1	2.7	*
89	N. May Arietids	5-12	34.2	19.0	29.0	49	26.4	1.9	K, Ka
90	S. May Arietids	5-12	34.3	10.8	29.8	36	11.4	2.3	J, Ka
91	N. ε-Arietids	5-12	41.4	21.9	26.5	8	13.2	1.3	J, K, Ka
92	S. ε-Arietids	5-12	45.8	12.7	27.2	11	34.4	1.1	*
93	ε-Taurids	5-12	55.2	28.8	21.6	10	151	0.6	K
94	μ-Virginids	5-12	227.1	-4.1	23.9	11	22.7	1.7	C, T
95	A	5-10	234.6	8.0	24.3	4	39.5	0.5	*
96	α-Scorpiids	5-12	236.9	-16	31.3	22	29.1	1.4	T
97	A	5-10	244.1	-0.3	31.0	8	27.7	1.7	*
98	Serpentids	5-12	245.4	11.0	32.5	10	12.2	2.0	T
99	A	5-12	244.1	0.4	31.1	6	31.4	0.9	*
100	N. May Ophiuchids	5-12	249.9	-16	32.9	28	22.0	1.3	S
101	S. May Ophiuchids	5-12	247.9	-29	33.3	7	30.7	2.2	S, T
102	A	5-12	252.1	5.2	39.8	6	4.9	3.3	*
103	A	5-12	252.1	-4.0	29.2	6	72.6	1.0	*
104	A	5-12	259.1	23.8	38.6	12	6.2	2.8	*
105	A	5-12	258.7	22.0	22.7	8	60.0	0.6	*
106	N. θ-Ophiuchids	5-12	262.0	-16.6	37.0	19	18.2	3.8	*
107	S. θ-Ophiuchids	5-12	263.4	-27.7	36.5	9	10.3	3.7	T
108	A	5-10	271.9	29.8	38.2	7	16.1	2.2	*

Table 2. Continuation.

	Showers and associations (A)	Day of observation	α_R deg	δ_R deg	V_∞ km/s	N	M $\times 10^{-3} g$	δ_0 g/cm^3	Note
				May 1969					
109	ε-Aquilids	5-10	281.0	22.2	34.7	40	10.6	2.9	K, Ka
110	A	5-12	281.1	31.1	35.2	10	9.3	1.8	K, Ka
111	A	5-12	290.5	30.0	36.1	19	9.2	2.2	K, Ka
112	A	5-12	291.5	41.9	42.4	11	11.2	4.1	*
113	A	5-12	295.4	22.6	36.2	11	15.4	1.5	K, Ka
114	A	5-12	297.5	19.7	48.8	6	11.7	2.7	*
115	A	5-12	300.6	0.9	66.1	8	0.7	4.2	*
116	A	5-12	303.1	31.3	36.8	21	7.7	3.0	K, Ka
117	A	5-12	303.9	43.8	38.7	5	2.4	1.8	*
118	A	5-12	312.7	36.6	40.0	4	11.3	2.7	*
119	A	5-12	314.8	11.1	60.7	30	2.0	4.6	K, Ka
120	A	5-12	322.3	20.7	59.5	11	0.7	2.4	K, Ka
121	A	5-12	326.1	10.5	62.0	18	1.4	3.7	K, Ka
122	A	6-12	334.6	25.3	55.6	13	1.3	3.9	Ka
123	A	5-12	335.2	38.7	40.2	15	8.4	3.8	*
124	A	5-12	335.9	51.9	40.5	9	4.8	0.2	K
125	A	5-12	340.6	43.3	42.5	10	4.3	3.4	*
126	η-Aquariids	5-12	340.9	1.7	66.9	136	3.2	2.8	J, Ka, S
127	A	5-12	344.6	54.3	37.1	7	18.0	0.3	*
128	A	5-12	350.6	31.3	52.0	8	4.7	3.9	*
129	A	5-12	351.3	32.0	35.5	11	4.1	2.9	*
130	A	5-12	355.6	21.7	39.3	7	17.5	1.2	K
131	A	5-12	356.1	47.7	40.1	33	9.2	3.4	K
				June 1969					
132	A	15-30	10.5	12.6	56.2	5	2.3	2.2	*
133	A	15-30	40.3	20.2	35.4	11	10.4	2.5	K, Ka
134	A	15-30	48.6	8.1	29.7	5	15.9	2.7	*
135	A	15-30	49.7	24.9	38.7	6	5.5	3.5	K
136	A	15-30	63.7	33.7	38.3	9	10.9	4.1	*
137	A	15-30	69.0	31.0	28.0	4	7.3	3.6	S
138	A	15-30	307.7	3.5	35.2	5	12.6	1.4	K
				July 1969					
139	A	1-3	9.1	20.5	60.9	8	1.9	1.1	K
140	A	1-5	17.9	7.2	66.5	6	1.8	2.8	*
141	A	1-7	17.8	23.7	58.2	5	5.2	3.4	K
142	A	4-5	75.0	14	37.5	6	8.5	2.0	*
143	χ-Sagittariids	1-5	273.7	-30.4	24.3	4	310	0.7	S
144	A	1-5	294	-18.4	33.5	5	25.4	1.4	*
145	A	1-5	305.6	28.5	44.5	4	8.9	1.1	*
146	A	1-5	310.4	-5.4	40.1	5	20.2	2.6	*
147	A	1-5	325.4	22.1	32.5	4	3.8	2.1	*
148	A	14-24	5.7	26.3	61.8	5	2.6	2.8	Ka
149	A	14-24	6.7	59.7	44.0	5	11.1	2.0	K
150	A	14-26	10.4	-0.1	57.8	6	3.0	4.3	*
151	A	14-24	16.2	35.0	63.8	7	-	-	K
152	A	14-24	18.9	22.5	60.8	13	4.7	2.8	K
153	A	14-24	31.9	30.1	63.4	11	2.3	2.5	K
154	ψ-Sagittariids	14-16	26.7	65.1	46.1	4	3.8	2.0	T
155	A	14-24	37.2	7.3	64.3	5	4.9	1.8	K
156	A	14-24	46.0	30.1	62.5	10	2.3	3.5	Ka
157	A	14-24	94.6	29.6	42.5	4	-	-	*
158	Capricornids	14-24	298.7	-25.4	23.1	7	44.6	0.7	T
159	S. ι-Aquariids	14-24	318.9	-16.7	34.2	15	32.7	1.3	Ka
160	A	14-24	320.6	4.84	29.4	5	10.5	0.8	Ka
161	π-Aquariids	14-24	327.3	-2.7	36.4	11	10.0	1.5	Ka, S
162	A	14-24	327.1	15.8	27.4	5	37.3	0.2	Ka
163	S. δ-Aquariids	14-26	337.1	-19.2	40.8	36	-	-	J, Ka

Table 2. Continuation.

	Showers and associations (A)	Day of observation	α_R deg	δ_R deg	V_∞ km/s	N	M $\times 10^{-3} g$	δ_0 g/cm^3	Note
				July 1969					
164	A	14-24	338.0	12.6	29.9	10	18.1	0.7	*
165	A	14-24	348.4	-24.2	37.6	10	15.4	4.5	*
166	A	14-24	354.1	27.8	58.3	6	2.7	2.9	K, Ka
167	A	14-24	354.7	-9.5	53.7	6	4.5	4.0	*
				August 1969					
168	A	3-14	24.9	33.7	57.7	4	-	-	K
169	A	3-14	27.8	62.6	57.2	4	2.4	1.2	Ka
170	A	11-14	42.1	40.3	60.7	7	2.2	2.6	K
171	Perseids	3-14	49.6	56.8	57.6	11	5.0	0.3	J, K, S
172	A	11-14	58.9	39.9	61.0	5	3.6	2.9	K, Ka
173	A	11-22	64.2	7.9	58.9	6	3.4	1.7	*
174	A	3-12	90.2	10.8	46.8	4	9.1	0.6	*
175	α-Capricornids	11-14	317.8	-4.8	23.6	8	24.1	1.2	C, K, J
176	N. ι-Aquariids	3-14	333.7	-6.1	34.2	8	2.4	1.6	J, Ka
177	A	3-14	339.1	54.7	44.5	4	4.5	2.9	*
178	N. δ-Aquariids	3-14	344.9	2.8	40.1	12	7.4	3.9	Ka
179	S. δ-Aquariids	3-12	347.9	-13.6	41.3	23	15.9	2.9	C, J, Ka
180	A	3-14	348.5	32.5	37.8	8	2.8	3.8	*
				September 1969					
181	A	12-27	19.4	10.7	41.1	11	5.1	3.0	K
182	A	22-24	24.6	89.7	39.7	9	13.6	0.5	*
183	γ-Arietids	12-27	31.0	18.3	37.3	6	2.9	2.8	S
184	A	12-27	71.7	9.1	50.5	6	-	-	*
185	A	22-27	74.2	36.6	61.9	4	-	-	Ka
186	A	12-27	84.0	11.1	53.3	6	0.8	5.0	Ka
187	A	22-27	83.5	27.2	60.5	5	-	-	K, Ka
188	β-Aurigids	12-27	87.1	42.5	58.5	5	-	-	K, Ka
189	A	12-24	98.2	5.4	60.1	7	1.2	2.7	K, Ka
190	A	12-24	110.1	37.7	63.7	6	-	-	Ka
191	A	12-27	110.9	20.6	59.9	4	4.3	2.5	Ka
192	A	22-27	147.3	-30.9	4	-	-	*	
193	A	22-27	157.0	9.1	35.8	9	6.5	2.9	*
194	A	22-27	156.7	29.2	40.4	5	-	-	*
195	A	12-27	164.5	22.3	41.3	5	3.2	3.3	K
				October 1969					
196	Oct. Andromedids	1-13	8.8	22.2	29.8	4	-	-	K, S
197	A	1-13	21.9	9.0	30.4	6	14.5	1.1	K
198	A	1-17	25.3	32.4	35.4	6	7.8	2.4	*
199	A	1-17	25.7	21.4	30.0	8	17.5	2.5	*
200	S. Arietids	1-17	31.8	13.5	31.8	14	12.0	1.6	Ka
201	N. Taurids	1-17	39.5	21.5	35.5	9	6.9	3.7	Ka
202	S. Taurids	1-13	74.2	29.6	57.0	5	1.1	4.0	Ka, T
203	A	1-13	77.8	10.3	56.1	4	1.2	3.7	Ka
204	S. ν-Aurigids	1-4	82.9	47.9	54.8	5	4.3	2.9	S
205	A	1-17	89.9	-17.6	56.1	5	4.8	1.2	*
206	A	1-13	93.8	9.5	51.9	7	3.1	0.8	Ka
207	A	1-17	97.8	25.9	63.1	7	2.4	0.7	Ka
208	A	1-17	115.5	-3.0	62.6	4	-	-	*
209	Oct. Lyncids	1-14	116.3	57.3	60.0	5	2.9	2.4	?
210	??	1-15	120.9	11.6	57.0	5	2.5	1.4	K
211	A	1-15	124.9	30.9	56.7	5	1.8	2.1	*
212	A	1-17	151.2	24.3	48.1	6	1.5	3.3	*
213	A	1-13	162.3	3.0	31.7	5	5.9	0.7	*
214	A	1-15	171.6	31.9	47.8	4	1.4	2.9	*

Table 3. The average densities (in g/cm^3) of the stream meteoroids: δ_0 – determined in this study and by Narziev (1991), δ_{01} – found by Babadzhanov (2002), δ_{02} – published in Lebedinets (1987), δ_m – the mineralogical density given by Benyuh (1974); N – count of radio meteors in the stream, K – porosity of the meteoroid particle.

Shower name	N	δ	δ_{01}	δ_{02}	δ_m	K %
η-Aquariids	32	3.3	-	2.0	-	-
Orionids	13	3.3	-	2.5	-	-
N. Taurids	14	2.6	1	3.5	2.7	10
S. Taurids	19	2.2	1	2.3	2.7	20
N. May Arietids	53	1.9	-	-	-	-
S. May Arietids	36	2.3	-	-	-	-
Quadrantids	28	1.7	1.4	2.8	3.4	50
N. δ Aquariids	52	2.0	1.7	3.3	4.1	50
S. δ Aquariids	152	2.3	1.7	3.3	4.1	40
N. ι-Aquariids	26	1.5	5.1	-	-	-
S. ι-Aquariids	50	1.9	3.2	-	-	-
0-Cetids	89	2.7	-	-	-	-
Piscids	83	2.8	-	-	-	-
α-Capricornids	36	1.2	1.0	2.5	2.8	60
ψ-Sagittariids	4	0.7	-	-	-	-
Geminids	71	2.4	1.6	4.4	3.3	30
α-Scorpiids	71	2.4	1.6	4.4	3.3	30
N. Librids	8	1.1	-	-	-	-
S. Librids	7	2.8	-	-	-	-
N. Ophiuchids	15	3.8	-	-	-	-
S. Ophiuchids	6	3.7	-	-	-	-
N. May Ophiuchids	23	1.3	-	-	-	-
S. May Ophiuchids	5	2.2	-	-	-	-
N. May ε-Arietids	6	1.3	-	-	-	-
S. May ε-Arietids	11	1.1	-	-	-	-
N. Leonids	9	2.8	0.4	-	-	-
S. Leonids	29	2.2	0.4	-	-	-

ference between the mineralogical and the bulk density is due to porosity K of the meteoroid particle only, we have found that the densities obtained in this study and those given by Benyuh (1974) may be related by

$$\delta = \delta_m(1 - K) \tag{2.11}$$

where $K{=}V_p/V_t$, V_p – the volume of voids, V_t – total volume of a particle. Calculated porosities K of the meteoroid particles are listed in Table 3.

According to Table 3 porosity of meteoroids of cometary origin equals to 10-60%. It gives some information about the mineralogical density of meteoroids of the related streams. As one can see in Table 3, the particles from related streams (Quadrantids, Northern and Southern δ Aquariids) have similar values of porosity. In case of the unrelated streams e.g. for the α-Capricornids and Geminids, porosities of their particles differ by factor two.

According to the results of laboratory simulation of cometary nuclei (Ibadinov 1998), porosities of the matrices, which are separated from the surface of the nucleus reach 40-98%. According to the theoretical estimates porosities get 26% for the most compact spherical particles. Hence, the results of laboratory simulations of cometary phenomena are in good agreement with our results obtained from the observations of meteor showers of cometary origin. Also, on a base of complex radar and photographic observations of meteors we can say that the meteoroids in the related streams have similar physical characteristics.

3. Conclusions

As result of our study we can draw a few conclusions.

1) From December 1968 till November 1969 we have carried out the radar observations of meteors. Two techniques were used: the diffraction and the bearing-time methods. As result, the radiants and velocities over 6100 individual meteors were determined.
2) Searching amongst the radiants and velocities we have found 214 meteor showers and associations. About half of these streams and associations have been observed by the radar for a very first time.
3) For the first time, using radar observations and taking into account the factors influencing the shape of the ionization curves – the masses and densities of the particles (members of the meteor showers and associations) were determined.
4) We have estimated the porosity of the meteoroids from the meteor shower twins. We have found that the densities and structures of the meteoroids of a common origin are similar.

References

Babadzhanov P.B., 2002, A&A, 317
Bibarsov R.Sh. et. al., 1990, Astron. Vestnik, 24, 326
Benyuh V., 1974, Astron. Vestnik, 8, 2, 96
COSPAR International Reference Atmosphere (1972), Berlin Akad. Verl.
Chebotaryev R.P., et al., 1970, Bull. Ast. Inst. of the Acad. of Sci. of the TjSSR, 55, 25
Chebotaryev R.P., 1970, Komety Meteory, 19, 46
Chebotaryev R.P., 1976, Komety Meteory, 24, 19
Cook A.F., 1973, in Proc. of IAU Colloq. 13, Albany, NY, 14-17 June 1971, eds Hemenway C.L., Millman P.M., and Cook A.F., NASA SP319, p. 183
Ibadinov H.I., 1998, Ph.D. Thesis, Academy of Sciences of RAN, Moscow, p. 296
Jopek T.J., Jenniskens P.M., 2011, in Proc. of the Meteoroids Conf., Breckenridge, Colorado, USA, May 24-28, 2010, eds Cooke W.J., Moser D.E., Hardin B.F., Janches D., NASA/CP-2011-216469. p. 7
Kashcheev B.L, Lebedinets V.N., Lagutin M.F., 1967 Moscow, Nauka, 250 pp
Korpusov V.N., 1970, Ph.D. Thesis, Obninsk, p. 171
Lebedinets V.N., 1987, Astron. Vestnik, 21, 1, 65
Narziev M., 1991, Reports of RT, XXXIV, 7, 412
Narziev M., 2003, Reports of RT, V. XL VI, 9, 5
Rietmeijer F.J.M., Nuth III J.A., 2000, EM&P, 82-83, 325

Sekanina Z., 1976, Icarus, 27, 265
Smirnov V., Vaisberg O., Anisimov S., 1986, in ESA Proc. of the 20th ESLAB Symposium on the Exploration of Halley's Comet, ESA SP-250, vol, 2, p. 195
Terentjeva A.K., 1966, in book "Investigation of meteors", Nayka, 1, p. 62-132.
Voloshchuk Y.I, Kashcheev B.L, Kruchinenko V.G., 1989, Meteors and meteoric matter, Kiev, Naukova, Dumka, 294 pp

PART 4

Meteoroid streams, meteoroid populations and origin

Meteoroids 2013, Proceedings of the Astronomical Conference,
held at A.M. University, Poznań, Poland, Aug. 26-30, 2013,
eds Jopek T.J., Rietmeijer F.J.M., Watanabe J., Williams I.P.,
Adam Mickiewicz University Press in Poznań, pp 179–192

The Origin of stream and sporadic meteors, comets or asteroids

Williams I.P.[1], **Jopek T.J.**[2]

[1]School of Physics and Astronomy, Queen Mary University of London, E1 4NS, UK
(I.P.Williams@qmul.ac.uk)
[2]Astronomical Observatory Institute, Faculty of Physics, A. Mickiewicz University,
Sloneczna 36, 60-286 Poznań Poland

Abstract. Asteroids and Comets that come close to the Earths orbit are called Near Earth Objects (NEOs). Any dust ejected from them, meteoroid streams will formed a meteoroid stream with orbits that are similar to that of the parent body. If the Earth passes through such a stream, the meteoroids will ablate and produce meteors that are as meteor showers. In this region, orbits evolve rapidly, hence, over time the orbits of stream meteoroids will progressively diverge both from each other and from the orbit of the parent body, so that instead of being observed as a meteor shower, these meteoroids become part of the sporadic background.

When a meteor shower is observed, a similarity in the orbits should indicate the parent and several test for this are discussed. If the parent is active, then it is a comet, but if no activity is found then it could either be an asteroid or a dormant comet. In this case, the behaviour of the meteor in the atmosphere will indicate whether the parent body was likely to be an asteroid or a comet.

For sporadic meteoroids the situation is more complicated as they can not be associated with a given parent body. All that can be done is to classify the orbits as being of comet or asteroid origin. Several criteria have been proposed and applied to the present day orbits of sporadic meteors. Using a single criterion can introduce a serious bias into the results with the fraction of comet orbits understated by up to 29%. Two parameter criteria have been suggested to remove this bias. Using these criteria on a set of ∼78000 sporadic meteoroids 66–67% have comet type orbits. This fraction can differ for meteors observed by different techniques, i.e. video, photographic and radar, in general it decreases with decreasing brightness of the observed meteors.

Keywords: near-Earth asteroids, comets, parent bodies, meteors, meteoroids, meteoroid streams, sporadic meteoroids, orbital classification

1. Introduction

A meteor is the result of the ablation of a solid particle (meteoroid) in the atmosphere of the Earth. They vary in size from tens of microns (which can only be detected by radar) to several tens of meters such as the recently observed Chelyabinsk fireball that was seen with the naked eye in daylight. Meteoroids can come from any parent that releases particles into the near-Earth environment. The majority of the meteoroids in the inner solar system come from two sources, asteroids and comets, though a few originate from the surface of other solar system bodies (mostly the Moon and Mars) while a fraction may also originate from interstellar

space (e.g Baggaley & Galligan, 2001; Janches et. al., 2001). In principle, meteors can be observed on any other body that has an atmosphere so that the impinging meteoroid ablates and Christou (2010) has investigated the possible occurrence of showers on Venus and Mars.

A meteor shower occurs when the number of meteors that are observed is significantly above the general background and where these meteors have a well-defined radiant on the sky. The existence of a radiant point indicates that the meteoroids were moving on parallel paths when they entered the Earth's atmosphere. To do this, they all must have similar heliocentric orbits, and so there exists in the inner Solar System families of meteoroids moving on similar orbits, meteoroid streams. Multi-station observations of these meteors allow the orbital elements of the heliocentric orbit to be determined. This gives a strong indication of parentage of the stream. The historical development of ideas concerning the association of meteoroid streams with asteroids and comets can be found in Williams (2011). In a comet, there are two principal ways in which a meteoroid stream can be formed. As a comet approaches the sun, solar heating causes the ices to sublimate and the resulting gas outflow carries away small dust grains with it as was first proposed by Whipple (1951). Others (e.g. Crifo 1995; Ma, Williams & Chen 2002) have modified this model, but the results are similar with the ejection velocity of the meteoroids generally being less than a few 100 ms^{-1}. Many comets have been observed to either fragment or totally disintegrate. Such a process will also release a large number of meteoroids. Again, the speed of the meteoroids relative to the nucleus will be small.

In the case of asteroids, the number of mechanisms that can cause meteoroid ejection is larger, for example inter-asteroid collisions, internal re-adjustment, tidal effects and a YORP spin-up leading to rotational instability. The mechanism that will form the strongest streams is a collision, as was initially suggested by Piotrowski (1953) and Fesenkov (1958). Proof that asteroids can indeed release dust in this manner came with the image of 2010A2 (Linear) an asteroid with a dust tail caused by a collision between two asteroids, in 2009 (Jewitt et al., 2010; Snodgrass et al., 2010). The velocity of the meteoroid relative to the parent asteroid will still be small compared with the heliocentric velocity. Thus, in all cases the orbit of the parent and the initial orbits of the meteoroids will be similar and a meteoroid stream is formed. (For a mathematical formulation of the physics involved, see Williams, 2002, 2004).

Individual meteoroids can experience significantly different perturbations, for example through a close planetary encounter resulting in significant orbital changes (Hughes, Williams & Fox, 1981; Jenniskens, 1998).

An other important effect is solar radiation, through radiation pressure and the Poynting-Robertson drag, first discussed in the context of meteoroids by Wyatt & Whipple (1950) and reviewed by Klacka & Williams (2002). Other processes may also remove meteoroids from the stream, for example, collisions between stream meteoroids and its parent (Williams et. al., 1993) or collisions with interplanetary dust particles (Trigo-Rodriguez et. al., 2005). Hence, as the stream gets older, meteoroids are lost from it, while the population of meteoroids moving on independent

orbits gets fed. This population gives rise the sporadic meteor population, which is more numerous than the population of meteors in showers, with only 25-35% being in showers. By the very way they come into existence, the sporadic meteors can not be associated with any given parent body and all that might be inferred is whether its original orbit was likely to be similar to those of asteroids or comets. The purpose of this paper is to critically review the methodologies used and results obtained in determining the relative proportions of meteoroids originating from asteroids and comets.

2. Methods for determining the parent of a meteor

2.1. Density considerations

It is to be expected that the bulk density of a meteoroid which originated from a rocky or metallic asteroid would be of the order of 3000 kg m^{-3} or higher while one originating from a comet would be between 500 and 1000 kg m^{-3}. A few meteoroids reach the surface of the Earth as meteorites. All those have bulk densities that roughly match those of asteroids. However, there is a selection effect here, only relatively strong meteoroids can survive the passage through the atmosphere. The number of meteorites that can be associated with a specific asteroid or comet based on its orbit prior to encountering the Earth is very small, of the order of 10 and so no conclusions can be drawn regarding the general percentage of meteoroids originating from comets or asteroids.

There are other difficulties in using the density as the main discriminator for determining the parentage of meteoroids. First, it is necessary to determine both the deceleration and brightness of the meteor as it passes through the atmosphere and any errors in measurement can significantly alter the results. Determining the deceleration requires a measurement of the velocities at various points, necessitating multiple site observations with accurate timings. This introduces a strong bias towards brighter meteors that are in streams. Second, the derived density depends critically on the model used for the ablation and in particular whether or not fragmentation takes place. Assuming that meteoroids were porous and crumbly, Jacchia et al.(1967) obtained a typical bulk density for meteoroids of 260 kg m^{-3}, while Verniani (1969) found from 140 kg m^{-3} to 630 kg m^{-3} for stream meteoroids and 280 kg m^{-3} for sporadics. Ceplecha (1958) modelled the ablation based using the heat conductivity equation through a solid body and found (Ceplecha, 1967) that meteoroid densities lay in the range $1400-4000$ kg m^{-3}, an order of magnitude higher. With the same model, Babadzhanov (1993) found that the densities ranged from 2500 kg m^{-3} for the Leonids, to 5900 kg m^{-3} for the Geminids. Thus, if it is assumed that the meteoroid structure is comet-like, a comet-like density is obtained, while assuming an asteroid structure give an asteroid density. Babadzhanov (2002) improved the model and found a range from 400 kg m^{-3} for the Leonids to 2900 kg m^{-3} for the Geminids.

There is also the problem that, while a comet nucleus is primarily composed of water-ice and is very porous, there are embedded within it small non-icy particles that become meteoroids and these could have a higher density. Conversely, asteroids

can have crumbly meteoroids on their surface. Hence, it is not surprising that up to now the major tool for determining a pairing of parent and stream has been orbit similarity.

2.2. Orbital similarity

A number of authors have proposed criteria to quantify the differences between two known orbits, for example Southworth & Hawkins (1963), Drummond (1981), Steel, Asher & Clube (1991), Jopek (1993), Valsecchi, Jopek & Froeschlé (1999), Jopek et al. (1999, 2008), Nesvorny & Vokrouhlicky (2006). These were summarised in Jopek & Williams (2013). The relationship between well-known meteor showers and comets have been firmly established using one of these criteria. The best known are the Perseids and 109P/Swift-Tuttle, the Leonids and 55P/Temple-Tuttle, the October Draconids and 21P/Giacobini-Zinner and both the Orionids and the Eta Aquariids with 1P/Halley. There are two associations between bodies that have been designated as asteroids and very major showers,(3200) Phaethon and the Geminids and (196256) 1993EH1 and the Quadrantids. Many asteroids have been suggested as being associated with the Taurid complex. There are many other established pairings between both comets and asteroids and streams. Lists can be found in books such as Jenniskens (2006).

There are a number of questions that arise when claims are made that a particular body is the parent of a given stream based on orbital similarity. First, is the orbital similarity due to chance. If it is, then we can draw no conclusions regarding the cometary or asteroidal origin of that stream. The systematic monitoring of the skies, has led to a vast increase in the number of known NEOs. Babadzhanov, Williams & Kokhirova (2008a) calculated that there is a 1/5 chance that a randomly chosen set of orbital elements will match the orbital elements of some NEO. Further, the typical period of variations in the orbital elements of Near-Earth asteroids is 5000 to 10000 years (see for example Babadzhanov, Williams and Kokhirova, 2012) so that even if orbits were not initially similar, orbital changes can cause them to become similar at the present time. Porubčan, Kornoš & Williams (2004) suggested that similarity of orbits should be maintained for 5000 years before a generic association could be claimed. Second, if the association is genuine, the question of whether the stream formed through dust ejection from the associated asteroid or did the dust came from a comet that has since become dormant or disintegrated leaving dormant fragments that are now indistinguishable from asteroids. Meteoroid stream can be formed through mutual collisions between asteroids. Streams formed in this way contain far less mass and are far more diffuse than those from a comet origin (Williams, 1993) but the Geminids, the Quadrantids or the Taurids are all very massive streams.

According to Wiegert, Houde & Peng (2008), the probability of a chance alignment between (3200) Phaethon and the Geminids is less than 0.001. Soon after the discovery of (3200) Phaethon, Fox, Williams & Hughes (1983) pointed out that it had all the characteristics necessary to be the parent of the Geminid meteoroid stream assuming that ejection takes place continuously over a wide range of true anomaly, or comet-like. Other papers confirm that the structure of the stream is

best explained by ejection from a comet (Hunt, Williams & Fox, 1985; Williams & Wu, 1993a; Ryabova, 2001; 2007), but no comet on the required orbit has been found. Phaethon brightened by at least 2 magnitudes on 2009 June 20 (Battams & Watson 2009), though no activity had been observed prior to that date (Hsieh & Jewitt 2005; Wiegert, Houde & Peng 2008). Ryabova (2012) concluded that meteoroids ejected during this outburst could be seen as a weak meteor shower in 2050, but such outbursts can not be the source of the vast majority of meteoroids in the very strong Geminid stream. Asteroid 2005 UD and 1999 YC have very similar orbits to that of Phaethon (Ohtsuka et al., 2006, 2008; Jewitt & Hsieh, 2006; Kinoshita et al., 2007; Kasuga & Jewitt, 2008), giving support to the comet fragmentation hypothesis.

Despite its strength and regularity in the current epoch, no records of the Quadrantids exist prior to about AD1800. Integrations (Murray, Hughes & Williams,1980; Hughes, Williams & Fox, 1981; Froeschlé & Scholl, 1982, 1986; Babadzhanov & Obrubov, 1987; Wu & Williams 1992) show that large changes in the orbital element of the Quadrantids take place over a few thousand years, which may explain the lack of early observations. However, it is also possible that the strong stream we observe today only formed a few centuries ago as was suggested by (Wiegert & Brown, 2004; 2005). No present-day comet has been unambiguously associated with the stream, though there have been many contenders (see Williams et al. 2004). McIntosh (1990) suggested that comet 96P/Machholz was a possible candidate since the orbits were similar several millennia ago. The characteristics of the orbital evolution of the comet and stream are also very similar, both showing changes with a 4000-yr period (Gonczi Rickman & Froeschlé 1992), but this requires the stream to have formed at least several millennia ago. The narrowness of the central peak in the activity profile led Jenniskens et al.(1997) to conclude that most of the meteoroids observed today are quite young. The mean orbit of the Quadrantids was integrated back to 1491 by Williams & Wu (1993b) and these elements are in remarkably good agreement with those given by Hasegawa (1979) for C/1490 Y1. Jenniskens (2004) suggested that 2003EH1 was a fragment from the break-up of C/1490 Y1 while Williams et al. (2004) showed that the orbit of 2003 EH1 in 1490 could produce the path on the sky described by Hasegawa. Comet 96P/Machholz is known to fragment and a possible scenario is that several millennia ago it fragmented, with a smaller part becoming C/1490 Y1. A fragmentation of C/1490 Y1 a few hundred years ago produced 2003 EH1 as well as a large number of meteoroids that are responsible for the strong narrow peak in the activity curve.

The Taurids can not be regarded as a single stream with many radiants located in both Taurus and Aries (Denning, 1928). Numerous authors (Olsson-Steel 1988; Babadzhanov, Obrubov & Makhmudov 1990; Štohl & Porubčan 1990; Steel Asher & Clube 1991) agree that the stream is a complex of several smaller meteoroid streams and filaments. Unlike the Geminids and the Quadrantids, the Taurids has an active comet, 2P/Encke associated with it. Many asteroids are also in the complex (Asher, Clube & Steel, 1993a; Clube & Napier (1984); Steel & Asher, 1996; Asher, Bailey Emel'yanenko, 1999; Babadzhanov, 2001; Porubčan Kornoš & Williams, 2006;

Table 1. The percentage of 7830 NEAs and 780 periodic comets not correctly classified by the various criteria.

Q [%]	E [%]	T [%]	Pe [%]	K [%]	
3.9	3.8	7.2	10.7	16.4	NEAs
1.0	1.5	2.2	5.8	13.8	Comets

Babadzhanov, Williams & Kokhirova, 2008b; Napier, 2010; Jopek, 2011). Asher, Clube & Steel (1993b) suggested that the whole complex could, have formed by the fragmentation of a giant comet 20-30 Ky ago.

Thus the population of meteoroids in known streams is dominated by those of cometary origin. For the sporadic meteors, there is by definition, no associated parent body and so the criterion for similarity of orbits discussed above can not be used and different methodologies have been developed.

2.3. Differentiating between types of orbits

In order to discriminate between the orbits of comets and asteroids, Whipple (1954) proposed $K = \log\left[a(1+e)/(1-e)\right] - 1$, the K-criterion. When $K \geqslant 0$ the orbit is of a comet type. Using this K-criterion Whipple (1954) found that 96% of known comets and 99.8% of known asteroids were correctly classified. The criterion can also be applied to meteoroids, and Whipple classified 90% of 144 bright photographic meteors as being of comet origin.

Several other criteria can be used. The T-criterion is based on the Tisserand invariant: $T = a^{-1} + 2a_J^{-1.5}\left[a(1-e^2)\right]^{(0.5)} \cos I$ where a_J is the semi-major axis of Jupiter's orbit and I the inclination of the meteoroid orbit relative to the Jupiter orbital plane. Kresak (1969) used the condition $T < 0.58$ to define a comet type orbit. Variants of this criterion are widely used in the NEO field (eg Jewitt, 2012; Babadzhanov, Williams & Kokhirova, 2013).

Two additional criteria, the P and Q criterion defined by $P = k^2 a^{1.5} e$, where k is the Gauss gravity constant and $Q = a(1+e)$ were proposed by Kresak (1967, 1969). For a comet orbit $P > 2.5$, and $Q > 4.6$ AU. Q is aphelion distance and so this condition simply requires that the orbit does not go beyond the asteroid belt.

Jopek & Williams (2013) proposed a new criterion, the E criterion (the orbital energy E) given by $E = -0.5k^2 a^{-1}$ with $a > 2.8$ AU for comet orbits.

The reliability of these methods was investigated by Starczewski & Jopek (2004). The Q-criterion proved to be the most reliable, producing the smallest number of exceptions. Jopek & Williams (2013) repeated this reliability test, applying all the criteria to the orbits of 780 comets given in Marsden & Williams (2008) and 7830 near-Earth asteroids given in the NEO Dynamic Site, 2012. Their results are summarized in Table 1. It is clear that the Q and E criterion are the most reliable while the K criterion produced the most exceptions.

3. Comet-asteroid classifications applied to meteoroid orbits

3.1. Historic investigations and recent works

To classify meteoroid orbits the various criteria have been used by several authors. Using the K-criterion, Whipple (1954) found that 90% of 144 orbits obtained using a small camera, 90% were of comet type. However this sample contained many stream meteoroids. Using photographic data obtained by Super Schmidt cameras Jacchia et al. (1967) found that 99.8% of orbits were of comet type, while Jones & Sarma (1985) found that the TV meteors were about equally divided into comet and asteroid types. Steel (1996a) found more comet orbits within photographic data but roughly the same number of orbits of both types amongst the Canadian TV meteors and the Adelaide radio meteors. However, in the Kharkov radio meteors he found more asteroid orbits a result contradicted by Voloshchuk et al. (1997) who that found 63% of the Kharkov meteors were on comet orbits. Using the Q-criterion and selecting only sporadic meteors, Starczewski & Jopek (2004) found that 78% radio meteors, 48% of photographic and 53% of video meteors moved on asteroid type orbits. For the photographic and video meteor samples, the results of Starczewski & Jopek are consistent with those given by Steel (1996a), but for radio meteors are very different from those of Voloshchuk et al. (1997).

Jopek & Williams (2013) studied approximately 78000 observations of meteors collected from many sources. From this data set, only elliptical orbits which passed the internal consistency check (see Jopek et al. 2003) were used. The primary aim of the investigation was to investigate sporadic meteors and so stream meteors were removed using the method described in Jopek et al. (2008).

3.2. Discussion of the results of the C-A classification

Jopek & Williams (2013) used all the criteria listed earlier so that differences between them could also be assessed. Their results are summarized in Table 2. The E-criterion gives the smallest fractions of meteoroids moving on comet orbits, with the fraction increasing through the Q, P and T-criterion, the K-criterion giving the largest. The differences between the results obtained are in the range 10-15%. Jopek & Williams (2013) illustrated the reason for the differences in reliability by means of plots of $1/a$ against e showing the threshold values of all the criteria discussed above. The observed meteoroids must lie between the boundaries $Q = 1$ and $q = 1$, and they occupy almost all this region. The E-curve occupies the lowest position in the region so that all the meteoroids classed by the E-criterion as comet were classed as comet by all the other criteria. Starczewski & Jopek (2004) used a similar classification method and partly used the same meteor data as Jopek & Williams (2013). Two discrepancies between them are clear. First, Starczewski & Jopek (2004) found lower fractions of comet orbits amongst all sporadic meteoroids and also amongst the data obtained by each observation techniques. In general Jopek & Williams found about 20% more sporadic meteoroids moving on comet orbits with the increase being smallest for the radio meteoroids and highest for the video data. Jopek & Williams used a larger sample of the video meteoroids, mainly obtained by SonotaCo group (SonotaCo 2009, 2011) where the mean magni-

Table 2. C - A one parameter classification. In the separate rows we give the percentages of meteors among the whole sporadic component, radar, video and photographic meteors, respectively. The last part gives the results by Starczewski & Jopek (2004).

Q [%]	E [%]	T [%]	P [%]	K [%]	Sample size and type	
44.0	41.8	56.8	49.0	61.8	77869	all meteoroids
23.4	21.4	36.1	28.1	44.8	45539	radio -,-
73.4	71.0	86.6	78.9	86.1	30899	video -,-
65.5	59.6	70.6	68.4	76.5	1431	photo -,-
23.6	-	35.5	28.7	42.8	55891	all meteoroids
22.2	-	34.0	27.1	41.4	52993	radio -,-
46.9	-	64.9	54.2	63.6	1221	video -,-
51.7	-	60.2	62.4	71.7	1677	photo -,-

tude was -1^m, so that they should probably be regarded as "photographic" rather than video. The orbits used by Starczewski & Jopek (also included in the Jopek & Williams set) obtained using cameras in Canada and Ondrejov had a limiting magnitude of 6^m–8^m.

The second discrepancy concerns the small but clear differences between the percentages of comet orbits found amongst both the radio meteors and the photographic meteors, where the same sources were used. However, different methods were used to eliminate the stream component. Starczewski & Jopek (2004) made only a limited search for streams, finding that only 15% of the sample belongs streams while Jopek & Williams (2013) found that 33.4% were in streams. Thus more comet orbits were eliminated. It is clear that the results depend on how well the stream component is eliminated.

4. Limitation of the one parameter C-A classification

The foregoing discussion shows that the conclusions depend on the criteria used. This is illustrated in Figure 1, reproduced from the paper of Jopek & Williams (2013). According to the Q-criterion, all meteoroids with $Q < 4.65$ are moving on asteroid type orbits. However, in Figure 1, there are many such meteoroids for with $i > 75°$. Very few real asteroids have such high inclinations and only one NEA, (2009 HC82), with $Q < 4.6$ [AU] and $i > 75°$ exists. There are no comets with such orbital properties. Therefore, the source of all sporadic meteoroids found in this region of the plot is an interesting question. The highest fraction of such orbits, 28% were in radio meteor data, with 15% in the video data and only 5% in the photographic data. These meteoroids are thus predominantly small.

With the E-criterion (see Figure 1), a similar percentage (23.2%) of "asteroid" meteoroids move on orbits for with $i > 75°$. For the remaining criteria the percentages of such "asteroid" meteoroids can be found in the paper of Jopek & Williams (2013) and are of the same order.

Some insight into the source of these sporadic meteoroids with $Q < 4.6$ AU and $i > 75°$ can be obtained by using the Hammer-Aitoff equal area diagram. It was first used by Hawkins (1956) and by many others since (eg Elford & Hawkins,

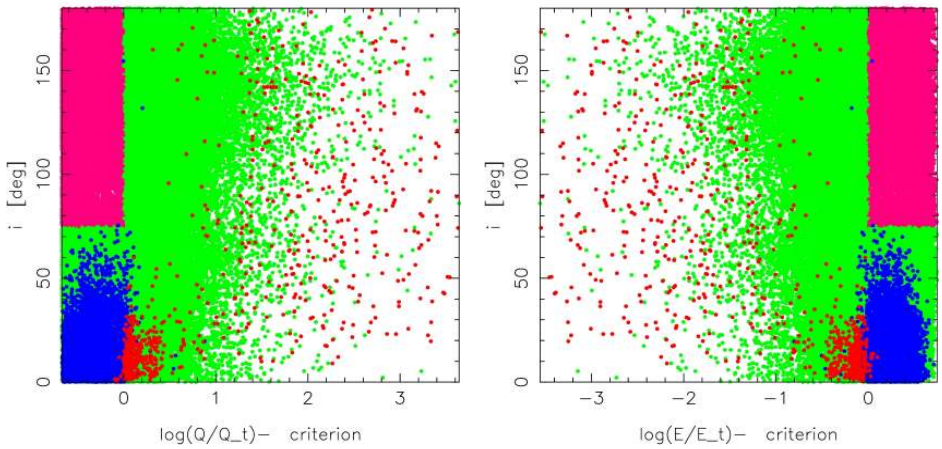

Figure 1. Left panel — 780 Comets (red), 7830 NEAs (blue) and 60412 sporadic meteoroids (green) on the i-$log(Q/Q_t)$ plane. Additionally, 17457 "asteroid" meteoroids for which inclinations $i > 75^\circ$ and aphelia distances $Q < 4.6$ [AU] are plotted as magenta rectangles. The right panel — 780 Comets (red), 7830 NEAs (blue) and 59810 sporadic meteoroids (green) on the and i-$log(E/E_t)$ plane. Additionally, 18059 "asteroid" meteoroids for which the inclinations $i > 75^\circ$ and the semi-major axes $a < 2.8$ [AU] are plotted as magenta rectangles.

1964; Sekanina, 1973; Galligan & Baggaley, 2005; Campbell-Brown 2008). Jopek & Williams (2013) found that for the 60412 meteoroids with $Q > 4.6$ [AU] or $i < 75^\circ$, (all the meteors that we are NOT interested in) the regions corresponding to the helion, antihelion, north and south apex and north and south toroidal concentrations, first identified by Elford & Hawkins (1964), were all visible. On the other hand, the 17457 meteoroid with $Q < 4.6$ [AU] and $i > 75^\circ$ were connected only with the apex concentration, with essentially none elsewhere. These meteoroids entered the Earth atmosphere with a speed $V_g > 30$[km/s].

4.1. The origin of meteoroids with $Q < 4.6$ AU and $i > 75^\circ$

According to Davies (1957), the aphelion distance of small meteoroids moving on high-inclined orbits would be reduced on realistic time-scales so that the orbits became more circular. Dycus & Bradford (1964) confirmed that P-R drag can decrease the aphelion of comet type orbits, changing the trajectories to asteroid type. Arter & Williams (1995) showed that P-R drag reduced the aphelion of meteoroids in the April Lyrids shower. Jones et al.(2001), Wiegert et. al. (2009) and Nesvorny et. al. (2011) have shown that the apex and toroidal meteoroids may originate through this mechanism from long period or Oort Cloud comets. Therefore the observed meteoroids moving on highly-inclined "asteroid" orbits evolved similarly and are of comet origin. With such a large influx of meteoroids that originated in comets, but now miss-classified as on asteroid type, it is clear that none of the one parameter criteria proposed to date are able to correctly classify all sporadic meteoroids and that the asteroid population is overstated.

Table 3. Cometary orbits among the sporadic meteoroids. The fractions in percentages, were found by the two parameters C-A classifications (see the text). In round brackets the limiting magnitude of the observation system are given. Notation e.g. $Mg > 2^m$ means that only meteors fainter then 2 magnitude has been classified.

Q-i [%]	E-i [%]	T-i [%]	P-i [%]	K-i [%]	Sample size	Sample type and remarks
66.4	66.9	70.3	69.4	78.4	77869	all meteoroids
51.3	49.9	56.0	54.6	67.8	45539	radio orbits
88.5	87.2	91.3	91.1	95.2	30899	video orbits
68.0	64.4	72.3	72.0	79.2	1431	photo orbits
48.3	43.4	54.9	55.2	61.9	286	photo bolides
67.5	63.1	71.3	70.7	79.7	670	photo Super Schmidt
80.6	78.7	84.2	83.8	88.8	475	photo small camera
59.9	58.1	63.7	63.0	68.6	322	video Canada ($+8.5^m$)
70.5	68.7	73.0	73.2	82.3	485	video Ondrejov ($+5$-6^m)
86.3	85.5	88.0	87.3	91.3	393	video DMS ($+6^m$)
88.9	87.7	91.9	91.5	95.7	7816	video SonotaCo 2007
90.0	88.8	92.7	92.6	96.0	9318	video SonotaCo 2008
88.6	87.2	91.5	91.3	95.7	12565	video SonotaCo 2009
55.9	54.1	60.0	60.6	74.1	170	video Ondrejov $Mg > 3^m$
69.0	67.8	74.7	72.4	82.8	87	video SonotaCo 2007, $Mg > 2^m$
70.9	70.9	75.7	75.7	80.6	103	video SonotaCo 2008, $Mg > 2^m$
64.4	61.6	70.5	71.1	83.5	315	video SonotaCo 2009, $Mg > 2^m$
62.2	59.6	67.2	66.2	83.3	1397	radio Adelaide1 ($+6^m$)
65.9	63.5	71.1	69.6	83.4	1106	radio Adelaide2 ($+8^m$)
46.3	44.8	51.8	50.0	65.2	14335	radio Harvard1 ($+12$-13^m)
41.9	40.6	47.1	45.2	56.7	13968	radio Harvard2 ($+12$-13^m)
56.3	55.0	59.4	58.6	69.4	4136	radio Kharkov ($+12$-13^m)
74.0	73.1	76.9	75.8	80.8	6637	radio Obninsk ($+6$-8^m)
52.0	49.5	56.2	56.3	82.6	3960	radio Mogadishu ($+6$-8^m)

5. Two parameter C-A classification

To overcome this, Jopek & Williams (2013) proposed that a two parameter approach should be adopted by adding inclination to each of the other criteria that have been discussed. Thus, if $i > 75^\circ$ the meteoroid is classed as comet type, irrespective of what the previous classifications determine. The new classifications are listed in full in Jopek & Williams (2013).

Jopek & Williams applied these new constraints to the sample of ~ 78000 sporadic meteoroids and found that, as expected, the fractions of comet meteoroids becomes significantly higher. The detailed results are reproduced in Table 3.

Both the Q-i and E-i criteria, now show that, 66–67% of the sporadic meteors were on comet orbits, the smallest fraction, 50–51%, was found among the radio meteors. For the video and photographic sub-samples, the fractions on comet orbits were 87–89% and 64–68%, respectively.

As mentioned earlier, Jopek & Williams and Starczewski & Jopek used different video samples in their analysis. To remove this discrepancy, in the "video" section in Table 3 the results for each video sub-sample used by Jopek & Williams are given. It can be seen that the fraction of meteoroids on comet orbits observed in Canada is about 30% less than in case of the meteors observed in Japan by SonotaCo. The meteors observed in Japan and Canada correspond to different ranges of magnitudes, the mean magnitude of meteors observed by SonotaCo being -1^m, but for meteors observed in Canadian the mean magnitude was close to 4.5^m.

Concentrating only on the faint meteors by removing all meteors with absolute magnitudes $Mg < 3^m$ from the Ondrejov results and $Mg < 2^m$ from the SonotaCo data, the fraction of meteors on comet orbits in the Ondrejov data is 14% less. In case of the SonotaCo data number classified as comet type orbits decreased by 14–20%.

Different results were found amongst the radio data. The smallest fraction 40–42% of meteors on comet orbits occurred among the Harvard2 "synoptic year" sample. For the Harvard1 sample, using the same criteria, the results were 4% higher. In the radio data from the Kharkov radar with a similar sensitivity to the Harvard equipment, comet orbit accounted for 55–56% of the total. A significantly less sensitive radar was used in Mogadishu and the percentage of meteors on comet orbits is smaller, 50–52%.

The radar equipments used in Adelaide and in Obninsk have a sensitivity comparable to that used in Mogadishu. In the Australian data many more meteoroids were found to be moving on comet type orbits. Some of these discrepant results are probably caused by selection effects arising from the observing strategy used. For example the Obninsk radio meteor data consist solely of meteors observed at their descending nodes, and hence all observed radiants have ecliptic latitude $\beta \geqslant 0$, but there is insufficient data available on most of the observing strategies to allow a definitive conclusion to be reached.

In the photographic results, the fraction on comet orbits was low, 43–48% .

6. Conclusion

The meteoroid associated with the three major streams, the Geminids, the Taurids and the Quadrantids, were mostly of cometary origin, though there are bodies that are classified as asteroids associated with them.

To classify the sporadic meteoroids properly into comet or asteroid populations a two parameters criterion needs to be used. Using only one parameter criteria causes the fraction of sporadic meteoroids on comet type orbits to be understated. For the photographic meteors, the underestimation is quite small, 2–5%. In case of radio data, the underestimation can reach 15–29%.

This underestimation comes about because there are many orbits that are classified as asteroid ($Q < 4.6$ AU) but are on high inclination orbits ($i > 75°$). These are mostly meteoroids that were originally on comet orbits but where P-R drag has reduced the aphelion distance Q so that they now satisfy the Q-criterion for being classed as asteroid type.

References

Arter T., Williams I. P., 1995, EM&P, 68, 141
Asher D.J, Clube S.V.M., Steel D.I., 1993a, in Štohl J. Williams I.P.,eds, Meteoroids and their parent bodies, Slovak Acad. of Sci., Bratislava, 93
Asher D.J, Clube S.V.M., Steel D.I., 1993b, MNRAS, 264, 93
Asher D.J. Bailey M.E. Emel'yanenko V.V., 1999, MNRAS, 304, L53
Babadzhanov P.B., 1993 in Štohl J. Williams I.P.,eds, Meteoroids and their parent bodies, Slovak Acad. of Sci., Bratislava, 295
Babadzhanov P.B., 2001, A & A, 373, 329
Babadzhanov P.B., 2002, A & A, 384, 317
Babadzhanov P. B., Obrubov Yu. V., 1987, Publ. Astron. Inst. Czech. Acad. Sci., 67, 141
Babadzhanov P.B., Obrubov Yu., Makhmudov N., 1990, Solar Syst. Res., 24, 12
Babadzhanov P.B., Williams I.P., Kokhirova G.I., 2008a, MNRAS, 386, 1436
Babadzhanov P.B., Williams I.P., Kokhirova G.I., 2008b, A & A 479, 249
Babadzhanov P.B., Williams I.P., Kokhirova G.I., 2012, MNRAS, 420, 2546
Babadzhanov P.B., Williams I.P., Kokhirova G.I., 2013, A & A 556, A25
Baggaley W.J., Galligan D.P., 2001, in Warmbein B., ed, Meteors 2001, ESA-SP495. 663
Battams K., Watson A. 2009, IAU Circ., 9054
Campbell-Brown M.D., 2008, Icarus, 196, 144
Ceplecha Z., 1958, Bull. Astron. Inst. Czechosl., 9, 154
Ceplecha Z., 1967, Smiths. Contr. Astrophys., 11, 35
Christou A.A., 2010, MNRAS, 402, 2759
Clube S.V.M., Napier W.M., 1984, MNRAS, 211, 953
Crifo J.F., 1995, ApJ, 445, 470
Davies J.G., 1957, Advances in Electronics and Electron Physics, 9, 95
Denning W.F., 1928, J. Brit. Astron. Asoc., 38, 302
Drummond J.D., 1981, Icarus, 45, 453
Dycus R.D., Bradford D.C., 1964, Icarus, 3, 306
Elford W.G., Hawkins G.S., 1964, Harvard Meteor Proj. Res. Rep. No 9, Nov., NASA-CR-60790
Fesenkov V. G., 1958, Soviet Astronomy, 2, 303
Fox K., Williams I.P., Hughes D. W., 1983, MNRAS, 205, 1155
Froeschlé Cl., Scholl H., 1982, A & A, 111, 346
Froeschlé Cl., Scholl H., 1986, A & A, 158, 259
Galligan D.P., Baggaley W.J., 2005, MNRAS, 359, 551
Gonczi F., Rickman H., Froeschlé Cl., 1992, MNRAS, 254, 627
Hawkins G. S., 1956, AJ, 61, 386
Hasegawa I., 1979, PASJ, 31, 257
Hsieh H.H., Jewitt D., 2005, ApJ, 624,1093
Hughes D. W., Williams I. P., Fox K., 1981, MNRAS, 195, 625
Hunt J., Williams I.P., Fox K., 1985, MNRAS, 217, 533
Janches D., Mathews J.D., Meisel D., Zhou Q., 2001, Icarus, 150, 706
Jacchia L.G., Verniani F., Briggs R.E., 1967, Smiths Contr. Astrophys., 10, 1
Jenniskens P., 1998, Earth, Planets and Space, 50, 555
Jenniskens P., 2004, AJ, 127, 3018
Jenniskens P., 2006, Meteor Showers and their Parent Comets, CUP, 693
Jenniskens P., Betlem H., De Lignie M., Langbroek M., Van Vliet M., 1997, A & A, 327, 1242
Jewitt D., Hsieh H., 2006, AJ, 132, 1624

Jewitt D., Weaver H., Agarwal J., Mutchler M., Drahus M., 2010, Nature, 467, 817
Jewitt, D.C. 2012, AJ, 143, 66
Jones J., Sarma T., 1985, Bull. Astron. Inst. Czechosl., 36, 103
Jones J., Campbell-Brown M., Nikolova S., 2001, in Warmbein B., ed, Meteors 2001, ESA-SP495, 575
Jopek, T.J., 1993, Icarus, 106, 603
Jopek T.J., Valsecchi G.B., Froeschlé Cl., 1999, MNRAS, 304, 751
Jopek T.J. Valsecchi G. B., Froeschlé Cl., 2003, MNRAS, 344, 665
Jopek T.J., Rudawska R., Bartczak P., 2008, EM&P, 102, 73
Jopek T.J., 2011, Memorie della Societa Astronomica Italiana, 82, 310
Jopek T. J., Williams I.P., 2013, MNRAS, 430, 2377
Kasuga T., Jewitt D., 2008, AJ, 136, 881
Kinoshita D., Ohtsuka K., Sekiguchi T., Watanabe J. et al., 2007, A&A, 466, 1153
Klacka J., Williams I.P., 2002, in Warmbein B., ed, ACM 2002, ESA-SP500, 141
Kresak L., 1967, Smithsonian Contribution Astrophysics, 11, 9
Kresak L., 1969, BAICz, 20, 177
Ma Y., Williams I.P., Chen W., 2002, MNRAS, 337, 1081
Marsden B.G., Williams G.V., 2008, Catalogue of cometary orbits 2008, MPC.
McIntosh B. A., 1990, Icarus, 86, 299
Murray C. D., Hughes D. W., Williams I. P., 1980, MNRAS, 190, 733
Napier W.M., 2010, MNRAS, 405, 1901
NEO Dynamic Site, 2012, `http://newton.dm.unipi.it/neodys`
Nesvorny D. Vokrouhlicky D., 2006, AJ, 132, 1950
Nesvorny D. Vokrouhlicky D. Pokorny P. Janches D., 2011, ApJ, 747, 1
Ohtsuka K., Sekiguchi T., Kinoshita D., Watanabe J.-I., et al., 2006, A&A, 450, L25
Ohtsuka K., Arakida H., Ito T., Yoshikawa M., Asher D.J., 2008, M&PSA Suppl., 43, 5055
Olsson-Steel D.I., 1988, Icarus, 75, 64
Piotrowski S. I., 1953, Acta Astronomica, 6, 115
Porubčan V. Kornoš L. Williams I.P., 2004, EM&P. 95, 697
Porubčan V., Kornoš L., Williams I.P., 2006, Contr. Astron. Obs. Skalnate Pleso, 36, 103
Ryabova G.O., 2001, in Warmbein B., ed, Meteoroids 2001 ESA SP-495, Noordwijk, 77
Ryabova G.O., 2007, MNRAS, 375, 1371
Ryabova G.O., 2012, MNRAS, 423, 2254
Sekanina Z., 1973, Icarus, 18, 253
Snodgrass C. et al., 2010, Nature, 467, 814
SonotaCo, 2009, WGN J.IMO, 37, 55.
SonotaCo, 2011, `http://sonotaco.jp/doc/SNM/`
Southworth R.B., Hawkins G.S., 1963, Smiths. Contr. Astroph.,7, 261
Starczewski S., Jopek T.J., 2004, EM&P, 95, 41
Steel D.I., Asher D.J., Clube S.V.M., 1991, MNRAS, 251, 632
Steel D.I., Asher D.J, 1996, MNRAS, 280, 806
Steel D.I., 1996a, Space Sci. Rev., 78, 507
Štohl J., Porubčan V., 1990; in Lagerkvist C.-I. Rickman H. Lindblad B.A., eds, Asteroids, Comets, Meteors III, Uppsala Universitat Reprocentralen, 571
Trigo-Rodriguez J.M., Vaubaillon J., Ortiz J.L. et al., 2005, EM&P 97, 269
Valsecchi G.B., Jopek T.J., Froeschlé Cl., 1999, MNRAS, 304, 743
Verniani F., 1969, Space Sci Rev., 10, 230
Voloshchuk Yu. I., Vorgul' A. V., Kashcheev B. L., 1997. Astronom. Vestnik, 31, 345

Wiegert P.A., Brown P., 2004, EM&P,95, 81
Wiegert P.A., Brown P., 2005, Icarus, 179,139
Wiegert P.A., Houde M., Peng R., 2008, Icarus, 194, 843
Wiegert P.A., Vaubaillon J., Campbell-Brown M., 2009, Icarus, 201, 295
Whipple F.L., 1951, ApJ, 113, 464
Whipple F.L., 1954, AJ, 59, 201
Williams I.P., 1993, in Štohl J. Williams I.P.,eds, Meteoroids and their parent bodies, Slovak Acad. of Sci, Bratislava, 31
Williams I.P., 2002, in Murad E. Williams I.P., eds, Meteors in the Earth's Atmosphere, Cambridge University Press, Cambridge, p.13
Williams I.P., 2004, WGN J. IMO, 32, 11
Williams I.P., 2011, A&G, 52, 2.20
Williams I.P., Hughes D.W., McBride N., Wu Z., 1993, MNRAS, 260, 43
Williams I. P., Wu Z., 1993a, MNRAS, 262, 231-248
Williams I. P., Wu Z., 1993b, MNRAS, 264, 659-664
Williams I.P., Ryabova G.O., Baturin A. P., Chernitsov A. M., 2004, MNRAS, 355, 1171
Wu Z., Williams I. P., 1992, MNRAS, 259, 617
Wyatt S.P., Whipple F.L., 1950, AJ, 111, 558

Meteoroids 2013, Proceedings of the Astronomical Conference,
held at A.M. University, Poznań, Poland, Aug. 26-30, 2013,
eds Jopek T.J., Rietmeijer F.J.M., Watanabe J., Williams I.P.,
Adam Mickiewicz University Press in Poznań, pp 193–197

Taurid meteor complex

Buček M.[1], **Porubčan V.**[1,2]

[1]Faculty of Mathematics, Physics and Informatics, Comenius University,
Mlynská dolina, 842 48 Bratislava, Slovakia
[2]Astronomical Institute of the Slovak Academy of Sciences,
Dúbravská cesta 9, 845 04 Bratislava, Slovakia (porubcan@fmph.uniba.sk)

Abstract. Structure of the autumnal part of the Taurid meteor complex based on photographic, radio and video meteor orbits is investigated and presented. Potential filaments or sub-streams to be associated with the complex were searched for utilizing the Southworth-Hawkins D-criterion. Altogether fourteen filaments or sub-streams associated with the complex were separated, with the length of the complex exceeding 100 degrees. Central part of the complex is formed by four the most dense filaments, the Northern and Southern Taurids, Southern Piscids and Omicron Orionids. The most probable bodies genetically related to the complex besides 2P/Encke are 2005 UY6, 2005 TF50 and 2007 RU17.

Keywords: meteoroids, meteor streams, meteor complexes, Taurids

1. Introduction

The Taurids active in autumn are a meteor stream with the longest activity period of all major meteoroid streams. Already Denning (1928) from visual observations recognized the complex structure of the stream, identifying thirteen active radiants situated in Aries and Taurus. Whipple (1940) and later Whipple and Hamid (1952) analyzing photographic Taurids indicated a possible relationship of the stream with comet Encke. At present, as well as P/Encke several Apollo asteroids are considered for possible progenitors of the stream (Babadzhanov et al., 1990, Štohl and Porubčan, 1990, Asher et al., 1993, Babadzhanov, 2001, etc.).

As the Taurids are dominant in bright meteors, the activity and structure are best known from photographic observations, which provide the most precise orbits. Whipple (1940) for his analysis of photographic Taurids had at disposal 9 orbits. The last version of the IAU MDC database, version 2003 (Lindblad et al., 2003) lists 4581 photographic orbits to which additional 292 orbits were added to the new updated database (Neslušan et al., 2013) and utilized for investigation of the Taurid complex. In order to get a more complex information on the structure and activity of the complex, the present analysis was extended also to radio (Harvard Radio Meteor Project 1965 and 1969, Sekanina 1970) and video (Japanese Network 2007-2011; SonotaCo 2009) meteor orbits.

2. Analysis and results

The Taurids, their potential streams or sub-streams to be associated with the complex were searched for by an iteration procedure (Porubčan and Gavajdová 1994)

Table 1. The mean orbits and radiants of the northern and southern branch of the Taurid meteor complex derived from the densest filaments (N Tau – northern branch; S Tau and S Psc – southern branch).

N Taurids	Photo	TV	Radar	S Taurids	Photo	TV	Radar
q [AU]	0.361	0.378	0.394	q [AU]	0.341	0.366	0.369
a [AU]	2.164	2.073	1.810	a [AU]	2.047	1.924	1.668
e	0.832	0.817	0.772	e	0.832	0.808	0.775
i [deg]	2.7	2.7	2.4	i [deg]	5.6	5.4	5.5
ω[deg]	293.5	292.1	292.7	ω[deg]	116.7	114.4	116.4
Ω[deg]	228.6	230.1	227.1	Ω[deg]	34.4	36.7	28.1
π[deg]	162.2	162.1	159.8	π[deg]	151.2	151.1	144.5
Vg [km/s]	28.14	27.34	25.27	Vg [km/s]	28.38	27.17	25.59
R.A. [deg]	57.5	58.4	55.6	R.A. [deg]	46.7	47.9	40.5
δ r.a. [deg]	0.79	0.81	0.79	δ r.a. [deg]	0.77	0.76	0.76
Dec. [deg]	22.4	22.7	22.1	Dec. [deg]	12.3	12.6	10.1
δ dec.[deg]	0.16	0.16	0.17	δ dec.[deg]	0.22	0.19	0.19

utilizing the Southworth-Hawkins D-criterion (1963). In order to get the cores of the streams a strict limiting value D of 0.10 (photo and video), 0.15 (radio) was applied. Further, only filaments with the geocentric velocity (±5km/s with respect to the mean Vg of the stream) and radiant (±10 degrees with respect to the Taurid radiant ephemeris allowed for the daily motion) were selected.

By this procedure were identified 173 photographic orbits (70 N and 103 S branch), 1288 TV orbits (625 N and 663 S branch) and 416 radar orbits (165 N and 251 S branch) belonging to the Taurid complex.

The radiants of the Taurid complex meteors selected by all three techniques are depicted in Figure 1 and the mean orbits and radiants derived from the densest filaments (N Tau northern branch; S Tau and S Psc southern branch) are listed in Table 1.

The complex is best represented by video orbits were 14 filaments could be recognized (Figure 2, Table 2). The most populated filaments are Northern and Southern Taurids, Southern Piscid and Southern Omicron Orionids. Due to a very long period of activity (September – December), the complex is extending over 100 degrees and the Taurid complex radiant passes through five constellations. The radiant areas of both branches (allowed for the daily motion) form compact areas of the size of 25 x 15 degrees.

3. Associated NEOs

Potential associations between Taurid filaments and NEOs were searched for among NEOs known by August 1, 2013 comprising 10069 objects (ASTORB.DAT database, JPL catalogue of comets). Orbital similarity was verified by comparing the mean orbits of the filaments with the orbits of NEOs applying the Southworth-Hawkins D-criterion to the osculating orbits of NEOs and filaments.

Taking into account fact that present osculating orbits cannot reflect real genetic associations between the Taurid complex filaments and NEOs, for the analysis

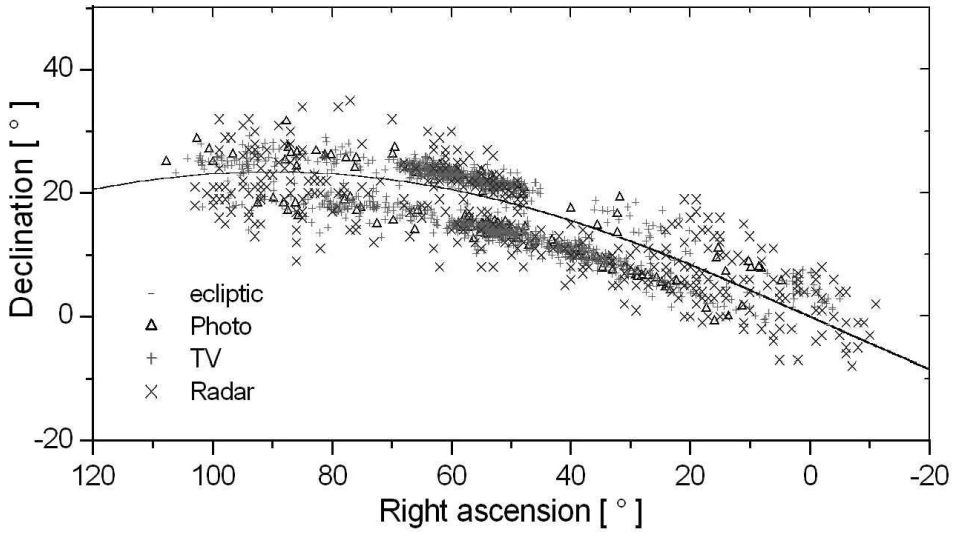

Figure 1. Radiants of the autumnal branch of the Taurid complex meteors selected from photographic (IAU MDC database), television (Japanese Network – SonotaCo) and radio (Harvard) observations.

Table 2. The mean radiants (right ascension and declination) and orbital elements of the filaments of the Taurid complex depicted in Figure 2, derived from the best represented population provided by video observations. Vg – the mean geocentric velocity and n – the number of orbits.

Filament	Q [AU]	q [AU]	a [AU]	e	i [deg]	ω [deg]	Ω [deg]	π [deg]	R.A [deg]	Dec. [deg]	Vg [km/s]	n
01 ω Psc (a)	4.37	0.366	2.227	0.834	3.4	293.6	170.9	104.4	0.7	3.5	27.86	9
02 ω Psc (b)	3.76	0.291	1.821	0.836	5.4	304.2	166.0	110.2	0.5	4.6	28.92	22
03 μ Psc (a)	4.56	0.410	2.239	0.814	4.7	108.5	10.1	118.6	19.5	3.4	26.58	8
04 δ Psc	3.68	0.267	1.766	0.844	4.0	127.4	352.7	120.1	10.6	1.5	29.47	13
05 μ Psc (b)	3.62	0.328	1.840	0.819	4.9	119.7	11.5	131.2	25.5	6.2	27.91	44
06 β Ari	3.86	0.338	1.923	0.820	4.0	298.0	197.3	135.3	27.5	14.8	27.86	28
07 S Psc	3.25	0.320	1.732	0.814	5.7	121.0	23.3	144.3	37.6	9.9	27.86	145
08 S Tau	3.79	0.389	2.016	0.806	5.3	111.3	43.1	154.4	52.8	13.9	26.84	304
09 N Tau	3.90	0.378	2.073	0.817	2.7	292.1	230.1	162.1	58.4	22.7	27.34	457
10 o Ori S	4.05	0.403	2.123	0.808	5.0	108.9	65.4	174.3	74.5	17.7	26.86	124
11 o Ori N	4.10	0.366	2.100	0.824	2.8	293.3	247.1	180.3	77.4	25.4	27.91	41
12 η Gem N	4.18	0.436	2.204	0.800	2.2	284.7	265.5	190.2	93.5	25.6	26.15	42
13 μ Gem	4.48	0.378	2.311	0.835	2.5	290.8	267.2	198.0	98.4	25.4	28.29	25
14 η Gem S	4.10	0.385	2.139	0.819	4.5	110.7	82.4	193.1	93.1	19.2	27.62	25

NEOs with D $\leqslant$ 0.30 were selected and their theoretical meteor radiants and encounter geocentric velocities at their approaches to the Earth orbit were computed (Neslušan et al. 1998). Further, additional conditions for potential associations between filaments and NEOs were applied: differences in the geocentric velocity of asteroid and filament ΔVg $\leqslant$ 5 km/s and in the theoretical meteor radiant of asteroid and radiant of filament ΔR.A. $\leqslant$ 10 degrees, ΔDec. $\leqslant$ 10 degrees. Applying these conditions 131 potential association were obtained, formed by 67 asteroids (some of them were associated to more filaments).

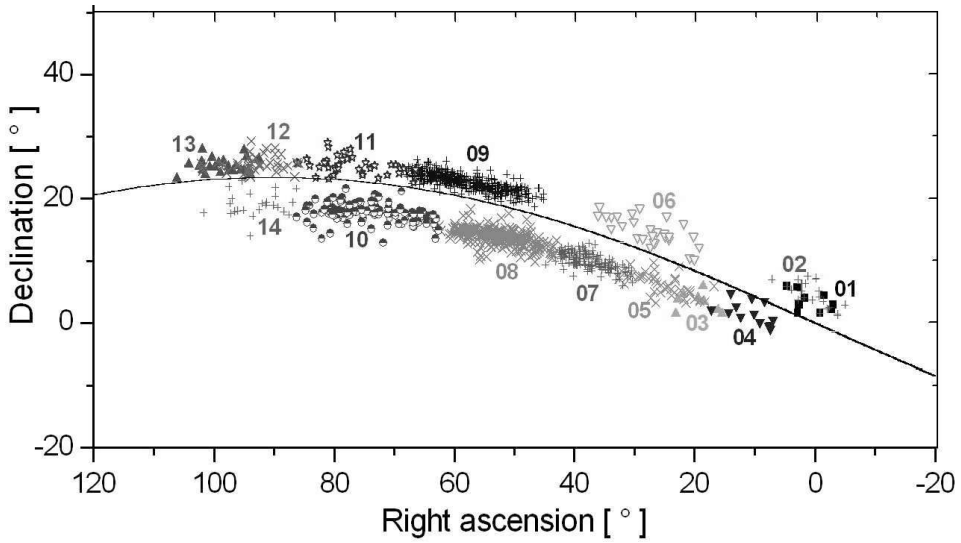

Figure 2. Radiants of the filaments of the Taurid complex derived from video observations. The numbers correspond to the filaments listed in Table 2.

In order to disclose probable associations, the motion of all the 67 asteroids and mean orbits of the Taurid complex filaments was integrated for 10000 year backward (package Mercury 6, Bulirsh-Stoer procedure) and the most probable bodies genetically related to the complex inferred from a long-term evolution of D, besides 2P/Encke are 2005 UY6, 2005 TF50 and 2007 RU17. All the three NEOs with the absolute magnitudes H of 17.94, 20.30 and 18.14, respectively are relatively small bodies with diameters in the range of approx. 500-1200 m.

4. Conclusions

Analysis of the Taurid complex based on photographic, video and radio meteor orbits exhibits its very long activity. The complex, with 14 identified filaments of which the most dense are the Northern and Southern Taurids, the Southern Piscids and Omicron Orionids, forms a broad stream extending over 100 degrees in solar longitude (September – December). The radiant area of the complex reduced to the common solar longitude of 220 degrees is 25 x 15 degrees. Following the orbital evolution backwards over 10000 yrs, the most close associations of NEOs known by August 1, 2013 with the Taurid complex are found for 2005 UY6, 2005 TF50 and 2007 RU17.

Acknowledgements

Authors are indebted for support of the research to the Slovak Research and Development Agency, project APVV-0516-10.

References

Asher D.J., Clube S.V.M., Steel D.I., 1993, MNRAS, 264, 93
Babadzhanov P.B., 2001, A&A, 373, 329
Babadzhanov P.B., Obrubov Yu., Makhmudov N., 1990, Solar System Res., 24, 12
Denning W.F., 1928, J. Brit. Astron. Assoc., 38, 302
Lindblad B.A., Neslušan L., Porubčan V., Svoreň J., 2003, EM&P, 93, 249
Neslušan L., Porubčan V., Svoreň J., 2013, EM&P, 111, 105, DOI 10.1007/s11038-013-9427-1"
Neslušan L., Svoreň J., Porubčan V., 1998, A&A., 331, 411
Porubčan V., Gavajdová, M., 1994, P&SS, 42, 151
Sekanina Z., 1970, Icarus 13, 450
SonotaCo, 2009, WGN, Journal of the IMO, 37, 55
Southworth R.B., Hawkins G.S., 1963, Smith. Cont. Aph. 7, 261
Štohl J., Porubčan V., 1990, Asteroids, Comets, Meteors III., Uppsala Univ., 571
Whipple F.L., 1940, Proc. Amer. Phil. Soc., 111, 375
Whipple F.l., Hamid S.E. 1952, Harvard Rep., No. 361

Meteoroids 2013, Proceedings of the Astronomical Conference, held at A.M. University, Poznań, Poland, Aug. 26-30, 2013, eds Jopek T.J., Rietmeijer F.J.M., Watanabe J., Williams I.P., Adam Mickiewicz University Press in Poznań, pp 199–204

The Capricornids asteroid-meteoroid complex

Babadzhanov P.B., Kokhirova G.I., Khamroev U.Kh.

Institute of Astrophysics, Academy of Sciences of the Republic of Tajikistan, Dushanbe, Tajikistan (kokhirova2004@mail.ru)

Abstract. The near-Earth asteroids (NEAs) 2008BO16, 2011EC41, and 2013CT36 are moving on similar orbits that, according to the values of the Tisserand invariant, could be classed as comet-like. Investigation of the orbital evolution shows that the NEAs are the quadruple crossers of the Earth's orbit. Consequently, a developed meteoroid stream, possibly associated with them, might produce four meteor showers. Theoretical parameters of the predicted showers were calculated and identified with the observable night-time σ-Capricornids and χ-Sagittariids, and daytime Capricornids-Sagittariids and χ-Capricornids showers. The comet-like orbits and association with the same meteoroid stream producing four active showers are strong indications that these asteroids have a common cometary origin. Earlier the NEAs (2101) Adonis and 1995CS (a potentially hazardous asteroid), were recognized as dormant comets on the base of their association with the same meteoroid stream. So, it may be concluded, that either four NEAs are large sized splinters of Adonis, or all five objects are fragments of a larger comet that was the parent body of the Capricornids meteoroid stream, and whose break-up occurred several tens of thousands years ago.

Keywords: near-Earth asteroids, dormant comets, meteoroid stream, meteor showers, orbits, evolution, radiants

1. Introduction

It is now accepted that some near-Earth asteroids (NEAs) may be dormant or extinct comets. Indeed, it may be expected that these NEAs might produce meteoroid streams during their active periods. So, the existence of an associated meteoroid stream producing an observed meteor showers and the comet-like orbit of a NEA are indicators of its cometary nature. Such NEAs and a meteoroid streams associated with them which have very similar orbits and a likely common progenitor form a complexes of near-Earth objects (NEOs). A good example of such sets is the Taurid asteroid-meteoroid complex which consists of many substreams and has both comet 2P/Encke and more than 40 NEAs moving on orbits within it that are in reality dormant or dead comet fragments (Asher *et al.* 1993; Babadzhanov 2001; Porubčan et al. 2004, 2006; Babadzhanov et al. 2008a; Rudawska et al. 2012a,b; Madiedo et al. 2013). It was shown that such meteoroid streams as the Piscids, ι-Aquariids, ν-Virginids, Scorpiids contain from one till several large NEAs of cometary origin, and these asteroid-meteoroid complexes are the results of a cometary break-up (Babadzhanov et al. 2008b, 2009, 2012, 2013). Here we report the identification of three new NEAs moving within the σ-Capricornids meteoroid stream which is associated with the asteroid (2101) Adonis.

Table 1. Summary of Orbital (J2000.0) and Physical Properties of the NEAs.

NEA	a [AU]	e	q [AU]	Q [AU]	i [deg]	Ω [deg]	ω [deg]	π [deg]	T_j	H	d [km]
2008BO16	2.4	0.809	0.46	4.40	8.6	133.9	254.4	28.3	2.9	22.9	0.13
2011EC41	2.4	0.880	0.29	4.56	9.9	38.8	357.8	36.7	2.8	19.9	0.53
2013CT36	2.5	0.819	0.44	4.47	6.4	351.6	38.9	30.4	2.9	19.2	0.73

2. Near-Earth asteroids moving on similar comet-like orbits

We searched the "Near-Earth Objects Dynamic Site" database (NEODyS 2013) to find a group of Earth-crossing asteroids that move on similar orbits that could be classed as cometary. Three Apollo group asteroids were identified 2008BO16, 2011EC41, and 2013CT36. Their main properties are given in Table 1, where as well as the usual orbital elements the absolute magnitude of an asteroid H, it equivalent diameter d, and the Tisserand invariant T_j are given. To estimate the equivalent diameters d of the asteroids we used the following relationship (Tedesco et al. 1992)

$$2\log d = 6.247 - 0.4H - \log p, \tag{2.1}$$

where p is the albedo of an asteroid. The values of diameters in Table 1 were determined under the mean value of the albedo $p = 0.07$ accepted for very dark asteroids (Jewitt 1992). Many criteria have been proposed to differentiate between asteroidal and cometary orbits and these have recently been reviewed by Jopek and Williams (2013). One of the most widely used is the Tisserand invariant defined relative to Jupiter (Kresak 1982; Kosai 1992) by the expression

$$T_j = \frac{a_j}{a} + 2[\frac{a}{a_j}(1-e^2)]^{0.5}\cos i, \tag{2.2}$$

where a, e, and i are the semi-major axis, eccentricity, and inclination of the object's orbit, respectively, and $a_j = 5.2$ AU is the semi-major axis of the orbit of Jupiter. Kresak (1969) suggested that for comets $2.08 < T_j \leqslant 3.12$, and for asteroids $T_j > 3.12$. A value of T_j at around 3 is still considered to be the boundary between asteroidal and cometary orbits (Jewitt 2012). According to this criterion, the above three NEAs orbits are classified as comet-like.

Jopek and Williams (2013) also discuss criteria for claiming an association between objects based on orbital similarity. A widely used criterion proposed by Southworth and Hawkins (1963) is the D_{SH}, defined by the expression

$$D_{SH}^2 = (e_2-e_1)^2 + (q_2-q_1)^2 + (2\sin\frac{i_2-i_1}{2})^2 + \sin i_1 \sin i_2 (2\sin\frac{\Omega_2-\Omega_1}{2})^2 +$$

$$+[(\frac{e_1+e_2}{2})2\sin\frac{(\Omega_2+\omega_2)-(\Omega_1+\omega_1)}{2}]^2, \tag{2.3}$$

where the subscripts 1 and 2 relate to these two orbits that are being compared. The orbits are considered to be similar if their value of $D_{SH} \leqslant 0.20$. In the situation where the angular orbital elements Ω and ω are changing rapidly Asher *et al.* (1993)

Table 2. Mutual values of the D criterion.

NEA	2008BO16	2011EC41	2013CT36
2008BO16	0	0.19	0.02
2011EC41	0.19	0	0.17
2013CT36	0.02	0.17	0

proposed a simplified D criterion, namely

$$D^2 = (\frac{a_1 - a_2}{3})^2 + (e_1 - e_2)^2 + \{2 \sin \frac{i_1 - i_2}{2}\}^2, \tag{2.4}$$

with limits similar to those used for D_{SH}. Mutual values of the D criterion (Table 2) confirm that all three asteroids have similar orbits therefore probably, a common origin. To prove that they have a common origin, it is necessary to show that a related meteoroid stream exists.

3. Investigation of the NEAs orbital evolution and a search for related showers

As was pointed out by Babadzhanov and Obrubov (1992), the nodal distance of stream meteoroids orbits will be equal to 1 AU at four different values of ω, during one cycle of its variation and so four meteor showers originating from a single meteoroid stream can be formed. These four meteor showers consists of a night-time shower with Northern and Southern branches producing at the pre-perihelion intersection with the Earth, and of a daytime shower also with Northern and Southern branches producing at the post-perihelion intersection. We investigated the secular variations of the orbital elements of the three NEAs using the Everhart integration method (Everhart 1974) over one cycle of variation of the argument of perihelion ω taking into account the gravitational perturbations from the major planets. The resulting variations of the heliocentric distances of the ascending node R_a and the descending node R_d versus the argument of perihelion ω are plotted on Figure 1. It is seen, that the asteroids cross the Earth's orbit four times during this period, i.e. the R_a and R_d are equal to 1 AU at four mean values of ω: $105.7 \pm 6.5, 75.2 \pm 5.9, 289.0 \pm 8.8$, and 253.3 ± 9.8. Using the orbital elements of the NEAs at these positions the theoretical geocentric velocities and radiants of meteor showers, possibly associated with each of these asteroids, were calculated. Then a search of published catalogues for observable showers close to theoretically predicted ones was undertaken. It turners out that all three NEAs are associated with the same meteoroid stream. The results are summarizing in Tables 3,4,5, where the theoretical Northern and Southern branches of the night-time shower are designated as T "A" and T "B", and the Northern and Southern branches of the day-time shower as T "C" and T "D". The predicted Northern branch of the night-time shower was identified with a known meteor shower, which was identified in radar observations by Sekanina (1973) and named the σ-Capricornids. This shower is listed as SCA with the number 179 in the catalogue of meteor

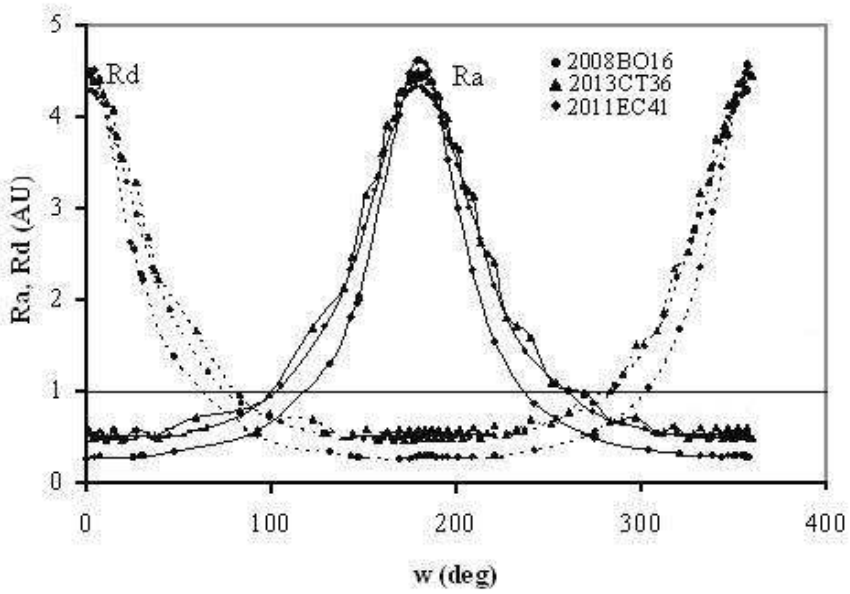

Figure 1. Variations in the nodal distances for three NEAs.

Table 3. Theoretical and observed geocentric radiants (J2000.0)and velocities of meteor showers associated with the NEA 2008BO16.

	Shower	α_g [deg]	δ_g [deg]	V_g [km/s]	$L_\odot$ [deg]	Date	D_{SH}	Type	Cat.
T	"A"	293.3	-13.8	26.0	106.9	July 9		N	
O	σ-Capds	298.5	-18.4	24.6	107.6	July 11	0.17	N	S2
T	"B"	295.1	-27.0	26.1	106.3	July 8		N	
O	χ-Sagds	290.7	-26.0	25.6	100.2	July 3	0.05	N	S3
T	"C"	305.4	-13.7	26.0	310.5	Jan.31		D	
O	Capds-Sagds	299.8	-14.1	25.1	309.8	Jan.31	0.14	D	S3
T	"D"	307.9	-27.1	25.9	309.5	Jan.30		D	
O	χ-Capds	314.8	-23.3	26.8	325.1	Feb.15	0.12	D	S2

showers of Jenniskens (2006). The nine bolides detected by the fireball networks of Canada, USA, and Tajikistan also confirm its activity. The predicted Southern branch of the night-time shower corresponds to the active shower χ-Sagittariids. The Northern and Southern branches of the day-time shower were identified with the day-time Capricornids-Sagittariids and χ-Capricornids, respectively. All these observable showers also were seen by Sekanina (1973, 1976) using radar observations. A satisfactory agreement between the theoretical and observable orbital properties is confirmed by the values of the D_{SH} criterion. The closeness of the ra-

Table 4. Theoretical and observed geocentric radiants (J2000.0)and velocities of meteor showers associated with the NEA 2011EC41.

	Shower	α_g [deg]	δ_g [deg]	V_g [km/s]	$L_\odot$ [deg]	Date	D_{SH}	Type	Cat.
T	"A"	291.0	-19.3	31.5	95.3	June 28		N	
O	σ-Capds	298.5	-18.4	24.6	107.6	July 11	0.19	N	S2
T	"B"	299.7	-21.2	32.2	101.8	July 4		N	
O	χ-Sagds	290.7	-26.0	25.6	100.2	July 3	0.20	N	S3
T	"C"	300.1	-13.4	29.8	329.6	Feb.22		D	
O	Capds-Sagds	299.8	-14.1	25.1	309.8	Jan.31	0.11	D	S3
T	"D"	325.6	-16.7	31.4	337.2	Feb.28		D	
O	χ-Capds	314.8	-23.3	26.8	325.1	Feb.15	0.19	D	S2

Table 5. Theoretical and observed geocentric radiants (J2000.0)and velocities of meteor showers associated with the NEA 2013CT36.

	Shower	α_g [deg]	δ_g [deg]	V_g [km/s]	$L_\odot$ [deg]	Date	D_{SH}	Type	Cat.
T	"A"	294.1	-14.5	26.9	106.3	July 9		N	
O	σ-Capds	298.5	-18.4	24.6	107.6	July 11	0.19	N	S2
T	"B"	300.4	-25.5	26.9	110.2	July 13		N	
O	χ-Sagds	290.7	-26.0	25.6	100.2	July 3	0.05	N	S3
T	"C"	303.7	-15.7	26.9	309.7	Jan.302		D	
O	Capds-Sagds	299.8	-14.1	25.1	309.8	Jan.31	0.18	D	S3
T	"D"	305.1	-26.6	27.1	308.9	Feb.29		D	
O	χ-Capds	314.8	-23.3	26.8	325.1	Feb.15	0.11	D	S2

diant coordinates, velocities, and activity dates also prove the relationships between the NEAs and the meteor showers.

4. Conclusions

The similar comet-like orbits of the NEAs and their association with a meteoroid stream that produces four active showers are strong indications that these NEAs have a cometary nature and a common origin. Earlier it was established, that the NEAs (2101) Adonis and 1995CS (PHA) of 800 and 40 m in size respectively are associated with the same meteoroid stream producing four meteor showers (Babadzhanov 2003) mentioned above, and so it can be concluded that they have a common cometary origin. Thus, either the considered NEAs are large sized splinters of the Adonis, or all five objects are fragments of a larger comet that was the parent body of the Capricornids meteoroid stream, and whose break-up occurred several tens of thousands years ago. The existence of such fragments of this family may be expected among the numerous new discovered asteroids. Note that the longitudes of perihelion of the NEAs 1995CS, 2008BO16, 2011EC41, and 2013CT36 orbits differ from the longitude of perihelion of the Adonis by no more

than on 5 deg., confirming the relationship between these objects and that they are moving inside the Capricornids meteoroid stream. At present the location of the 2008BO16 corresponds to the period of activity of the day-time meteor shower χ-Capricornids (January-February), and the asteroid was discovered exactly at that time. The date of the NEA 1995CS observations (February 1995) also corresponds to the period of activity of the day-time meteor shower χ-Capricornids.

Acknowledgements

We would like to acknowledge the useful comments of the referee.

References

Asher D.J., Clube S.V.M., Steel D.I., 1993, MNRAS, 264, 93
Babadzhanov P.B., 2001, A&A, 373, 329
Babadzhanov P.B., 2003, A&A, 397, 319
Babadzhanov P.B., Obrubov, Yu.V., 1992, Cel. Mech.& Dyn. Astron., 54, 111
Babadzhanov P.B., Williams I.P., Kokhirova G.I., 2008a, MNRAS, 386, 1436
Babadzhanov P.B., Williams I.P., Kokhirova G.I., 2008b, A&A, 479, 249
Babadzhanov P.B., Williams I.P., Kokhirova G.I., 2009, A&A,507, 1067
Babadzhanov P.B., Williams I.P., Kokhirova G.I., 2012, MNRAS, 420, 2546
Babadzhanov P.B., Williams I.P., Kokhirova G.I., 2013, A&A, 556, A25
Everhart E., 1974, Cel. Mech., 10, 35
Jenniskens P., 2006, Meteor showers and their parent comets, New-York: Cambridge Univ. Press, p. 790
Jewitt D.C. 1992, in Comets in the Post-Halley Era, eds. R.L. Newburn et al., Dordrecht, Kluwer, 19
Jewitt D.C., 2012, AJ, 143, 66
Jopek T.J. Williams I.P., 2013, MNRAS, 430, 2377
Kosai H., 1992,Cel. Mech. & Dyn. Astron., 54, 237
Kresak L., 1969, BAC, 20, 177
Kresak L., 1982, BAC, 33, 104
Madiedo J.M., et al., 2013, MNRAS, 431, 246
NEO Dynamic Site, 2013, April, `http://newton.dm.unipi.it/neodys`
Porubčan V., Kornoš L., Williams I.P., 2004, EM&P, 95, 697
Porubčan V., Kornošs L., Williams I.P., 2006, Contrib. Astron. Obs. Scalnate Pleso, 36, 103
Rudawska R., Vaubaillon J., Jenniskens P., 2012a, European Planetary Science Congress 2012, held 23-28 Sept., 2012 in Madrid, Spain, EPSC2012-886R
Rudawska R., Vaubaillon J., Jenniskens P., 2012b, Asteroids, Comets, Meteors 2012, Proceedings of the conference held May 16-20, 2012 in Niigata, Japan, LPI Contribution No. 1667, id. 6222
Sekanina Z., 1973, Icarus, 18, 253
Sekanina Z., 1976, Icarus, 27, 265
Tedesco E.F., Veeder G.J., Fowler J.W., Chillemi J.R., 1992, in The IRAS Minor Planet Survey. Final Report, Phillips Laboratory, Hanscom Air Force Base, MA, PL-TR-92-2049
Southworth R.B., Hawkins G.S., 1963, Smith. Cont. Aph. 7, 261

Meteoroids 2013, Proceedings of the Astronomical Conference,
held at A.M. University, Poznań, Poland, Aug. 26-30, 2013,
eds Jopek T.J., Rietmeijer F.J.M., Watanabe J., Williams I.P.,
Adam Mickiewicz University Press in Poznań, pp 205–212

60 years of modelling the Geminid meteoroid stream

Ryabova G.O.

Reasearch Intsitute of Applied Mathematics and Mechanics, Tomsk State University,
Russian Federation (ryabova@niipmm.tsu.ru)

Abstract. A brief historical review of the mathematical modelling of the Geminid meteoroid stream is given. The 'hollow stream' model by Jones (1985) and '4-showers' model by Babadzhanov and Obrubov (1986) were revised.

Keywords: meteoroids, mathematical modelling, Geminids

1. Introduction

The Geminid meteor shower is one of the most intense and most studied of the annual showers. The first registered appearance was in 1862 AD according to King (1926). The parent body of the Geminid stream is generally accepted to be the asteroid (3200) Phaethon, discovered as 1983TB. A concise review of the (3200) Phaethon – Geminid meteoroid stream complex origin can be found in (Ryabova, 2008). Among all meteoroid streams the Geminid stream seems to hold the lead in the amount of works devoted to mathematical modelling of either the stream as a whole or some of its structural features. Recently a review was given by Ryabova (2006), where the general principles of mathematical modelling were discussed, and in particular methods of calculating the stream's age and the ejection velocity, as well as the *status quo* in the Geminid, Perseid and Leonid streams modelling. But the objective of that work was not the historical review. However the history of the mathematical modelling of the Geminid stream is interesting and instructive.

It appears that the first work devoted to a simulation of the Geminids was that of Plavec (1950). He computed secular perturbations of the Geminid orbit to obtain the possible period of the shower visibility. This was the fist stage of modelling when a single orbit was calculated or integrated. Later general features of the Geminid stream structure were studied by integration of small numbers of meteoroid orbits and/or theoretical reasoning on this basis. Only several selected publications will be mentioned: Belkovich (1986), Gustafson (1989), Hughes and McBride (1989), Kramer and Shestaka (1992), Lebedinets (1985), Olsson-Steel (1987), Terent'eva and Bayuk (1991). Each of tens of named and unnamed works laid a stone into the wall of contemporary understanding of the stream structure and the process of its formation. Several of them have a special significance, namely works of Fox, Williams and Hughes (1982, 1983), Jones (1985), Jones and Hawkes (1986), Babadzhanov and Obrubov (1986), Williams and Wu (1993). We'll discuss strengths and weaknesses of these models and lessons learned from them.

The qualitative model of the Geminids by Ryabova (2007, 2008) which summarized results of 20-years efforts will also be discussed *very* briefly.

2. Fox, Williams & Hughes (1982, 1983)

A model developed in these works was based on really large numbers (500 000) of model meteoroids unlike earlier statistically pure models. It was assumed that all the orbital elements of all the ejected particles change exactly like those of the mean orbit of the stream. Certainly, it is not so, but as the first approximation the idea worked perfectly well. This idea and the other one – activity profile changes as function time and mass – were later developed by other researchers. As we know from observations the Geminid shower maximum does not changed its position with time. Fox, Williams and Hughes explained this phenomenon: the trajectory of the stream mean node motion matches the skew form of the dense central region of the stream, i.e. the small nodal regression is caused by a pure geometric factor.

3. Jones (1985)

The aim of the work in question was to study the scatter of meteoroid orbits caused by gravitational perturbations. The evolution of the orbits of 71 meteoroids was calculated over a period of 5000 yr into the future. Each of the test particles was launched on the mean Geminid orbit (Hughes, 1978) with standard Keplerian elements: $a = 1.35$ au, $e = 0.896$, $i = 23°.6$, $\Omega = 260°.3$, $\omega = 324°.8$, and the mean anomaly was assigned randomly. The numerical integration of the equations of the motion was carried out using a fourth- order Runge-Kutta technique. Only one perturbing planet (Jupiter) was taken into account. The author did not publish the initial time for the integration, or whether all the test-particles were launched from the mean orbit at the same time. The first is not important, because we are going to discuss only qualitative features of the model, and the second is obvious from the results.

According to the author, 'it had been expected that the result would have been a gradual diffusion-like expansion of the stream instead of Gaussian distributions the cross-sections were closed curves indicating that the orbits of the particles in the stream fall on the surface of a torus'. The computation time was several hundred hours, so the effect of the other planets on the stream structure was estimated on the basis of calculations for a single meteoroid. It was expected that 'Saturn will cause the thickness of the toroidal shell to increase to about 4 per cents of Jupiter-only radius of torus. Similarly, the effect of the other perturbations can also be included by convolution'. The passage of the Earth through the hollow stream should result in bimodal activity curve of the shower. Taking into account that Jones (1985) could not explain his results in due time, and according to our knowledge nobody did at a later date either, and that Jones' bimodal 'hollow stream' is still referred to (e.g. in Arlt and Rendtel (2006)), we decided to revise the model.

We calculated the evolution of the orbits of 71 meteoroids 1000 yr into future from the initial date 14.12.1985 (JD2446413.5) taken quite arbitrarily. The test meteoroids were distributed around the mean orbit (its orbital elements are given above) with 5 degree–step in the mean anomaly. For the numerical integration of the equations of motion the Everhart procedure 19th order with variable step size has been used. Planetary coordinates were taken from the JPL planetary Development Ephemeris – DE406. Now we are not as limited by computer power as 30 years ago, so we made 3 runs: with only one perturbing planet – Jupiter, with Jupiter and Saturn, and with 5 planets (Venus – Saturn). Each run takes about 40 min. The results are presented in Figure 1.

We can see that perturbations from the internal planets change the results dramatically. The reason is that Jupiter and Saturn are really 'outer' planets, enveloping the stream orbits. Venus, Earth and Mars intersect the stream, acting like a blender. So the 'hollow stream' is an artifact of the model.

4. Jones & Hawkes (1986)

While Fox, Williams and Hughes (1983) assumed that the orbital elements of the model meteoroids change in an identical way to the mean Geminid orbit, Jones and Hawkes (1986) estimated the mean rate of change of the angular Keplerian elements of particles as functions of their initial orbital energy and angular momentum. They supposed that the stream was generated 1000 years ago, and varying a and e and calculating the subsequent evolution of the test meteoroids as described by Jones (1985) found $\langle di/dt\rangle$, $\langle d\omega/dt\rangle$ and $\langle d\Omega/dt\rangle$. Combining this with the Whipple (1951) comet model, the authors calculated the activity of the meteor shower, duration of the shower and the motion of the descending node in the interval of 2000 years for meteoroids with mass 10^{-4} g. This work made the next step after the Fox, Williams and Hughes (1983) model, but still was a very preliminary model.

5. Babadzhanov and Obrubov (1986)

For the first time this model was presented in (Babadzhanov and Obrubov, 1986) and reproduced later in several papers (e.g. Babadzhanov and Obrubov, 1987, 1992). The authors estimated the stream age in 20 thousand years. Then using two motion integrals

$$(1 - e^2)\cos^2 i = \text{const}, \qquad e^2(2/5 - \sin^2 i \sin^2 \omega) = \text{const},$$

where the first follows from the Jacobi integral, and the second is the Lidov integral, and also assuming that $\Omega+\omega = \text{const}$, the authors obtained a complicated 3D-shape. Supposing that meteoroids should fill out this volume with time, a stream was obtained, which gives four showers observed on the Earth: the Geminids, Daytime Sextantids, Canisids and δ-Leonids. Now when computers are fast it is easy to revise the model. This revision has a pure cognitive purpose, because the age of

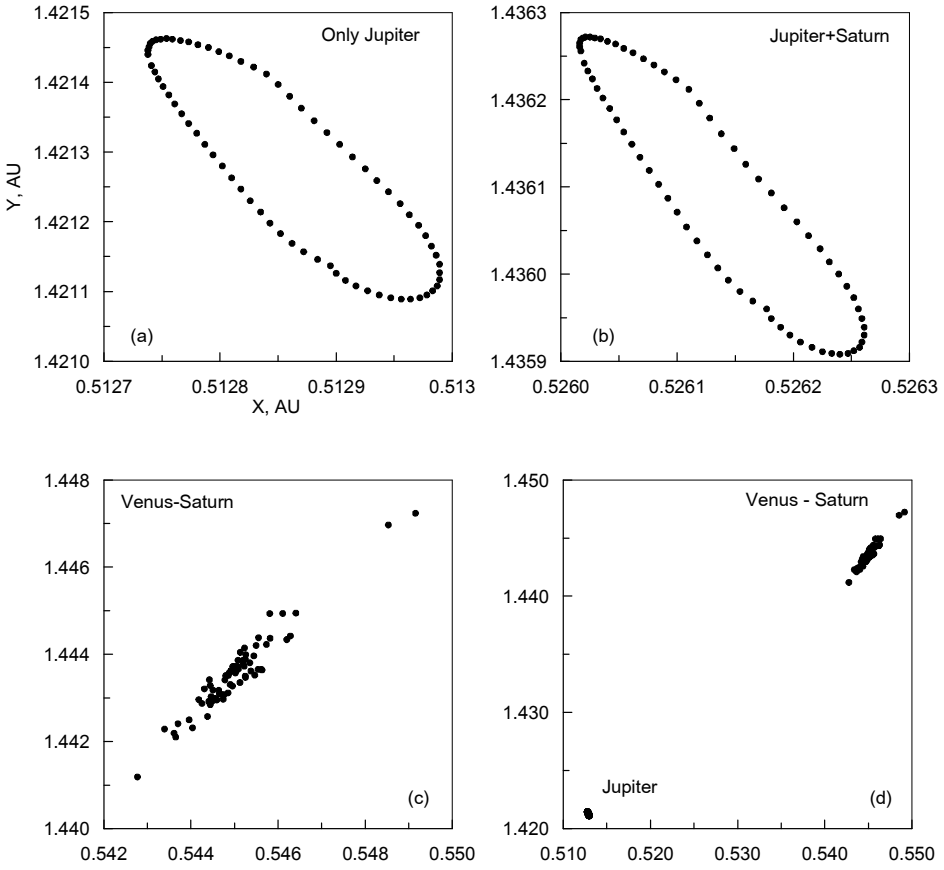

Figure 1. Cross-section of the sample of orbits in the ecliptic plane at the descending node after 1000 years of evolution. Perturbing planets in (a)–(c) are self-explaining. (d) nodes of two samples of orbits for comparison. The coordinate system is the standard heliocentric one.

the Geminid stream determined by several methods hardly exceeds 2–3 thousand years (Ryabova 1999).

The orbital elements for the parent asteroid were taken to be the same as in (Ryabova 2007; Table 1). The reference orbit (20 000 years ago) for the model was calculated using the Gauss-Halphen-Goryachev method (Sukhotin 1981), where gravitational perturbations from six planets (Venus–Saturn) were taken into account. This method allows for only secular perturbations of the first order, so the semi-major axis does not change during the integration. Our orbital elements for the reference orbit (J2000.0)

$a = 1.27134872000$ au, $e = 0.89687143487$, $i = 16°.11349382510$,
$\Omega = 129°.74953808873$, $\omega = 83°.79137861121$

are in agreement with the orbit, used in the Babadzhanov and Obrubov model (Obrubov 1993), reduced to J2000.0

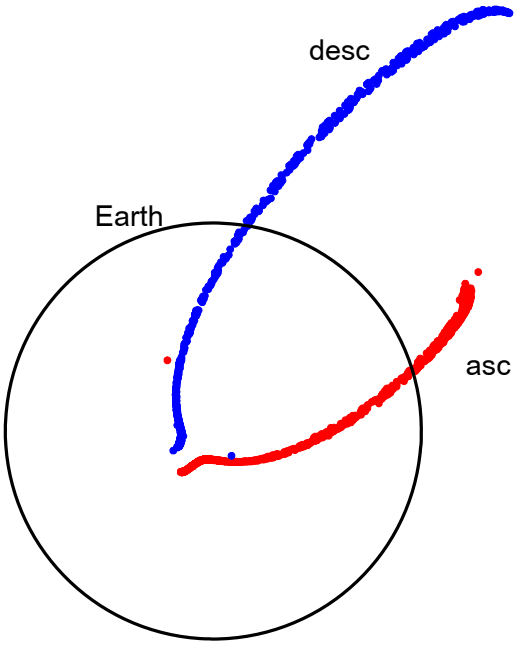

Figure 2. Geminid model cross-section in the ecliptic plane for 1000 orbits. Both descending and ascending nodes are shown.

$a = 1.2712$ au, $e = 0.898$, $i = 16°.7$, $\Omega = 100°.0$, $\omega = 112°.7$.

In fact, they are in the good agreement for a Gauss-type method, considering the integration interval (20 000 years) and the fact that Obrubov (1993) used an other initial orbit. We checked our Halphen-Goryachev integrator comparing the results of the Phaethon orbit integration with the results obtained by the Everhart procedure. They are in the excellent agreement (Ryabova 2007; Fig. 2).

Ejection of one thousand of meteoroids was simulated from perihelion of the reference orbit. The particles were ejected uniformly into the sphere with velocity 650 m s^{-1} (like in the Babadzhanov & Obrubov model). The equations of motion of these particles were integrated to present time (epoch JD2454300.5) using again Halphen-Goryachev method. In this run the Poynting-Robertson effect and radiation pressure were taken into account as well as gravitational perturbations. The key-parameter for the radiation perturbations is the ratio of the particle's cross-section to its mass, and we took the mass equal to 10^{-3} g, and the particle's radius equal to 0.089 cm. The resulting model stream (Figure 2) is very narrow (less than 2° in the solar longitude) and produces only two showers *none of them is the Geminids* (as well as Daytime Sextantids, Canisids or δ-Leonids). The first model shower meets the Earth on the solar longitude $L \approx 251°$, and the geocentric equatorial coordinates of its radiant are $\alpha \approx 196°$, $\delta \approx -2°$; for the second shower $L \approx 5°$, $\alpha \approx 305°$, $\delta \approx -13°$. For the Geminid shower $L \approx 263°$, $\alpha \approx 112°$, $\delta \approx 32°$.

6. Williams and Wu (1993)

This work considers numerical models of the Geminid stream. For each model 2000 meteoroids were ejected from the Phaethon orbit at three epochs AD 0, 500 and 1000. The evolution of 100 random test particles (sample I) for each model was calculated up to 1983 using the Runge-Kutta-Nystrom numerical integrator, including gravitational perturbations from Venus, Earth, Mars and Jupiter. The Poynting-Robertson and Yarkovsky-Radzievskii effects were ignored, but the effect of radiation pressure was included. The particle's size was taken typical for visual meteors. The rates of change of the orbital elements of 1900 residual particles (sample II) were calculated as weighted mean of the closest particles from the sample I (limitations of the computer power 20 years ago!). One more run was made for AD 0 and the smaller meteoroid size (typical for radar observations). The resulting cross-sections of the model stream and orbital distributions of the model showers were studied. The results obtained are close to the results obtained recently (see the next section) for 10 mln-particles models, but they were interpreted in a slightly different way – as a proof of the model stream matching the observed Geminid stream. Now we know that the small scatted in Ω was not caused by underestimation of the stream age. For the stream age of 10 000 years it is even smaller (Ryabova, 1999). We know also that there exists a systematic shift between the model and the real maximum of activity, and this has no relation to rms scatters.

One of the main results of this work is the visibility period for the Geminid shower. For the stream age of 2000 years, the shower could be observed from AD 1200. This result is worth revising considering new estimations of ejection velocities (Ryabova, 2013) and an improved orbit for Phaethon.

7. Ryabova (2007, 2008)

If the Geminid stream behaved like the Quadrantid stream or, say, the Orionid stream, where changes in the meteoroids' orbits are sharp, and close encounters with major planets are numerous, this model could not be developed in 1989 (the first published version). Fortunately the changes in the Geminid's orbital elements are so smooth that they may be approximated by polynomials. The method of nested polynomials was invented by Ryabova (1989), but the idea originates from Fox et al. (1983). This method is very fast and calculation of orbital evolution for 10 millions of orbits takes only several minutes on a usual desktop computer. The calculation time weakly depends on the time interval, so it is practically the same for 2 or 10 thousand of years.

In the first versions of the model some observed features of the Geminid shower were explained: the shape of the activity curve, the absence of the nodal shift with time. The main discovery was that the stream has two layers, and the shower peculiar bimodal shape conforms to cometary scenario of the stream origin. Later this model was applied to understand the whole of the stream structure: 3D-shape, density distribution within the stream, mass distribution, radiant structure etc. For example, several activity 'spots' in the radiant area, which some researchers

ascribed to microshowers of the unknown origin (see references in Ryabova (2008)) were explained.

This model has two serious discrepancies with the real stream. The first is that the location of the stream is not correct, and the second is that the width of the model shower is half that of the real shower. We had hopes that the shower width will increase, if a precise numerical method for calculation of orbital evolution will be used. Unfortunately, these hopes were not realized (a preliminary numerical model is under preparation for publication, some of its details were published by Williams and Ryabova (2011). We believe that the reason for the disagreement is the dramatic transformation of the Phaethon's orbit due to jet forces. It is hardly possible to calculate the initial body orbit, if it is the case.

8. Conclusions

The history of the Geminid stream modelling is long, but the peak of the most influential works was in the 1980s. I believe (this time I do not use an academic 'we' to stress my personal opinion) that 1980s models described above were very important and inspiring for meteoroid stream modelling specifically and for meteor astronomy in the gross regardless of their shortcomings.

The main lesson learned from revising the old models is the following: referring to 30-years old results one should be very careful.

Acknowledgements

This work was supported by the Ministry of Education and Science of the Russian Federation. This research has made use of SAO/NASA's Astrophysics Data System Service. The author thanks the Organizing Committee of Meteoroids 2013 conference for financial support.

References

Arlt R., Rendtel J., 2006, MNRAS, 367, 1721
Babadzhanov P.B. , Obrubov Yu.V., 1986, Dokl. AN SSSR, 290, 54 (in Russian)
Babadzhanov P.B. , Obrubov Yu.V., 1987, Handbook for MAP, 25, 2
Babadzhanov P.B. , Obrubov Yu.V., 1992, CeMDA, 54, 111
Belkovich O.I. , 1986, Astron. Vestn., 20, 142 (in Russian)
Fox K., Williams I.P., Hughes D.W., 1982, MNRAS, 200, 313
Fox K., Williams I.P., Hughes D.W., 1983, MNRAS, 205, 1155
Gustafson B.Å.S., 1989, A&A, 225, 533
Hughes D.W., 1978, in Cosmic Dust, ed. McDonnell J.A.M., John Wiley, New York, p. 123
Hughes D.W., McBride N., 1989, MNRAS, 240, 73
Jones J., 1985, MNRAS, 217, 523
Jones J., Hawkes R.L., 1986, MNRAS, 223, 479
King A., 1926, MNRAS, 86, 638
Kramer E.N., Shestaka I.S., 1992, Astron. Vestn., 26, 85 (in Russian)
Lebedinets V.N., 1985, Sol. Syst. Res., 19, 101
Obrubov Yu.V., 1993, Meteoroid streams' evolution, D.Sci. thesis, Dushanbe (in Russian)
Olsson-Steel D., 1987, MNRAS, 226, 1

Plavec M., 1950, Nature, 165, 362
Ryabova G.O., 1989, Sol. Syst. Res., 23, 158
Ryabova G.O., 1999, Sol. Syst. Res., 33, 224
Ryabova G.O., 2006, in Proc. of the IAUS 229, p. 229
Ryabova G.O., 2007, MNRAS, 375, 1371
Ryabova G.O., 2008, EPSC 2008, article id. 226
Ryabova G.O., 2008, EMP, 102, 95
Ryabova G.O., 2013, Sol. Syst. Res., 47, 219
Sukhotin A.A., 1981, Astron. Geod., Tomsk Gos Univ., Tomsk, 9, 67 (in Russian)
Terent'eva A.K., Bayuk O.A., 1991, Bull. Astron. Inst. Czechosl., 42, 377
Whipple F.L., 1951, ApJ, 113, 464
Williams I.P., Wu Z., 1993, MNRAS, 262, 231
Williams I.P., Ryabova G.O., 2011, MNRAS, 415, 3914

Meteoroids 2013, Proceedings of the Astronomical Conference,
held at A.M. University, Poznań, Poland, Aug. 26-30, 2013,
eds Jopek T.J., Rietmeijer F.J.M., Watanabe J., Williams I.P.,
Adam Mickiewicz University Press in Poznań, pp 213–216

Forecast of enhanced activity of eta-Aquariids in 2013

Sato M.[1], **Watanabe J.**[2]

(1) Kawasaki Municipal Science Museum, Japan (mail@kaicho.net),
(2) National Astronomical Observatory of Japan (jun.watanabe@nao.ac.jp)

Abstract. We tried to simulate distributions for Eta-Aquariids (ETA) of dust trails from 1P/Halley, we found out that some dust trails formed by meteoroids ejected in –1197 and –910 would approach the Earth in 2013. It means that the enhancement of eta-Aquariids would be expected. Actually, the enhanced activity of eta-Aquariids was observed in 2013. Its peak time corresponded with the time when the dust trails approached the Earth based on our simulation. Therefore, it was sure that the enhancement was caused by these dust trails.

Keywords: meteoroid stream, meteor showers, comet, orbits, evolution, radiants

1. Introduction

Eta-Aquariids (ETA) is one of the established meteor showers. The regular activity is middle level for meteor showers, its ZHR is about 50. The parent body is 1P/Halley which is the same as Orionids. The enhancement activities of Orionids were observed between 2006 and 2010, we explained that it was caused by the dust trail formed by meteoroids ejected in about 3000 years ago (Sato and Watanabe 2007).

We tried to simulate distributions for eta-Aquariids of dust trails from 1P/Halley by using the same method as Orionids. As a result, we found out that some trails would approach the Earth in 2013. Therefore, it was expected that eta-Aquariids would be enhanced in 2013.

2. Dust trail model

We applied the simplest approach of the dust trail model. Each trail was assumed to be formed by meteoroids ejected during the perihelion passage of the parent comet. The trail was calculated by test meteoroids ejected parallel to the comet motion, both ahead of and behind the comet. In some models the meteoroids ejection is assumed to the sunward (Ex. Ma, et al. 2002). However, we only considered the ejection along the path because the effect of the divergence of the orbits compared with the parent comet is larger than other assumption, which covers the case of sunward ejection. It is also noted that the ejected meteoroids perpendicular to the path move a heliocentric orbit that is indistinguishable from that of the comet. To calculate the perturbations, we included the three largest main-belt asteroids in addition to the eight planets, Pluto and the moon. We did not take the effect of radiation pressure on the meteoroids into account in our calculation. The orbital

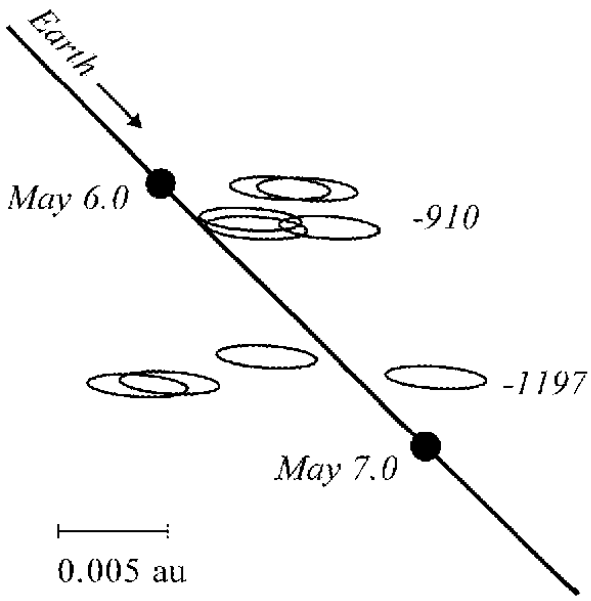

Figure 1. Distributions of dust trails in 2013. Two kinds of dust trails formed by meteoroids ejected in –1197 and –910 would approach the Earth in 2013.

elements of parent comet were those calculated by Yeomans and Kiang (1981). The calculated trails were those generated from –1403 (1404 BC).

3. Forecast from simulation

Figure 1 shows the distributions of dust trails of eta-Aquariids in 2013. Two kinds of trails (–1197 and –910 trails) would be expected to approach the Earth's orbit. These dust trails were complicated because of the perturbations. Table 1 shows the situation of the dust trails. It gives that the enhancement peak would be expected to occur between 5:00 and 22:00 on May 6. We announced this forecast based on our simulation to meteorobs mailing list (by IMO) and NMS mailing list (by Nippon Meteor Society in Japan).

4. Observation results

An enhanced activity of eta-Aquariids was actually observed in 2013. Figure 1 shows the results of visual observations by IMO (IMO 2013) and NMS (Uchiyama 2013). According to the summary by IMO, the peak was observed between about 2:00 and 18:00 on May 6, the ZHR reached about 130. The similar result was obtained by NMS, its peak time was recorded about 18:00 on May 6, the ZHR reached about 110.

Table 1. Data of main dust trails in 2013. The date is the time when the Earth passed the ascending node of the given trail particles. ΔR is the difference in heliocentric distance between the Earth and each trail in the ecliptic plane. The value of fM means the approximate degree of extension about dust trails.

Ejection Year	Expected peak time Date [UT]	Time [UT]	LS (2000)	Δ R [au]	Ejection Velocity [m/s]	fM	Radiant α [deg.]	Radiant δ [deg.]	Vg [km/s]	Orbital Period [yrs]
−910	2013 May 06.24	05:44	45.681	−0.0037	−2.36	0.038	337.78	−0.88	66.08	72.0
−910	2013 May 06.24	05:45	45.682	−0.0018	−2.12	0.095	337.77	−0.89	66.04	71.9
−910	2013 May 06.26	06:16	45.703	−0.0017	−2.05	0.038	337.78	−0.88	66.04	71.8
−910	2013 May 06.27	06:27	45.710	−0.0017	−2.11	0.017	337.79	−0.88	66.04	71.9
−910	2013 May 06.29	07:02	45.734	−0.0046	−2.50	0.11	337.82	−0.86	66.10	72.0
−910	2013 May 06.40	09:42	45.841	−0.0041	−2.29	0.035	337.88	−0.83	66.10	71.9
−1197	2013 May 06.53	12:37	45.959	+0.0021	+3.44	0.013	337.89	−0.80	65.99	71.7
−1197	2013 May 06.89	21:19	46.310	−0.0026	+3.43	0.012	338.14	−0.67	66.12	71.7

Molau (2013) reported that this year the peak of IMO Video Meteor Network is by a factor of two to three higher than in the previous years. Its peak of flux density observed about May 6.

Each peak time was consistent with the expected time based on our simulation. It was sure that such enhancement of eta-Aquariids was caused by approach of dust trails obtained by our simulation.

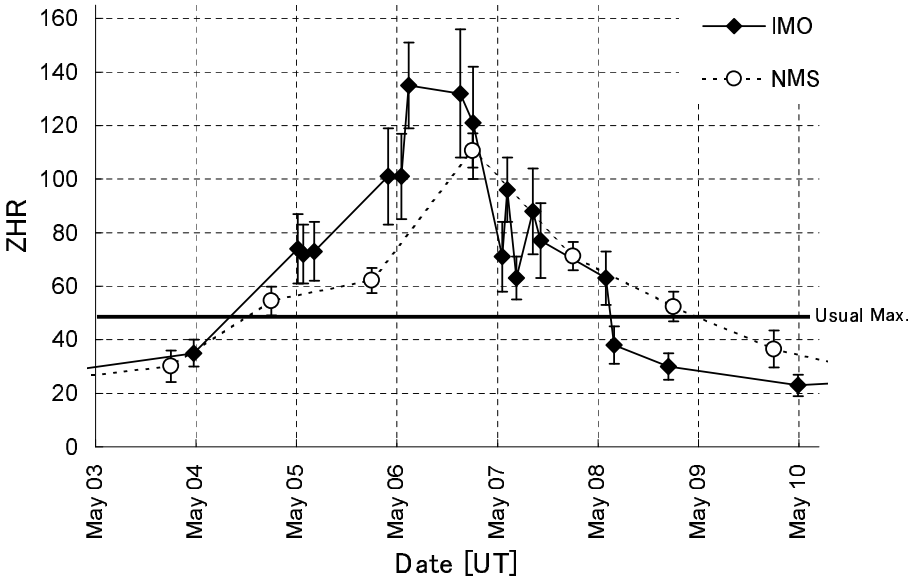

Figure 2. Results of visual observations. Black square with a solid line means data by IMO (IMO 2013) and white circle with a dotted line means data by NMS (Uchiyama 2013).

References

IMO 2013, May, http://www.imo.net/live/eta-aquariids2013/
Ma Y., Williams I.P. Chen, W., 2002, MNRAS 337, 1081
Molau S., 2013, May, http://www.imonet.org/reports/201305.pdf
Sato M., Watanabe J., 2007, Publ. of the Astron. Soc. of Japan 59, No.4, L21
Uchiyama S., 2013, May, http://homepage2.nifty.com/s-uchiyama/meteor/shwr-act/05etaact/eta-act.html
Yeomans D.K., Kiang T., 1981, MNRAS 197, 633

Meteoroids 2013, Proceedings of the Astronomical Conference, held at A.M. University, Poznań, Poland, Aug. 26-30, 2013, eds Jopek T.J., Rietmeijer F.J.M., Watanabe J., Williams I.P., Adam Mickiewicz University Press in Poznań, pp 217–224

New meteor showers identified in the CAMS and SonotaCo meteoroid orbit surveys

Rudawska R.[1], **Jenniskens P.**[2]

[1]Institut de Mécanique Céleste et de Calcul des Éphémérides, 77 Avenue Denfert-Rochereau, 75014 Paris, France (rudawska@amu.edu.pl)
[2]SETI Institute, 189 Bernardo Ave, Mountain View, CA 94043, USA

Abstract. A cluster analysis was applied to the combined meteoroid orbit database derived from low-light level video observations by the SonotaCo consortium in Japan (64,650 meteors observed between 2007 and 2009) and by the Cameras for All-sky Meteor Surveillance (CAMS) project in California, during its first year of operation (40,744 meteors from Oct. 21, 2010 to Dec. 31, 2011). The objective was to identify known and potentially new meteoroid streams and identify their parent bodies. The database was examined by a single-linking algorithm using the Southworth and Hawkins D-criterion to identify similar orbits, with a low criterion threshold of $D < 0.05$. A minimum member threshold of 6 produced a total of 88 meteoroid streams. 43 are established streams and 45 are newly identified streams. The newly identified streams were included as numbers 448-502 in the IAU Meteor Shower Working List. Potential parent bodies are proposed.

Keywords: meteoroid stream, meteor shower, comets, asteroids

1. Introduction

Ongoing meteoroid orbit surveys aim to identify as many as possible meteoroid streams. Each stream originated from a parent comet or asteroid. By integrating the parent body orbit back in time, dust can be generated at different epochs and then followed forward to its orbital evolution into an Earth intersecting stream at the present time to confirm the association. Each conclusive link provides a record of the parent body past activity and a 3-dimensional distribution of the dust in the inner solar system now and into the future (Jenniskens 2006).

In recent years, networks of low-light-level video cameras have contributed many new meteoroid orbits, complimenting radar studies such as results from the Canadian Meteor Orbit Radar (Brown et al. 2010). The most productive camera network has been that of the Japanese SonotaCo consortium (SonotaCo 2009). Meteoroid stream searches in Europe have been mostly focused on single-station observations (e.g. the International Meteor Organization Video Meteor Database), but multi-station results are now being gathered by the European Video Meteor Network Database (Kornos et al. 2013).

In California, the Cameras for All-sky Meteor Surveillance (CAMS) network started operations in October of 2010. At the end of 2011, 40,744 meteoroid orbits were calculated. The work presented here was our first attempt to confirm some of the previously reported showers listed in the IAU Working List of Meteor

Showers (Jopek & Jenniskens 2011), and to find potential new meteoroid streams. We did so by combining the CAMS data with those released by the SonotaCo consortium.

2. Methods

The 60-camera CAMS network consists of three stations of 20 low-light-level video cameras each, located at Fremont Peak Observatory, at Lick Observatory, and in Sunnyvale (or alternatively in Mountain View or Lodi) in California. The three stations used Watec Wat-902H2 Ultimate cameras equipped with f1.2 12 mm focal length lenses. The video is stored in four-frame compressed format and analyzed using the CAMS software package (Jenniskens et al. 2011). The CAMS system provides data with astrometric precision about 1.4' O-C (2.8' per pixel).

The 100-camera SonotaCo network consists of more than 30 stations, which use both WATEC-100N and WATEC-902H2 cameras equipped with 3.8–12 mm lenses (SonotaCo 2009). Data are recorded and analyzed by the UFO software package. The precision of the measured radiant positions is about a factor of two less precise than the CAMS network (Jenniskens et al. 2011). At the time of this work, in early 2012, the 2007 – 2009 meteoroid orbits were made publicly available (64,650 meteors).

3. Meteor showers identification

The combined database contains 105,394 meteoroid orbits. This meteor database was examined using a single-linking orbit grouping method by means of the Southworth and Hawkins criterion (Southworth & Hawkins 1963) to identify similar orbits.

In a first step, the IAU List of Established Meteor Showers was used to identify known meteor showers in the combined database. For each stream identified in this step the mean orbit was calculated and stream members identified. To obtain the mean parameters we calculated the angular elements as normalized sin and cos, the mean radiant position was averaged as a vector, while the rest of the parameters as arithmetic mean. Those orbits which were not identified in the first step were used in the subsequent group-search using the single-linking method. Our grouping algorithm (Rudawska et al. 2012) is based on the single linkage, or nearest neighbour, method proposed by Southworth and Hawkins (1963). In addition, they introduced the distance function, D_{SH}, which now is the most often used criterion to identify what orbits are similar and may be linked.

Two orbits are thought associated if D is less than an assumed constant threshold, sometimes taken as $D < 0.25$ (Lindblad 1971). In the first step, in which the major showers were identified, we used a threshold of 0.10. In the subsequent grouping algorithm, we used a low value of 0.05. Hence, only the most identical orbit groupings were extracted from the surveys. For our preliminary parent body search, we used a higher threshold of 0.20.

4. Results

The results for all clusters with at least 6 members (again, for threshold $D < 0.05$), excluding previously identified meteoroid streams, are summarized in Table 1. The table shows the mean orbital elements and the mean radiant of each new meteoroid stream. The first two columns give the assigned IAU number and code of the stream. The next five columns show the mean orbital elements: eccentricity (e), perihelion distance (q), inclination (i), argument of perihelion (ω), and longitude of ascending node (Ω), respectively. The following four columns include the solar longitude, the right ascension and declination of the radiant, and the geocentric velocity. The twelfth column shows the number of identified meteors in each stream. The final column gives the name of the shower.

In the period between April and June we found 11 new meteoroid streams (Figure 1). In the period between April 22 and May 6, we identified the Camelopardalids shower (#451), which may originate from comet 209P/LINEAR (formerly known as 2004 CB). This comet has a close encounter with Earth during May 2014, when Earth will cross potential dust trails from past returns. The shower provides some evidence that this weakly active comet produced large dust grains in the past. The predicted radiant of the possible outburst meteors in 2014 is at R.A.=125, Decl.=+78, and entry speed is 15.9 km/s (Jenniskens 2006). The observed radiant is at R.A.=172.6, Decl.=+83.7 with entry speed of 14.7 km/s (Table 1).

From April to June, we found 11 new meteoroid streams (Figure 1). Meteoroid orbits of the April ϵ Delphinids (#450) and the June ϵ Cygnids (#458) are retrograde with unknown long-period comet parent bodies. These are compact showers.

The low velocity θ Virginids (#452) may originate from 2011 HP4. The May μ Leonids (#453) may derive from either 2009 EF21 or 2008 EH. The May ϕ Virginids may originate from 2005 JU1. The May ψ Scorpiids (#456) are a good match to the present orbit of 2009 KM. The May δ Leonids may originate from asteroid 2013 KB.

The May α Comae Berenicids (#455) move in an orbit roughly aligned with that of comet 73P/Schwassmann-Wachmann 3. The showers #459 (June ϵ Ophiuchids) and #460 (λ Ophiuchids) may be the same shower, perhaps from Jupiter-family comet P/2005 JQ5 (Catalina), with $D_{SH} \approx 0.06$. Shower 459 is the more certain one.

Between July and September we found 12 meteor showers. Compared to the spring meteor showers, these showers have a smaller number of members. With one exception, the August ν Aquariids (#467), which includes 13 meteoroid orbits that cover a period between August 8 and 16. These may originate from comet 72P/Denning-Fujikawa.

The July ρ Herculids (#463) are perhaps from asteroid 2011 MC. The retrograde August ξ Cassiopeiids (#465) may originate from a Halley-type comet. There is no candidate parent body. The September ρ Pegasids (#477) could derived from either asteroids 2011 EU29, 2004 NL8, or 2009 DA1. The September o Orionids may originate from comet P/2005 T4 (SWAN).

The autumn showers (Figure 2) extractions include the ι Aquariids (#484), with 176 meteors an unusually large group and possibly composed of multiple streams.

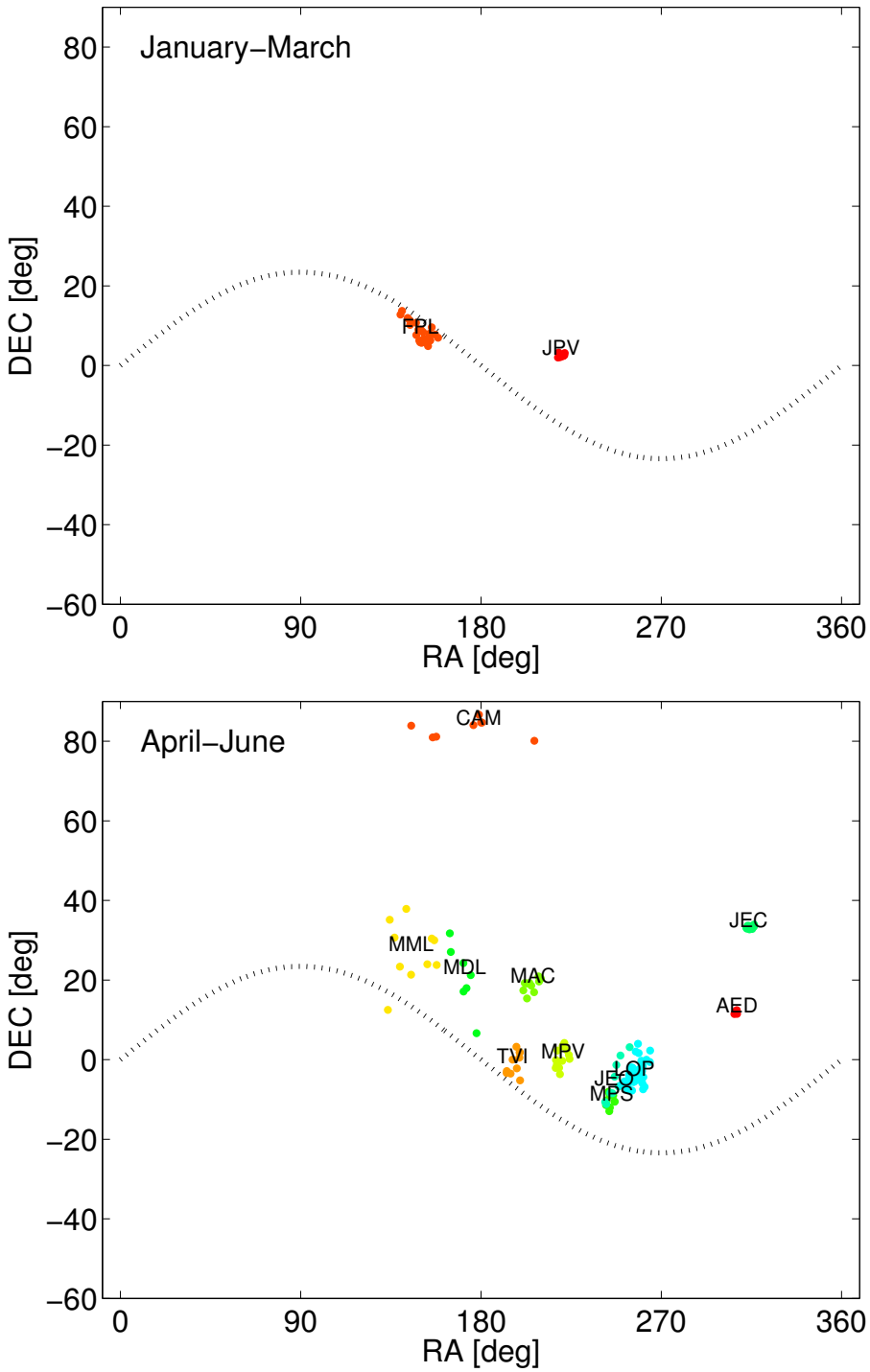

Figure 1. The radiant position of meteor showers found between January and June. The dashed line is the ecliptic plane.

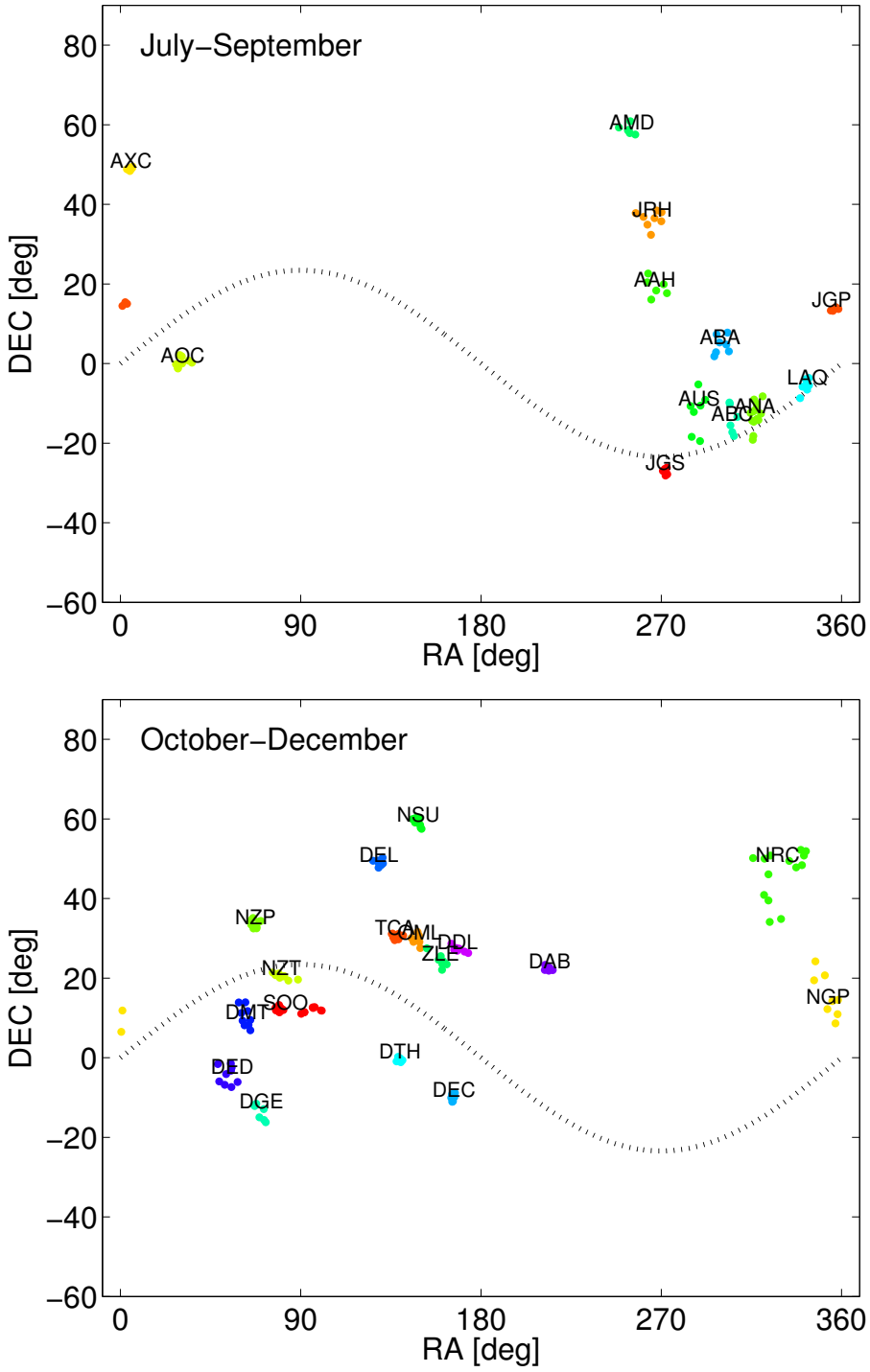

Figure 2. The radiant position of meteor showers found between July and December. The dashed line represents ecliptic plane.

Table 1. Mean orbital elements and radiant position of the newly identified meteoroid streams. Shower 462=175 and shower 499 is part of 20.

IAU	Code	e	q	i	ω	Ω	$\lambda_\odot$	α	δ	V_g	No	Name
*448	AAL	0.969	0.070	9.2	332.8	13.6	13.6	219.7	–12.9	40.7	6	Apr. α Librids
449	ABS	0.605	0.899	1.5	16.1	187.5	13.6	164.9	+4.4	12.3	7	Apr. β Sextantids
*450	AED	0.997	0.745	122.3	119.1	20.1	20.2	307.2	+11.8	61.5	6	Apr. ϵ Delphinids
*451	CAM	0.619	0.998	20.7	168.1	39.1	39.1	172.6	+83.7	14.7	8	Camelopardalids
*452	TVI	0.683	0.856	2.4	230.5	39.6	39.5	196.9	–1.0	14.9	10	θ Virginids
*453	MML	0.545	1.004	2.8	183.0	31.1	40.3	145.5	+27.2	7.7	10	May μ Leonids
*454	MPV	0.744	0.652	10.4	259.7	41.6	41.6	220.2	+0.3	21.7	12	May ϕ Virginids
*455	MAC	0.612	0.902	10.0	223.4	42.8	42.8	205.2	+18.7	13.7	10	May α C. Berenicids
*456	MPS	0.805	0.522	9.4	275.5	61.5	61.5	244.5	–10.6	25.4	10	May ψ Scorpiids
*457	MDL	0.488	1.003	3.1	189.1	54.2	54.1	171.2	+20.9	7.4	7	May δ Leonids
*458	JEC	0.997	0.914	95.6	216.8	82.3	82.3	314.3	+33.2	53.2	9	June ϵ Cygnids
*459	JEO	0.656	0.833	7.3	236.8	84.1	84.1	246.9	–5.2	15.6	9	June ϵ Ophiuchids
460	LOP	0.742	0.741	11.1	248.2	84.5	84.5	257.2	–3.7	19.7	37	λ Ophiuchids
461	JGS	0.692	0.796	1.8	61.8	288.8	108.9	272.1	–27.1	16.3	7	July δ Sagittariids
462	JGP	0.904	0.524	150.0	273.8	120.8	120.8	358.6	+14.2	62.6	8	July δ Pegasids
*463	JRH	0.633	0.981	21.3	203.8	124.6	124.6	265.1	+36.4	15.6	8	July ρ Herculids
464	KLY	0.698	0.939	24.7	215.1	126.8	126.9	277.5	+33.3	18.6	6	κ Lyrids
*465	AXC	0.887	0.907	104.9	219.1	135.8	135.8	4.9	+48.9	55.5	9	Aug. ξ Cassiopeiids
466	AOC	1.016	0.724	157.9	64.2	318.5	138.5	30.7	+0.3	67.5	8	Aug. o Cetids
*467	ANA	0.781	0.618	2.6	223.3	154.0	139.4	317.1	–13.1	21.8	13	Aug. ν Aquariids
468	AAH	0.598	0.987	11.9	200.6	142.1	142.1	267.2	+19.2	11.2	6	Aug. α Herculids
469	AUS	0.601	0.930	3.0	217.8	145.1	145.1	287.9	–12.2	11.1	7	Aug. υ Sagittariids
*470	AMD	0.654	1.011	30.3	177.2	145.4	145.4	253.7	+58.8	19.5	6	Aug. μ Draconids
471	ABC	0.638	0.846	2.1	234.5	146.5	146.4	305.4	–14.1	13.9	6	Aug. β Capricornids
472	ATA	0.648	0.790	7.4	243.5	147.3	147.3	310.6	–1.8	15.9	7	Aug. θ Aquilids
473	LAQ	0.877	0.297	2.6	300.3	148.0	147.6	342.3	–5.5	30.6	9	λ Aquariids
474	ABA	0.701	0.872	10.2	228.1	148.7	148.7	300.0	+4.7	15.1	7	Aug. β Aquariids
475	SAQ	0.709	0.723	1.3	215.1	165.6	158.1	329.2	–11.0	17.9	10	Sept. Aquariids
476	ICE	0.832	0.421	3.4	134.0	357.2	176.1	4.8	–1.4	26.9	8	ι Cetids
*477	SRP	0.723	0.726	6.1	249.8	177.4	177.4	343.4	+5.0	18.3	7	Sept. ρ Pegasids
478	STC	0.606	0.938	1.7	185.7	174.6	177.7	316.0	–14.1	10.3	13	Sept. θ Capricornids
*479	SOO	0.928	0.774	159.3	58.1	5.6	185.6	79.2	+12.1	67.6	18	Sept. o Orionids
*480	TCA	0.822	0.845	154.8	131.8	207.3	207.3	137.5	+30.5	67.2	8	τ Cancrids
*481	OML	0.819	0.889	151.5	140.3	218.6	218.6	148.0	+29.7	67.3	7	Oct. μ Leonids
*482	NGP	0.705	0.938	4.4	207.7	228.4	228.4	354.9	+14.4	11.4	10	Nov. γ Pegasids
483	NAS	1.103	0.898	154.2	325.5	51.4	231.4	149.9	–3.4	71.1	8	Nov. α Sextantids
484	IOA	0.652	0.836	3.4	193.7	200.4	234.7	27.6	+17.3	13.8	176	ι Arietids
*485	NZT	0.926	0.172	5.5	135.9	60.0	240.0	81.0	+20.5	35.5	8	Nov. ζ Taurids
*486	NZP	0.859	0.389	13.3	288.2	240.4	240.4	67.3	+33.6	29.4	9	Nov. ζ Perseids
487	NRC	0.616	0.982	14.4	189.1	241.4	241.4	323.2	+43.4	11.8	14	Nov. ρ Cygnids
*488	NSU	0.972	0.813	99.9	230.0	241.6	241.6	148.3	+59.2	55.3	10	Nov. σ U. Majorids
489	ZLE	1.344	0.953	155.3	200.0	248.6	248.6	159.6	+24.4	74.0	7	ζ Leonids
*490	DGE	0.818	0.716	23.5	66.8	69.3	249.3	69.5	–13.6	23.8	7	Dec. δ Eridanids
491	DCC	0.942	0.387	167.8	104.9	69.5	249.5	131.7	+12.8	64.1	6	Dec. δ Cancrids
492	DTH	0.967	0.695	149.6	66.3	71.9	251.9	139.2	–0.4	67.1	6	Dec. θ Hydrids
493	DEC	1.016	0.925	154.3	331.4	71.9	251.9	166.0	–10.0	70.6	6	Dec. ϵ Craterids
*494	DEL	0.947	0.365	94.0	287.2	253.1	253.1	129.2	+49.1	51.7	8	Dec. Lyncids
495	DMT	0.609	0.831	4.1	53.6	82.1	262.1	62.4	+10.3	13.5	9	Dec. μ Taurids
496	DED	0.633	0.903	7.4	38.0	82.6	262.6	53.6	–4.4	12.2	9	Dec. ϵ Eridanids
*497	DAB	1.002	0.686	112.3	113.3	263.9	263.9	213.5	+22.3	59.5	7	Dec. α Bootids
*498	DMH	0.983	0.930	123.5	27.2	84.8	264.8	152.7	–23.8	63.8	7	Dec. μ Hydrids
499	DDL	1.152	0.611	137.3	253.0	275.9	275.9	168.8	+27.2	67.0	8	Dec. δ Leonids
*500	JPV	0.950	0.669	145.3	110.3	285.6	285.6	220.3	+2.5	66.2	7	Jan. ϕ Virginids
501	FPL	0.829	0.388	4.1	110.0	137.3	317.3	147.8	+9.0	28.3	14	Feb. π Leonids
*502	DRV	0.923	0.777	153.9	124.0	252.5	252.5	185.1	+12.9	68.1	19	Dec. ρ Virginids

Others are more typical. A few are highly inclined streams with retrograde orbits such as the December Lyncids (#494). None have candidate parent bodies. The November γ Pegasids (#482) are possibly related to asteroids 2010 UM7,

2012 UU169, or 2007 PA8, all potentially dormant Jupiter Family comets. The Tisserand parameter for 2007 PA8 is 2.95 and for 2010 UM7 is 2.94, respectively. Moreover, the 2007 PA8 diameter is around 5 km in diameter (applying relationship between absolute magnitude and diameter given by Pravec & Harris (2007). It would be interesting to study this object in reference to its possible past activity that may have supplied this meteoroid stream.

In January, we found the January ϕ Virginids (#500), which is represented mostly by SonotaCo meteor orbits due to lack of CAMS observations at this time. The shower is active from January 3 till 7, peaking at solar longitude 285.6 degrees.

5. Discussion

Because the CAMS survey is ongoing, these are preliminary results. In preparation of publication, these detections were reported to the IAU Meteor Data Center. To be more certain that these single-linking D-criterion extractions represented true meteoroid streams, we aimed to collect sufficient data within the CAMS network alone to confirm the detections. By the end of 2012, a total of 101,000 meteoroid orbits were measured by CAMS alone and the streams were again investigated, case by case. This work is the topic of a future publication.

In total, 29 out of the 48 candidate showers in Table 1 were confirmed. These are marked with a star in the first column of Table 1. In addition, we found that two of the newly identified streams are likely part of now established showers: shower 462=175 and shower 499 is part of 20.

A total of 21 showers were not detected in the CAMS data collected so far (those without a star in Table 1). Based in part on SonotaCo data, it is possible that some of these showers were active only at some time in the period 2007-2009, before CAMS operations were started, or that they peak at solar longitudes not yet covered in the current CAMS observations due to bad weather on those days.

Alternatively, it is possible that, in spite of the low D threshold value used in this study, the remainder are mere chance associations of unrelated orbits. Single-linking of related orbits alone does not guarantee association.

More meteoroid streams may exist in the data. The discriminant criterion, used at this low threshold value, does not select streams dispersed significantly in longitude of perihelion, for example.

6. Conclusions

The Cameras for All-sky Meteor Surveillance (CAMS) and SonotaCo Network Japan meteor databases were examined by single-linking algorithm combined with Southworth and Hawkins D-criterion. A total of 88 meteor meteoroid streams were found, 43 of which were known established showers, two others have since been established. A significant fraction of the remainder (at least 29 out of 46) are newly recognized meteoroid streams. Potential parent bodies are proposed.

Acknowledgements

We thank Quentin Nenon (SETI Institute) for support of the stream verifications from the more recent CAMS data, and Jeremie Vaubaillon (IMCCE) for providing a postdoctoral position to RR and for facilitating a working visit by PJ to IMCCE. CAMS is supported by the NASA Near Earth Object Observation program.

References

Brown P., Wong D. K., Weryk R. J., Wiegert P., 2010, Icarus, 207, 66

Jenniskens P., 2006, Meteor Showers and their Parent Comets. Cambridge University Press

Jenniskens P., Gural P. S., Dynneson L., Grigsby B. J., Newman K. E., Borden M., Koop M., Holman D., 2011, Icarus, 216, 40

Jopek T. J., Jenniskens P. M., 2011, in Cooke W. J., Moser D. E., Hardin B. F., Janches D., eds, Proc. Meteoroids 2010 Conf., held in Breckenridge, Colorado USA, May 24-28, 2010, NASA/CP-2011-216469. p. 7

Kornos L., Koukal J., Piffl R., Toth J., 2013, in Gyssens M., Roggemans P., eds, Proc. of the Inter. Meteor Conf., 31st IMC, La Palma, Canary Islands, Spain, 2012, pp 21–25

Lindblad B. A., 1971, Smithsonian Contributions to Astrophysics, 12, 14

Pravec P., Harris A. W., 2007, Icarus, 190, 250

Rudawska R., Vaubaillon J., Atreya P., 2012, A&A, 541, A2

SonotaCo 2009, WGN, Journal of the International Meteor Organization, 37, 55

Southworth R. B., Hawkins G. S., 1963, Smithsonian Contributions to Astrophysics, 7, 261

Meteoroids 2013, Proceedings of the Astronomical Conference,
held at A.M. University, Poznań, Poland, Aug. 26-30, 2013,
eds Jopek T.J., Rietmeijer F.J.M., Watanabe J., Williams I.P.,
Adam Mickiewicz University Press in Poznań, pp 225–233

Confirmation and characterization of IAU temporary meteor showers in EDMOND database

Kornoš L.[1], Matlovič P.[1], Rudawska R.[1], Tóth J.[1], Hajduková M. Jr.[2], Koukal J.[3], Piffl R.[3]

[1]Faculty of Mathematics, Physics and Informatics, Comenius University in Bratislava, Slovak Republic (kornos@fmph.uniba.sk)
[2]Astronomical Institute of the Slovak Academy of Sciences, Bratislava, Slovak Republic
[3]CEMeNt – Central European Meteor Network

Abstract. The European viDeo MeteOr Network Database (EDMOND) is a database of video meteor orbits resulting from cooperation and data sharing among several European national networks and the International Meteor Organization Video Meteor Network, IMO VMN, (Kornoš et al. 2013b). At present, the 4th version of the EDMOND database, which contains 83 369 video meteor orbits, has been released.

The first results of the database analysis, in which we studied minor streams, are presented. Using the radiant-geocentric velocity method we identified 267 meteor showers, among them 67 established showers and 200 from the working list of the IAU MDC. Making a more detailed examination, we clearly identified 22 showers of 65 *pro tempore* showers of the working list of the IAU MDC (updated in August 2013). The identification of 18 meteor showers was questionable, while 25 showers were not found. For all the identified temporary meteor showers, we list the weighted mean orbital elements, the radiant position and the geocentric velocity.

Keywords: meteor showers, meteor orbital databases, cluster analysis

1. Introduction

The rapid development of video techniques in recent years has resulted in the massive use of video cameras in meteor observations. The number of new meteor networks has increased, and the efficiency of those already existing has improved. In three years, the Japanese meteor network database, containing around 30 low-light level camera observations, grew to 65 000 orbits (SonotaCo 2009); SonotaCo et al. (2010). The recently established system CAMS (Cameras for Allsky Meteor Surveillance) in the United States obtained 47 000 orbits of meteors just in the first year of its operation (Jenniskens et al. 2011). In Europe, between 2000 and 2013, the IMO Video Meteor Network collected over 1.2 million single-station meteors (Molau 2014). Also, in Europe, the continuous monitoring of meteors and fireballs is conducted by the 25 stations the Spanish Meteor and Fireball Network (SPMN; Pujols et al. (2013), which has been working now for 5 years. While till mid-2011, NASA's All-Sky Fireball network, established in 2008, with its 6 video cameras, detected 1796 multi-station meteors (Cooke and Moser 2012). Another good example of well developed regional networks are the Canadian Automated Meteor Obser-

vatory (CAMO), (Brown et al. 2010) and the Croatian Meteor Network (CMN), (Andreić and Šegon 2010).

Thanks to the broad international cooperation of video meteor observers from several European countries, a multi-national network EDMONd (European viDeo-Meteor Observation Network) was created. As a result of its work, the first version of the EDMOND database, containing data from the years 2009, 2010, 2011 and half of 2012, was presented at the IMC conference in La Palma, Spain in 2012 (Kornoš et al. 2013a). In the last year, observers affiliated to the International Meteor Organization Video Meteor Network (IMO VMN) have started to share their data, whereas the data of EDMONd and IMO VMN have been merged. Nowadays, the data is collected from observers from a substantial part of Europe and, due to this international cooperation, meteor activity is monitored over almost the entire Europe. In effect, the database has accumulated 1 639 358 records of single-station meteors between 2000 and 2013 (EDMONd – 447 266 and IMO VMN – 1 192 092).

2. EDMOND database

The computation of meteor orbits is performed by the UFOOrbit software (SonotaCo 2009). As the single-station video data are obtained and reduced using two different tools, the MetRec (Molau 1999) and UFOAnalyzer tools (SonotaCo 2009), the UFO data can be used without any changes. However, the data obtained by the MetRec software has to be first converted into the UFO format using the program INF2MCSV written by SonotaCo. The present database contains about 72 % of MetRec data. As the conversion is not fully compatible, the computation of orbits is performed in two steps. First, preliminary orbits are computed using UFOOrbit with basic parameter settings Q_o and $dt = 5$ sec (which means that all combinations of single-station meteors within 5 second intervals are computed), and with additional settings: beginning and terminal heights have to be $H_{1,2} \in (15; 200)$ km, the empirically derived quality parameter $QA > 0.3$, and the largest difference in velocity among considered stations in the orbit computation is $dV < 7$ km/s.

After that, to reject the less precise orbits and false orbits, another filter of parameters is applied: the angle of observed trajectory has to be $Q_o > 1$ deg, the duration of the meteor $dur > 0.1$ sec, the convergence angle $Q_c > 10$ deg, the difference between the two poles of ground trajectory $dGP < 0.5$ deg, and the difference in velocity between unified velocity and velocity from one of the stations $dv12\% < 7.07\,\%$. In comparison to the previous versions of the database, the most important modification is the restriction of the difference in velocities for stations used in meteor orbit computation. The definition of all parameters is in the UFO Manual. More details can be found in (Kornoš et al. 2013b).

At present, the 4th version of the EDMOND database containing 83 369 video meteor orbits, has been released. Most of them ($\sim 84\%$) are double-stations orbits. About 48 800 orbits belong to the sporadic background and 34 500 are shower meteors (59 % and 41 %, respectively).

The EDMOND database was examined in several tests and compared with other meteor orbits databases. The examination allowed us to demonstrate the characteristic features of the EDMOND, which are particularly important for future analyses based on the data.

The derivation of orbital elements, which define the shape of the orbit, is highly dependent on the uncertainty of the determination of the meteor velocity. One of the parameters used in the data reduction is dv12% (the difference in the velocities, given in percentage). The geocentric velocity is the decisive parameter in the calculation of the orbit. Thus, the dv12% parameter is an important indicator of its accuracy. The smaller the difference between velocities from different stations, the more accurate the orbit determination is. Therefore, in the distribution of dv12%, a decrease in the number of orbits with increasing values of dv12% should be the most rapid. The comparison of the distribution of dv12% parameter of the EDMOND (Kornoš et al. 2013a) and SonotaCo catalogue showed similar decrease; with a slightly slower one in the EDMOND.

The distributions of orbital parameters within several meteoroid streams from EDMOND were also analysed. In Kornoš et al. (2013a), the dispersions of orbital elements of the Lyrids from EDMOND were studied. Comparing them with the SonotaCo video orbits, the consistency of both datasets was demonstrated. Moreover, if we compare both sets of video data (Figure 1), the dispersions in $1/a$ of the meteor orbits within individual streams obtained from the EDMOND data are about 1.3 times larger than the values from the SonotaCo catalogue. Figure 1 shows the observed differences in the semi-major axes within the meteor streams compared with the orbital deviations in the streams determined from different datasets. The median semimajor axes of video meteor orbits in both the EDMOND and SonotaCo data are systematically biased, probably as a consequence of the method used to determine the orbits. In comparison with the IAU MDC photographic database (Lindblad et al. 2005), they are shifted towards the short-period side; the velocities determined in the video data are slightly underestimated.

An important indicator of the quality of data is the relative number of hyperbolic orbits, because the probability of registering real hyperbolic orbits is very small (Hajduková et al. 2014a). The apparent hyperbolicity of the orbits is, generally, caused by a high spread in velocity determination, shifting a part of the data through the parabolic limit. This, however, does not explicitly mean large measurement errors. Of the 83 369 meteor orbits collected in the EDMOND, 5.7% are determined as hyperbolic. This percentage is roughly comparable to that in the SonotaCo database. Initially, the proportion of hyperbolic meteors in the latter was 11.58%, but after the selection of quality orbits (Vereš and Tóth 2010), this was reduced to 3.28%. Of the 4712 hyperbolic meteors in the EDMOND, 43% are shower meteors. Shower meteors which have heliocentric velocities with excesses over the parabolic limit offer proof of the false hyperbolicity of their orbits. The hyperbolic orbits in our data were analysed separately in the paper Hajduková et al. (2014b).

A comparison of both the EDMOND and the SonotaCo catalogue, in terms of orbital parameters, showed an equivalence of the data.

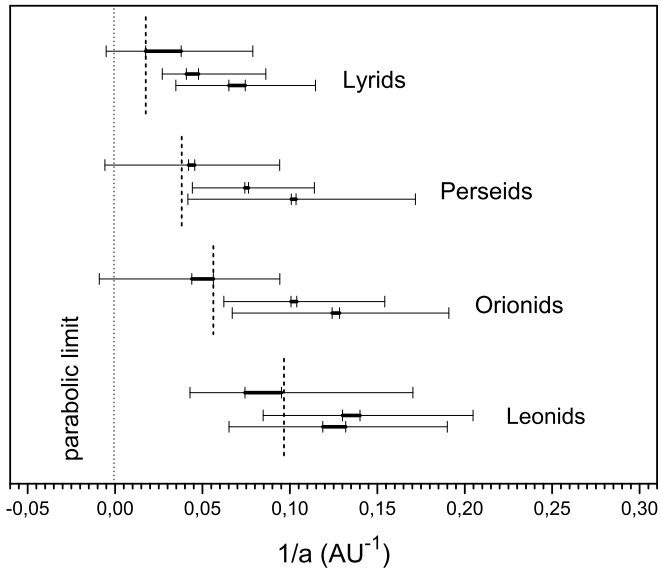

Figure 1. Comparison of the observed dispersion for the chosen meteoroid streams from different databases (upper line – photographic meteors from the IAU MDC, middle line – video meteors from the SonotaCo catalogue (2007–2009), lower line – the EDMOND data) described by absolute median deviation in terms of $1/a$: Thin line – the interval between two limiting values of $(1/a)_{1/2}$, which includes 50 percent of all orbits. Bold line – the interval between two limiting values of the uncertainty $(1/a)_L$ of the resulting values of median $(1/a)_M$. Dotted vertical line – the parabolic limit. Dashed vertical lines – parent comets (the figure is taken from the paper (Hajduková 2014)).

3. Identification of streams in EDMOND

Meteor showers in the EDMOND database were identified using the IAU Meteor Data Center Database (IAU MDC; (Jopek and Kaňuchová 2014)). At the end of August 2013, the IAU MDC list of showers contained 461 showers, 95 of them established and 366 in the working list.

In the first search, the radiant position-geocentric velocity method was used (we hereafter call it *radiant-V_g* method). Meteors were selected according to the peaks activity of meteor showers (±15 deg) given in the IAU MDC list, and fulfilling the conditions for radiant position (±5 deg) and geocentric velocity (±10%·V_g). A shower was considered only if at least 5 orbits had been identified. In this way, 267 meteor showers were identified, where 200 of them are meteor showers from the working list and 67 are the established showers.

We focused on *pro tempore* showers from the IAU MDC working list. Of 65 *pro tempore* showers in the list, 61 were identified using the *radiant-V_g* method. To determine their fundamental parameters more precisely, the first part of the Welch method (Welch 2001) with Southworth-Hawkins D criterion (Southworth and Hawkins 1963) was used. According to the equation (4) in Welch (2001) paper

$$\rho = \sum_{i=1}^{N} \left(1 - \frac{D_i^2}{D_c^2}\right) \; ; \qquad D_i \leqslant D_c \; , \tag{3.1}$$

where ρ is a density at a point in orbital elements space, N is the number of meteors of a *pro tempore* shower found in the first step, D_i is the value obtained for the i-th meteor in the *pro tempore* shower by comparing its orbit with orbits of each member of the identified shower, and D_c is the threshold value that determines the dynamical similarity among meteor orbits. We searched for the core of each *pro tempore* shower identified in the first step of the analysis (i.e. by *radiant-V_g* method).

The procedure creates a group of meteors around each meteor orbit from the examined shower, which fulfil the condition of the limiting value of Southworth and Hawkins criterion $D_c = 0.12$. On the basis of the equation (3.1), the value of the density (ρ) is determined for each group. The higher the density value, the more important the group in the examined shower is. However, the highest value of ρ does not always mean it is the core of the stream because the initial set could be contaminated by a nearby separate small shower; or because the MDC data are not yet accurate enough.

We therefore compared all the available parameters of each *pro tempore* shower at the IAU MDC with the mean values of the same parameters of each found group. We compared as well the mean orbits, radiant positions and geocentric velocities with newly meteor showers found in the SonotaCo (2007-2009) and CAMS (2010-2011) databases (Rudawska and Jenniskens 2014). The mean values of the orbital elements and other parameters of each group were obtained as a weighted arithmetic mean, where the weight was determined by $(1 - D_i^2/D_c^2)$ (Welch 2001).

The results obtained from this procedure are given in Table 1 and Table 2. Table 1 contains 22 showers for which the identification was certain, i.e. the parameters of which agree well with those from the IAU MDC list. Another 18 showers, for which the comparison showed quite considerable differences in some parameters, and thus making their identification questionable, are shown in Table 2. For instance, the difference in solar longitude or right ascension of radiant position reaches 10°, while the difference in eccentricities and perihelion distances, probably due to their high geocentric velocity, is greater than 0.1. In the EDMOND database (as of August 2013) we could not identify 25 *pro tempore* meteor showers. The reason is either the number of orbits in the particular showers was insufficient (less than 5) or the differences between some of the compared parameters were too big (larger than in Table 2).

A few low inclined meteor showers (#449, #467, #473, #475, #476, #478) seem to be represented as separate branches, where one (or both) of the branch includes from 1 to 3 members. However, as the amount of meteors in the Northern and/or Southern branch is small (<5), and there is no evident splitting, in those cases we considered such shower as one meteor shower. Therefore, we added (or subtracted) 180 degrees to the angular elements (ω, Ω) of the smaller branch, and then the weighted mean of ω and Ω of the shower was calculated.

Table 1. Mean values of the parameters: solar longitude (L_S), radiant position $(RA, Dc)_{2000}$, geocentric velocity (V_g), orbital elements and (D) – Southworth-Hawkins criterion of reliably identified *pro tempore* showers from the IAU MDC in the database EDMOND. N – number of meteors. In the second line of each shower, there are standard deviations.

Shower	L_S	RA	Dec	V_g	q [AU]	e	ω [°]	Ω [°]	i [°]	N	D_{SH}
448 AAL	14.4	219.7	-13.0	37.70	0.097	0.945	329.6	14.4	6.7	8	0.05
	6.0	3.2	1.6	2.35	0.028	0.025	5.4	6.0	3.5		0.04
449 ABS	7.3	166.5	5.5	14.65	0.844	0.658	52.4	187.3	0.7	5	0.04
	5.1	2.4	2.7	0.82	0.023	0.050	4.6	5.1	0.8		0.04
456 MPS	61.7	243.7	-10.5	24.63	0.541	0.790	273.2	61.7	9.0	26	0.05
	4.4	2.9	1.4	1.12	0.040	0.025	4.8	4.4	1.2		0.03
458 JEC	83.0	315.5	33.1	52.11	0.911	0.888	218.7	83.0	95.4	10	0.05
	1.9	1.4	1.0	0.80	0.008	0.047	1.4	1.9	1.1		0.03
460 LOP	85.9	257.6	-5.4	19.62	0.722	0.724	251.8	85.9	10.3	27	0.05
	3.7	2.2	2.4	1.13	0.037	0.032	5.0	3.7	1.0		0.03
462 JGP	120.5	263.5	13.3	62.31	0.484	0.922	275.2	120.5	149.4	12	0.06
	3.5	161.1	1.1	0.57	0.040	0.034	4.2	3.5	1.7		0.03
463 JRH	125.8	265.9	36.2	14.18	0.982	0.553	204.5	125.8	19.7	8	0.05
	5.2	2.8	2.3	0.97	0.012	0.046	5.4	5.2	1.5		0.03
465 AXC	136.1	4.7	48.9	54.72	0.898	0.843	221.4	136.1	104.2	14	0.06
	2.1	3.0	1.3	0.63	0.015	0.049	2.7	2.1	1.2		0.03
466 AOC	136.8	29.0	0.9	65.84	0.696	0.901	70.2	316.8	159.8	6	0.05
	4.5	3.5	2.1	0.56	0.025	0.048	2.9	4.5	3.6		0.05
467 ANA	139.5	318.1	-12.2	21.35	0.612	0.752	265.6	139.5	2.6	23	0.06
	3.2	2.1	2.1	1.39	0.037	0.037	4.2	3.2	1.6		0.03
474 ABA	147.9	301.3	4.5	15.07	0.860	0.676	230.9	147.9	10.1	11	0.05
	6.6	1.9	2.4	1.49	0.041	0.053	7.4	6.6	1.0		0.03
477 SRP	177.1	345.9	5.1	18.41	0.699	0.699	254.8	177.1	5.8	15	0.06
	4.2	1.8	2.0	1.51	0.046	0.043	6.6	4.1	1.1		0.03
478 STC	170.7	315.3	-13.3	10.19	0.927	0.561	218.3	170.7	1.1	6	0.05
	8.1	1.9	3.5	1.17	0.024	0.041	6.6	8.1	0.9		0.03
479 SOO	185.7	80.4	10.6	66.87	0.792	0.876	56.5	5.7	156.5	20	0.07
	3.1	2.2	1.6	0.69	0.031	0.049	4.6	3.1	2.9		0.03
480 TCA	204.1	135.1	29.2	67.31	0.808	0.839	125.9	204.1	158.0	18	0.06
	3.5	3.1	1.2	0.52	0.023	0.044	3.8	3.5	2.2		0.03
497 DAB	261.8	210.6	22.9	59.47	0.690	0.967	113.1	261.8	113.6	5	0.03
	0.7	1.1	1.2	0.31	0.025	0.021	3.3	0.7	0.5		0.05
500 JPV	288.2	221.9	1.2	65.05	0.657	0.866	106.6	288.2	146.5	8	0.05
	3.4	2.4	1.4	0.92	0.028	0.056	3.1	3.4	2.6		0.04
502 DRV	253.2	185.1	12.3	68.18	0.776	0.920	123.8	253.2	154.8	7	0.05
	4.0	3.2	1.7	0.82	0.024	0.051	4.1	4.0	2.6		0.04
508 TPI	146.5	351.5	4.0	38.01	0.102	0.951	328.0	146.5	21.1	143	0.06
	4.7	3.3	2.0	1.49	0.021	0.014	3.9	4.7	3.0		0.03
529 EHY	258.2	134.1	2.4	61.72	0.362	0.951	107.4	78.2	143.0	18	0.07
	3.1	2.6	1.0	0.97	0.029	0.031	4.0	3.1	1.8		0.03
530 ECV	304.9	193.9	-18.6	67.39	0.790	0.813	56.0	124.9	157.9	6	0.05
	3.7	3.2	1.7	0.49	0.038	0.026	5.8	3.7	3.9		0.04
546 FTC	144.1	30.2	67.4	52.20	1.009	0.868	173.0	144.1	95.4	14	0.06
	2.8	4.3	1.5	1.10	0.002	0.058	2.3	2.8	2.2		0.04

Table 2. Mean values of the parameters: solar longitude (L_S), radiant position $(RA, Dc)_{2000}$, geocentric velocity (V_g), orbital elements and (D) – Southworth-Hawkins criterion of questionably identified *pro tempore* showers from the IAU MDC in the database EDMOND. N – number of meteors. In the second line of each shower, there are standard deviations.

Shower	L_S	RA	Dec	V_g	q [AU]	e	ω [°]	Ω [°]	i [°]	N	D_{SH}
451 CAM	40.6	182.7	83.2	13.02	1.000	0.517	167.9	40.6	19.0	4	0.04
±	5.8	7.8	2.6	0.69	0.003	0.033	3.5	5.8	1.2		0.04
464 KLY	125.9	276.3	34.8	18.61	0.945	0.695	213.6	125.9	25.1	6	0.06
	6.8	2.2	1.9	1.32	0.018	0.043	4.3	6.8	1.5		0.04
468 AAH	136.3	267.8	20.6	12.47	0.977	0.631	204.4	136.3	13.5	7	0.05
	7.4	2.6	2.2	1.05	0.013	0.047	5.4	7.4	1.2		0.04
470 AMD	144.4	254.8	58.2	18.98	1.012	0.631	178.4	144.4	29.5	17	0.07
	4.2	4.2	2.6	1.12	0.002	0.041	3.6	4.2	2.0		0.03
471 ABC	137.8	306.3	-12.5	16.95	0.752	0.676	248.9	137.8	3.4	9	0.05
	3.8	2.2	2.4	1.42	0.035	0.043	4.6	3.8	1.5		0.03
472 ATA	143.8	310.3	-1.8	18.66	0.742	0.735	248.3	143.8	8.8	10	0.06
	6.3	1.9	3.6	1.29	0.046	0.044	7.1	6.3	1.5		0.04
473 LAQ	145.3	341.0	-5.1	31.12	0.279	0.881	303.2	145.3	4.1	20	0.07
	2.8	2.4	1.8	1.09	0.026	0.023	3.8	2.8	2.4		0.04
475 SAQ	157.1	330.6	-10.7	21.02	0.669	0.810	255.7	157.1	0.8	8	0.06
	4.0	1.6	1.4	1.22	0.033	0.060	5.1	4.0	0.7		0.05
476 ICE	175.5	4.6	-0.7	26.23	0.419	0.811	107.7	355.5	2.6	21	0.07
	5.0	2.9	2.1	1.39	0.043	0.032	5.7	5.0	1.7		0.03
481 OML	219.7	148.5	29.1	67.13	0.892	0.793	140.7	219.7	152.1	6	0.06
	3.7	3.2	1.7	1.00	0.024	0.048	5.2	3.7	2.6		0.04
484 IOA	233.6	28.5	15.6	14.51	0.824	0.677	233.9	233.6	1.5	5	0.05
	4.5	1.7	2.5	1.34	0.037	0.038	6.2	4.5	1.0		0.05
499 DDL	277.4	169.5	26.6	63.06	0.536	0.955	266.1	277.4	135.3	62	0.06
	2.8	2.5	1.4	0.85	0.022	0.044	3.0	2.8	1.6		0.03
531 GAQ	49.8	305.8	14.1	60.78	0.980	0.781	201.2	49.8	123.3	6	0.04
	2.7	1.9	0.5	0.30	0.012	0.048	3.7	2.7	0.9		0.04
533 JXA	112.6	35.0	9.2	68.85	0.863	0.939	313.8	292.6	171.8	19	0.06
	6.6	4.7	2.0	0.55	0.038	0.032	6.5	6.6	2.3		0.03
537 KAU	207.4	90.7	32.0	64.98	0.483	0.965	272.9	207.4	160.4	10	0.06
	4.6	4.4	1.1	1.01	0.045	0.040	5.6	4.6	2.5		0.04
538 FFA	215.1	50.9	30.2	38.12	0.187	0.957	311.3	215.1	24.1	5	0.05
	5.8	4.8	2.7	1.87	0.021	0.029	4.0	5.8	3.3		0.05
545 KCA	156.4	8.6	49.4	51.36	0.685	0.925	250.7	156.4	93.6	4	0.05
	1.9	2.5	1.4	0.94	0.019	0.049	2.0	1.9	1.3		0.04
547 KAP	137.6	43.9	45.6	63.53	0.976	0.852	157.0	137.6	132.0	11	0.06
	2.1	2.6	1.4	0.50	0.009	0.040	3.0	2.1	2.2		0.03

4. Conclusions

In the work, the European viDeo MeteOr Network Database (EDMOND) is introduced. Its 4th version contains 83 369 video meteor orbits. The Database was created thanks to the broad international cooperation of several European national networks and the International Meteor Organization Video Meteor Network, with the aim of connecting observers within a wide area. This has made it possible to

combine those observations which otherwise would have stayed as single-station data.

We expect to use this expanding database, particularly to study minor streams. The first results are here presented. Using the *radiant-V_g* method we identified 267 meteor showers of the IAU MDC, where 67 of them are established showers and 200 are showers from the working list.

Making a more detailed analysis of *pro tempore* showers from the IAU MDC working list, we determined their orbital elements, radiant positions, geocentric velocities and solar longitudes. The results were divided into two groups, based on a comparison of the mean values with those available in the IAU MDC. Table 1 contains 22 showers of the 65 *pro tempore* showers in the working list of the IAU MDC (August 2013), identification of which was clear and reliable. Identification of 18 meteor showers listed in Table 2 is questionable, as some their parameters differ considerably from those at the IAU MDC.

This work showed that the EDMOND database is able to provide relevant data convenient for the confirmation of meteor showers from the working list of the IAU MDC, which can improve their orbital and geophysical parameters.

Acknowledgements

This work was supported by the Slovak Research and Development Agency, project No. APVV-0517-12.

References

Andreić Ž., Šegon D., 2010, In Proceedings of the International Meteor Conference, Šachtička, Slovakia, 18–21 September 2008, 16

Brown P., Weryk R.J., Kohut S., Edwards W.N., Krzeminski Z., 2010, WGN, Journal of the International Meteor Organization, 38, 25

Cooke W.J., Moser D.E., 2012, in Proceedings of the International Meteor Conference, Sibiu, Romania, 15–18 September 2011, 9

Hajduková M. Jr., 2014, in Proceedings of the International Meteor Conference, 32d IMC, Gyssens M., Roggemans P. eds, 22-25 Aug., Poznań, Poland, 2013, in press

Hajduková M. Jr., Kornoš L., Tóth J. 2014a, M&PS, 49, 63

Hajduková, M. Jr., Kornoš L., Tóth J. 2014b, in Proceedings of the Meteoroids 2013 Conference, Poznań, Poland, 26–30 August 2013, eds Jopek T.J., Rietmeijer F.J.M., Watanabe J., Williams I.P, AM University Press, Poznań, p. 289

Jenniskens P., Gural P. S., Dynneson L., Grigsby B. J., Newman K. E., Borden M., Koop M., Holman D., 2011, Icarus, 216, 40

Jopek T.J., Kaňuchová Z., 2014, in Proceedings of the Meteoroids 2013 Conference, Poznań, Poland, 26–30 August 2013, eds Jopek T.J., Rietmeijer F.J.M., Watanabe J., Williams I.P, AM University Press, Poznań, p. 353

Kornoš L., Koukal J., Piffl R., Tóth J., 2013a, in Proceedings of the International Meteor Conference, Canary Islands, Spain, 20–23 September 2012, 21

Kornoš L., Koukal J., Piffl R., Tóth J., 2013b, in Proceedings of the International Meteor Conference, 22–25 August 2013, Poznań, Poland, in press

Lindblad B.A., Neslušan L., Porubčan V., Svoreň J.,2005 EMP, 93, 249

Molau S., 1999, in Proceedings of the International Conference Meteoroids 1998, Tatranska Lomnica, Slovakia, 17–21 August 1998, 131

Molau S., 2014, in Proceedings of the Intern. Meteor Conf. 2013, Poznań, Poland, 22-25 August 2013, in print

Pujols P., Amblàs M., Trigo-Rodríguez J.M., Dergham J., Madiedo J.M., Montanyà J., van der Velde O., 2013, Lunar and Planetary Institute Science Conference Abstracts, 44, 2054

Rudawska R., Jenniskens P., 2014, in Proceedings of the Meteoroids 2013 Conference, Poznań, Poland, 26–30 August 2013, eds Jopek T.J., Rietmeijer F.J.M., Watanabe J., Williams I.P, AM University Press, Poznań, p. 217

SonotaCo 2009, WGN, Journal of the International Meteor Organization, 37, 55

SonotaCo, Molau S., Koschny D., 2010, European Planetary Science Congress 2010, 798

Southworth R.B., Hawkins G.S., 1963, Smithsonian Contrib. Astrophys. 7, 261

Tóth J., Kornoš L., Vereš P., Šilha J., Kalmančok D., Zigo P., Világi J., 2011, Publ. Astron. Soc. Japan 63, 331

Vereš P., Tóth J., 2010, WGN, Journal of the International Meteor Organization, 38, 54

Welch P.G., 2001, MNRAS, 328, 101

Meteoroids 2013, Proceedings of the Astronomical Conference,
held at A.M. University, Poznań, Poland, Aug. 26-30, 2013,
eds Jopek T.J., Rietmeijer F.J.M., Watanabe J., Williams I.P.,
Adam Mickiewicz University Press in Poznań, pp 235–242

The ecliptic-toroidal structure of the meteor complex of comet 96P/Machholz

Neslušan L., Kaňuchová Z., Tomko D.

Astronomical Institute, Slovak Academy of Sciences, 05960 Tatranská Lomnica, Slovakia
(ne@ta3.sk, zkanuch@ta3.sk, dtomko@ta3.sk)

Abstract. Meteors belonging to the ecliptical showers enter the Earth's atmosphere from several directions, (i) of solar apex, (ii) toward the Sun, i.e. helion, and (iii) outward from the Sun, i.e. antihelion. Other particular sources of meteors, the northern and southern toroidal, are situated far from the ecliptic. The latter were suspected not to be real. By studying the meteoroid complex of comet 96P/Machholz, we found that the toroidal sources are real, but also that they can be a part of meteor complex composed of both ecliptical and toroidal showers, originating from a single parent body. In contrast, an identical ecliptic-toroidal structure can have a more than one parent body. Details about the structure of 96P (and, possibly, also asteroid 2003 EH1) are presented here.

Keywords: meteoroid streams, ecliptical showers, toroidal showers, ecliptic-toroidal structure, parent body, comet 96P/Machholz, asteroid 2003 EH1

1. Introduction

The small bodies in the Solar System on orbits with perihelion within the snow line usually produce small meteoroid particles around their orbit. If the orbit of a body releasing the particles passes closely the Earth's orbit, some of these particles collide with the Earth's atmosphere and an observable meteor shower is produced.

If the entire orbit of the parent body is far from that of the Earth, no shower is usually observed. However, the orbits of some bodies can exhibit a large libration, usually due to strong gravitational perturbations by Jupiter. The orbits of associated meteoroids exhibit the librations as well so that they can closely approach the Earth's orbit. Therefore meteors can be produced despite the fact, that the orbit of their parent is far from Earth.

In the case of some specific meteoroid streams, the libration of the orbits can lead to their multiple approach to the orbit of our planet and, thus, several meteor showers originating in a single parent body can be observed. The Jupiter-family comet 96P/Machholz is one such parent body. In this contribution, we describe our study of the theoretical stream of this comet.

It should be remembered that comet 96P was suggested as the parent body of the well-known meteor shower Quadrantids by McIntosh (1990). The relationship between the comet and the shower was studied by several authors (Wu and Williams 1992; Gonczi et al. 1992; Jones and Jones 1993; Froeschlé et al. 1993; Williams and Collander-Brown 1998). Babadzhanov and Obrubov (1992, 1993) published a more complex study concerning not only to the relationship between the comet and

Quadrantids, but other showers as well. These authors described, for the first time, the qualitative features of the 96P meteor-shower complex.

In 2003, asteroid 196 256 (2003 EH1) was discovered moving around the Sun on an orbit that is very similar to the mean orbit of Quadrantids. Immediately after the discovery, it was believed that this asteroid is exclusive parent body of this meteor shower (Jenniskens, 2004). The relationship between 2003 EH1 and Quadrantids was then studied by several authors (Williams et al. 2004; Porubčan and Kornoš 2005; Ryabova and Nogami 2005; Wiegert and Brown 2005). Babadzhanov et al. (2008) suggested the generic relationship not only between the asteroid and Quadrantids, but they claimed that the asteroid could be the parent body of some other showers. Today, we know that both objects, 96P and 2003 EH1 (Kaňuchová and Neslušan 2007; Neslušan et al. 2013a; 2013b), can be, from the point of view of dynamical evolution, the parent bodies of Quadrantids as well as another at least three (possibly five) real meteor showers.

2. The modeling of a theoretical stream

To model a theoretical stream of a given parent body, we integrate its nominal orbit backward in time down to a chosen moment of perihelion passage. At perihelion, we assume an ejection of 10 000 test particles from the parent's surface. The particles represent the meteoroids. Their modeled ejection is assumed to be random, in all possible directions, and with the ejection velocity equal to 1/1000 of the parent's perihelion velocity. Although the real meteoroids escape from the parent body not only at perihelion and with the ejection velocity in a wider range, whereby a preferred direction of their ejection can occur, our simple method is sufficient to fill in the whole six-dimensional phase-space of studied orbital elements with the particles. Of course, the phase-space is not filled immediately after the modeling. A certain relaxation time is needed to spread the particles around the entire orbit of the parent. The relaxation time varies with a different ejection velocity, but it is always much shorter than the minimum period of the dynamical evolution of the stream, which we are interested in.

After the modeling of the set of test particles, we integrate all them for the period ranging from the moment of their assumed escape from the parent until the present. We use the integrator RA15 produced by Everhart (1985) within the software package MERCURY developed by Chambers (1999). The perturbations of all eight big planets are included.

When the integration is completed, we select those particles which are moving on orbits that currently approach within 0.05 AU the Earth's orbit . The orbits of these particles are similar to the orbits of meteors of the shower and can, thus, be used to make the prediction of shower mean parameters. The limit of 0.05 AU is larger than the Earth's radius, determining the actual cross section of our planet. It is a compromise between the relevance of the particles chosen for our prediction and their number. The actual number of meteoroids in a stream is by many orders of magnitude higher than we can include in our computations. Having only $\sim 10^4$

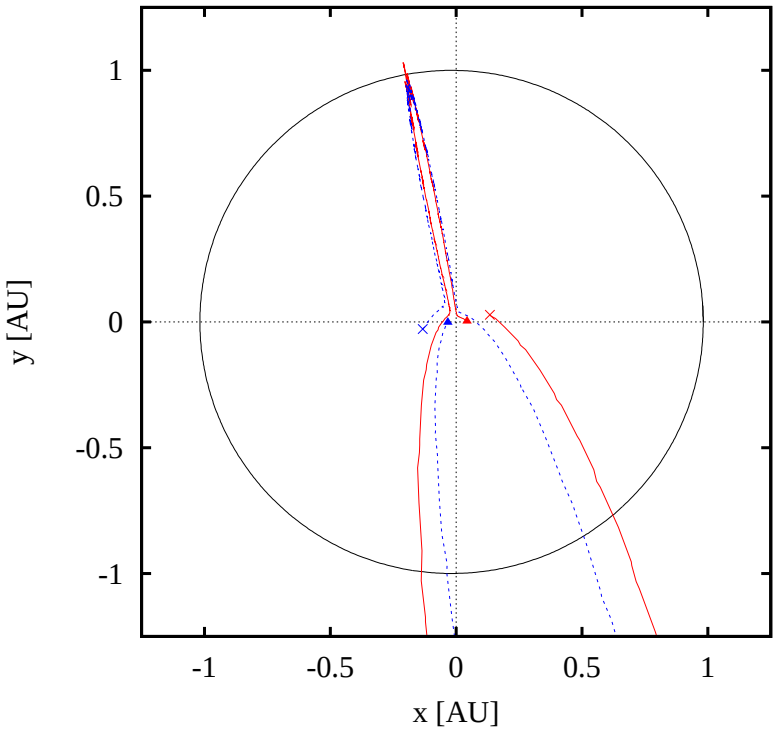

Figure 1. The evolution of the ascending (dotted blue curve) and descending (solid red curve) node of the orbit of comet 96P during one period of the libration of its longitude of ascending node (∼8200 years). The Earth's orbit is illustrated with the circle.

test particles, we must artificially enlarge the Earth's cross section to obtain at least a small group of the particles corresponding to a potential shower.

For comet 96P, we model 8 theoretical streams with perihelion passages about 500, 1000, 2000, 2900, 3000, 3100, 3200, and 4000 years before the present.

3. Evolution of orbital nodes

The libration cycle of longitude of ascending node and the argument of perihelion of the nominal orbit of 96P lasts about 8200 years. During this period, the nodes of its orbit move toward the Sun and outward from it, whereby they cross the Earth's orbit several times. The evolution of the position of the ascending as well as the descending node is shown in Fig. 1.

In principle, there are 8 crossing points of the curves showing the evolution of the nodes with the Earth's orbit. However, as seen in the upper region of Fig. 1, two crossing points of the ascending as well as two points of the descending node are so close each other that it is practically impossible to distinguish them. So, we consider only 6 cross-points and, therefore, predict 6 corresponding showers.

4. The Meteoroid complex of 96P

Detailed information about the predicted showers of the 96P complex was already published in our earlier paper (Neslušan et al. 2013a). Therefore we only briefly summarize their basic geophysical and orbital characteristics in Table 1. We predict six showers of the 96P/Machholz complex. Four of these showers are well-known: daytime Arietids, Southern and Northern δ-Aquariids, and Quadrantids. In addition, we predicted another two showers to which we refer as ,,filament 4" and ,,filament 6". Filament 4, if exists, is the southern branch of the Arietids. Filament 6 occurs to be the southern counterpart of the Quadrantids when the toroidal structure of the complex is considered (Sect. 5).

5. The ecliptic-toroidal structure

It is known that meteoroids come to the Earth in relatively higher rates from some specific directions of sky. From the point of view of this circumstance, the showers can be classified as ,,ecliptical" and ,,toroidal". The meteors of the ecliptical showers come from (i) the direction of the Earth's apex, (ii) direction toward the Sun named ,,helion", and (iii) direction opposite to the Sun named ,,antihelion". The toroidal sources of meteors were reported especially from the radar observations. The mean ecliptic longitude of their radiant is identical to that of the Earth's apex and the mean radiant is far from the ecliptic, whereby the (iv) northern and (v) southern toroidal showers can be observed.

In the case of 96P meteor complex, we predict showers from (ii) to (v) of the above described types. The distribution of radiants of the Earth-orbit approaching particles (within 0.05 AU) considered in all 8 models is shown in Fig. 2 in the ecliptical coordinate frame with the longitude λ_g replaced by angle $\lambda_a = \lambda_g - (\lambda_\odot + 270^o)$ to emplace the Earth's apex into the origin of the coordinate system. $\lambda_\odot$ is the solar longitude in the time of predicted meteor shower (specifically, we consider the moment when the Earth is in its closest approach to the orbit of a given meteor). In Fig. 2, we see that the radiants of δ-Aquariids N and S, daytime Arietids, and daytime filament 4 are situated near the ecliptic. Each shower has its northern and southern branch as well. Therefore we can regard these showers as ecliptical showers of the 96P complex. In particular, the Arietids and filament 4 belong to the helion cardinal direction and δ-Aquariids N and S to the antihelion cardinal direction.

Further, we can see that the mean modified longitude, λ_a, of the radiants of Quadrantids and filament 6 (Fig. 2) is approximately equal to zero. These showers can, thus, be classified as the toroidal showers of the complex. The Quadrantids belong to the northern and filament 6 to the southern toroidal cardinal direction.

For the identification of the predicted showers a search in three databases: the IAU MDC photographic (Lindblad et al. 2003), video (SonotaCo 2009) and radio-meteor (Hawkins 1963; Sekanina and Southworth 1975; Lindblad 2003) for real showers was carried out. The predicted filaments 4 and 6 were not found in these observational data. The latter can, however, be detected only from the southern hemisphere. In the data considered, there is a relatively small number of mete-

Table 1. The geophysical and orbital characteristics of the theoretically predicted showers of comet 96P/Machholz. Denotation used: α_g and δ_g – equatorial coordinates of geocentric radiant, V_g and V_h – geocentric and heliocentric velocity, γ – angular distance of mean geocentric radiant from the Sun in time when the Earth is in the shortest distance from the mean orbit of shower, A – amount of the particles in the given shower with respect to the total considered number (the summary amount of all eight models), q – perihelion distance of mean shower orbit, e – its eccentricity, ω – argument of perihelion, Ω – longitude of ascending node, and i – inclination to the ecliptic.

	Arietids	δ-Aquariids N	Quadrantids	Filament 4	δ-Aquariids S	Filament 6
α_g [deg]	31.2 ... 47.4	328.5 ... 343.1	224.5 ... 228.2	53.5 ... 56.5	335.3 ... 347.7	87.9 ... 153.6
δ_g [deg]	16.6 ... 24.6	−8.3 ... −3.2	48.3 ... 50.3	14.4 ... 16.2	−16.5 ... −13.7	−53.6 ... −41.9
V_g [km s^{-1}]	37.9 ... 43.9	39.0 ... 44.3	41.7 ... 42.5	44.1 ... 46.0	36.1 ... 43.2	26.1 ... 45.8
V_h [km s^{-1}]	35.5 ... 39.1	36.0 ... 38.7	38.9 ... 39.0	37.3 ... 39.6	37.8 ... 38.2	39.3 ... 40.2
γ [deg]	28.6 ... 32.3	144.1 ... 151.3	85.8 ... 88.7	31.4 ... 34.6	149.0 ... 158.4	90.2 ... 115.5
A [%]	2.53	0.05	0.49	0.06	2.04	0.34
q [AU]	0.043 ... 0.151	0.014 ... 0.035	0.960 ... 0.977	0.014 ... 0.036	0.043 ... 0.188	0.897 .... 0.981
e [1]	0.960 ... 0.986	0.974 ... 0.995	0.682 ... 0.688	0.989 ... 0.995	0.950 ... 0.986	0.715 ... 0.810
ω [deg]	18.1 ... 37.0	339.8 ... 349.2	170.7 ... 178.2	191.8 ... 200.3	136.6 ... 157.7	−0.7 .... 34.9
Ω [deg]	60.9 ... 86.1	106.5 ... 132.8	281.6 ... 282.7	265.7 ... 272.7	301.4 ... 320.5	85.1 ... 97.8
i [deg]	9.7 ... 33.7	21.8 ... 45.5	72.9 ... 74.5	24.3 ... 36.0	18.2 ... 28.6	37.9 ... 81.2

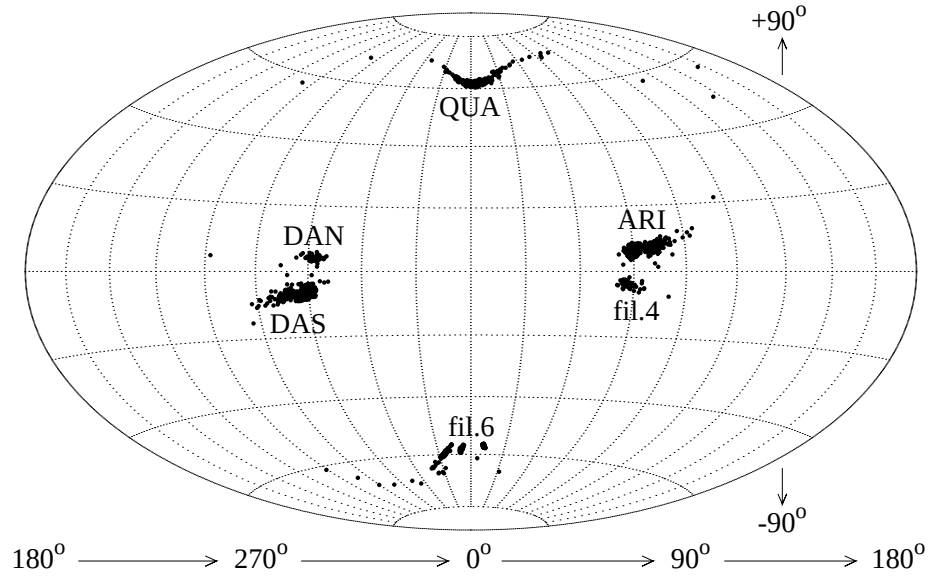

Figure 2. The distribution of radiants of the particles in eight considered models of the theoretical streams of comets 96P/Machholz, which approach, in their orbits, to the Earth's orbit within 0.05 AU. The distribution is shown in the Hammer projection of the ecliptical coordinate frame with modified longitude to emplace the Earth's apex into the origin of the coordinate system. The abbreviations refer to: DAN and DAS - δ-Aquariids N and S, QUA – Quadrantids, ARI – Arietids, and fil.4 and fil.6 – theoretical filaments 4 and 6 (see Sect. 4).

ors, therefore the corresponding real shower can still exist but not be evidenced in the data. Filament 4 corresponds to a daytime shower with an extremely short perihelion distance. Also this shower still can be discovered in a larger, more abundant, radio data. †

We note that an almost identical ecliptic-toroidal structure was recently identified for the meteoroid complex of asteroid 196 256, also known by its preliminary designation 2003 EH1 (Neslušan et al. 2013b). The orbit of this asteroid is situated in the same orbital phase space as that of comet 96P (e.g. Kaňuchová and Neslušan 2007). Both orbits are shifted in phase about two millennia (McIntosh, 1990), therefore they seem to be very different at the present. The meteoroids of

† In some presentations at this conference, the authors (Bruzzone et al. 2013, Brown et al. 2013; Campbell-Brown et al. 2013) mentioned the observations conducted by the Canadian Meteor Orbit Radar. In the figures of the radiant distribution of detected meteors, a clear accumulation of radiants corresponding to a southern branch of Arietids can actually be seen. This accumulation is a good candidate for the real shower predicted by us as filament 4.

the streams of both parent bodies, 96P and 2003 EH1, spread over the whole orbital phase space after a period, therefore the structure of the 96P and 2003 EH1 streams is, practically, the same. Only the models for the shortest evolutionary periods (for the release of meteoroids during the perihelion passage 500 and 1000 years in the past) give different pictures. While the early model of 96P stream predicts the occurrence of Arietids, that of 2003 EH1 stream predicts the occurrence of Quadrantids in the first stage of the evolution of streams.

6. Conclusions

The meteoroid-shower complex of comet 96P/Machholz has an interesting structure consisting of six showers with the radiants distributed on the sky symmetrically with respect to the Earth's apex. Four showers of the complex, δ-Aquariids N and S, daytime Arietids, and theoretical filament 4, which can be regarded as the southern branch of Arietids, represent the ecliptical showers of the complex. However, it is interesting not only that a single parent body can be associated with more than a single (or two) shower(s), but it can associate the showers of two kinds, ecliptical and toroidal.

The case of the 96P complex shows that the toroidal showers are ordinary showers, which can be, moreover, related to the ecliptical showers. The toroidal showers of the 96P complex are the Quadrantids and theoretical filament 6 with the mean radiant in the southern sky.

Finally, the orbit of asteroid 196 256 (2003 EH1) is situated in the same phase space as the orbit of comet 96P and can, thus, be another parent body of the complex as meanwhile demonstrated by Babadzhanov et al. (2008), Neslušan et al. (2013b). There can exist not only multiple showers of a single parent body, but the multiple showers of multiple parent bodies as well.

Acknowledgements

This work was supported, in part, by VEGA − the Slovak Grant Agency for Science, grants No. 0011 (L.N. and D.T.) and No. 0022 (Z.K.).

References

Babadzhanov P.B., Obrubov Yu.V., in: Asteroids, Comets, Meteors 1991, Lunar and Planetary Inst., Houston, p. 27

Babadzhanov P.B., Obrubov Yu.V., in: Meteoroids and Their Parent Bodies, eds. J. Štohl and I. P. Williams, Astron. Inst., Slovak Acad. Sci., Bratislava, p. 49

Babadzhanov P.B., Williams I.P., Kokhirova G.I., 2008, MNRAS, 386, 2271

Bruzzone S., Brown P., Weryk R.J., Wong D.K., 2013, Meteoroids 2013, in the Conference Program and Abstract, #022, (`http://www.astro.amu.edu.pl/Meteoroids2013/index.php?section=program`)

Brown P.G., Weryk R.J., Wong D.K., 2013, Meteoroids 2013, in the Conference Program and Abstract, #021, (`http://www.astro.amu.edu.pl/Meteoroids2013/index.php?section=program`)

Chambers J.E., 1999, MNRAS, 304, 793

Campbell-Brown M., Brown P.G., Weryk R.J., Wiegert P.A., 2013, Meteoroids 2013,

in the Conference Program and Abstract, #003, (http://www.astro.amu.edu.pl/Meteoroids2013/index.php?section=program)

Everhart E., 1985, in: Dynamics of Comets: Their Origin and Evolution, eds A. Carusi and G. B. Valsecchi, Proc. of IAU Colloq. 83, held in Rome, Italy, June 11-15, 1984., Kluwer, Dordrecht, p. 185

Froeschlé C., Gonczi R., Rickman H., 1993, in: Meteoroids and Their Parent Bodies, eds. J. Štohl and I. P. Williams, Proc. of the Inter. Astron. Symp. held at Smolenice, Slovakia, July 6-12, 1992, Publ. by Astron. Inst., Slovak Acad. Sci., Bratislava, p. 169

Gonczi R., Rickman H., Froeschlé C., 1992, MNRAS, 254, 627

Hawkins G.S., 1963, Smithsonian Contrib. Astrophys., 7, 53

Jenniskens P., 2004, AJ, 127, 3018

Jones J., Jones W., 1993, MNRAS, 261, 605

Kaňuchová Z., Neslušan L., 2007, A&A, 470, 1123

Lindblad B.A., 2003, private communication

Lindblad B.A., Neslušan L., Porubčan V., Svoreň J., 2003, Earth, Moon, Planets, 93, 249

McIntosh B.A., 1990, Icarus, 86, 299

Neslušan L., Kaňuchová Z., Tomko D., 2013a, A&A, 551, A87

Neslušan L., Hajduková jr. M., Jakubík M., 2013b, A&A, 560, A47

Porubčan V., Kornoš L., 2005, Contrib. Astron. Obs. Skalnaté Pleso, 35, 5

Ryabova G., Nogami N., 2005, in Proc. Inter. Meteor Confer. held at Varna, Bulgaria, 23−26 Sept. 2004, eds M. Triglav-Čekada, J. Kac, and A. McBeath, International Meteor Organization, p. 63

Sekanina Z., Southworth R.B., 1975, Physical and dynamical studies of meteors. Meteor-fragmentation and stream-distribution studies. Final Report., Smithsonian Astrophys. Obs., Cambridge, MA

SonotaCo, 2009, WGN – Journal of IMO, 37, 55, (http://sonotaco.jp/doc/SNM/)

Southworth R.B., Hawkins G.S., 1963, Smithsonian Contrib. Astroph., 7, 261

Wiegert P., Brown P., 2005, Icarus, 179, 139

Williams I.P., Collander-Brown S.J., 1998, MNRAS, 294, 127

Williams I.P., Ryabova G.O., Baturin A.P., Chernitsov A.M., 2004, MNRAS, 355, 1171

Wu Z., Williams I.P., 1992, MNRAS, 259, 617

Meteoroids 2013, Proceedings of the Astronomical Conference,
held at A.M. University, Poznań, Poland, Aug. 26-30, 2013,
eds Jopek T.J., Rietmeijer F.J.M., Watanabe J., Williams I.P.,
Adam Mickiewicz University Press in Poznań, pp 243–249

Prediction of meteor shower of comet 161P/2004 V2

Tomko D.[1], **Neslušan L.**[1]

[1]Astronomical Institute, Slovak Academy of Sciences, 05960 Tatranská Lomnica, Slovakia
(dtomko@ta3.sk, ne@ta3.sk)

Abstract. We deal with theoretical meteoroid stream of Halley-type comet 161P/2004 V2. For two perihelion passages in the far past, we model the stream and follow its dynamical evolution until the present. We predict the characteristics of potential meteor showers according to the dynamical properties of artificial particles currently approaching the orbit of the Earth. Our dynamical study reveals that the comet 161P/2004 V2 could have an associated Earth-observable meteor shower, although no significant number of artificial particles are identified with real, photographic, video, or radar meteors. However, the mean radiant of the shower is predicted on the southern sky (its declination is about -23^o) where a relatively low number of real meteors has been detected and, therefore, recorded in the databases used. The shower of 161P has a compact radiant area and a relatively large geocentric velocity of $\sim$53 km s^{-1}.

Keywords: meteoroid streams, meteors, parent body, comet 161P/2004 V2

1. Introduction

The major meteor showers observed in the Earth's atmosphere are caused by the Earth impacting particles which originated from larger parent bodies. A prevailing part of these parents are comets.

If the entire orbit of comet is situated in a large distance from the orbit of our planet, the particles of the stream usually do not collide with its atmosphere, hence a detection of the stream is almost impossible in this case. In some Earth-orbit-distant streams, the gravitational perturbations of major planets as well as non-gravitational effects can however deflect a significant number of particles from the corridor around the parent body orbit, into an alternative corridor crossing the Earth's orbit. Thus, some cometary or asteroidal objects in distant orbits can still have associated a stream colliding with the Earth's atmosphere.

A Halley type comet 161P/2004 V2 (Hartley-IRAS) was discovered by M. Hartley (U.K. Schmidt Telescope Unit, Australia). He found the trail of a comet on a photographic plate exposed on November 4th, 1983 (Kronk, `http://cometography.com/pcomets/161p.html`). He estimated the magnitude as 15. Before a confirmation plate could be obtained, J. Davies and S. Green (University of Leicester, England) reported on November 11th that the Infrared Astronomy Satellite had imaged a comet on November 10.35 UTC. They estimated the magnitude as 15.5. This comet appeared to be identical to that found by Hartley. It is the Halley-type comet with orbital period of 21.5 years. At the present, the orbit of 161P does not approach the Earth's orbit closer than $\sim$0.4 AU.

2. Modelling of the Stream Dynamics

To study the orbital evolution of test particles in the modelled stream, we follow the procedure suggested by Neslušan (1999). After some improvements in the context of our study, the procedure consists of the following steps.

1. The integration of motion of the parent body backward in time. The integration periods are $200P_o$ and $500P_o$ for this comet ($P_o = 21.5$ years). The initial orbital elements are taken from the Catalogue of Cometary Orbits, 16th edition (Marsden and Williams 2005). We consider the gravitational perturbations of 8 planets, Mercury to Neptune. Their initial position and velocity vectors are taken from the Astronomical Almanac for year 2004 (2002). Integrator RA15 developed by Everhart (1985) within the MERCURY package (Chambers 1999) is used to perform the numerical integration.

2. Modelling the theoretical stream in each moment of parent perihelion passage reached at the previous step. Specifically, we generate orbits of 10,000 test particles. These particles are assumed to be ejected from the parent-body surface uniformly to all directions with the unique ejection velocity equal to 1/1000 perihelion velocity of parent body.

3. Numerical integration of the stream particles from the moment of their assumed ejection (in step (2)) until the present. Integrator RA15 within the MERCURY package is again used. The final characteristics of 8 perturbing planets and the parent body in the integration in step (1) are taken as initial in this step. Since we aim to predict new streams, we do not consider any non-gravitational effects. We assume that an including of these effects characterized with the entire ranges of possible free parameters would only enlarge the dispersion of predicted stream characteristics.

4. The analysis of main evolutionary features of the theoretical stream.

5. The selection of the test particles approaching the present Earth orbit closer than 0.05 AU. Selected particles are regarded as the part of the stream colliding with the Earth and, thus, causing an eventual meteor shower.

6. The analysis of the dynamical evolution of the Earth-orbit approaching small part of the modelled stream (EAPS) and, if there are enough particles, prediction of the characteristics of an eventual meteor shower associated with the studied parent body.

7. The identification of the Earth-orbit approaching particles with the actually observed meteors. The photographic al IAU MDC (Lindblad et al. 2003), radio-meteor (Hawkins, 1963; Sekanina and Southworth 1975; Lindblad, 2003), and the SonotaCo video-meteor (SonotaCo 2009) databases are used at this identification.

3. The Predicted Stream

Since an occurrence of an Earth-surface-observable meteor shower is often related to a close passage of the parent body around the Earth's orbit, we show the evolution of the minimum distance between the orbit of comet and the Earth's orbit, in Figure 1. The upper limit of this minimum distance in the case of well-known

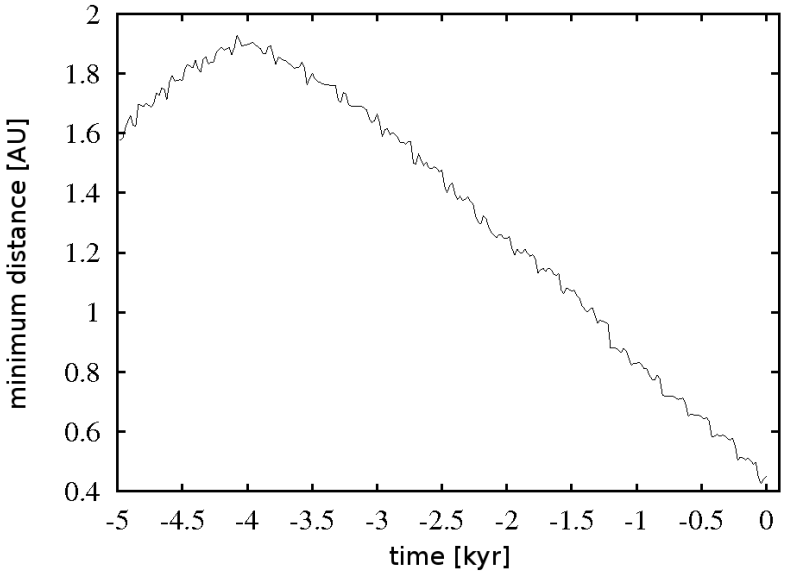

Figure 1. Evolution of the minimum orbital intersection distance (MOID) between the orbits of comet 161P and Earth during the last 5 millennia.

major meteor showers is ∼0.15 AU (the orbital arc of 1P/Halley associated with the Orionids). Typically, the distance is several hundredths of astronomical unit. As one can see on Figure 1, the orbit of comet 161P has been far from the Earth's orbit during the last 5,000 years.

The stream associated with this comet is modelled for times of 200 P_o and 500 P_o, i.e. about 4,300 and 10,750 years before the present. The orbital as well as geophysical characteristics of seven particles of the EAPS appear to be too different from the mean characteristics of the EAPS, and therefore although they pass within 0.05 AU of the Earths orbit, we do not regard them as members of the found shower. The EAPS consists of 729 particles in total.

The predicted geophysical parameters of 161P shower are given in Table 1. In Table 2 we list the mean orbital characteristics, and their dispersion (characterized by standard deviation) of the particles released from comet which are on the collision course with the Earth. The positions of radiants of the modelled particles are illustrated in Figure 2. In this figure, the radiants of a few not-shower particles are also shown (with squares). The radiant area of 161P shower associated with the stream modelled for time 200 P_o before the present is almost the same as that associated with the stream modelled for time 500 P_o before the present.

The daily motion of radiant can be useful during comparison of observed meteors with the predicted shower. Variations of the radiant coordinates of the predicted 161P shower with solar longitude are displayed in Figure 3. If the shower is relatively young, its period activity can be short, lasting only a few days. For the shower related to the stream modelled in 200 P_o before the present (crosses in Figure 3),

Table 1. Geophysical characteristics of the predicted meteor shower associated with comet 161P. Denotation used: t_{evol} – the period for which the orbital evolution is followed (the theoretical stream was modelled before this time), t_{act} – period of the activity of shower during a year, $<\lambda_\odot>$ –mean ecliptical longitude of the Sun at the moment of collision of shower particles with the Earth, α_g a δ_g – equatorial coordinates of geocentric radiant, V_g a V_h – geocentric and heliocentric velocity, γ – angular distance of the radiant from the Sun in time corresponding to the mean longitude. Time t_{evol} is given as the multiple of the catalogue orbital period of the parent comet, P_o, the angular quantities are given in degrees, and velocities in $\mathrm{km\,s^{-1}}$.

t_{evol}	t_{act}	$<\lambda_\odot>$	α_g	δ_g	V_g	V_h	γ
200	Sep. 23.5 – Sep. 26.0	181.48	76.2	−23.4	53.1	40.6	103.6
500	Sep. 21.1 – Oct. 5.1	183.18	78.2	−22.5	53.6	40.6	103.0

the activity corresponds to $180° \leqslant \lambda_\odot \leqslant 182°$. It is interesting that the shower of 161P is compact despite the fact that the minimum distance between the 161P orbit and the Earths orbit was large, ∼1.8 AU, 4300 years before the present (see Figure 1).

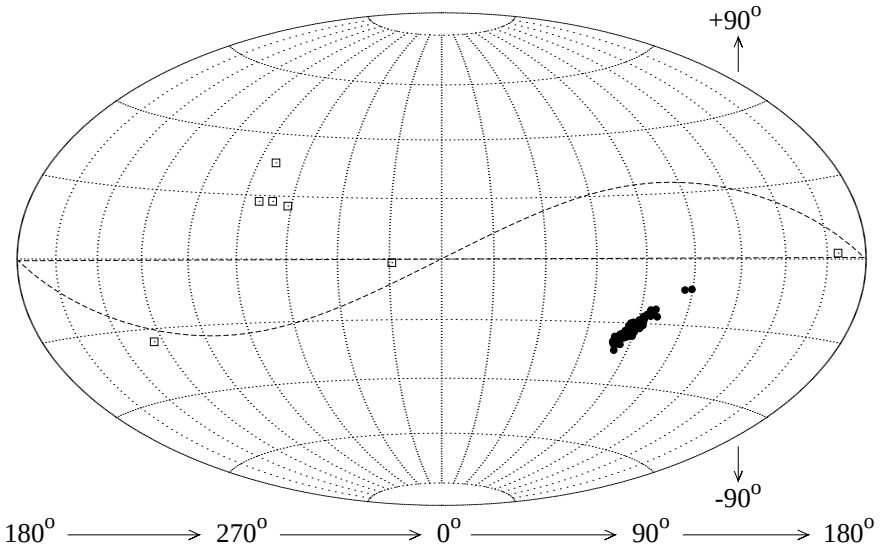

Figure 2. The Hammer-Aitoff diagram of the radiants in the equatorial reference frame. The crosses (small bullets) correspond to the particles for which the MOID < 0.05 AU.The radiants of few particles with the characteristics largely different from the mean characteristics of the shower are shown with squares. The sinusoid-like curve illustrates the ecliptic.

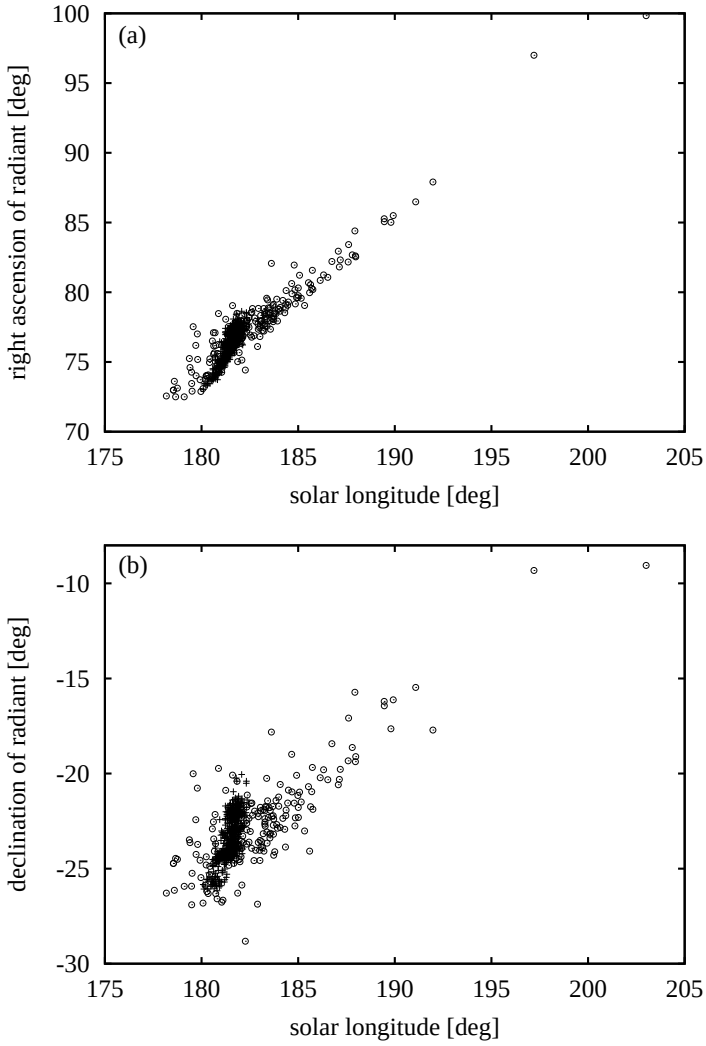

Figure 3. Dependence of the equatorial coordinates of theoretical radiants on the solar longitude in the case of predicted shower from comet 161P/2004 V2. Left panel for right ascension, right panel for declination. All quantities are given in degrees. The radiants of shower corresponding to the stream modelled in time $200\,P_o$ ($500\,P_o$) are shown with crosses (small bullets).

The geocentric velocity of the predicted shower is relatively high, from ∼53 to ∼54 km s^{-1}. Consequently, a well-seen light effect can be expected at the meteor events. The shower should be quite well observable, if actually exists.

Our cluster analysis among the theoretical particles and the real meteors taken from the used databases gave no positive result. In all three considered databases (Lindblad et al., 2003; Hawkins 1963; Sekanina & Southworth 1975; Lindblad 2003;

Table 2. Mean orbital characteristics with their standard deviation of the predicted meteor showers associated with the parent body considered. Denotation: t_{evol} – as in Table 1, q – perihelion distance, a – semi-major axis, e – eccentricity, ω – argument of perihelion, Ω – longitude of ascending node, i – inclination to the ecliptic. Quantities q and a are given in astronomical units and angular quantities in degrees.

t_{evol}	q	a	e	ω	Ω	i
200	0.90±0.02	7.6±0.4	0.882±0.007	39.9±1.3	1.5 ±0.4	97.5±2.2
500	0.89±0.02	7.3±0.8	0.88±0.02	38.9±1.8	3.2±3.1	99.0±4.5

SonotaCo 2009) we have found only a few orbits for which D_{SH} -discriminant (Southworth and Hawkins, 1963) was reasonable low. To separate the shower from the database, we use method of "break point" (Neslušan et al. 1995; Neslušan et al. 2013). No break point was however seen on the plot – identified number vs. critical D_{SH} -discriminant dependence.

The mean characteristics of the modelled shower cannot be either related to any real shower published by Brown et al. 2010; Jenniskens 1994, 2006; SonotaCo 2009, or listed in the IAU MDC database (see Jopek and Jenniskens 2011; Jopek and Kaňuchová 2014).

4. Conclusions

Comet 161P/2004 V2 could have produced the Earth-observable meteor shower. In this study no significant number of the modelled particles has been identified with the real, photographic, video, or radar meteors. However, the theoretical radiants of the shower is located on southern sky (declination of mean radiant about $-23°$) where a relatively low number of meteors has been detected and therefore was recorded in the available databases. The question on the existence of this predicted shower still remains opened.

Acknowledgements

This work was supported by VEGA − the Slovak Grant Agency for Science, grant No. 0031.

References

Astronomical Almanac 2004, 2002, U.S. Government Printing Office and The Stationary Office, Washington and London

Brown P., Wong D. K., Weryk R. J., Wiegert P., 2010, Icarus, 207, 66

Chambers J.E., 1999, MNRAS, 304, 793

Everhart E., 1985, in Dynamics of Comets: Their Origin and Evolution, eds Carusi A., and Valsecchi G.B., Kluwer, Dordrecht, p. 185

Hawkins G.S., 1963, Smithsonian Contrib. Astrophys., 7, 53

Jenniskens P., 1994, A&A, 287, 900

Jenniskens P., 2006, Meteor Showers and their Parent Comets, Cambridge University Press, Cambridge, UK

Jopek T.J., Jenniskens P., 2011, in Proc. Meteoroids 2010 Conf., held in Breckenridge, Colorado USA, May 24-28, 2010, NASA/CP-2011-216469, p. 7

Jopek T.J., Kaňuchová Z., 2014, in Proc. Meteoroids 2013 Conf., held in Poznan, Poland, Aug. 26-30, 2013, eds Jopek T.J., Rietmeijer F.J.M., Watanabe J., Williams I.P, AM University Press, Poznań, p. 353

Lindblad B.A., 2003, private communication

Lindblad B.A., Neslušan L., Porubčan V., Svoreň J., 2003, EM&P 93, 249

Marsden B.G., Williams G.V., 2005, Catalogue of cometary orbits, 16-th ed., Smithsonian Astrophys. Obs., Cambridge

Neslušan L., 1999, A&A, 351, 752

Neslušan L., Svoreň J., Porubčan V., 1995, EM&P, 68, 427

Neslušan L., Svoreň J., Porubčan V., 2013, EM&P, 110, 41

Sekanina Z., Southworth R.B., 1975, Final Report. Smithsonian Astrophys. Obs., Cambridge, MA

SonotaCo, 2009, WGN - Journal of the IMO, 37, 55

Southworth R. B., Hawkins G. S. ,1963, Smith. Cont. to Aph., 7, 261

Meteoroids 2013, Proceedings of the Astronomical Conference,
held at A.M. University, Poznań, Poland, Aug. 26-30, 2013,
eds Jopek T.J., Rietmeijer F.J.M., Watanabe J., Williams I.P.,
Adam Mickiewicz University Press in Poznań, pp 251–262

A parent body search across several video meteor data bases

Šegon D.[1], Gural P.[2], Andreić Ž.[3], Skokić I.[4], Korlević K.[5], Vida D.[4], Novoselnik F.[4]

[1]Astronomical Society "Istra" Pula, Park Monte Zaro 2,
52100 Pula, Croatia (damir.segon@pu.htnet.hr)
[2]351 Samantha Drive, Sterling, VA 20164-5539, USA
[3]University of Zagreb, Faculty of Mining, Geology and Petroleum Engineering,
Pierottijeva 6, 10000 Zagreb, Croatia
[4]Astronomical Society "Anonymus", B. Radića 34, 31550 Valpovo, Croatia
[5]Višnjan Science and Education Center, Istarska 5, 51463 Višnjan, Croatia

Abstract. A meteor stream search that uses all the known near-Earth objects (NEOs) as parent bodies, with their individual orbital elements as the starting point, has found statistically significant associations when applied to video meteor data bases. By using the combined CMN–SonotaCo data sets containing 133,652 video meteor orbits, 30 comets were associated with meteor showers of which only 23 were previously listed in the IAU MDC data base. Additionally, 43 asteroids with inclinations over 15 degrees may be associated to streams containing ten or more meteor orbits, each possibly representing a new meteor shower. Lastly, by using a modified search that compared the orbital similarity of each meteor to all other video meteors in the data base, 1093 groupings with more than ten meteors were found that may be indicative of several new minor showers. Of those groups, 6 new showers were found to be potentially associated to a parent body. Several dozen additional groups are planned for publication and submittal to the IAU for their consideration as newly discovered streams. Altogether 56,486 (42%) of the meteors in the combined video meteor data base are in one of the meteor stream groupings found, while the rest are likely sporadics. Further analysis is needed to prove that the groupings found are indeed minor showers.

Keywords: meteor showers, meteoroids, parent body search, video meteor observations

1. Introduction

The ongoing collection of multi-station video meteor orbits through 2013 had reached a point of statistical significance, such that it was time to revisit the search for new minor meteor streams as well as stream associations to potential new parent body candidates. Past searches for new meteor streams within orbital data bases can be found in Lindblad (1971a); Jopek et al. (2003); Svoreň et al. (2000) using photographic orbits, in Sekanina (1976) using radio meteors, and in Greaves (2000) using video derived orbits. In addition, many papers have also been published concerning the connections between meteor streams and either near-Earth asteroids or comets in Drummond (1981); Hasegawa et al. (1992); Jopek et al. (2002); Jopek (2011); Jopek and Williams (2013). Based on these and other previous successes, this work was initiated to re-examine minor meteor streams by utilizing a large

combined data base of video meteor orbits. The analysis was started by identifying a "seed" orbit to form the basis of a collection of associated meteors in Keplerian space. The definition of the seed orbit distinguishes the sections of this paper as follows. Section 2 concerns cometary associations to meteor streams using each individual comet's orbital parameters as a seed orbit, section 3 is similar in nature but starting with near-Earth asteroids (NEAs) as the seed orbits for the search, while section 4 involves a twist on past searches in that it treats each individual meteor as a seed orbit to look for associations amongst its neighbors and thereby find new and existing minor streams. Section 5 ends the paper with a brief summary of the findings.

Several data components are utilized in searches of this nature. For the near-Earth objects the latest complete set of orbital elements for both comets and NEAs were downloaded from the JPL small-body data base search engine JPL (2013) which contained 3205 comets and 8824 asteroids. These would provide the seed orbits for parent-body/meteor-stream associations. Clearly a statistically good sample of meteors is beneficial for this type of study, which was in the form of multi-station triangulated video meteor orbits. Since 2007, two independent video meteor camera networks have been monitoring the skies over Japan and Croatia, the SonotaCo Meteor Network and Croatian Meteor Network (CMN) respectively. As a result of five years of collection, their combined catalogues contain over one hundred thirty thousand meteoroid orbits comprised of 114,280 meteors from the SonotaCo data base and 19,372 meteors published by the CMN, spanning the years 2007-2011. References to the data bases can be found in SonotaCo (2009), SonotaCo (2013), Šegon et al. (2012), Korlević et al. (2013), and CMN (2013). Note that the video derived orbits fall between radar and photographic measurement accuracies, with the video's advantage being both a large statistical sample set to work from and possessing good quality Keplerian elements.

The processing approach breaks somewhat from the search methodologies employed in the past, particularly for the individual meteor based seed orbit. Previous studies have often relied on a "single meteor linking technique" dating back to Southworth and Hawkins (1963) and Lindblad (1971a). They begin with a meteor orbit and chain together orbitally similar meteors by treating the pairings independently. This was recognized as potentially suffering from long linked chains where meteors at either end of the chain, can end up being unrelated in their orbital parameters. Thus, tight orbital similarity criteria were applied to minimize this risk. Also in the past, the concept of starting from a single meteor and performing orbital similarity comparisons within a large data base, was considered too computationally burdensome for computer processing systems. This is no longer the case as the total computational time for this study amounted to just a few hours and the entire data base fit easily within modern day computer memory. It is a given that a large portion of the meteors in the analyzed data bases are in fact sporadics, but the authors recognized that a significant fraction of meteors are actually members of a stream and as such, they have neighbors within such a large data base to help form the initial mean orbit of a minor stream. Furthermore a search along the daily drift of the orbital elements in time is included to track the stream across

its entire activity period. The assumption is that each and every meteor orbit in the data base could be a potential seed orbit of a minor shower grouping and thus all should be checked for clustering.

A boot-strapping technique was employed that starts with either a single meteor orbit or a near-Earth object orbit as a starting seed. The process first finds meteors with nearly equivalent orbital parameters by applying the usual similarity criteria (described later) and grouping those meteors into a single mean orbit using arithmetic averaging. The new mean orbit is run against the entire meteor data base again and the process is repeated until an unchangeable set of meteors has been found. A converged mean orbital parameter set is calculated along with a mean solar longitude which is close in time to the peak flux.

The second phase takes the newly found mean meteoroid orbit near the time of peak flux, and searches outwards through the data base in solar longitude shifting by one degree wide bins. So for one day ahead, all meteors are D-criteria tested against the converged mean orbit that only fall within the next day's one degree solar longitude bin after the peak. Meteors meeting both the D-criteria and solar longitude bin constraints are averaged, forming a new mean orbit for the day after peak. The search continues by advancing another degree in solar longitude, again finding all meteors meeting the D-criteria constraint relative to the mean orbit of the day before, as well as falling within the one degree solar longitude bin width. This process continues stepping forward in time until the meteor counts in a one degree solar longitude bin falls below two. Then the same process is repeated starting at the time of peak flux and instead working backwards in time, one solar longitude bin at a time. No meteors are mixed in the mean orbits obtained per day since they are segregated by solar longitude bins of one degree width. This approach permits the association of meteors over a long activity profile to a common stream, and thus accounts for changes occurring in a stream's orbital elements over time. The advantage of the technique is that it adds meteors to a group that the similarity criteria may have rejected if only a single mean orbit was used to characterize the stream over its entire activity period.

Three orbital similarity criteria were used in tandem to provide a more robust level of restriction, such that meteors must meet all three thresholds to be grouped together. The classic D-criteria developed by Southworth and Hawkins (1963), and later updated by Drummond (1991) and Jopek (1993), were applied to each independent parent body orbit, meteor orbit, or mean orbit when compared against every available meteor orbit from the video data base, using thresholds of $D_{SH} < 0.15$, $D_D < 0.075$, and $D_H < 0.15$ respectively. These threshold values were selected based on suggestions in papers by various authors such as Lindblad (1971a), Lindblad (1971b), Jenniskens (2006), as well as others. The same threshold levels are used in all the processing, unless stated otherwise.

2. Cometary associations to meteor streams

In the first phase of the study, associations between cometary objects and meteor streams were investigated by starting with a comet as the parent body seed orbit, and candidate meteor orbits were extracted from the video data base by fulfilling

the three D-criteria simultaneously. From the resulting list of meteor groupings, when the initial meteor count in a group was higher than ten, the process continued with a search for a possible meteor shower as described previously. For each significant meteor grouping, the resulting orbital parameters, activity period, radiant drift, and other shower characteristics were recorded per degree of solar longitude, and then compared with the orbital parameters of known meteor showers from the IAU MDC database (see Jopek and Jenniskens (2011), Jopek and Kaňuchová (2014)). It is important to note that in some cases, this iterative pro-

Table 1. The list of comets associated to meteor showers as found by the search described in this paper. The number of meteor orbits associated with the particular comet satisfying $D_{SH} < 0.15$ criteria is given in the column "Meteors". Possible new showers found based on this analysis are labeled with a "*". Known showers potentially associated with a parent body are labeled with a "**".

Comet	Meteors	Shower
109P/Swift-Tuttle	5881	Perseids
55P/Tempel-Tuttle	140	Leonids
1P/Halley	998	Orionids,η Aquariids
C/1917F1(Mellish)	327	December Monocerotids
C/1861G1(Thatcher)	281	April Lyrids
8P/Tuttle	202	Ursids
C/1846J1(Brorsen)	110	December σ Virginids
3D/Biela	102	Andromedids
C/1771A1(Greatcomet)	86	July Pegasids
C/1739K1	85	Leonis Minorids
C/1987B1(Nishikawa-Takamizawa-Tago)	85	** ϵ Geminids???
169P/NEAT	74	α Capricornids
C/1979Y1(Bradfield)	74	July Pegasids
C/1911N1(Kiess)	64	Aurigids
45P/Honda-Mrkos-Pajdusakova	56	August δ Capricornids
C/1852K1(Chacornac)	53	η Eridanids
C/1964N1(Ikeya)	46	* July ξ Arietids
C/1983H1(IRAS-Araki-Alcock)	43	η Lyrids
249P/LINEAR	41	not an unique choice
73P/Schwassmann-Wachmann3	38	τ Herculids - not confirmed by this work
255P/Levy	32	* α Cepheids
C/1864N1(Tempel)	31	** δ Piscids
D/1770L1(Lexell)	31	North. μ Sagittariids
185P/Petriew	27	not an unique choice
C/1961T1(Seki)	25	December ρ Virginids?
P/2005JQ5(Catalina)	25	not an unique choice
C/1957U1(Latyshev-Wild-Burnham)	21	* κ Aurigids
21P/Giacobini-Zinner	19	October Draconids - not found in this search
C/1790A1(Herschel)	18	β Aurigids - not confirmed by this work
C/1853G1(Schweizer)	17	* γ Aquilids
C/1943W1(vanGent-Peltier-Daimaca)	17	November Hydrids - not found in this search
197P/LINEAR	16	not an unique choice
C/1862N1(Schmidt)	15	ζ Arietids
C/1975T2(Suzuki-Saigusa-Mori)	15	λ Ursae Majorids
C/2012C2(Bruenjes)	15	* θ Craterids
103P/Hartley2	14	not an unique choice
C/1939H1(Jurlof-Achmarof-Hassel)	14	* θ Cetids
C/1718B1	12	π Hydrids?
C/1870K1(Winnecke)	12	* 51 Andromedids
C/1948L1(Honda-Bernasconi)	12	* 55 Arietids
209P/LINEAR	11	* May λ Draconids
C/1966T1(Rudnicki)	11	—
222P/LINEAR	10	not an unique choice

cess did not produce a well converged and iteratively stable set of meteoroid orbits and therefore the seed comet was excluded as a possible parent body of a meteor shower. However, the search did find the existing known comet-stream associations as well as some new findings. Note there was a final check in the process, to ensure the link between the comet and the single meteors in the resultant meteor grouping were unique. Thus each individual meteoroid orbit in an alleged stream was compared with all known NEOs up through May 1, 2013, to test for orbital similarity to a parent object other than the comet under test.

The complete list of established and possible meteor showers associated with comets found by this search is given in Table 1. As would be expected, the major meteor showers such as the Orionids, Perseids, Leonids and several minor showers were connected to their previously known parent comets. In total, 21 comet parent bodies were reconnected to previously associated meteor streams, which provided evidence that the search method was functioning properly.

In some cases, the D-criteria distance between the "final" mean meteor shower orbit when compared to the cometary "seed" orbit, differed by more than the selected thresholds for D_{SH}, D_D and D_H. But this was likely due to the different dynamical evolution of both the meteoroid stream and the comet's orbit and would require full dynamical modeling of the two, to truly verify the parent-stream associations. Considering the fact that the initial comet's orbital parameters led us to the meteor shower, does suggest that there is some connection between the comet and the meteor stream. Meteor showers with discrepant D-criteria distances between parent and shower (π Hydrids and December ρ Virginids) have been labeled in Table 1 with a question mark after their name to highlight this difference. In addition, those comet cases where single meteors within the associated meteor shower grouping possessed orbital similarities to other NEOs, have been noted in the table as "not an unique choice", meaning that some other NEO may also be the parent body of that particular meteor shower.

Two new possible associations were discovered between cometary parent bodies and minor meteor showers currently listed in the IAU MDC working list, marked by a double asterisk "**" in Table 1. Those are comet C/1987B1(Nishikawa-Takamizawa-Tago) potentially tied to the ϵ Geminid meteor shower, as also found by Olsson-Steel (1987), and C/1864N1(Tempel) potentially connected to the δ Piscids.

More significant are possible links between comets and 9 previously unknown minor meteor showers, noted with a single asterisk "*" in Table 1. The associations cover a wide range of orbits including Jupiter family comets, Halley type comets, very long period comets, as well as comets on parabolic orbits, and span a full range of inclinations. This indicates that the approach does not suffer seriously from selection effects within the realm of cometary association, given the limitation that this is based on meteors sampled strictly at Earth's orbit.

One example of a new shower found by starting the search from a comet's orbital elements is shown in Figure 1, containing plots of the orbits of meteor stream members and radiant connected to comet C/1853G1(Schweizer). Comet Schweizer is a long period comet (approximately 780 year period) having a de-

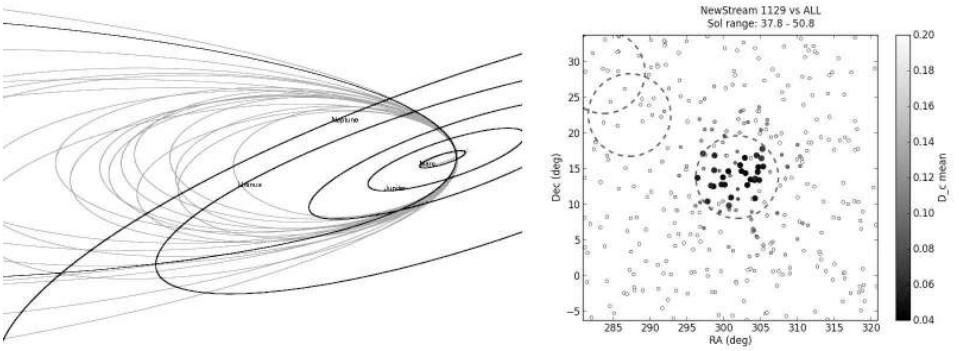

Figure 1. Meteoroid orbit plot (left) for the new stream members associated with comet C/1853G1(Schweizer). The comet's orbit is the black line. The corresponding radiant plot is given on the right side. The difference in D_C to the mean shower orbit is coded with shades of gray where the black end of the scale indicates a high similarity of orbital elements.

scending node distance from Earth's orbit of 0.07 AU, which favors the possibility that we are observing meteors coming from that parent body. Another very interesting discovery are meteors possibly originating from the extremely long period comet C/1939H1(Jurlof- and Achmarof-Hassel) for which were found two associated meteor showers. This comet has nodal crossing distances with respect to Earth's orbit of 0.04 AU and 0.07 AU at the ascending and descending nodes respectively. The two meteor groupings have extremely similar angular orbital parameters, lending credence to our strong opinion that both meteor showers found are really connected to this comet. Due to the small number of meteors found in the search, the second possible meteor shower has not been listed in Table 1.

3. Asteroidal associations to meteor streams

The search for asteroidal connections to meteor streams is more complicated as indicated by previous studies in this arena by Jopek et al. (2002) and others. First, there are many more known NEAs than comets which increase the odds of a chance alignment with a group of meteors. Second, many asteroids have very similar orbits and have been conjectured to be grouped into families, which could effectively span a larger subspace in orbital elements and impose a larger D-criteria threshold (at the moment the existence of families for NEO asteroids is still debated, see for instance Jopek (2011) and Schunová et al. (2011) for both positive and negative opinions). Third, there is an issue of the reliability of the D-criteria used above, due to the existence of large variances in some Keplerian elements arising from low inclination orbit comparisons - a common attribute of NEAs.

Despite these short-comings, this first look at NEA to video meteor stream association was undertaken in the same way as was done for the study of comets above. That is, each NEA is taken as a seed orbit to search for similar orbits amongst the video meteor data base. This resulted in many possible connections when run

Table 2. The list of asteroids with inclination over 15^o associated to meteor showers as found by the search described in this paper. The number of meteor orbits associated with the asteroid is given in the column "Meteors", representing counts for $D_{SH} < 0.15$.

Asteroid	Meteors	Asteroid	Meteors	Asteroid	Meteors	Asteroid	Meteors
3200 Phaethon	8250	2005GE59	31	2004SA	25	2003CQ20	19
2011XA3	213	2002LV	31	2001XU	25	2011GE62	19
2010DG77	53	2011SZ15	30	2013FC8	24	2006TA8	19
2009ST103	47	2009QJ9	30	2013HH19	23	2008GV	19
2000CO33	44	2009VP44	30	2003BK47	23	2010HZ104	18
2001MG1	44	2013EW27	28	2001WH1	22	2001SS287	17
2004UE	42	2008EC69	27	2010TK167	21	2007XN	17
2004CL1	40	2009AD16	26	2010QA5	21	2008TB	17
2007LQ19	36	2005JA45	26	2010UG7	20	2004BE68	15
2010JN71	32	2002JY8	26	2008HK	20	2011FQ17	15
2001XQ	32	2008DD	25	2012KU42	20		

with the same thresholds of D-criteria used previously. In several cases, the low-inclination orbits failed to produce a stable, convergent set of meteors. The D-criteria performance analysis by Galligan (2001), as well as an analysis done by Porubčan et al. (2004) suggests that for inclinations below 10 degrees, a tighter threshold should be used (0.09 and 0.12 per cited paper respectively). Asher et al. (1993) suggests that different D-criteria entirely should be applied for low inclined orbits such as the Northern and Southern Taurid showers, but for the opposite reason, to allow a wider spread in longitude of perihelion. In order to avoid erroneous NEA to meteor stream associations for the similarity criteria thresholds set for this study, the search was limited to asteroids with inclinations higher than 15 degrees. The list of asteroids with the number of associated meteors from the video data base is given in Table 2. As would be expected, the most striking asteroid-to-meteor shower connection is clearly revealed by this search: the asteroid Phaeton and the Geminids meteor stream. Besides Phaeton, our search revealed a possible association between a new meteor shower and asteroid 2001XQ. Since this asteroid lies on an orbit typical for Jupiter family comets, it could be possible that 2001XQ is not an ordinary asteroid, but a dormant comet or extinct comet nucleus.

4. Minor showers found within the video meteor data base

The minor meteor shower search through the video meteor data base was based on the same procedures as used in the NEO search except for two differences. The meaning of the parent body "seed" orbit was modified to represent one of the meteor orbits in the data base rather than an NEO. This essentially states that a single meteor itself is a good starting representative of the mean orbit of a stream, such that given a large data base and comparing every seed meteor to every other meteor, a significant number of similar orbit meteors will combine to form a mean orbit in the first pass through the data (modern computer systems make this level of processing possible on over 130,000 orbits). As before, if the number of meteors satisfying all three D-criteria thresholds was higher than 10, that seed meteor was assigned an associated count and stored in a running list. The process continued evaluating all possible meteors in the data base (each essentially assigned as a seed

Table 3. The list of showers from the IAU MDC list (as of 1st August 2013) found by the second search run. The meteors were claimed to be associated to the particular shower if $D_{SH} < 0.15$, $D_H < 0.15$ and $D_D < 0.075$ are satisfied simultaneously. The number of meteor orbits associated with the particular shower is given in the column "Meteors".

Code	No.	Shower Name	Meteors	Code	No.	Shower Name	Meteors
GEM	4	Geminids	7612	CAN	411	c Andromedids	36
PER	7	Perseids	6289	ACB	429	α Coronae Borealids	35
ORI	8	Orionids	4710	MLE	438	μ Leonids	34
LEO	13	Leonids	1119	SSS	168	Southern σ Sagittariids	33
QUA	10	Quadrantids	996	AMO	246	α Monocerotids	33
NTA	17	North Taurids	895	NAS	483	November α Sextantids	32
HYD	16	σ Hydrids	888	ZCY	40	ζ Cygnids	29
COM	20	Comae Berenicids	814	LUM	524	λ Ursae Majorids	29
STA	2	South Taurids	682	GAQ	531	γ Aquilids	29
ETA	31	η Aquariids	488	NIA	33	North ι Aquariids	28
SDA	5	South δ Aquariids	439	ZAR	193	ζ Arietids	28
FTA	286	ω Taurids	409	OUI	241	October Ursae Minorids	28
CAP	1	α Capricornids	351	TPY	340	θ Pyxidids	28
MON	19	December Monocerotids	319	NSA	67	North μ Sagittariids	27
SPE	208	September ϵ Perseids	280	CTA	388	χ Taurids	27
LYR	6	April Lyrids	270	THA	390	November θ Aurigids	27
URS	15	Ursids	258	AUP	415	August Piscids	27
KCG	12	κ Cygnids	232	FPL	501	February π Leonids	27
NOO	250	November Orionids	226	XHE	346	x Herculids	26
JCO	90	January Comae Berenicids	156	BAR	434	β Arietids	26
ORN	256	North χ Orionids	146	GBO	104	γ Bootids	25
EGE	23	ϵ Geminids	142	BCN	232	Dayt. β Cancrids	25
ZCS	444	ζ Cassiopeiids	135	GUM	404	γ Ursae Minorids	25
AND	18	Andromedids	132	FMV	516	February μ Virginids	25
ERI	191	η Eridanids	120	UUM	527	υ Ursae Majorids	25
DSV	428	December σ Virginids	113	UAN	507	υ Andromedids	24
EHY	529	η Hydrids	113	FLY	511	15 Lyncids	24
DKD	336	December κ Draconids	112	FOA	534	51 Andromedids	24
XVI	335	December χ Virginids	104	BAQ	519	β Aquariids	22
BCD	268	β Cancrids	101	DAB	497	December α Bootids	21
JPG	462	July γ Pegasids	92	DSE	34	δ Serpentids	20
LMI	22	Leonis Minorids	89	PDF	45	ϕ Draconids	20
NUE	337	ν Eridanids	89	OCT	281	October Camelopardalids	18
OER	338	o Eridanids	78	AIC	505	August ι Cetids	18
AHY	331	α Hydrids	75	OLE	515	o Leonids	18
HVI	343	h Virginids	75	ALO	517	April λ Ophiuchids	18
PPS	372	ϕ Piscids	73	FHE	345	f Herculids	17
NDA	26	North δ Aquariids	70	MPR	435	μ Perseids	17
DAD	334	December α Draconids	70	AED	450	April ϵ Delphinids	17
POR	430	September π Orionids	66	XCB	323	ξ Coronae Borealids	16
KUM	445	κ Ursae Majorids	65	ARC	348	April ρ Cygnids	16
DRV	502	December ρ Virginids	65	CVN	403	Canum Venaticids	16
ECV	530	η Corvids	64	JIP	431	June ι Pegasids	16
AUR	206	Aurigids	63	JEC	458	June ϵ Cygnids	16
NPI	215	North δ Piscids	63	DEL	494	December Lyncid	16
PSU	339	ψ Ursae Majorids	63	JLE	319	January Leonids	15
DXL	204	Dayt χ Leonids	61	THC	535	θ Cetids	15
DLI	47	μ Virginids	55	TAH	61	τ Herculids	14
GDR	184	July γ Draconids	53	KSE	27	κ Serpentids	13
JRH	463	July ρ Herculids	52	XLI	140	April χ Librids	13
TCA	480	τ Cancrids	52	MIC	370	Microscopiids	13
ELY	145	η Lyrids	50	RPU	512	ρ Puppids	13
JBO	170	June Bootids	49	UCE	194	υ Cetids	12
SLY	81	September Lyncids	48	SCA	179	σ Capricornids	11
BAU	210	β Aurigids	48	SPI	216	South δ Piscids	11
DPI	410	δ Piscids	47	OMO	227	October Monocerotids	11
DMH	498	December μ Hydrids	47	GCM	395	γ Canis Majorids	11

Table 3. Continuation

Code No.	Shower Name	Meteors	Code	No.	Shower Name	Meteors
ICY 525	ι Cygnids	46	NBO	432	ν Bootids	11
NHY 121	ν Hydrids	45	NZT	485	November ζ Taurids	11
KAU 537	κ Aurigids	45	MBC	520	May β Capricornids	11
PIH 101	π Hydrids	44	DSX	221	Dayt. Sexantids	10
DCL 443	December Leonids	44	AAL	448	April α Librids	10
AGC 523	August γ Cepheids	44	FFA	538	55 Arietids	10
ASC 55	α Scorpiids	43	AAN	110	α Antliids	9
OCU 333	October Ursae Majorids	41	SSA	237	σ Arietids	9
XUM 341	January ξ Ursae Majorids	38	DCM	398	December Canis Majorids	9
NLY 437	November Lyncids	38	JMC	362	June μ Cassiopeiids	8
AXC 465	August ξ Cassiopeiids	38	AHE	518	April 102 Herculids	7

orbit). This first pass produced a very long list of possible meteor groupings (they are not referred to as potential showers in this stage of analysis), having in all 56,486 meteors out of the 133,652 meteor orbits available, which were assigned into one of 3,172 groups.

The second pass through the data base attempted to avoid contamination of minor streams by major showers and is the other modification to the process. In count sorted order from highest to lowest, each running list meteor orbit was again assigned as a seed orbit, and the more extensive processing discussed in the introduction was applied to estimate the daily mean orbital estimates across the stream's activity period. Thus sweeping up all meteors associated with a particular shower. These were then removed from the pool of available meteor orbits before the next lowest count meteor orbit on the running list was set up as the new seed orbit. The process continued until all meteor seeds with significant counts had been processed. The remaining meteors in the pool effectively make up the sporadic meteor population.

After the second pass, the mean orbital parameters for some groups were found to be very similar to other groupings, so each group's mean orbital values were compared to all the other groups. These similarities were likely due to the poorly estimated orbital parameters of single meteors falling just outside the D-criteria of a given group. If a test group contained a smaller number of meteors than a reference group, and also had mean orbital parameters fulfilling a somewhat relaxed D-criterion relative to the reference group, that test group was excluded from further analysis. The similarity threshold was set to the slightly higher values of $D_{SH} < 0.20$, $D_D < 0.10$ and $D_H < 0.20$ to perform this culling. These thresholds were selected to ensure that potentially close but distinct groups of orbits, remain on the list for further analysis. However, this process did cull the number of groups significantly, leaving a total of 1,093.

To verify if this processing yielded valid streams, we compared the results with the data for existing meteor showers already listed in the IAU MDC database. The potential matching was done in one of two ways. The first was by means of an orbital similarity test for cases where the orbital parameters were also available for showers in the MDC. For each group found in the video data base search, the D_{SH}, D_D and D_H values were calculated against all the meteor showers in the MDC list and reported when $D_{SH} < 0.15$, $D_D < 0.075$ and $D_H < 0.15$. The second

matching method was applied in cases where the mean orbital parameters were not available from the IAU MDC, where the MDC only contained the right ascension (RA), declination (DEC) and solar longitude at the time of maximum activity. In those cases, the radiant drift values were obtained for each group from the video meteor analysis, and the radiant's RA and DEC values were calculated for the solar longitude of maximal activity given in the IAU MDC for a specific shower. If the resulting radiant separation was smaller than 5 degrees, the radiant distance as well as the shower IAU code name, were reported along with the group analyzed. Moreover, in order to ensure that some meteor groups found in this way were truly representative of a meteor shower, an interactive tool was developed to present various orbital element plots to an analyst, containing details on a variety of orbital parameter pairings to better visualize the association of meteors in each group's dataset.

If the orbital parameters for a given group matched a known meteor shower from the IAU MDC data base by one of the two methods above, and in addition passed the visual inspection for neighboring showers in the Keplerian subspace via the visualization tool, the group was declared to have been matched to a particular meteor shower. An example of such a group to known meteor stream matching is shown in Figure 2.

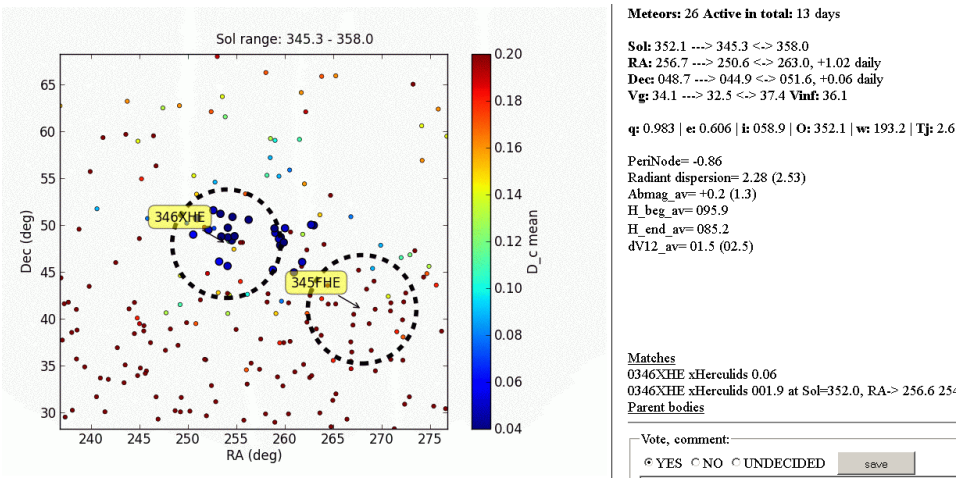

Figure 2. An example of one product from the data visualization tool used in the detailed group to shower matching. Existing shower radiants from the MDC are shown in dashed black circles while individual meteor orbit D-criteria distances are plotted as colored dots. Larger dots are for the grouped meteors alleged to be in a common stream.

The list of showers in the IAU MDC database (as extracted on August 1, 2013) that were also found by this search method is given in Table 3. For the 93 established meteor showers, this search confirmed the existence of 54 of them. Regarding the rest, in 6 cases the radiant lies below minus 30 degrees declination (thus making them very hard to detect in the northern hemisphere based CMN and SonotaCo data bases), 27 are daytime meteor showers, and the remaining 6 showers (South.

ι Aquariids, October Draconids, η Virginids, October Capricornids, α Lyncids and the February η Draconids) were not detected. The latter case is most likely due to their variable (and very low) activity level. Further details of the results from this search will be published in the near future and will include several dozen newly discovered streams. Stream parameters on a number of the most prominent new minor showers detected has already been sent to the IAU MDC and placed on their list of meteor showers awaiting validation as an established shower. A separate web page is being hosted by the CMN containing all the detailed plots and search results and will be made available to the public in the near future.

5. Conclusions

The current analysis has resulted in the confirmation of existing relationships between known meteor showers and parent bodies, as well as several new associations of statistical significance that are in need of further study. The search methodology employed of using a parent body "seed" orbit to identify potential meteors on similar orbits through the use of a large meteor orbit data base, is highly effective for verifying existing parent-body to meteor shower associations as well as quantifying the duration and Keplerian element temporal behavior of meteor streams. This search resulted in findings of new possible meteor shower to parent body connections which were not known previously. The reasons why the new associations between comets and meteor showers may not have been found during previous searches (e.g. Drummond (1981)) is likely due to the different types of data samples searched, the size of the meteor orbit data bases, or searches based on less accurate orbits obtained from radar observations.

An important point to emphasize is that all these new findings need to be checked via dynamical modeling of hypothetical meteor streams produced by any connected parent body to validate they are truly associated to the actual streams found. In addition, this work can be extended to include the growing number of meteor orbit databases, which will also help to validate the results of this search.

Finally, we found a large number of very low flux meteor showers potentially associated with both asteroids and comets, where additional sample support is needed for confirmation. We hope that in the near future with further multi-station meteor orbit data base growth and the publication of the CAMS system data by Jenniskens et al. (2011), which contains higher accuracy meteor orbits dating back to November 2010, the additional candidate associations can be verified.

Acknowledgements

The authors would like to acknowledge all members of Croatian Meteor Network (CMN), in alphabetical order (first name first): Alan Pevec, Aleksandar Borojević, Aleksandar Merlak, Alen Žižak, Berislav Bračun, Dalibor Brdarić, Damir Matković, Damir Šegon, Dario Klarić, David Gostinski, Dejan Kalebić, Denis Štogl, Denis Vida, Dorian Božićević, Filip Lolić, Filip Novoselnik, Gloryan Grabner, Goran Ljaljić, Ivica Ćiković, Ivica Pletikosa, Janko Mravik, Josip Belas, Korado Korlević, Krunoslav Vardijan, Luka Osokruš, Maja Crnić, Mark Sylvester, Mirjana

Malarić, Reiner Stoos, Saša Švagelj, Sonja Janeković, Tomislav Sorić, VSA group 2007, Zvonko Prihoda, Željko Andreić, Željko Arnautović, Željko Krulić.

This work was partially supported by the Ministry of Science, Education and Sports of the Republic of Croatia, Faculty of Mining, Geology and Petroleum Engineering, University of Zagreb, Višnjan Science and Education Center and by private funds of CMN members.

References

Asher D.J. et al., 1993, MNRAS 264, 93
CMN download page, 2013, http://cmn.rgn.hr/downloads/downloads.html
Drummond J.D., 1981, Icarus 45, 545
Drummond J.D., 1991, Icarus 89, 14
Galligan D.P., 2001, MNRAS 327, 623
Greaves J., 2000, Radiant 22, 27
Hasegawa I. et al., 1992, PASJ 44, 45
Jenniskens P., 2006, Meteor Showers and their parent comets, Cambridge University Press
Jenniskens P. et al., 2011, Icarus 216, 40
Jopek, T.J., 1993, Icarus, 106, 603
Jopek, T.J., Valsecchi G.B., Froeschle Cl. , 2002, Asteroids III, Univ. of Arizona Press, Tuscon, 645
Jopek, T.J., Valsecchi G.B., Froeschle Cl., 2003, MNRAS 344, 665
Jopek T.J., Jenniskens P., 2011, Proc. Meteoroids Conf., held in Breckenridge, Colorado USA, May 24-28, 2010, 7
Jopek T.J., 2011, EPSC-DPS Joint Meeting 2011, 15
Jopek T.J., Williams I.P., 2013, MNRAS 430, 2377
Jopek T.J., Kaňuchová Z., 2014, Proc. Meteoroids Conf., held in Poznań, Poland, Aug. 26-30, 2013, eds Jopek T.J., Rietmeijer F.J.M., Watanabe J., Williams I.P, AM University Press, Poznań, p. 353
JPL, 2013, http://ssd.jpl.nasa.gov/sbdb_query.cgi
Korlević K. et al., 2013, WGN 41:2, 48
Lindblad B.A., 1971a, Smithson. Contrib. Astrophys., No. 12, 14
Lindblad B.A., 1971b, Smithson. Contrib. Astrophys., No. 12, 1
Olsson-Steel D., 1987, MNRAS 228, 23p
Porubčan V. et al., 2004, EM&P 95, 697
Schunová E., 2011, EPSC-DPS Joint Meeting 2011, 1875
Sekanina Z., 1976, Icarus 27, 265
SonotaCo, 2009, WGN 37:2, 55
SonotaCo, 2013, http://sonotaco.jp/doc/SNM/index.html
Southworth R.B., Hawkins G.S., 1963, Smith. Cont. Aph. 7, 261
Svoreň et al., 2000, Planetary and Space Science 48, 933
Šegon D. et al., 2012, WGN 40:3, 94

Meteoroids 2013, Proceedings of the Astronomical Conference,
held at A.M. University, Poznań, Poland, Aug. 26-30, 2013,
eds Jopek T.J., Rietmeijer F.J.M., Watanabe J., Williams I.P.,
Adam Mickiewicz University Press in Poznań, pp 263–265

Comet outbursts and the meteor showers

Guliyev A.S.[1], **Kokhirova G.I.**[2], **Poladova U.D.**[1]

[1]Shamakhy Astrophysical Observatory of National Academy of Sciences of Azerbaijan, Azerbaijan
(ayyub54@yahoo.com)
[2]Institute of Astrophysics, Academy of Sciences of the Republic of Tajikistan, Dushanbe, Tajikistan

Abstract. The features of 116 comets that have shown an outbursts in their brightness, are considered in the paper. The hypothesis on that the outburst in activity of comets are caused by their passing through meteoroid streams is studied. For this purpose the orbital elements of such comets relative to the planes of motion of 68 meteor showers from Cook' catalogue are analyzed. It was found that four of the nearest and distant nodes of comet orbits relative to the planes of motion of nine meteor showers exceeds the average statistical background with confidence probability from 0.90 to 0.95, and more than 0.95, respectively. The October Draconids, Aurigids, κ-Serpentids, δ-Draconids, σ-Hydrids, Coma Berenicids, Leonids, Leo Minorids, and Perseids showers are the most effective. The results of calculation show that often, the comets outbursts may be caused by collisions of comets with meteoroids under the passing through the meteoroid streams that are producing listed meteor showers as well as solar activity.

Keywords: comets, comet outburst, meteor showers

1. Introduction

The notion that an outburst in activity of comets and even fragmentation of the nucleus caused by the passage of the comet through a meteoroid stream is quite old, Bosler and Roure (1937) suggesting the fragmentation of comet 3D/Biela was caused by its passage through the Leonid meteoroid stream. Babadzhanov et al. (1991) revisited this suggestion, concluding that it was unlikely that this was the cause of the fragmentation of 3D/Biela since it passed through the least populated part of the stream, the mechanism in general could be responsible for affecting the behavior of comets.

Williams et al. (1993) suggested the brightening of comet 1P/Halley at that time was caused by the passage of the nucleus through its own meteoroid stream, while Hughes and Williams (1998) had suggested that the surfaces of two asteroids, (951) Gaspra and (243) Ida was due to their respective passages through their own meteoroid streams.

The possible effects of comet nuclei passing through meteoroid streams was investigated again by Guliyev (2010). According to this hypothesis, the short-perihelion comet groups were formed as a result of a collision of the proto-comet nuclei with meteoroid streams. Such impacts can result in the disintegration of the nucleus and also produce a short-time brightness increase through the opening of the part of comet nuclei's surface.

2. Objects and target of investigation

The data on 116 events where brightness outbursts, took place as well as on the appearance of large structures in comets comas were investigated. Some of the data was taken from the catalogue of Andrienko and Vashenko (1981) and some outbursts were observed at the Shamakhy Astrophysical Observatory and reported in Guliyev and Rustamova (2005); Guliyev et al. (2007). The point of the investigation is to analyze the distribution of the dynamic parameters of comets that experienced outbursts compared to the planes of orbits of 68 known meteor showers. The data for the showers was taken from the catalogue of Cook (1973).

3. Method

The method of study is the same that was used in Guliyev and Dadashov (2009). At the first stage using the equations of spherical astronomy the orbital elements of outburst comets are calculated relative to the orbital plane of the each meteor shower. The ascending node of the given shower orbit is taken as the initial point for calculation of the angular orbital elements. The heliocentric distances of both nodes of the comets orbits are then calculated and the number of comet nodes, (N) which lie close to the shower orbit is calculated. By varying the longitude of the ascending node Ω and the inclination i of the selected meteor shower orbit a set of "pseudo-showers" was generated, and the above calculation repeated.

The number of nodes n_i found by this way are comparing with the value of N using the relevant methods of mathematical statistics. Values of Ω in the range 0 to 330 deg. were considered in steps of 30 deg., while the inclination i vary from 0 to 90 deg. with the steps used so that the poles of corresponding planes on the celestial sphere are equidistant each from other. As a result, of the calculations,as well as N and n_i the following values are determined: n, σ, t, and α – the mean value of n_i within the 67 areas under consideration, the standard ratio $t = (N - n)/\sigma$, the dispersion and the confidence probability, respectively.

4. Results of calculations

The distribution of both the nearest and distant nodes of the outburst comets relative to the planes of 68 meteor showers listed in the catalogue of Cook (1973) was considered by using the above described method. Initially, the accepted range of values for the nodes was taken as the shower's size from the perihelion to aphelion. As a rule, a stream excluded from the consideration if the value of the range was less than 1. If it lies between 1 and 1.67, then the initial interval should decreased. As a result, out of the initial 68 showers, 12 are of interest and their detail results are given in Table 1. As it is seen from the Table 1, the values of t relatively to (q, Q) are significant in five cases. Their confidence probabilities α exceed 0.95. The results on t may be considered as satisfactory for eight cases if their initial ranges are narrowed. Obviously, the secondary ranges often lie close to the perihelion of orbits where the showers particles density increases. The October Draconids meteor

Table 1. The results of calculations on meteor showers.

Meteor shower	q [AU]	Q [AU]	Ω [deg]	i [deg]	t_{near}(q,Q)	$t_{near}(r_1, r_2)$	t_{dist}(q,Q)	$t_{dist}(r_1, r_2)$
δ-Draconids	0.996	4.54	14.4	37.5	-	-	2.10	-
κ-Serpentids	0.450	-	14.7	64.0	-	-	-	2.23(q;4.0)
ϕ-Bootids	0.950	1.55	40.7	19.0	-	-	1.84	-
April Lyrids	0.919	55.08	32.4	79.0	-	2.04(q;1.14)	-	-
D. ζ-Perseids	0.340	2.86	78.7	0	1.67	-	-	-
Perseids	0.953	55.05	139.7	113.8	1.89	-	-	-
Aurigids	0.802	-	158.6	146.4	-	-	-	2.8(2.3;3.8)
Oct. Draconids	0.996	6.02	197.0	30.7	-	3.35(q;1.18)	-	-
Leo Minorids	0.650	116.6	211.7	124.0	-	-	-	1.8(1.3;3.2)
Leonids	0.985	22.02	235.2	162.6	-	-	-	1.7(2.1;3.3)
σ-Hydrids	0.244	59.76	79.7	125.5	-	-	2.12	-
C. Berenicids	0.580	-	282.7	134.0	-	2.4(.62;1.80)	-	-

shower is especially effective because its value of t is equal to 3.35. The Aurigids shower develops nearly the same ($t = 2.8$).

5. Conclusions

The reported results confirm that the collision with the meteoroid streams listed may be responsible for the outburst in the activity of some comets. A passing through the showers dense layers may lead to a partial renovation of the comet nucleus surface due to impacts of the particle. As a consequence the sublimation activation increases. The hypothesis is supported by the observational data confirming the existence of great number of craters on the comets nuclei surface that were photographed by the space missions during the last years. So, as further work, it is necessary to study possible association of the comets outbursts with the meteor showers, which are not included into the catalogue of Cook.

Acknowledgements

We would like to acknowledge the useful comments of the referee.

References

Andrienko D.A., Vashenko, V.N., 1981, Comets and the solar corpuscular radiation, Moscow, Izdatel'stvo Nauka 164, (in Russian)

Babadzhanov P.B., Wu, Z., Williams I.P., Hughes D.W., 1991, MNRAS, 253, 69

Bosler J., Roure H., 1937, Journale des Observateurs, XX, 105

Cook A.F., 1973, in Evolutionary and Physical Properties of Meteoroids, eds: Hemenway, C.L., Millman, P.M., Cook, A.F., Washington, DC, NASA SP-319, 183

Guliyev A.S., 2010, Origin of short-perihelion comets, Baku, Publ. Comp. Elm, 151

Guliyev A.S., Rustamova U.J, 2005, Circular of ShAO, 110, 3

Guliyev A.S., Rustamova U.J., Churyumov K.I., Chubko L.V., 2007, Azerbaijani Astron. Jour., 3-4, 10

Guliyev A.S., Dadashov A.S., 2009, in Proc. IAU Sympos. No. 263, eds Fernndez J.A., Lazzaro D., Prialnik D. and Schulz R., Cambridge University Press, 5, 81

Hughes D.W., Williams I.P., 1998, P&SS, 46, 929

Williams I.P., Hughes D.W., McBride N., Wu, Z., 1993, MNRAS, 260, 43

Meteoroids 2013, Proceedings of the Astronomical Conference, held at A.M. University, Poznań, Poland, Aug. 26-30, 2013, eds Jopek T.J., Rietmeijer F.J.M., Watanabe J., Williams I.P., Adam Mickiewicz University Press in Poznań, pp 267–273

Two mechanisms of the ejection of meteoroids from comets

Gronkowski P.[1], **Wesołowski M.**[1]

[1]Faculty of Mathematics and Natural Sciences, University of Rzeszów, Pigonia 1 Street, 35-310 Rzeszów, Poland (gronk@ur.edu.pl)

Abstract. The mechanisms of the ejection of meteoroids from comets are reviewed. We focused on two questions. The first one is related to the dragging of dust-ice particles by molecules of gases which sublimate from a cometary nuclei. The second one is related to jets from cavities in nuclei of comets. In the presented work maximal size of cometary particles which can be lifted from the cometary nuclei in different heliocentric distances by gentle sublimation and the jets of cometary geysers was examined.

Keywords: comets, dust, meteoroids

1. Introduction

There are known a several ways of ejection of particles from cometary nuclei:

1) dragging of cometary particles by outflowing molecules of gases released by sublimation from the surface of the cometary nucleus,
2) jets from the cavites in nucleus,
3) electrostatic levitation,
4) rocket-mechanism.

In this paper we focused on two first mentioned above mechanisms. The first mechanism has been well-known for many decades and wide described in the literature. Contrary, the second mechanism was seen only in the last few years due to space missions. Occurrence of geysers-like phenomena in the form of strongly colimated jets of gas and dust are recently reported for a few comets. On September 21, 2001 the spacecraft Deep Space 1 approached the nucleus of Comet 19P/Borrelly at a distance about 2170 km. The nucleus of this comet, coma and dust jets were pictured by onboard camera. A main jet which dominated in the near-nucleus coma was emitted from a broad central cavity and it had geyser-like form (Yelle et al. 2004 and literature therein). On 2010 November 4 the Deep Impact spacecraft in the frame of the EPOXI mission visited the nucleus of Comet 103P/Hartley (A'Hearn et al. 2011). On the excellent quality images performed by spacecraft camera, are visible bright geyser-like jets. NASA's astronomers stated that this was the first time in history of cometary researches that comet activity dominated by sublimation of carbon dioxide was observed so close to the Sun (1.06 AU). The nucleus of this comet was surrounded by clouds of large number of water ice relatively large particles which were ejected from nucleus by geyser-like jets of CO_2 (Gronkowski et al. 2011). Also long-standing observations of famous Comet 29P Schwassmann-Wachmann 1 revealed fact that the activity of this comet is

related with number of jets produced by its nucleus (Ivanova et al. 2011 and literature therein). The paper presented here is just the development of the work by Gronkowski et al. 2011. This aim of the presented paper is to compare the effectiveness of two mentioned above mechanisms of ejection of meteoroids from comets.

2. Gentle sublimation

In the first step of our considerations we determine the maximum radius of a cometary grains $a_{\max}$ which are lifted from the surface of a comet as the results of gentle sublimation of cometary volatile species. Dynamics of dust-grains laying on the surface of cometary nucleus is determined by the following forces: gravitation of a comet nucleus, drag force coming from the cometary gases and the centrifugal force related with the rotation of a comet nucleus. Other forces acting on the grains like solar tidal force (which is the product of the Sun gravitation and inertia force related with orbital motion of a comet), solar radiation force and Coriolis force are negligible for the considered large grains sized in the range of several centimetres. It is easy to show that the condition for $a_{\max}$ has the following form:

$$\frac{1}{2}C_{\mathrm{D}}\pi a_{\max}^2(v_{\mathrm{g}}-v_{\mathrm{gr}})^2\rho_{\mathrm{g}}+m_{\mathrm{gr}}\omega^2R_{\mathrm{N}}cos^2\phi=\frac{GM_{\mathrm{n}}m_{\mathrm{gr}}}{R_{\mathrm{N}}^2}. \tag{2.1}$$

We note here that in the presented work the notation from paper Gronkowski et al. 2011 is adopted. Occurs in this equation parameter $\mathrm{C_D}$ is the modified free-molecular drag coefficient for spherical particles of size a_{max} and generally is given by the following expression:

$$C_{\mathrm{D}}=\frac{2s^2+1}{s^3\sqrt{\pi}}\exp(-s^2)+\frac{4s^4+4s^2-1}{2s^4}++\mathrm{erf}(s)+\frac{2\sqrt{\pi}}{3s}\sqrt{\frac{T_{\mathrm{gr}}}{T_{\mathrm{g}}}}. \tag{2.2}$$

It should be noted that the magnitude of "s" is the ratio of relative velocity between the gas and the grain with respect to the most probable velocity of the gas. Based on (Eq.(2.1)) we can express $a_{\max}$ by the following formula:

$$a_{\max}=\frac{9C_{\mathrm{D}}M\mu\dot{Z}v_{\mathrm{g}}}{32\pi G\rho_{\mathrm{gr}}\rho_{\mathrm{n}}R_{\mathrm{n}}(1-\frac{3\pi cos^2\phi}{G\rho_{\mathrm{n}}P^2})}. \tag{2.3}$$

3. Cometary geysers-like phenomena

The approach to the general problem of geyser-like phenomena for comets presented in this section is based on the author's model that was applied strictly to the case of geysers on 103P/H (Gronkowski et al. 2011). The model assumes that interior of a cometary nucleus is probably full of cracks, holes and cavities. The assumption that a cometary nucleus contains of mentioned above 'structural imperfections' seems to bee very reasonable. Firstly, holes and cavities can be relics from the times when the solar system originated and comets were formed due to mutual aggregation

of cometesimals of various sizes. Secondly, a different kind of cometary ices have a different rates of sublimation. Such way of cometary material sublimation favours the creation of holes and cavities in a nucleus. There are various hypotheses about

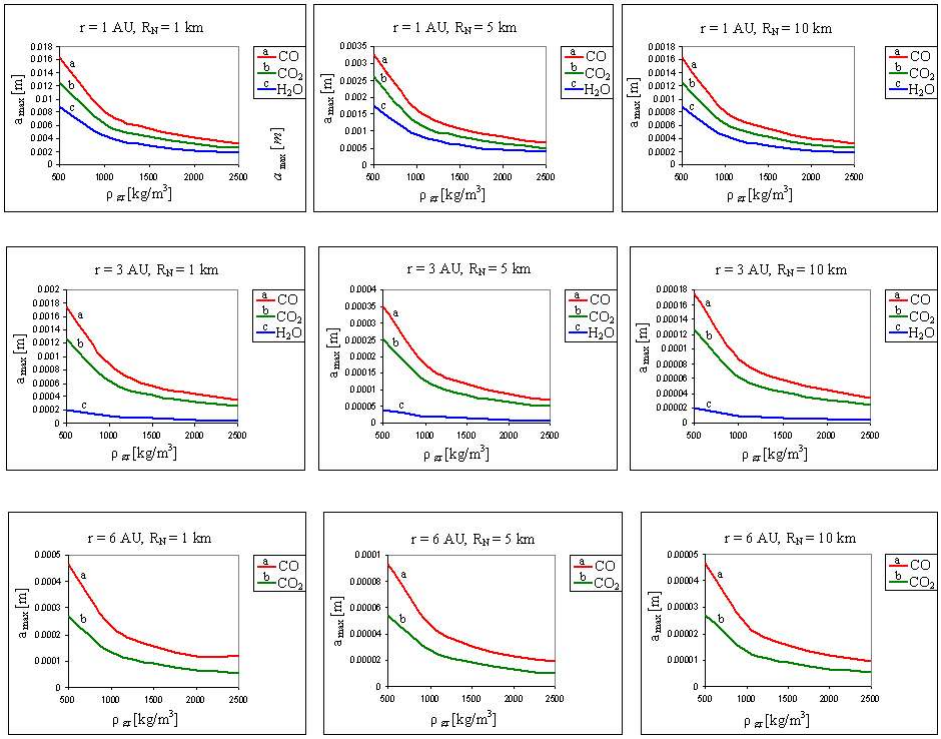

Figure 1. The maximal radii $a_{\max}$ (in meters) of grains lifted out from a comet nucleus by gentle sublimation as the function of their densities $\rho_{\rm gr}$ (kg/m^3), radii of nuclei $R_{\rm N}$, heliocentric distances of a comet r and kind of sublimating species. It was assumed that a cometary nucleus does not rotate.

the origin of comets nuclei. Only two of them are the most favoured. According to the first one the cometary embryos were created in the giant planet formation zone. Afterwards, comets nuclei were dynamical scattered by growing protoplanets to the region of the Ort cloud. Second hypothesis assumes that nuclei of comets were created as a result of direct accretion in the solar nebula at relatively large heliocentric distance. One way or the other the cometary nucleus is made up of an aggregate of 10-100 m 'cometesimals' and contains significant voids in the form of holes and caves in the intercometesimals regions. Holes and caves should have the size distribution that echoes the way in which the comet was created. The results of the EPOXI mission allow us to assume that the surface of geyser's cave could have been covered by more sublimation active species than water ice as carbon monoxide or carbon dioxide. Solar energy falling on the surface of a comet's nucleus is conducted into interior. Therefore, cometary ices in cavities could sublimate.

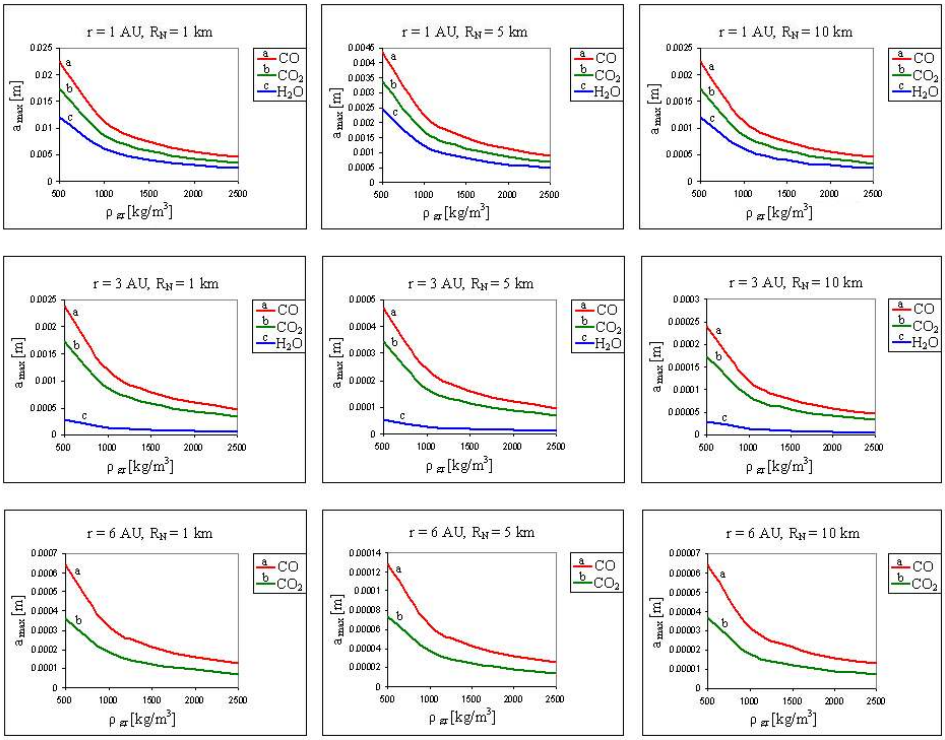

Figure 2. The same relation as in Fig.1 but for a rotating cometary nucleus with P=10^h.

Consequently there accumulated gases could escape outside through narrow cracks or channels. Finally, geysers-like phenomenon can be observed. The fundamental role in the description of physical conditions in a comet plays the energy balance equation at the surface of its nucleus. In this place we should bear in mind two cases:

(i) cometary ices sublime from the part of nucleus surface which is situated over the cavity of geyser,

(ii) this part of nucleus does not show any sublimation activity.

In the case (i) the energy balance equation has the following form:

$$A_{\mathrm{C}}\frac{S_0(1-A)\cos\theta}{d^2} = (A_{\mathrm{C}}-A_{\mathrm{MIN}})\left(\epsilon\sigma T_{\mathrm{s}}^4+\frac{\dot{Z}L(T)}{N_0}\right)+ \\ +(A_{\mathrm{C}}-A_{\mathrm{MIN}})h(\psi)K(T)\frac{\Delta T}{\Delta x}. \tag{3.1}$$

For the case (ii) we have following equation:

$$A_{\mathrm{C}}\frac{S_0(1-A)\cos\theta}{d^2} = (A_{\mathrm{C}}-A_{\mathrm{MIN}})\epsilon\sigma T_{\mathrm{s}}^4+(A_{\mathrm{C}}-A_{\mathrm{MIN}})h(\psi)K(T)\frac{\Delta T}{\Delta x}. \tag{3.2}$$

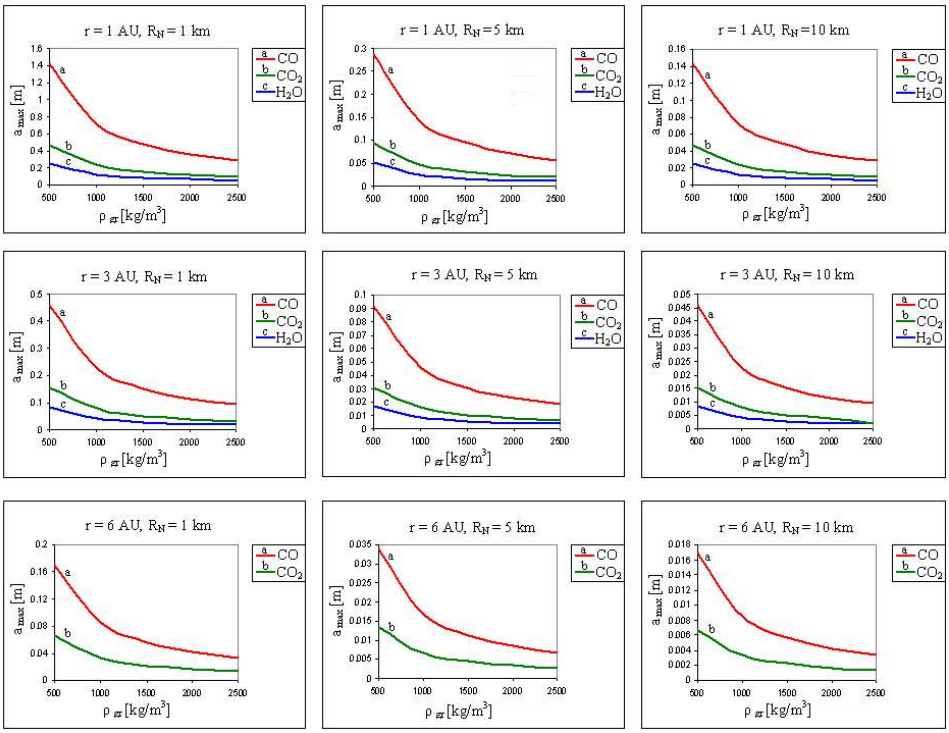

Figure 3. The same as in Fig.1 but for geysers-like phenomena.

In equations (3.1)–(3.2) the left sides stand for the absorbed by the nucleus solar radiation energy. The right side of equation (3.1) is a sum of the reradiated by nucleus energy, the energy used for the sublimation of cometary ices and the heat conducted into interior of the comet nucleus. In equation (3.2) the right side is the same as in equation (3.1) but the term related to the sublimation of cometary ices has been omitted. In the presented above equations $T_{\rm s}$ stands for the surface temperature of the nucleus, $\Delta T = T_{\rm s} - T_{\rm c}$ and $\Delta x = 10$m is the thickness of the crust of the cometary material over the cavity. Here T_c denotes the temperature inside the cavity. For simplicity we assume that all the heat conducted from the surface of the comet nucleus to the cavity is used for the latent heat of sublimation. By this assumption the following equation is valid:

$$L\dot{M} = (A_{\rm C} - A_{\rm MIN})h(\psi)K(T)\frac{\Delta T}{\Delta x}, \tag{3.3}$$

where $\dot{M}$ is the mass flux from the geyser (in kg/s units). In the sake of calculation the velocity of gas molecules $v_{\rm gey}$ in the jet at the exit of geyser we should use the Bernoulli equation:

$$\frac{1}{2}v_{\rm cav}^2 + \frac{\gamma}{\gamma - 1}\rho_{\rm cav} = \frac{1}{2}v_{\rm gey}^2 + \frac{\gamma}{\gamma - 1}\rho_{\rm gey}. \tag{3.4}$$

Here parameter γ denotes the ratio of the specific heats of flowing gas. The left side of this equation is dependent on the physical conditions in the cave and the right side is dependent on the physical condition at exit of geyser. Additionally, we should take into account the relation which results from the continuity equation:

$$\dot{M} = A_{\mathrm{MIN}} \rho_{\mathrm{g}} v_{\mathrm{gey}}. \tag{3.5}$$

In this way we have obtained two system of equations: (3.1), (3.3), (3.4), (3.5) for the case (i) and (3.2)–(3.5) for the case (ii). Both systems of equations should be solved together with the law of the ideal gas, adiabatic law and the equation of the state given by Clausius-Clapeyron formula. Moreover, dynamic relationship for molecules of gas escaping from the surface of comet into a vacuum should be taken into consideration. The condition for emission of large pieces of cometary material from geyser has analogical form as previously for gentle sublimation case. Therefore, the formula for the maximum radius $a_{\max}$ of cometary chunks which are lifted by geyser's jet from a comet has following shape:

$$a_{\max} = \frac{9 C_{\mathrm{D}} v_{\mathrm{gey}} (1-\alpha)}{32\pi G \rho_{\mathrm{gr}} \rho_{\mathrm{n}} R_{\mathrm{n}} (1 - \frac{3\pi \cos^2\phi}{G\rho_{\mathrm{n}} P^2}) \alpha L} h(\psi) K(T) \frac{\Delta T}{\Delta x}. \tag{3.6}$$

The parameter α stands for the ratio of minimum cross sectional area in the channel of geyser to the cross sectional area of the geyser's cavity ($\alpha = A_{\mathrm{MIN}}/A_{\mathrm{C}}$).

The results of calculations are presented in Figures (1)–(3).

4. Conclusions

In this paper two mechanisms of the ejection of meteoroids from comets are reviewed. The first one is gentle sublimation from comets. The second one are jets from cometary geysers-like phenomena. Taking into considerations Figs.(1)–(3) we simply can make some conclusions. Firstly, jets from the geysers can lift much larger pieces of cometary material in relation to the mechanism driven by gentle sublimation. Secondly, the most effective drag mechanism is controlled by CO sublimation and the least efficient mechanism is controlled by H_2O sublimation.

A lot of numerical tests related to calculations of $a_{\max}$ were carried out. These tests showed some interesting facts.

(a) The efficiency of 'drag mechanism' for geysers is strongly dependent on the model of the energy balance over the vicinity of geyser outlet. In the case of (ii) values of $a_{\max}$ are essentially larger in relation to the case (i). Therefore the Fig.3 presents the results only for the case (ii).
(b) The efficiency of 'drag mechanism' for H_2O sublimation in the heliocentric distance 6 AU is completely negligible.
(c) In the case of geysers the influence of a comet rotation for the value of $a_{\max}$ is negligible.

The calculations related with two mechanisms which potentially are capable of lifting out of cometary material from a nucleus of a comet into space are carried

out. It is shown that dragging mechanism can lift the dust grains out from cometary nuclei at maximum range of a millimetre. Contrary, supersonic jets emanating from geyser cavity can throw away from the comet large several centimetres sized pieces of water ice. The results of EPOXI mission to the comet 103P/H fully confirm this fact.

Acknowledgements

This work was partially supported by Centre for Innovation and Transfer of Natural Sciences and Engineering Knowledge.

References

A'Hearn M.F., et al., 2011, Sci, 332, 1396
Gronkowski P., Sacharczuk Z., Topolewicz S., 2011, AN, 332, 785
Ivanova et al., 2011, Icarus, 211, 559
Yelle R.V., Sonderblom L.A., Jokipii J.R., 2004, Icarus, 167, 30

Meteoroids 2013, Proceedings of the Astronomical Conference,
held at A.M. University, Poznań, Poland, Aug. 26-30, 2013,
eds Jopek T.J., Rietmeijer F.J.M., Watanabe J., Williams I.P.,
Adam Mickiewicz University Press in Poznań, pp 275–286

Dynamical modelling of meteoroid streams

Clark D.L.[1], **Wiegert P.A.**[1]

[1]Dept. of Physics and Astronomy, University of Western Ontario,
London, Ontario, N6A 3K7, Canada (dclark56@uwo.ca)

Abstract. Accurate simulations of meteoroid streams permit the prediction of stream interaction with Earth, and provide a measure of risk to Earth satellites and interplanetary spacecraft. Current cometary ejecta and meteoroid stream models have been somewhat successful in predicting some stream observations, but have required significant assumptions and simplifications. Extending on the approach of Vaubaillon et al. (2005a), we model dust ejection from the cometary nucleus, and generate sample particles representing bins of distinct dynamical evolution-regulating characteristics (size, density, direction, albedo). Ephemerides of the sample particles are integrated and recorded for later assignment of weights based on model parameter changes. To assist in model analysis we are developing interactive software to permit the "turning of knobs" of model parameters, allowing for near-real-time 3D visualization of resulting stream structure. Using the tool, we will revisit prior assumptions made, and will observe the impact of introducing non-uniform and time-variant cometary surface attributes and processes.

Keywords: meteoroid streams, modelling, software tools, visualization

1. Introduction

A pair of articles Vaubaillon et al. (2005a) and Vaubaillon et al. (2005b) describe a then-novel technique to separate the time consuming integration of numerous dust particles from the analysis of meteoroid stream structural change due to ejecta model manipulation. They accomplished this by generating a model independent uniform distribution of dust particles throughout multiple apparitions of a comet. These test particles are integrated forward multiple centuries, and the resulting ephemerides are stored. An ejecta model based on the work of Crifo & Rodionov (1997) and Jorda et al. (1992) was then used to assign frequency weights to each of these particles. Density profile change within a region and time of interest (typically near the Earth at the intersection of the stream with the ecliptic) can then be quickly re-evaluated based on the manipulation of model parameters and the resulting new frequency weights. The Vaubaillon work involves the generation and integration of 7 x 10^6 particles, where particles are binned across ejection direction, velocity and mass. In our work we also want to bin particles by albedo, as albedo impacts a particle's reaction to solar radiation and thus the evolution of the meteoroid stream. Therefore, we raise the expected number of particles to consider to order 10^8. In the following sections we discuss the implications of this population size. We will also introduce a variety of jetting, albedo, rotation and nucleus shape models, evaluating the simplifications of the Vaubaillon approach. Throughout, the software uses the abstract concept of a model to implement both the simulation of physical processes and the visualization of simulated results. The software

provides a consistent user interface for manipulating models while in real-time providing 3D visualization feedback on the resulting stream structure. We maintain a separation of the model itself from the operations of model definition, parameter manipulation, and real-time analysis and visualization. Therefore we are able to quickly adapt to fundamental model changes or replacements.

2. The Challenges

The viability of this project depends on the ability to manipulate physical models of ejection and cometary state, visually verify the near-nucleus local impact of the model changes, and visualize the long-term impact on the meteoroid stream structure, all in near-real time. We therefore began project implementation by prototyping various aspects of the software to ensure our rather lofty expectations could be met. We also want to quickly determine computer resources and/or approach changes which might be required to overcome performance obstacles. There are four primary challenge to this work: 1) can we manipulate arbitrary models in a user-interface with real-time visual feedback of the local impact? 2) can we generate and store the long-term ephemerides for the 10^8 particles in question? 3) can we quickly assign frequency weights to a population of 10^8 particles? and 4) can we visualize the impact of a model change on the meteoroid stream in a near-real time fashion?

2.1. Models and Model Manipulation

One of the goals of the project is to not only experience the impact of model parameter changes on a resulting meteoroid stream, but also to compare various models. It was recognized that there is great benefit in completely separating the implementation of a given model from the cross-model concepts of model manipulation and visual rendering of the stream impact. This realization lead to the abstracting of the concept of a model, having all models present a common interface for parameter manipulation and inspection, and having all models use a common interface for driving the 3D rendering of stream impact.

2.1.1. Common Model Manipulation

Any model can be thought of as 1) a collection of data values which may be constant (e.g. pi) or variable, and which are independent or dependent on other variables, and 2) algorithms to compute dependent model parameters from independent parameters or other dependent parameters. The software framework provides an implementation of a C++ model class which supports the definition of constant, independent, and dependent values, and the definition of C++ functions to perform model parameter calculations. All the user must do to implement a particular model is to define a set of parameters and write the parameter computation code. Parameter computations may optionally use Application Program Interfaces (APIs) to assign frequency weight distributions to the particle cloud and to manipulate the 3D rendering of the resulting stream. The implementation of the abstract model class and its use is described in Section 4, but as an example: to implement

a model which computes c = a + b, the user must define a new model class which is derived from the abstract model class, define three class members representing parameters (a, b, c), instantiate the parameters with a descriptive name for display (e.g. a, b, Result c, and write a single C++ function whose content is one statement c = a + b;. With the model defined in this way, a wealth of functionality is provided by the underlying abstract class, and the surrounding software framework:

- generated screen dialogs for the keying, selecting and inspection of model values,
- model value range limiting as part of the model definition,
- real-time calculation and inspection of dependent values as independent values change,
- the forced manipulation of dependent values, calculating a needed dependent value,
- the manipulation of independent values to arrive at a needed dependent value,
- uncertainty propagation throughout the model,
- model persistence (reading from a file, writing to a file),
- particle cloud weight distribution via a common API,
- 3D scene manipulation via a common API,
- a model multi-threading framework for smooth display updating during model changes,
- recording, undo, and playback of model changes,
- scripting of model changes.

2.1.2. Ejection Models

Various cometary dust ejection models have been used to seed the prediction of meteoroid streams: e.g. Whipple (1950); Brown et al. (1998); Vaubaillon et al. (2005a) based on the Crifo & Rodionov (1997). Although varying in complexity, each of these models may be used to generate frequency distributions of particles of specific attributes through multiple apparitions of a comet. The Vaubaillon model is the more complex in terms of model parameters, but it is still easily represented and manipulated in the auto-generated model interface. A sample display is seen in Figure 1.

2.1.3. Nucleus Shape Model

The shapes of very few cometary nuclei are known. We presume the shape of the nucleus influences the local production of dust, primarily due to localized shading of the surface by higher elevation points. The shape also impacts the direction of jets at any given epoch. Historically, celestial object shapes were expressed in a data file of surface radii over a grid of regularly spaced longitude-latitude values. The software supports the manipulation of such a grid via a shape model derived from the abstract model concept (See Figure 2). In this case, the definition of the shape model is not done by tedious coding of numerous parameters (the radius at each longitude / latitude), but is generated programmatically from a shape model file. The more common current shape model practice is to define an object shape as a set of surface points expressed in Cartesian coordinates. Triangular patches of surface areas are defined by a list of edges expressed as a pair of indices into the list of

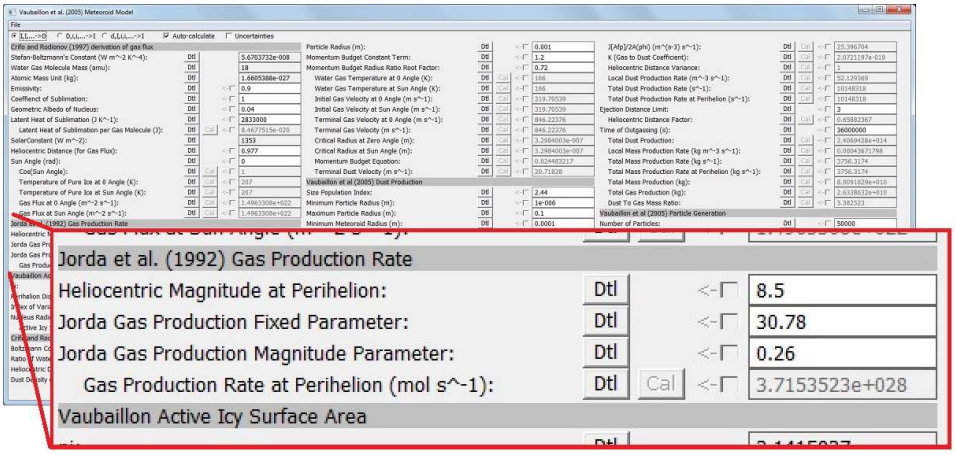

Figure 1. The model user interface and the Vaubaillon ejection model from Vaubaillon et al. (2005a) using Crifo & Rodionov (1997) and Jorda et al. (1992). The user interface is generated automatically from the model, and can support an arbitrary number of model parameters.

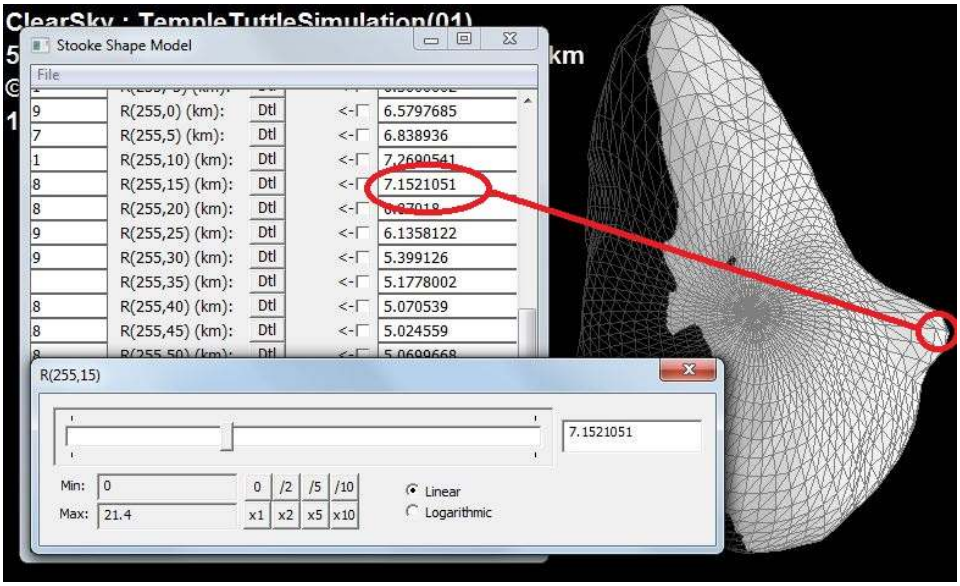

Figure 2. The shape of a cometary nucleus expressed as surface radii over a grid of regularly spaced longitudes and latitudes. Manipulation of the radii results in a real-time change to the visualization of the nucleus.

surface points. The generation of a shape model from this form of shape definition is under development.

2.1.4. Modelling Rotation

Rotation of the cometary nucleus provides an interesting degree of variability to local generation of dust, as active areas travel in and out of direct Sun exposure. This project will adopt known rotations of cometary nuclei, and in the case where rotation is not well known, will allow for the introduction of reasonable rotations to evaluate rotation impact on the generated stream. The rotation model used is a simple collection of any number of rotation axes expressed in right ascension and declination, with rotational period expressed in days, and an optional base line zero rotation epoch. The baseline epoch allows for the arbitrary setting of zero rotation at a given epoch, if a cometary orientation has been observed by some means. The control of the rotation is performed by a standard auto-generated model dialog, with a operation model parameter (described in Section 3), the display update pump, driving a simulated time step to the 3D rendering of the nucleus. In this way the user visualizes the rotating nucleus and the impact of the rotation changes, including the dynamic impact on jetting or broader more homogeneous dust production. Axis precession is not currently supported, but is recognized as a requirement. Precession definition will be added to each axes.

2.1.5. Modelling Jets

Diffuse and collimated dust jets have long been observed in images of cometary nuclei. Many models exist attempting to explain their behaviour. This project will not attempt to predict the existence of jets on a given comet; their presence can only be confirmed by direct observation of the nucleus or by non-homogeneous dust distribution in a comet coma and tail. This project will evaluate various aspect of simulated jets (size, diffusion, density, velocity) to evaluate whether jets have significant impact on the generated meteoroid stream, and whether that impact contributes to localized density difference in the stream, or whether the jetted particles are distributed along the comet orbit dampening those differences. Vaubaillon et al. (2005a) requires some restriction on the fan out of dust material in order to properly model observed Leonid meteor shower peaks, so there is reason to research this further. For the purpose of prototyping, we have used a simple jet model, allowing the user to define an arbitrary number of jets, each with a jet source diameter, fan-out half angle, dust generation rate, and dust ejection velocity. These jets may be positioned and modeled using the common model user interface (see Figure 3), with conical representation of the jets providing the visual feedback to the user that the desired jetting is being defined.

2.1.6. Modelling Dust Albedo

Although dust albedo is an important indicator of nucleus composition and evolutionary history, the interest in albedo for this project lies in the implications on meteoroid stream evolution. Darker albedo particles absorb more solar radiation and therefore are more affected in their orbital motion by radiation pressure. Whereas Vaubaillon et al. (2005a) used a fixed assumed dust albedo we permit both the interactive change of a cross-nucleus homogeneous albedo, and the surface mapping of various albedos. No prototyping of albedo modeling has yet been

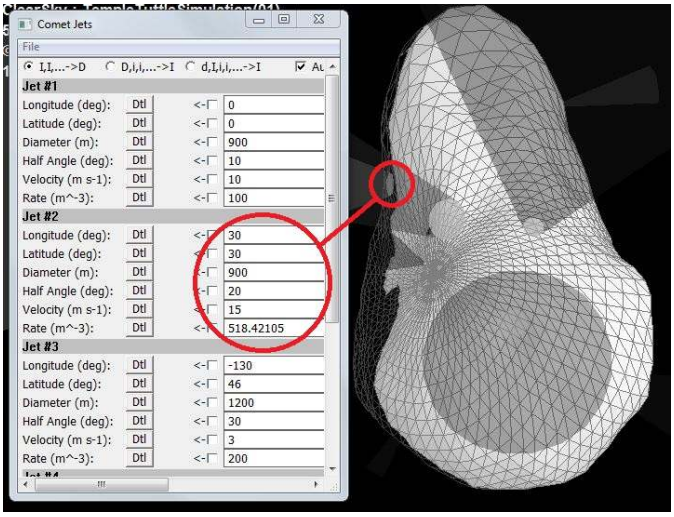

Figure 3. The modeling of comet jets, allowing the user to specify the position, surface diameter, fan out, dust velocity and dust production rate. The 3D rendering permits the visual verification of desired jet properties.

done. However, the confidence is high that this does not add performance concern to the project, as the specification of localized albedo may be maintained in exactly the same fashion as the comet shape, through a grid of albedos assigned to a longitude / latitude grid, or through the definition of small triangular patches of albedo value. The real-time feedback of the dust model change has been simulated through the implementation of visual property surface mapping of irregular objects (See Figure 4). The speed of visual feedback on the rotation of a surface object (including shadowing) is quite satisfactory. This is a greater complexity problem than albedo mapping, so we conclude the real-time feedback on albedo model changes will not be an issue.

2.2. The Generation and Storage of Ephemerides

Increasing the population size of our dust particles from Vaubaillon's 7 x 10^6 to 10^8 raised two areas of concern, the creation and integration of a much larger set of ephemerides (discussed here), and the need to be able to dynamically assign frequency weights to these particles in real-time as nucleus and ejection models are manipulated (discussed in the next section). The generation and management of the ephemerides seem manageable. From a storage perspective, we look at the data needed to represent a dust particle and its ephemeris. Considering the data which must be stored for each particle (particle ID, size, density (or mass), albedo, ejection epoch, heliocentric ejection direction, sun angle at ejection, ejection velocity) we assume 100 bytes per particle is an ample allocation. We therefore can estimate the size of the particle table to be approximately 10^2 X $10^8 = 10^{10}$ or 10 GB of data. Considering the ephemeris, we must store for each particle position the following: particle ID, epoch, position x, y, z, velocity vx, vy, vz. We can assume an upper

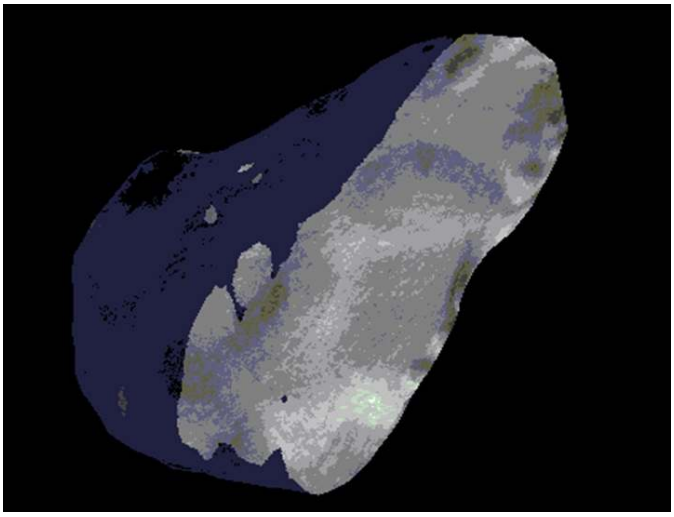

Figure 4. A surface mapping of visual images onto an irregularly shaped object, used as a proxy for gauging whether maintaining dust albedo distributions will be a performance concern for the project.

size of 10^2 bytes per particle ephemeris epoch. By maintaining sparse ephemerides which may be curve fitted around identified areas of interest, we would hope to restrict ephemeris sizes to 10^2 points per particle. In addition, the use of Chebyshev polynomials are also being considered to minimize the amount of data required to describe a particle ephemeris. Our upper bound estimate for the overall particle ephemeris storage for a given comet is 10^2 X 10^2 X $10^8 = 10^{12}$ or 1 TB of storage. This is an easily manageable amount of data.

We then turn to the computational resource required to generate the ephemerides for a single comet. Vaubaillon et al. document 10-50 processor weeks required for the generation of their ephemerides. Taking into account the approximately 15-fold increase in particle population size for this project, we would estimate 150-750 processor weeks on comparable hardware. With computational speed increases in current hardware over the past 10-years, and recognizing that several high-performance computation farms of >100 processors are available for use for this project, the integration requirements seem manageable (1-2 weeks dedicated use of 100 processors). Fortunately, integration is the one aspect of this project which does not need to be done near-real-time. This is a onetime computation expense that need not be repeated as physical models are manipulated.

2.3. Propagation of Weights

The real-time propagation of new particle frequency weights is the major computation hurdle to overcome. It would not be feasible to compute and reassign weights across 10^8 particle in real-time on a typical workstation. Here we must take advantage of the fact that at any given point in time, one is interested in a specific area of space (typically near the Earth) near a specific epoch (e.g. at a meteoroid

stream peak). This means that a substantially few number of particles need to have weights assigned as a model is manipulated. Considering the overall length of a typical comet orbit, and the tendency of particles to spread along an orbit, it seems reasonable that order 10^5 particles may need weight reassignment during a given analysis. Assigning weights to this number of particles, and displaying in real-time the impact of this weighting has been prototyped (See Figures 5 and 6). More research needs to be done to ensure the efficient selection of particles of interest. Particles are very easily selected based on ejection epoch, but selection on other particle attributes require more computation to determine if a model change disqualifies or qualifies particles

2.4. Visualization of Model Impact on Streams

As mentioned in Section 2.3, we are typically concerned with a particle population of approximately 10^5 particles at a given point in time. A prototype model was created to allow for the selection of 10^5 particles by their orbital element proximity to a changeable target set of elements. The model uses the common provided API for weight assignment. Updating the display on a workstation in real-time was achieved (see Figures 5 and 6).

3. Presentation and Operation Models

We have demonstrated that a model driven approach to real-time 3D rendering of stream impact is viable. We round out the discussion of models with brief comments of support models falling into two categories: visualization models and operational models. Visualization models are the controls which aid in the 3D visualization of celestial scenes, be they of the cometary nucleus, the meteoroid stream, or any other solar system context the user desires. These controls are implemented as derivations of the common abstract model, allowing for interactive scene manipulation, scripting of animations, and persistence of scenes to/from disk. There are three main visualization models developed or in planning: 1) a scene composition model indicating the target and eye of the scene (including anchoring the target and eye to an object, field of view, orientation, reference frames, visual adjustments for differing visualization media, time steps, etc.), 2) a particle colouration model permitting the dynamic assignment of colouration schemes to particle attributes and attribute combinations, and 3) a slicing model permitting the user to manage a planar slice tool with which one can perform cross-sectional analysis of a meteoroid stream (See Figure 7). The orientation of the slicing tool is managed independently from the scene manipulation model, allowing for maximum flexibility in visualizing stream structure.

Operational models are models which manage how user interactions are reflected in the modifications and display of other models. Operational models include 1) the shape impact curve model: a model which describes how the changing of a surface vertex impacts the surrounding environment on the nucleus surface. The user may specify the shape and extent of an impact curve, allowing the creation of realistic cratering, peaks, rifts, etc.; and 2) the rotation pump: a control of the simulated

time increments used to animate cometary nucleus rotation. Increasing the pump value increases the simulated time passage and therefore the apparent displayed rotation.

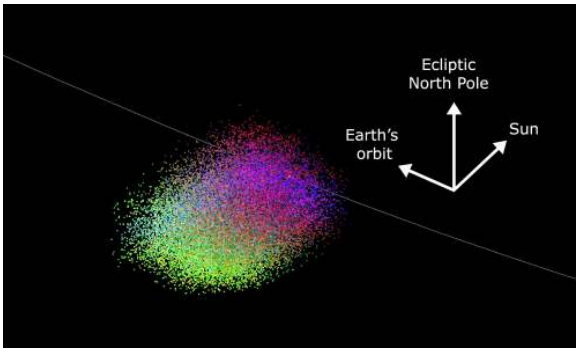

Figure 5. A 3D representation of a portion of a meteoroid stream with 10^5 particles selected and shaded according to proximity to a target set of orbital elements.

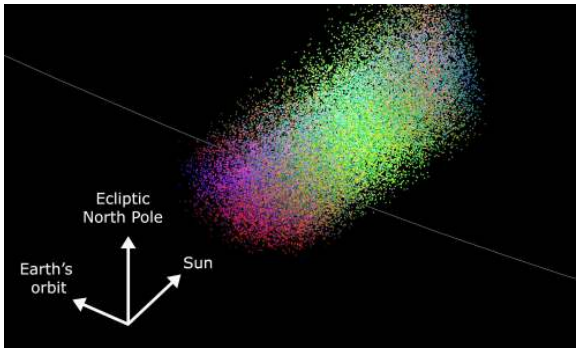

Figure 6. A second representation of a meteoroid stream, showing the inclusion, exclusion and change of colouration due to changes in the target set of orbital elements.

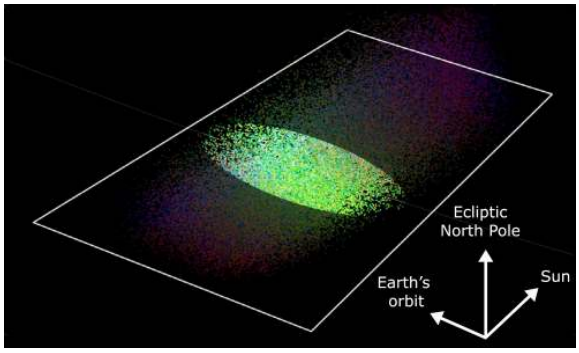

Figure 7. The slicing model tool, permitting the user to perform analysis of meteoroid stream internal structures via the manipulation of the slicing pane and viewing orientation.

4. The Implementation of Models

This section describes in further detail the implementation of models based on an abstract C++ model class. The discussion here presumes a cursory knowledge of C++ or another Object Oriented language.

4.1. The Definition and Initialization of a Model

All models in our software derive from a C++ class CModel which encapsulates all interfaces required by the software framework. The CModel class supports both the static or execution-time dynamic manipulation of model values representing the model parameters. Model values are implemented in a CModelValue class. To implement and initialize a model, the user must define a class derived from CModel, and either declare and initialize statically (see Figures 8 and 9); or programmatically build the model thought the dynamic allocation of a new values (new CValue()) and use of a CModel method CModel::addValue(CValue& value). Identified as an area of possible improvement, the user is required to explicitly state the interdependencies of the model values (See Figure 10). We would prefer to generate the dependency map at execution time directly from the model value implementation methods. The final piece of model implementation is the description of the algorithms to calculate the dependent values of the model. This is done by implementing a function member <model-class>::calculate<value> for each CModelValue member <value> within the class. The algorithm can use standard C++ arithmetic syntax when referring to CModelValue members (See Figure 11). Buried within the CModelValue implementation, and transparent to the user, are error propagation and formula optimization facilities. The C++ arithmetic operators are overridden to optionally calculate uncertainties, and will force the calculation of dependent variables only when they are needed within another nested dependency.

4.2. Particle Weights Assignment

The CModel abstract class utilizes a software framework interface to assign weights to particles. The framework manages the tabling of the integrated particles, the specifics of the comet ephemeris over time, and the models currently at play. To populate weights, the developer must implement a single class method used to signal model changes by the multithreaded framework. This method must iterate through the particle population process over the comet apparitions, selecting particles of interest, and populating only non-zero weights. The framework avoids setting weights to zero for all particles not weighted by keeping a sequence number of model changes, with weighting of a particle resulting in the particle being flagged with the current change sequence. All particles with a change sequence other than the current sequence are assumed to have frequency weight of zero.

5. Conclusions to Date

Usability: The prototyping work completed to date demonstrates we are building a powerful tool for meteoroid stream modelling. Dust ejecta and cometary nucleus models are easily implemented, and can be easily maintained. Performance: It

```
class CMeteoroidModel : public CModel
{
public:
    CMeteoroidModel(void);
    virtual ~CMeteoroidModel(void);
    VALUE_CLASS_DEFINITION(CMeteoroidModel);
    // Crifo and Rodionov (1997) derivation of gas flux Z(rh) from equation (9)
    SECTION_DEFINITION(CrifoRodionov1997GasFlux);
    CONSTANT_DEFINITION(StefanBoltzmannsConstant);
    CONSTANT_DEFINITION(WaterGasMoleculeMass);
    CONSTANT_DEFINITION(AtomicMassUnit);
    VALUE_DEFINITION(Emissivity);
    VALUE_DEFINITION(CoefficientOfSublimation);
    VALUE_DEFINITION(GeometricAlbedoOfNucleus);
    VALUE_DEFINITION(LatentHeatOfSublimation);
    CALCULATION_DEFINITION(LatentHeatOfSublimationPerGasMolecule,CMeteoroidModel);
    CONSTANT_DEFINITION(SolarConstant);
    VALUE_DEFINITION(HeliocentricDistanceForGasFlux);
    VALUE_DEFINITION(SunAngle);
    CALCULATION_DEFINITION(CosSunAngle,CMeteoroidModel);
    CALCULATION_DEFINITION(TemperatureOfPureIceAtZeroAngle,CMeteoroidModel);
    CALCULATION_DEFINITION(TemperatureOfPureIceAtSunAngle,CMeteoroidModel);
    CALCULATION_DEFINITION(GasFluxAtZeroAngle,CMeteoroidModel);
    CALCULATION_DEFINITION(GasFluxAtSunAngle,CMeteoroidModel);
    // Jorda et al. (1992)
    SECTION_DEFINITION(JordaEtAl1992);
    VALUE_DEFINITION(HeliocentricMagnitudeAtPerihelion);
    VALUE_DEFINITION(JordaGasProductionFixedParameter);
    VALUE_DEFINITION(JordaGasProductionMagnitudeParameter);
    CALCULATION_DEFINITION(GasProductionRateAtPerihelion,CMeteoroidModel);
```

Figure 8. An example of a model class defined statically through statically defining model class values.

```
REGISTER_MODEL("Vaubaillon et al. (2005) Meteoroid Model",CMeteoroidModel);

CMeteoroidModel::CMeteoroidModel(void) :
    // Crifo and Rodionov (1997) derivation of gas flux Z(rh) from equation (9)
    SECTION_INITIALIZATION(CrifoRodionov1997GasFlux,"Crifo and Rodionov (1997) der
    CONSTANT_INITIALIZATION(StefanBoltzmannsConstant,"Stefan-Boltzmann's Constant",
    CONSTANT_INITIALIZATION(WaterGasMoleculeMass,"Water Gas Molecule Mass","amu"),
    CONSTANT_INITIALIZATION(AtomicMassUnit,"Atomic Mass Unit","kg"),
    VALUE_INITIALIZATION(Emissivity,"Emissivity",""),
    VALUE_INITIALIZATION(CoefficientOfSublimation,"Coeffienct of Sublimation",""),
    VALUE_INITIALIZATION(LatentHeatOfSublimation,"Latent Heat of Sublimation","J K
    CALCULATION_INITIALIZATION(LatentHeatOfSublimationPerGasMolecule,"Latent Heat
    VALUE_INITIALIZATION(GeometricAlbedoOfNucleus,"Geometric Albedo of Nucleus",""
    CONSTANT_INITIALIZATION(SolarConstant,"SolarConstant","W m^-2"),
    VALUE_INITIALIZATION(HeliocentricDistanceForGasFlux,"Heliocentric Distance (fo
    VALUE_INITIALIZATION(SunAngle,"Sun Angle","rad"),
    CALCULATION_INITIALIZATION(CosSunAngle,"Cos(Sun Angle)","",CMeteoroidModel),
    CALCULATION_INITIALIZATION(TemperatureOfPureIceAtZeroAngle,"Temperature of Pur
    CALCULATION_INITIALIZATION(TemperatureOfPureIceAtSunAngle,"Temperature of Pure
    CALCULATION_INITIALIZATION(GasFluxAtZeroAngle,"Gas Flux at 0 Angle","m^-2 s^-1
    CALCULATION_INITIALIZATION(GasFluxAtSunAngle,"Gas Flux at Sun Angle","m^-2 s^-

    // Jorda et al. (1992)
    SECTION_INITIALIZATION(JordaEtAl1992,"Jorda et al. (1992) Gas Production Rate",
    VALUE_INITIALIZATION(HeliocentricMagnitudeAtPerihelion,"Heliocentric Magnitude
    VALUE_INITIALIZATION(JordaGasProductionFixedParameter,"Jorda Gas Production Fi
    VALUE_INITIALIZATION(JordaGasProductionMagnitudeParameter,"Jorda Gas Productio
    CALCULATION_INITIALIZATION(GasProductionRateAtPerihelion,"Gas Production Rate
```

Figure 9. A model class constructor initializing the properties of model values through the use of initialization macros paralleling the definition macros in Figure 8.

appears that the desires to provide near-real-time model manipulation feedback and cometary stream structure impact visualization are achievable. All prototyping has been done on a single workstation representative of the upper-end workstations available today (in this case 2-processor 8-core laptop). Other uses: In developing the prototypes for ejecta and cometary nucleus environment models, it became

```
{
    // Crifo and Rodionov (1997) derivation of gas flux Z(rh) from equation (9)
    SET_DEPENDENCIES3(LatentHeatOfSublimationPerGasMolecule,LatentHeatOfSublimation,
                      AtomicMassUnit,WaterGasMoleculeMass);
    SET_DEPENDENCIES1(CosSunAngle,SunAngle);
    SET_DEPENDENCIES2(TemperatureOfPureIceAtZeroAngle,GeometricAlbedoOfNucleus,
                      HeliocentricDistanceForGasFlux);
    SET_DEPENDENCIES3(TemperatureOfPureIceAtSunAngle,GeometricAlbedoOfNucleus,
                      CosSunAngle,HeliocentricDistanceForGasFlux);
    SET_DEPENDENCIES8(GasFluxAtZeroAngle,GeometricAlbedoOfNucleus,SolarConstant,
                      HeliocentricDistanceForGasFlux,Emissivity,
                      StefanBoltzmannsConstant,TemperatureOfPureIceAtZeroAngle,
                      CoefficientOfSublimation,LatentHeatOfSublimationPerGasMolecule);
    SET_DEPENDENCIES9(GasFluxAtSunAngle,GeometricAlbedoOfNucleus,SolarConstant,
                      CosSunAngle,HeliocentricDistanceForGasFlux,Emissivity,
                      StefanBoltzmannsConstant,TemperatureOfPureIceAtSunAngle,
                      CoefficientOfSublimation,LatentHeatOfSublimationPerGasMolecule);
```

Figure 10. The definition of the inter-value dependency map implemented as macros executed within the constructor method of the model class.

```
CModelValue CMeteoroidModel::calculateGasFluxAtSunAngle()
{
    return ((((1-m_GeometricAlbedoOfNucleus)*m_SolarConstant*m_CosSunAngle)
            /(m_HeliocentricDistanceForGasFlux*m_HeliocentricDistanceForGasFlux))
                -m_Emissivity*m_StefanBoltzmannsConstant
                    *::pow(m_TemperatureOfPureIceAtSunAngle,4.0))
            / (m_CoefficientOfSublimation*m_LatentHeatOfSublimationPerGasMolecule);
}
```

Figure 11. An example of a derived value calculation, using standard C++ syntax to implement formulae. CModelValue instances (named m_<value>) may be used in the formulae in the same manner as one uses numeric variables. Overrides of the C++ arithmetic operators implement uncertainty propagation.

apparent that this modelling in conjunction with the powerful 3D scene rendering is a powerful tool for cometary coma and cometary tail research. Stepping back, it is also conceivable that this approach could be used in like research areas where the manipulation of a source environment impacting wide scale long-term evolution, such as the evolution of the solar system or more specifically, Near Earth Object, asteroid belt, Kuiper Belt and Oort Cloud populations.

Acknowledgements

We thank Jeremie Vaubaillon for his patience, support, and his explanations and assistance in recreating his results for the purposes of verifying our methods. We thank Phil Stooke for his allowing us to use his shape model and surface mapping of the asteroid Gaspra as our test model for a cometary nucleus.

References

Brown P., Jones J., 1998, Icarus, 133, 1, 36

Crifo J.F., Rodionov A.V., 1997, Icarus, 129, 1, 72

Jorda L., Crovisier J., Green D.W.E., 1992, in Lunar and Planetary Inst., ACM, 1991, 285

Vaubaillon, J., Colas, F., Jorda, L., 2005a, A&A, 439, Issue 2, 751

Vaubaillon J., Colas F., Jorda L., 2005b, A&A, 439, Issue 2, 751

Whipple F. L., 1950, ApJ, 111, 375

PART 5

Meteor databases, observation techniques, software and data reduction

Meteoroids 2013, Proceedings of the Astronomical Conference,
held at A.M. University, Poznań, Poland, Aug. 26-30, 2013,
eds Jopek T.J., Rietmeijer F.J.M., Watanabe J., Williams I.P.,
Adam Mickiewicz University Press in Poznań, pp 289–295

Hyperbolic Orbits in the EDMOND

Hajduková M. Jr.[1], Kornoš L.[2], Tóth J.[2]

[1]Astronomical Institute of the Slovak Academy of Sciences, Bratislava, Slovak Republic
(maria.hajdukova@savba.sk)
[2]Comenius University, Faculty of Mathematics, Physics and Informatics, Bratislava,
Slovak Republic (kornos@fmph.uniba.sk)

Abstract. The present work is based on an analysis of 83369 meteor orbits collected in the European video meteor network database – EDMOND (Kornoš et al. 2013a), 5.7% of which have orbits determined as hyperbolic. Among them, we searched for gravitationally accelerated meteoroids. The investigation showed that only 8 meteoroids from all 4712 hyperbolic orbits had close encounters with one of the major planets, giving a proportion of only 0.0017 of all hyperbolic orbits. However, for none of these 8 meteoroids did the integration procedure show significant changes in their orbits; thus, the close encounters did not cause their hyperbolicity. Indeed, our analysis showed that erroneous determinations of the heliocentric velocity is responsible for the vast majority of hyperbolic orbits among the detected meteors in the EDMOND.

Keywords: meteoroids, meteors, hyperbolic orbits

1. Introduction

The high abundance of hyperbolic orbits among detected meteors has always been an issue, and in spite of great progress in the development of observational techniques and orbit determination it remains so. Their presumably high presence in databases started an unsuccessful search for interstellar meteoroids but, in fact, it reflects the quality of observational data. Indeed, the proportion of hyperbolic orbits in data was found to be dependent on the precision of the data (Štohl 1971; Hajdukova 1994; current study).

Except for an interstellar origin of meteoroids, there are other sources that are related to the processes at work in our Solar System which can produce Earth crossing hyperbolic orbits. In this case, the particles, naturally, originate within the Solar System.

One of these sources is a possible mechanism of mutual collisions of small bodies in the Solar System as was investigated in the paper Pittich and Solovaya (2013). Depending on their direction, the fragments will migrate into either the inner or outer part of the Solar System, with different orbital velocities. The orbital behaviour of the Main Belt body fragments showed, according to these authors, the possibility for some of them to be shifted on hyperbolic orbits, and migrate out of the Solar System as hyperbolic meteoroids. A fraction of them may cross the inner part of the Solar System. In these cases they cross the Earth's orbit and they will be observed at Earth as hyperbolic meteors.

Meteoroids perturbed due to a close planetary encounter are probably more frequent. Their production depends sensitively on both the speed and direction with

which the meteoroids approach the scattering planet (Wiegert 2011). The flux of gravitationally scattered meteoroids at the Earth is not yet known. However, their proportion among the registered meteors, according to several studies based on meteors observed by different techniques and considering different particle sizes, seem to be rare. Among 7489 video meteors from the SonotaCo TV catalogue (SonotaCo 2009), none of the hyperbolic orbits was caused by a meteoroid encountering a planet (Hajduková et al. 2013). Among the 4581 photographic orbits of the IAU Meteor Database (Lindblad et al. 2005), not a single meteor was found whose hyperbolicity was caused by planetary perturbation (Jakubík 2001). In an optical search for interstellar meteoroids based on 1739 meteor orbits of high accuracy (Musci et al. 2012), the majority of the nominally hyperbolic events could not have been more than very slightly perturbed due to recent close planetary encounters. The last mentioned authors found no clear evidence of interstellar meteoroids among their data and concluded that the few hyperbolic meteors identified were most likely the result of measurement errors.

These results agree with our previous studies searching for interstellar meteoroids (Hajduková 1994, 2008, 2011), which demonstrated how extremely small the number of possible interstellar meteoroids is among the hyperbolic orbits in the registered data and how great the number of hyperbolic orbits is due to erroneous velocity determination. Thus, our task here was also to estimate the limits of possible errors in EDMOND data. In our analysis, we focused on meteoroids on hyperbolic orbits produced by planetary perturbations.

2. European video meteor network database

For our analysis, we used the European video meteor network database (EDMOND) of video meteor orbits (Kornoš et al. 2013a). The database is the result of cooperation and data-sharing among several European national networks and the International Meteor Organization Video Meteor Network (IMO VMN). During the years 2001-2013, about 109000 preliminary orbits were collected in the database, the subsequent treatment of which created the current version EDMOND 4.0, which consists of 83369 orbits (Kornoš et al. 2013b). Two sets of multiple selection criteria were used, which eliminated meteors with the largest errors in their velocity determination. After this selection, the proportion of hyperbolic orbits in the data decreased significantly, from 14% of the previous version to 5.7% of the current version of the database.

Considering that the proportion of hyperbolic orbits in data depends on the quality of the original observations, an examination of individual hyperbolic orbits should use only data of the highest accuracy. Thus, additionally, we applied stronger criteria to the data to obtain a subset of meteor orbits of even higher accuracy, viz. (1) the duration of the trail had to be over 0.3 seconds, (2) the maximum difference between 2 poles of ground trajectory had to be smaller than 0.1 degree, (3) the overlap percentage of trails observed from two stations for a particular meteor had to be larger than 50%, and (4) the convergence angle Q_C had to be larger than 20 degrees. The resulting subset of the 28555 higher quality video orbits con-

Table 1. Overview of all hyperbolic orbits from the EDMOND (ED), and of those selected from the subset of higher quality orbits (HQ).

	ED	HQ
Number of all orbits	$N_{all} = 83369$	28555
Number of hyperbolic orbits	$N_{e>1} = 4712$	1431
Proportion of hyperbolic orbits	$N_{e>1}/N_{all} = 0.057$	0.050
Number of shower meteors	$N_{show} = 34562$	11160
Number of sporadic meteors	$N_{spor} = 48807$	17395
Number of hyperbolic shower meteors	$N_{show,e>1} = 2018$	620
Number of hyperbolic sporadic meteors	$N_{spor,e>1} = 2694$	811
Proportion of shower meteors among the hyperbolic meteors	$N_{show,e>1}/N_{e>1} = 0.428$	0.433
Number of retrograde meteors	$N_{i>90} = 43571$	12267
Number of hyperbolic retrograde meteors	$N_{i>90,e>1} = 3606$	1127
Proportion of retrograde orbits among the hyperbolic meteors	$N_{i>90,e>1}/N_{e>1} = 0.765$	0.788

tains 1431 hyperbolic meteors (5.0%) and was used for a search for true hyperbolic orbits. An overview of the EDMOND data is listed in Table 1.

3. Concentration of shower meteors among hyperbolic orbits

Inaccuracy in the heliocentric velocity is a significant source contributing to the uncertainty in semi-major axes determination. The value of the semi-major axis is very sensitive to the value of the heliocentric velocity v_H, especially near the parabolic limit. For meteoroids with high velocities, any error in the determination of v_H can easily push the orbit over the parabolic limit and create an artificial hyperbolic orbit. To follow the influence of such errors on our sample of orbits considered to be hyperbolic, we created diagrams showing the radiant positions of orbits for the selected intervals of values of $1/a$ close to the parabolic limit and beyond (Figure 1). The analysis showed a high concentration of shower meteors among the hyperbolic orbits, which is clearly due to measurement errors, mostly in the velocity determination. A gradual decrease in the concentration of shower radiants with decreasing values of $1/a$ would be expected, but their concentration among the orbits of highest hyperbolic excesses is still evident. Meteors fulfilling the criteria of belonging to meteor showers and, at the same time, having heliocentric velocity with an excesses over the parabolic limit, offer proof of the false hyperbolicity of their orbit. All of them belong to high-inclined streams with long periods and heliocentric velocities close to the parabolic limit, mostly with retrograde orbits.

Generally, the errors in the measured velocity increase towards higher velocities, which belong mostly to retrograde orbits, and so they increase the proportion of hyperbolic orbits among particles moving on retrograde orbits. The proportion of retrograde orbits in the data is 52%, whereas that in the hyperbolic data is 77%.

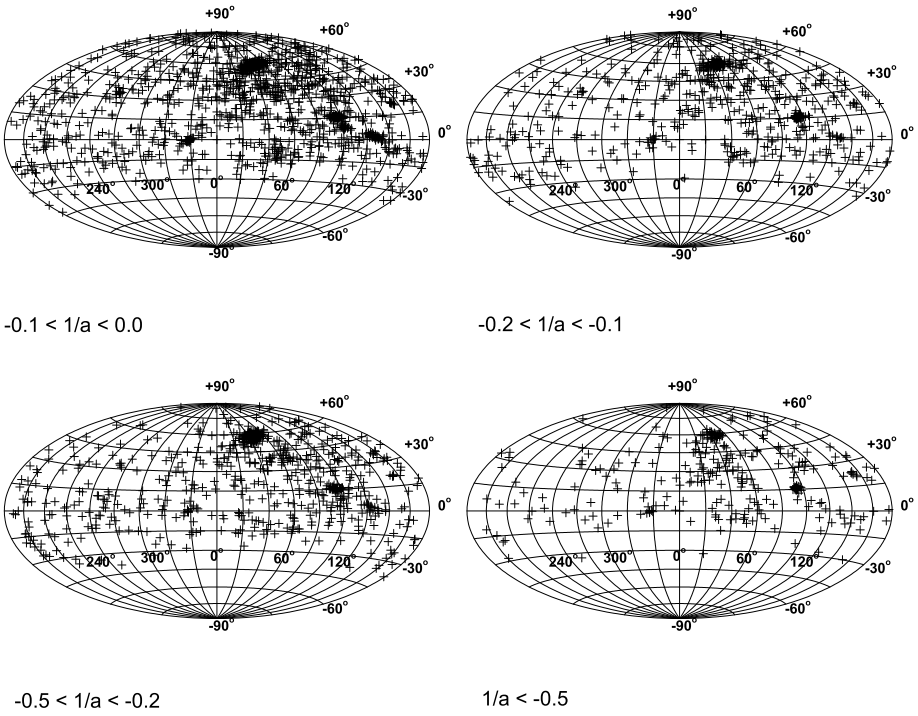

Figure 1. Position of radiants (in α and δ) of hyperbolic meteoroids from the EDMOND, within chosen limits of reciprocal semi-major axis 1/a in AU^{-1}. The presence of radiants of shower meteors with high heliocentric velocities, Perseids ($\alpha = 46^\circ$, $\delta = 58^\circ$), Orionids ($\alpha = 95^\circ$, $\delta = 15^\circ$), Leonids ($\alpha = 152^\circ$, $\delta = 22^\circ$), Lyrids ($\alpha = 272^\circ$, $\delta = 32^\circ$) and Eta Aquariids ($\alpha = 337^\circ$, $\delta = -2^\circ$), is evident, even among the orbits of highest hyperbolic excesses.

We examined four meteor showers, which can be clearly distinguished in Figure 1: Perseids, Orionids, Leonids, and April Lyrids. The 2331 Perseids from the period July 29 – August 26 were identified using the Southworth-Hawkins D-criterion for orbital similarity (Southworth and Hawkins, 1963), fulfilling the condition $D_{SH} < 0.25$. As much as 9% of these Perseid shower meteors have orbits determined as hyperbolic with $a < 0$ and $e > 1$. For the other three meteor showers, the limiting value of $D_{SH} < 0.2$ was applied. The highest proportion of formally hyperbolic orbits (13.9%) was found in the set of 79 meteoroids belonging to the April Lyrids. It corresponds to the smallest difference between the parabolic velocity and the mean heliocentric velocity $\Delta v_H = 0.22\,\mathrm{km\,s^{-1}}$ of the April Lyrids meteor shower. Four hyperbolic meteors among the 91 Leonids in the data resulted in a slightly smaller proportion of hyperbolic orbits (7.7%). In the set of 802 Orionids, there are 107 hyperbolic meteors (13.3%). A dependence of the contribution of hyperbolic orbits in meteor showers on the mean heliocentric velocity of a particular shower, $N_{e>1}/N = f(v_H)$ is visible. This relationship that was found in our previous studies (Hajduková 2008, 2011) is confirmed by the results from the new data set. It

Table 2. Close meteoroid encounters within the frame of 1 Hill's sphere of a particular planet, obtained by a backwards integration performed for all hyperbolic meteoroids from the EDMOND. For each meteoroid is listed: the year of observation, its closest distance to planet encountered, its heliocentric velocity v_H measured at Earth and the hyperbolic excess of its heliocentric velocity Δv_H; (qual) - orbits of higher quality.

Meteor No	Year	Planet	Distance [AU]	v_H [km s^{-1}]	Δv_H [km s^{-1}]
399 (qual)	2008	Jupiter	0.2006	42.76	0.66
2481 (qual)	2009	Saturn	0.2938	42.68	0.58
7088	2010	Jupiter	0.1974	43.17	1.07
24980	2011	Jupiter	0.2584	44.56	2.46
18028 (qual)	2011	Saturn	0.3586	42.21	0.11
38652	2012	Jupiter	0.1387	43.27	1.17
27630 (qual)	2012	Jupiter	0.2195	42.23	0.13
6686	2012	Jupiter	0.1728	42.29	0.19

offers proof that determinations of hyperbolic orbits are subject to measurement errors in the velocity.

The investigation showed that for all four showers the standard deviations of heliocentric velocities exceed the differences between the parabolic velocity and the mean heliocentric velocity of the particular shower by a factor of 1.3 to 3.7, which clearly explains the abundance of hyperbolic orbits among these four meteor showers.

Applying the results to the subset of sporadic meteors and assuming that their orbits were determined, in general, with the same precision as for the shower meteors, we can conclude that there is a lack of statistical argument for the presence of real hyperbolic orbits among the EDMOND data.

4. Hyperbolic orbits caused by planetary perturbation

4712 meteors with heliocentric velocities determined as hyperbolic from the EDMOND and 1431 hyperbolic orbits from the subset of higher quality orbits we created for this analysis (see section 2), were searched for unbound meteoroids due to a close accelerating encounter with one of the massive planets of the Solar System. In order to follow their orbital evolution, all hyperbolic orbits were integrated backwards for 80 years. At this time, all meteors reached a heliocentric distance of at least 100 AU. We followed the same procedure that was used for analyzing hyperbolic meteors from the SonotaCo catalogue (Hajduková et al. 2013). For the integration, the multistep procedure of Adams-Bashforth-Moulton's type, up to the 12th order with a variable step-width, developed by Shampine and Gordon (1975) and implemented by Montenbruck and Pfleger (2000), was used. In the model, the planets Mercury through Neptune were considered as perturbing bodies; Earth and the Moon were treated separately. The positions of the perturbing planets were obtained from the Planetary and Lunar Ephemeris DE406, prepared by the Jet Propulsion Laboratory (Standish 1998). The orbital evolution of the meteoroids was, as in our above mentioned study, traced in two steps. In

the first step, a backward motion of a meteoroid on Keplerian heliocentric orbit into the distance of 3 Hill's radii from Earth was calculated, because the orbital elements in the data refer to the orbit of each meteoroid before it came under the influence of Earth's gravity. In the second step, the above mentioned gravitational model was used and the integration was performed. On such a short passage of the orbit, it is not necessary to include the influence of non-gravitational forces.

The investigation showed 39 orbits encounters within the frame of 3 Hill's sphere of Jupiter, two within the frame of 3 Hill's sphere of Saturn, and none with any of the other major planets. Only 8 meteoroids from all 4712 hyperbolic orbits (and only 4 from the 1431 higher quality orbits) had close encounters with one of the two major planets closer than 1 Hill's radius, giving a proportion of only 0.0017 of all hyperbolic orbits. Six occurred with Jupiter and 2 with Saturn. Their heliocentric velocities observed at Earth are from 42.20 to 44.56 $\mathrm{km\,s^{-1}}$ and the corresponding hyperbolic excesses range from 0.11 to 2.46 $\mathrm{km\,s^{-1}}$. The small number of events is partly the result of the high inclinations of the orbits which results in only a short section of a meteor's orbit being near to the ecliptic plane. About 77% of all hyperbolic orbits in the EDMOND have inclinations greater than 90°. Nevertheless, for none of the meteoroids, which had had a close encounter did the integration procedure show significant changes in their orbits.

The hyperbolic orbits were also searched for a change from a hyperbola to an ellipse during the backward integration process, connected with the meteoroid's motion retreating away from the Sun with respect to the barycenter of the whole Solar System. This phenomenon was studied previously by Hajduková et al. 2013, using a different set of video orbits. It could, theoretically, reveal orbits of interstellar meteors but only on the assumption that meteor orbits are precisely determined. In the catalogue investigated, there are only 30 hyperbolic orbits (which correspond to a fraction 0.006 of all hyperbolic orbits) that changed during the integrations from a hyperbolic to an elliptic orbit. For four of them, it took place outside Jupiter's orbit; for others, more distantly, at least beyond Saturn's orbit. In all cases, the orbits were retrograde or with very high inclinations, and none of them was caused by a close meteoroid encounter with a planet. The negligible proportion of orbits changed from a hyperbolic to an elliptic orbit reflects the insufficient accuracy of the orbits investigated.

The results of the analysis and an overview of the meteoroids' close encounters are shown in Table 2.

5. Conclusions

Our analysis of 4712 hyperbolic orbits from the 83369 meteors from the European video meteor network database did not produce any convincing arguments in favor of the existence of true hyperbolic meteors, in spite of the presence of many orbits with determined values of $a < 0$ and $e > 1$ in the data. Meteoroids with hyperbolic orbits were searched for close approaches with one of the massive planets of the Solar System. The integration procedure showed that 8 from all 4712 hyperbolic meteoroids, and only 4 from the 1431 higher quality orbits, had close encounters with one of the major planets closer than 1 Hill's radius. None of these encounters

produced significant changes in the meteoroid orbits. Not a single meteoroid was found in the database whose hyperbolicity was caused by planetary encounters.

Furthermore, taking into account (1) a high concentration of shower meteors among the hyperbolic orbits, (2) a dependence of the contribution of hyperbolic meteors in meteor showers on the mean heliocentric velocity of a particular shower, and (3) a high proportion of hyperbolic orbits among particles moving on retrograde orbits, we can conclude that there is a lack of statistical argument for the presence of real hyperbolic orbits in the catalogue.

The hyperbolic velocities observed at Earth are most likely a consequence of observational and measurement errors, mostly in the velocity. Other sources which can produce the hyperbolicity of a meteor orbit, including a planetary perturbation, are negligible in comparison. To avoid entering poor quality data into the database, stronger filters for the selection of the orbits can be used, but this will come at the expense of the quantity of the data. In any case, an improvement in the velocity measurement and determination is essential.

Acknowledgements

This work was supported by the Slovak Research and Development Agency, project No APVV-0517-12, and by the Slovak Scientific Grant Agency VEGA, project No 1/0225/14.

References

Hajduková M. Jr., 1994, A&A, 288, 330

Hajduková M., 2008, EM&P, 102, 67

Hajduková M. Jr., 2011, Publ. Astron. Soc. Japan, 63, 481

Hajduková M. Jr., Kornoš, L., Tóth, J., 2014, M&PS, 49, 63

Jakubík M., 2001, M. Sc. thesis, Comenius University, Bratislava, Slovak Republic

Kornoš L., Koukal J., Piffl R., Tóth, J., 2013a, IMC Proceedings, eds Gyssens M., Roggemans P., La Palma, Canary Islands, Spain, 20-23 Sept. 2012, p. 21

Kornoš L., Koukal J., Piffl R., Tóth J., 2013b, IMC Proceedings, eds Gyssens M., Roggemans P., Poznan, Poland, 22-25 Aug. 2013, in press

Lindblad B. A., Neslušan L., Porubčan V., Svoreň J., 2005, EM&P, 93, 249

Montenbruck O., Pfleger T., 2000, Astronomy on the Personal Computer, Springer

Musci R., Weryk R.J., Brown P. Campbell-Brown M.D., Wiegert P., 2012, Aph. J. 745, 161

Pittich E. M., Solovaya N. A., 2013, IMO Proceedings, eds Gyssens M., Roggemans P., La Palma, Canary Islands, Spain 20-23 Sept. 2012, p. 182

Shampine L. F., Gordon M. K., 1975, Computer solution of ordinary differential equations, Freeman and Comp., San Francisco

SonotaCo, 2009, WGN, Journal of the International Meteor Organization, 37, 55

Southworth R.B., Hawkins G.S., 1963, Smithson. Contrib. Astrophys. 7, 261

Standish E.M., 1998, JPL Planetary and Lunar Ephemeris, DE405/LE405, JPL I0M, 312, F-98-048

Štohl J., 1971, Bull. Astron. Inst. Czechosl., 21, 10

Wiegert P., 2011, in Proc. of Conf., Meteoroids: The smallest solar system bodies, eds Cook W.J., Moser D.E., Hardin B.F., Janches D., Breckenridge, Colorado, USA, 24-28 May 2010, NASA CP-2011-216469, p. 106

Meteoroids 2013, Proceedings of the Astronomical Conference,
held at A.M. University, Poznań, Poland, Aug. 26-30, 2013,
eds Jopek T.J., Rietmeijer F.J.M., Watanabe J., Williams I.P.,
Adam Mickiewicz University Press in Poznań, pp 297–305

Status and history of the IMO Video Meteor Network

Molau S.[1,2], **Barentsen G.**[1,3]

[1]International Meteor Organization
[2]Abenstalstr. 13b, 84072 Seysdorf, Germany (sirko@molau.de)
[3]University of Hertfordshire, College Lane, Hatfield, AL10 9AB, U.K. (geert@barentsen.be)

Abstract. The Video Meteor Network of the International Meteor Organization (IMO) has been monitoring the night sky for shooting stars since 1999. It was the first network of automated video cameras to observe meteors in visible light in a continuous fashion, and it remains one of the largest networks to date. By the end of 2012, 81 cameras across 15 countries had recorded more than 1.4 million meteors in 4 600 nights. The resulting database is publicly available and has been used in a range of studies, including the confirmation of about 100 known meteor showers, the detection of more than 20 previously unknown showers, and the characterization of the radiants and velocities of the parent meteoroid streams. Recent advances include the ability to monitor a meteor shower's flux density in real-time. This paper summarizes the history, the characteristics and the main results of the network, which is led entirely by citizen scientists (i.e. amateur astronomers).

Keywords: citizen science, meteor showers, meteoroid fluxes, video meteor observations

1. Introduction

The Video Meteor Network of the International Meteor Organization, in short *the IMO network*, is a joint effort by amateur astronomers to obtain video meteor observations on a regular basis. This paper summarizes the history, the characteristics and the main results of the network, which has been operating continuously for nearly fifteen years.

We start in Section 2 by discussing the three phases which characterize the history of the network. In Section 3 we describe the project and compare it with other video networks, and in Section 4 we summarize the main results. Finally, in Section 5 we conclude and offer a future outlook.

2. History

Video observations of meteors have been attempted as early as the 60's and the 70's of the previous century, but the method only gained widespread adoption in the 90's when the required equipment became more affordable. The observations were initially limited to dedicated observing campaigns for selected events, because the data analysis was a largely manual and hence time-consuming process, carried out off line after the observations.

In March 1999, however, a first camera in Germany started to monitor the night sky on a continuous basis (Molau 2001). Its data processing was automated and

Table 1. Growth of the IMO Video Meteor Network.

Year	Cameras	Observers	Countries	Nights	Eff. Time [h]	Meteors
1999	8	7	3	117	1 022	8 352
2000	11	8	5	248	506	12 852
2001	19	12	7	293	524	31 646
2002	19	12	8	318	5 866	23 258
2003	23	15	8	357	9 614	36 389
2004	21	11	7	351	7 376	25 205
2005	23	17	9	356	9 543	40 770
2006	28	19	9	365	14 983	69 844
2007	30	22	9	364	16 932	75 053
2008	37	24	10	366	22 984	92 323
2009	43	24	10	365	32 291	138 765
2010	57	32	12	365	35 489	192 050
2011	80	46	16	365	69 063	312 099
2012	81	46	15	366	93 562	353 627

took place in real-time to avoid the need to store the observations on video tape. This marked the start of the IMO network, which has grown continuously since. In this section we offer a brief summary of its history, which can be divided into three phases: (i) the initial setup and data collection; (ii) using the data to establish meteor showers; and (iii) exploiting the data to estimate meteoroid fluxes.

2.1. Phase 1: setup and data collection

This first phase of the network was characterized by the setup of the network, the software development and the initial data collection. The IMO network has been growing constantly from year to year, and so did the output of the network (Table 1). As of June 2007, meteor observations have been obtained in every single night.

The first years of the network saw continuous development and improvement of the software, based on the ever-increasing practical experience. The meteor detection program, called MetRec (Molau 1998), was enhanced significantly and a number of additional tools were developed to support the preparation and the post-processing of the observations. The overarching aim was to reduce manual interaction as much as possible, in order to attract a sufficiently large number of observers which could operate a camera for many years.

2.2. Phase 2: establishing meteor showers

The second phase started in 2006, when the database contained astrometry for about a quarter million of single-station meteors. After more than 6 years of data collection, it was deemed that the network had obtained sufficient coverage at all solar longitudes to switch from occasional analyses of selected showers to a comprehensive statistical analysis of meteor showers across the year.

The analysis procedure used is explained in detail in Molau (2006). In brief, it is based on Bayes' decision rule and does not require a-priori knowledge about meteor showers, which are searched for in a two-step procedure. In the first step,

the database is split into solar longitude intervals. Within each interval, all active radiants are determined as follows: for each meteor M and each possible radiant R ($\alpha/\delta/v_\infty$), we calculate and accumulate the conditional probability $P(M|R)$ to find the most probable radiants which can explain the data. The conditional probability is inferred from the distance between the radiant and the backwards-prolonged meteor path, as well as the difference between the expected and the observed angular velocity (a procedure similar to the meteor shower assignment performed by visual observers). In the second step, similar radiants in consecutive solar longitude intervals are connected to identify meteor showers which are active over a certain amount of time.

By 2008, the data set had almost doubled in size and the meteor shower search was repeated with an improved algorithm, which fixed certain weaknesses in the first analysis (Molau 2008). The improvements included the introduction of information on the altitude of the meteor layer and the error distribution. Moreover, an observability function was introduced to correct for the observing geometry and to allow for a direct comparison of the meteor shower activity.

In 2009, on the occasion of the 10th anniversary of the IMO network, we carried out the most elaborate meteor shower search till then based on nearly half a million meteors (Molau & Rendtel 2009). A third step in the shower detection procedure was added, namely a manual quality check and refinement of the automatically obtained results. We also linked our results to the newly created meteor shower working list of the IAU Meteor Data Center (MDC), (Jopek and Kaňuchová 2014).

The above analyses had shown the Perseus/Auriga region to be particularly challenging in the months of September and October, because there appeared to be a number of nearby radiants with similar properties. Hence in Rendtel & Molau (2010) we published a specific analysis of meteor showers in that area.

By November 2011, the size of our database had grown to over a million meteors, and hence the latest and most comprehensive meteor shower search with the best coverage of solar longitudes (Figure 1) was started and eventually published in Molau (2013). Not only had the data set grown dramatically, but also the MDC working list had become fully established and new showers were now actively being reported to the MDC from different networks. For the first time, we conducted a bidirectional match between the IMO database and the MDC working list, i.e. we introduced an additional procedure to check for evidence of showers which appear in the MDC working list but were not automatically found by us. In total we could confirm 106 meteor showers from the MDC list plus 23 additional streams belonging to the Antihelion source.

2.3. Phase 3: estimating flux densities

Starting from 2010, we complemented the radiant searches with flux density estimates. The meteor detection software was extended to estimate the limiting magnitude of the camera in real-time†. When combined with the observing geometry (field of view, observing direction, meteor shower velocity, radiant altitude and angular distance) and the effective observing time, all of which can be determined

† Explained in http://www.imo.net/imc2010/talks/Molau.pdf

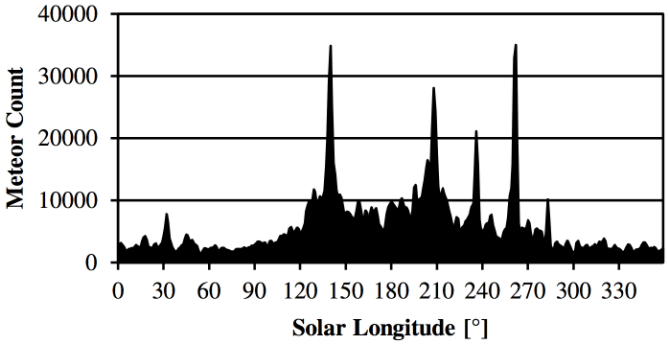

Figure 1. Distribution of meteors over solar longitude in the 2013 meteor shower analysis.

precisely for a video system, we were able to calculate the flux density of known meteor showers on the fly. In April 2011, an online web service was implemented for observers to upload their flux density data automatically. The web service has a user interface which allows the meteor shower activity of all major showers to be analysed with configurable parameters (Molau & Barentsen 2012).

On the occasion of the Draconids outburst later that year, we implemented a real-time flux density display which allowed enthusiasts world-wide to follow the development of the outburst online without delay (Molau & Barentsen 2013).

2.4. Current Status

By the end of 2012, the IMO Video Meteor Network had united 46 observers from 15 countries. The majority of the 81 cameras were located in (central) Europe, where there is a significant overlap of the observing fields. There are also a few individual systems in America and Australia (Table 2). The database had grown to more than 1.4 million meteors recorded in 4 600 nights. The combined effective observing time equals 325 000 hours or over 37 years of continuous observation. All IMO network data are quality checked and available without restriction in different formats, and can be downloaded in part from the website†.

3. Network characteristics

The IMO Video Meteor Network was the first meteor network to continuously monitor the night sky in visible light, and it is one of the largest video networks to date. With very few exceptions, all participants in the network are amateur astronomers organized in local societies, who operate their private video equipment. Even though there are a few typical configurations such as Mintron or Watec cameras with 3.8 mm or 8 mm f/0.8 Computar lenses, we have a wide range of different camera types and properties overall. Many observers operate one or two camera at their home location, but we also have a few participants who operate up to five video systems at different locations. Nearly all stations are fully automated and operate every night.

† http://www.imonet.org

The IMO network is a single station network by design, which is the biggest difference to most other networks. No matter where in the world someone is interested in meteors, and no matter what kind of camera he or she operates, anyone can join

Table 2. List of observers who had contributed more than 1 000 meteors to the IMO Video Meteor Database by December 2012.

Observer	Country	Nights	Eff. Time [h]	Meteors
S. Molau	Germany	3 461	36 452.0	214 099
J. Strunk	Germany	2 501	21 389.1	72 194
J. Kac	Slovenia	2 052	23 909.4	94 069
F. Castellani	Italy	1 754	14 028.4	46 322
B. Brinkmann	Germany	1 519	8684.7	31 646
I.Yrjölä	Finland	1 438	7 561.4	28 468
E. Stomeo	Italy	1 415	20 871.6	127 816
S. Slavec	Slovenia	1 415	6 389.8	17 725
S. Crivello	Italy	1 301	15 172.2	80 078
R. Goncalves	Portugal	1 299	18 463.2	71 695
M. Triglav	Slovenia	1 188	5 218.8	18 345
D. Koschny	Netherlands	1 184	7 518.5	36 165
C. Hergenrother	USA	1 102	7 432.3	19 440
A. Igaz	Hungary	1 030	13 104.2	48 273
O. Benitez-S.	Spain	1 026	5 295.4	13 959
M. Govedic	Slovenia	906	7 481.6	28 028
W. Hinz	Germany	900	5 018.5	26 931
M. Eltri	Italy	899	6 198.0	27 604
H. Schremmer	Germany	823	3 344.0	11 493
E. Rothenberg	Germany	808	3 717.6	12 388
R. Lunsford	USA	803	5 102.1	33 229
M. Otte	USA	701	3 389.5	13 826
I. Tepliczky	Hungary	679	4 045.9	19 375
Z. Perkó	Hungary	652	3 654.1	23 570
S. Kerr	Australia	648	4 666.9	34 036
J. Rendtel	Germany	647	3 823.4	17 223
J. Morvai	Hungary	595	3 141.0	8 915
P. Ochner	Italy	567	2 399.6	7 982
E. Berkó	Hungary	544	7 607.5	32 985
K. Jonas	Hungary	501	2 719.9	8 112
C. Saraiva	Portugal	464	8 142.3	19 163
S. Csizmadia	Hungary	477	1 819.9	5 773
S. Evans	UK	457	2 807.3	11 411
M. Maciejewski	Poland	403	5 261.2	13 140
L. Scarpa	Italy	380	2 468.2	8 636
S. Quirk	Australia	341	3 041.8	10 109
M. Breukers	Netherlands	319	2 863.1	8 290
S. Kiss	Hungary	300	1 875.0	2 077
B. Roberto	Italy	294	1 583.4	5 320
S. Biro	Hungary	287	1 723.4	5 037
G. Maravelias	Greece	273	1 625.9	7 268
R. Pucer	Slovenia	272	1 650.9	6 231
A. Leroy	France	255	1 194.3	1 676
K. Jobse	Netherlands	251	1 801.9	20 090
M. Nitschke	Germany	213	942.5	5 425
M. Bombardini	Italy	203	1 187.0	5 670
F. Ocaña G.	Spain	174	958.4	1 218
S. Ueberschaer	Germany	173	882.3	1 684
U. Sperberg	Germany	167	1 069.2	4 659
R. Štork	Czech Rep.	157	1 547.6	26 480
Z. Zelko	Hungary	127	825.1	2 137
M. Currie	UK	123	533.9	2 133
G. Kladnik	Slovenia	64	348.9	1 668
R. McNaught	Australia	52	401.2	5 285
M. Weber	Czech Rep.	29	49.4	1 050

the IMO network and contribute to our database, as long as the observing standards are followed. There is no need to establish a local network of identical camera with synchronized fields of view, because single meteors from single cameras are included in the database and used for analyses. Hence, there are both individual observers as well as national video networks which provide their data to the IMO network.

This strategy has allowed us to build a data set of unprecedented size. The number of single-station meteor records in the IMO database is an order of magnitude larger than the number of orbits obtained by large video networks with synchronized fields of view. Of course this limits the kind of studies which may be performed using the database. For example, whilst we can reliably determine shower radiants from single-station meteors in a *statistical* sense, we cannot obtain orbits for *individual* meteors. As a result, the large data set allows us to determine activity intervals and flux profiles precisely, but the accuracy of certain shower parameters such as the velocity is lower than what may be obtained from double-station data.

Although the IMO network was originally envisaged as a single-station network, the database does contain some tens of thousands of double-station observations, due to the high camera density in central Europe. For this reason, the full IMO network data set was imported into the EDMOND database (Kornoš et al. 2012) in 2013, for the purpose of analysing the trajectories and orbital parameters using these double-station observations.

Another unique property of the IMO network is the standardization of the computer hard- and software. All participants use the same digitizer hardware and the MetRec software (Molau 1998) for meteor detection and analysis.

The observations are reported to the headquarters on a monthly basis. Before they are stored into the database, the observations are manually checked for quality by a team of network administrators, which is in addition to the initial post-processing checks made by the observer. This means that the results of every night are checked by eye at least twice, hence ensuring a high level of quality and consistency despite the large variety of camera systems and observers.

Finally, the results are summarized and published on a monthly basis in WGN, the journal of the IMO, together with the result of an initial analysis. This provide the contributors with active feedback.

4. Results

As briefly mentioned in Section 2, multiple analyses have been carried out using the IMO network database over the years. In this section we summarize the highlights.

4.1. Meteor shower analyses

In the second phase of the IMO network, our data analysis activities focused on the detection of meteor showers. We confirmed about one hundred meteor showers from the MDC working list, improved their shower parameters, detected more than 20 unknown meteor showers, and confirmed new discoveries of other teams.

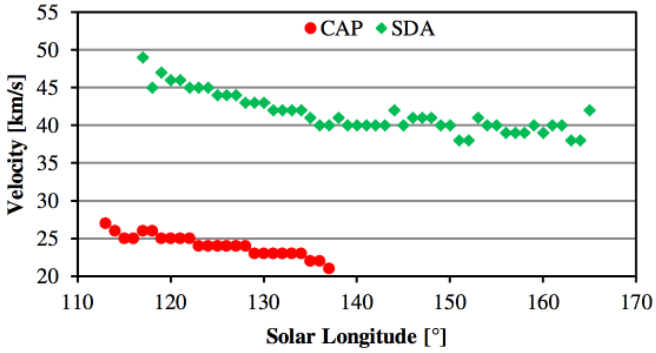

Figure 2. Velocity of meteors of the α-Capricornids (CAP) and Southern δ-Aquariids (SDA) showers over their activity interval.

We did not only provide information about the radiant position, drift and velocity of meteor showers. but also provided long-term activity profiles.

During the 2009 analysis we found that not only the radiant position, but also the velocity of certain meteor showers varies over time (Molau & Rendtel 2009). Figure 2 depicts the velocity of α-Capricornids and the Southern δ-Aquariids meteors against time. In both cases the velocities reduce significantly over the activity period. The observed pattern requires further investigation, but it is likely explained by a combination of (i) the change of Earth's velocity vector as it revolves around the Sun, and (ii) the fact that meteoroids in different regions of a stream are on slightly different orbits.

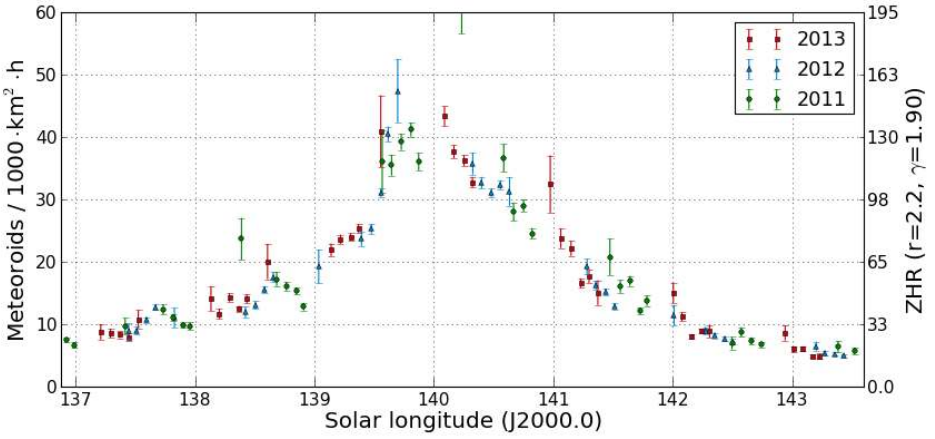

Figure 3. Flux density profile of the Perseids maximum in 2011-2013.

4.2. Flux density calculation

For every major meteor shower since 2011, detailed flux density profiles have been obtained. Because most of our cameras are located at European longitudes, we cannot cover all solar longitudes in a single year. However, by combining the data sets of different years we manage to obtain complete, high-resolution activity profiles. An example is given in Figure 3, which shows the activity profile of the Perseids peak based on data obtained between 2011 and 2013.

4.3. Zenith exponent

While analyzing flux density profiles of individual meteor showers, we detected systematic deviations as a function of the radiant altitude. We found that these errors can be tackled by adopting a zenith exponent γ different than 1.0. In Molau & Barentsen (2012) we determined the zenith exponent for a number of meteor showers individually, such that the systematic errors were minimized. We obtained values between 1.5 and 2.0, with an average value of $\gamma = 1.75$ over all showers.

4.4. Real-time flux density profiles

The Draconids outburst of 8 October 2011 was a major event which triggered several ground-based and airborne observing campaigns. We conducted an experiment to provide reliable flux density estimates in real time on the internet. About twenty IMO network observers intended to join the experiment, though only four cameras in Germany, Slovenia and Portugal enjoyed sufficiently clear skies to upload their observations in real time. Based on their data, the flux density profile was automatically calculated and published online. The Draconids peak was immediately and clearly apparent in the graph, which is still available online†.

Later, the remaining data were uploaded and analysed. The final data set from 57 cameras contained 1 605 Draconids meteors, which was sufficient to calculate the flux density profile with a temporal resolution of just five minutes (Figure 4). We could accurately determine the peak time, the flux density, and the full with at half maximum (FWHM) of the Draconids outburst, published in Molau & Barentsen (2013).

5. Conclusions and outlook

The IMO Video Meteor Network is a joint effort by nearly 50 amateur astronomers to obtain video meteor observations on a continuous and automated basis. It was the first network of its kind and has remained one of the largest networks since, with more than 1.4 million single-station meteors having been recorded by 81 cameras between 1999 and 2012. The resulting data set has been quality-checked by eye and is available to the public.

This paper summarised the history, the characteristics and the main results of the network. We discussed how the data has been used in a range of studies, including the confirmation of about 100 known meteor showers, the detection of

† See http://www.imonet.org/draconids

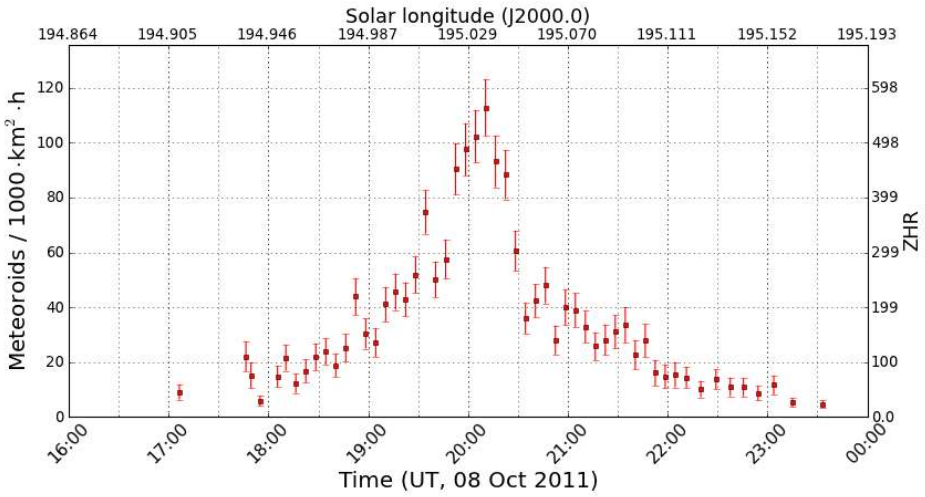

Figure 4. High resolution flux density profile of the Draconids on October 8, 2011.

more than 20 previously unknown showers, and the characterization of the streams and their flux densities. A notable highlight was the outburst of the 2011 Draconids, during which the network delivered a high-resolution activity profile in real time.

In future work, we aim to carry out further analysis by exploiting the rapidly growing database, improving the data quality and refining the analysis techniques.

Acknowledgements

We are deeply indebted to all video meteor observers contributing to the IMO network (Table 2) and providing the basis for the scientific success of the joint effort.

References

Jopek T.J., Kaňuchová Z., 2014, in Proceedings of the Meteoroids 2013 Conference, Poznań, Poland, 26–30 August 2013, eds Jopek T.J., Rietmeijer F.J.M., Watanabe J., Williams I.P, AM University Press, Poznań, p. 353

Kornoš L., et al., 2012, Proc. of the Intern. Meteor Conf. 2012, La Palma, Spain, 22

Molau S., 1998, Proc. of the Intern. Meteor Conf. 1998, Stará Lesná, Slovakia, 9

Molau S., 2001, Proc. of the Meteoroids 2001 Conf., Kiruna, Sweden, 315

Molau S., 2006, Proc. of the Intern. Meteor Conf. 2006, Rhoden, The Netherlands, 38

Molau S., 2008, Proc. of the Intern. Meteor Conf. 2008, Šachtička, Slovakia, 76

Molau S., Rendtel J., 2009, WGN, Journal of the Intern. Meteor Organization, 37, 98

Molau S., Barentsen G., 2012, Proc. of the Intern. Meteor Conf. 2012, La Palma, Spain, 11

Molau S., 2013, Proc. of the Intern. Meteor Conf. 2013, Poznan, Poland, in print.

Molau S., Barentsen G., 2013, EM&P, 14, in print

Rendtel J., Molau, S., 2010, WGN, Journal of the Intern. Meteor Organization, 38, 161

Meteoroids 2013, Proceedings of the Astronomical Conference,
held at A.M. University, Poznań, Poland, Aug. 26-30, 2013,
eds Jopek T.J., Rietmeijer F.J.M., Watanabe J., Williams I.P.,
Adam Mickiewicz University Press in Poznań, pp 307–314

Automatic detection of asteroids and meteoroids A Wide Field Survey

Vereš P.[1,2], Tóth J.[2], Jedicke R.[1], Tonry J.[1], Denneau L.[1], Wainscoat R.[1], Kornoš L.[2] Šilha J.[2,3]

[1]Institute for Astronomy, University of Hawaii at Manoa,
2680 Woodlawn Drive, Honolulu, HI 96814, USA (veres@ifa.hawaii.edu)
[2]Faculty of Mathematics, Physics and Informatics, Comenius University,
Mlynska Dolina, 84248 Bratislava, Slovakia
[3]Astronomical Institute, University of Bern, Sidlerstrasse, CH-3012 Bern, Switzerland

Abstract. We propose a low-cost robotic optical survey aimed at 1-300 m Near Earth Objects (NEO) based on four state-of-the-art telescopes having extremely wide field of view. The small Near-Earth Asteroids (NEA) represent a potential risk but also easily accessible space resources for future robotic or human space in-situ exploration, or commercial activities. The survey system will be optimized for the detection of fast moving - trailed - asteroids, space debris and will provide real-time alert notifications. The expected cost of the system including 1-year development and 2-year operation is 1,000,000 EUR. The successful demonstration of the system will promote cost-effectiveicient ADAM-WFS (Automatic Detection of Asteroids and Meteoroids – A Wide Field Survey) systems to be built around the world.

Keywords: NEO survey, asteroids, meteoroids, space debris

1. Introduction

It has been more than 200 years since the first asteroid, now defined as a dwarf planet, Ceres, was discovered. Progressive development of instrumentation and techniques in astronomy revealed the existence of the asteroid main belt and other dynamically stable and unstable populations of minor bodies throughout the Solar System including NEAs encountering the Earth. In 2013, 10,000th NEO was discovered by the Pan-STARRS survey (Kaiser et al. 2010). Although, the number of NEA has been rising rapidly within the last decade due to the dedicated asteroid surveys such as Spacewatch (Gehrels et al. 1986), LINEAR (Stokes et al. 2000), LONEOS (Koehn and Bowell 1999), NEAT (Pravdo et al. 1999), space-based NEOWISE (Wright et al. 2010) or ongoing next generation surveys such as Catalina Sky Survey (Larson et al. 1998) and Pan-STARRS, there is a large uncertainty in the population count and orbital properties of small NEA within the size range of $1 - 300$ m are not understood well. In previous studies (Rabinowitz et al. 1994; Bottke et al. 2002; Stuart and Binzel 2004) the population count of 10 m size NEA differed more than one order of magnitude. Although, NEOWISE mission supposedly derived accurate diameters of asteroids by the thermal modeling and assumed that there are less small NEAs that it was predicted before (Mainzer et al. 2013), recent studies by Harris (2008) and Brown et al. (2013), based on recent ground-based discoveries and the fall of the Chelyabinsk meteoroid in 2013,

suggest a much higher count. Other previous studies also indicated that small NEA population could be enhanced by tidal disruption of rubble-pile asteroids during close approaches to the Earth, such as a theory about the common origin of Příbram and Neuschwanstein meteorites coming from heterogenous stream of meteoroids (Spurný et al. 2003) when the frequency of rubble-pile asteroids disruption were estimated (Tóth et al. 2011). Similarly in subsequent studies, Schunová et al. (2012), Schunová et al. (2014) analysed the creation mechanisms of NEA's families and showed supporting evidence for mentioned theories. Moreover, the meteoroid streams may contain large particles from break-ups and enriched population of small NEOs (Porubčan et al. 1992; Rudawska et al. 2012; Babadzhanov et al. 2013).

In the past (Tóth and Kornoš 2002, 2003; Vereš et al. 2006), we proposed a simple low-cost survey for discovering population of small asteroids flying-by within one lunar distance from the Earth. In this paper we introduce an advanced and more sophisticated, yet low cost concept that will characterize the population of small NEA that from the large part is undetectable by current telescopic systems.

2. Concept

Automatic Detection of Asteroids and Meteoroids - A Wide Field Survey (ADAM-WFS) will consist of 4 identical wide-field astrographs (Houghton-Terebizh f=300 mm, f/1.44) on a fast-track mount with high-precision guiding (Fig. 1). Each telescope will be equipped with a large-scale single chip CCD camera (4096x4096 pix) providing a total FOV of almost 100 square degrees. The predicted limiting magnitude with the wide-band optical filter will be +17.5 mag. at S/N=5.0 with 30 sec exposures and a pixel scale of 4.36 arcsec/pix. This configuration is able to survey almost an entire sky visible from a specified location in 3 visits per night (Fig. 2), with the rapid image processing providing moving targets in almost a real-time. We will use the Moving Object Processing System (MOPS, (Denneau et al. 2007)) that has been utilized by the Pan-STARRS and ATLAS (Tonry 2011). Stationary transients will be processed during the daytime. We propose to build the system at an existing observatory with a dedicated 60-80 cm follow-up telescope and existing infrastructure.

2.1. Advantages of ADAM-WFS

The survey budget is considered **low-cost** compared to the existing or planned all-sky surveys that focus on deeper limiting magnitude, or space-based observatories, which are up to two orders of magnitude more expensive. In contrast to existing or planned deep surveys with narrower fields of view, our survey will cover **entire visible night sky** few times per night. In spite of its lower limiting magnitude, large pixels would **decrease** the effects of **trailing loss** for fast moving targets. Thus, ADAM-WFS will detect more fast moving objects than any survey equipped with telescopes of similar size.

Usually, the development of a new survey takes years due to the new hardware and software development and methods to be implemented. Our goal is to **avoid**

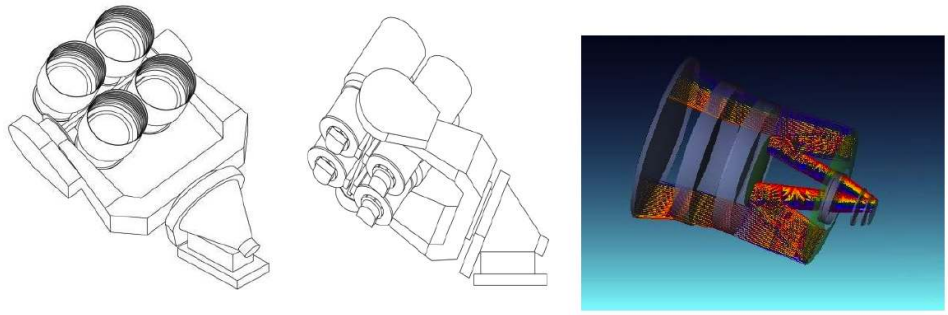

Figure 1. A design of the ADAM survey telescope - the mount and 4 optical assemblies in front and rear views (left) and optical path of the Houghton-Terebizh optical system (right).

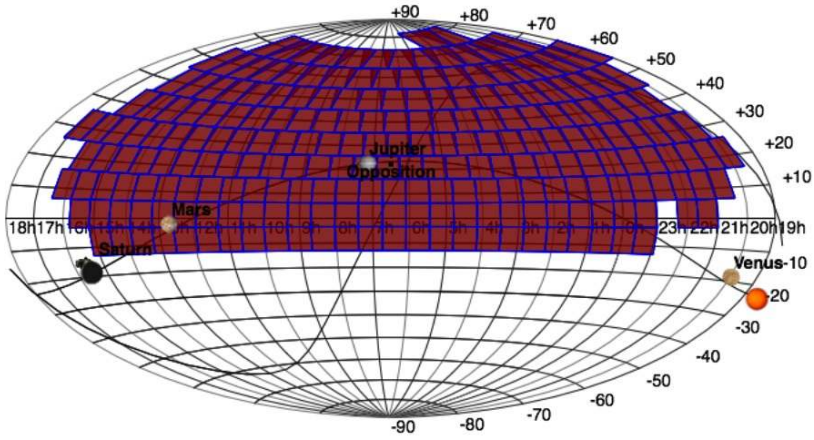

Figure 2. Sky coverage of the ADAM survey on one night, taken from the MOPS simulation interface.

reinventing the wheel and use existing routines for image processing, moving object processing, hardware, mount and optics to speed-up the delivery of the complete system and cut down the cost. We will also count on a **compact team** of astronomers and engineers with work and science experience on existing surveys (Pan-STARRS) or surveys under the development (ATLAS), on full-time and subcontracts.

Significant advantage is the **existing infrastructure** that will serve the prototype for the development and operation. It will be built on existing observatory – Astronomical and Geophysical Observatory of the Comenius University, Modra, Slovakia (AGO Modra) – that contains workshop, complete infrastructure and nonstop technical support. Future deployment of ADAM-WFS systems is also strongly encouraged on existing observatories (e.g. Canary Islands, South Africa). New generation surveys are often focused on multiple tasks (e.g. Pan-STARRS). Our survey

will be **optimized towards small NEA detection** with byproducts available for additional science.

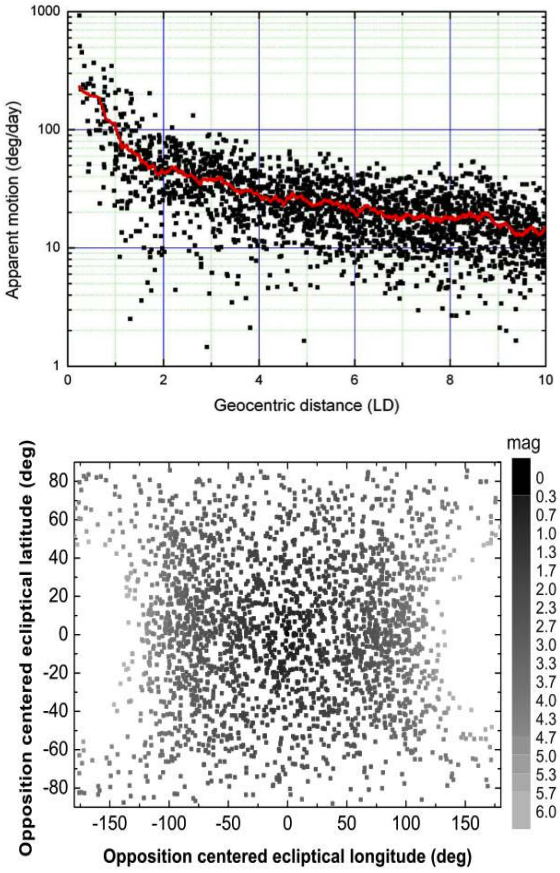

Figure 3. Rate of motion of asteroids on near-miss orbits as a function of the minimum geocentric distance denoted in lunar distances (left) and magnitude loss (a phase effect) of asteroids as a function of opposition centric ecliptical distance.

2.2. Targets of the survey

The main target of the survey is **discovery and characterization of small NEA and other close-approaching populations**. The survey will search for potential **Earth impactors** of small and intermediate diameters (1–100 m) and **pre-entry detections of bright bolides**. The all-sky coverage and optimization toward high angular rate of motion would make the system a good detector for **monitoring, characterization and discovery of space debris**. This combination of survey properties will also benefit the detection of **telescopic meteors** as well. Because the limiting magnitude will not be a competition for multi-meter apertures and space based telescopes, it will serve the photometry of objects that

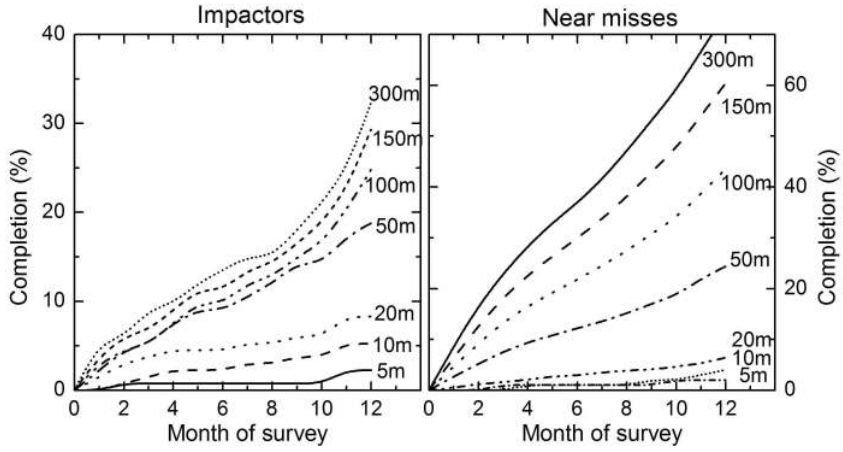

Figure 4. Survey efficiency in finding Earth impacting asteroids (left) and asteroids that fly-by in the Earth vicinity (right).

are too bright and saturated for next generation surveys, such as **bright main belt asteroids**. The extremely low focal ratio and large light gain of the aperture would help **discovery of active asteroids** (Jewitt 2012), especially at low solar elongations. The important feature of the project will be the accessibility of the data – the database will be available for external scientists to mine additional resources for **science byproducts**, such as **variable stars, novae, supernova, lensing events, gamma-ray bursts**.

3. Expected outcomes

We simulated a one-year ADAM-WFS survey based at AGO Modra Observatory, by using MOPS with the realistic pointings, avoiding Moon and using orbits of large MB asteroids, synthetic orbits of asteroids that will approach the Earth within 10 lunar distances based on real asteroids and Earth impacting asteroids (Chesley and Spahr 2004; Denneau et al. 2013). The apparent rate of motion of asteroids at the closest distance and phase effect of asteroids near the Earth are shown in Fig. 3. Figure 4 shows the efficiency of the proposed system in discovering Earth impacting asteroids and close approachers as the function of diameter and the duration of the survey. Depending on the population model, this system will be able to discover $30-120$ NEAs with $D > 10\,m$ within 10 lunar distances per year and a comparable number of smaller asteroids with diameter $D < 10\,m$. Figure 5 shows the number of known large main belt asteroids that will be discovered within one year survey. Due to the cadence of the survey we will obtain ~ 650 light curves of bright main belt asteroids every year, suitable especially for slow rotators detection. We also performed the simulation of space debris detection by using the SPACE-TRACK debris catalog. The simulation detected 350 - 550 space debris particles per night (Fig. 6).

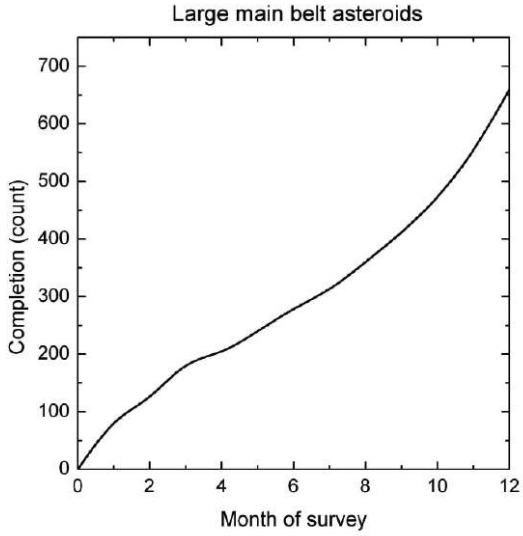

Figure 5. Survey efficiency of large main belt asteroids.

4. Conclusion

The project of ADAM-WFS represents a new way of observation and exploration of the small NEO population in the close vicinity of the Earth. The project will fill up the current gap in our knowledge of small solar system bodies between the bolide-sized objects observed in the atmosphere and the large asteroids and comets ob-

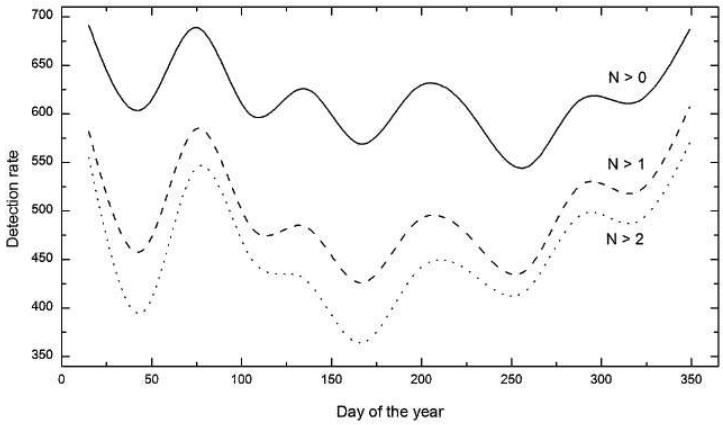

Figure 6. Number of detection of space debris per night by ADAM-WFS based on space-track data. The number of detections per particle per night ($N > 0$, at least one detection; $N > 1$, two and more detections; $N > 2$, more than two detections). Variations in the rates are produced by the combination of weather conditions and Earth's shadow vs. field of view geometry.

served telescopically. Identical telescopes can be installed all over the world or cooperate with other similar projects like ATLAS to increase the sky coverage and not depend on the daylight cycle to search for small NEOs, Earth impactors and optical transient events like variable stars, novae or supernovae. Data gathered during the operation will provide terabytes of images and database entries for years of research and data mining. Naturally, additional coordinated follow-up observations will be needed to complete the orbital and physical determination of newly found asteroids.

Acknowledgements

We thank for the financial support from NASA grant No. NNX12AR65G and Slovak Research and Development Agency Grant No. APVV 0516-10 and APVV 0517-12.

References

Babadzhanov P.B., Williams I.P., Kokhirova G.I., 2013, A&A, 556, A25

Bottke W.F., Morbidelli A., Jedicke R., Petit J.M., Levison H.F., Michel P., 2002, Icarus, 156, 399

Brown P.G., Assink J.D., Astiz L., Blaauw R., Boslough M.B., Borovička J., Brachet N., Brown D., Campbell-Brown M., Ceranna L., Cooke W., de Groot-Hedlin C., Drob D.P., Edwards W., Evers L.G., Garces M., Gill J., Hedlin M., Kingery A., Laske G., Le Pichon A., Mialle P., Moser D.E., Saffer A., Silber E., Smets P., Spalding R.E., Spurný P., Tagliaferri E., Uren D., Weryk R.J., Whitaker R., Krzeminski Z., 2013, Nature, 503, 238

Chesley S., Spahr T., 2004, ?? in Mitigation of Hazardous Comets and Asteroids, 22

Denneau L., Kubica J., Jedicke R., 2007, XVI ASP Conf. Ser., 376, 257

Denneau L., Jedicke R., Grav T., Granvik M., Kubica J., Milani A., Vereš P., Wainscoat R., Chang D., Pierfederici F., Kaiser N., Chambers K.C., Heasley J.N., Magnier E.A., Price P.A., Myers J., Kleyna J., Hsieh H., Farnocchia D., Waters C., Sweeney W.H., Green D., Bolin B., Burgett W.S., Morgan J.S., Tonry J.L., Hodapp K.W., Chastel S., Chesley S., Fitzimmons A., Holman M., Spahr T., Tholen D., Williams G.V., Abe S., Armstrong J.D., Bressi T.H., Holmes R., Lister T., McMillan R.S., Micheli M., Ryan E.V., Ryan W.H., Scotti J.V., 2013, PASP, 12, 357

Gehrels T., Marsden B.G., McMillan R.S., Scotti, J.V., 1986, AJ, 91, 1242

Harris A., 2008, Nature, 453, 1178

Jewitt D., 2012, AJ, 143, 66

Kaiser, N., Burgett, W., Chambers, K., et al., 2010, Proc. SPIE, 7733

Koehn B. W., Bowell E., 1999, BAAS, 31, 1091

Larson S., Brownlee J., Hergenrother C., Spahr T., 1998, BAAS, 30, 1037

Mainzer A., Bauer J., Grav T., Masiero J., Cutri R.M., Wright E.L., Nugent C.R., Stevenson R., Clyne E., Cukrov G., Masci F., 2013, arXiv:1310.2980

Pravdo S.H., Rabinowitz D.L., Helin E.F., et al. 1999, AJ, 117, 1616

Porubčan V., Štohl, J., Svoreň J., 1992, Contrib. Astron. Obs. Skalnate Pleso, 22, 25

Rabinowitz D.L., Bowell E., Shoemaker E.M, Muinonen L., 1994, in Hazards due to comets and asteroids, University of Arizona press, 285312

Rudawska R., Jenniskens P., Vaubaillon J., 2012, European Planetary Science Congress, 2012, 711

Schunová, E., Granvik, M., Jedicke, R., et al., 2012, Icarus, 220, 1050

Schunová E., Jedicke R., Walsh K.J., Granvik M., Wainscoat R.J., 2014, Properties and evolution of near-Earth object families created by tidal disruption., Icarus, submitted
Spurný P., Oberst J., Heinlein D., 2003, Nature, 423, 151
Stokes G.H., Evans J.B., Viggh H.E.M., Shelly F.C., Pearce E.C., 2000, Icarus, 148, 21
Stuart J.S., Binzel R.P., 2004, Icarus, 170, 295
Tóth J., Kornoš L., 2002, Acta Astron. et Geoph. Univer. Comen., XXIV, 61
Tóth J., Kornoš L. 2002, CD-ROM proceedings MACE 2003, May 1-4, 2003, Mallorca, Spain, 35
Tóth J., Vereš P., Kornoš L., 2011, MNRAS, 415, 1527
Tonry J.L., 2011, PASP, 123, 58
Vereš P., Tóth J., Kornoš L., 2006, Contrib. Astron. Obs. Skalnate Pleso, 36, 171
Wright E.L., Eisenhardt P.R.M., Mainzer A.K. et al. 2010, AJ, 140, 1868

Meteoroids 2013, Proceedings of the Astronomical Conference, held at A.M. University, Poznań, Poland, Aug. 26-30, 2013, eds Jopek T.J., Rietmeijer F.J.M., Watanabe J., Williams I.P., Adam Mickiewicz University Press in Poznań, pp 315–318

Meteor detection in wide-field survey telescopes

Ocaña F.[1], **Ponz J.D.**[2], **Zamorano J.**[1]

[1]Departamento de Astrofísica y Ciencias de la Atmósfera, Facultad de Ciencias Físicas, Universidad Complutense de Madrid, 28040 Madrid, Spain, (fog@astrax.fis.ucm.es)
[2]Neomenia S.L.

Abstract. Meteor observing requires a huge field of view (FoV) as its appearance in the sky cannot be foreseen. In the new era of the time-domain astronomy many telescopes will cover the whole sky with a cadence of a few days. These requirements lead to fast large telescopes with wide FoVs, like the Schmidt cameras that were widely used for meteor observing in the past. Common general-purpose telescopes have small plate scale and employ large integration times, what plays against meteor detection. We present here an estimation of the number of meteors detected as a byproduct of these surveys, with the detailed example of the Test-Bed Telescopes, an ESA project for NEO and space debris surveillance.

Keywords: meteors, video technique, CCD, Schmidt camera

1. Telescopic meteors

Meteors have been widely observed with the use of telescopes throughout history. First conscientious studies started probably in the nineteenth century (Taibi, url). In the twentieth century these efforts were retaken and observers were encouraged to use telescope techniques for more accurate observations and survey populations of smaller particles (Millman 1937; Olivier 1950).

In the last decades there has been some specific studies measuring telescopic meteor fluxes (Henize et al. 1993), but in the vast majority of the cases these are serendipitous detections (Borovička and Zamorano 1995; Jenniskens et al. 2004; Iye et al. 2007).

Nevertheless identifications could be an issue in wide-field telescope images. Fortunately these telescopes usually have focal lengths large enough to show meteors (at 100km high) out of focus (Jenniskens et al. 2004; Iye et al. 2007). Also low-earth orbit satellites are easily discarded taking images only when the Sun is not illuminating these orbits (usually within 2 hours after or before the twilight). Due to their nature meteors within the hundredths of micron range are monitored using radar sensors. Most optical meteor surveys observe meteor down to magnitude 6 (millimeters range), however smaller meteoroids are able to produce meteors as they suffer ablation down to 100 microns (Bronshten 1983). For the sake of simplicity, we assume they have similar luminous efficiencies and there is constant mass index (s) in the range of the meteors detectable by wide-field survey telescopes (magnitude < 10). To determine the number of meteors N_m detectable by the telescope we need to calculate the flux of meteoroids in the detection range of the telescope, it is the integral down to the limiting magnitude (lm) of the meteor luminosity function F(m). Therefore these meteors are observable in the optical range with the use of

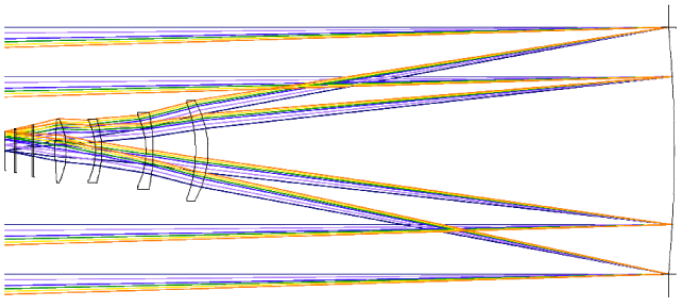

Figure 1. 60 cm f/2.5 prime-focus telescope optical layout. It has a 4-lens Wynne corrector that gives an aberration-corrected FoV of almost 3° in diameter.

silicon devices (i.e., CCDs) and the aid of large collection area optical devices.

$$F(m)\mathrm{d}m = \mathrm{d}N_m \approx m^{-s}\mathrm{d}m \tag{1.1}$$

Inputs for this study are the sporadic meteoroid fluxes detected in the visual range (down to magnitude +6) by IMONET (Molau et al. 2013) and in the radar range for fainter meteors (Blaauw et al. 2011).

1.1. Average sporadic meteor

We define some 'standard' values to simplify the problem. They are educated guesses to get a rough order of magnitude of the detectable meteors. The best approximation for such a problem would be a proper simulation with real population and conditions. The limiting magnitude of the meteor depends on the sky brightness, the time of integration and the speed of the meteor. Then the photons reaching a certain pixel coming from a meteor should be numerous enough over the photons coming from the sky during the whole time of integration. As the distribution is close to potential, the 'radar' meteors would be the most numerous. For this range the sporadic flux is well above the meteor shower flux. Thus we can assume some average properties (i.e., 30 km/s speed), an average elevation of the FoV of 50 degrees and a mean radiant distance to the sporadic sources of 45 degrees. This leads to an average apparent speed of $8°/s$. The area is the projected FoV at 100 km high, the average beginning height of meteors. Therefore we would calculate the number of meteors starting in the FoV, but not the ones crossing it. Consequently we consider the meteors being around 5-10 degrees long to calculate the number of meteors crossing the FoV.

2. Test-Bed telescopes for SSA activities

Within the Space Situational Awareness (SSA) programme of ESA, it is foreseen to deploy several robotic telescopes to provide surveillance and tracking services for man-made as well as natural near-Earth objects (NEOs). The Test-Bed Telescope

Table 1. Comparison of theoretical numbers with real data from IMONET (video camera ACR operated by Wolgang Hinz) (Molau et al. 2013).

System	FoV (sq. degrees)	Meteor lm	Meteor rate h^{-1}
TBT	6.25	7	≈ 1
SuperWasp	482	8	≈ 15
HINWO/ACR	557	6	≈ 5

(TBT) project will procure a validation platform for an autonomous optical observing system in a realistic scenario, consisting of two telescopes located in Spain and Australia, to collect representative test data for precursor SSA services. These small telescopes are a clear example of this new astronomical survey era. They will be 60-cm telescopes with a 2.5×2.5 square degrees FoV taking short exposure images during clear nights all year round. The result of this study for the TBT telescopes with ca. 12 square degrees of FoV is the detection of sporadic meteors around a couple of them per hour. Low-noise CCD read-out, short exposures and dark sky are essential to increase the SNR of meteors and the subsequent detection probability. Else the limiting magnitude is diminished rapidly due to the short time the meteor spends over a pixel compared to the constant sky background.

3. Meteor detections by telescopes: estimations

Once the flux of meteoroids down to a certain mass/size is known, we can evaluate the performance of these systems (meteor rate) as the product of the flux of meteoroids by the atmospheric area A monitored by the telescope.

$$\text{meteor rate} = A \cdot \int_{-\infty}^{lm} F(m)\mathrm{d}m \tag{3.1}$$

TBT telescopes have a plate scale of 2.2 arsec/pixel. For a meteor at 8°/s, the light will be over the pixel for only 0.08 ms. Therefore the relationship between plate scale and meteor speed is the main constraint for the limiting magnitude. For a typical exposure of 2 s, the stellar limiting magnitude for TBT telescopes (A=25 km^2) will be around 18, however it would be no more than 7 for our average meteor. This leads to a value of only 0.06 meteors starting in the field per hour, and around 1 meteor per hour through the field.

However the SuperWASP survey is covering 482 square degrees with a plate scale of 13.7 arsec/pixel. The same 'average' meteor will spend 0.5 ms over each pixel. For its typical exposure of 30 s, the stellar limiting magnitude for SuperWASP will be 18, however it would be only 8 for meteors. This leads to a value of around a tenth of meteors per hour through the field.

In Table 1 it can be seen that a system like SuperWasp could achieve a similar detection rate that a dedicated meteor detection video camera. Short exposures are very important for increasing meteor detection rate, what could be the case for

time-domain surveys. Common general-purpose telescopes have small plate scale and most scientific cases lead to employ large integration times, what plays against meteor detection.

4. Conclusions

Meteor detection rates to be achieved with the future wide-field survey telescopes are similar to the ones for current video networks. Therefore meteors detected as byproducts in these surveys will be a free source of meteoric data. For this purpose survey images should be analyzed by meteors scientists using survey archives or even dedicated algorithm in their processing pipelines. All these telescopes will sum up thousands of square degrees, observing each night. The combined detecting area at 100 km high will be more than 10000 km^2, similar to some of the video systems devoted to meteor detection.

A proper simulation should be carried to investigate further in this topic using real populations. In this Meteoroids 2013 conference other group carried out an experimental test with a CMOS sensor at the 1.05-m Kiso Schmidt. They get results in the range expected (Watanabe et al. 2014).

References

Blaauw R., Campbell-Brown M., and Weryk R., 2011, MNRAS, 412, 2033

Borovička J. and Zamorano J., 1995, EM&P, 68, 217

Bronshten V.A., 1983, Fizika meteornykh iavlenii, Moscow, Izdatelstvo Nauka, 1981, Dordrecht, D. Reidel Publishing Co., 1983, English translation

Henize K. G., Stanley J. F., O'Neill C. A., and Nowakowski B. S., 1993, in Optical Engineering and Photonics in Aerospace Sensing. International Society for Optics and Photonics, 76

Iye M., Tanaka M., Yanagisawa M., Ebizuka N., Ohnishi K., Hirose C., Asami N., Komiyama Y., and Furusawa H., 2007, arXiv preprint arXiv:0704.3491

Jenniskens P., Jehin E., Cabanac R.A., Laux C.O., and Boyd I.D., 2004, M&PS, 39, 609

Millman P. M., 1937, Journal of the Royal Astronomical Society of Canada, 31, 93

Molau S. et. al., 2013, "Monthly Reports of the AKM/IMO Video Meteor Network", posted on IMONET website `//www.imonet.org/reports/`

Olivier Ch.P., 1950, Proceedings of the American Philosophical Society, 94, 327

Taibi R., "The early years of meteor observations in the USA", `http://www.amsmeteors.org/about/ams-history/the-early-years-of-meteor-observations-in-the-usa/`

Watanabe J., Kasuga T., Terai T., Miyazaki S., Ohta K., Murooka F., Ohnishi T., Yamasaki T., Mito H., Aoki T., Soyano T., Tarusawa K., Matsunaga N., Sako S., Kobayashi N. and Doi M., Enomoto, 2014, in Meteoroids 2013, Proc. of the Astron. Conf., held in Poznań, Poland, Aug. 26-30, eds Jopek T.J., Rietmeijer F.J.M., Watanabe J., Williams I.P., AM University Press, Poznań, p. 325

Meteoroids 2013, Proceedings of the Astronomical Conference,
held at A.M. University, Poznań, Poland, Aug. 26-30, 2013,
eds Jopek T.J., Rietmeijer F.J.M., Watanabe J., Williams I.P.,
Adam Mickiewicz University Press in Poznań, pp 319–323

A new software application for allsky camera networks

Peterson C.L.
Department of Planetary Science, Denver Museum of Nature and Science, Denver, Colorado, USA
(clp@alumni.caltech.edu)

Abstract. We report on a new software suite for operating allsky cameras intended for meteor analysis. The software consists of a client component local to each camera, and a central server component which each camera supplies with data. The software is modular and major components are open source. Particular attention is directed towards utilizing published, publicly available code for critical analysis routines.

Keywords: allsky cameras, camera networks, meteoroid orbit analysis, video meteors

1. Introduction

A number of software and hardware tools are available to automate the detection and recording of meteor events (Molau 2012; SonotaCo 2005; Brown et al. 2010; Chavez 2009). Cloudbait Observatory and the Denver Museum of Nature and Science have operated a network of allsky cameras (Peterson 2010) in Colorado since 2001 using a combination of publicly available software as well as proprietary, internally developed tools. Maintaining this system has grown difficult as the detection software is dependent on obsolete hardware. Furthermore, the use of proprietary analysis code makes it difficult to compare data with that from other camera networks.

Our response has been to reconsider the entire system, designing software optimized for our specific requirements, and for allsky meteor networks in general.

2. Current problems

Issues limiting the quality of data, and the efficient growth of the network include:

- current software (Metrec) is dependent on obsolete video digitization hardware,
- current software only supports low resolution analog video cameras,
- analog video digitizers introduce astrometric errors (Peterson 2011),
- use of unpublished, unreviewed analysis code reduces confidence in data,
- system provides limited real-time response to events,
- orbit determination is unautomated,
- data upload mechanism creates security issues for client camera sites.

3. Design goals

The intent was to develop an open source software package that could be easily implemented by anyone operating an allsky camera network.

Key to this goal was limiting the functionality of the software at the camera site to nothing more than detection and reporting. This offloads all the critical analysis work to a centrally managed server, ensuring uniformity in processing and little need to maintain and update software in the field.

Additionally, it was planned to utilize standard video driver code integral to the camera computer operating system, allowing for much broader support of video devices. In particular, it is a goal of the network to migrate from the current NTSC video cameras to higher resolution cameras with digital interfaces.

Finally, an important design goal was to provide a web access portal to the meteor data, with access for both camera operators, network operators, other researchers, and the public.

4. Design strategy

The system was planned to consist of two components: a video acquisition and meteor detection client, and an analysis server. The client module was intended to operate in a Windows environment, since that is the primary operating system at 85% of our current camera sites, and is supported by all of them.

The client system's code was planned to separate video acquisition into a high priority thread and the meteor detection into a background process. This was intended to allow modest computer hardware to operate with complex detection and false event handling even at high frame rates and high resolution.

In order to simplify network configuration for the camera operators, all communication between the client and server was planned to utilize only the HTTP protocol.

The server code was designed to operate on any system configured as a typical web server, with no dependence on compiled code or executable modules. MySQL was chosen for the database component. PHP was chosen for all the code modules, because its similarity to C makes code translation fairly easy, it is installed by default on virtually all web servers, and because it is an interpreted language. The use of an interpreted language means that the network code is automatically multiple platform, with no need for different compiled versions.

5. Client module

The client module consists primarily of the video acquisition interface and meteor detection code, supplemented by several optional user utilities.

Video frames are scanned as they are received. Meteors are tentatively identified by a simple motion detection algorithm which is not computationally intensive. A ring buffer is utilized so that frames recorded before an event is detected become part of the meteor record. Recorded frames are maintained in memory and analyzed using a series of tests running in a low priority thread, eliminating most false events. Data which are determined to represent a meteor are written to disk. Event details are transmitted via Internet to the meteor network server. Data include event endpoints in local horizon coordinates, peak magnitude, start time, and event

duration. To avoid server overloading on large networks, the raw video is retained on the client machine and not automatically uploaded to the server. Summary data are uploaded using the HTTP PUT method, and the client polls the server periodically for specific instructions. In response to the proper semaphore, the client may subsequently upload the raw video frames for an event. By restricting all communications to HTTP traffic on standard ports, security and firewall issues at client sites are largely avoided.

Automated start and stop based on location and twilight times, and unattended operation are fully supported.

Three utility applications are provided. An astrometric calibrator collects a series of video frames, co-adds them, and produces a plate solution. The latest solution is always included with the summary data uploaded by the detection module. A post-processor allows all events to be manually examined and optionally rejected. A data viewer presents saved videos and the results of local analyses.

6. Server module

The server module manages all of the client stations, and performs the bulk of the event analysis.

The server module receives event summaries from client stations. Data are immediately inserted in a MySQL database. Timing correlation is used to detect simultaneous recording of single events across multiple stations. When a correlated event is suspected, the server posts flags on a hidden web page which is monitored by the clients, triggering the upload of all video data from cameras potentially in capture range of the meteor. The server then performs a series of analyses on each combination of station pairs that recorded that event.

The *radiant and timing calculator module* accepts the station coordinates, event start and stop coordinates, and the event start and stop time. It calculates the geocentric atmospheric trajectory for each station pair combination. It also calculates the average velocity and estimates the initial velocity.

The *state vector calculator module* applies required coordinate transforms utilizing a PHP port of NOVAS (Bangert et al. 2011): ITRS to GCR to ecliptic coordinates. State vectors are calculated from each station pair combination.

The *orbit calculator module* accepts a state vector, calculates the heliocentric positions for the Earth, Moon, and planets utilizing the VSOP82 algorithm (Meeus 1991) , and applies these to a PHP port of the MERCURY integrator (Chambers J.E., Migliorini F. 1997), performing backward integration to convergence on stable orbital elements.

The server module also provides a human interface to the collected and analyzed data. Access is controlled so that information available publicly is optionally limited in comparison with data available to camera operators and designated researchers. In its typical configuration, event summaries are available for all events recorded by every camera, and complete analyses are available for all multiple station events. The user interface provides searchable access to the meteor database, orbital anal-

ysis for multiple-station events, a ground track plotter, a graphical orbit plotter, and a video viewer.

Finally, the server module manages a visual witness input mechanism and witnessed meteor database.

7. Results

Some components of this software remain in active development. Beta code has been operational on a three-camera subnet (baselines 66 km, 85 km, 101 km, inside the current Colorado network boundaries, which functions as a reference system) since May 2013. All cameras are identical, but the three test stations utilize different video capture hardware than the reference network stations.

The sensitivity of the test system is equivalent to the reference system, but the major sources of false events that plague the reference system (airplanes, clouds, water drops on the camera dome) are almost completely eliminated. Most captured events to date are sporadic meteors, lacking any reference orbit for accuracy comparison. Orbit solutions for most sporadics are consistent with the antihelion and apex sources. Confirmed multi-station shower member detections include 22 Southern Delta Aquariids (SDA), 11 Alpha Capricornids (CAP), 30 Eta Aquariids (ETA), and 25 Perseids (PER). In all cases, calculated orbital elements show good agreement with published orbits for the associated showers. The largest error is in the determination of the semi-major axis (mean standard deviation 15%), which is attributed primarily to the poor accuracy of the initial velocity estimate inferred from the average velocity during luminous flight.

Math intensive analysis modules ported to PHP yield identical results to their native versions (C and FORTRAN).

The system has been tested successfully with a 1280 x 960 pixel, 30 frame/s Firewire camera, providing substantially better data than a conventional NTSC analog video camera. It is known that digitization of an analog video signal can produce significant astrometric errors.

8. Ongoing development

A major source of error in the orbit calculation is the use of an initial velocity estimated from the average velocity. Under development is an automated frame analyzer that resolves the meteor centroid as a function of time. This will allow an accurate initial velocity to be determined and a deceleration profile calculated.

The frame analyzer will also provide a light curve (subject to dynamic range limitations of the hardware). Some cameras in the current network utilize a Lambertian sphere in the field of view to provide an accurate light curve for fireballs which saturate the detector in the direct image. Plans are to include this feature in all the new network cameras.

The current astrometry module solves for altitude using a third-order polynomial model. Higher resolution cameras will require a higher order solution, ideally utilizing published astrometry code.

Multiple station analysis for events with data from more than two stations is currently handled by calculating results for each station pair combination, and then averaging with a simple weighting factor based on the location of the event in each camera field. A more sophisticated statistical scheme needs to be developed.

References

Bangert J., Puatua W., Kaplan G., Bartlett J., Harris W., Fredericks A., Monet A., 2011, "Users Guide to NOVAS Version C3.1", Washington, DC, USNO, http://aa.usno.navy.mil/software/novas/novas_c/NOVAS_C3.1_Guide.pdf

Brown P., Weryk R.J., Kohut S., Edwards E.N., Krzeminski Z., 2010, "Development of an Allsky Video Meteor Network in Southern Ontario, Canada, The ASGARD System", WGN, 38, 25

Chambers J.E., Migliorini F., 1997, "Mercury – A New Software Package for Orbital Integrations", Bull. American Astron. Soc., 29, 1024

Chavez J., 2009, "Video Sentinel Users Manual", Sandia National Laboratories

Molau S., 2012, "MetRec Software", http://metrec.org

Meeus J., 1991, "Astronomical Algorithms", Willmann-Bell, Inc., pp. 205-208

SonotaCo, 2005, "UFOCapture Software", http://sonotaco.com

Peterson C., 2010, "The Colorado Allsky Camera Network", Proceedings of the IMC, Armagh, 2010, 87

Peterson C., 2011, "A comparison of the impact of jitter and timing errors on the accuracy of several popular video capture devices", NASA Workshop: Meteor Video Observations and Analysis, PARI, 2011 Aug 4-5, http://cloudbait.com/science/mvoa2011.pdf

Meteoroids 2013, Proceedings of the Astronomical Conference,
held at A.M. University, Poznań, Poland, Aug. 26-30, 2013,
eds Jopek T.J., Rietmeijer F.J.M., Watanabe J., Williams I.P.,
Adam Mickiewicz University Press in Poznań, pp 325–328

Faint meteor observation by large-format CMOS sensor with 1.05-m Kiso schmidt telescope

Watanabe J.[1], Kasuga T.[1], Terai T.[1], Miyazaki S.[1], Ohta K.[2], Murooka F.[2], Ohnishi T.[2], Yamasaki T.[2], Mito H.[3], Aoki T.[3], Soyano T.[3], Tarusawa K.[3], Matsunaga N.[1], Sako S.[3], Kobayashi N.[3], Doi M.[3], Enomoto T.[4]

[1]National Astronomical Observatory of Japan (jun.watanabe@nao.ac.jp)
[2]Canon Inc.,
[3] Kiso Observatory, Institute of Astronomy, School of Science, University of Tokyo,
[4] JAXA/ISAS/SOKENDAI

Abstract. We tried to use a new high-sensitivity CMOS sensor of the world's largest size as a one-chip ($\sim$ 20cm$\times$20cm square) attached to the prime focus of the 1.05 m (F3.1) Schmidt telescope at the Kiso Observatory, University of Tokyo, for faint meteor observation. The resulting field of view was 3.3 by 3.3 degrees, with a limiting magnitude of about 12 in our preliminary analysis. Assuming the height of faint meteors at 100 km, the derived flux of sporadic meteors is about 5×10^{-4} km^{-2} s^{-1}. Although the analysis is still on going, it is clear that this CMOS sensor is useful and effective for observing faint meteors.

Keywords: CCD, faint meteors, instruments, observation technique

1. Introduction

For observing faint meteors, we need either a large telescope or comparable optics, which always give a limitation of the field of view. It is a kind of trade-off between the high sensitivity by using larger telescope and narrower field of view. Reconciling these conflicting requirements, we need a large-format imaging detector. Usually we realize it by putting many CCD chips in sequence at the focal plane. However, we have always undetectable region as a gap of the chips. These gaps can be filled for the static targets like galaxies by using mosaic imaging technique, but not for the high-spe ed moving objects like meteors. Therefore, large format one-chip sensor was desired for future observations.

2. A new large format CMOS sensor

A ultra-high-sensitivity CMOS sensor of the ultra-large format was developed by Canon Inc. in 2010 (http://www.canon.com/news/2010/aug31e.html, 2010, Yamashita et al. (2011)). The format is 202×205 mm square in size which is the world largest one-chip CMOS sensor. This can be produced from an $\sim$12-inch ($\sim$300 mm) wafer, and is approximately 40 times the size of Canon's largest commercial CMOS sensor as shown in Figure 1. The number of pixels is 1280×1248. Because the increased size of the new CMOS sensor allows more light to be gathered, it enables

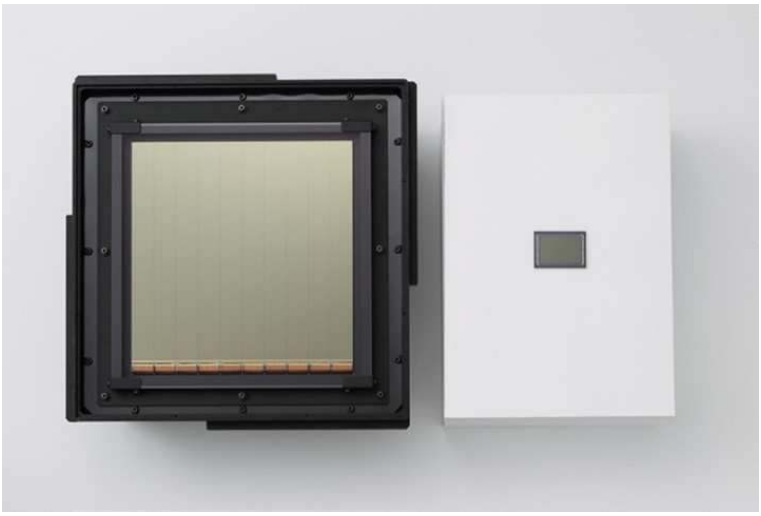

Figure 1. A new large-format CMOS sensor (left) and a 35mm full size CMOS sensor often used in digital single-lens reflex camera product (right). This image was provided by Canon Inc.

shooting in low-light environments. The sensor makes it possible to capture image with one one-hundredth the amount of light required by a 35 mm full-frame CMOS sensor, facilitating the shooting of 60 frame-per-second video with a mere 0.3 lux of illumination. One of the applications for the new ultra-high-sensitivity CMOS sensor is video recording of astronomical phenomena in the night sky. We used this large-format CMOS sensor attached to the prime focus of the 1.05-m (F3.1) Schmidt telescope (Takase et al. 1977) at the Kiso Observatory, Institute of Astronomy, School of Science, University of Tokyo, for faint meteor observation. The resulting field of view was 3.3 by 3.3 degrees.

3. Test observations

Several test observations including operation checks of the system were carried out during 11–13 January 2011, 3–7 September 2011, and 12–17 December 2012. The images were taken at the high time resolution as 60 frames per second. In this system, the limiting magnitude is estimated to be about 12 in our preliminary analysis. Because of the limitation of the data storage, full-power observations (14-bit data per 1/60 second) were performed for about one or two hours each night. During the first period, we counted a sporadic meteor every 5 seconds at an elevation 30 degree. This is about one order higher detection rate of faint meteors compared with previous work (Pawlowski et al. 2011).
Assuming the height of faint meteors at 100 km, the derived flux of the sporadic meteors is about $5\times10^{-4}\mathrm{km}^{-2}\ \mathrm{s}^{-1}$.

The last run was performed during the active period of the Geminid meteor shower. We could take useful data on December 12 and 13. We pointed the telescope

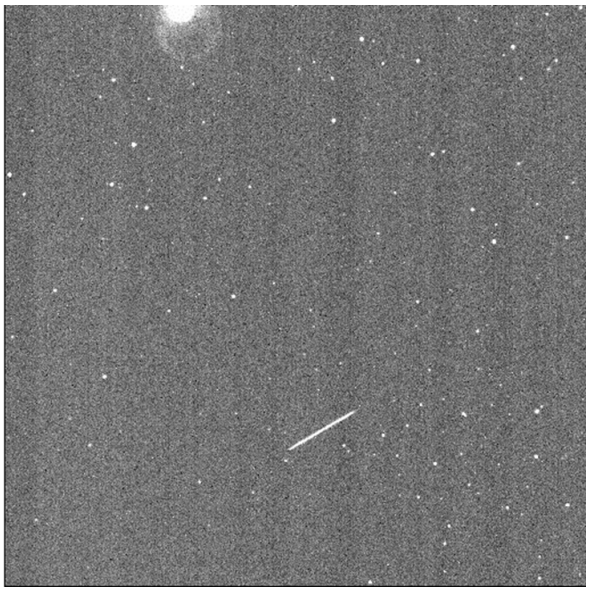

Figure 2. An example image of a Geminid meteor detected on December 12 2012. The center is the north pole, and exposure time is 1/60 sec. The star at the edge of this image is the Polaris.

to the north celestial pole on December 12, and to the points of 20 degrees north and east from the radiant point. Figure 2 shows an example of a Geminid meteor detected on December 12. One of the authors inspected a part of data taken at around 20h UT by naked eye, and detected 58 meteors, including 11 Geminid meteors, among about 17000 frames which corresponds to 287 seconds from 20h 00m UT on December 12. Because these data was taken at the elevation of about 60 degrees, the expected area is about 200 km^2 at the height of 100 km. Therefore, the flux of the meteors was 1×10^{-3} km^{-2} s^{-1}. This value is two times larger than that derived in the first run.

During the Leonid meteor shower, Watanabe et al.(1999) derived the flux of sporadic meteors as 1.3×10^{-5} km^{-2} s^{-1} by video observations with a limiting magnitude of 7. This value was basically that of sporadic meteors due to the lack of strong activity in the Leonid meteor shower in 1998. If we assume the magnitude index of 3, then the expected flux for magnitude of 10 will be 3.5×10^{-4} km^{-2} s^{-1}, which is almost comparable to that obtained in this observation.

At present, we cannot progress further mainly due to the delay in the development of the automatic detection program. We have demonstrated that this CMOS sensor is useful and effective for observing faint meteors. The flux of faint meteors is rarely derived, especially for sporadic meteors. Campbell-Brown (2007) noted that while a significant amount of video data has been collected, sporadic fluxes have never been calculated for video data. Unfortunately, the system was not stable so that various noise patterns that frequently occurred on each of the frames, which was not fixed even in the last observation run. However, these noise patterns can

be removed by a similar reduction method as used for the flat field correction. It is not a serious problem for faint meteor observations.

References

Campbell-Brown M., 2007, in Proc. Workshop on Dust in Planetary Systems (ESA SP-643), September 26-30 2005, Kauai, Hawaii. Editors: Krueger H., Graps, A., 11

Pawlowski J.F. et al., 2001, M&PS, vol. 36, no. 11, 1467

Takase B. et al., 1977, Ann. Tokyo Astron. Obs. 2nd Ser., Volume XVI, Number 2, 74

Watanabe J. et al., 1999, Pub. Astron. Soc. Japan, vol. 51, L11

Yamashita Y. et al., 2011, in Proc. Solid-State Circuits Conference Digest of Technical Papers (ISSCC), IEEE International, 408

Meteoroids 2013, Proceedings of the Astronomical Conference,
held at A.M. University, Poznań, Poland, Aug. 26-30, 2013,
eds Jopek T.J., Rietmeijer F.J.M., Watanabe J., Williams I.P.,
Adam Mickiewicz University Press in Poznań, pp 329–333

Correction effect to the radiant dispersion in case of Low Velocity Meteor Showers

Sato M.[1], **Watanabe J.**[2]

[1]Kawasaki Municipal Science Museum, Japan (mail@kaicho.net),
[2]National Astronomical Observatory of Japan (jun.watanabe@nao.ac.jp)

Abstract. We usually apply various corrections for determining apparent radiant point to the actual trajectories of shower meteors. In case of low velocity meteor showers, the velocity corrections should be carefully performed together with the error estimate. Here we show that such correction strongly affects the dispersion of radiant points especially in case of low geocentric velocity meteor showers.

Keywords: near-Earth asteroids, dormant comets, meteoroid stream, meteor showers, orbits, evolution, radiants

1. Introduction

We usually apply various corrections for determining apparent radiant point to the actual trajectories of shower meteors. In case of low velocity meteor showers, the velocity corrections should be carefully performed together with the error estimate. Here we show that such correction strongly affects the dispersion of radiant points especially in case of low geocentric velocity meteor showers.

2. Examination

The radiant is described by the synthetic vector between the velocity of meteoroids and the velocity of the Earth. We assumed the range of intrinsic dispersion in the estimate of velocity "d". Figure 1 shows the relation between the radius of the radiant and "d". It becomes obvious that the radius is dependent on the geocentric velocity "Vg". And we derived the corresponding radii of radiant points in various meteor showers. Figure 2 shows the result when "d" = 2 km/sec. We can easily recognize the correction effect of the dispersion is larger with lower velocity meteor showers. While in the case of large velocity such as Leonids and Perseids, the derived dispersion of the radiants is small, it becomes quite large in the case of Draconids and Phoenicids. Accordingly, we found out the simple method of correcting this. We calculate the corrected radiant by subtracting the Earth vector (Figure 3). It means that the actual heliocentric velocity of meteor shower is obtained. Figure 4 shows the result of modified radiant points. It becomes clear that the derived dispersion of radiants can be obtained by this correction.

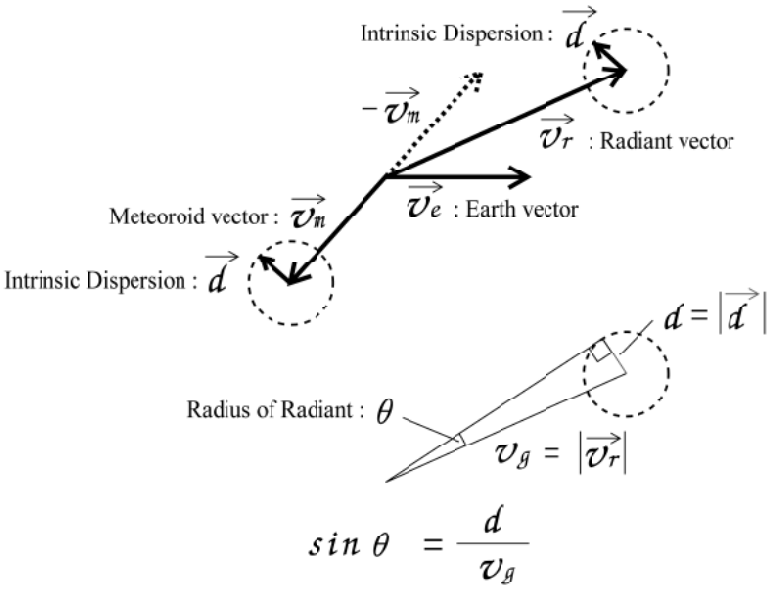

Figure 1. Relation between the radius of the radiant and the geocentric velocity of meteor showers.

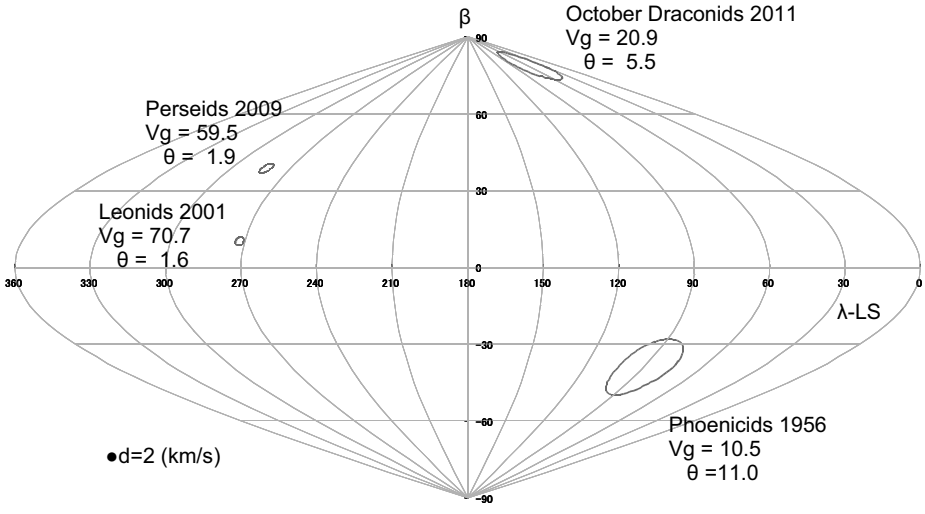

Figure 2. Derived radii of radiant points corresponding to the error of 2 km/sec. V_g is the geocentric velocity of meteor showers.

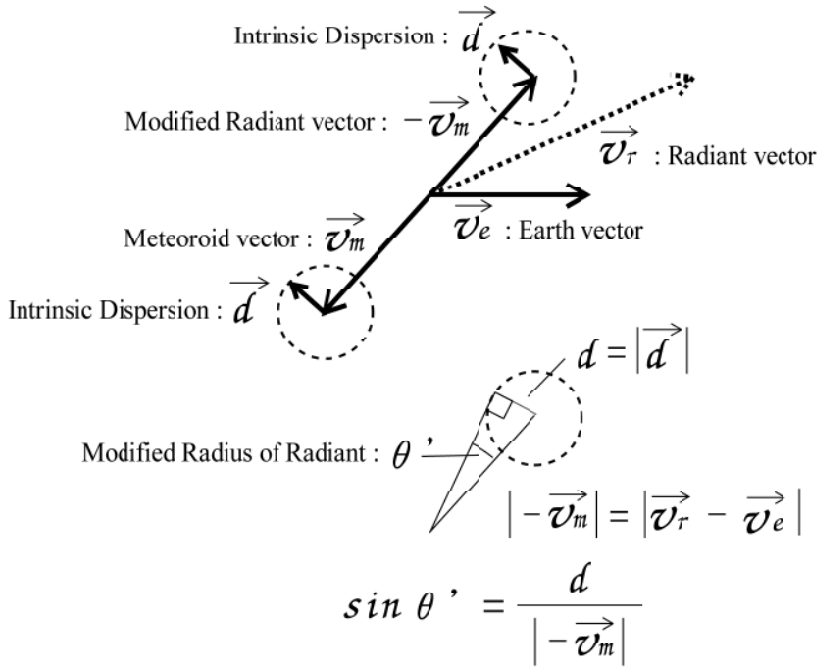

Figure 3. Method of correction.

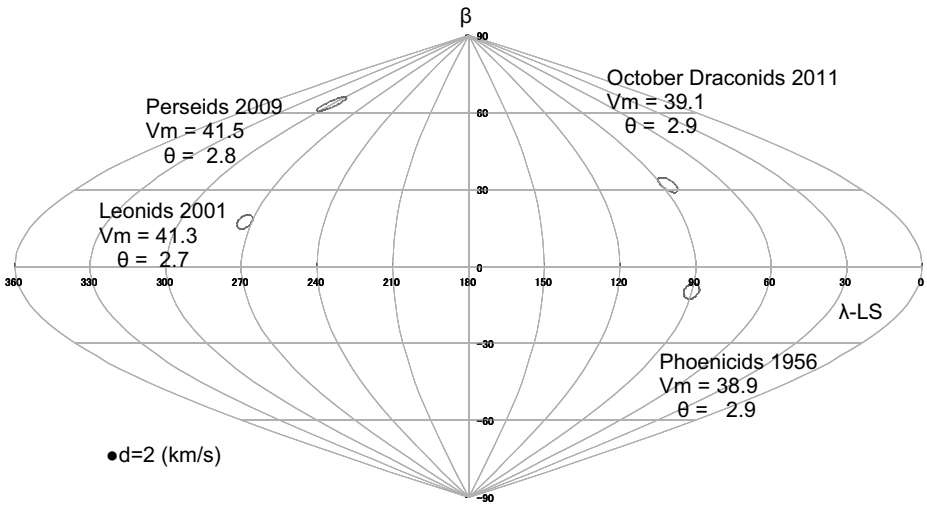

Figure 4. Derived radii of modified radiant points corresponding to the dispersion of 2 km/sec. V_m is the actual velocity of meteor showers.

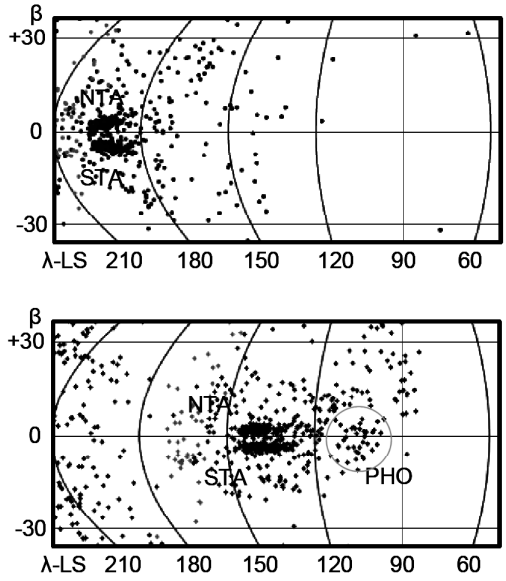

Figure 5. Distributions of radiants between October 20 and November 20 in 2008. Upper panel shows uncorrected and lower panel shows corrected cases. The radiant of Phoenicids (PHO) can be recognized only in corrected figure. Data of radiants was referred to from SonotaCo Networ'

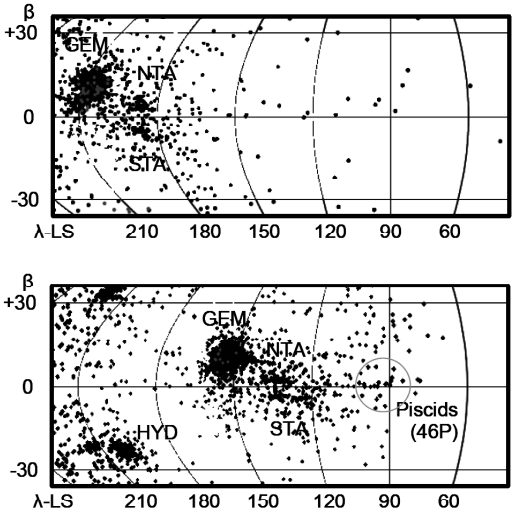

Figure 6. Distributions of radiants between December 1 and 21 in 2012. Upper panel shows uncorrected and lower panel shows corrected cases. The radiant of December Piscids can be recognized only in corrected figure. Data of radiants was referred to from SonotaCo Network.

3. Detection of meteor showers

We carried out careful inspection to the observed data for low velocity meteor showers by taking this correction effect into account, and found the existence of activities of Phoenicids in 2008 and December Piscids in 2012. Figures 5 and 6 show the result of the obtained radiants of uncorrected and corrected of this effect.

4. Conclusions

It became clear that Phoenicids in 2008 and December Piscids in 2012 can be recognized only in this corrected figure. It also means that such low velocity meteor showers were overlooked without this correction. Therefore, we should perform this correction when we inspect low velocity meteor showers.

Kresak and Porubcan (1970) estimated that the dispersion of radiants was generally about 1 km/sec. In this case, it seems to be slightly large. We have to investigate in more detail.

Acknowledgements

We would like to acknowledge the useful data from SonotaCo Network.

References

Kresak L., Porubčan V., 1970, Bull. Astron. Inst. of Czechoslovakia 21, 153

Meteoroids 2013, Proceedings of the Astronomical Conference,
held at A.M. University, Poznań, Poland, Aug. 26-30, 2013,
eds Jopek T.J., Rietmeijer F.J.M., Watanabe J., Williams I.P.,
Adam Mickiewicz University Press in Poznań, pp 335–343

Semi-empirical method for the photometry of low-light meteors from observations with the isocon television systems

Kozak P.M.

Astronomical Observatory of Kyiv Taras Shevchenko National University, Kyiv, Ukraine
(kpm@univ.kiev.ua)

Abstract. The universal semi-empirical method for the photometry of low-light meteors is proposed. The method was developed for the photometrical measurements and reductions of meteor images obtained with the observational television systems of super-isocon type, which are well-known due to their non-linearity of the response onto the input signal, and afterimages from the dynamical objects in a television frame, which are not removable because of construction features of the systems. Semi-empirical method was displayed in the fact that the photometrical dependences of the television system for the moving and stationary objects were investigated by means of the test with photographing of the star sky with the camera, which was rotating with different angular velocities including zero velocity (i.e. when the camera was in the stationary state). Basing on the obtained results the calibrating curve was plotted, and light curves of two low-light meteors of 5-6 magnitude were calculated. The proposed method is universal and can be used for the photometrical processing of data obtained with any television or video system.

Keywords: meteor, meteor photometry, photometric reduction, television system

1. Introduction

Photometry of meteors made by television (TV) technique differs principally from the photographic one. On the one hand, the TV rate allows investigating a meteor in its development since the time rate of one frame is always less than the meteor existence time, which would have to simplify the photometric processing. On the other hand, the meteor leaves the straight line image in the frame, similar to the photographic one but limited in its length by the frame rate, whereas the stars of comparison still form point object images. Obviously, the scheme of photometric measurements should greatly differ from the photographic one.

At the photometric measurements of meteors obtained with the help of modern video cameras equipped with the CCD and amplifier the mostly often the method of summing pixels is used. The method had been proposed in Hawkes et al. (1993) and later used in Fleming et al. (1993) and Murray et al. (1998). This method uses the fact that the meteor image in each frame has a view of a dash of the fixed length and intensity. Summing the intensities over background over all pixels belonging to the meteor dash image, and comparing it with sums of intensities over the star images pixels one can obtain the meteor magnitude. We have to warn about that such a method will give the correct result only for the video system with the linear response of the signal onto the input light flux. So, before the use of such a method

one should carry out testing the observational system for linearity, which can be done, for instance, through the test with camera rotation (Kozak et al. 2001; Kozak 2008,b).

When we use for the observations the highly sensitive cameras of orticon (super-orticon) type or isocon (super-isocon) type the application of such an approach is impossible since, except the obvious non-linear response of the electronic signal onto the optical one, the given systems posses a significant delay in the accumulation and readout of a signal from the electronic transmitting tube target. In spite of the fact that such systems are outdated and posses by a range of imperfections they are the most sensitive among similar cameras, so they are still used for meteor observations (Hajdukova et al. 1995; Kozak et al. 2007, 2012). Whereas the methods for astrometrical and kinematical processing of meteors registered using super-isocon television systems were developed in Kozak (2002) and Kozak (2003) accordingly, the method for meteor photometry for these observational systems was not described in details. In the given paper the semi-empirical method for the meteor photometry registered with TV systems of super-isocon type is proposed.

2. Theory of television meteor photometry: formulation of the problem

The illuminance to be created by a low-light meteor during time t of its flight along the trajectory L in the atmosphere at distance R from the observer may be presented in general as a function $E_1(L,t)$ where E_1 is the energy of radiation per time unit, through area unit and from the trajectory length unit ($\mathrm{Js^{-1}m^{-2}m^{-1}}$), or from the trajectory angular unit if the trajectory cannot be calculated and R is unknown (for instance for single station observations, $\mathrm{Js^{-1}m^{-2}deg^{-1}}$). Evidently, the meteor in such a case is considered as a single-dimension-extensive object in which the radiation in any moment t occurs from both the meteor coma and its atmospheric tail. For the lowest meteors being observable with a TV system the afterglow from the meteor tail is very low and becomes extinct fast, so the meteor can be considered as a point radiative moving object. In this case the functional dependence $L = L(t)$ exists, and the light curve of a meteor can be presented as a function $E_0(t)$ or $E_0(L)$, where E_0 is an illuminance per time unit through area unit ($\mathrm{Js^{-1}m^{-2}}$). Usually the meteor light curve is plotted as a function of height. In the case of nebula or cloudy structure of the meteor coma (LeBlanc et al. 2000; Spurny et al. 2000; Taylor et al. 2000; Campbell-Brown et al. 2013) registered with the help of observational system of high spatial resolution one can introduce spatial illuminance (spatial magnitude) as a function of azimuth A and zenith distance Z_R of the meteor: $E_2(A, Z_R, t)$, where E_2 is measured in $\mathrm{Js^{-1}m^{-2}deg^{-2}}$. It is obvious that values E_0, E_1 and E_2 are connected between themselves via single and double integration.

Observational systems equipped with transmitting tubes are very slowed in accumulation and readout of the signal, therefore they have long afterimage (sometimes tens of frames dependently on the input signal intensity). The meteor in the frame leaves the tail to be visible during many frames. And so, the use of any other model

for meteor photometrical measurements except the model for point radiative moving object is impossible, and just value E_0 has to be measured. Since the TV system of super-isocon type is designed for the observations of critically low-light meteors producing very low and brief atmospheric tails such a limitation is not critical.

In the given work we will not consider all photometrical reductions like conversion of magnitudes from own photometrical system to catalogical one; correction of magnitude for the atmospheric absorption; correction of meteor magnitude to absolute one; view field correction etc. since we described them partly earlier in Kozak et al. (2001). Here we will pay attention to the appropriateness of the measured photometrical characteristics which would not depend on the described above problems.

3. Idea of semi-empirical approach for meteor photometry

As was shown above it is difficult to carry out the correct photometrical processing of a meteor registered with the isocon TV system. Taking into consideration the big amount of TV system tunings (the same star can create different responses dependently on amplification coefficient, electromagnetic focusing etc.) it becomes obvious that we can compare photometrical measurement of a meteor only with stars of comparison presented in the same series of TV frames where the meteor moves. But there are two problems still exist: what parameter has to be measured in the meteor and stars images, and how to compare these measured parameters? For the stationary star images the most optimal approach is in measurements of their photometrical volumes,

$$V_* = \sum_{x,y \in *} I(x, y)$$

i.e. sums of intensity over background in pixels belonging to the image, and further plotting the calibrating curve as a function $\log_{10} V_* = f(m_*)$.

The measurement of similar parameter for meteors is impossible since we cannot separate its image appeared in the current frame from one in the previous frames because of long existence of meteor "tail" (electronic afterimage). We could summarize all frames with the meteor images as was proposed in Kozak et al. (2001) and than try to select a part of summed meteor tail corresponding in its length to the time of a frame.

Similar scheme was proposed in Hawkes et al. (2001). But such a scheme can be realized only for cameras with the linear response onto an input signal. As it was shown in Kozak (1998) for super-isocon TV system $V_* \sim E_*^{0.75}$, i.e. the function is not linear, and so the same object will produce different integral image depending on the state of the object (the higher image motion velocity in the frame the lower intensity will be produced).

Therefore, we should measure some parameter to be proportional to the input energy flux from the object on the one hand, and be easily measurable for both stationary and moving images, on the other hand. The most obvious parameter responded such rules (Kozak 1998) is the intensity over background in one pixel

with the highest value $I_{MAX}(x, y)$ (for the stationary star image this is a star center $I_{MAX}(x, y) = I_0(0, 0)$). But due to fluctuations these parameter measurements will be of low precision. Besides, maximal intensity of the image is the most sensitive to the possible oversaturation, and its increasing practically stops after reaching some limit value. The area of the transverse photometrical profile over background made perpendicularly to meteor image motion through $I_{MAX}(x, y)$ seems to be much better. First, the error of measuring S will be $\sqrt{N}$ times less that for single pixel, where N is a number of summed pixels. Second, this value continues to grow up after reaching oversaturation of intensity thanks to transverse enlargement of the image. The calibrating curve can be plotted in this case as $S_* = S_*(m_*)$ measured upon stationary star images. But after measuring similar value for the meteor image S_M one cannot go into the calibrating curve with that value because of different exposures of moving meteor and stationary stars of comparison. Obviously, the transverse photometrical profile area depends, except magnitude m_M, on the speed of the point spread function (PSF) motion over the frame: $S_M = S_M(m_M, \upsilon_M)$. As a way out from such a situation we can propose the "stop" of the meteor image, i.e. determination of its photometrical value $S_M(m_M, 0)$ if it were immovable. For the determination of view of the function $S_M = S_M(m_M, \upsilon_M)$ one can use a test with camera rotation during photographing star sky (Kozak et al. 2001; Kozak 2008,b) since the stars are point objects corresponding to considering model of the meteor. Selecting a large range of stars of different intensities and a collection of star image motion speeds over frame covering real meteor ones (formed by different angular velocities of camera rotation) we will obtain some dependency $S_* = S_*(m_*, \upsilon_*)$ including event of $\upsilon_* = 0$. There are images of stationary and moving fields of camera view with stars, and a frame with the real meteor in Figure 1. In order to study the dependence of the photometrical profile area for moving star image on the image motion speed over a frame we have obtained according graphs for some stars from the constellation of Ursa Major (the first group) and Aquila (the second group) registered in different time. There were 21 stars processed in the first group. The range of image velocities over frame was (0; 2.00; 2.41; 2.84; 3.11; 4.78; 4.86; 6.81; 8.07; 9.04 21.45) pixel/frame, which at angular pixel size of 4 arcmin and the rate 25 fps corresponds to (0; 3.33; 4.02; 4.73; 5.18; 7.97; 8.10; 11.35; 13.45; 15.07; 35.75) deg/sec. According range for the second group (11 stars) was (0; 1.50; 5.05; 5.10; 6.96; 28.29) pixel/frame, or (0; 2.49; 8.42; 8.50; 11.61; 80.48) deg/sec. The limited amount of the velocities was conditioned by the difficulties of carrying out the test with the TV camera of rate 25 full frame a second (we used only odd or even fields of the frame for the processing): any slight change of the rotation velocity immediately leads to photometrical profile change. Nevertheless the given velocity ranges satisfactory reflect the range of meteor angular velocities. After processing of the test results we have found that bright objects, intensity of which is close to oversaturation, behave themselves in different, not easy explainable way, and do not allow realizing adequate photometrical reduction. Further we consider the photometrical processing only for objects of low and middle intensity. The graph of $S_*(m_*, \upsilon_*)/S_*(m_*, 0)$ vs. υ_* is shown in Figure 2. As it can be seen from the Figure 2 the ratio $S_*(m_*, \upsilon_*)/S_*(m_*, 0)$

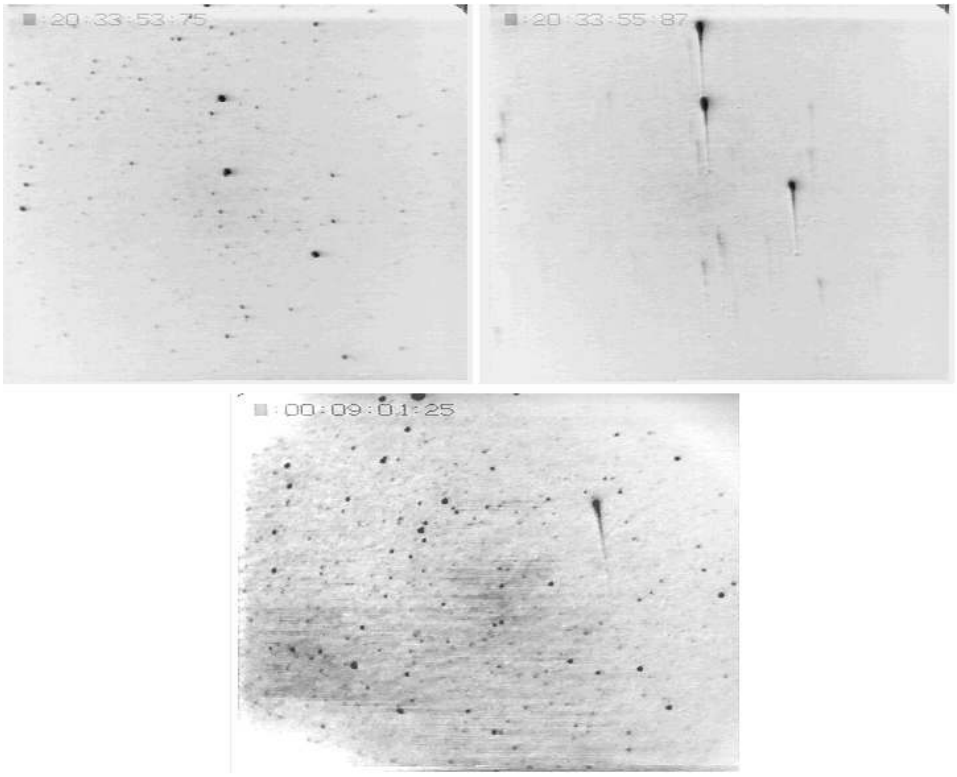

Figure 1. The "simulated meteor" test. There is a stationary frame at top-left (Ursa Major sky area); the same area obtained with the rotating camera in top-right; a frame with a real meteor at bottom-center. TV frames are shown in the inverted view.

demonstrates similar behavior for the stars of different magnitudes of low and middle range, and so it can be described by one function. For simplification of reducing $S(m, v)$ to $S(m, 0)$ we can select the fit function which has to meet the following requirements: $S(m, v)/S(m, 0) = 1$ if $v = 0$, and $S(m, v)/S(m, 0) \to 0$ when $v \to \infty$. The easiest such a function is the exponent

$$S_*(m, v)/S_*(m, 0) = \exp(-C_* v_*) \tag{3.1}$$

shown in Figure 2 (dotted curve), $C_* \approx 0.33$ in our case. The given value of the coefficient is probably not the optimal due to absence of points for the range 10-20 pixel/frame, and as a result it is badly fit the data at big velocity values. It is acceptable for using in meteor photometry in the first approach, but the following power function seems to be more preferable:

$$S_*(m, v)/S_*(m, 0) = C_B v^{-C_A} \tag{3.2}$$

where $C_A \approx 0.51$, $C_B \approx 0.49$ (Figure 2, solid curve). Using this function we have to remember that $S(m, v)/S(m, 0) = 1$ for $v \approx 0.25$ pixel/frame, but not for $v = 0$.

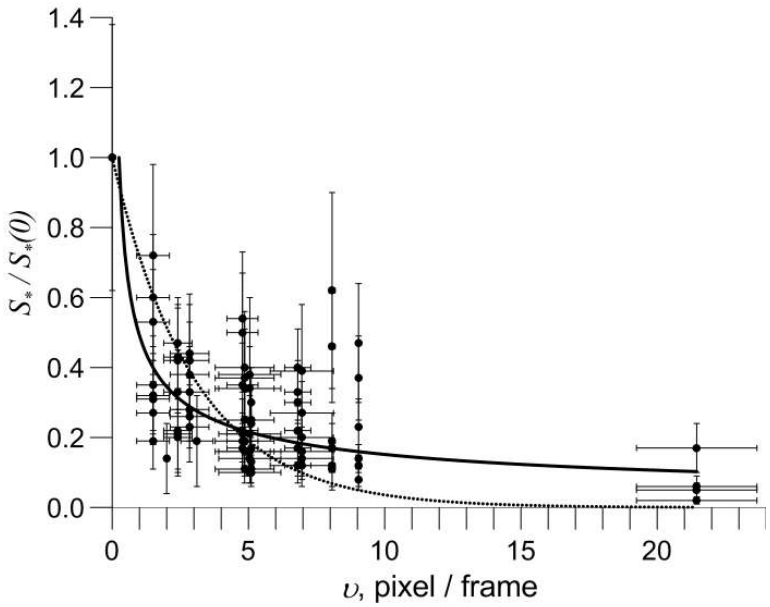

Figure 2. Relative transverse photometrical profile areas for star images vs. their image motion velocity over a frame.

In such a way we automatically suppose $S(m,0) \simeq S(m,0.25)$, but in practice we cannot use this function for $\upsilon < 0.25$.

In such an approach the only problem to be solved is the bad quality of measurements for stationary objects, which is caused by some asymmetry of star image shapes in odd and even fields of a frame, and low amount of pixels forming the image. The calibrating curve will be plotted with big errors. It is much better to measure the values of photometrical volumes V_* for stationary objects. In addition, just this value is directly connected with the light flux from the point object entering the observational system lens, and accordingly with its illuminance E_0. Taking into account that both values are connected between themselves and are proportional to the star illuminance we propose to plot the calibrating curve using just values V_*. And for the further transformation of corrected meteor values $S_M(m_M,0)$ to "$V_M(m_M)$" we will need to study a view of dependency between them using stationary star images. The easiest way is to assume that the distribution of intensity in star image can be fitted by some two-dimensional bell-shape function, for instance by Gaussian function $I(x,y) = I_0 \exp(-(x^2+y^2)/2\sigma^2)$. Then the profile of it will be described by single-dimensional Gaussian. Using this fact we can write $V/S = \sqrt{2\pi}\sigma$ and use this formula for calculating V via S when the fitting procedure is used and σ is known. If measurements are carrying out in a simplified manner we can derive the analogues formula but with the use of maximal intensity I_0 in the star image center over background, which is measured easily, and then use $V/S^2 = 1/I_0$. The obtained ratio calculated upon the stars used in Figure 2 was the following $V_*(m)/S_*(m,0) \approx 3.41 \pm 0.35$.

4. Discussion and examples of application of semi-empirical method for meteor photometry

If the functional dependence of transverse photometrical profile $S(\upsilon)$ on the point object image velocity over the frame υ is determined for the used observational system with the help of the formula (3.1) or (3.2) (or any other) the order of meteor photometrical reductions seems to be the following. The simplified version consists in measuring $S_*(m_*, 0)$ of stars of comparison in frames with the meteor image, selecting their magnitudes m_* from a catalogue, and plotting the calibrating curve upon these values. Then we measure in each frame meteor parameters υ_M and $S_M(m_M, \upsilon_M)$. Further using the formula (3.1) or (3.2) we make a meteor "immovable", i.e. calculate $S_M(m_M, 0)$. Finally, we go into the calibrating curve with this value and obtain the meteor magnitude m_M. The second approach is

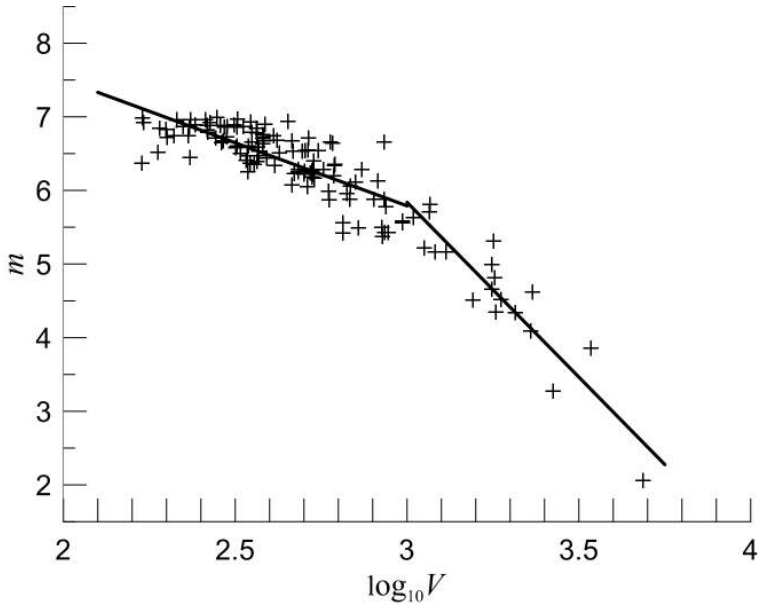

Figure 3. Calibrating curve plotted using photometrical volumes of stationary images of stars of comparison during observations on 19 September 2003.

more precise. First we measure more precise values $V_*(m_*)$ for stars of comparison in frames with the meteor image, and the calibration curve is plotted in the form of $m_* = m_*(\log_{10} V_*)$. Then we transform the measurements in each frame of meteor image $S_M(m_M, \upsilon_M)$ and υ_M to $S_M(m_M, 0)$ using (3.1) or (3.2). Further we convert $S_M(m_M, 0)$ to the "photometrical volume of immovable meteor" $V_M(m_M)$, go into the calibrating curve with it and finally obtain the meteor magnitude m_M.

As an example we considered two meteors which were consecutively registered on 19 September, 2003 at $20^h42^m04^s$ and $20^h42^m31^s$ of UT. The same as in the tests the lens Jupiter-3 (F = 50 mm, F/1.5) was used for the observations. Their image velocities over frame were $\upsilon_1 \approx 3.90 \pm 1.47$ pixel/frame ($\upsilon_1 \approx 6.50 \pm 2.45$ deg/sec),

and $\upsilon_2 \approx 5.14 \pm 1.75$ pixel/frame ($\upsilon_2 \approx 8.57 \pm 2.92$ deg/sec). A short time period between events allows us to use the same calibrating curve for both meteors (Figure 3).

As it is seen from Figure 3 the calibrating curve can be conveniently fitted by two straight lines: $m \approx -1.71\log_{10}V + 10.93$ for the range $\log_{10}V < 3$, and $m \approx -4.75\log_{10}V + 20.08$ for the range $\log_{10}V > 3$. The light curves of the meteors are shown in Figure 4.

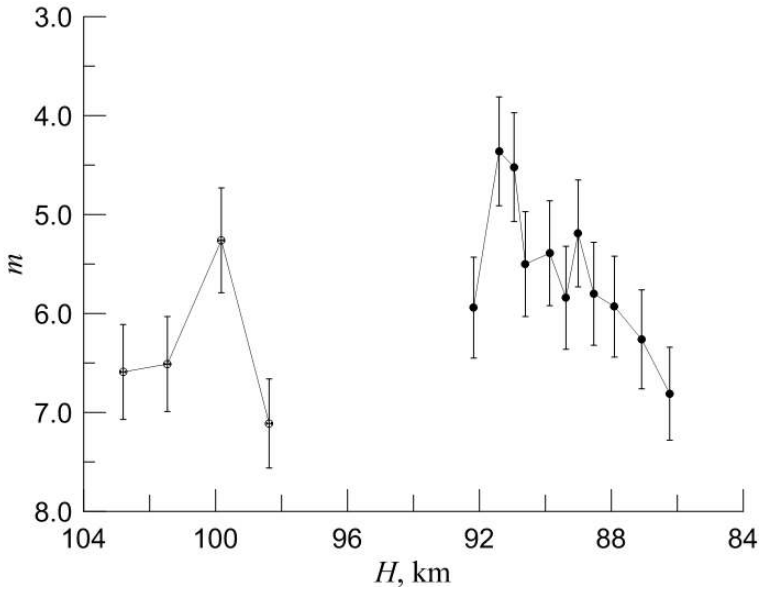

Figure 4. Light curves of two sporadic meteors registered on 19 September 2003 with interval of half-minute.

5. Conclusions

Described above method for meteor photometry was developed first of all for TV system with the transmitting tube of isocon (super-isocon) type, but due to its universality can be used for any observational TV/video system. The evident imperfection of this semi-empirical method is limited amount of points, corresponding to TV frames containing the meteor image, and therefore the precision of light curve plotting. For the observational systems with the linear response onto the input signal one can carry out photometry of the meteor image in a similar way in the summed frame, measuring there a profile in each pixel along the meteor image increasing significantly in that way a number of points in the light curve. In this case comparison of such meteor measurements has to be done with the summed moving star images from the similar integral frame. However, even realizing so dense photometrical measurements of a meteor one must remember that these val-

ues do not correspond strictly to momentary meteor magnitude because of large size of PSF for point objects (they are significantly larger than pixel size).

One more problem which must be solved for the super-isocon system in near future is the problem of bright star images having another view of the dependence between their moving and stationary photometrical measurements. In the presented example we have considered very low-light meteors of 5-6 magnitude (limit meteors were $+7^m$). However for meteors from Perseid or Leonid showers most of meteors will be highly oversaturated and so investigations of super-isocon TV system in a range of bright object images must be continued.

Acknowledgements

The author expresses his gratitude to the Organizing Committee of Meteoroids 2013 conference for financial support. The work was done in the frame of Ukrainian governmental budgetary scientific program, grant 11BF023-03.

References

Campbell-Brown M.D., Borovicka J., Brown P., Stokan E., 2013, Meteoroids 2013, in the Conference Program and Abstracts, #023, (`http://www.astro.amu.edu.pl/Meteoroids2013/index.php?section=program`)

Fleming D. E. B., Hawkes R. L., Jones J., 1993, in Proc. of the Inter. Astron. Symp. held at Smolenice, Slovakia, July 6-12, 1992, eds J. Stohl and I.P. Williams, 261

Hajdukova M., Kruchinenko V.G., Kazantsev A.M., Taranucha Ju.G., Rozhilo A.A., Eryomin S.S., Kozak P.N., 1995, EM&P, 68, 297

Hawkes R.L., Mason K.I., Fleming D.E.B., Stultz C.T., 1993, in Proc. of the Inter. Meteor Conf., Smolenice, Slovakia, 2-5 July 1992, eds: D. Ocenas, P. Zimnikoval, 28

Hawkes R.L., Bussey J.E., MacPhee S.L., Polloc C.S., Taggart L.W., 2001, in Proc. of the Meteoroids 2001 Conf., 6-10 Aug. 2001, Kiruna, Sweden, ed.: B. Warmbein, ESA SP-495, 281.

Kozak P.N., 1998, Kin. Phys. Celest. Bodies, 14, 6, 427

Kozak P.M., Rozhilo A.A. and Taranukha Y.G., 2001, in Proc. of the Meteoroids 2001 Conf., 6-10 Aug. 2001, Kiruna, Sweden, ed. B. Warmbein, ESA SP-495, 337

Kozak P.N., 2002, Kin. Fiz. Nebesn. Tel, 18, 5, 471

Kozak P.N., 2003, Kin. Fiz. Nebesn. Tel, 19, 1, 62

Kozak P., Rozhilo O., Kruchynenko V., Kazantsev A., Taranukha A., 2007, Adv. Space Res., 39, 4, 619

Kozak P., 2008, EM&P, 102, 1-4, 277

Kozak P., 2008b, in Advances in Meteoroid and Meteor Science, eds: J.M. Trigo-Rodrigues, F.J.M. Rietmeijer, J. Llorka, D. Janches, Springer, 277

Kozak P., Rozhilo O., Taranukha Y., 2012, in the JD5 IAU XXVIII General Assembly, Abstract No 5963

LeBlanc A.G., Murray I.S., Hawkes R.L., Worden P., Campbell M.D., Brown P., Jenniskens P., Correll R.R., Montague T., Babcock D.D., 2000, MNRAS, 313, L9

Murray I.S., Beech M., Taylor M.J., Jenniskens P., Hawkes R.L., 1998, EM&P, 82/83, 351

Spurny P., Betlem H., Jobse K., Koten P., Leven J., 2000, M&PS, 35, 1109

Taylor M.J., Gardner L., Murray I., Jenniskens P., 2000, EM&P, 82-83, 379

Meteoroids 2013, Proceedings of the Astronomical Conference,
held at A.M. University, Poznań, Poland, Aug. 26-30, 2013,
eds Jopek T.J., Rietmeijer F.J.M., Watanabe J., Williams I.P.,
Adam Mickiewicz University Press in Poznań, pp 345–351

Evidence for VLF propagation perturbations associated with single meteors

Rault J.-L.
International Meteor Organization Radio Commission (f6agr@orange.fr)

Abstract. Evidence is given in this study that under some particular circumstances, a single meteor, when entering the Earth atmosphere, is capable of disturbing the propagation of VLF (Very Low Frequency) electromagnetic waves propagating in the Earth ground-ionosphere waveguide.

Keywords: radio meteors, VLF, propagation disturbances

1. Introduction

Natural and man-made VLF (Very Low Frequency) electromagnetic waves propagate on Earth at very long distances, thanks to a natural low attenuation waveguide. This waveguide consists of the ground surface layer and of the lowest layer of the ionosphere which behave like two parallel conductive plates. According to the ray tracing method commonly used (Delcourt, 2000) to describe VLF radio propagation on short to moderate distances (< 2000 km), the amplitude of a VLF radio wave at a given observation location can be represented as the vectorial sum $\vec{A_0} = \vec{A_G} + \vec{A_S}$.

Vector lengths of $\vec{A_G}$ and $\vec{A_S}$ represent respectively the amplitude of the ground wave propagating along the Earth surface, and of the sky wave reflected from the D layer (during day time) or E layer (during night time) of the ionosphere. The angle between the two vectors represents the phase (delay) between the ground wave and the sky wave components. Therefore, any change in the altitude or conductivity of the ionosphere or in the conductivity of the ground modifies consequently the amplitude of the VLF signal at the reception location.

2. VLF propagation perturbations

Various natural phenomenons (see Figures 3, 4 and 5) such as ultraviolet rays radiated by the Sun, polar cap absorption events, X rays coming from solar flares, γ rays radiated by distant stars, and thunderstorms lightnings create long duration or short transient VLF propagation disturbances by modifying the electron density or the altitude of the ionospheric D or E layers (Barr 2000).

3. Searching for VLF disturbances induced by meteors

The aim of the present work was to study if meteors entering the Earth atmosphere could also cause any VLF radiowaves propagation disturbances. VLF phase (Chilton 1961) and amplitude (De 2012) transient variations occurring during

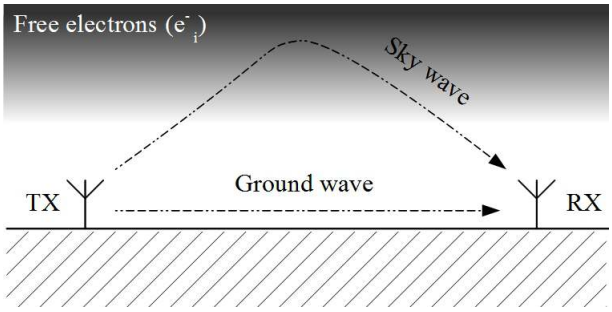

Figure 1. Representation of the sky and ground waves propagating in the Earth ground/ionosphere natural waveguide.

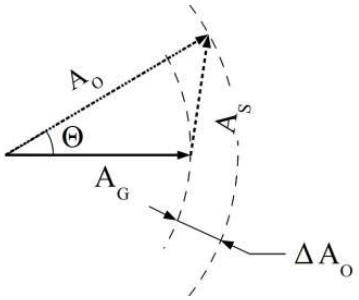

Figure 2. The VLF signal at the RX reception location is the vectorial sum of the sky wave and of the ground wave radiated by the transmitter TX.

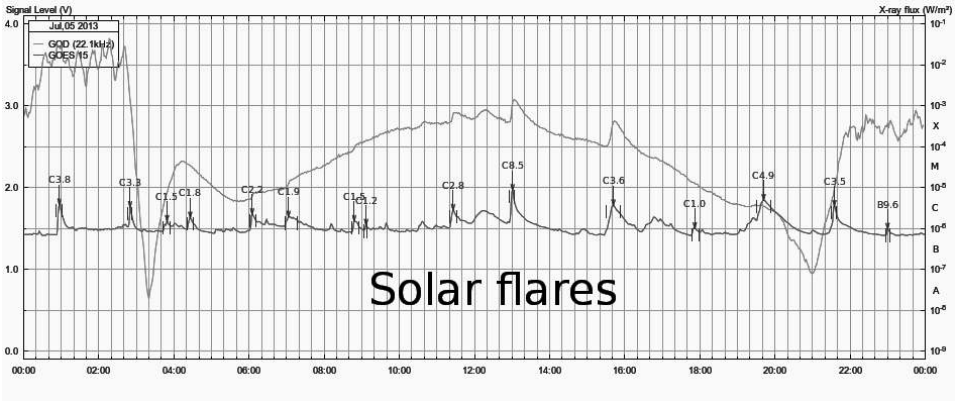

Figure 3. Example of VLF amplitude spikes (upper curve) induced by X ray bursts (lower curve) from solar flares (Loudet 2013).

meteor showers were reported in the past, but these variations were observed on a statistical basis and at large time scales only (i.e. averaged values). They were not directly linked to any single meteors.

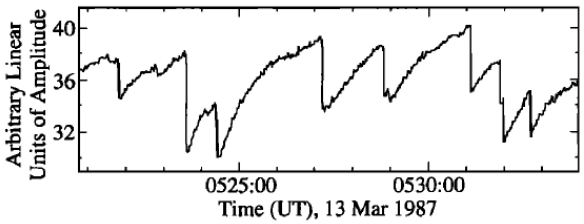

Figure 4. Example of VLF amplitude spikes triggered by LEP (lightnings induced electron precipitations) (Lev-Tov 1995).

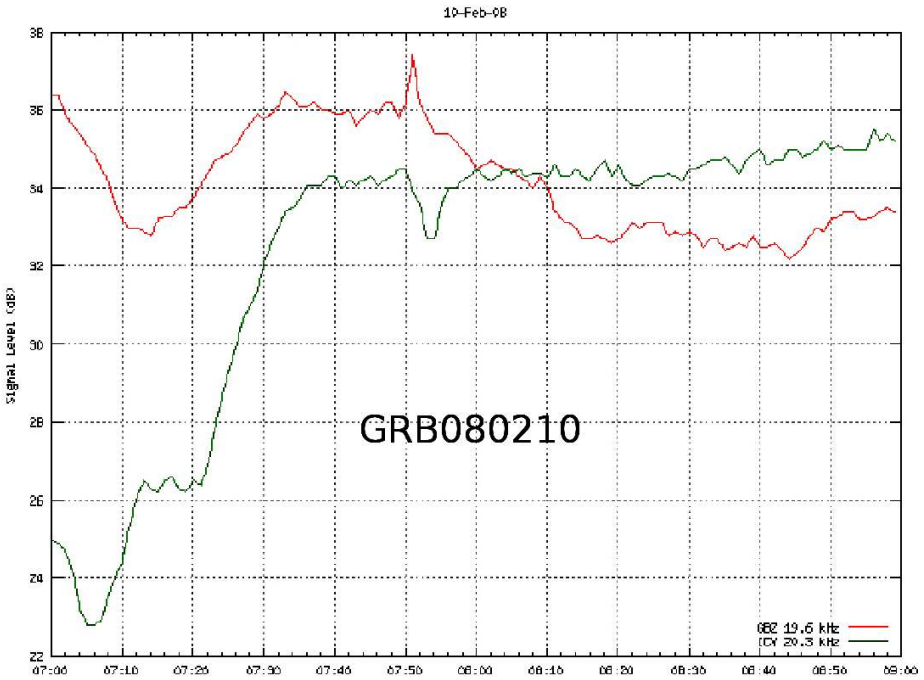

Figure 5. VLF amplitude anomalies at 07h50mn on the 10^{th} of February 2008 due to a GRB (γ ray burst) from a distant star (Godet 2008).

3.1. Observation of a first transient VLF disturbance induced by a single meteor

In the framework of a joint radio/video meteor observations campaign, VLF/VHF radio and video data were synchronously recorded at the Pic du Midi observatory during the 2010 Geminids meteor shower (Rault, 2010). The radio set-up consisted mainly of an e-field ELF/VLF broadband receiver (5 Hz to 24 kHz bandwidth) specifically designed for meteor observations, a VHF commercial receiver dedicated to meteor pings detection and a digital hifi stereo recorder. The signal amplitudes

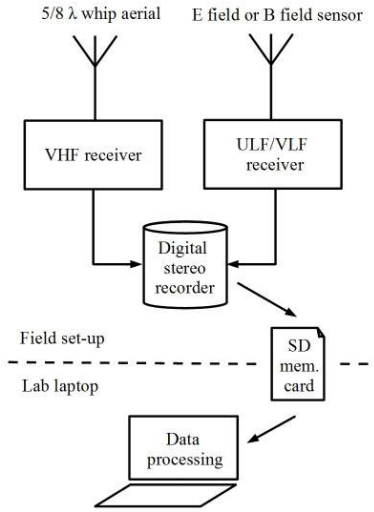

Figure 6. VHF forward scatter / VLF observation set-up.

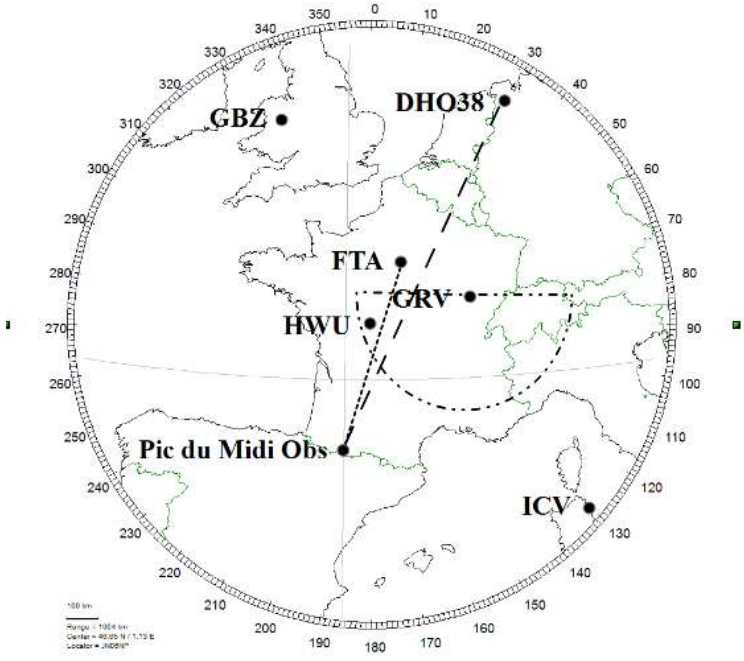

Figure 7. Pic du Midi observatory, VLF transmitters (GBZ, DHO38, FTA, HWU, ICV) and Graves VHF radar (GRV) locations. The dotted half-circle centered on GRV represents the illumination area of the radar.

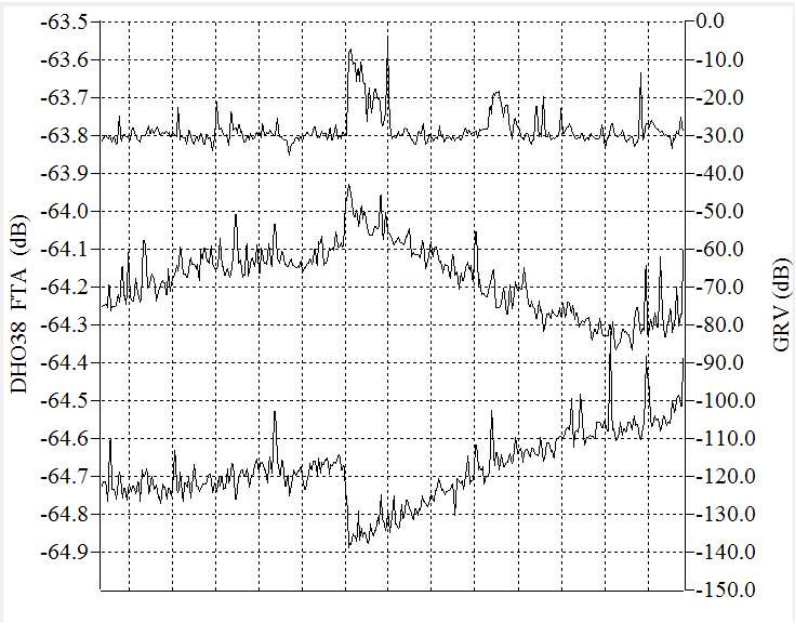

Figure 8. First observation at Pic du Midi observatory of a constructive interference on FTA (middle trace) and of a destructive interference on DHO38 (lower trace) triggered by a single meteor (meteor VHF echo on upper trace). Time scale: 10s/square.

of five VLF transmitters (GBZ, DHO38, FTA, HWU and ICV) were recorded simultaneously 24 hours a day. Meteors were detected in VHF (Very High Frequency) forward scatter mode, using the french radar GRAVES (GRV) as targets illuminator. Short amplitude transients on the amplitude of the German VLF transmitter DHO38 and on the french VLF transmitter FTA were serendipitously observed when a large meteor entered the atmosphere on December 13 at 23h13m44s UT. No visible transients were observed at the same time on the amplitudes of GBZ, HWU or ICV. On figure 8, the upper trace shows successive meteor echoes detected in VHF forward scatter mode. The middle trace shows a constructive interference between $\vec{A_G}$ and $\vec{A_S}$ detected on FTA, and the lower trace shows a destructive interference on DHO38. The horizontal time scale is 10 s/div, and the vertical VLF amplitudes scales are 0.1 dB/div.

3.2. Observation of further meteor transient VLF disturbances

During the 2013 Lyrids meteor shower, a campaign dedicated to the observation of potential VLF meteor perturbations was performed in a remote area located in Lozère, France. About 50 large overdense meteors echoes were manually analyzed and several new meteor-induced VLF amplitude disturbances were found (see examples on figure 9).

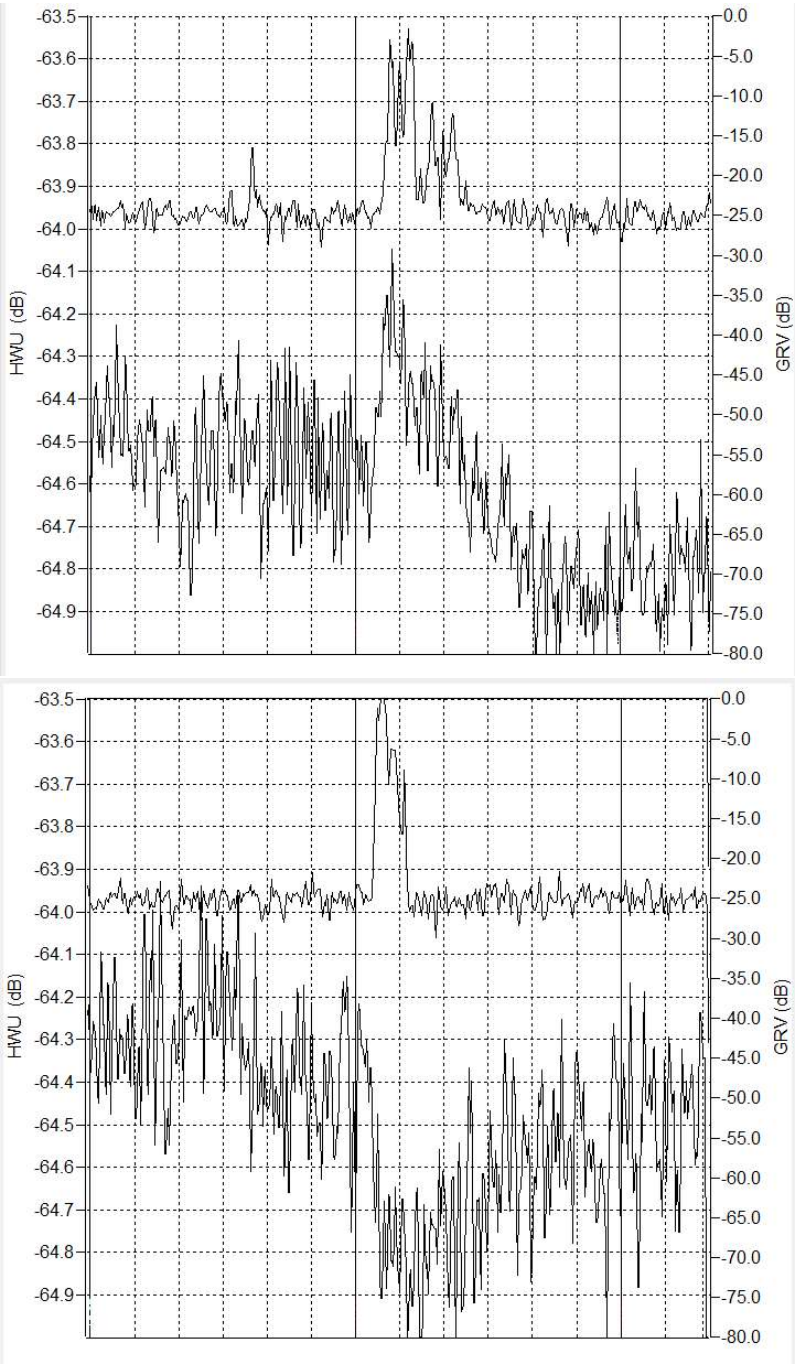

Figure 9. Examples of some other VLF destructive or constructive interferences induced by meteors on the HWU signal recorded in Lozere during the Lyrids 2013. Upper trace: VHF meteor echo; lower trace: VLF amplitude. Time scale: 10s/square.

4. Conclusions

Such "M-SIDs" (Meteor induced Sudden Ionospheric Disturbances) seem to be faint and rare. They are supposed to be created by sudden variations of density and/or altitude of the lowest region of the ionosphere, these variations being due to the outbreak of large meteor overdense trails (presenting a free electrons line density greater than $2x10^{14}$ electrons/meter). Until now, all the observed transient amplitude spikes are presenting a similar shape, starting with a steep slope and followed by a progressive recovery (with an average duration of about 60 seconds). No M-SIDs at all were observed during day times. It is supposed that between sunrise and sunset, the ionospheric D layer produced by the solar UV and X rays is masking any meteor trails effects, because its altitude is lower than the average altitude of the meteor trails. All the observed M-SIDs seem to occur when the meteor trails appear close to a line drawn between the observation location and the VLF transmitter location.

Former various VHF/VLF records performed during Geminids 2008, 2009, 2010, 2011, 2012, Leonids 2009, 2012, Perseids 2009, 2010, 2011, 2012 will be analyzed to identify more VLF disturbances induced by single meteors, and to determine their main characteristics.

Acknowledgements

The author gratefully acknowledges François Colas and Jérémie Vaubaillon from IMCCE for the invitations to participate to several observation campaigns at Pic du Midi observatory and at Haute-Provence observatory.

References

Barr R., et al., 2000, Journal of Atmospheric and Solar-Terrestrial Physics, 62, 1689
Chilton, C.J.,1961, Journal of Geophysical Research 66, 379
De S.S., 2006, Indian Journal of Radio and Space Physics, Vol.35, Dec., 396
Delcourt J.J., 2000, Ionosphère région D, Lavoisier, ISBN 2-7462-0656-0, 141
Godet J.-P., 2008, Private correspondence
Lev-Tov S.J., 1995, Journal of Geophysical Research, Vol. 100 NO A11, 21, 375-21, 3
Loudet L., 2013, http://sidstation.loudet.org/data-fr.xhtm
Rault J.-L., 2010, WGN, the Journal of the IMO 38:2, 67

Meteoroids 2013, Proceedings of the Astronomical Conference,
held at A.M. University, Poznań, Poland, Aug. 26-30, 2013,
eds Jopek T.J., Rietmeijer F.J.M., Watanabe J., Williams I.P.,
Adam Mickiewicz University Press in Poznań, pp 353–364

Current status of the IAU MDC Meteor Showers Database

Jopek T.J.[1], **and Kaňuchová Z.**[2]

[1]Astronomical Observatory, Faculty of Physics, A.M. University, Poznań, Poland
[2]Astronomical Institute, Slovak Academy of Sciences, 05960 Tatranská Lomnica, Slovakia

Abstract. During the General Assembly of the IAU in Beijing in 2012, at the business meeting of Commission 22 the list of 31 newly established showers was approved and next officially accepted by the IAU. As a result, at the end of2013, the list of all established showers contained 95 items. The IAU MDC Working List included 460 meteor showers, among them 95 had *pro tempore* status. The List of Shower Groups contained 24 complexes, three of them had established status. Jointly, the IAU MDC shower database contained data of 579 showers.

Keywords: established meteor showers, IAU MDC, meteor database, meteor showers nomenclature

1. Introduction

Since its establishing, the activity of the Task Group of Meteor Shower Nomenclature (later transformed into the Working Group on Meteor Shower Nomenclature, hereafter WG) proved to be advisable.† As results of this activity, several practical principles (rules) have been adopted:

- the meteor shower codes and naming conventions (Jenniskens 2006a, 2007, 2008; Jopek and Jenniskens 2011),
- a two-step process was established, where all new showers discussed in literature are first added to the Working List of Meteor Showers, each being assigned a unique name, a number, and a three letter code,
- all showers which satisfy the verification criterion will be included in the List of Established Showers and then officially accepted during next GA IAU.

The naming rules as well as the Established and Working Shower Lists are posted on the IAU MDC website (Jopek and Kaňuchová 2013).

In 2009, during the GA IAU held in Rio de Janeiro, for the first time in history of Meteor Astronomy 64 showers were officially named by the IAU. Their names and geocentric parameters were given in Jopek and Jenniskens (2011), and were posted on the IAU MDC website (Jopek and Kaňuchová 2013).

Three years later, in Beijing, next 31 showers obtained their official names (see Table 1, 2). During the business meeting of the Commission 22 held in Beijing, the members attending this meeting further agreed that the Working Group on

† The Task Group of Meteor Shower Nomenclature was established during the GA IAU held in Prague in 2006.

Meteor Shower Nomenclature should continue its activity during the next triennium (2012-15). The members of the new WG are: T.J. Jopek (chair), P.G. Brown (v-chair), J. Baggaley, D. Janches, P. Jenniskens (C22 president), J. Kac, Z. Kaňuchová, G.I. Kokhirova, P. Koten, J.M. Trigo-Rodriguez and J. Watanabe.

Shortly before the GA IAU in Beijing the authors of this paper started an upgrade of the MDC shower database. Mainly it consisted in: adding the orbital elements, adding the literature references and additional parameters to already known meteor showers. During this upgrade we found that for some meteor showers the data given in the MDC are incorrect. Partly, such data were corrected, but in some cases deeper studies are needed, and such corrections should be clinched by all members of the WG.

In this study we describe the results of our work. First we remark new utility options implemented on the IAU MDC shower database. Next we point out the need of polishing the rules of meteor shower nomenclature, and propose some standardization for such nomenclature.

2. Upgrade of the IAU meteor shower database

The MDC database upgrading encompassed correction of erroneous data (typos, mistakes), but also complement of the orbital data and bibliographic information. Correction of the erroneous data was an easy task because we have been supported by users who wrote to us about many particular errors. We appreciate their initiative very much.

Next stages of the database upgrade procedure were more labour consuming, sometimes they were tedious and needed computer software implementation.

2.1. Supplementation of the meteor showers orbits and bibliographic references

Until August 2012, the IAU MDC shower database contained only shower codes, shower names, mean geocentric parameters and the name of the possible parent body. No orbital information i.e. no mean values of the orbital elements were given and no literature references to the data sources were available. To cure the situation

Leonids					Single Shower - Status - Established							Next Previou
RA	DE	dRA	dDE	VG	a	q	e	Peri	Node	Incl	N	References
[deg] J2000				[km/s]	[AU]	[AU]		[deg] J2000				
154.24	21.60	0.659	-0.325	70.66	10.1	0.9853		173.50	236.15	162.36	-	H.Betlem ??
153.0	+22.0	+0.70	-0.42	70.7	11.5	0.985		172.5	235.2	162.6	-	Cook, 1973
153.6	+22.1	+0.60	-0.45	70.26	10.3	0.984	0.904	172.4	235.0	162.1	0009	Kresak and Porubca
153.9	+21.6	+0.944	-0.603	70.92	15.2	0.984		172.36	235.7	162.53	0029	Lindblad et al., 1
55P/Temple-Tuttle												

Figure 1. A fragment of the IAU MDC website screen-shot. An example of the shower upgraded with the orbital elements and the literature ADS references. Currently, for many showers several sets of the geocentric and heliocentric parameters are given.

we added orbital and literature information for over 200 showers using different data sources. Furthermore, for several dozen of showers, the additional sets of mean geocentric and heliocentric parameters determined by different authors have been included into the database. In the main part, we copied data published by

Table 1. Geocentric data of 31 showers (streams) officially named during the IAU XXVIIIth GA held in Beijing in 2012. The solar ecliptic longitude λ_S , the geocentric radiant right ascension and declination α_g, δ_g are given for the epoch J2000.0.

No	IAU No & code		Shower (stream) name	λ_S (°)	α_g (°)	δ_g (°)	V_g (km/s)
1	11	EVI	eta Virginids	354	182.1	2.6	29.2
2	23	EGE	epsilon Geminids	206	101.6	26.7	68.8
3	26	NDA	Northern delta Aquariids	123.4	344.7	0.4	40.5
4	100	XSA	Daytime xi Sagittariids	304.9	284.8	–18.6	26.3
5	128	MKA	Daytime kappa Aquariids	354	338.7	–7.7	33.2
6	151	EAU	epsilon Aquilids	59	284.9	15.6	30.8
7	175	JPE	July Pegasids	107.5	340	15	61.3
8	184	GDR	July Gamma Draconids	125.3	280.1	51.1	27.4
9	197	AUD	August Draconids	142	272.5	65.1	17.3
10	202	ZCA	Daytime zeta Cancrids	147	119.7	19	43.8
11	242	XDR	xi Draconids	210.8	170.3	73.3	35.8
12	252	ALY	alpha Lyncids	268.9	138.8	43.8	50.4
13	257	ORS	Southern chi Orionids	260	78.7	15.7	21.5
14	333	OCU	October Ursae Majorids	202	144.8	64.5	54.1
15	334	DAD	December alpha Draconids	256.5	207.9	60.6	41.6
16	335	XVI	December chi Virginids	256.7	186.8	–7.9	67.8
17	336	DKD	December kappa Draconids	250.2	186.0	70.1	43.4
18	337	NUE	nu Eridanids	167.9	68.70	1.1	65.9
19	338	OER	omicron Eridanids	234.7	60.70	–1.5	26.9
20	339	PSU	psi Ursae Majorids	252.9	167.8	44.5	60.7
21	341	XUM	January xi Ursae Majorids	300.6	169.0	33.0	40.2
22	346	XHE	x Herculids	352	254	48	36
23	348	ARC	April rho Cygnids	37.0	324.5	45.9	41.8
24	372	PPS	phi Piscids	106.0	20.1	24.1	62.9
25	388	CTA	chi Taurids	220.0	63.2	24.7	42.1
26	390	THA	November theta Aurigids	237.0	89	34.7	33.8
27	404	GUM	gamma Ursae Minorids	299.0	231.8	66.8	31.8
38	411	CAN	c Andromedids	110	32.4	48.4	59
39	427	FED	February eta Draconids	315.11	239.92	62.49	35.6
30	445	KUM	kappa Ursae Majorids	223.21	144.46	45.44	65.30
31	446	DPC	December phi Cassiopeiids	252.48	19.8	58.0	16.4

Jenniskens (2006, Table 7), but in the future we intend to take full advantage of the original data sources. Such approach will facilitate removing internal data inconsistency, a problem that we have been noticed during upgrading procedure. In our opinion, the inconsistency of meteor shower data needs thorough solution.

As the literature references we used the URL addresses of the SAO/NASA Astrophysics Data System (ADS). Figure 1 illustrates an example of a meteor shower data record, now supplemented with a few sets of the dynamical parameters and the literature references.

An upgrade of the MDC shower database will be continued by adding the shower parameters taken directly from the original papers. Also, if relevant data prove to be available, for each shower we will include several sets of additional geocentric and heliocentric parameters.

Table 2. Heliocentric data of 31 showers (streams) officially named during the IAU XXVIIIth GA held in Beijing in 2012. The values of the angular orbital elements are given for the epoch J2000.0. For several showers their mean orbital elements are not given in the source literature.

No	IAU No	Shower (stream) name	a [AU]	q [au]	ω (°)	Ω (°)	i (°)
1	11	eta Virginids	2.562	0.382	349.1	280.5	3.5
2	23	epsilon Geminids	10.0	0.731	241.7	209.0	172.9
3	26	Northern delta Aquariids	2.536	0.071	332.6	1 39.0	23.0
4	100	Daytime xi Sagittariids	1.744	0.383	66.6	296.0	4.3
5	128	Daytime kappa Aquariids	1.7	0.18	42	359.7	1.8
6	151	epsilon Aquilids	0.873	0.354	318.3	59.5	59.6
7	175	July Pegasids	44	0.536	267.2	107.5	131.6
8	184	July Gamma Draconids					
9	197	August Draconids	1.515	1.007	185.6	141.9	30.4
10	202	Daytime zeta Cancrids	5.00	0.05	206.5	326.9	21.1
11	242	xi Draconids	1.279	0.988	175.3	210.8	69.0
12	252	alpha Lyncids	25.4	0.281	295.9	268.8	84.4
13	257	Southern chi Orionids	2.23	0.594	86.4	80.1	5.2
14	333	October Ursae Majorids	5.9	0.979	163.7	202.1	99.7
15	334	December alpha Draconids					
16	335	December chi Virginids					
17	336	December kappa Draconids					
18	337	nu Eridanids					
19	338	omicron Eridanids					
20	339	psi Ursae Majorids					
21	341	January xi Ursae Majorids					
22	346	x Herculids					
23	348	April rho Cygnids	6.51	0.8099	125.55	37.0	69.9
24	372	phi Piscids	2.09	0.8559	125.02	106.0	152.6
25	388	chi Taurids	4.97	0.0807	328.49	220.0	12.3
26	390	November theta Aurigids	1.13	0.1160	330.07	237.0	27.8
27	404	gamma Ursae Minorids	4.20	0.9593	199.54	299.0	51.1
38	411	c Andromedids					
39	427	February eta Draconids	–250	0.971	194.09	315.07	55.20
30	445	kappa Ursae Majorids					
31	446	December phi Cassiopeiids					

3. Test of meteor shower names correctness

During a normal maintenance of the MDC shower database and during its upgrade we have met several problems related to shower names. Some problems were reported to us by the database users, some we have recognized by ourselves.

To ascertain if a shower name listed in the MDC is formally correct, one has to compare it with the name obtained by applying to this shower the nomenclature rules published e.g. in Jenniskens (2006a, 2007, 2008); Jopek and Jenniskens (2011). For old, well known showers discovered many years ago, no one would expect that their names will pass such name test. But in case of the new showers discovered quite recently it should be different. We just wanted to know to what extend the shower nomenclature rules are respected by shower discoverers, and on

the other hand, how well the shower nomenclature WG controls the shower naming procedure.

To ensure the test objectivity and to perform it automatically we developed a software in which the shower nomenclature rules were implemented (Jenniskens 2008; Jopek and Jenniskens 2011):

1) a meteor shower should be named after the constellation of stars that contains the radiant,
2) to distinguish among showers from the same constellation, the shower may be named after the nearest (brightest) star with a Greek or Latin letter assigned.
3) to distinguish among showers from the same constellation one may add the name of the month,
4) for daytime showers, those with a radiant less than 32 degrees from the Sun, it is a custom to add "Daytime".
5) Finally one can add "Southern" or "Northern" to distinguish between the south and north branches of a shower, both originated from the same parent body.

By default, the points 3) and 4) relate to the shower activity period.

Our test consisted of two parts. In the first part, using the shower radiant coordinates, we have found in which constellation this point is located.
The constellation borders were established by Delporte (1930) on behalf of the IAU Commission 3 (Astronomical Notations). Delporte drew the constellation boundaries along vertical lines of right ascension and horizontal parallels of declination, on the epoch pf 1875. For a different epoch, due to precession phenomena, the net of the spherical coordinates do not overlap with the constellation boundaries. Hence, Delporte's publication is not convenient for determining a constellation from the radiant position. For this purpose an approach described by Roman (1987) is excellent. We have implemented it in our testing software, and to take into account an influence of the precession we have used the formulae taken from the Explanatory Supplement to the Astronomical Almanac (Seidelmann et al. 1992, ed.).

In the second part of our test, we have found the star nearest to the radiant position. Corresponding minimum distance along a great circle was calculated between the radiant and the nearest star, both located in the same constellation. Also we have verified if we deal with the "Daytime", "Southern" or "Northern" radiant, as well on which month the shower activity period falls. To find the month of the shower activity we found the date of the shower activity corresponding to the Sun ecliptic longitude given in the MDC. We used the formulae for the Sun ecliptic longitude given in Meuss (1991); Astronomical Almanac (1996). Throughout all test the Sun ecliptic latitude was set to zero, the year of the shower activity was assumed to be 2000 AD.

3.1. Choice of the star catalogue

At the end of AD 2013 the IAU MDC comprised of 95 established showers, 460 working list showers and 24 groups – shower complexes. Inclusively the IAU MDC list (including complexes) contained 579 meteor showers. We have posed a question – are the names of these showers correct from the point of view of the meteor shower nomenclature rules?

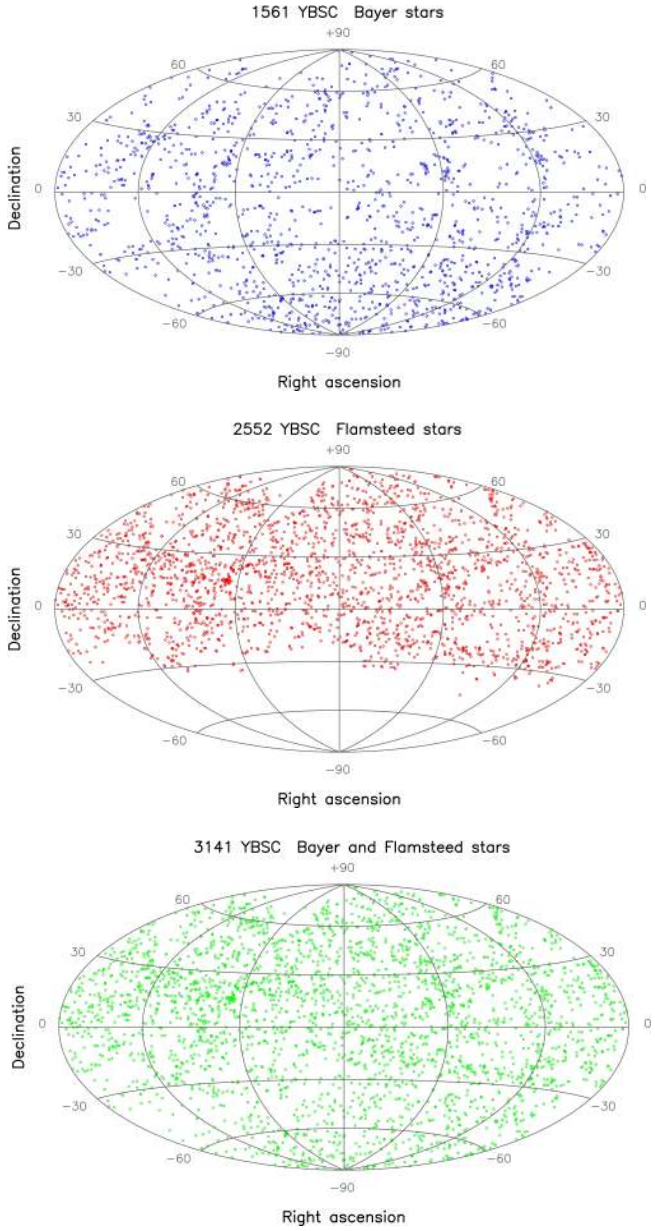

Figure 2. The Hammer-Aitoff diagram of Bayer (top) and Flamsteed (middle) stars taken from the Yale Bright Star Catalogue. The stars designated by Flamsteed are distributed on the sky only visible from Great Britain. The Bayer stars are distributed more uniformly. The bottom diagram contains all 3141 Bayer and/or Flamsteed stars taken from this catalogue. The sky coverage is better on this diagram, still one can see a few regions significantly less populated by stars.

Quickly we have realized that in many cases the shower names can not be verified, and that the main reason of it lies in insufficient precision of 2-nd rule of the meteor shower nomenclature. To apply this rule one has to decide on the star catalogue to use and the limiting magnitude of stars. Such settings were never made by the WG, therefore to address the above issue we have applied the Yale Bright Star Catalogue (BSC), 5th Revised Ed. (Hoffleit and Warren 1991).

The BSC contains 9096 stars† brighter then ∼6.5 magnitude, which is roughly every star visible to the naked eye from the Earth. The catalogue is fixed in number of entries, but its data is being updated. The version of 1991 was the next but four, and it was compiled and edited by Ellen Dorrit Hoffleit of Yale University. Among others, the BSC catalog contains the equatorial positions of stars for J2000, the visual magnitudes, and detailed information on individual entries. This information includes constellation code and a star name — generally Bayer and/or Flamsteed name.

Originally Bayer stars were labelled by Greek and Latin letters e.g. "alpha Centauri", "d Centauri". However, to avoid some confusion, astronomers revised Bayer's system adding several modifications. E.g. in Orion constellation the Greek letter "pi" was supposed to apply to all six stars in the arc forming the lions pelt or shield on Orion left arm. In this case, astronomers added superscripts to Bayers letters (pi^1, pi^2, pi^3,...) to distinguish between the individual stars. In the case of Flamsteed designation system each star is labeled by a number and the Latin genitive of the constellation it lies in, e.g. "51 Pegasi".

From the BSC we have drawn a subset of 3141 stars for which Bayer and/or Flamsteed names were available.‡ Our subset contains 1561 Bayer's stars and 2552 stars designed by Flamsteed. 972 stars have both Bayer and Flamsteed designations. Flamsteed's catalogue covered only the stars visible from Great Britain, and therefore stars of the far southern constellations have no Flamsteed numbers. Bayer stars cover the whole sky more or less uniformly. Figure 2 illustrates distributions of Bayer and Flamsteed stars on the whole celestial sphere.

3.2. Results of the shower name correctness test

After setting the star catalogue, we used a software in which we implemented all the shower nomenclature rules. We wanted to test the name correctness of the meteor showers listed in the IAU MDC. Altogether 554 meteor shower names were initialy tested, but after including the showers for which we had several radiants, we have tested 646 shower names.¶ We compared all components of the shower names given in the MDC database with those yielded by out test-software. We were able to control correctness of the Daytime-Nighttime shower activity, Northern-Southern

† The BSC contains 9110 objects, of which 9096 are stars. Fourteen objects cataloged in the original compilation of 1908 are novae, supernovae or non-stellar objects that have been retained to preserve the numbering.

‡ Three stars from the Trapezoid group in the Orion constellation were omitted to avoid the same star names.

¶ As *a natura rei* — our test was possible only if the solar ecliptic longitude at the moment of the shower activity and the radiant coordinates were given. In the IAU MDC, in case of meteor shower complexes such information is only available for three of them.

branches, the month of the shower activity and the star and constellation names. As was expected, we observed that for some showers more than one name component is incorrectly specified in the IAU MDC database. In Table 3 we collected general results of the test. We made several tests for a few subsets of the whole radiant set (646 radiants) and for different sets of the BSC stars.

Table 3. Results of the name correctness test for the IAU MDC meteor showers. The first row refers to all 646 radiants of 554 meteor showers (status for the end of 2013). The second row (350 radiants) refers to "old" showers only, observed before the Working Group on Meteor Shower Nomenclature was organized. The last row involves the showers for which the names were assigned by the Working Group (WG flag in the first column). The letters B and F in the first columns mean that Bayer and Flamsteed stars were used in the test. The second column gives the number of tested shower radiants (NR), the third column (IN) gives the total number of incorrect shower names, the following columns include the number of showers for which the test gave negative results due to incorrect: N-S – Northern-Southern branches, D-N – Daytime and Nighttime activity, M – month of the shower activity, Star – name of the radiant nearest star, Const – constellation name in which the radiant is located. For IN, Star, Cons columns the percentage ratio between quoted values and the NR are given in brackets.

	NR	IN	N-S	D-N	M	Star	Const
BF	646	464 (72%)	5	12	6	415 (64%)	156 (24%)
B	350	257 (73%)	3	10	2	216 (62%)	125 (36%)
BF+WG	296	186 (63%)	2	2	4	175 (59%)	31 (10%)

3.3. Discussion of the results

At first glance, the results given in third column of Table 3 are very discouraging. For majority of meteor showers listed in the MDC, their names do not fulfill the nomenclature rules (see section 3).

In Table 3, the first row presents the most complete result of our test. We used all 3141 Bayer and Flamsteed stars from the BSC catalogue and tested 646 shower radiants included in the MDC database. The names of 73% of meteor showers did not fulfill the nomenclature rules. However one can easily explain significant part of such a result. In this test we made use of Flamsteed stars as well, but these stars were not used when names for ∼500 of the shower radiants collected in the MDC were assigned. Flamsteed stars have been in use quite recently for naming meteor showers.

So we made two additional tests. The first one concerned 350 showers for which the names were assigned outside the WG, and the second test for 296 showers which were named by the WG. In the first test only Bayer stars were used, in the second one, both Bayer and Flamsteed stars. Results of these additional tests are given in the second and third row in Table 3. The numbers of incorrect names are still very high, but the high number of incorrect names for showers fixed before the WG activity time is not a surprise. At that time the shower names were assigned more or less subjectively, using different star maps and possibly applying individual rules developed by shower discoverers.

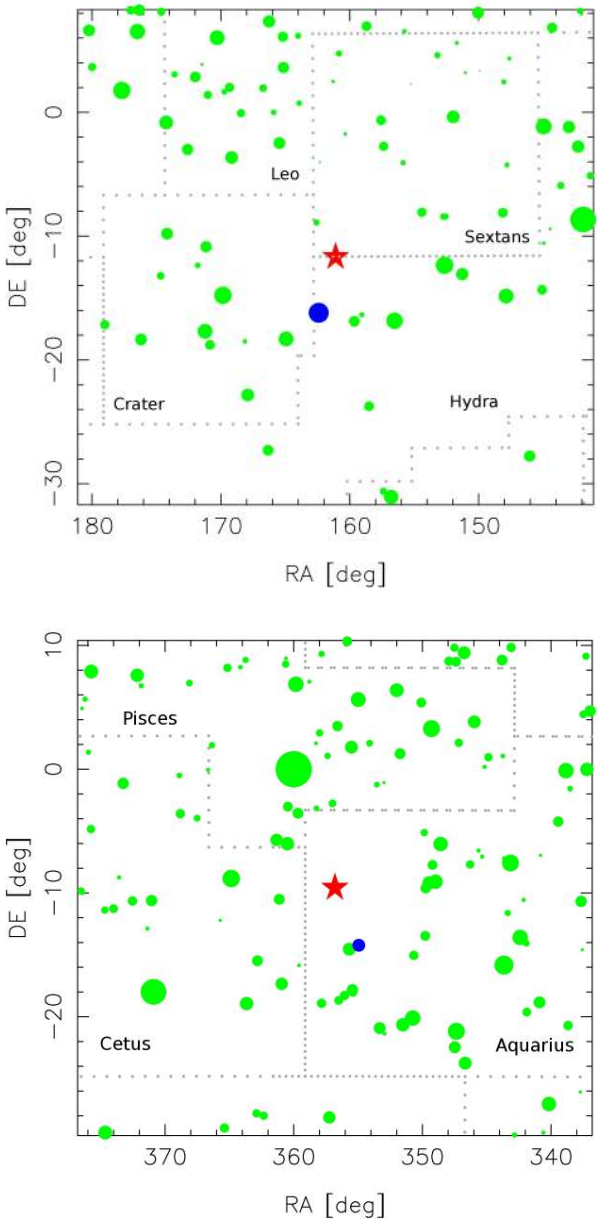

Figure 3. Top — difficult case of the radiant assignement (marked by star symbol) of January ν Hydrids (#544, JNH). It lies almost on the border of two constellations. Bottom — the radiant of the August ι Cetids (#505, AJC) undoubtedly lies in the Aquarius constellation.

The last row in Table 3 enables us to draw a weak conclusion that activity of the WG brought positive results – among 296 showers a fraction of incorrect names is a bit smaller. However, this fraction is disconcertingly high, and after the WG started its activity, one should expect that all fractions in the last row of Table 3 should be close to zero. Again we can explain such result easily. During the seven years of its activity the WG had no access to the standard implemented by our software. Without any commonly used standard, all the work of the WG was subjective.

Without an objective tool (a software plus a star catalogue) it is very difficult to find which star is the closest one to a given point on the celestial sphere. Therefore in Table 3 we see the highest numbers in the seventh column. Additionally these numbers were increased by each incorrect assignment of the constellation name in which the shower radiant lies in. Therefore one can assume that the incorrect star names, for the most cases, resulted just due to mistakes. They were not the results of the willful nomenclature rules violations.

But it seems to be the opposite in case of the incorrect constellation name assignment. Certainly, a few mistakes were also possible here. E.g. on Figure 3 the radiant of January ν Hydrids lies very close to the border between Hydra and Sextans constellations. By "naked eye" it is very difficult to decide in which constellation this radiant lies in. Therefore in case of incorrect constellation names we can have some amount of mistakes, but in most cases, it seems that the shower nomenclature rules were violated, also by the WG. An example of such nomenclature rule violation is shown on the bottom graph of Figure 3. On this graph, the radiant point lies undoubtedly inside the Aquarius constellation, however despite it, the shower was named August ι Cetids.

Our tests have shown that the number of incorrect months, branches and day-night activities assignments are small. They were caused by mistakes like in case of the shower Southern δ Leonids (see Figure 4), or due to inconsistency of the shower parameters. In some cases, data given in the MDC shower database were taken from different sources, e.g. the solar longitude at the peak of the shower activity and the radiant coordinates are taken from different sources. Therefore, probably they are inconsistent. But in our software to find e.g. precise radiant elongation from the Sun at the moment of shower activity one needs consistent data. From our experience, the data inconsistency in the MDC is a serious problem and should be investigated separately.

Several incorrect "Daytime" prefixes can be explained by the choice of the value 32 degrees† for the critical elongation of the daytime radiant from the Sun. In the MDC database we have found the shower (#152, NOC, Northern Daytime ω Cetids) with radiant elongation 47 degrees, labeled by Sekanina in his original paper Sekanina (1976) also as "Daytime" shower. It is clear that the value 32 degrees is just too rigorous.

† This value was taken from Jenniskens (2008); Jopek and Jenniskens (2011).

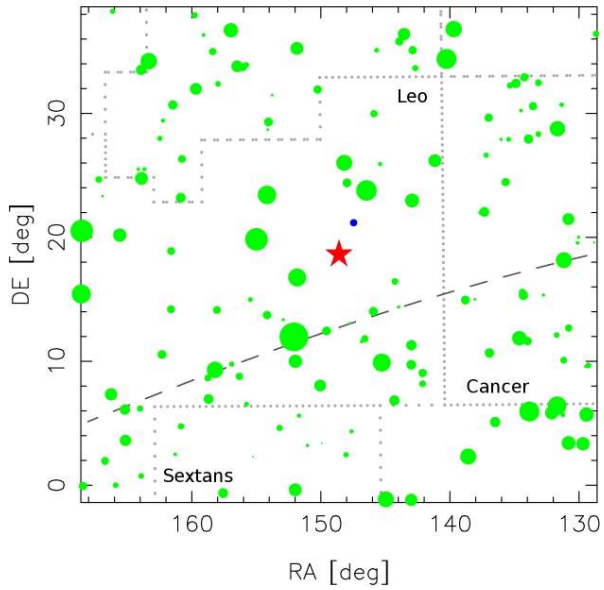

Figure 4. Southern δ Leonids (#113, SDL), the third set of parameters for this shower contains the radiant coordinates RA=148.6, DE=18.6. Its ecliptic latitude is BE=5.5 degrees, what means that this radiant, marked by a star symbol, lies in the northern ecliptic hemisphere not the southern one.

4. Conclusions

In 2012 during the GA IAU in Beijing, 31 new meteor showers were officially named. Thus, at present the list of the established meteor showers contains 95 objects. Including showers placed on the Working list and the List of Showers Groups the MDC contains 579 meteor showers (see Jopek and Kaňuchová 2013).‡

On the IAU website `http://www.iau.org/public/themes/naming/` one can find information on how different astronomical objects and features are named, *inter alia* the minor planets and comets. There is no information about the nomenclature of meteor showers. To include such information on this website, we believe, it is essential to formulate and implement the objective rules of the meteor shower nomenclature. Our study has shown that nomenclature rules published so far are not sufficient for this purpose. They are not sufficiently precise, hence not objective. Such situation is very disadvantageous for the meteor astronomers community.

Existing nomenclature problems can be solved twofold: by keeping tradition as much as possible, or more radically. In the first approach we should transform existing traditional, imprecise rules into a set of objective ones, e.g. by choosing a standard star catalogue which will be used for meteor shower name assignments. More radical approach, perhaps unavoidable, requires more energy and a good will from the meteor astronomers community. Probably, it would require the break up with the tradition.

‡ Status at the end of 2013.

Another important task is an improvement of the IAU MDC shower database. The MDC database needs further improvement, both as to its contents and as to its user friendly interface. Without fail, such improvement will require long-term activity.

Acknowledgements

We would like to acknowledge the users of the IAU MDC who informed us about several erroneous data: Reiner Arlt, Zeljko Andreić, David Asher, Rhiannon Blaauw, Steve Hutcheon, Diego Janches, Sirko Molau, Ned Smith and Francisco Ocaña, Regina Rudawska.

References

Astronomical Almanac, 1996, p. C24

Delporte E., 1930, Dlimitation scientifique des constellations, Cambridge University Press

Hoffleit D., Warren Jr., W.H., 1991, "The Bright Star Catalog, 5th Revised Edition (Preliminary Version)", http://tdc-www.harvard.edu/catalogs/bsc5.html

Jenniskens P., 2006, Meteor Showers and their Parent Bodies, Cambridge UP, UK, pp 790

Jenniskens P., 2006a, WGN, Journal of the International Meteor Organization 34, 127

Jenniskens P., 2007, Div. III, Comm.22, WG Task Group for Meteor Shower Nomenclature, IAU Information Bulletin 99, January 2007, 60

Jenniskens P., 2008, EM&P, 102, 5

Jopek T.J., Jenniskens P.M., 2011, in Proc. Meteoroids 2010 Conf., held in Breckenridge, Colorado USA, May 24-28 2010, eds Cooke W.J., Moser D.E., Hardin B.F., Janches D., NASA/CP-2011-216469, p. 7

Jopek T.J., Kaňuchová Z., 2013, http://www.astro.amu.edu.pl/~jopek/MDC2007/, or http://www.ta3.sk/IAUC22DB/MDC2007

Jeong-Han Kim, Geonhwa Jee, Changsup Lee, Yong-Ha Kim, 2013, Advances in Polar Science, 24 (4-English), 241

Meuss J., 1991, Astronomical Algorithms, Willmann-Bell, p. 151

Roman N.G., 1987, Publication of the Astronomical Society of Pacific, 99, 695

Seidelmann P.K., et al., 1992, Explanatory Supplement to the Astronomical Almanac, ed. by Seidelmann P.K., University Science Books, Mill Valley, California

Sekanina Z., 1976, Icarus, 27, 265

Index

Autor index

Keyword index